

***Advances in Printing
and Media Technology***

Vol. XXXVIII

Edited by Nils Enlund and Mladen Lovreček

Darmstadt
MMXI

Advances in Printing and Media Technology
Proceedings of the 38th International Research Conference of iarigai
Budapest-Debrecen, Hungary, September 2011

Published by the International Association of
Research Organizations for the Information,
Media and Graphic Arts Industries

Darmstadt, Germany 2011

Co-edited by

Nils Enlund, Helsinki, Finland
Mladen Lovreček, Zagreb, Croatia

Scientific Committee

Dr. Anne Blayo, Grenoble
Prof. Timothy Claypole, Swansea
Prof. Edgar Dörsam, Darmstadt
Prof. Nils Enlund, Helsinki
Prof. Wolfgang Faigle, Stuttgart
Dr. Patrick Gane, Helsinki
Prof. Jon Yngve Hardeberg, Gjøvik
Prof. Ulrike Herzau-Gerhardt, Leipzig
Prof. Gunter Hübner, Stuttgart
Dr. Per-Åke Johansson, Stockholm
Prof. Marie Kaplanova, Pardubice
Dr. John Kettle, Espoo
Prof. Helmut Kipphan, Schwetzingen
Dr. Marianne Klamann, Stockholm
Prof. Björn Kruse, Linköping
Prof. Yuri Kuznetsov, St. Petersburg
Dr. Magnus Lestelius, Karlstad
Prof. Ulf Lindqvist, Espoo
Prof. Patrice Mangin, Trois Rivières
Dr. Erzsébet Novotny, Budapest
Prof. Pirkko Oittinen, Helsinki
Prof. Jouko Peltonen, Turku
Dr. Bernard Pineaux, Grenoble
Prof. Anastasios Politis, Athens
Dr. Anu Seisto, Espoo
Prof. Johan Stenberg, Stockholm
Dr. Scott Williams, Rochester
Dr. Renke Wilken, Munich

The facts published in this book are obtained from sources believed to be reliable. However, publishers can accept no legal liability for the contents of papers, nor for any information contained therein, nor for conclusions drawn by any party from it.

No part of this publication may be reproduced, stored in a retrieval system or transmitted in any form or by any means of electronic, mechanical, photocopying, recording or otherwise without the prior written permission of the publisher.

Printed edition

ISBN 978-3-9812704-3-3
ISSN 2225-6067

Online edition

ISBN 978-3-9870704-4-0
ISSN 2409-4021

Contents

Introduction

Preface	3
Printing is alive and well - and so is print research <i>Nils Enlund</i>	
A light source colour fidelity index for the graphic arts <i>János Schanda</i>	5
Determining CIEDE2000 for printing conformance <i>Robert Chung, Ping-hsu Chen</i>	11

1. Printing techniques

Film splitting during offset printing - the influence of paper surface properties on film splitting geometry <i>Peter Rättö, Erik Blohm, Gary Chinga Carrasco</i>	21
Modeling local print density variations in rotogravure print <i>Ulrich Hirn, Markus Lechthaler, Wolfgang Bauer</i>	27
Development of a comparative tool to predict ink misting <i>Laurette Vieille-Grosjean, Alice Vermeulin</i>	35
Two-dimensional digital emulation for alignment of paper sheet in the printing press <i>Rostislav Moginov, Eva Poznyak</i>	43
CCD sensors for ink film opacity measurement and color evaluation <i>Paritosh Prayagi, Dietmar Nowack, Alexander Böddicker, Markus Schnitzlein, Chris Maurer, Arved Hübler</i>	51
Hybrid printing - print quality mechanisms when offset and inkjet are combined <i>Marianne Klamann, Erik Blohm, Per-Åke Johansson, Jon Lofthus, Viviane Alecrim, Jonas Örtengren</i>	59
Simulation aided design of inkjet systems <i>Philip Marmet, Fritz Bircher, Johannes Renner, Philipp Haslebacher, Gert Schlegel, Florian Fässler</i>	69
Reproducibility of DoD inkjet printing systems <i>Johannes Renner, Fritz Bircher, Gert Schlegel</i>	79
The influence of printing pressure on flexographic print quality <i>Akos Borbely, Rozalia Szentgyörgyvölgyi</i>	87
A statistical approach to the modelling of ink transmission on flexo-printed sack paper <i>Verena Feirer, Ulrich Hirn, Herwig Friedl, Wolfgang Bauer</i>	93
Influence and interaction phenomena of screen printing machine settings on surface roughness <i>Ingmar Petersen, Gunter Hübner, Timothy C. Claypole, Eifion Jewell</i>	103
The new technology of perfect binding with vibratory milling heads and investigations of durability of adhesive bonded books <i>Georgij Petriaszwili, Yuriy Pyryev</i>	111

2. Printing materials

- The role of substrate structure in liquid transfer during heatset offset printing 123
Carl-Mikael Tåg, Maunu Toiviainen, Mikko Juuti, Catherine Ridgway, Patrick A. C. Gane
- The effect of coating pore structure and geometry on the drying efficiency of heatset web-offset ink solvent 133
Philip M. Gerstner, Hai Zhang, Patrick A. C. Gane
- Nanoscale single and multilayer adsorption of polyelectrolytes to pulp fibers 143
Praveen Chandak, Levente Csoka, George Grozdits
- The influence of UV coating application on printed cardboard surface properties and colourimetric values 153
Igor Karlović, Erzsébet Novotny, Ivana Tomić, Dragoljub Novaković
- Extending the use of fibre based substrates using novel surface treatment methods: case studies 159
Vesa Kunnari, Annaleena Kokko, Tomi Erho, Timo Kaljunen, Thea Sipiläinen-Malm, Mikko Keränen
- Improving the light fastness of sublimation transfer printed polyester substrate 167
Imadeddine Afara, Philip Urban, Edgar Dörsam
- Impacts on the impression of printed effect pigments 175
Martin Haas, Edgar Dörsam, Evgeny Kurmakaev, Thorsten Euler, Martin Schmitt-Lewen, Immanuel Fergen, Joachim Sonnenschein
- Screen printing with effective printing inks 183
Raša Urbas, Jana Rozman, Marta Klanjšek Gunde
- Pore structural changes in inkjet coatings by the inclusion of binders and additives 191
Catherine J. Ridgway, Vesa Kukkamo, Patrick A. C. Gane
- Influence of flexographic inks on optical density of full tone fields and contrast in printing on the biodegradable films 201
Joanna Izdebska, Halina Podsiadlo
- Evaluation of image segmentation algorithms for folded substrate analysis 209
Magdolna Apró, Dragoljub Novaković, Pál Szabolcs

3. Special printing applications

- Inkjet printed electronics at UAB-CNM: technology and design flow developments 221
Eloi Ramon, Francesc Vila, Elkin Gonzalo Díaz, Jofre Pallarès, Lluís Terés, Jordi Carrabina
- Electrical and print quality of flat-plate capacitor screen-printed on paper 231
Marta Klanjšek Gunde, Marijan Maček, Maša Žveglič, Tadeja Muck, Tjaša Vidmar, Janja Plevnjak, Nina Hauptman, Raša Urbas, Gorazd Golob, Marica Starešinič
- Characterisation of catalyst layers for fuel cell printed by flexography 237
Chloé Bois, Anne Blayo, Rémi Vincent, Christine Nayoze, Didier Chaussy
- Gravure printing of thick film electrodes for PEM fuel cell production 247
Frank Siegel, Albert Kohl, Eugen Enns, Wolfgang Deger, Holger Dziallas, Andreas Willert, Reinhard Baumann

UHF RFID antenna printing on offset paper substrate using inkjet and screen-printing technologies <i>Markus Johannes Müller, Susana Otero, Vicente de Gracia</i>	253
Optimization of aperture size and distance in the insulating mask of a five layer vertical stack forming a fully printed thermoelectric generator <i>Andreas Willfahrt, Gunter Hübner</i>	261
Smart-printed-pack - intelligent packaging container attached with opening detector and paper-based electroluminescent indicator lamp <i>Vincente de Gracia, Susana Otero, Nuria Herranz, Markus Johannes Müller, Juan Diaz</i>	271
Printability of thermochromic offset inks and their interactions with dampening solution <i>Ondrej Panák, Bohumil Jašúrek, Jan Vališ, Marie Kaplanová, Marta Klanjšek Gunde</i>	277
Polymer films with watermark for protected printing production <i>Alexandr Kondratov, Evgeny Bablyuk, Marina Dryga, Evgenia Anokhina</i>	285
Braille dot height impact on the functionality and legibility of the pharmaceutical packaging <i>Gorazd Golob, Bojan Rotar, Damjan Šulc</i>	293
 4. Color processing	
Evaluating color-difference formulas in LCD-based soft-proofing <i>Maria Fedutina, Philipp Urban, Edgar Dörsam</i>	303
Colour effect changes at security graphics due to print media and colour sequence <i>Erzsébet Novotny, Rozalia Szentgyörgyvölgyi, Pál Görgényi-Tóth</i>	309
Characteristic analysis of the primary color inks in color print <i>Mahziar Namedanian, Sasan Gooran</i>	317
Regression method for predicting the colorimetry of spot colour overprints <i>Kiran Deshpande, Phil Green</i>	323
Extended color gamut printing for flexo packaging <i>Alexandra Pekarovicova, Veronika Lovell, Paul D. Fleming</i>	331
Evaluation of quality for color halftone <i>Li Yang</i>	339
The impact of optical brightener on the color perception of halftones <i>Michael Dattner, Daniel Bohn, Peter Urban</i>	349
 5. Environment, publishing and society	
Printing and environmental sustainability <i>Ivana Bolanča Mirković, Igor Majnarić, Sandra Mustač, Zdenka Bolanča</i>	361
Development of innovative sustainable printing practices to reduce VOCs emissions in the SMEs printing industry based on BREF best available techniques <i>Markus Johannes Müller, David Pérez, Vincente de Gracia, Alejandro Fuentes, Susana Otero</i>	369

Water conservation and approach to zero liquid discharge (ZLD) in a paper manufacturing plant - A case study	379
<i>Anayath Rajendrakumar, Satyavolu V. Subrahmanyam, Senniappan Chinnaraj, Amrutharaj Harikrishan, Kaipensery S. Rajesh, Kiran Prayagi, Palaniappan Karunanithi, Natarajan Baskaran</i>	
Analysis of JDF files	387
<i>Thomas Hoffmann-Walbeck, Sebastian Riegel</i>	
Multiple platform magazine publishing: integration of print and digital content in traditional magazine advertising	395
<i>Natalia Gilewicz</i>	
Local newspaper publishing: editorial structure and environmental impact - a case study	403
<i>Malin Picha, Åsa Moberg</i>	
Social media in print - a publishing system for communities	411
<i>Timo Kuula, Maiju Aikala, Jouko Hyväkkä, Anu Seisto</i>	
Exchange rates for media currencies	419
<i>Ulf Lindqvist, Anna Viljakainen, Hannu Kuukkanen, Paula Järvinen, Pekka Siltanen</i>	
Index of authors	425



Introduction

Preface

Nils Enlund

Co-editor, Chairman of the **iarigai** Program and Publishing Committee

E-mail: nilse@kth.se

Printing is alive and well - and so is print research

The rapid demise of print has in recent years been foretold by many consultants and other prophets. In a digital world with next to instantaneous global communication, who needs print? Still, print is everywhere around us. Not only in this book, but on every package, on every signpost, every t-shirt, in all manuals for new electronic media devices. Certainly, the broad spectrum of printed products will undergo changes and balance shifts as digital products and services capture portions of the consumer market but the demand for quality print will remain.

In addition, new uses for printing technology are developing. Printing is currently seen not only as a method for putting text and images on paper but as a more generic technology for rapidly and accurately placing "stuff on stuff", i.e., different types of substances on different types of substrates. Printed electronics is a topical and representative example of such novel applications.

Both the developing of new printing applications and the optimization of traditional techniques require advanced scientific and technical research. And high quality research is currently carried out at universities and research organizations all over the world. The yearly **iarigai** conference is the main international forum for the exchange of research results in the print and media technology field. The volume that you now hold in your hands contains the research contributions presented at the 38th International Research Conference of **iarigai**, the International Association of Research Organizations for the Information, Media and Graphic Arts Industries, held in Budapest and Debrecen, Hungary, from September 11 to 14, 2011. The contributions for this conference were evaluated and selected by a scientific committee of international experts through a double-blind review process.

These proceedings provide a good overview of current research at universities and research organizations in the field. Contributions cover a broad field: publishing issues, environmental considerations, printing techniques and materials, security printing, printed electronics, as well as color processing and management.

Color is also the topic of the two keynote presentations at the conference. These non-reviewed contributions are included at the front of these proceedings.

The editors and publishers hope that you will find the contents of these proceedings valuable, informative, and interesting.



A light source colour fidelity index for the graphic arts *

János Schanda

University of Pannonia, Egyetem u. 10, H-8200 Veszprém, Hungary

E-mail: schanda@vision.vein.hu

Abstract

Colour mismatch problems appear when inappropriate illumination is applied. Colour matching functions need updating to be able to produce measurement results that will agree with visual testing. Three levels of correction are discussed and determined. Furthermore, the new CIE indoor D 50 and D 65 illuminants could deliver more reliable results as the traditional illuminant C, and by using the proposed smoothing the realization of sources seems to be also possible.

Keywords: colour fidelity, colorimetry, illuminant

1. Introduction

Graphic arts standardized the CIE Daylight Illuminant D50 for its colour checking work. But the art work is often looked under the illumination of light sources whose spectrum differs considerably from D50. This leads to colour mismatch problems, and it turned out that by simple colorimetric computations these mismatches can not be corrected. In our research we investigated these questions and came to the conclusion that corrections have to be made at three levels:

- correct the colour matching functions (CMFs) used in the colorimetric calculations;
- use more realistic irradiation spectral power distributions as the generally accepted D50;
- update the present colour rendering metric to describe the real colour appearance of the observed images better.

In the following these three aspects of modern graphic arts colorimetry will be discussed.

2. Correcting the colour matching functions

CIE has defined two sets of CMFs for 2° and 10° Observers. In graphic arts only the 2° Observer is used, as the coloured patches one has to envisage are usually smaller than 4°, the limit for the use of the 2° Observer. As well known the 2° Observer, defined in 1931, has been coupled to the photometric observer, the $V(\lambda)$ -function, and this function deviates from average visual sensitivity in the blue part of the spectrum. Although this is known since 1951 (CIE, 1951), a supplementary spectral luminous efficiency function was published only in 1990 (CIE, 1990), and the CMFs have not been corrected till date.

In 2006 we found (Bieske et al, 2007) that the visual and instrumental match of an RGB LED with an incandescent lamp differed considerably. Figure 1 shows the chromaticity of an incandescent light as a blue square, several observers matched with RGB LEDs this light and from the spectrum we calculated the chromaticity, and obtained the orange diamonds. As can be seen the individual match settings of the observers lay all outside the chromaticity of the incandescent lamp.

The experiment has been repeated with differently filtered incandescent lights with similar result (Csuti P, 2008). CIE TC 1-36 is developing a colorimetric description based on the cone fundamental spectral responsivity. Based on these CMFs a tentative transformation to a CIE XYZ like colour space has been elaborated (CIE, 2006), and it could be shown (Csuti et al, 2009) that the CIE TC 1-36 tentative CMFs give a better description of the visual colour match as the CIE 1931 CMFs. We could show that even better agreement can be reached with a slightly modified blue cone spectral sensitivity curve, see Figure 2.

* Invited keynote presentation given at the 38th International research conference, Budapest, September 2011

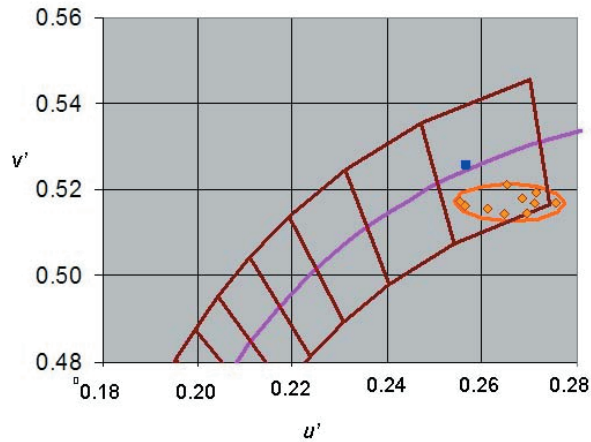


Figure 1: u',v' chromaticity co-ordinates of visually matching incandescent light (blue square) and RGB LED light (orange diamonds)

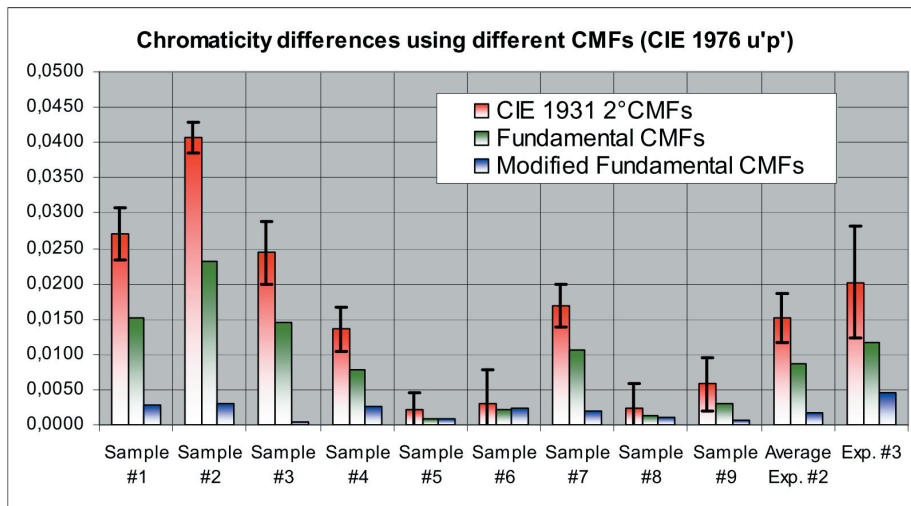


Figure 2: Chromaticity differences of nine samples of filtered incandescent light and mixtures of RGB-LED lights, using the CIE 1931 CMFs, the Fundamental based CMFs recommended by CIE TC 1-36 and the CMFs using a modified S-cone spectrum

As can be seen from Figure 2 the CIE 1931 CMFs, used in graphic arts, describe considerable mismatch for the visual match, the CIE TC 1-36 CMFs are much better, but real agreement can only be reached with our modified CMFs.

In subsequent investigations we could show that the relationship shown in Figure 2 holds also in many other situations (Csuti et al, 2011). Based on all these results one can state that if colours should be reproduced in such form that they should agree in different media the calculation should be done using the modified cone fundamental based CMFs. This is especially true if in graphic arts prepress investigations are made using an LCD monitor with RGB LED primaries.

3. Illumination of the print copy

If the soft copy is correctly evaluated the hard copy has to be evaluated correctly too. The general practice of using a D50 simulator is not necessarily the best solution. A few years ago we proposed an indoor daylight illuminator (Gombos et al, 2009) based on which the CIE defined its indoor daylight. Figure 3 shows the spectral power distribution (SPD) of the traditional (standard) D65 and D50 illuminants and the recommended indoor illuminants. As can be seen, for the indoor illuminants the UV radiation below 360 nm is strongly reduced, this will provide lower contribution of optical brighteners in the colour appearance of the paper, and will enable unified use of daylight illuminants, i.e. abandon the use of the outdated illuminant C.

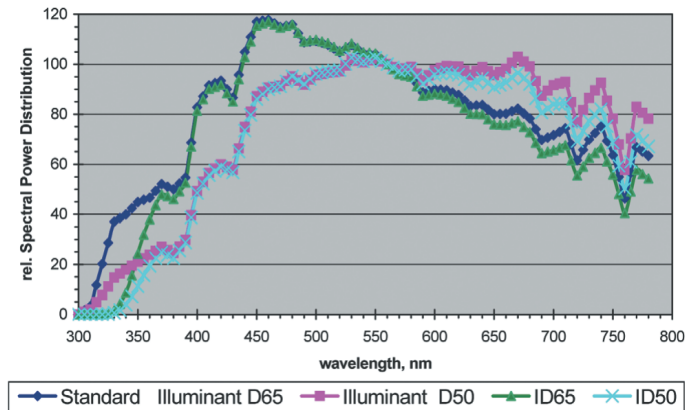


Figure 3: Spectra of the indoor and outdoor (standard) daylight spectra for D65 and D50

Daylight spectra show irregular sharp edges that can not be reproduced in sources. Most daylight simulators use fluorescent lamps, where the mercury lines might cause difficulties if colours with slightly different reflection spectrum have to be evaluated. Using modern averaging routines one can try to optimize the smoothing of the daylight functions so that they can be reproduced using modern light sources. Figure 4 shows the CIE D65 SPD and a possible smoothed SPD that was created using the LOWESS averaging program. For testing the influence of the smoothing we calculated the colour difference of 100.000 different spectral reflectance samples of real objects if irradiated by the original and the smoothed D65 SPD and found that for the curve as shown in Figure 4 the largest CIELAB difference was $\Delta E_{ab}=0.3$ and the average was below 0.1. Thus one can recommend to use the smoothed SPD function. Experiments are under way how this smoothed function can be realized using practical light sources.

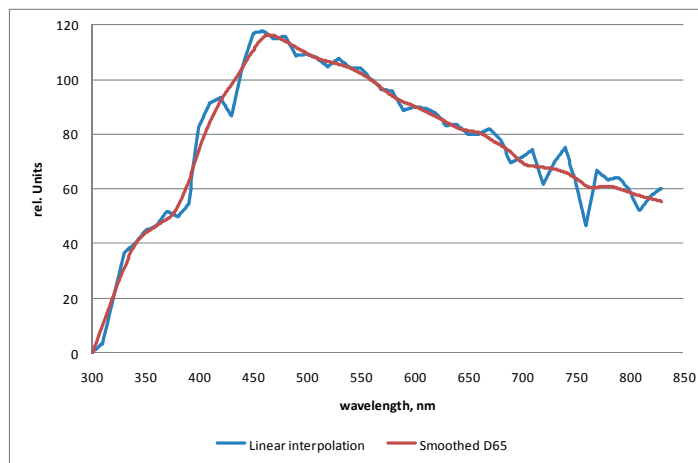


Figure 4: CIE D65 Daylight SPD (blue curve) and with LOWESS smoothed (red) curve.

4. Colour rendering

After putting both the soft-copy assessment and the hard-copy illumination into proper colorimetric description the images have to be evaluated according to their appearance. The most difficult question in the colorimetric evaluation of colour reproductions is the proper description of colour rendering. Classically the colour rendering had been defined as:

“effect of an illuminant on the colour appearance of objects by conscious or subconscious comparison with their colour appearance under a reference illuminant”

see (CIE, 1987). CIE defined 8 plus 6 test samples for this evaluation, defined to use Planck radiators as reference if the correlated colour temperature of the test source is below 5000 K and a phase of daylight if it is above 5000 K. The calculation is performed according to the scheme as seen on Figure 4 (Schanda, 2007).

Problems with the CIE recommendation (CIE, 1974) are that the calculation of the colour differences are based on the obsolete CIE U^*, V^*, W^* space, the method for chromatic adaptation is also outdated, and the test samples proved to be inadequate for proper evaluation. CIE is working on the updating of its recommendation, and at the CIE Session at Sun City, South Africa in 2011 decided to develop two metrics, one that describes colour fidelity and the other for colour preference.

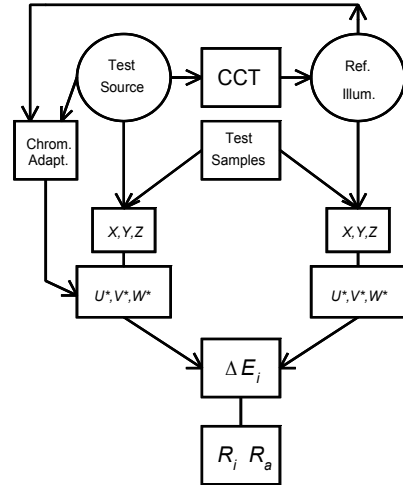


Figure 5: Flow chart for determining the colour rendering indices

4.1 Colour fidelity index

The CIE Technical Committee TC 1-69 decided that one of its recommendations should describe the colour difference of the test samples from the reference sample, just as in the traditional colour rendering index, only modern colorimetric models should be used. We are participating in a consortium working on the development of such a metric, and our recommendations is now to use

- 2 times 90 test samples of three different lightness values, two chroma values and 36 hue angles for most closely spaced samples (one set of highly colour constant samples and one set of metameric samples to these) plus four skin tones. Among these samples 83 samples are of graphic arts origin, others are textile, paint and natural object samples. Figure 5 shows in CIECAM02 space the location of the test samples illuminated by a test and a reference light source.

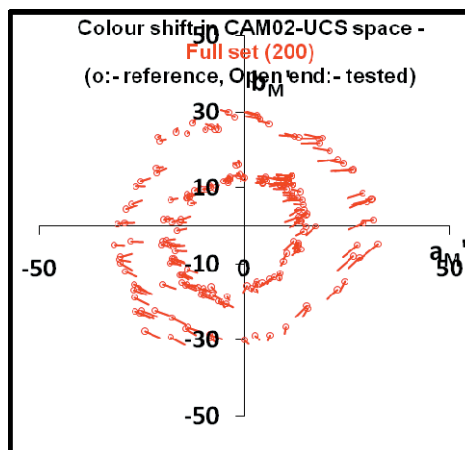


Figure 6: Samples in a_M', b_M' plane, showing the samples of different hues of a light source pair

- Calculations are made using the CIE 10° observer (a compromise as the modified CMFs have not been accepted yet internationally) and in CIECAM02 space.
- RMS averaging is performed for the individual colour rendering indices (CRIs) that are calculated from the colour differences using a nonlinear equation so the CRIs cannot be negative, but for very bad colour reproduction tend to zero. Maximum values, i.e. 100 % good colour rendering, is described in this proposed system also with an $R_a = 100$.

Our consortium hopes that this proposal will be accepted by the CIE technical committee and can be published soon as an official recommendations.

4.2 Colour preference index

The question of colour preference is - according to the opinion of this author - much more complicated. NIST is promoting the CQS metric (see Davis and Ohno, 2005), but we could show that the 15 test samples the model is using is not enough to produce an unambiguous description of the quality of the source to be tested.

We conducted colour preference investigations using ISO reference pictures comparing a tri-ban CFL, an RGB LED and two blue LEDs with yellow/red phosphors to an incandescent lamp, asking observers about their impression for vividness, naturalness and preference. At this stage we would like to draw attention only to the following questions: In one of our experiments observers were divided into two groups: “expert” observers who dealt in their daily work with colour, and “naïve” observers, who have learned about colorimetry (university students) but were not occupied in a colour related enterprise. Figure 7 shows the results. As can be seen the ranging of the light sources is different if you ask the naïve or the expert observers.

The replies depended also on the subject of the picture shown. The following figures show the three pictures used in this experiment and the scores the joint group of naïve and expert observers gave for the question “preferred illumination”. As can be seen not always the same light source was thought to give the most preferred colour reproduction, despite the fact that the illumination with the five sources was the same.

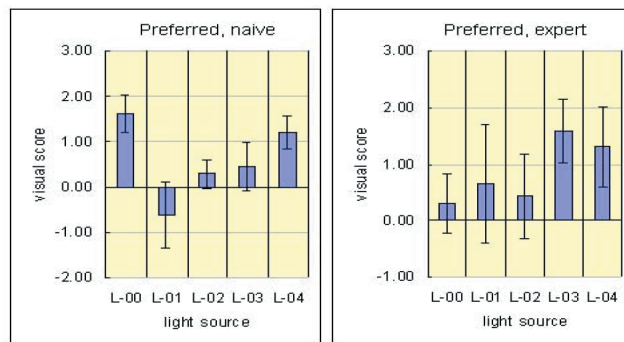


Figure 7: Replies of the two groups of observers on the question “preferred illumination”

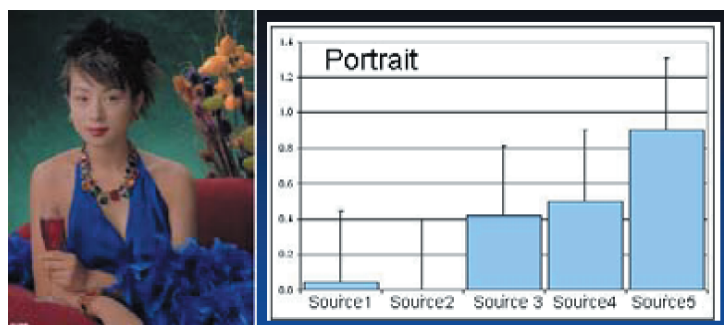


Figure 8: Picture “girl with glass” and preference scores for the different sources

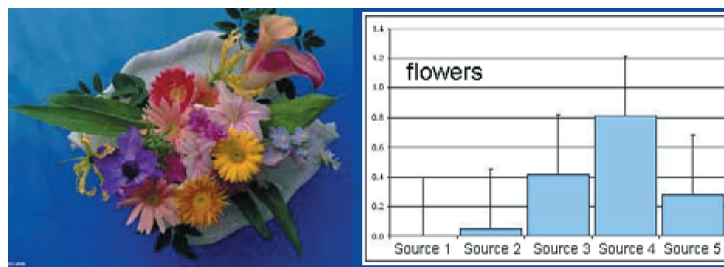


Figure 9: Picture “flowers” and preference scores for the different sources.



Figure 10: Picture "threads" and preference scores for the different sources

At this stage we do not want to go into more detail on the preference question and how it correlates with different proposed metrics. Investigations are still in progress and we hope to be able to report on results at a later meeting. At this moment we would like to draw only your attention on the fact that a proper evaluation of the light source colour preference needs still further investigation. For the graphic arts community we can only state that carefully selected reference sources and different image contents are needed to get to a meaningful result.

5. Conclusions

With the introduction of modern solid state light sources both as background illumination of displays and for image viewing traditional colorimetry is not enough to do meaningful evaluations in graphic arts. Colour matching functions need updating to be able to produce measurement results that will agree with visual testing. For image viewing in indoors the new CIE indoor D 50 and D 65 illuminants could deliver more reliable results as the traditional illuminant C, and by using the proposed smoothing the realization of sources - not simulators - seems to be also possible.

Colour fidelity description seems to be on the horizon, the development of a really good and meaningful colour preference index needs - however - further research.

References

- Bieske K, Csuti P, Schanda J (2007) Colour appearance of metameric white lights and possible colorimetric description. Proc. CIE Expert Symp. on Visual Appearance, Paris 2006, CIEx032:2007. pp. 137-139.
- CIE (1951) Technical Committee No. 7, Colorimetry and Artificial Daylight, Secretariat Reports. Proc. CIE 12th Session Vol. 1.
- CIE (1974) Method of measuring and specifying colour rendering properties of light sources, 2nd ed. Publication *CIE* **13.2**.
- CIE (1987) International Lighting Vocabulary. Publication. *CIE* **17.4**-1987.
- CIE (1990) CIE 1988 2° Spectral Luminous Efficiency Function for Photopic Vision. Publication. *CIE*. 086-1990.
- CIE (2006) CIE TC 1-36 draft technical report of Chapter 7.3: Development of chromaticity diagrams based upon the principles of the CIE XYZ system.
- CIE (2009) Indoor daylight illuminants. Publication. *CIE*. 184:2009.
- Csuti P, Schanda J (2008) Colour matching experiments with RGB-LEDs. *Color Res. & Appl.* **33/2** 108-112.
- Csuti P, Schanda J (2009) A better description of metameric experience of LED clusters. CIE Midterm Meeting, Budapest.
- Csuti P, Schanda J, Petruli R, McGroddy K, Harbers G (2011) Improved color matching functions for better visual matching of LED sources. CIE Conference 2011 Sun City, South Africa.
- Davis W, Ohno Y (2005) Toward an improved color rendering metric. Proc SPIE S941 9.
- Gombos K, Pointer M, Sik-Lányi C, Schanda J, Tarczali T (2009) Proposal for an indoor daylight illuminant. *COLOR Res. & Appl.* 43/1 18-25.
- Schanda J (2007) Colour rendering of light sources, Chapter 8 in Colorimetry - Understanding the CIE system, ed. J. Schanda, Wiley - Interscience.

Determining CIEDE2000 for printing conformance *

Robert Chung and Ping-hsu Chen

Rochester Institute of Technology
69 Lomb Memorial Drive, Rochester, NY 14623, USA
E-mails: rycppr@rit.edu; pinghsuchen@gmail.com

Abstract

ISO 12647-2 specifies tolerance of solid KCMY in CIELAB DE metric. Due to the fact that CIELAB lacks visual uniformity, ISO/TC130 decided to use CIEDE2000 metric, where appropriate, for all new ISO/TC130 standards and revisions of existing standards. This study used a printing database of over 200 printed samples to find out how solid conformance, determined by each metric, compared to each other. This research is not limited to finding CIEDE2000 values that are backward compatible with CIELAB DE. More importantly, this study recommends tolerance of solid KCMY in CIEDE2000 metric that are visually uniform. As a result, the value of $2.4 \Delta E_{00}$ is recommended for solid CMY and the value of $3.6 \Delta E_{00}$ is recommended as for black solid. These recommendations accommodate both visual uniformity and compatibility of the two ΔE metrics.

Keywords: CIELAB, ΔE^*_{ab} , ΔE_{00} , *Optimized ΔE_{00}*

1. Introduction

CIE developed the CIELAB color space as an approximation of uniform color space in 1976. The Euclidean distance in CIELAB color space, i.e., ΔE^*_{ab} , provides a quantitative way to define color difference. Several color difference metrics, such as CIE94, CMC, and CIEDE2000, have been proposed to provide a better correlation between the perceived color difference and instrumental color difference. There is no single ratio between ΔE^*_{ab} metric and these newer color difference metrics.

In Berns' paper (1996) and textbook (2000), he described a method for setting color tolerance between color difference data and visual data. This research adopted the method to find optimized CIEDE2000 tolerances values for ISO 12647-2 (2004 and 2007) solids of KCMY with a tolerance of $5 \Delta E^*_{ab}$.

2. Research question

The Euclidian distance is not good enough to discern and describe perceived color difference for graphic arts industry. For example, equal color differences values ΔE^*_{ab} of solids KCMY are perceived unequal in their visual color difference. The 24th ISO/TC130 Plenary Meeting, Sao Paulo, Brazil (TC130 N1733, 2010) resolved to use CIEDE2000 for all new ISO/TC130 standards and revisions of existing standards, where appropriate.

A difficulty in adopting ΔE_{00} is that there is no single tolerance value in ΔE_{00} metric that matches exactly the outcome with ΔE^*_{ab} metric. For example, two samples with identical ΔE^*_{ab} , as shown in Table 1, do not have the same ΔE_{00} values, calculated according to CIEDE2000 equations (ISO 13655, 2009).

Table 1: Example of samples with identical ΔE^*_{ab} but not identical ΔE_{00} values

ISO aim (L^*, a^*, b^*)	Samples (L^*, a^*, b^*)	ΔE^*_{ab}	ΔE_{00}
54, -36, -49	59, -36, -49	5	4.6
	54, -41, -49	5	1.8

Using ISO aim for cyan ($L^*, a^*, b^* = 54, -36, -49$) as an example, a tolerance of $5 \Delta E^*_{ab}$ encompasses a group of (L^*, a^*, b^*) values on the circumference of a circle that have an Euclidean distance of 5 from the ISO aim. When calculating the ΔE_{00} values between the ISO aim and the group of (L^*, a^*, b^*) values, they

* Invited keynote presentation given at the 38th International research conference, Budapest, September 2011

do not produce a single CIEDE2000 value. This issue can be further explored and expressed in Figure 1. The upper-center figure shows the ISO aim of cyan solid. There are 360 points, at an interval of 1 degree, on the circumference of the circle and they are all $5 \Delta E^*_{ab}$ away from the cyan ISO aim.

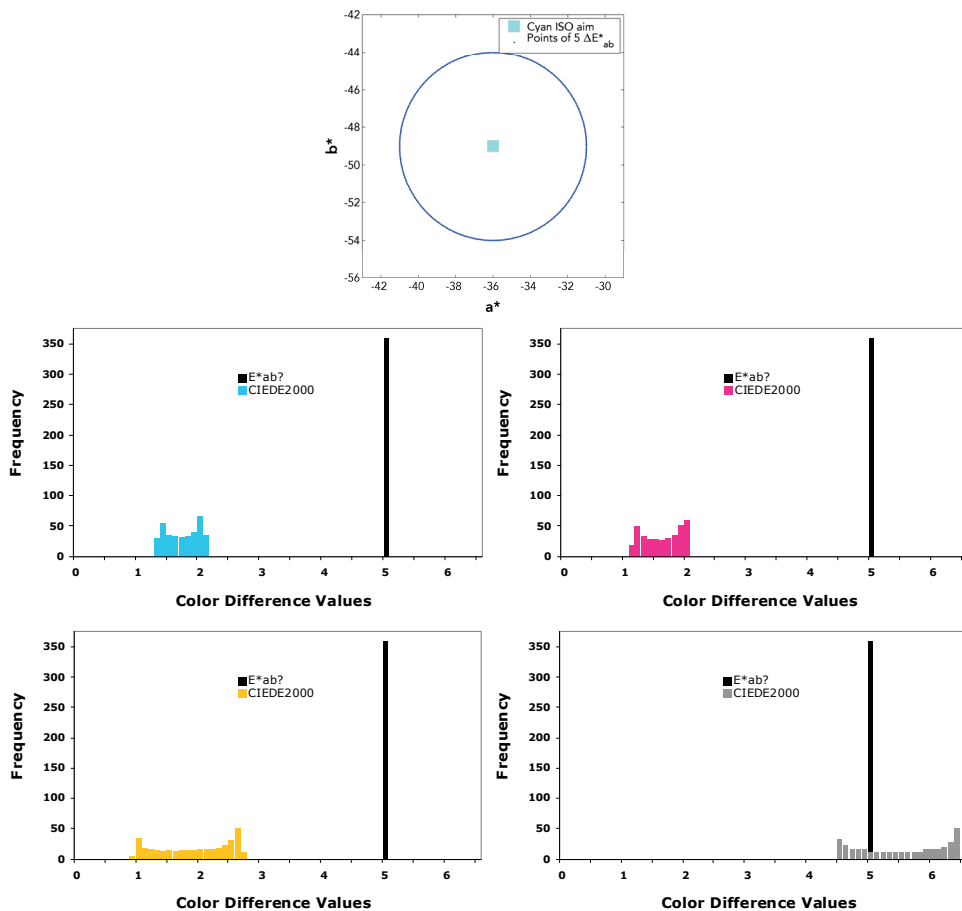


Figure 1: Example of samples with identical ΔE^*_{ab} but not identical ΔE_{00} values

The middle-left figure shows the histogram of ΔE_{00} values for those points on the circumference of the circle compared to the histogram of ΔE^*_{ab} that are $5 \Delta E^*_{ab}$ from the cyan ISO aim. To elaborate, the ΔE_{00} values of those equal ΔE^*_{ab} points are (1) smaller in magnitude, (2) not converging, and (3) non-normal distributed.

The middle-right, lower-left, and lower-right of Figure 1 show the cases for magenta, yellow, and black solids, respectively. By observing the ΔE distributions of CMYK solid, we can further conclude that: (1) colors having equal ΔE^*_{ab} convert to a range of ΔE_{00} , (2) ΔE_{00} magnitude of CMY solid is less than ΔE^*_{ab} , and (3) ΔE_{00} magnitude of black solid is similar to ΔE^*_{ab} . In other words, there is no easy solution in determining a “single value” in CIEDE2000 metric for each of the KCMY solids. This leads to the research question, “How can we determine color tolerance as a single CIEDE2000 metric for KCMY solids that represents the best compromise in ΔE^*_{ab} ?”

3. Literature review and research question

There are three instances where converting color tolerance from ΔE^*_{ab} into ΔE_{00} numbers for KCMY solids were studied. Specifically, Andreas Kraushaar (2010), Danny Rich (2010), and David McDowell (2011) discussed their approaches and findings at ISO/TC 130 meetings.

Kraushaar used 112 CIELAB measurements of KCMY solids from the bvdM/Fogra certification database, computed both ΔE^*_{ab} and ΔE_{00} between measurement and ISO 12647-2 colorimetric aims. Based on the CRF (cumulative relative frequency) of ΔE^*_{ab} and ΔE_{00} , he showed that the probability of passing at $5 \Delta E^*_{ab}$ for cyan solid is equivalent to the probability of passing at $2.6 \Delta E_{00}$. Only cyan solid was documented in his case study.

Rich took thousands of data points passing the ISO criteria around the printed solids. Ratios and their ranges between the two metrics, ΔE_{ab}^* and ΔE_{00} , were recommended based on those simulated pass data. Due to the fact that the magnitude of ΔE_{00} is hue-, chroma-, and lightness-dependent, Rich was not able to recommend a single ΔE_{00} , but a range of ΔE_{00} that equate to $5 \Delta E_{ab}^*$.

McDowell took ratios between two metrics, ΔE_{ab}^* and ΔE_{00} , from colorimetric data measured from proofing samples of IT8.7/4 target, and tried to find the “best ratios” of tints and solids between ΔE_{ab}^* and ΔE_{00} . It was shown that the ratio is proportional to KCMY ink amount and there is no single ratio between the two metrics.

The above literature review indicates that equal ΔE_{ab}^* transforms into unequal ΔE_{00} of less magnitude around KCMY solids, with the exception for K. But none can claim that there is a CIEDE2000 metric for each of the KCMY solids. Thinking outside the box, this research used a printing database of over 200 printed samples to find out how solid conformance, determined by each color difference metric, compared to each other.

To state the research question differently, i.e., “Is there a single ΔE_{00} that will pass as many jobs that ΔE_{ab}^* also passes and, at the same time, fail as many jobs that ΔE_{ab}^* also fails?” If such a value exists, we will call it, *Optimized ΔE_{00}* .

4. Methodology

In order to determine *Optimized ΔE_{00}* , we need a database with a large amount of printed samples, including jobs that pass and jobs that fail the criterion of $5 \Delta E_{ab}^*$. We also need an optimization strategy.

Once *Optimized ΔE_{00}* is determined, we need to realize that finding CIEDE2000 values that are backward compatible with CIELAB DE, is not the endgame. More importantly, we need to recommend tolerance of solid KCMY in CIEDE2000 metric that are visually uniform while backward compatible.

This section describes (1) an example of color tolerance optimization, (2) how to derive *Optimized ΔE_{00}* tolerances from database. The result of *Optimized ΔE_{00}* tolerances are discussed before the determination of ΔE_{00} tolerances for ISO 12647-2 solid conformance.

An Example of Color Tolerance Optimization

In his textbook, Berns describes an optimization routine that derives color tolerances between instrumental and visual data. Below is a step-by-step adoption of the optimization routine used in this research:

Step 1. Given a database with 35 $L^* a^* b^*$ measurements for cyan solids. Their ΔE_{ab}^* values and conformance compared to ISO tolerance ($5 \Delta E_{ab}^*$) are listed in Table 2.

Table 2: ΔE_{ab}^* values and conformances of 35 cyan samples

Sample	ΔE_{ab}^*	Conformance	Sample	ΔE_{ab}^*	Conformance	Sample	ΔE_{ab}^*	Conformance
#1	5.1	Fail	#13	2.4	Pass	#25	4.9	Pass
#2	2.5	Pass	#14	2.9	Pass	#26	3.4	Pass
#3	1.7	Pass	#15	6.7	Fail	#27	5.2	Fail
#4	6.1	Fail	#16	2.1	Pass	#28	3.0	Pass
#5	3.5	Pass	#17	1.9	Pass	#29	3.1	Pass
#6	1.3	Pass	#18	3.8	Pass	#30	1.9	Pass
#7	1.4	Pass	#19	7.3	Fail	#31	5.2	Fail
#8	2.7	Pass	#20	10.3	Fail	#32	4.8	Pass
#9	3.7	Pass	#21	7.0	Fail	#33	4.5	Pass
#10	3.2	Pass	#22	6.2	Fail	#34	5.2	Fail
#11	4.9	Pass	#23	4.0	Pass	#35	3.1	Pass
#12	3.3	Pass	#24	2.6	Pass			

Step 2. The data in the Table 2 are then sorted into two groups: “pass” ($5 \Delta E_{ab}^*$ or less) and “fail” (greater than $5 \Delta E_{ab}^*$).

Step 3. The CIEDE2000 values of 35 measurements can also be calculated based on the measurements and the ISO aim. Two groups (pass and fail) data are listed in Table 3 with corresponding CIEDE2000 values and placed in ascending order.

Table 3. Data of pass & fail groups with CIEDE2000 values in ascending order (Table 3).

Table 3: CIEDE2000 values in ascending order

Pass	CIEDE2000	Pass	CIEDE2000	4	CIEDE2000
1	0.5	14	1.7	1	2.1
2	0.5	15	1.9	2	2.4
3	0.8	16	1.9	3	3.5
4	0.9	17	1.9	4	3.5
5	1.0	18	2.0	5	3.6
6	1.0	19	2.0	6	4.1
7	1.0	20	2.2	7	4.2
8	1.0	21	2.5	8	4.2
9	1.3	22	2.6	9	5.3
10	1.3	23	2.9	10	6.7
11	1.4	24	3.2		
12	1.5	25	3.4		
13	1.7				

Step 4. The cumulative percentages (also known as CRF or cumulative relative frequency) for pass and fail groups are then calculated as follows:

$$CRF_{pass,i} = 100 (i / n_p)$$

$$CRF_{fail,i} = 100 - 100 (i / n_f)$$

where n_p and n_f represent the numbers of samples passed and failed, respectively, and i represents sample ID, which is 1 to 25 for pass group and 1 to 10 for fail group in this example.

Step 5. The CRF percentages (%CRF) with corresponding CIEDE2000 values are listed in Table 4.

Table 4. CRF of pass and fail groups with CIEDE2000 values

Pass CRF %	CIEDE2000	Pass CRF %	CIEDE2000	Fail CRF %	CIEDE2000
4	0.5	56	1.7	90	2.1
8	0.5	60	1.9	80	2.4
12	0.8	64	1.9	70	3.5
16	0.9	68	1.9	60	3.5
20	1.0	72	2.0	50	3.6
24	1.0	76	2.0	40	4.1
28	1.0	80	2.2	30	4.2
32	1.0	84	2.5	20	4.2
36	1.3	88	2.6	10	5.3
40	1.3	92	2.9	0	6.7
44	1.4	96	3.2		
48	1.5	100	3.4		
52	1.7				

Step 6. The %CRFs are plotted as a function of CIEDE2000 values (Figure 2).

If only the CRF of passed samples are plotted (colored in cyan) in Figure 2, one might conclude that the equivalent tolerance is the maximum ΔE_{00} of the pass group. This is what Kraushaar did. On the other hand, if only the CRF of failed samples are plotted (colored in blue), then the equivalent tolerance is the minimum ΔE_{00} of the fail group.

When both CRF curves are plotted, the intersection of the pass and the fail groups provides *Optimized ΔE_{00}* tolerance that maximizing the agreement between two metrics. In this case, below the intersection ($2.4 \Delta E_{00}$ & 81%), the CRF curve (colored in cyan) represents the case that “data pass with ΔE^*_{ab} metric also pass with ΔE_{00} metric”, and the CRF curve (colored in blue) represents the case that “data fail with ΔE^*_{ab} metric also fail with ΔE_{00} metric”. This points out the importance of having a large database with both pass and fail samples when determining *Optimized ΔE_{00}* .

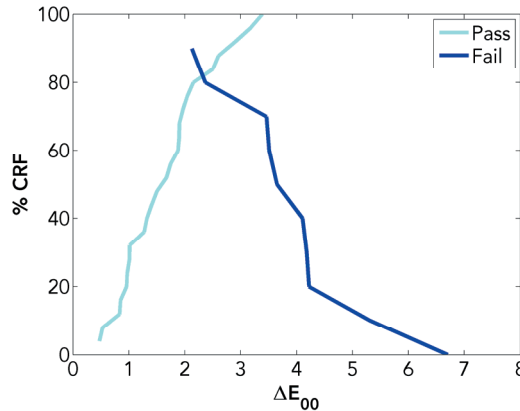


Figure 2: %CRF of pass and fail groups

Deriving Optimized ΔE_{00} Tolerances from Database

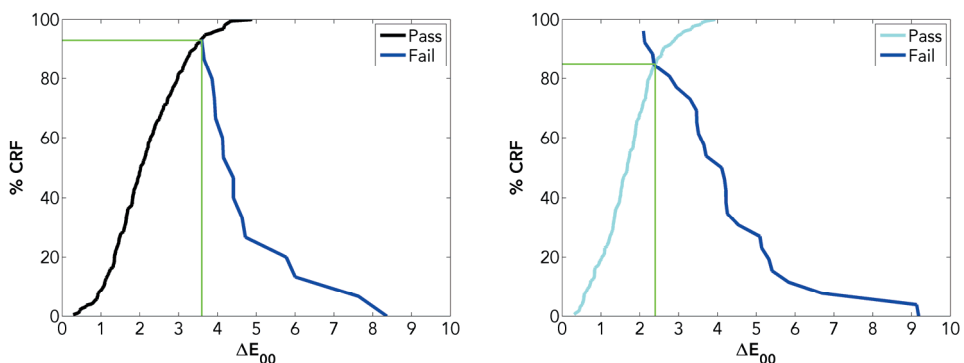
In this research, a total of 208 jobs from three databases, PSA, PSO, and G7, as shown in Table 5, were used. PSA (2011) database (n = 35) is unfiltered, thus, containing failed samples according to ISO 12647-2 criteria. On the other hand, PSO database (n = 88) is filtered, i.e., it only contains passed samples according to ISO 12647-2 criteria. G7 database (n = 85) is filtered where only samples that pass G7 Grayscale requirements are included. In addition, G7 database is not filtered according to ISO 12647-2 criteria for solid conformance, and hence it also provides data failed $5 \Delta E^*_{ab}$. These three databases were all used in the optimization routine, as described in the previous section.

Table 5: Three databases used in this research

PSA	35	Unfiltered	2010 PSA survey
PSO	88	Filtered by solid & TVI	Courtesy of bvdM/Fogra
Database	Number of Jobs	Filtered/Unfiltered	Remark
G7	85	Filtered by grayscale	Courtesy of IDEAlliance

5. Results and discussion

Figure 3 shows the %CRF versus the ordered ΔE_{00} values. The green lines help to locate the intersections, *Optimized ΔE_{00}* , and the percentages of outcome equality. When using $5 \Delta E^*_{ab}$ tolerances, the intersections of KCMY are at $3.6, 2.4, 2.2,$ and $1.5 \Delta E_{00}$, respectively.



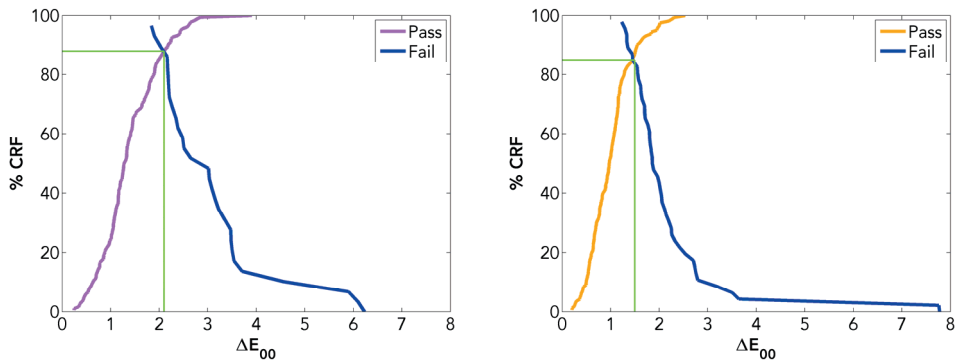


Figure 3: Optimized ΔE_{00} derived from the combined databases

Optimized ΔE_{00} corresponding to 5 ΔE^*_{ab} tolerances of printed solids are listed in Table 6. Optimized ΔE_{00} tolerances keep equal outcome higher than 84% in this case. Considering the two CRF curves form the shape of ‘X,’ the following observations apply to all four graphs:

- (A) The lower left of the ‘X’ represents samples that pass both 5 ΔE^*_{ab} and its Optimized ΔE_{00}
- (B) The lower right of the ‘X’ represents samples that fail both 5 ΔE^*_{ab} and its Optimized ΔE_{00}
- (C) The upper left of the ‘X’ represents “samples fail ΔE^*_{ab} metric, but pass at its Optimized ΔE_{00} ”
- (D) The upper right of the ‘X’ represents “samples pass 5 ΔE^*_{ab} metric, but fail at its Optimized ΔE_{00} ”

Table 6: Optimized ΔE_{00} tolerances corresponding to 5 ΔE^*_{ab} tolerances of solids

	ISO 12647-2 Solid Tolerances			
	K	C	M	Y
ΔE^*_{ab}	5	5	5	5
ΔE_{00}	3.6	2.4	2.2	1.5

These four observations can also be described as Figure 4. In the figure, the circle indicates the ΔE^*_{ab} tolerance, and the ellipse indicates ΔE_{00} tolerance. Case A, B, C, and D correspond to the A, B, C, and D observations above, respectively.

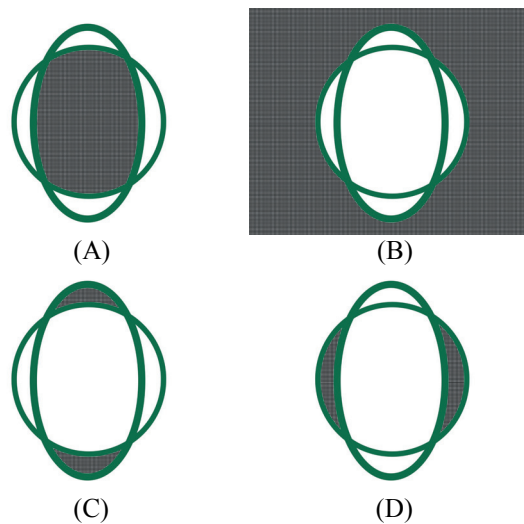


Figure 4: "Venn diagrams" between ΔE^*_{ab} and ΔE_{00} metrics

Determining ΔE_{00} Tolerances for ISO 12647-2 Solid Conformance

The key motivator of this research is to replace ΔE^*_{ab} by ΔE_{00} that better aligns instrumental color difference with perceived color difference while backward compatible. This means that a single ΔE_{00} tolerance for all KCMY solids would be most desirable.

Optimized ΔE_{00} tolerance, as shown in Table 6, only provides backward compatibility between the two color difference metrics. One possible solution for a single ΔE_{00} tolerance is to consider the average of all four *Optimized* ΔE_{00} , or

$$Ave_ \Delta E_{00} = \frac{3.6 + 2.4 + 2.2 + 1.5}{4} = 2.4 \quad [1]$$

By using the average, i.e., $2.4 \Delta E_{00}$, it will have minimum impact on cyan solid conformance and be more forgiving for magenta and yellow solid conformance. However, a single ΔE_{00} will cause many jobs in the database to fail due to the tightened tolerance in black solid. A more suitable solution is to use $2.4 \Delta E_{00}$ for CMY solids tolerance and to use $3.6 \Delta E_{00}$ for black solid tolerance.

The difference in distribution between K solid and CMY solids can be further verified by the real data. Figure 5 shows the ΔE_{00} distribution of 208 real KCMY solids with (1) red color to indicate those who fail the $5 \Delta E_{ab}^*$ conformance, (2) green dotted line to indicate the specified tolerance at $2.4 \Delta E_{00}$ for CMY solids, and (3) a green dotted line at $2.4 \Delta E_{00}$ and a grey dotted line at $3.6 \Delta E_{00}$ for black solid. As discussed, the cut-off at $2.4 \Delta E_{00}$ for CMY solids is more stringent for cyan solid than magenta and yellow solids. If the same cut-off at $2.4 \Delta E_{00}$ were used for black solid, a much larger percentage of the jobs would have been failed. Thus, the tolerance of $3.6 \Delta E_{00}$ is more appropriate for black solid.

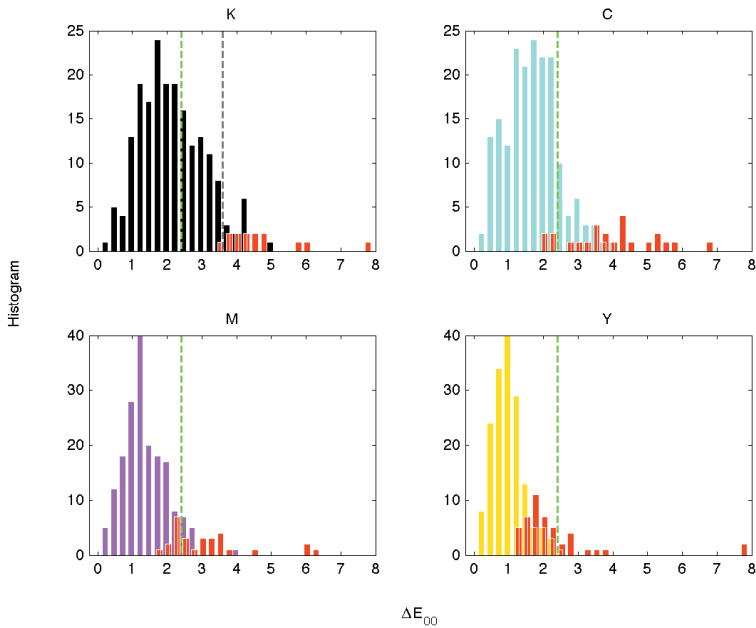


Figure 5: Distributions of ΔE_{00} values from 208 real data

Based on the above analyses and reasoning, it is recommended that $2.4 \Delta E_{00}$ be used for CMY solids tolerance, and $3.6 \Delta E_{00}$ be used for K solid for ISO 12647-2 solid conformance.

6. Summary

ISO/TC130 resolved to use CIEDE2000 because it has better correlation to human visual perception. Previous researches for converting color tolerance from ΔE_{ab}^* into ΔE_{00} for KCMY solids are mainly based on filtered database or simulated data. Due to the fact that there is no single ratio between two metrics, they had difficulties in making their recommendations convincing.

In this research, Berns' method was adopted to find *Optimized* ΔE_{00} tolerances corresponding to the tolerances of $5 \Delta E_{ab}^*$. The combined databases, consisted of 208 real printed jobs, were used to better represent the capability of the printing process. While there is no obvious ratio between the two metrics, *Optimized* ΔE_{00} tolerances keep the pass/fail outcome between two metrics as close as possible. Overall, the equality of outcome is close to 90%.

It should be noted that *Optimized* ΔE_{00} tolerances are mainly provided a starting point to determine the CIEDE2000 tolerances for ISO 12647-2 solid conformance. It represents the best compromise between CIELAB DE and CIEDE2000, but it is not necessary the final recommendation.

Because the CIEDE2000 calculation of black solid behaves differently than CMY solids, this research recommends that a more suitable solution is to use 2.4 ΔE_{00} for CMY solids tolerance and to use 3.6 ΔE_{00} for black solid tolerance for ISO 12647-2 solid conformance.

Acknowledgment

The authors wish to express their appreciation to the following individuals and organizations: Interim Dean Frank Cost of RIT College of Imaging Arts and Sciences, for his support and financial assistance of the project; Mr. Elie Khoury, Alwan Colour Expertise, for his continuing collaboration and support of standardization work; and Dr. Anne Blayo, EFPG, for her encouragement to present the paper at the 38th Iarigai International Research Conference in Budapest, Hungary.

References

- A. Kraushaar, Results on CIEDE2000, ISO/TC 130 (N1005), 2010
- D. C. Rich, White paper on ISO-12647 tolerances, ISO/TC 130 (N994), 2010
- D. L. McDowell, CIEDE2000 Draft 02, ISO/TC 130 (N1053), 2011
- ISO 12647-2. Graphic technology - Process control for the production of half-tone colour separations, proof and production prints - Part 2: Offset lithographic processes. 2004 and 2007
- ISO 13655. Graphic technology -- Spectral measurement and colorimetric computation for graphic arts images. 2009
- ISO/TC 130 (N1733), Resolutions 24th Plenary Meeting, 2010-10-16, Sao Paulo
- R. Chung and P. Chen, Statistical Analysis of PSA Press Sheet Check-up Database, RIT Printing Industry Center, Rochester, NY, PICRM- PICRM-2011-08, 2011
- R. S. Berns, Billmeyer and Saltzman's Principles of Color Technology, Third Edition. Wiley & Sons, New York, 2000, pg. 124-125
- R. S. Berns, Deriving instrumental tolerances from pass-fail and colorimetric data, Color Res. Appl. 21, 459-472, 1996



1

Printing techniques

Film splitting during offset printing - the influence of paper surface properties on film splitting geometry

Peter Rättö¹, Erik Blohm¹, Gary Chinga-Carrasco²

¹ Innventia

Box 5604, SE-114 86 Stockholm, Sweden

E-mails: peter.ratto@innventia.com; erik.blohm@innventia.com

² PFI

Høgskoleringen 6b, N-7491 Trondheim, Norway

E-mail: gary.chinga.carrasco@pfi.no

Abstract

The filament pattern during printing was studied. The printing was performed in a Prüfbau laboratory printing press with IGT medium viscosity oil. The filament pattern was recorded with a high speed camera. Newsprint handsheets with similar surface roughness but different amounts of fine material were used during the trials. Different amount of fine material was obtained by fractionising the TMP pulp and additional beating of kraft pulp. Both qualitative and quantitative analyses of the filament pattern were performed.

The filament pattern at the nip exit appeared as a bright area. The density of the filament pattern was further analysed with computerized image analysis. The intensity and spreading of the brighter area were quantified. An increased amount of fine material resulted in a denser filament pattern. Calendering densified the filament pattern further.

A dense filament pattern indicates a later oil splitting point from the nip centre and a higher splitting force due to a higher splitting velocity. A dense and smooth paper would thus be subjected to higher tensional forces at the nip exit than a porous and relatively rough paper.

Keywords: film splitting, ink film, porosity, roughness, printing

1. Introduction

In order to meet the competition with other media, the demands on efficiency and productivity of modern printing presses increase continuously. A consequence of higher web speeds is an increase in the forces acting on the paper surface. The higher productivity is thus usually accompanied with increased demands on the paper and fundamental knowledge of the dynamics in a printing press is therefore of outmost strategic importance to meet market demands.

Tensional forces at the exit of the nip are due to splitting of the ink film. The maximum tensional force is achieved just before the film splitting starts. This splitting force depends on the ink film thickness, the ink viscosity and the ink splitting velocity. The splitting of the ink film might result in removal of loose particles and loosely bonded particles and segments from the paper surface and in particle deposits on the printing blanket, a phenomenon defined as linting. In the most extreme cases, the printer needs to stop the printing press and clean the blanket repeatedly. An increased printing speed combined with a high ink viscosity will increase the forces at the exit of the printing nip. A better understanding of the forces at the exit of the nip are therefore of interest in order to increase pressroom productivity.

The surface strength of a paper can be measured using standardized tacky oil and an accelerated printing velocity. The strength of the paper is defined as the velocity where the film splitting force results in picking of the surface. Blockhuis and Tollenaar (1962) and Kehlä et al. (1974) measured the pick strength of papers at different oil film thicknesses. A minimum in pick velocity with the ink film thickness was obtained which coincided with a maximum in fibre removal, or with a maximum in the film splitting force. Kehlä et al. (1974) suggested that the picking velocity decreased with an increased coverage of the paper surface at low ink film thicknesses and increased at higher ink film thicknesses. However, to obtain an explanation of how film splitting forces act on the paper, a fundamental understanding on how press geometry, film properties and ink rheology interact is needed.

During splitting of a liquid film, a tensional force is achieved. The force needed to split the film has been formulated by Stefan (1874) as:

$$F = \frac{V_s \cdot \eta \cdot A}{h_x^3} \quad [1]$$

where V_s is the splitting velocity, η is the ink viscosity, A is the area of contact and h_x is the ink film thickness. Stefan's law was derived for thick oil films and can thus not be directly applied to the transfer of a thin ink layer in a printing press. The viscosity-velocity product, VVP, was an early attempt to describe how printing speed and ink viscosity affect the film splitting forces:

$$VVP = V \cdot \eta \quad [2]$$

where V is the printing speed. The viscosity-velocity product only describes speed and viscosity and cannot describe the interaction of the ink film thickness and the printing press geometry on ink splitting forces. Carlsson and Hultgren (1968) proposed a model that was quite similar to Stefan's law, where the film splitting force was divided into two perpendicular components:

$$F_{2,4} = \frac{K_{1,2} \cdot V \cdot \eta}{h_x} \quad [3]$$

where $K_{1,2}$ are constants depending on the printing nip geometry. Mangin et al. (1990) proposed a generalisation of Stefan's law of film splitting. They derived an expression of film splitting forces:

$$T = K \cdot \frac{V_s \cdot \eta^m}{h_x^n} \quad [4]$$

where K is a function of the paper and the printing nip geometry, η is the ink viscosity and m and n are constants describing the influence of the ink viscosity and the ink film thickness respectively. All these expressions consider a completely covered substrate which is not always the case during printing of paper.

In order to model the film splitting forces in a printing nip, the influence of the printing nip geometry and the influence of paper properties also need to be considered. Aspler et al. (1993) modelled the press geometry to calculate the splitting velocity. They used a laboratory printing press tackmeter consisting of two rolls and with a force transducer imbedded in one of the rolls to measure the tack force experimentally. To describe the separation forces of the ink film a model based on the separation speed, V_s , of the surfaces of two rigid rolls was used:

$$V_s = 2 \cdot V \cdot \sin\left(\frac{d}{R}\right) \approx \frac{2 \cdot V \cdot d}{R} \quad [5]$$

where V is the printing speed, d is the distance from the centre of the nip and the point of separation and R is the roll diameter, see Figure 1. The parameter d depends on the ink film thickness and the paper porosity: d increases with ink film thickness and decreases with a more porous paper.

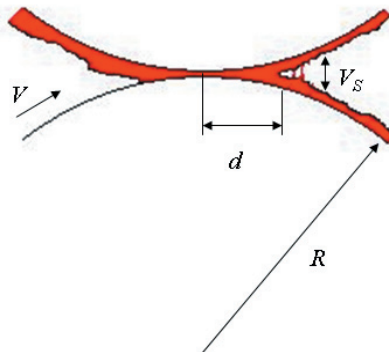


Figure 1: A schematic illustration of the press geometry and film splitting as described in equation (5)

Aspler et al. (1993) measured the tack force and the distance between the nip centre and the point of separation for newsprint at three different calendering levels. As the papers were calendered harder, the distance increased and thus the separation force increased. This was probably due to the absorbance of the rough papers due to a high porosity. It shall be remembered that Aspler et al. (1993) used a laboratory device and the impact of film splitting distance might not be relevant due to a difference in roll diameters between the laboratory equipment and a full-scale printing press.

The fact that the paper properties also influence the splitting forces indicate that better descriptions of how the paper and printing press interact is needed in order to understand the phenomenon of linting. This becomes especially evident when press speeds are increased. The purpose of this work has therefore been to shed more light on how some paper properties might influence the splitting forces and thus contribute to the understanding of this complex problem. With an appropriate description of the complexity of forces acting on the paper surface in a printing nip, some answers might be given on how to design the paper and how to optimize the printing operation in order to prevent linting.

2. Materials and methods

Handsheets were manufactured in a dynamic sheet former from a commercial TMP pulp and a commercial kraft pulp. In order to obtain a relatively open surface, the fines of the first TMP pulp were separated from the pulp by fractionizing. A relatively closed surface was obtained by adding the fractionised fines to a non-filtrated TMP pulp. Further closing of the paper surface was achieved by additional beating of the kraft pulp with 2000 revs in a PFI mill.

The pulps were then mixed according to Table 1, and sheets were made in a dynamic sheet former. The sheets were pressed according to standard conditions and calendered to a PPS roughness of $4.7 \pm 0.2 \mu\text{m}$. The papers were characterised according to light scattering, thickness and surface profile. Additional sheets of paper 3 and 7 were calendered to a PPS roughness of $2.9 \pm 0.2 \mu\text{m}$.

Table 1: Composition of laboratory sheets. The amount of TMP fines is given in relation to the normal amount, i.e. 100% is an untreated sheet

Paper	TMP (%)	kraft (%)	Amount TMP fines (%)	Beating of kraft [rev]	Density [kg/m^3]	Light scattering coeff. [m^2/kg]	PPS [μm]
NP1	50	50	0	0	752	28.18	4.83
NP3	50	50	200	0	754	38.39	4.46
NP7	50	50	200	2000	776	37.22	4.59

The analysis of film splitting was performed in a Prüfbau laboratory printing press at a load of 750 N. Oil transfer was measured gravimetrically by weighting the printing cylinder before and after each printing trial. The press speed was 0.5 m/s, and four repetitions were made for each speed and paper. Medium viscosity oil from IGT was used for the printing press trials and the filament pattern was captured with a high speed camera at a time resolution of 1 ms between each frame. The exit of the nip was captured and the oil transfer was evaluated by weighting the printing roll before and after printing. A picture of the experimental set up is shown in Figure 2.



Figure 2: Photograph of the experimental set up with the Prüfbau press and the high speed camera

Each printing sequence was composed of 50 images. 4 printing replicates were performed for each sample. The 50 images for each replicate were averaged to produce one average image. The 4 average images for each sample were slightly rotated to a horizontal position. The 4 images were then intensity averaged to produce one global image from each sample, printed at a given speed. The images were scanned from left to right and top to bottom, and the intensities were quantified.

3. Results

Figure 3 shows the average oil transfer in the printing nip for the different handsheets at the two press speeds. The handsheet with the most open surface, NP1, showed a significantly higher ink transfer than the rest of the handsheets. The rest of the handsheets showed similar amounts of oil transfer regardless of fines content, type of TMP or calendering. The splitting point between the different handsheets should thus not be affected by differences in ink transfer as long as the same printing speed is used.

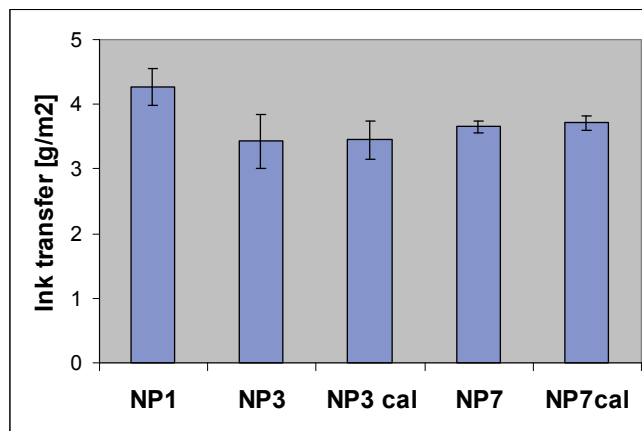


Figure 3: The oil transfer of the different handsheets. The error bars indicate the 95% confidence limits

Figure 4 shows the filament pattern of different handsheets. The handsheet with the most open surface, where the TMP fines had been removed showed the most open filament pattern, indicating an early splitting point, Figure 4a). As the handsheets were closed up by addition of TMP fines, Figure 4b), the filament pattern became denser, indicating a later splitting point. As the sheets were further closed by additional beating of the kraft pulp, Figure 4c), the filament pattern became even denser, indicating even later splitting points.

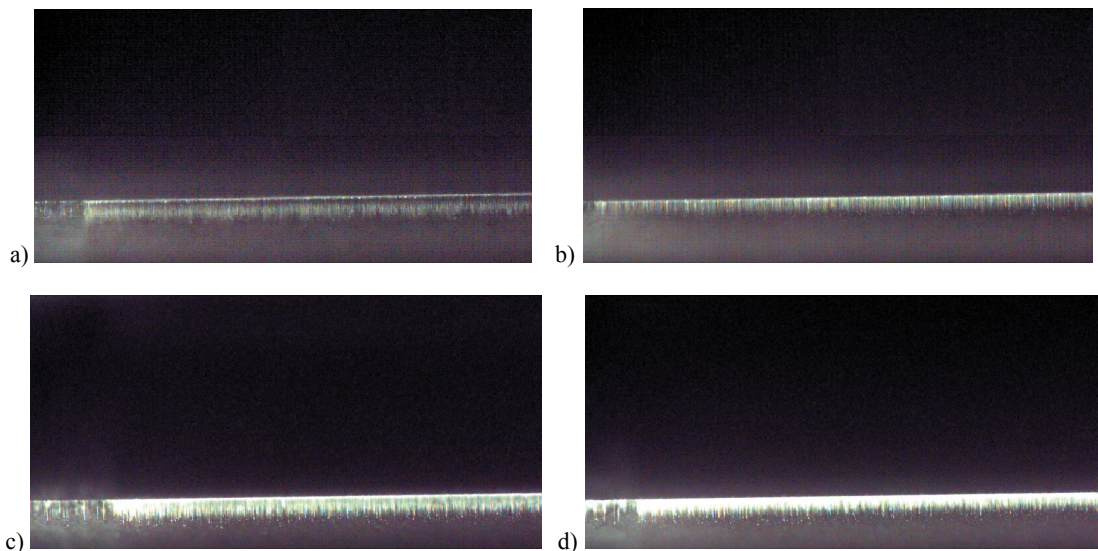


Figure 4: The filament pattern of different newsprint handsheet samples at a press speed of 0.5 m/s. The images were captured with a high speed camera. a) represents handsheet NP1, b) handsheet NP3, c) handsheet NP7 and d) handsheet NP7 that had been additionally calendered

Calendering decreased the surface roughness and closed the surface even further, Figure 4d). Consequently, the additionally calendered papers yielded an even denser filament pattern, compare Figures 4c) and 4d). This indicates a later film splitting point and thus a higher splitting force. It should be remembered that calendering will also influence the surface roughness, which might also influence the splitting pattern or at least the splitting force according to the models described in equations [1] to [5].

The global images acquired from each series are presented in Figure 5. The processed images confirm the qualitative analysis of Figure 4. The most open sheet, NP1, showed the most open filament pattern. As the paper surface was closed by the addition of fines (NP3), the filament pattern became denser. Additional beating (NP7) and additional calendering (NP3 calendered and NP7 calendered), densified the filament pattern further.

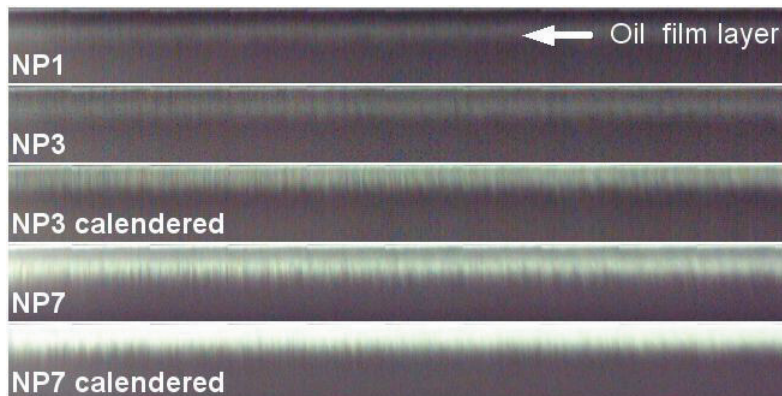


Figure 5: Average intensity images of samples NP1 to NP7

Figures 6 a and b show the intensity levels from the upper edge (position 0 pixel). Note that the oil layers show an increasing intensity from NP1 (without fines, no additional beating) to NP7 (additional fines and additional beating) (Figure 6a). The intensity levels are higher and more homogeneous for the corresponding calendered sheets (Figure 6b).

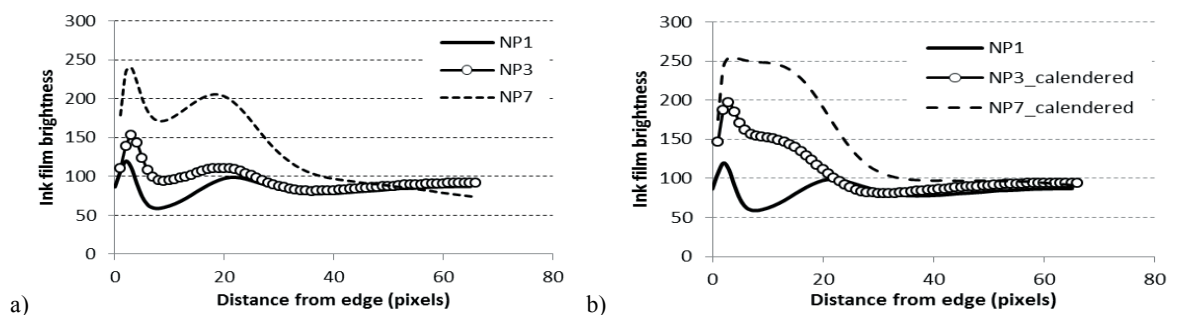


Figure 6: The Ink film brightness (intensity) as a function of the distance from the splitting point at a printing speed of 0.5 m/s. a) Handsheets NP1, NP3 and NP7. b) Handsheets NP1, NP3 and NP7, which were additionally calendered. NP1 is given in b) as a reference

4. Discussion

The paper surface will influence the splitting forces at the nip exit. Hence, proper comparison of the surface strength of different papers, as measured with an IGT testing device, requires that the papers have similar surface roughness.

Looking at the images of the filaments in Figures 4a) to d), and the corresponding average intensity, Figures 6a) and b), it is quite obvious that the paper surface influences the filament formation. It is also reasonable to assume that a denser filament pattern would indicate a later splitting point. Papers with a relatively close surface also showed a denser filament pattern and therefore a later splitting point. The quantitative analysis in Figures 6a) and b) confirmed the qualitative analysis where a more dense surface shows an increased

intensity compared to an open surface. It was also observed that calendering not only increases the intensity but calendered papers also showed a more homogenous pattern from the edge of the samples, compare Figure 6a with Figure 6b.

The absorption of the paper can be varied in a number of ways, e.g. through furnish composition and calendering. The most absorbing handsheet was obtained by removing the TMP fines and this series also showed the most open filament pattern. When the paper surface was relatively closed, first by addition of TMP fines and additional grinding, the filament pattern became denser. Additional calendering both closed the surface and improved smoothness. Consequently, the filament pattern of calendered handsheets showed a considerably denser pattern than the corresponding uncalendered handsheets.

5. Conclusions

The film splitting force at the nip exit can be followed for an oil film in a Prüfbau press with a high speed camera. A qualitative evaluation of the filament pattern correlated well with the corresponding quantitative image analysis. Smaller differences in filament pattern were on the other hand harder to observe and the quantitative analysis was of great help in this case.

It was also seen that the paper surface properties had a great influence on the filament pattern and thus the splitting force. An open surface seems to yield a less dense filament pattern than a denser and smoother surface. The film splitting force at the nip exit can thus be varied with furnish composition and by process parameters since a more dense paper would give a later splitting point. From the insights of these experiments, papers can be designed for higher press speeds.

Acknowledgements

Holmen Paper, Norske Skog and StoraEnso are greatly acknowledged for financial support.

The authors wish to thank Miroslav Hoc for fruitful scientific and technical discussions, Mrs Anni Hagberg for performing the printing trials and Mr Magnus Hillergren for the high speed photography. Berit Leinsvang and Trond Karlsen, PFI are acknowledged for manufacturing and calendering the handsheets.

References

- Aspler J.S., Maine C., De Grace J.H., Zang Y.H., Taylor S. (1993): "Printing tack, Part I: Influence of paper structure on ink 'tack' measured in a printing nip", *Adv. Printing Sci. Techn.*, 22, 139-158.
- Blokhuis G., Tollenaar D. (1962): "Surface strength distribution and its effect on pick testing", *TAPPI*, 46(3): 201-204.
- Carlsson G.E., Hultgren K. (1968): "Notes on the testing of the surface strength of paper at printing", *Svensk Papperstidning*, 71(6), 235-240.
- Kelhä V., Manninen M., Oittinen P. (1974): "Tack force measurement and picking", *TAPPI*, 57(4), 86-90.
- Mangin P.J. (1991): "A critical review of the effect of printing parameters on the linting propensity of paper", *JPPS*, 17(5), J156-J163.
- Mangin P.J., Silvy J., De Grace J.H. (1990): "Offset linting studies: Part II - Further contributions to linting theories", *Proc. 6th Int. Printing and Graphic Arts Conf, Vancouver, B.C., Canada*, 109-119.
- Staff of the Institute of Paper Chemistry (1946), *Paper Trade Journal*, 123(18, 19), 24.
- Stefan M.J. (1874): "Versuche über die scheinbare Adhäsion", *Sitzungsberichte der K. Akad. D. Wissensch. Math. Naturwiss.*, 69, II, Abth., 713-735.

Modeling local print density variations in rotogravure print

Ulrich Hirn, Markus Lechthaler and Wolfgang Bauer

Graz University of Technology, Institute for Paper, Pulp and Fiber Technology

Kopernikusgasse 24, A-8010 Graz, Austria

Email: ulrich.hirn@tugraz.at

Abstract

The paper related reasons for print unevenness are usually due to inhomogeneities in the paper structure. Instead of measuring overall paper parameters like e.g. PPS roughness we are evaluating high resolution measurements of local paper properties. These 2D paper property maps are linked to images of the print and the effect of local paper property variations on local print density variations is analyzed using statistical models.

The statistical evaluation of rotogravure printed SC papers showed, that for both industrial and laboratory print three paper properties are the governing factors of print unevenness: local brightness variations, beta formation and local variations of printing ink penetration. All three are relevant in low and high tones, however local brightness variations are highly dominant in light tone values and local printing ink penetration is highly dominant in dark tone values. The other parameters examined in this study (surface topography, local opacity, local refractive index and local thickness variations) were of minor importance. The modeling results presented in our work are stable and reproducible.

The introduced methodology is also applicable to analyze paper related reasons of print unevenness for other paper grades and other printing technologies. Measurement of local paper properties and linking these data to local print density variations can also be applied to offset, flexo or digital printing. Thus it might be applied to other research aimed to identify paper properties governing print unevenness in different printing technologies.

Keywords: print quality, local paper properties, statistical model, rotogravure, SC paper

1. Introduction

The paper related reasons for print unevenness are usually due to inhomogeneities in the paper structure. Instead of measuring overall paper parameters like e.g. PPS roughness or a formation index research has increasingly shifted towards high resolution measurement of local paper properties, which permits to analyze local defects and inhomogeneities of the paper structure. Linking local print density variations to high resolution measurements of local paper properties has been a promising approach to investigate print unevenness.

Earlier studies focused on the effect of local grammage and/or topography on local print density variations (Kajanto, 1989; Hansson and Johansson, 1999; Dickson, 2006; Mettänen et al., 2007).

In this paper the reasons for rotogravure print unevenness of SC papers is investigated. The key novelties of this work are summarized in three points.

1. Several variables in addition to formation and topography are analyzed. We are measuring seven paper properties as high resolution 2D maps. The measured paper properties are: Beta formation (local grammage), local brightness, local opacity, surface topography, paper thickness variations, local refractive index, local printing ink penetration. The effect of all these local paper properties on local print density variations are analyzed using statistical models.
2. We apply a modeling technique that permits to analyze the degree of redundancy (interrelation) between the model variables. This technique permits to identify key variables and to eliminate redundant variables. We are thus able to provide exact information which paper properties are responsible for print unevenness and, equally important, which are not.
3. Identical paper samples are printed on both, a laboratory printing press and an industrial printing press. We will demonstrate that industrial and laboratory print revealed similar, yet not identical results.

2. Materials and methods

We analyzed three commercial SC papers from different European paper producers. The papers had a basis weight of 56g/m². Local paper properties were measured and linked to local print reflectance measurements of industrial and laboratory prints. Measurement of local paper properties and linking these data to local print reflectance is described in section 2.1. The analysis of industrial prints and laboratory prints has some important differences, hence they are described separately in section 2.2 and 2.3. Statistical modeling and the interpretation of these results is explained in section 2.4.

2.1 Measurement and registration of local paper properties

Figure 1 illustrates the measurement and registration procedure by aligning the measurements of local basis weight (top, left) and the image of the paper after print, i.e. print reflectance (top, right). All other local paper property measurements are aligned in the same way. Each paper sample is marked with a hole pattern which defines the area of the paper to be analyzed (top images). The hole pattern is applied using a computer controlled CO₂ laser (Hirn et al., 2009b), the holes have a diameter of 200-500μm. The measurement maps are matched using a coordinate system defined by the hole pattern, as illustrated by the arrows in the top row images in Figure 1. Matching (also called registration) of two images consists of translation and rotation of the images, and rescaling if they have different pixel size, see Figure 1 (middle). The detailed procedure as well as an error estimate is described in (Hirn et al., 2008).

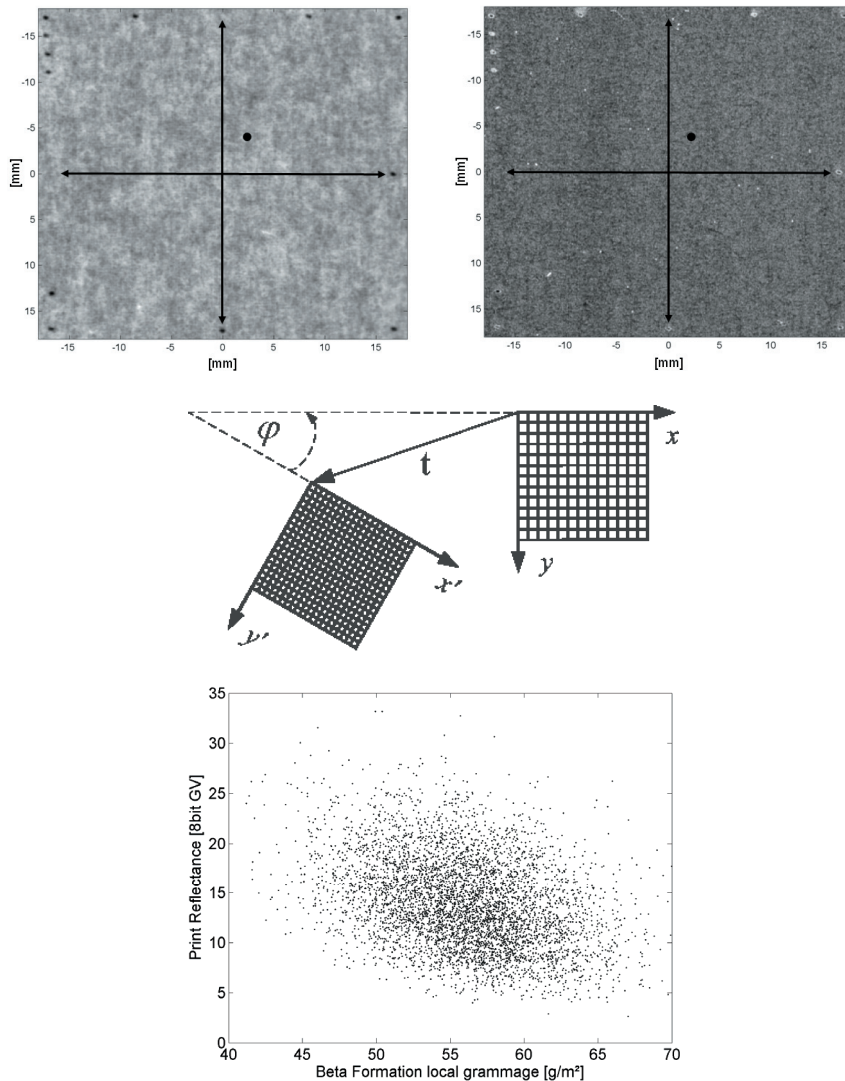


Figure 1: Laser holes (top) are used to define a coordinate system on the paper for all measurements. Registering two 2D measurement maps, i.e. images, consists of rotation and translation of the image coordinates (middle). After registration local grammage values are correlated to print reflectance after print (bottom), $r^2=0.12$

After image registration the coordinate systems in each image are congruent. So a point with specific coordinates in both images refers to the same position on the paper sample. Figure 1 (bottom) shows the data for local grammage before print and print reflectance after print extracted from the matched images. Each point in the scatter plot represents the values for local grammage and local print reflectance of a small area in a specific position on the paper. A relationship can be observed, regions with higher local grammage tend to be darker after printing ($r^2=0.12$).

In this work we were measuring seven local paper properties, the parameters of the measurements are given in Table 1. Additionally to seven paper properties local print reflectance of the printed paper has been measured. For data analysis all registered measurement maps are rescaled to the same pixel size of 250 μm . For a viewing distance of 30cm under good illumination the human eye can resolve structures with a size between 125 μm and 250 μm (Olzak, Thomas 1986). Thus at a pixel size of 250 μm we are preserving all structures visible to the human eye but deleting the invisible, smaller ones.

Table 1: Measurements of local paper properties and print reflectance

Local Paper Property	Measurement Method	Pixel Size of data map [$\mu\text{m}/\text{pix}$]
Local Brightness [8 bit image]	Flatbed scanner Epson Perfection 4990 Photo	21.17
Local Opacity [%]	Optical Microscope (Wanske et al., 2008)	6.42
Local Basis Weight [g/m^2]	Beta Radiography (Keller et al. 2004)	50.00
Surface Topography [μm]	Chromatic White Light Sensor (Fries, 2001)	20.00
Local Thickness Variation [μm]	Chromatic White Light Sensor (Fries, 2001)	20.00
Local Effective Refractive Index [-]	Surfotronics System (Elton and Preston, 2006)	200.00
Local Printing Ink Penetration [8 bit image]	Flatbed Scanner Epson Perfection 4990 (Enzi et al. 2004)	21.17
Print Reflectance [8 bit image]	Flatbed Scanner Epson Perfection 4990 Photo	21.17

2.2 Analysis of laboratory rotogravure prints

For analysis of laboratory prints the unprinted paper was first marked with holes. Then the six local paper properties were measured as described in Table 1: Local grammage (Keller et al., 2004), local brightness, local opacity, surface topography (Fries, 2001), thickness variations and local refractive Index (Elton and Preston, 2006). Subsequently black fields with 25%, 40%, 60% and 100% tone were printed in a rotogravure laboratory printing press, the LTG 20 Einlehner printability tester (Klein 2009). The LTG 20 is a sheet fed rotogravure press with one cylinder, it has an operation speed of 30 m/min. For each sheet 3 rotations of the cylinder are printed.

The Einlehner press provides Electrostatic Printing Assist (ESA), however the prints were performed without ESA due to difficulties in finding a proper ESA setup. The resulting prints were scanned. Finally local printing ink penetration was measured (Enzi et al., 2004), this measurement is also described in the following section.

2.3 Analysis of industrial rotogravure prints

In rotogravure the paper is printed from the reel, thus it is impossible to measure local paper properties before printing. Thus we had to find a way to measure them afterwards, as a result the whole procedure was reversed. First the paper was printed, then the printing ink was removed and local paper properties were measured.

Printing was carried out on a commercial Cerruti 4-color rotogravure press with a web width of 650mm operated at a speed of about 40 m/min. It is a Double Ender gravure press, a machine layout which is also called 'Pony' concept, e.g. described by (Chung, 2009). These machines are printing both sides of the web with only four printing cylinders by turning the web at the end of the machine, displacing it orthogonally to the printing direction and leading it back through the same cylinders.

The same cylinder is used to print both sides of the paper web, these machines are thus often chosen for printing trials of paper producers because two sidedness in the print from a pony press always descends from the paper and not from the cylinder. We analyzed black fields printed with 30%, 50%, 60% and 100% tone value.

For the analysis of industrial rotogravure prints the printed paper sample is marked with laser holes *after printing*. Then the printing ink is removed from the surface of the paper using a mixture of a solvent (toluene) and black rotogravure printing ink (Enzi et al. 2004). Please note that this procedure not only removes the printing ink from the surface, it also reveals the structure of printing ink penetrated into the SC paper. The solvent used to remove the print contains black ink, thus the ink penetrates into all accessible regions of the paper. After removal of the print the local paper properties are measured.

It is easy to see, that after removal of the printing ink (Figure 2, right) local optical properties like local brightness and local opacity cannot be measured any more. On the other hand it is quite straightforward to realize that local grammage (formation) does not change during the ink removal procedure and can thus be measured after print. Also local printing ink penetration is revealed with this technique (Enzi et al., 2004). However, for the three local paper properties surface topography, thickness variations and local refractive index it had to be verified that they can accurately be measured after ink removal. Verification has been performed using laboratory prints. Paper properties were measured *before* printing, then the paper was printed, the printing ink was removed and finally the paper properties were measured again. Comparing the local paper property maps measured on the unprinted paper and after ink removal yielded a correlation coefficient r^2 between 0.7 and 0.95. This result confirmed that surface topography, thickness variations and local refractive index measurements remain largely unaffected, they can be measured after removal of the printing ink. We have the hypothesis that toluene, which is a fully non-polar solvent, does not lead to any swelling of the fibers or dissolving of the fillers thus leaving paper properties unaffected by printing. Environmental SEM images of the paper surface, taken before print and after ink removal, are supporting this hypothesis. No changes are visible in the paper surface.

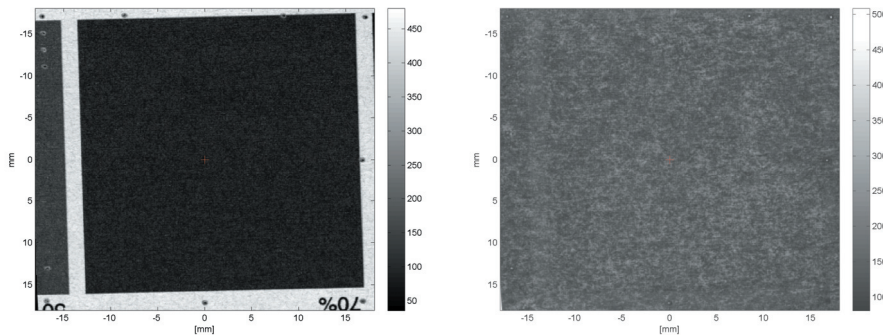


Figure 2: Measurement procedure for industrial print of SC paper. The printed sample is marked with laser holes (left). Subsequently the ink on the surface is removed with a toluene based solvent (right). No more ink is on the surface, dark regions indicate penetration of the printing ink into the paper

2.4 Modeling local print density from local paper properties

Applying the procedures described in section 2.1 to 2.3 we obtained congruent sets of data for local print density and local paper properties. One dataset comprises an area of 10cm², employing a pixel size of 250µm it contains roughly 15000 data points.

The key idea of our modeling approach is based on multiple linear regression. Modeling local print reflectance d by local paper properties p_1, p_2, \dots, p_7 (local grammage, ..., local printing ink penetration) we employ the combined influence of all seven variables as a linear combination

$$d = \beta_0 + \beta_1 p_1 + \beta_2 p_2 + \beta_3 p_3 + \beta_4 p_4 + \beta_5 p_5 + \beta_6 p_6 + \beta_7 p_7$$

By applying differently configured linear models we analyze the influence of each predictor. The mathematical details of the method and the interpretation of the results are described by (Hirn et al., 2009a) and in more detail by (Lechthaler, 2007).

The results of such a model are shown in Figure 3, the influence of the individual paper properties on print unevenness is represented as bars. Figure 3 gives the result for 30% tone value laboratory rotogravure print of one SC paper. A key feature of the modeling procedure is, that the r^2 value for each local paper property can be split into two parts. A redundant part (light gray part of the bar) consisting of information that is also provided by the other variables and an irredundant part (dark gray) of the information which is exclusively provided by this paper property. According to Figure 3 local brightness variation and formation have the

strongest interrelation with local print density variations. Please note that most of the information provided by formation is redundant, i.e. it is also contained in the other variables. Interestingly local opacity is a significant influence factor, although the r^2 to local print density is low ($r^2 \sim 0.17$) it provides considerable *exclusive* (non-redundant) information to the model. Local refractive index and local ink penetration show little and mostly redundant r^2 , thus these predictors are irrelevant. Furthermore the predictors local topography and local thickness variations are statistically not significant, this is indicated by the error bars of the predictors intersecting with the x-axis.

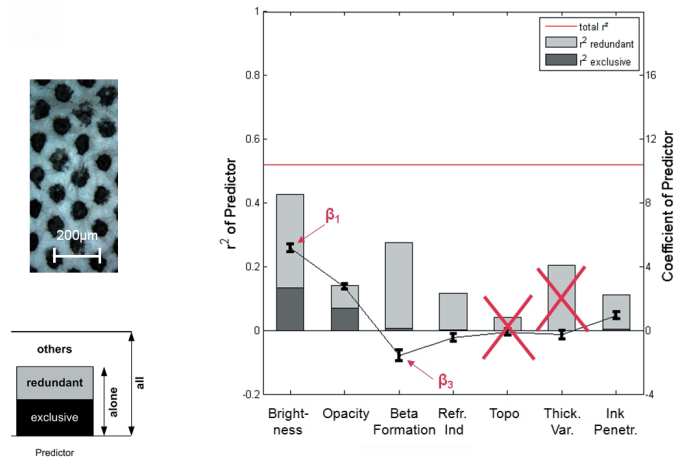


Figure 3: Model for the local print density as a function of local paper properties in 30% laboratory rotogravure print of SC paper

In conclusion, the print density variations in 30% tone value of laboratory rotogravure print are controlled by variations of the optical properties local brightness and local opacity. This seems plausible, considering the fact, that more than 60% of the paper surface is unprinted, Figure 3 (left). It should be noted that roughly half of the information of the full model (horizontal line at $r^2=0.53$ in Figure 3) can be explained by formation. This leads to the conclusion that, while print unevenness is mainly related to variations of the optical properties, the *paper structural reason* for these optical variations can to a large part be attributed to formation.

3. Results

The highly compressed results of the industrial- and laboratory rotogravure prints are given in Figure 4 and Figure 5. The graphs give six bars for each predictor, in Figure 4 that is three papers with both, 30% and 50% tone industrial print (top) and the same three papers with 25% and 40% tone of lab print (bottom). Local brightness and formation are the strongest predictors for the lab print (bottom), these measurements are not available for the industrial print. It is interesting to see, that for industrial print (top) printing ink penetration is an important factor already in the low tone values. This can be explained by the lower viscosity of the industrial ink compared to the ink for the Einlehner lab press.

Local variations in refractive index of the paper did not yield an interrelation with local print density. Surprisingly topography did not come out as a critical factor either. We believe, this is due to the fact, that missing dots are the key criterion to guide paper calendaring and thus the smoothness of the paper. Our hypothesis is, that papers are calendared to the point, where surface topography is not playing an issue any more, i.e. no missing dots are occurring. It is interesting to see, that paper thickness variations are an important predictor, it is however highly redundant to other factors. Further analysis will be required to give a suitable interpretation for this result.

Figure 5 shows the results for high tone values. Again the same three papers were analyzed for lab print (60% and 100% tone) and industrial print (70% and 100% tone). Variations in printing ink penetration are clearly the dominant reason for print unevenness in high tones. Please note that the predictor printing ink penetration *alone* has nearly the same r^2 as the full model, this is evident from the small distance between the bars of ink penetration and the horizontal line giving the r^2 of the full model. Thickness variations and beta formation are also good predictors, however they are highly redundant (large light grey columns) to the other measurements

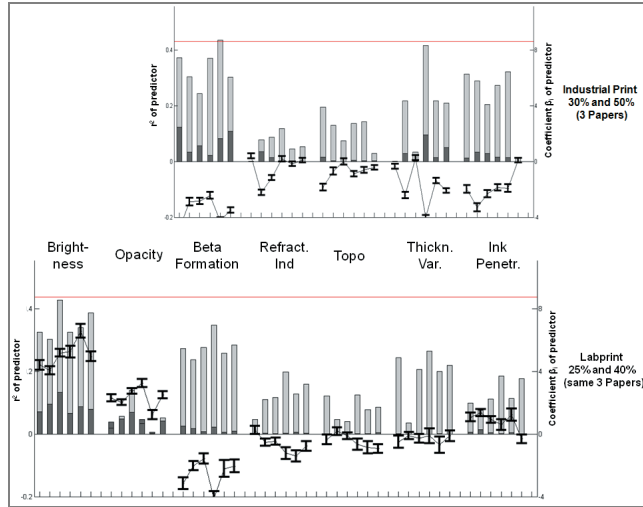


Figure 4: Analyzing the interrelation of local paper properties with print unevenness of rotogravure print in low tone values (25%-50%). The top graph shows the results for industrial print, the bottom graph for the lab print

Interestingly local paper brightness is still somewhat relevant, even in the high tone values. Local variations in refractive index of the paper and surface topography again did not yield an interrelation with local print density.

3.1 Discussion

It has to be noted that the models reveal similar results for all papers. The groups of six bars, representing three papers with two high and two low tone values, have quite similar height for each predictor. This indicates that the results give stable and statistically representative models for the influence of local paper properties on rotogravure print unevenness. Repeatability and stability of the models from our analysis has also been examined in an earlier publication (Hirn et al., 2009a), the results were good.

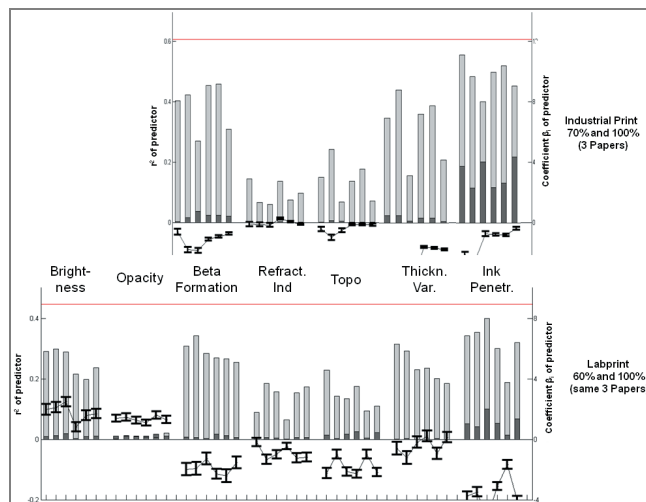


Figure 5: Analyzing the interrelation of local paper properties with print unevenness of rotogravure in high tone values (60%-100%). The top graph shows the results for industrial print, the bottom graph gives the results for the lab print

The modeling results for both low and high tone values show that the measured local paper properties are highly inter-correlated. Some predictors like refractive index and topography are even entirely redundant to the other variables. That means that these measurements can be dropped from the models without a loss in overall r^2 . This highlights the importance of using a modeling technique that quantifies and eliminates the inter-correlation between the local paper properties.

4. Conclusions and outlook

A comprehensive methodology to examine the interrelation between print unevenness and local paper properties has been introduced. High resolution measurement of paper properties, subsequent linking local paper properties to local print density and finally statistical modeling of the interrelation is a powerful tool to investigate the paper related reasons for print unevenness. The ability of the modeling procedure to quantify redundant information from individual measurements has been shown to be a valuable tool to identify the key paper properties responsible for print unevenness.

Our analysis of rotogravure printed SC papers showed, that for both industrial and laboratory print three paper properties are the governing factors of print unevenness. These are local brightness variations, beta formation and local variations of printing ink penetration. All three are relevant in low and high tones, however local brightness variations are highly dominant in low tone values and local printing ink penetration is highly dominant in high tone values. The other parameters examined in this study (Surface topography, local opacity, local refractive index and local thickness variations) were of minor importance.

Analyzing print unevenness we obtain stable and reproducible models. The similarity of results between laboratory- and industrial print demonstrates that removing the printing ink after printing and then determining local paper properties is a valid procedure for rotogravure printed SC papers.

We want to point out that the presented methodology to analyze paper related reasons for print unevenness is also applicable to other paper grades and other printing technologies. Measurement of local paper properties and linking these data to local print density variations can also be applied to offset-, flexo- or digital printing. The analysis method is particularly well suited for sheet fed printing where it is easy to measure the local properties of a piece of paper *before* printing, e.g. digital printing and sheet fed web offset. For web fed printing either the printing ink has to be removed after the print or the method is limited to measuring local paper properties that remain unaffected by printing like e.g. formation. Also the method is applicable to all lab printing techniques. Thus our methodology could be applied to other research aimed to identify paper properties governing print unevenness in different printing technologies.

Acknowledgements

We would like to thank SCA Laakirchen and SCA R&D Centre AB for permitting us to publish the results from our joint research. Furthermore we gratefully acknowledge funding from the Austrian Industrial Research Foundation FFG, project 'Farbübertragung', project number 827 636.

References

- Chung, R. (2009) Milestones in Technology - Pony Press, Gravure Magazine 22(4) p. 46-48.
http://cias.rit.edu/~gravure/bob/pdf/Milestones_in_Technology_09.pdf
- Dickson, A. (2006) Evaluating the relationship between grammage, topography and print properties in newsprint. In 60th Appita Annual Conf., Melbourne, pages 19–23.
- Elton, N. and Preston, J. (2006) Polarized light reflectometry for studies of paper coating structure part 1+2. Tappi J., 5(7;8):8-16;10-16.
- Enzi, S.; Bauer, W. and Hirn, U. (2004) Einfluss der Penetration auf das Bedruckbarkeitsergebnis im Tiefdruck. In ProceedingsC TP-PTS-Symposium Papier und Bedruckbarkeit, pages 15.1 –15.17.
- Fries, T (2001) Fast, accurate, automatically generated measurements of surface roughness, contour and topography. Materialprüfung, 43(6), pages 234-235.
- Hansson, P. and Johansson, P.A. (1999) A new method for the simultaneous measurement of surface topography and ink distribution on prints. Nordic Pulp Paper Res. J. 14(4), 315-319.
- Hirn, U.; Lechthaler, M; and Bauer, W. (2008) Registration and correlation of local paper property maps. Nordic Pulp and Paper Res. J., 23(4):374–381.
- Hirn, U.; Lechthaler, M; Wind, E. and Bauer, W (2009a) Linear regression modelling of local print density in gravure printed SC paper. In Papermaking Research Symposium Kuopio, ISBN 978-951-27-1038-6.
- Hirn, U.; Kritzinger, J.; Donoser M. and Bauer, W (2009b) Introducing a concept to link 3D paper structure to 2D paper properties. In Trans. 14th Fundamental Research Symposium, Oxford, p.721-749.
- Kajanto, I (1989) The effect of formation on print quality with woodfree offset papers.

Nordic Pulp and Paper Res. J., 4(1):8-15.

Keller, D.S.; Kellomäki, M.; Pawlak, J.; Hägglund, J.E. (2004) Three storage phosphor systems for beta-radiographic imaging paper. Nordic Pulp and Paper Res. J. 19:170-175.

Klein, R. (2009), Praxis- und Labordruckergebnisse von Naturtiefdruckpapieren im Vergleich (in German) Wochenblatt für Papierfabrikation 137 (3-4):120-128.

Lechthaler, M. (2007) Bewertung des ortsabhängigen Verformungsverhaltens von SC Papier (in German). Ph.D. thesis, Graz University of Technology.

Mettänen, M.; Ihalainen, H.; and Ritala, R. (2007) Alignment and statistical analysis of 2-d small scale paper property maps. Proc. 2007 International Paper Physics Conference, Gold Coast, pages 624–632.

Olzak, L. and Thomas, J. (1986) Seeing Spatial Patterns, Boff, K., Kaufman, L. and Thomas, J. (eds.), Handbook of Perception and Human Performance, Wiley, pp. 7.1-7.52.

Wanske, M.; Großmann, H.; Scherer S. (2008) Messtechnische Bewertung von Tissue Produkten mit dem optischen Messsystem InfiniteFocus (in German). Wochenblatt der Papierfabrikation 136(9), 473-477.

Development of a comparative tool to predict ink misting

Laurette Vieille-Grosjean, Alice Vermeulin

ICGQ - The Quebec Graphic Communications Institute
999 Émile-Journault, East Montreal, QC, H2M 2E2, Canada
E-mails: lvieillegrosjean@icgq.qc.ca; avermeulin@icgq.qc.ca

Abstract

Ink misting has become a major issue for high speed offset presses. It typically occurs when an ink film splits between rollers and creates ink filaments, which eventually break up into tiny droplets, causing severe degradation of the press environment. Extensive research has helped to better understand misting mechanisms.

An attempt was made to develop a comparative and predictive method to evaluate misting based on physical simulations correlated to rheological properties of a panel of coldset and sheetfed inks. As a complex phenomenon, ink's tendency to mist cannot be defined by only one rheological parameter, such as tack or elasticity. And a predictive method may include a combination of several data coming from both ink and ink-water emulsion results. Simulating misting on Inkometer seemed to be a good first approach for sheetfed inks, as absence of misting was correlated to no result on a small-scale offset press (Apollo). A lot of observations were done during this study especially on misting simulations of coldset inks and influence of ink-water emulsions on rheological profiles of sheetfed inks. Further experiment shall be carried out to larger series of inks and ink-water emulsions to complete this approach.

Keywords: ink, misting, offset printing, rheology, comparative tool

Introduction

Misting typically occurs at the exit of the nip when an ink film splits between rollers and creates filaments, which eventually break up into tiny droplets expelled from the ink battery (see Figure 1). Among many factors, ink misting generally increases while the running speed increases to gain productivity. It occurs predominantly on high-speed offset presses and it has been particularly well known for many years on newspaper web offset presses (Reif, 1964), and more recently, even on high efficient sheetfed offset presses reaching very high speeds (for example: up to 18000 sheets / hour for the Roland 700 HiPrint HS presented at IPex 2010). This uncontrolled loss of material can cause severe degradation of the press environment, affects print quality and eventually leads to machine stops, which lowers the overall press performances. Thus, it has become of major interest for printers to better anticipate this problem before encountering it in pressrooms.

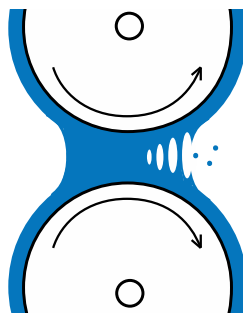


Figure 1: ink film splitting mechanism. After entering the roller nip, the ink film is submitted to both shear stresses and elongation forces. A cavitation phenomenon appears at the roller separation inducing a formation of strings. If they break up in several points they may produce small droplets of misting

The cause of formation of ink misting has been the subject of many investigations since the early 1930s. Misting is indeed a result of multiple parameters. It depends on the press condition, as it was observed that the tendency to mist is increased by the ink quantity and film thickness (Voet, 1956), the atmospheric conditions -low humidity and electrostatic field-, the temperature of the rollers (Traber et al, 1992), an increase in speed (Christiansen, 1995) and a reduction of their diameter (Bisset et al, 1979). But to reduce

misting, change in ink formulation (more especially amount of pigments, type and level of resin and extender) - leading to flow characteristics changes - can often and largely overcome the problem. Many researchers have indeed described rheological properties as of prime importance to explain ink behaviour into rollers nip: misting would decrease with higher ink viscosity (Voet, 1956; Bousfield et al., 1990) and higher cohesive energy or tack (Blayo et al., 1997). Elasticity is also put forward to be a key characteristic of the misting (MacPhee, 1997b).

These studies have helped to better understand the mist mechanisms within the press rollers but none of them provides practical tools for printers to select optimized consumables in full knowledge of the potential risks inside their press environment. An attempt was recently made by Savarmand et al, (2010) to build up a mathematical predicting model correlating the amount of misting from an ink slinging up from a laboratory device with the pressure peak generated in the nip, using dimensional numbers (such as Reynold number). But no clear correlation was obtained for large series of inks. As a matter of fact, as a complex phenomenon, misting remains hardly predictable in an absolute way, and a comparative predictive method appears to be more feasible. In the present study, our attempt is to develop a laboratory tool to predict ink-misting propensity based on the comparison of different inks according to their rheological profile. A secondary objective is then to define what characteristics of an ink are the most representative to define a potential risk of misting.

2. Method

2.1 Materials

2.1.1 Offset inks

Six web offset coldset inks were chosen among samples supplied by an ink manufacturer. A special attention was taken to select inks said to produce noticeable differences in terms of misting tendency on high-speed web offset presses when run under similar printing conditions. The tested panel was composed of three color process "regular" inks, i.e.: having a tendency to mist - named black A, cyan A, and magenta A in this report- and three color process "low mist" inks - named black B, cyan B, and magenta B -. For practical reasons yellow inks were not investigated in this study as obtained patterns are difficult to assess by visual or scanner analysis.

Misting phenomenon on four conventional sheetfed offset inks supplied by a printer was also investigated. Two inks, magenta D and cyan D, showing high levels of misting on a sheetfed offset press, were analyzed and compared with two inks of reference (magenta C and cyan C) showing no apparent misting under similar printing conditions.

Observations on misting phenomenon of coldset inks were done during real time production runs on a high-speed offset press, but some practical difficulties prevented to collect and quantify the effect. No quantification was either possible for sheetfed inks on sheetfed offset press.

2.1.2 Ink-water emulsions

For additional study, the influence of a fountain solution added to the sheetfed offset inks on misting was also investigated. For this purpose, a commercial concentrate solution recommended for use by the ink supplier was added to distilled water, and final pH and conductivity were respectively adjusted to 4.6 and to 1817 \square S to formulate a proper fountain solution.

Ink water-emulsion were prepared using a Duke Ink-Water Emulsification Tester, consisting of a mixer equipped with speed-controlled rotating blades. Ink and aqueous solution were weighed, poured into the tester, and mixed during 450 rotations at a constant speed of 90 rotations/minute under monitored lab temperature (23 +/- 2°C). Different water fractions within the emulsions were prepared, such as described below:

- ◆ The highest water absorption rate: determined using the Water Pickup method (ASTM D492-89 standard) while mixing 50g of ink with 50mL of aqueous solution. Volume, pH and conductivity were recorded from the remaining water after the test. Water pickups obtained were different according to the ink and results are reported in part 3.2.
- ◆ A 50 g emulsion with 15.0% (wt/wt) of aqueous solution into the ink.
- ◆ A 50 g emulsion with 5.0% (wt/wt) of aqueous solution into the ink.

For the 5 and 15% emulsions, attention was taken to verify that all the fountain solution was absorbed into the ink after the mixing step.

These emulsion were used for further tests on rheometer and Apollo press (see part 2.2)

2.2 Misting simulation

As no laboratory standard method currently exists to evaluate this parameter, we chose to explore two different possibilities to simulate and analyze ink misting.

Inkometers or similar tack measuring instruments are often encountered in the literature to assess misting propensity (Leach et al, 1993; Blayo et al, 1997; Claypole et al, 2010) and it is also a very common method among the ink manufacturers. It offers the advantage to use a small quantity of ink (less than 2 cm³), which can be run under monitored conditions (speed, time and temperature). A Thwing-Albert Inkometer was used to run the different samples under controlled conditions. Flat misting traps were positioned at specific spots to collect the ejected droplets from the rollers (see Figure 2). A plastic strip, as stable and non-absorbent substrate, was set up behind the rollers to trap and weight the amount of material ejected during rotation. Meanwhile, an offset sheet was placed in front of the rollers to collect ink droplets and analyze the misted patterns -offset paper being slightly absorbent, it offered better contrast for image analysis compared to a coated paper -.

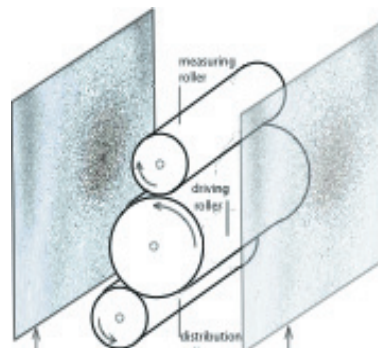


Figure 2: Collecting the misting around Inkometer rollers

Several tests were performed using 2 cm³ of ink, at different speeds: 1200, 2000 and 2700 rpm -revolutions per minute -, and for two different collecting times: 2 and 10 minutes. The rollers temperature was kept constant at 32°C. Ink samples were allowed to run 30 seconds at 300 rpm to adjust ink temperature and its distribution on the rollers, before traps were placed and misting was collected at the measuring speed.

A second laboratory misting simulating method was set up using a small Apollo web offset press. It consists on a web unwinder, two printing units with an inking battery and a fountain solution system, and a sheeter. It offers the advantage to reproduce at a smaller scale real printing conditions of a usual offset press, and distributes the ink between small diameter rollers (around 4 cm), that increases the solicitation frequency of inks and which should accentuate the misting tendency. Print trial parameters were set up as follow:

- ◆ Running speed: 76.2 m (250 feet) / minute
- ◆ Run length: 8000 copies (equivalent to a 25 minutes run)
- ◆ Image area: 228x216mm, made of solid color patches of 1.05 target density (for all inks).
A large image area was used to ensure uniform ink coverage along the rollers
- ◆ Paper: 90g/m² offset, reel width: 250 mm
- ◆ Temperature of the rollers: 31°C

Each printing unit was fed with the sheetfed inks of same color: the purpose was to compare cyan C with cyan D, and magenta C with magenta D under the same printing conditions. This test was however not performed on coldset inks A and B. Press was allowed running until stable ink-water emulsion and target printing density were reached. Once press was set up, misting traps were placed in front of the ink rollers to collect the ejected droplets. Then, a second press trial was done using an over water-ink emulsion to simulate “bad” printing conditions and see the effect on collected misting (expected to be worse than in proper ink-water balance conditions).

2.3 Misting evaluation

The misted traps of paper were measured using an Agfa Duoscan T1200 flat bed scanner coupled with the Verity IA 2004 image analyzer software. A mottle index was determined to express the variation of optical density observed in the pattern of a specified area of interest. The higher the index, the worst the mottle and the misting effect. Each sample was scanned at 300 dpi to get a macro analysis of the patterns. This method was coupled with both visual assessments and weighting results of plastic traps to ensure its consistency.

2.4 Rheological characterization

In the mean time, ink rheological characteristics were measured on a controlled-stress rotational rheometer from ATS Rheologica.

Flow properties were obtained using a parallel plate geometry of 30 mm at a gap of 0.001 mm. Both steady and oscillatory measurements were done but we chose to use oscillatory for rheological characterization, as this approach implying elasticity of the material is closer to the situation applied to ink during film splitting (Oittinen, 1976). Preliminary oscillatory experiments were carried out to determine the appropriate linear viscosity domain of the inks, before conducting frequency sweep tests (from 0.001 to 50 Hz). Dynamic viscosity (η'), tangent of the loss angle ($\tan \delta$), storage (G') and loss moduli (G'') were analyzed versus the frequency. Rheological tests were performed at 32°C, which is the temperature of heated ink on both the Inkometer and Apollo press, and which is also close to high temperatures that can be encountered on inking batteries of web offset presses.

2.5 Tack measurements

Ink tack was measured on the Inkometer according to ISO 12634 standard, in a controlled temperature room (23 +/- 2°C). Experiments were carried out using 1.32 cm³ of ink at a rotating speed of 1200 rpm, at 32°C, and tack values were recorded every minute during 10 minutes.

3. Results and discussion

3.1 Results for coldset inks

Tack values measured at 1, 5, and 10 minutes and the misting index expressed from analyzed misted traps from Inkometer simulations are reported in Table 1. As misting difference between inks run at 1200, 2000 and 2700 rpm showed good correlations (misting quantity increasing with both speed and collecting time), we chose to report only 2000 rpm-2min results. Comparing similar colors, inks having the highest tack value gave the less misting effect on samples (for example: black B versus A and magenta B versus A). However cyan inks having quite similar tack values, showed strong differences in misting. It is even more surprising to see cyan A having lower misting effect compared to cyan B, which was supposed to be a “low mist” ink in pressrooms. It can be also noted that tack values were quite stable with time excepted for magenta B (+15% from 1 to 10 minutes).

Table1: Results of tack and misting obtained for the set of coldset inks

	Tack			Misting index
	at 1min	at 5min	at 10min	at 2000 rpm, 2 min
Cyan A	4,9	4,9	4,8	1846
Cyan B	4,7	4,7	4,6	2564
Magenta A	5,9	6,0	6,1	1629
Magenta B	5,9	6,3	6,8	1460
Black A	5,0	4,8	4,7	1582
Black B	5,4	5,3	5,1	927

The evolution of the elastic character of the ink samples was estimated by the variation of the tangent of the loss angle: $\tan \delta$ (see Figure 3.a). It can be noted that inks from A series having similar elasticity values (but different viscosities) gave also quite similar results in misting. Black and magenta from A series, having higher misting level, showed also higher elasticity and higher dynamic viscosity (see Figure 3.b) compared to B series. But, here again, cyan inks results do not correlate with other colors' tendency (cyan B showing the worst misting also shows the lowest elasticity and viscosity), and no clear-cut conclusion can be drawn on the influence of viscoelasticity parameters based on these observations.

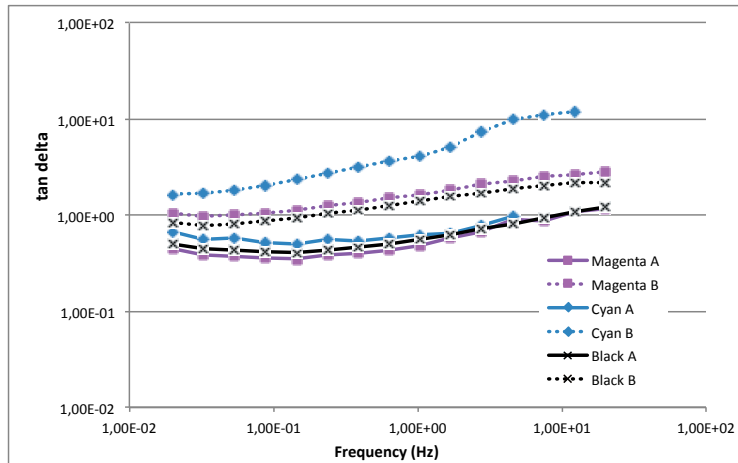


Figure 3.a: variation of $\tan \delta$ of coldset inks (A and B) as a function of frequency, at 32°C

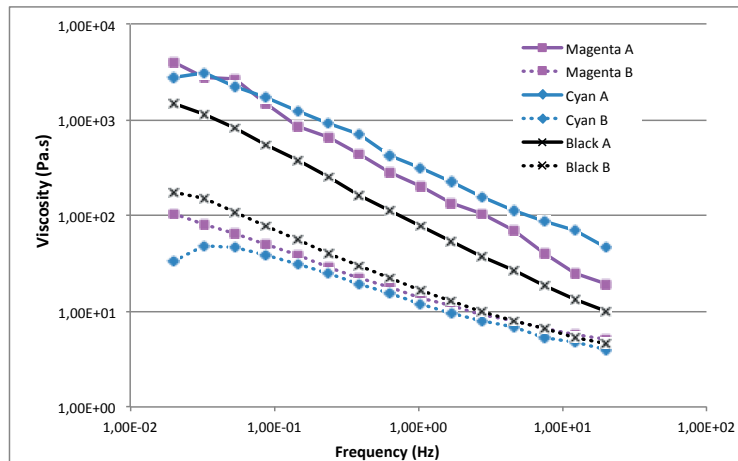


Figure 3.b: variation of viscosity of coldset inks (A and B) as a function of frequency, at 32°C

Lack of correlations obtained between rheological results and misting simulations let us think about the efficiency of the Inkometer method to discriminate two inks in their misting propensity. Several suppositions can be done: while simulating misting on an Inkometer, a part of ink solvent may evaporate eventually during the test as no fresh ink is reintroduced into the system, as it is the case in a traditional inking system on press. This may have an impact on the flow properties of the ink. This system does not either allow introducing water on rollers to form a proper ink-water emulsion.

Hayashi et al (1993) showed that increasing the fraction of water droplets in the ink decreases the tack and increases the elasticity, which changes the filament break-up length. It may thus probably affects strongly misting results compared to the sole ink's misting propensity. Thus, further tests will be performed within the next few months, on coldset inks using ink-water emulsions to broaden our analysis.

3.2 Results for sheetfed inks

The second part of the study aimed to compare misting of different sheetfed inks on both Inkometer and Apollo press and see the relevance and correlation of both methods. This study was also complemented by ink-water emulsion rheological tests, whose results are reported in Table 3 and Figures 5.a and 5.b.

No clear differences in tack can be seen between inks and values appeared to be quite stable with time. Misting results are absent because no obvious misting was generated on Inkometer tests, and despite many attempts to explore variable speeds and collecting time. In the same way, Apollo tests performed with the same inks and introducing fountain solution did not show any noticeable misting effect during print trials. These observations made while running inks in a proper ink-water balance (target densities) were similar to the ones obtained after a pronounced rise of water proportion in the emulsion was done.

Table 2: Results of tack and misting obtained for the set of sheetfed inks

	Tack			Misting index	
	at 1 min.	at 5 min.	at 10 min.	Apollo press (76,2 m/min, 25 min)	Inkometer (2000 rpm, 2 min)
Cyan C	14,6	14,7	15,0	-	-
Cyan D	15,0	15,0	15,5	-	-
Magenta C	13,8	14,0	14,8	-	-
Magenta D	13,5	14,0	14,6	-	-

Slight differences were observed on viscoelastic characteristics of C and D inks, C series being more elastic - tan delta values remaining quite stable with the frequency-, and more viscous than D series (see Figures 4.a and 4.b). Differences in viscoelasticity were even more pronounced between the cyan inks. But, these differences may not be discriminative enough between inks, as it does not seem to affect their misting behaviour. Despite sheetfed inks formulation are strongly different from coldset inks because they are run in very different press environments, one can notice that sheetfed inks showed higher cohesive energy, and less variation in rheological characteristics than coldset inks: perhaps inks having more “body” and better rheological stability would be key parameters to prevent ink misting?

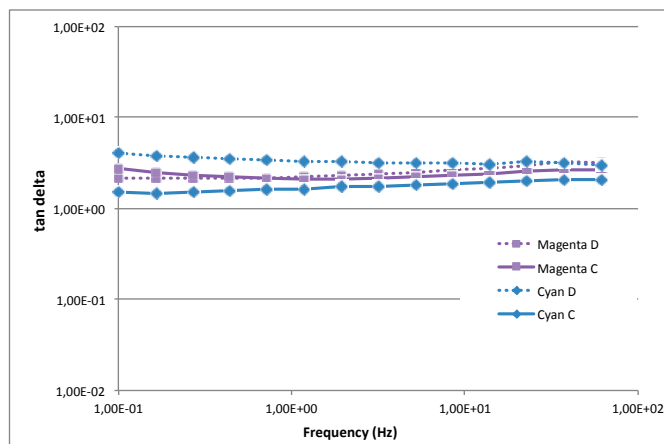


Figure 4.a: Variation of tan delta of sheetfed inks (C and D) as a function of frequency, at 32°C

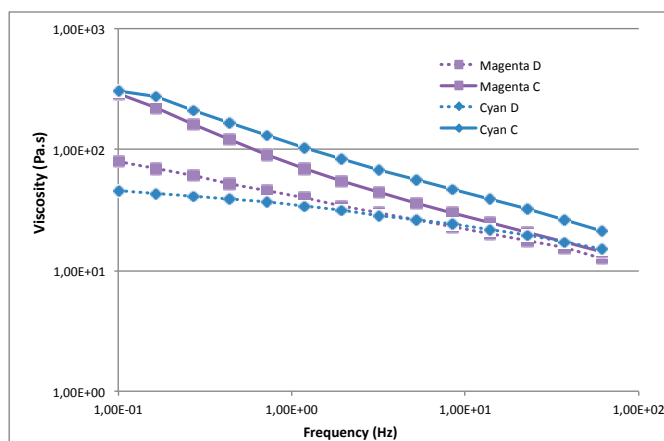


Figure 4.b: variation of viscosity of sheetfed inks (C and D) as a function of frequency, at 32°C

Some interesting results were obtained while oscillatory measurements were done on emulsion samples tested at different water proportions. For most of inks (cyan D, magenta C and D) an increase of water droplets fraction led to a slight decrease in viscosity and a rise in elasticity (increase of G'), and more especially near 1Hz frequencies. This last point is consistent with results found in the literature at low frequencies range (Hayashi, 1993) and (Aurenty *et al.*, 1998), explaining the rise of elasticity by an effect of interfacial tension of droplets resisting to the deformation.

Only cyan C showed quite different results with no major change in tan delta compared to a drop of viscosity. It also can be noted that D inks had higher water pick up values compared to C series, i.e. their water absorption capacity is higher. This set showed also a more pronounced drop of elasticity between 5 and 15% emulsions, meaning their flow properties may be more sensible to a change in the emulsion.

Table 3: Viscoelastic characteristics obtained on water-ink emulsions, at 1Hz and 32°C

	Water emulsion (%) wt/wt	G' (Pa)	G'' (Pa)	Tan delta	Viscosity (Pa.s)
Cyan C	5	667	1160	1,73	180,0
	15	282	470	1,66	74,0
	64,5 (WPU)	199	362	1,82	55,8
Cyan D	5	163	482	2,96	68,6
	15	205	516	2,52	75,0
	74,5 (WPU)	373	543	1,46	88,9
Magenta C	5	233	498	2,14	74,2
	15	260	481	1,85	73,8
	55 (WPU)	278	453	1,63	71,7
	5	154	376	2,44	54,9
	15	199	361	1,82	55,6
Magenta D	58,5 (WPU)	192	311	1,62	49,3

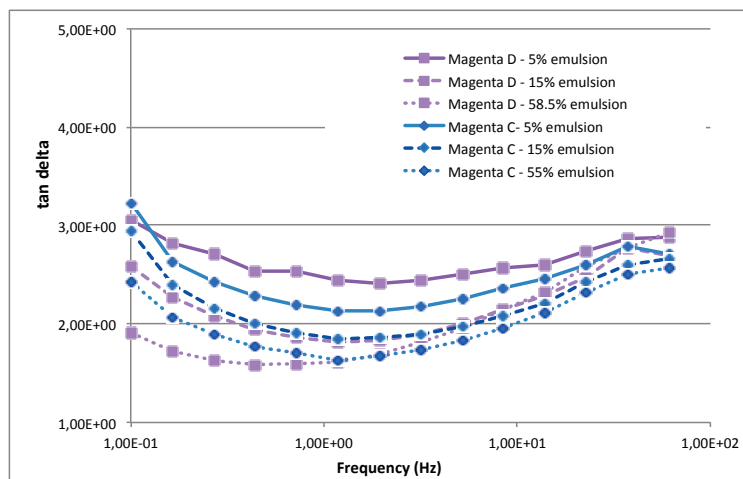


Figure 5.a: variation of tan delta of ink-water emulsions (magenta C and D) as a function of the frequency, at 32°C

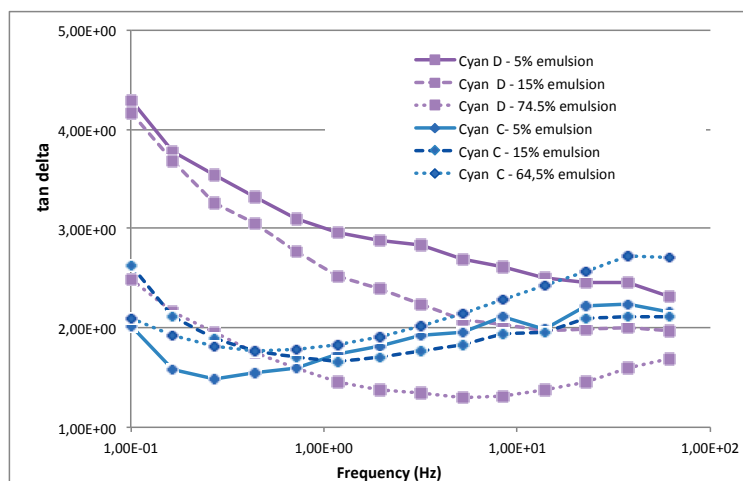


Figure 5.b: variation of tan delta of ink-water emulsions (cyan C and D) as a function of the frequency, at 32°C

After this study, as no obvious misting effect occurred from two different simulating methods and rheological characteristics did not show strong differences, some hypothesis can be made that misting observed for cyan and magenta D on the printer side, during real production run, would rather come from specific press conditions (such as excessive speed, increased pressures and roller temperature) rather than real differences between intrinsic properties of these particular sheetfed inks.

4. Conclusion

An attempt was made to develop a comparative method to evaluate misting propensity based on physical simulations correlated to rheological properties of a panel of 6 coldset and 4 sheetfed inks.

A lot of observations were done during this study but, due to a lack of results, no clear conclusions were drawn. One rheological parameter, such as tack or elasticity, is clearly not defining a tendency to mist and a predictive method may include a combination of several data coming from both ink and ink-water emulsion results. Simulating misting on Inkometer seemed to be a good first approach for sheetfed inks, as absence of misting was correlated to no result on a small-scale offset press (Apollo). Relevance of this laboratory method should be however further investigated using inks with noticeable and different misting propensities. Additional experiment shall be definitely carried out to include more data and complete this approach: With ink manufacturers support, coldset inks having higher distinctive misting propensity will be formulated and tested, to refine the method. Influence of the water-ink emulsion shall be also investigated and included into the analysis.

Acknowledgements

The authors would like to thank Sun Chemical, Imprimerie Mirabel, and Rethink Inks for their support in this project.

References

- Aurenty P., Palierne J.F., Gandini A., (1998), "Viscoelasticity of water/ink emulsions at low and high frequency", TAGA Conference Proceedings
- Blayo A., Waig Fang S., Gandini A., Le Nest J.F., (1997), "Study of ink misting phenomena", TAGA Conference Proceedings
- Blayo A., Gandini A., Medlege F., (2000), "Rheological characterization of printing inks: correlations between laboratory measurements and press performance", TAGA Conference Proceedings
- Claypole T., Vlachopoulos G., Bould D., (2010), "Ink misting formation in roller trains", IARIGAI vol. XXXVII
- Hayashi T., Morita K., Amari T., (1993), "Rheological properties and printabilities of polybutadiene /carbon black ink", J. Jpn. Soc. Colour Mater vol.66, Issue No. 11
- MacPhee J., (1997b), "A unified view of the film splitting process, Part II", American Ink Maker vol. 75 Issue No.1
- McPhee J., (1998), "Fundamentals of lithographic printing", Volume 1: Mechanism of printing
- Savarmand S., Bousfield D., Durand R., Warren R., (2010), "A laboratory method to characterize and predict ink misting", IARIGAI vol. XXXVII
- Voet A., (1956), "Ink misting and its prevention", American Ink Maker vol. 34, Issue No.

Two-dimensional digital emulation for alignment of paper sheet in the printing press

Rostislav Moginov, Eva Poznyak

The Moscow State University of Printing Arts after Ivan Phedorov
St. Pryanishnikova 2A, Moscow, Russia

E-mail: evastp@mail.ru

Abstract

This paper concerns alignment problems of a paper sheet in sheet-fed presses. The method of wave processes was used. The waves arise in a sheet when that aligns. There are used the numbering methods for solving a two-dimension problem concerning a blow of an elastic plate on various register stop forms. The main parameters of sheet alignment are defined. The close fit of the numerical and experience data is achieved. These results may be used in the feeder alignment mechanism design, debugging of sheet-fed presses and in the educational process.

Keywords: alignment, emulation, shock-wave

1. Introduction

The one of main system of sheet-fed presses is a feeding device which supplies a periodical sheets feeding to printing apparatus. The alignment mechanism provides the correct position of the sheet relative to the printing plate. The sheet front edge is aligned on the table 2 with the help of two fixed front guide stops 3. This ensures exact alignment of a right-angular sheet with specified sizes $b \times l$ ($l > b$) (Figure 1). The main object of this research is an alignment process of moving plate on two front guide stops.

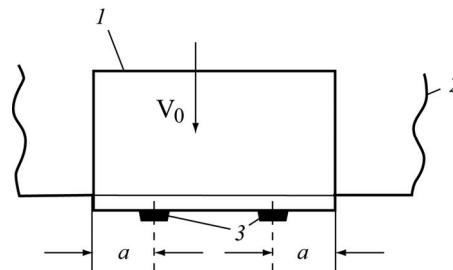


Figure 1: A sheet alignment scheme: 1 - a paper sheet; 2 - a feeding table; 3 - a front guide stop.

The main purpose of this work is to study stressedly-deformed condition of the paper sheet and its positioning parameters of sheet's alignment at the fixed front guide stops. This matter is considered for follows cases: different guide stop's sizes, various speeds of approaching the moving sheet towards the stopper and optimizations of the necessary parameters for qualitative information printing.

As is known the quantitative description of the collision processes is a very difficult problem (J. MacPhee, 1998; Muller A., 1980; Митрофанов В. П., 1999).

Thus to study the process of collision of a sheet about an obstacle it is necessary to develop mathematical modeling methods and produce some experimental research in laboratory conditions. Earlier some studies of such kind have been produced in particular in works (Веклич Н. А., 1970; Кильчевский Н. А., 1969; Горский Н. М., 1969; Паничкин В. И., 1973; Могинов Р. Г., 1999).

2. Methods

In contrary to this work the task of a definite size plate collision about a stop is digitally (with computer using) resolved in the framework of two-dimensional time-varying nonlinear theory of plates using Timoshenko's equations (Тимошенко С. П., 1979) and Godunov's (Годунов Г. П., 1961) digital methods of serration decay.

This task has a great importance for study of shock-wave processes in press's parts, when collision speed is below 6 m/s. When collision speed is much higher 6 m/s (that is $V \gg 6$ m/s) the task may be used to calculate main features of aircraft's thin-slab structure's deformation in case of high speed collisions of particles with different sizes and shapes about it and allows to predict the meteorite defense and man caused streams.

Let's put into consideration a co-ordinates system with X and Y axis coinciding with front and side sheet's edges. Let's consider a sheet sample with constant depth h , cut by sections along axis X, Y . There are various forces acting to this sample.

The system of nonlinear differential equations is the basis for solving of two-dimensional sheet's dynamics task. These equations set represents mathematical model describing a dynamic of the sheet's alignment with two front stops in the framework of Timoshenko's nonlinear theory of plates.

To resolve numerical task let's use the following notations: t - time; ξ - a current coordinate; u - a longitudinal displacement; v - a transverse displacement; $U = \partial u / \partial t$ - a longitudinal velocity; $V = \partial v / \partial t$ - a transverse velocity; ω - an angular moving sheet velocity; N - a longitudinal force; Q - a slaughter force; F - a longitudinal distributed load; G - a transverse distributed load; θ - an normal rotation angular; M - a bending moment; H - a torsional moment; T - a shearing force; ρ_0 - a material (paper) density; E - a coefficient of elasticity; μ - Poisson's ratio; K_s - a shear coefficient; l, h - a length and a thickness of plate (sheet); h_0 - a thickness of plate (sheet) in any section; $\xi = \xi_0$; $C_0 = E/\rho_0(1 - \mu^2)$ - a propagation speed of dilatational - compression waves; $C_s = K_s E/2\rho_0(1 + \mu)$ - a propagation speed of shear waves; $\alpha = C_s \cdot C_0$ (Figure 2).

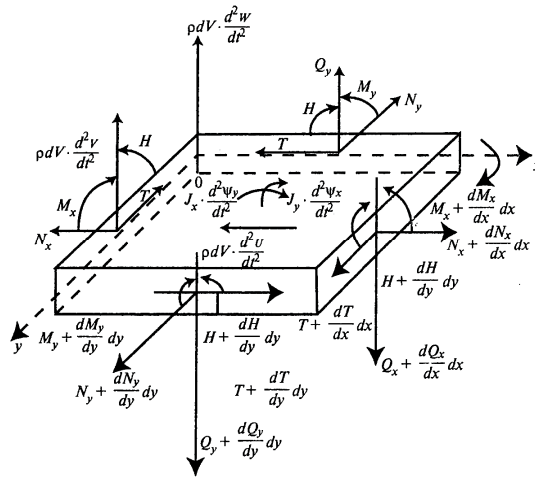


Figure 2: The scheme of the strengths and moments

The dynamic equations of the paper sheet are:

$$\frac{\partial N_x}{\partial x} - \frac{\partial}{\partial x} \left(Q_x \frac{\partial w}{\partial x} \right) + \frac{\partial T}{\partial y} + P_x - \frac{1}{1 - \mu^2} \frac{\partial u}{\partial t} = 0,$$

$$\frac{\partial N_y}{\partial y} - \frac{\partial}{\partial y} \left(Q_y \frac{\partial w}{\partial x} \right) + \frac{\partial T}{\partial y} + P_y - \frac{1}{1 - \mu^2} \frac{\partial v}{\partial t} = 0,$$

$$\frac{\partial}{\partial x} \left(Q_x + N_x \frac{\partial w}{\partial x} + T \frac{\partial w}{\partial y} \right) + \frac{\partial}{\partial y} \left(Q_y + N_y \frac{\partial w}{\partial y} + T \frac{\partial w}{\partial x} \right) + P_z - \frac{1}{(1 - \mu^2)} \frac{\partial w}{\partial t} = 0,$$

$$\frac{\partial M_x}{\partial x} + \frac{\partial H}{\partial y} - Q_x - \frac{1}{12(1 - \mu^2)} \frac{\partial \Omega_x}{\partial t} = 0,$$

$$\frac{\partial M_y}{\partial y} + \frac{\partial H}{\partial x} - Q_y - \frac{1}{12(1 - \mu^2)} \frac{\partial \Omega_y}{\partial t} = 0$$

[1]

Then the equations, connecting efforts and displacements, are:

$$\begin{aligned}
 Q_x &= \frac{K_s \alpha^2}{(1 + \mu)} \left(\frac{\partial w}{\partial x} + \psi_x \right), \\
 Q_y &= \frac{K_s \alpha^2}{(1 - \mu)} \left(\frac{\partial w}{\partial y} + \psi_y \right), \\
 N_x &= \frac{1}{(1 - \mu^2)} \left[\frac{\partial u}{\partial x} + \frac{1}{2} \left(\frac{\partial w}{\partial x} \right)^2 - \mu \left(\frac{\partial V}{\partial y} + \frac{1}{2} \left(\frac{\partial w}{\partial y} \right)^2 \right) \right], \\
 N_y &= \frac{1}{(1 - \mu^2)} \left[\frac{\partial V}{\partial y} + \frac{1}{2} \left(\frac{\partial w}{\partial y} \right)^2 + \mu \left(\frac{\partial u}{\partial x} + \frac{1}{2} \left(\frac{\partial w}{\partial x} \right)^2 \right) \right], \\
 T &= \frac{1}{2(1 + \mu)} \left(\frac{\partial u}{\partial y} + \frac{\partial V}{\partial x} + \frac{\partial w}{\partial x} \frac{\partial w}{\partial y} \right), \\
 M_x &= \frac{1}{12(1 - \mu^2)} \left(\frac{\partial \psi_x}{\partial x} + \mu \frac{\partial \psi_y}{\partial y} \right), \\
 M_y &= \frac{1}{12(1 - \mu^2)} \left(\frac{\partial \psi_y}{\partial y} + \mu \frac{\partial \psi_x}{\partial x} \right), \\
 H &= \frac{1}{24(1 + \mu)} \left(\frac{\partial \psi_x}{\partial y} + \frac{\partial \psi_y}{\partial x} \right)
 \end{aligned} \tag{2}$$

Let's note that nonlinear equations (1) and (2) are the sequence the law of conservation of momentum. These are the integral equalities and right for any loop.

The continuity equations have a view

$$\begin{aligned}
 \int_{\Gamma_1} \frac{\partial w}{\partial x} dx + w dt = 0, \quad \int_{\Gamma_2} \frac{\partial V}{\partial y} dy + V dt = 0, \quad \int_{\Gamma_2} \frac{\partial w}{\partial y} dy + w dt = 0, \\
 \int_{\Gamma_1} \frac{\partial \Psi_x}{\partial x} dx + \Omega_x dt = 0, \quad \int_{\Gamma_1} \frac{\partial u}{\partial x} dx + u dt = 0, \quad \int_{\Gamma_1} \frac{\partial \Psi_y}{\partial x} dx + \Omega_y dt = 0, \\
 \int_{\Gamma_2} \frac{\partial u}{\partial y} dy + u dt = 0, \quad \int_{\Gamma_2} \frac{\partial \Psi_x}{\partial y} dy + \Omega_x dt = 0, \quad \int_{\Gamma_1} \frac{\partial V}{\partial x} dx + V dt = 0, \\
 \int_{\Gamma_2} \frac{\partial \Psi_y}{\partial y} dy + \Omega_y dt = 0.
 \end{aligned} \tag{3}$$

Nonlinear differential equation system (1) - (3) is the basis for solving of two-dimensional sheet dynamics task. That represents mathematical model describing a dynamic of the sheet alignment with two front stops in the framework of Timoshenko's nonlinear theory of plates (Тимошенко С.П., 1979).

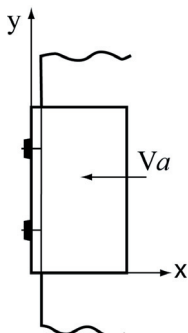


Figure 3: Sheet positioning against guide stops

To determine values of $\partial w/\partial x$ and $\partial w/\partial y$ in (1) - (3) let's suppose that the midline surface t haven't any breaks (see *Figure 3*).

Boundary conditions:

for edge $x = 0$

$$M_x = M_x^*, \Omega_x = 0, W = 0, U = -V_0, V = 0 \quad [4]$$

for edge $x = l$

$$M_x = 0, H = 0, Q_x + N_x \frac{\partial w}{\partial x} + T \frac{\partial w}{\partial y} = 0, N_x + Q_x \frac{\partial w}{\partial x} = 0, T = 0 \quad [5]$$

for edge $x = const$

$$M_y = 0, H = 0, Q_y + N_y \frac{\partial w}{\partial y} + T \frac{\partial w}{\partial x} = 0, N_y + Q_y \frac{\partial w}{\partial y} = 0, T = 0 \quad [6]$$

where M_x and V_0 are given impact at the edge.

Moreover, the task by under consideration has the following entry conditions:

$$\partial u/\partial t = -V_0, \partial v/\partial t = 0, \partial w/\partial t = 0 \text{ for } t=0, x=0, b_0 < y < b_1, b_2 < y < b_3, \quad [7]$$

where b_0, b_1, b_2, b_3 are the stop sizes.

In the case of collision a paper sheet about a solid obstacle the entry conditions are:

$$\partial u/\partial t = -V_0, \partial v/\partial t = 0, \partial w/\partial t = 0 \text{ при } t=0, x=0, 0 < y < b, \quad [8]$$

where b is the width of the paper sheet.

3. Results

The numbering solving analysis appeared that the picture of wave interactions is typical for fast loading. The blow duration is so little that the process time is as the effort spread.

As it is described earlier, equation set (1) - (3) with boundary (4), (6) and initial (7) or (8) conditions is solved numerically using Godunov's rupture breakup method. Some numerical results are on *Figures 4,5* for the time 0.101 ms, when the longitude wave reaches a sheet boundary $x = h, y = l$.

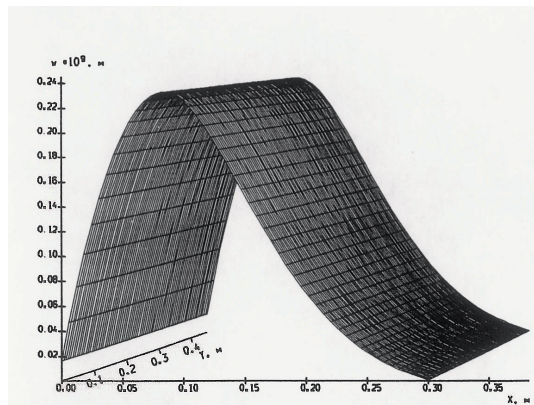


Figure 4: The bend sheet w for Offset paper on the left side ($U = 1.5$ m/s; $M_x = 3.516$ Nm) when the wave reaches the right sheet side ($t = 0.101$ ms). The one dimensional statement Parameters: $l = 0.3$ m; $b = 0.45$ m; $h = 1.5 \cdot 10^{-4}$ m; $C_o = 2970.9$ m/s; $C_s = 1303.4$ m/s; $\alpha = 0.43871$; $E = 7.0280 \cdot 10^9$ Nm; $K_s = 0.889$; $\rho_o = 875.0$ kg/m³

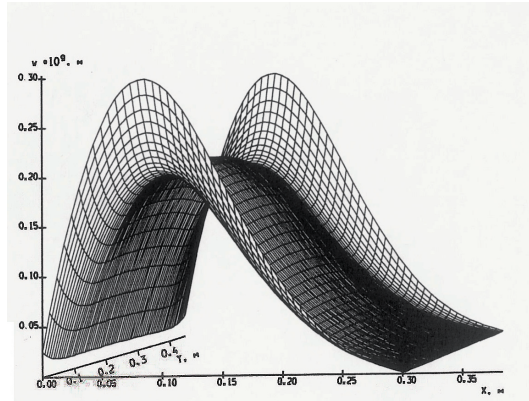


Figure 5: The bend sheet w for Offset paper on the left side ($U = 1.5$ m/s; $M_x = 3.516$ Nm) when the wave reaches the right sheet side ($t = 0.101$ ms). The two dimensional statement
Parameters: according Figure 4

The distributions of maximal flexure along a sheet on x and y coordinates are on Figures 4,5. It may view that the sheet bent reaches a maximum value in the two-dimension case as compared with the one-dimension one due to the wave reflection from sheet lateral free surfaces. The difference of the bent values between one-dimension and two-dimension cases is about 25%, it viewing the bent value symmetry about the sheet center and the maximum bent zone in the sheet corners in the two-dimension case.

The comparing values of the bending moment M_x depending on the sheet length x shows: the value M_x decreases gradually along the sheet length in the one-dimension case (Figure 6) and that appears much more difficult in the two-dimension one (Figure 7) when at first a few along the sheet length, after that gradually increases, but that decreases appreciably at $0.23 \leq x \leq 0.30$. So, the bending moment change along the sheet is non-linear one in the two-dimension case.

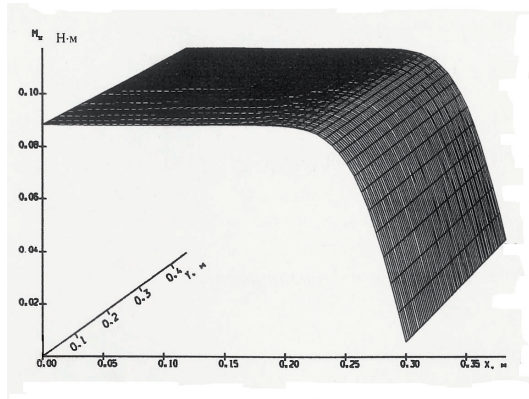


Figure 6: The bending moment M_x for Offset paper on the left side ($U = 1.5$ m/s; $M_x = 3.516$ Nm) when the wave reaches the right sheet side ($t = 0.101$ ms). The one dimensional statement

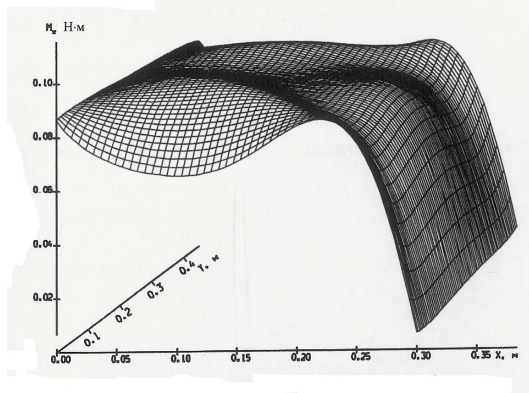


Figure 7: The bending moment M_x for Offset paper on the left side ($U = 1.5$ m/s; $M_x = 3.516$ Nm) when the wave reaches the right sheet side ($t = 0.101$ ms). The two dimensional statement

In the event of the blow of paper sheet to the surfaces of two side-by-side positioned front guide stops specified length and width, which are substantially smaller than appropriate sizes of a sheet. In a case like that the value of paper sheet deflection is considerably less than in case of solid collision of the whole paper sheet width about hard barrier (Figure 5). It seems that this feature is a result of an influence of blow-wave processes on left paper side. This side has intermediate free runs, where a contact with the guide stops lacks. An investigation of bending moment M_x inside a paper for the two-dimensional statement in case of two and nine (press GTO-52, comp. Heidelberg) guide stops (Figure 5 and Figures 8, 9 correspondingly) shows that the law of changing a value M_x according to paper length has more complex and various forms. There is a form looking like a “springboard” and for $x < 0.11$ m it obtains negative values for some paper peace’s. This research results is considered as previous data, which shall be specify, particularize and according multi parametrical investigate.

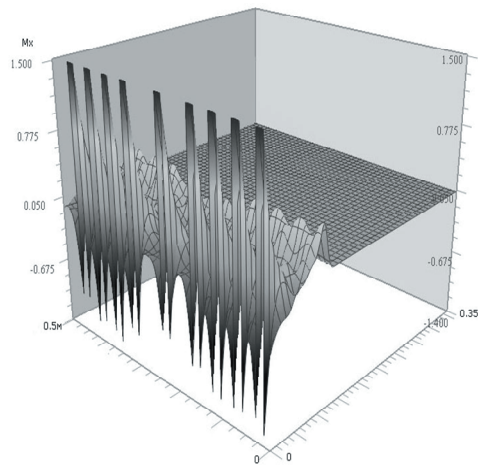


Figure 8: The bending moment M_x for Offset paper on the left side ($U = 1.5$ m/s; $M_x = 3.516$ Nm) when the wave reaches the point $1/4$ (another projection for the case according Figure 4)

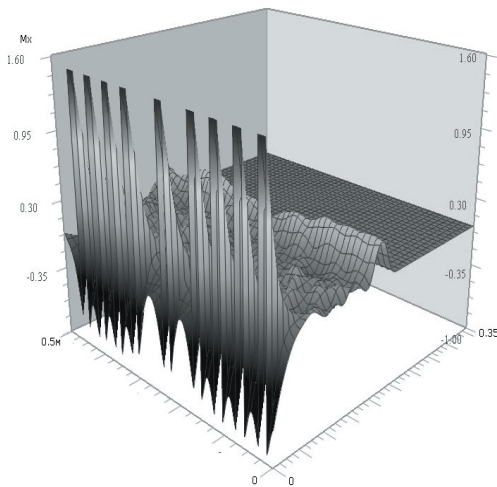


Figure 9: The bending moment M_x for Offset paper on the left side ($U = 1.5$ m/s; $M_x = 3.516$ Nm) when the wave reaches the point $1/2$ (another projection for the case according Figure 5)

4. Conclusion

There on the base of nonlinear theory of a blow of an elastic plate was fulfilled the study of wave processes for a press the sheets feeding systems. It was reached good agreement among the calculation and experimental results for the two dimensional statement in the cases of two and nine stops (press GTO - 52, comp. Heidelberg). It is seems that this results can be useful equal for the theory and design of guide stops in a feeding press mechanism and for an education process.

References

- Тр. Симпозиума по нелинейным и тепловым эффектам при переходных волновых процессах. - Горький, ГТУ, с. 143-151.
- MacPhee, J., (1998), Fundamentals of lithographic printing. GATFPRESS, Sewickeley (PA).
- Muller A., Drechsel K., (1980), Leitfaden der Offsettechnik. Polygraph-Verlag, Frankfurt/Main.
- в бумажном листе при ударе о жесткую преграду. - Тр. Конференции по современным проблемам механики многофазных сред и распространение волн в сплошной среде. - Ташкент, с. 83-86.
- Веклич Н.А., (1970), О распространении взаимодействий упруго-пластических волн в стержне при ударе
- Годунов Г.П., (1961), Разностная схема для двумерных нестационарных задач газовой динамики и расчет обтекания с отошедшей ударной волной. - ИС. ВММФ - Т.П., №6, с. 1620-1650.
- Горский Н.М., Коновалов А.Н., (1969), О численном решении плоской статической задачи теории упругости в напряжениях. - Тр. Конференции по численным методам решения задач теории упругости и пластичности. - Новосибирск, с. 55-64.
- Кильчевский Н.А., (1969), Теория соударения твердых тел. - Киев, Наукова думка, 246 с.
- Мамадалиев Н., Могинов Р., (1999), О распространении и взаимодействии упруго-пластических волн
- Митрофанов В.П., Тюрин А.А., (1999), Печатное оборудование. - Москва, МГУП, 441с.
- о преграду. Изв. АН СССР. МТТб №4, с. 182-185.
- Паничкин В.И., (1973), Расчет нелинейных одномерных волновых процессов деформации балок.
- Тимошенко С.П., Гудьер Д.Ж., (1979), Теория упругости. - Москва, Наука, 382 с.



CCD sensors for ink film opacity measurement and colour evaluation

Paritosh Prayagi^{1,2}, *Dietmar Nowack*², *Alexander Böddicker*^{1,2}, *Markus Schnitzlein*^{1,2},
*Chris Maurer*², *Arved Hübler*¹

¹ Institute for Print and Media Technology,
Chemnitz University of Technology/Chromasens GmbH
Reichenhainerstrasse 70, D-09126 Chemnitz, Germany

E-mails: paritosh.prayagi@s2007.tu-chemnitz.de; alexander.boeddicker@mb.tu-chemnitz.de;
arved.huebler@mb.tu-chemnitz.de

² Chromasens GmbH
Max-Stromeyer-Str. 116, D-78467 Constance, Germany

E-mails: dietmar.nowack@chromasens.de; markus.schnitzlein@chromasens.de;
chris.maurer@chromasens.de

Abstract

The development in the area of inline colour and optical density measurement raises the question of suitability of CCD sensors for print measurement applications. The correct evaluation and characterization of CCD sensors will be helpful especially for understanding the behavior of sensors while estimating colour and measuring the ink density. The responses obtained from the sensors are dependent on several optical factors such as the spectral sensitivity of sensors, assembly of lens apart from the light source being used. This paper researches extensively on the behavior of CCD sensors to characterize sensor linearity, sensor noise, influence of stray light for various optical combinations, sensor stability over temperature with regard to the requirements of printing applications.

Keywords: CCD sensor, sensor linearity, stray light, sensor noise, temperature stability

1. Introduction

The trend of measuring colour of finished printed products is slowly shifting from the printed copies being inspected offline to online and inline colour and density measurement systems. The online measurement system inspects the printed copies off the printing press but facilitates the changes such as ink and dampening settings on the press forming closed loop for colour control. The inline systems allow print quality inspection inside the printing press which aims to achieve 100% print quality control.

There can be two different ways to measure colour and density inside the printing press. Density is either measured using camera systems based on the responses in the absorption channels or is measured spectrally. Colour is similarly measured spectrophotometrically or measured/estimated using camera systems. The advantage of camera based measurement is the ability to measure within the whole image, inspect the image for defects as well as measure colour and density. The work done concentrates on characterizing CCD sensors for on-press applications of ink density measurement and spectral estimation of colour using camera systems.

The characterization of CCD sensors will be helpful especially for understanding the behavior of sensors while estimating colour and measuring the ink density. The responses obtained from the cameras are dependent on several optical factors such as the spectral sensitivity of sensors, assembly of lens apart from the light source being used.

This paper researches extensively on the behavior of CCD sensors namely:

- ✧ sensor linearity
- ✧ sensor noise
- ✧ influence of stray light for various optical combinations
- ✧ sensor stability over temperature

The work done is to conclude the characteristics and suitability of the CCD sensors for applications in on-press ink density measurement and aims towards achieving a real multi-spectral colour measurement system.

2. Research methods

Different experimental set-ups were prepared to characterize the sensors. The first set-up aimed to test the sensor linearity and sensor noise (Figure 1) while the second set-up was built to study the influence of stray light for various optical combinations (Figure 2).

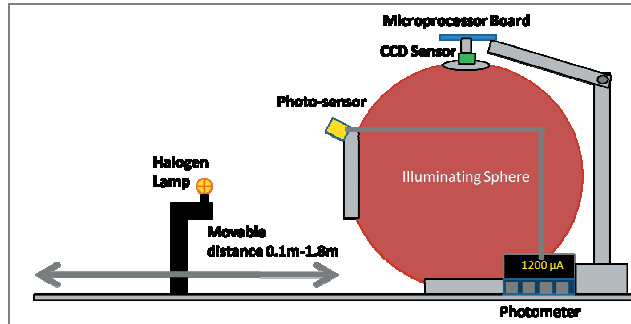


Figure 1: Experimental setup with illuminating sphere

The experiment to study the sensor linearity was set-up using an integrating sphere and standard light source Illuminant A (Tungsten Lamp - 75 W/ 6.25 A). The sensor used was a CCD line sensor connected with a microprocessor board. In-house developed software (Analysis and Test System Tool) by the company Chromasens GmbH enabled to capture images through the Leutron frame-grabber. The mounted light source was movable in order to prove the inverse square law with regard to sensor linearity. The sensor was mounted on the top of the integrating sphere. A dark room situation was prepared to reduce the influence of stray light on the measurements. The sensor linearity over distances ranging from 0.1m (starting from the illuminating sphere) to 1.8 was studied. Distances over 1.8m did not lead to any detectable responses while, under 0.1m led to the saturation of sensor. The linearity for integration times was studied ranging from 80 μ s - 4000 μ s. The sensor works with 2 horizontal shift registers. Therefore, it is possible to read the content simultaneously over two video channels resulting into 6 sub-channels (Odd and Even for each of the red, green and blue channels) through the whole image. With regard to the stability of the sensor responses it is important to study the sensor behavior dependent on higher temperatures. Therefore it was heated from room temperature up to the highest operating temperature (60°C). This range of temperature is conform to the operating and environmental temperatures on the printing units in the printing machine.

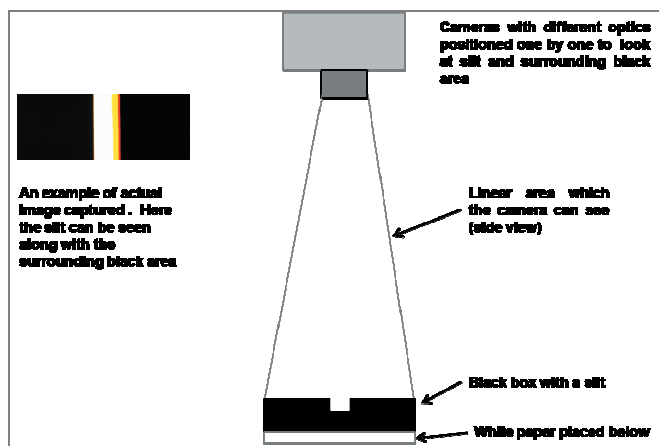


Figure 2: Experimental set-up to study the influence of stray light

Figure 2 shows the experimental set-up for the second part of the experiments conducted. Stray light influences the measurements in such a way that it causes changes in the grey levels. A CCD sensor in this case is used along with several optical combinations. A camera objective, a simple/single lens and the glass cover on the sensor are varied in different combinations to study this influence. The line sensor is set to observe the black box placed below with a 3 mm slit. A white paper is placed below the black box in order to reflect light falling on it through the slit. The light source is placed to focus on the slit and the area which the camera will detect the light source is not shown in the (Figure 2).

3. Research results

During the experimental work it was realized that it is difficult to prove the inverse square law of light in a practical situation. Therefore measurement methodology was modified. For every measurement a blend was prepared to measure the stray light which was deducted from the measurements with open radiation. From the view of printing press manufacturer the most important issue is the consistency and stability of the result. The sensor was very much stable for various exposure times and a fixed distance. The linearity of sensor was then evaluated from the images obtained from different distances of the light source to the illuminating sphere.

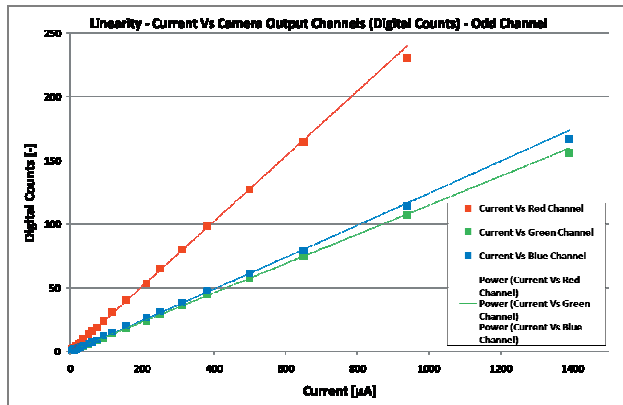


Figure 3:
Linearity of sensor for odd channel

The images were evaluated from their grey levels (digital counts) against the current in μA . The illuminating sphere was also connected with a photometer to simultaneously read from the CCD sensor as well as from the photometer. The linearity of sensor was evaluated for odd and even channels (Figure 3 and Figure 4). It was found that the CCD sensor response was linear to the current showed on photometer.

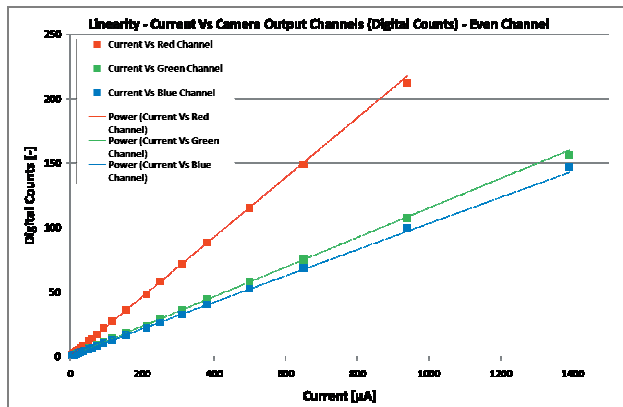


Figure 4:
Linearity of sensor for even channel

The measurements regarding the sensor behavior dependent on distance are plotted in Figure 5. The inverse square law of light is proved.

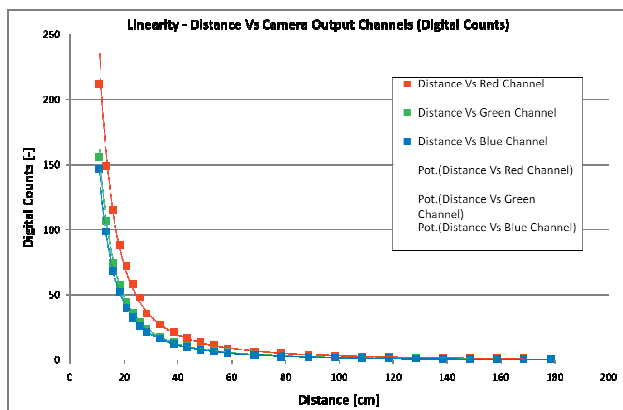


Figure 5:
Test for inverse square law of light for 3 output channels

The underlying dark current (camera offset) was also studied. All the experiments were carried out at a gain value of 100 without shading correction and white level adjustment. In the red region of the spectrum saturation could be recognized which is descending in the green and blue regions respectively. This influence is mainly due to the radiation function of the light source.

3.1 Photometric resolution (sensor noise)

The noise factor plays a very important role to determine the photometric resolution of the digit values obtained from each of the RGB channels. For determining the noise, each of the odd and even channels from the obtained values were analyzed. In order to this a special algorithm was developed to detect the noise in images. This algorithm calculated the arithmetic mean and the standard deviation of the selected area of the image.

Detecting camera responses under certain values cannot be realized because of the influence by the dark signal and read out noise. The values for the channels are registered in Table 1.

Table 1: Minimum channel values for measured noise

Channel	Minimum Value
Red	104
Green	84
Blue	136

With all the channels it is possible to achieve lower densities as seen in Figure 6, Figure 7 and Figure 8. The noise of the sensor behaves proportionally to the square root of the camera response. From the figures 6, 7 and 8, it can be observed that the green channel shows the best difference in the grey levels in the higher densities while blue is the worst.

A density value of 2.0 D means 1% transmission/reflection. This results in a grey level of 2.55. Especially printing on coated papers (offset printing) and transparent films or white backed films (flexographic printing/gravure printing/screen printing/printing with UV inks), the density of 2.0D is achievable with the used sensors. Some printing processes can go up to a density of 3.0 D. The density of 3.0 D equates to 0.1% light transmission/reflection. That means that a grey level of 0.25 is necessary to measure the density of 3.0 D. This is not possible with the experimental set-up.

Figure 6: Noise in the red channel

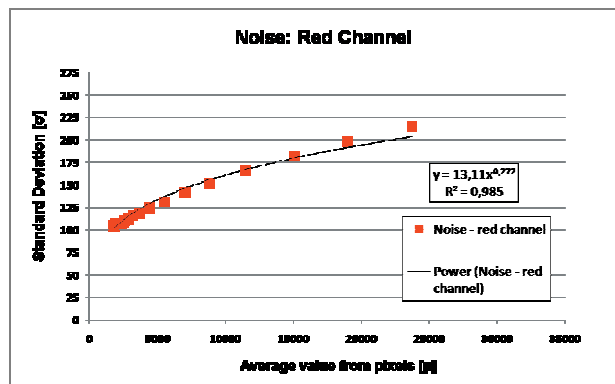
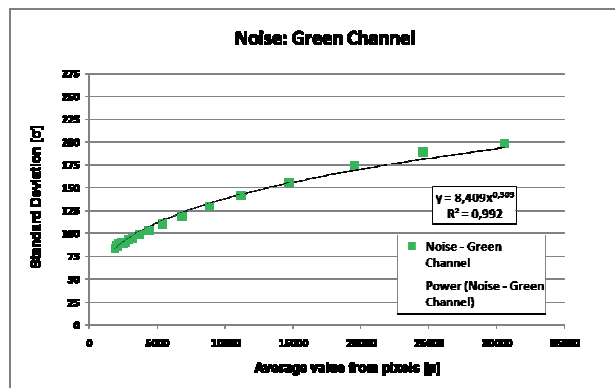


Figure 7: Noise in the green channel



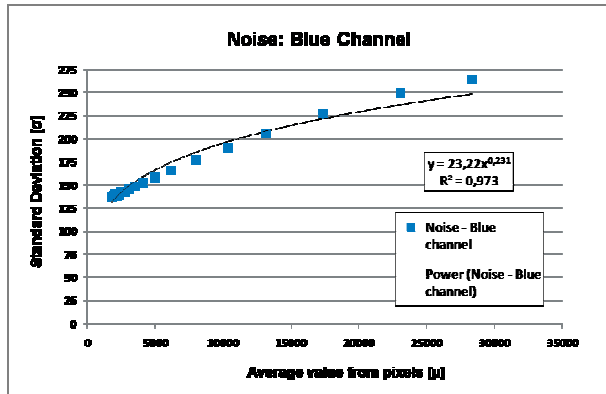


Figure 8: Noise in the blue channel

3.2 Influence of stray light

Apart from sensor linearity and sensor noise, stray light is amongst the major factors affecting realtime measurement. Unlike the traditional colour and density measurement devices such as spectrophotometers, colorimeters and densitometers, the camera allows a higher degree of stray light to reach the sensor device. This is due to the fact that the camera detects a larger area within the image (in case of CCD line sensors, whole or part of the line array). The light from the surrounding area influences the area to be measured because the whole light enters the optical assembly. It is necessary to minimize this error in order to obtain the correct camera response. Experiments were conducted to show that the error due to stray light can affect the measurements up to 1%. Various optical combinations were experimented upon to study the influence of optics on stray light.

Figure 9 shows the influence of stray light on the obtained image (camera response) using an open CCD sensor with a single lens. Here, no assembly of lenses is used (like in the case of a normal camera with objective).

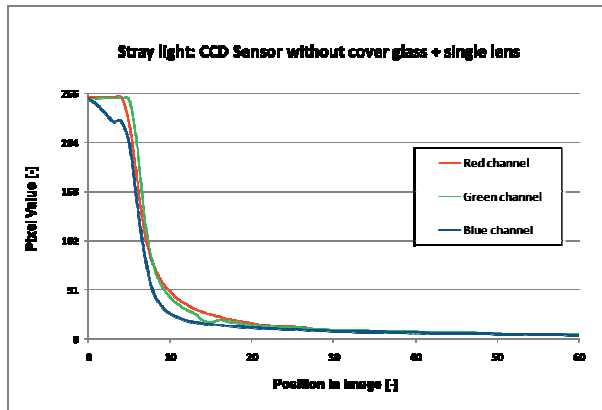


Figure 9: Influence of stray light - sensor with single lens, without cover glass

Figure 10 shows the influence of stray light on the obtained image with an open CCD sensor and with camera objective.

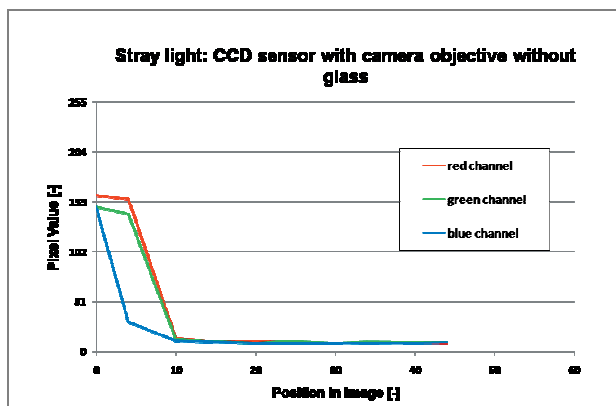


Figure 10: Influence of stray light - camera without sensor glass

Figure 11 shows the influence of stray light on obtained image using CCD sensor with sensor glass and a camera objective.

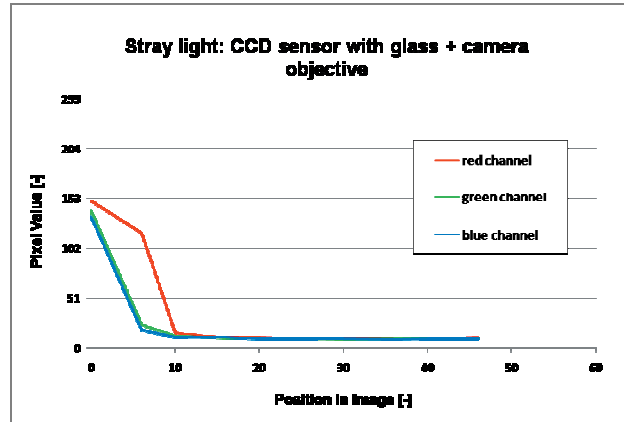


Figure 11:
Influence of stray light - CCD sensor
with glass and with camera objective

The results show that the sensor without cover glass and a single lens has minimal influence of stray light in comparison to researched optical combinations. Observing the pixel values the optical assembly according to Figure 9 allows more light to pass through in the area of the slit. In this case, the pixel values can be seen in the saturation level. In the other two cases, the objective allows less amount of light to pass through and hence, the pixel values are not in the level of saturation.

This shows that the influence of stray light will change according to the different optical assemblies.

3.3 Stability of CCD sensor over temperature

The Figure 12 shows the stability of CCD sensor over temperature.

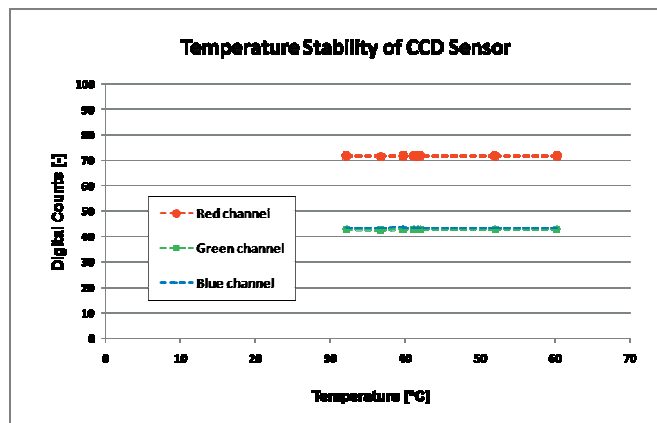


Figure 12: stability of CCD sensor over temperature

The sensor was heated up to 60° C. The sensor temperature was controlled by comparative measurements with a digital thermometer. The change of grey levels in the images depending on temperature was researched. There was no influential change observed in the grey levels for any of the temperature. Therefore, it can be concluded that the used CCD sensor is very stable at operating temperatures in the printing machine environment.

4. Conclusions

The print specific sensor characterization plays a very important role in selection of sensor for on-press measurement applications. The CCD sensor itself is limited to measuring higher densities due to uncertainty of several factors like the dark current, photon noise and stray light. Apart from this, the CCD sensor consists of broad band red, green and blue filters which are not ideal for density measurement on prints. The spectral sensitivity of absorption filters for print density measurement requires narrow band filters.. There are several physical problems involved in manufacturing of CCD sensors with this specific spectral sensitivity.

In applications of colour estimation using multi-channel/multi-spectral camera systems, the linear opto-electronic transfer function being in charge of the camera response depends on the system characteristics such as noise, stray light and linearity. Therefore, it is very important to characterize the CCD sensor with regard to the applications.

Further work is being done in cooperation with Chromasens GmbH to develop a multi-spectral measurement system for on-press applications. Work is being carried out to use individual narrow band channels within the multi-spectral system to measure density and estimate colour simultaneously.

Acknowledgements

We sincerely thank Prof. Dr. Bernd Jödicke at the University of Applied Sciences, Constance for support in the optical laboratories. We also thank Mr. Martin Hund, Mr. Bernhard Frei and Mr. Martin Merkler at Chromasens GmbH for help in the analysis and setup of experiments.

References

- Gomez, (2008), Quality control and colour assessment for flexography and gravure printing based on machine vision, Proceedings of 35th IARIGAI Research Conference, Valencia, Spain, pp 381-388
- Graichen, (1973), A new method for measuring colour on printed materials at high speed webs, 12th IARIGAI Research Conference, Versailles, France, IPC Science & Technology Press Limited, pp 169-173
- Hübler A. C. et. al, (2002), Possibilities for automatic control of colour print quality; IFRA Special Report 3.35
- Löffler. E.M, (2003), Messverfahren zur Bestimmung der relative spektralen Empfindlichkeit von Digitalkamerasystemen, Diploma Thesis, HdM Stuttgart
- Malmqvist K., (1993), The 3-colour CCD camera as a densitometer for measuring density of cyan, magenta and yellow in printed solid areas and in screen areas, Proceedings of 22nd IARIGAI Research Conference, Munich, Germany, pp 342-351
- Schnitzlein et. al, (2010) Spektrale Schätzung in Inline Bildinspektionssystemen mittels 6-12 kanaliger CCD-Zeilensensoren, 16th Farbworkshop, Ilmenau
- Wyszecki & Stiles, (2000) Colour Science - Concepts and Methods, Quantitative Data and Formulae, Second Edition, Wiley Publication



Hybrid printing - print quality mechanisms when offset and inkjet are combined

Marianne Klamán¹, Erik Blohm¹, Per-Åke Johansson¹, Jon Lofthus¹,
Viviane Alecrim², Jonas Örtégren²

¹ Innventia, Box 5604, SE-114 86 Stockholm, Sweden

E-mails: marianne.klamán@innventia.com; erik.blohm@innventia.com; perake.johansson@innventia.com; jon.lofthus@innventia.com

² Digital Printing Center, Mid Sweden University

Järnvägsgatan 3, SE-891 18 Örnsköldsvik, Sweden

E-mails: viviane.alecrim@miun.se; jonas.ortegren@miun.se

Abstract

The present work was performed in order to create improved possibilities for hybrid printing by increased knowledge of ink-paper interactions and compatibility between inkjet and offset inks. The goal was to define performance, expressed as print quality parameters for inkjet printing, UV and water based, in combination with offset printing. The work presented in the current paper was conducted in cooperation between Innventia and DPC.

The real challenge regarding hybrid printing is the demand that two entirely different printing techniques must be able to be printed onto the same substrate, with a resulting high print quality, regarding both print techniques. This is not a trivial prerequisite why the identification of the ruling performance mechanisms has been crucial for the work carried out. The demands on the surface structure, absorption properties and other parameters will differ depending on the kind of inkjet technology, the inks involved, and the impact of the offset printing.

For selected paper samples two approaches were used to evaluate ink-paper interaction and compatibility between inkjet and offset inks. These approaches are referred to as wet-on-dry and wet-in-wet printing.

Wet-on-dry printing trials were performed on pre-printed offset sheets. The trials for wet-on-dry printing have been carried out with both UV and water-based inkjet inks, whilst wet-in-wet printing only with UV inkjet inks on top of fresh offset prints inline.

The inkjet print quality was evaluated in terms of print sharpness (line width and blurriness), print density and print mottle. The influence of print speed was addressed.

Keywords: hybrid printing, inkjet print, print quality, print sharpness

1. Introduction

In a forecast for digital printing (PIRA, 2009), the process is prophesied to be a dominating printing technique 2018. Somewhat more modest figures are given by (Romano, 2011) saying that the customisation of packaging and catalogues increase all the time and the total amount of digitally printed copies will increase to 47% of all print volume by 2020. End customers require possibilities to customise information and consider it crucial as a way to increase sales and be more responsive to changing branding needs (Pettersson, 2011), (Edward, 2010) and target consumers with marketing information (Harrison, 2010).

Hybrid technology is useful, since an integration of customer specific information can be done at a late stage, by incorporating inkjet printing heads into a packaging line or even later at the point of sale. A possibility is also to add the information onto a pre-printed item. The bulk printing can then still be carried out with conventional printing technology which is more cost effective.

Inkjet technology presents a high level of flexibility. Besides the flexible integration of inkjet print heads into existing production lines it also offers a capability to print on substrates with various properties.

The real challenge regarding hybrid printing is the demand that two entirely different printing techniques must be able to be printed onto the same substrate, with a resulting high print quality, regarding both print

techniques. This is not a trivial prerequisite why the identification of the ruling performance mechanisms has been crucial for the work carried out. The demands on the surface structure, absorption properties and other parameters will differ depending on the kind of inkjet technology, the inks involved, and the impact of the offset printing.

Differences in print quality between offset and inkjet may be used for creating certain desired effects but may also cause a disturbing impact regarding the perception of the total print quality.

The present work was performed in order to create improved possibilities for hybrid printing by increased knowledge of ink-paper interactions and compatibility between inkjet and offset inks. The goal was to define performance, expressed as print quality parameters for inkjet printing, UV and water based, in combination with offset printing. The work presented in the current paper was conducted in cooperation between Innventia and DPC.

2. Methods

For selected paper samples two approaches were used to evaluate ink-paper interaction and compatibility between inkjet and offset inks. These approaches are referred to as wet-on-dry and wet-in-wet printing.

Wet-on-dry printing trials were performed on pre-printed offset sheets. The trials for wet-on-dry printing have been carried out with both UV and water-based inkjet inks, whilst wet-in-wet printing only with UV inkjet inks on top of fresh offset prints inline. At Innventia the reel-to-reel Linda machine, with an integrated inkjet printing module and an offset printing unit, was used, see Figure 1. The pre-printed sheets were glued on the paper web and printed wet-on-dry, and the wet-in-wet trials were performed in-line, reel-to-reel. These trials were carried out at two print speeds, 40 and 80 m/min. Wet-on-dry printing with water based pigmented inkjet inks on the offset printed samples, was performed at DPC using a desktop printer. The printer selection was done after evaluating micrographs of full tone cyan, magenta, yellow and black images. The inkjet ink printers that use pure colours were selected for the trials (i.e. no dots of other colours were visible in the full tone image).

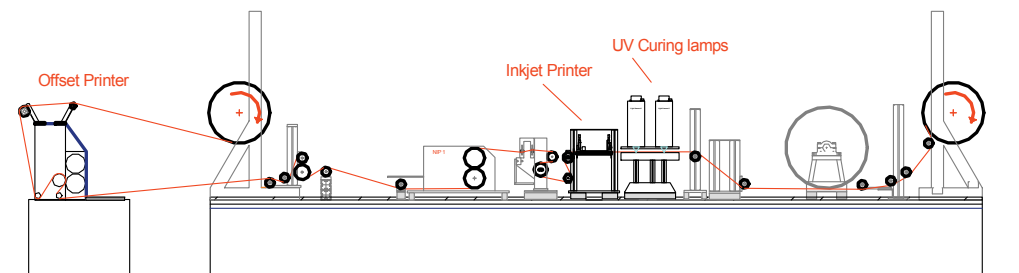


Figure 1: The Linda machine with offset printing unit and Inkjet print module (J. Lofthus)

Print trials and evaluations of substrate surface properties were performed on the substrates listed in Table 1. In the text the substrates are referred to using their respective acronyms.

Table 1: Samples identification

Paper	Acronym
Coated Paper	CP
Coated Board	BP
Uncoated Board	BR
Uncoated Wood free Paper 1	UC1
Uncoated Wood free Paper 2	UC2
Uncoated Wood-containing paper	UC3
Standard Newsprint	UC4

The wet-on-dry trials were carried out on both coated and uncoated grades whilst the wet-in-wet trials only on uncoated grades.

The offset test print lay-out was designed with tone areas of 0, 40 and 100% of yellow and the inkjet test lay-out with a grey tone scale, lines from 0,25 to 2 pts and a 40% tone value for mottle measurements, as seen in *Figure 2 and 3*. 1 pt line corresponds to 353 μm . PD and CD refer to print direction (vertical lines) and cross direction (horizontal lines) on the test print lay-out.

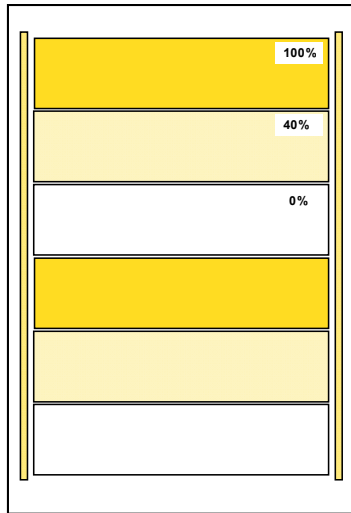


Figure 2: Offset test print lay-out

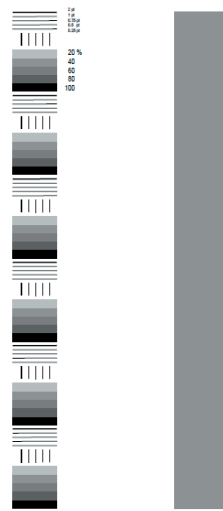


Figure 3: Inkjet test print lay-out

The inkjet printing was done on the 0% unprinted paper surface, the 40% and the 100% offset printed surfaces. The inkjet print quality was evaluated in terms of print sharpness (line width and blurriness), print density and print mottle. The influence of print speed was addressed. The methods in *Table 2* were used for the evaluations. The print sharpness was measured according to ISO 13660 and extended to measure also areas with different offset print coverage.

Table 2: Print quality evaluation methods

Property	Method	According to
Line width	QEA Personal IAS system	ISO 13660 print quality standard
Blurriness measured on the prints with UV curing ink	QEA Personal IAS system	ISO 13660 print quality standard
Blurriness measured on the prints with water based ink	FACIT method	differently from the ISO 13660 defines the edge zone from 33 to 67% reflectance
Print density	Techkon Spectrodens A 801023 Premium. Black channel	ISO-E setting with polarizer and paper white reference.
Print mottle	Epson scanner and STFI Mottling Expert Software	

Microphotographs were used to illustrate the increase or decrease in line width of 1 pt inkjet lines (lines in print direction) on offset printed substrates.

Contact angle measurement was performed with Fibro DAT 1100, Dynamic Absorption and Contact Angle Tester and with three liquids. The method is in compliance with TAPPI T558 & ASTM D-5725.

A porometer test using the ink 3809 (former 1520) from SunChemical was done to study the absorption capacity of the pre-printed surfaces. This test gives an indication about the porous structure of the paper (i.e. number of larger and smaller pores). This test was developed by SunChemical and Coates Lorilleux and involves the transfer of a standard ink (i.e. Porometertest farbe 3809) to the paper and rubbing it off after a few seconds. The optical density of the ink spots is measured after the rub off using an X-rite 500 spectrodensitometer. Higher optical density means higher absorption capacity of the paper, larger pores (Beyeler 1986). The test was carried out only on the unprinted areas of the substrates.

3. Results

Trials with UV curing inkjet inks, wet-on-dry

The wet-on-dry print trials with UV inkjet showed both narrower *line width* and less *blurriness* on coated paper and board compared with uncoated substrates, as elucidated by the microphotographs of the 1 pt inkjet lines in *Figure 4*, and measured values for line width, see *Figure 5*. A slight tendency to increased line width with increased offset area coverage for the *coated substrates* could also be seen. For the *uncoated substrate* the opposite is found, the line width and the blurriness for inkjet are decreased when printed on a higher area coverage of offset print. No influence of speed was found.

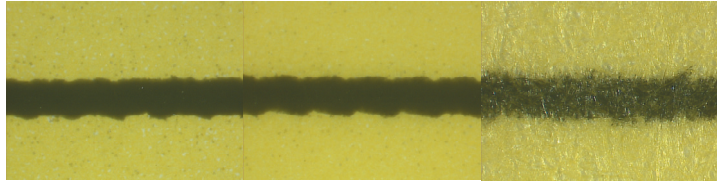


Figure 4: Narrower line width and less blurriness for inkjet lines printed on offset print on coated paper and board. From left to right: Coated paper (CP), coated (BP) and uncoated board (BR), 40 m/min. 100% tone coverage of the yellow offset print



Figure 5: Line width for 1 pt inkjet lines printed at 80 m/min on the offset printed substrates CP, BP and BR

An increased *print mottle* could be observed with increased offset area coverage on the uncoated, rougher surface, see *Figure 6*.

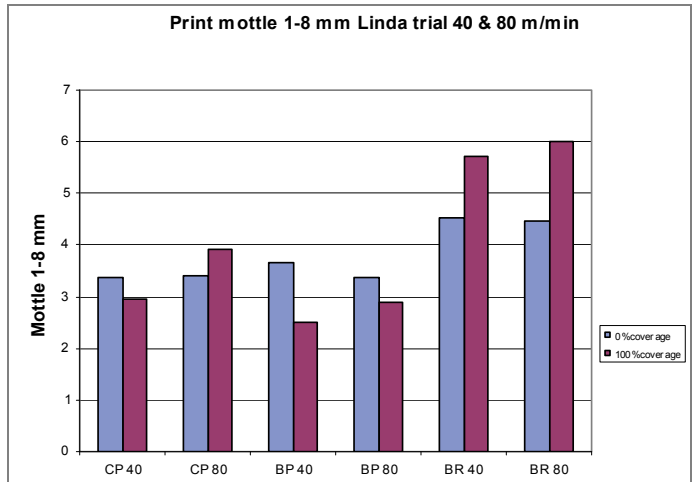


Figure 6: Print mottle for inkjet print, on the 100% offset printed surfaces of substrates CP, BP and BR., in the wavelength region 1-8 mm. 40 m/min and 80 m/min print speed

The *print density* increased on the coated grades with increased offset area coverage but not on the uncoated grade, see *Figure 7*. The print speed did not seem to influence neither mottle nor density.

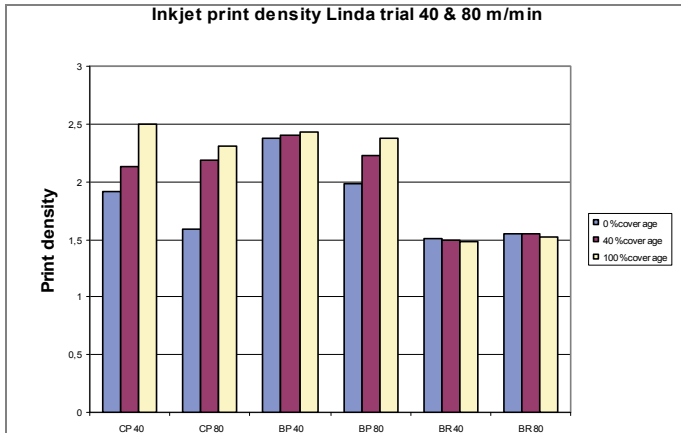


Figure 7: Inkjet print density. 40 m/min and 80 m/min print speed

Trials with UV curing inkjet inks, wet-in-wet

The wet-in-wet trials were carried out with offset followed by UV inkjet. What could be seen was that the *line widening* on the uncoated and roughest substrates was in the same range for both the wet-on-dry and wet-in-wet printing.

There was an increase in *blurriness* with increased area coverage on the rougher substrates UC3 and UC4, see Figure 8. Similar to what could be seen for the wet-on-dry printing an increased inkjet *print mottle* could be observed with increased area coverage for the offset print on rough surfaces.

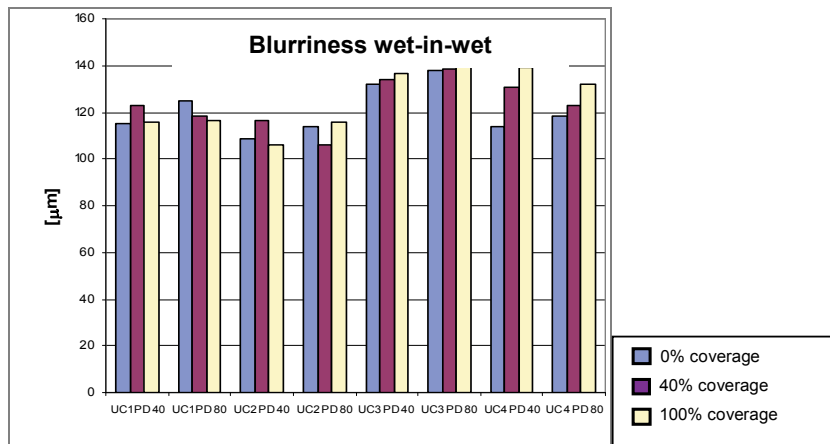


Figure 8: Blurriness for 1 pt inkjet lines printed at 40 and 80 m/min wet-in-wet on offset printed substrates

The *contact angle* measurements gave the results seen in Table 3. The coated samples show lower contact angles (better wetting) for water as well as for ethylene glycol, which is often used in water based inkjet inks.

Table 3: Contact angle measured for some of the substrates

Paper/board	Contact angle measured with		
	Water	Diiodomethane	Ethylene glycol
UC1 40	94,7	55,4	86,5
UC1 80	92,7	57,4	84,1
UC2 40	97,8	57,4	89,7
UC2 80	98,7	58,6	90,8
UC3, 100% offset area coverage (wet-in-wet)	102,9	52,7	73,8
UC3, 40% offset area coverage (wet-in-wet)	100,5	51,5	65,6
BR, 100% offset area coverage	89,7	59,0	73,1
BR, 40% offset area coverage	95,2	52,3	78,7
BP	74,2	52,3	59,1
CP, 100 % offset area coverage	74,9	39,5	62,8
CP, 40% offset area coverage	79,6	45,9	58,0

Trials with water based inkjet ink, wet-on-dry trials

The lower the surface porosity, the higher the reticulation of the ink or so called clustering effect (Frenkel 2010). Offset papers are more fine porous substrates compared to inkjet papers. Due to this, the inkjet ink solvent penetrates slowly into the paper leading to a stronger clustering effect which is visible as *print mottle*, (see Figure 9 and Figure 10). The porosity of the paper was reduced even further with increasing offset area coverage, clustering/mottle got even stronger, see Figure 9 (c) and Figure 10 (c), where the paper surface is completely covered by the offset ink film. A slightly higher clustering effect was observed for BP. On the other hand, this effect was not pronounced at the uncoated BR (see Figure 11).

In the porometer test much higher optical density (OD) for BR compared to CP and BP's coated surfaces was measured, see Table 4. This indicated that BR's ink absorption was much higher than the two other papers which explain the lack of clustering effect for it. Mercury porosimeter measurements would give a much more accurate result for the characterization of pore size of the printed and non-printed offset surfaces nevertheless the porometer test gives a good indication of the absorption capacity of these papers.

Table 4: OD values for the non-printed areas

Sample	CP	BP	BR
OD	0.40 ± 0.01	0.32 ± 0.03	1.02 ± 0.04

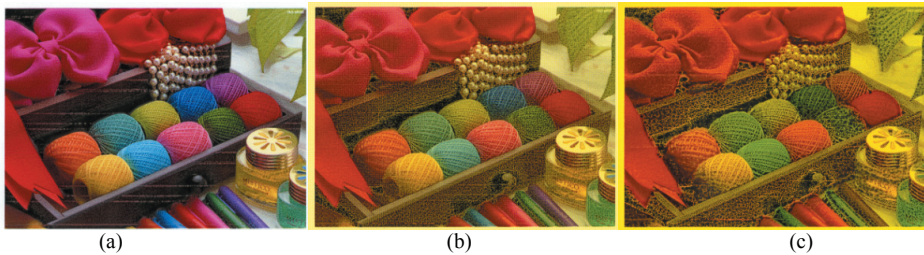


Figure 9: Clustering effect on the desktop printed image leading to a higher print mottle, for c compared to a. (a) 0% (b) 40% and (c) 100% area coverage of the offset pre-printed samples for CP

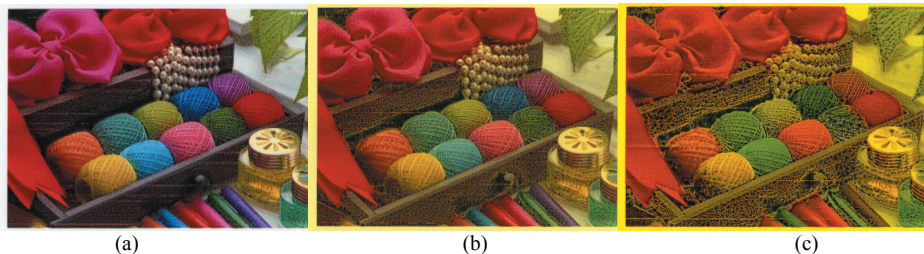


Figure 10: Clustering effect on the desktop printed image leading to a higher print mottle, for c compared to a. (a) 0% (b) 40% and (c) 100% area coverage of the offset pre-printed samples for BP

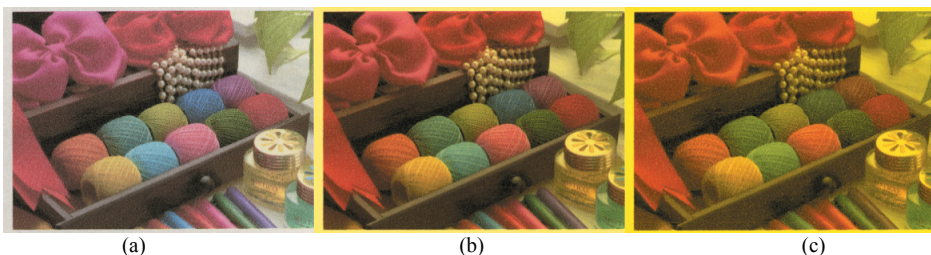


Figure 11: The clustering effect seen on CP and BP was not seen for BR. (a) 0% (b) 40% and (c) 100% area coverage of the offset pre-printed samples for BR

Due to the clustering effect, the results for line width and blurriness were not considered completely reliable for the samples CP and BP. Most of the print outs, except BR did not dry immediately after printing and print rub off occurred easily. It was necessary to dry the samples in an oven at 65°C before conducting the measurements.

The line width seemed to be unaffected with increased area coverage for the BR samples, see Figure 12, whereas the blurriness seemed to increase, see Figure 13, with increased offset area coverage.

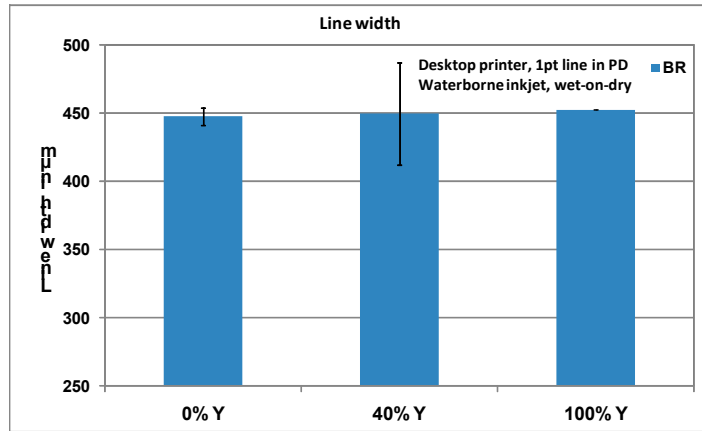


Figure 12: Line width for 1 pt inkjet lines printed at the desktop printer on offset for BR

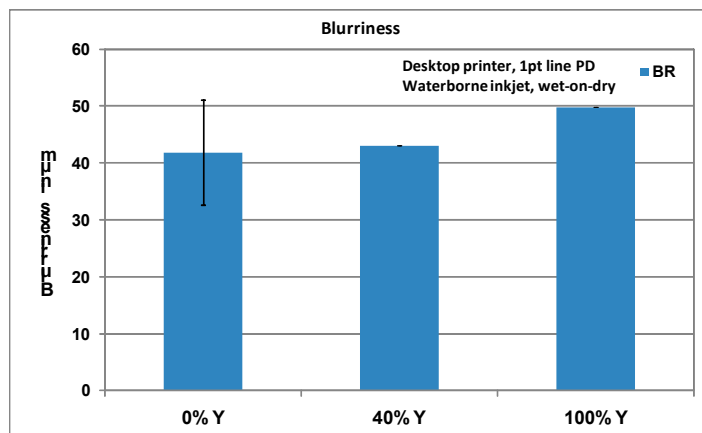


Figure 13: Blurriness for 1 pt inkjet lines printed at the desktop printer on offset for BR

4. Discussion

Some observed main phenomena in the different print situations were:

- **UV inkjet, wet-on-dry**
 - *Coated substrates*: Increased line width with increased offset print area coverage. Also the print density increased on the coated grades with increased offset area coverage (but not on the uncoated grade).
 - *Uncoated substrates*: Line width as well as blurriness unaffected or decreased with increased offset print area coverage.
 - *Uncoated, rougher surfaces*: An increased print mottle could be observed with increased offset area coverage
- **UV inkjet, wet-in-wet**
 - *Uncoated, rougher surfaces*: There was an increase in blurriness with increased area coverage on the rougher substrates. The line widening on the uncoated roughest substrates was in the same range as for the wet-on-dry printing.
 - *Uncoated, rougher surfaces*: Similar to what could be seen for the wet-on-dry printing an increased inkjet print mottle could be observed with increased area coverage for the offset print on the rough surfaces.

Water based inkjet, wet-on-dry

General: Offset papers are fine porous substrates compared to inkjet papers. Due to this, the inkjet ink solvent penetrates slowly into the paper leading to the clustering effect which is accentuated when an additional offset ink is applied.

The mechanisms leading to these phenomena can be several.

For the wet-on-dry printing the effects on print sharpness, as increased line width with increased offset print area coverage, seen on the coated paper, CP, may be related to the more closed surface caused by the offset ink on the substrate. This may result in less penetration and more spreading on the surface of the inkjet ink. On the opposite, for the uncoated papers and boards, a more open surface causes a larger absorption of both the offset ink and the inkjet ink and thus leaves the line width unaffected or decreased with increased offset area coverage for the UV-printed samples.

The water based inkjet ink solvent penetrates slowly into the paper leading to a stronger clustering effect which is visible as print mottle. The porosity of the paper was reduced even further with increasing offset area coverage, clustering/mottle got even stronger where the paper surface is completely covered by the offset ink film.

The coated samples show lower contact angles (better wetting) for water as well as for ethylene glycol. For the wet-in-wet printing, the increase in blurriness on the rougher substrates can be due to decreased penetration into the substrates due to closing of the surface by the offset ink.

Figure 14 illustrates how the UV inkjet ink spreads well on the offset printed areas (the yellow ones) but on the plain paper (the white areas) the fast absorption leaves “unprinted” areas and the paper shine through the inkjet ink area.

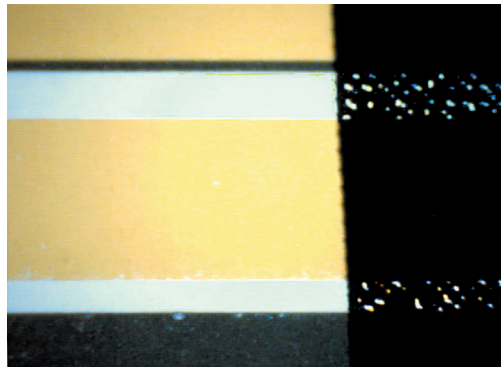


Figure 14: On the yellow offset printed areas the inkjet ink is spreading evenly but on the plain paper the absorption seems to be so fast that the ink doesn't have time to spread out and leaves uncovered areas

For water based inks the hydrophobic character of the offset ink film may often lead to poor wetting of the inks.

One mechanism that was observed for both wet-on-dry and wet-in-wet printing was the increased print mottle on uncoated papers and with increased area coverage of the offset ink. One conclusion that can be drawn from the microphotograph seen in *Figure 15*, is that this is caused by increased concentration of offset and inkjet printing ink on fibre peaks and closed parts of the surface. An additional or combined effect may also be a surface energetic effect between the polar inkjet ink and the non polar offset ink which causes reticulation of the ink thus increasing print mottle.



Figure 15: Print mottle caused by a concentration of offset and inkjet ink on fibre peaks (the darker parts)

It must be assumed that with a better substrate matching the results for the wet-on-dry trial using water based inks would have been more successful and the effects due to the ink reticulation and subsequently clustering effect would have been overcome or minimized. Even for BR, where this effect was lower, it could be noticed the effect on colour density, as the colorant seems to have penetrated into the substrate, leading to a very poor colour reproduction indicating a non optimized paper selection.

5. Conclusions

The mechanisms for the resulting print quality in terms of print sharpness, print mottling and print density look different depending on whether the print trials have been carried out wet-on-dry or wet-in-wet. It also depends on whether the inkjet printing is carried out with the UV curing or the water based inks.

However, some mechanisms are independent of these facts. The mechanisms are often more different for coated versus uncoated papers and boards than for wet-on-dry or wet-in-wet. The wet-in-wet printing, which was considered as one of the challenges to be carried out with a good result, could be performed well. Also the inkjet printing on the 100% offset printed area, considered as a challenge to print on, gave a good result at least for UV curing inkjet.

For the wet-on-dry printing effects on print sharpness, as increased line width with increased offset print area coverage could be seen on the coated paper, CP. On the opposite, for the uncoated papers and boards, the line width was unaffected or decreased with increased offset area coverage for the UV-printed samples. For the wet-in-wet printing, there was an increase in blurriness on the rougher substrates and a further increase with higher area coverage.

One mechanism that could be observed for both wet-on-dry and wet-in-wet printing with UV curing ink was the increased print mottle with increased area coverage. One conclusion that can be drawn is that this is caused by increased concentration of offset and inkjet printing ink on fibre peaks and closed parts of the surface. An additional or combined effect may also be a surface energetic effect between the polar inkjet ink and the non polar offset ink which causes reticulation of the ink thus increasing print mottle.

An increased print density with increased area coverage probably could be seen on the coated grades. The same pattern was not seen on the uncoated rough surfaces, but rather a slightly decreased print density with increased area coverage on uncoated surfaces.

The water based inkjet ink solvent penetrates slowly into the paper leading to a stronger clustering effect which is visible as print mottle. The porosity of the paper was reduced even further with increasing offset area coverage, clustering/mottle got even stronger where the paper surface is completely covered by the offset ink film.

UV inkjet appears to lead to better results than water based inkjet for the samples studied in this work. UV inkjet seemed, at least in the trials performed here, to be less sensitive to substrate selection. The porometer test can be one tool to be used in the selection of paper and boards appropriate for inkjet print. To print with water based inks in a hybrid printing approach seem to be more challenging, although worth it, when considering the requirements of i.e. food packaging applications.

Acknowledgements

Financial support from RISE, Research Institutes of Sweden, the EU structural funds and the County Administrative board is gratefully acknowledged.

References

- Adamic, Raymond J. and Gibney, Theresa A., 1993
- Anti-coalescent ink composition and method for making the same*. 5.188.664 [ed.] Hewlett-Packard. United States, Inkjet inks formulation.
- Beyeler, T. (1986).
- Porometertest*. S. a. C. Lorilleux
- Edward, S., 2010

Advertising is king: trends in package printing, Retail Pack, p. 20.

Frenkel, M. (2010).

Tailoring substrates for inkjet printing. The chemistry of inkjet inks. Singapore, World scientific.

Harrison, D., 2010

The new normal: marketing trends for consumer engagement, Print Summit, Geneva, Switzerland.

PIRA (update 2009)

The future of digital printing to 2018 (2008)

PIRA International, Report 2008, 189 p.

Romano, F., 2010

The future of print: forecasted technology trends in printing technology, *Punjab Print*, vol. 16, no. 3, May-June 2010, pp 9-10.

Petersson, M., 2010

Personalised increased sales: transactional printing in Sweden, Gr. Forum, no. 1-2, 2011, p. 42.

Simulation aided design of inkjet systems

*Philip Marmet*¹, *Fritz Bircher*¹, *Johannes Renner*¹, *Philipp Haslebacher*¹,
*Gert Schlegel*¹, *Florian Fässler*²

¹Institute of Print Technology, Bern University of Applied Sciences
Pestalozzistrasse 20, CH-3400 Burgdorf, Switzerland
E-mail: philip.marmet@bfh.ch

²Polytype SA, Route de la Glâne 26, CH-1701 Fribourg, Switzerland

Abstract

This paper presents an approach to simulation aided design of inkjet systems by creating an entirely virtual printing machine. Simulations are used in every domain of inkjet systems, from the single inkjet valves to the print machine's structural dynamics and the simulation of the final printout on substrates. All these simulations are coupled with different interfaces. Therewith the printing machine with its mechanical structure, drive systems and control algorithms can be optimized as a whole. The impact of vibrations on the final print result can be achieved with the simulation of the printout.

A deeper understanding of the whole printing process can be achieved due to the ability to simulate the entire inkjet system. Furthermore it is possible to solve a specific problem by simulating an individual setting, if necessary simulations can be coupled. A global approach to simulation with well-defined interfaces and couplings between the different engineering fields increases the interdisciplinary thinking and exchanging of knowledge. In this way, simulations are an efficient and powerful tool to develop and optimize the complex inkjet systems for tomorrow's needs.

Keywords: simulation, multiphysics, inkjet, valve, vibrations

1. Introduction

Nowadays simulations are an essential tool for the design process and optimization of inkjet systems regarding the need for shorter development times and the simultaneous demand for improved quality. With simulations, the development process can be accelerated by reducing the number of prototypes needed as well as allowing for a deeper understanding of the processes, which results in better solutions. Industrial inkjet applications are highly complex mechatronical systems, therefore the quality of the final printout depends on many different components and parameters. The interfaces between these subsystems are often the key point for the success of the whole system. Therefore it is often essential to use multiphysics simulations with well-defined interfaces between the different physics and working fields to achieve appropriate results.

Therefore, at the Institute of Print Technology at Bern University of Applied Sciences simulations are used in every domain of inkjet systems, from the single inkjet valves to the print machine dynamics and the simulation of the final printout on substrates. All these simulations are coupled with different interfaces. The aim of this paper is to give an overview of the simulation aided design concept for inkjet systems.

2. Methods for the simulation aided design process

This chapter gives an overview about the whole simulation aided design process. In Figure 1 this process is displayed schematically. For an ideal print result, precise inkjet dots are needed. To understand and influence the generation of dots, the whole inkjet valve is simulated including the valve control, the valve actuation with the mechanics, and the fluidics with fluid flow and droplet break up.

When the results of a single dot are registered, the next step is to study how the mechanics of the printing machine will bring them to the right place. This depends on the drive system and the structure of the printing machine (vibrations). The structure of the machine can be simulated by a modal analysis in FEM. From this modal analysis, a state space model is generated, which can be used in common software for drive- and

control-system simulation (e.g. Matlab), allowing for the optimization of the print head motion. The next step is to evaluate what effect these parameters will have on the final printing result. The generated single dot, print head motion and vibrations can be used as inputs for a printout simulation which is permitting a visual impression of the final printing result.

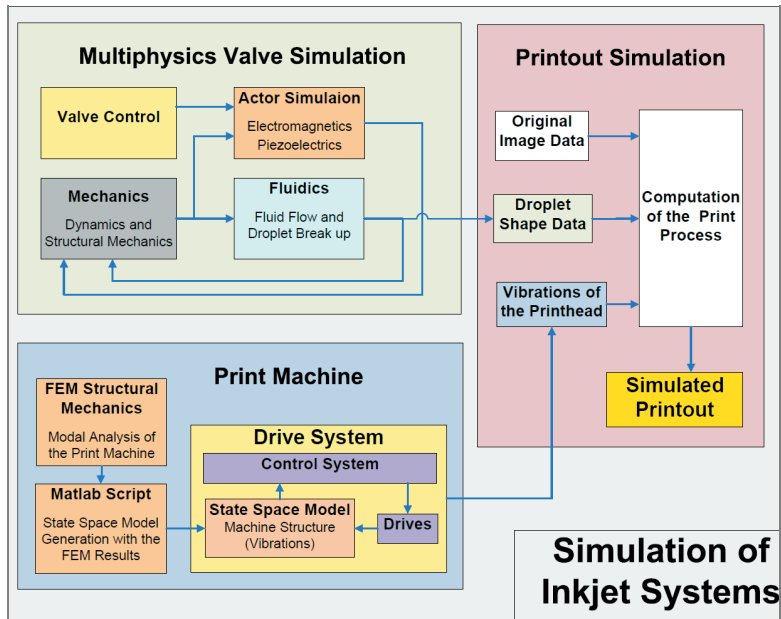


Figure 1: Simulation aided design process for inkjet systems

3. Multiphysics inkjet valve simulation

Comsol Multiphysics is the tool used for multiphysics valve simulation at the Institute of Print Technology. With Comsol, many different physical effects such as electromagnetic fields, fluidics, piezoelectric actuators, structural mechanics etc. can be linked together and computed. The mechanics and valve control can be integrated with Ordinary Differential Equations (ODE's).

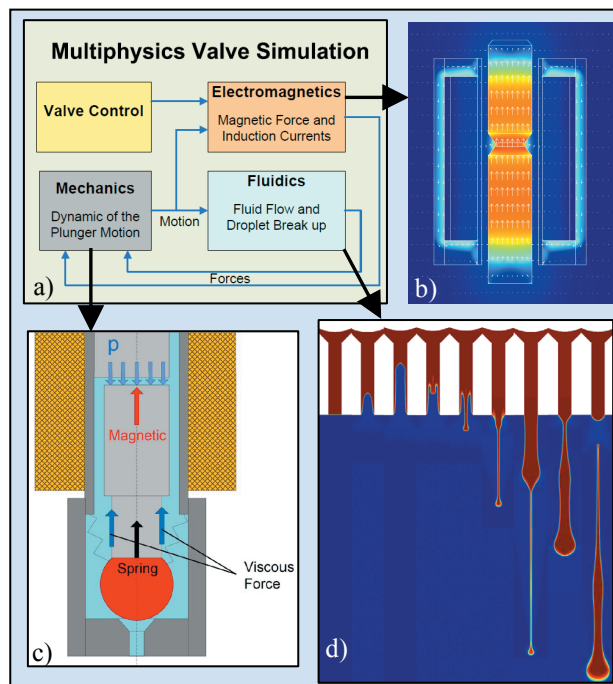


Figure 2: Multiphysics valve simulation

In Figure 2 the print head simulation is illustrated by an example of electromagnetic micro-valves, which are used for large-scale inkjet printing and for Braille printing.

To ensure accurate representation of the entire micro-valve-system starting with the valve-control-circuit on to the droplet's flight, the system is divided into four subsystems. The valve-control-circuit defines the length of the valve opening time with peak and hold current. This current is the input for the electromagnetic subsystem. Based on a transient FEM analysis, the induction currents due to self-induction and induction from the variation of the magnetic potential (due to magnetic circuit variation caused by the plunger-motion) are considered. To respect the nonlinear saturation effects of the magnetic material, a B-H curve of the used material is implemented. In Figure 2 b) the magnetic flux density in the electromagnetic circuit can be studied. The maximal flux density is in the air gap where the electromagnetic force is generated.

In the mechanical subsystem, the dynamics of the plunger-motion are described by ODE's. The ODE's take into account the forces on the plunger from the electromagnetic and the fluidic subsystem as well as the behaviour of the mechanical parts such as springs, stop-positions etc. The four subsystems are thus coupled together for every time-increment.

The plunger-movement defines the opening and closing of the valve and is the link for the fluidic subsystem. The fluidics is modelled with a two-phase-flow CFD formulation, which pays attention to the surface tension forces and the wetted walls for the generation of droplets, including satellite droplets. Because of the moving plunger the opening cross-section of the valve varies during the opening sequence. This is modelled with ALE, which is a moving mesh algorithm. The mesh displacement is ruled by the piston-motion of the ODE of the mechanical subsystem. In addition to the varying cross-section, the velocity of the plunger also affects the fluid. This is implemented by using moving-wall conditions. The velocity of the plunger-wall is again ruled by the mechanical subsystem. This effect is quite important for describing the fluid flow in the nozzle appropriately. In the sequence of the droplet's generation (as depicted in Figure 2 d), the opening plunger draws back the fluid, which will cause the pressure to decrease dramatically and thereby provoke the fluid to evaporate in some sections. One way to approximately describe this behaviour is to treat the fluid as weakly compressible and to describe the density of the fluid as a function of the local pressure. That's how the regions where cavitation will occur can be estimated (Figure 3) and the effect on the droplet break up can approximately be described, without dealing with the exact thermodynamics of the cavitation bubbles, which are of no interest in this study. When the plunger stops upon reaching its final position, the fluid can finally flow out (Figure 2 d).

This behaviour can only be studied properly by coupling together the different physics. To validate the simulation, the simulated droplet break up can be compared with a high speed camera recording with the same physical parameters (displayed in Figure 4).

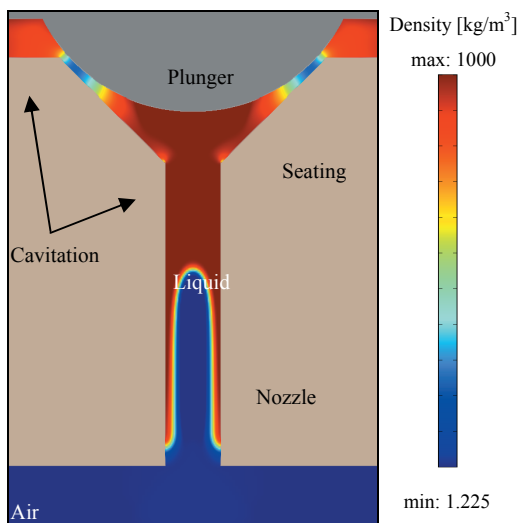


Figure 3: Cavitation in the nozzle

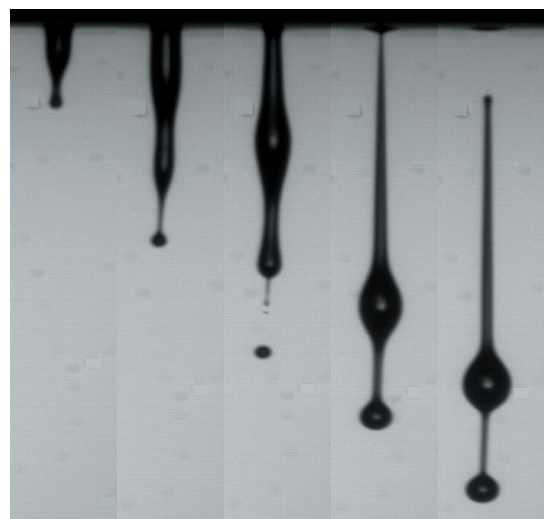


Figure 4: High-speed camera recording

The behaviour of the recorded droplet break up is reproducible. The first eye-catching aspect is that the droplet is not as symmetric as in the simulation, where the computation is done axial symmetrically. In the first sequence, the droplet is already rather pointed, because of the fact, that the fluid is first drawn back into

the nozzle. Therefore, a small satellite droplet breaks up from the main droplet. This behaviour corresponds very well with the simulation. After that, the main droplet narrows down and a second small droplet is separated (which cannot be caught exactly with the simulation). Finally, the trail of the main droplet definitely breaks up from the nozzle, which corresponds again very well with the simulation.

4. Printing machine simulation

Practical experience shows, that the products of a printing machine can be poor, even if the best print heads and print electronics are used. A possible reason might be the machine's vibrations caused by the drive system and the excitation of the printing machine's mechanical structure. This is particularly the case with large format printing machines because of their heavy print heads and drives, where the stiffness of the mechanical structure is in competition with the machine's weight and costs.

Structural modal analysis in FEM is considered state of the art, but this analysis is usually used for the mechanical design of printing machines only. The control engineer cannot use it, because the controlling simulation-programs are not compatible with FEM tools. However, vibrations can only be eliminated in a cost-effective way, if printing machine with its mechanical structure, drive system and control algorithms can be optimized as a whole.

For this reason a new method was developed at the Institute of Print Technology, which allows for the mechanical structure analysis to be utilized by common control simulation programs. Figure 5 shows the workflow of this method.

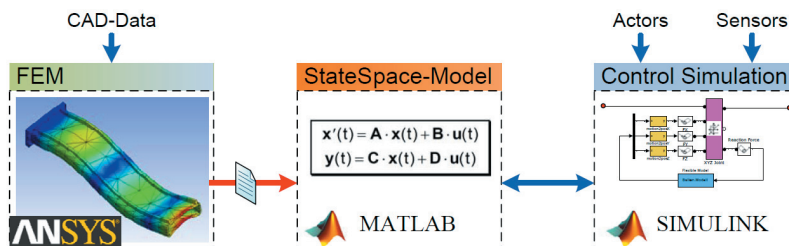


Figure 5: Coupled printing machine simulation

The tools used for this simulation are Ansys as FEM tool for the modal analysis and Matlab / Simulink for the control simulation. With a Matlab script, a state space model can be generated out of the eigenvectors and eigenvalues from the FEM modal analysis. This state space model can be used in Simulink, where it can be linked to the model of the drive system and the control algorithms.

To demonstrate the method, a simplified printing machine as shown in Figure 6 is modelled.

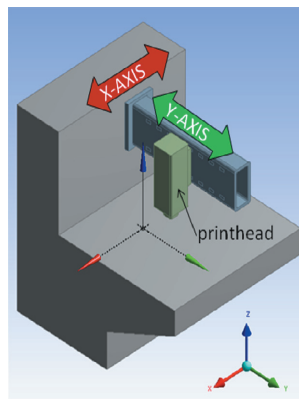


Figure 6: Sample printing machine

The starting point of the workflow is the analysis of the eigenfrequencies in Ansys. The first two modes are rigid body modes from the free motion along the two axes. The three most important modes are shown in Figure 7:

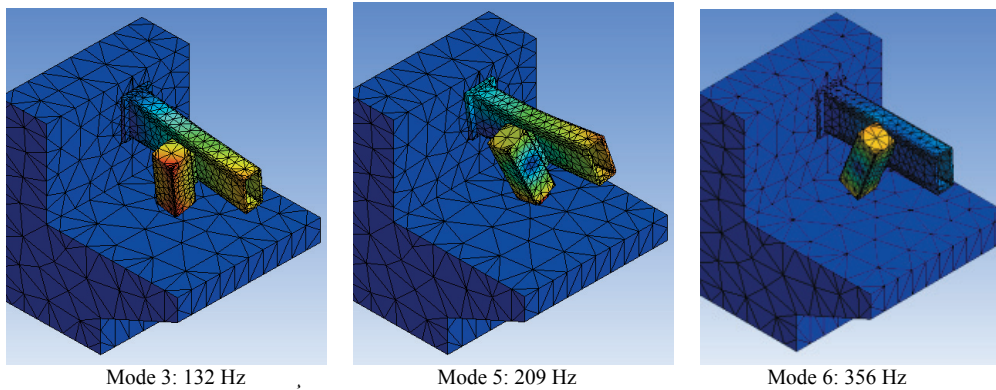


Figure 7: Result of the eigenfrequency's analysis

The dynamic time-response of the structure can be computed by superposition of the single modes. The characteristic behaviour of the structure can be captured sufficiently by including only the first few modes. Higher modes need a lot more energy to be excited and are usually more strongly damped than lower modes. Except for having shock-loadings, these modes can be cancelled without relevant changes in the model's behaviour. Therefore the simulation is by far not as costly (in terms of simulation-time) as direct time integration methods.

With a script in Ansys, the eigenvectors and eigenvalues can be written in a file, which can be imported into Matlab. The model order is reduced by cancelling the higher modes, which are not relevant. For the remaining modes, the damping has to be defined for each mode. Currently, there are no methods available to predict the damping of complex systems analytically. Therefore the damping parameters have to be drawn from experience if there are no experimental data available.

This reduced system can now be converted into a state space model. Therewith, a full model of the machine's structure is available for the common control tools in Matlab / Simulink. In Figure 8 the corresponding modes of the FEM frequency-analysis are marked in the bode diagram of the state space model.

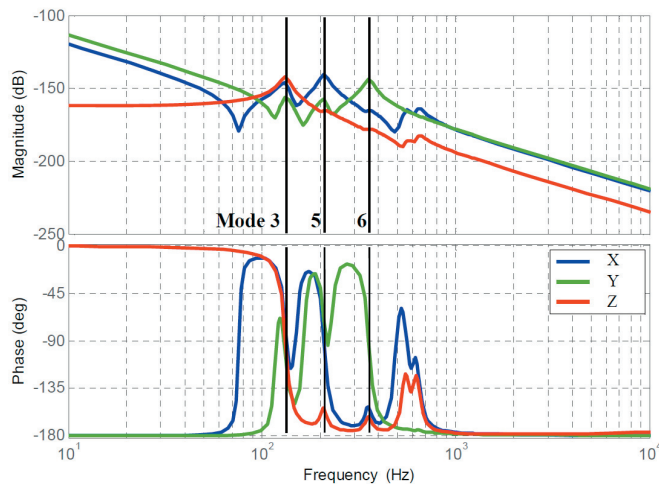


Figure 8: Compliance of the print head [m/N]

A disadvantage of a state space model is, that it is only able to represent the machine at one specific position. A different concentration of the mass due to the axis travelling, which leads to another behaviour of the system, cannot be considered. Multi Body Simulations (MBS) do not have this restriction, but in common programs the structural parts are only implemented as rigid bodies with springs and dampers, which is only a very poor approximation of the machine's structure. To close this gap, the two approaches can be combined. The moving axes are represented as rigid bodies with the MBS program, e.g. SimMechanics for the Matlab environment. With additional degrees of freedom between the rigid bodies the deflection of the bodies, which is described by the state space model generated from the FEM simulation, can be computed. Therewith, the full behaviour of the model can be captured.

Figure 9 illustrates the behaviour of the sample printing machine during a motion in Y- direction. In Figure 9 a), the motion of the print head is displayed. In Figure 9 b), the displacement in X, Y and ϕ - direction (according to Figure 11) from the ideal position of the print head due to the deflection and vibrations of the bodies are illustrated.

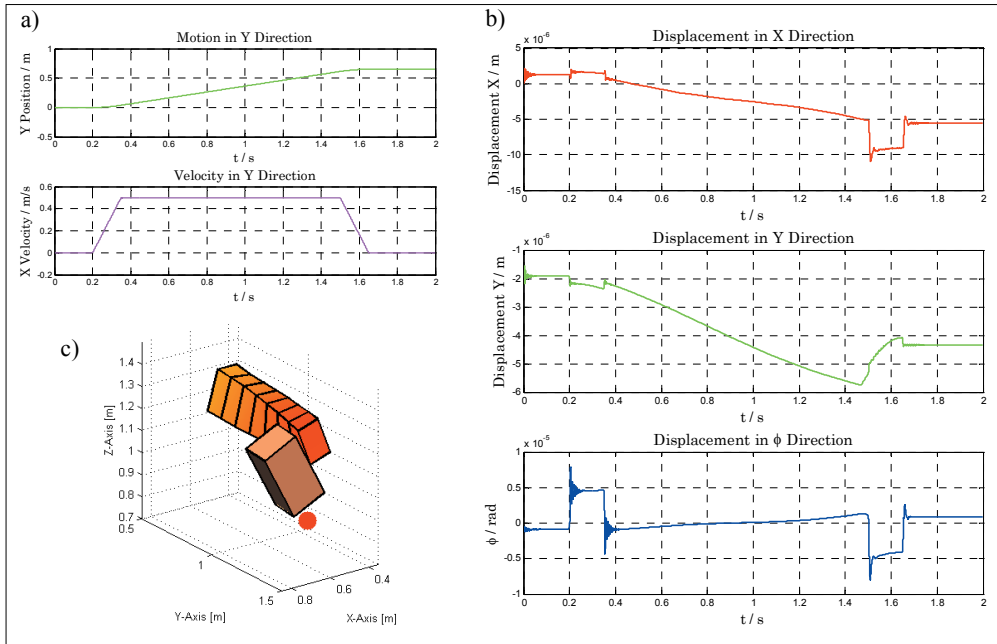


Figure 9: Deflection and vibrations of the print head during a simple motion

The static deflection increases while moving towards the outer end of the beam (also visible in the visualisation in Figure 9 c)). The vibrations are caused by the acceleration forces only in this example. But other excitations like ripple forces of linear motors can be modelled as well. In this way, unfavourable eigenfrequencies in the mechanical structure can be detected and eliminated at an early stage. Additionally, the stiffness of the system can be increased by compensating the eigenmodes with well-defined control-algorithms and drive systems.

With this method, the behaviour of the machine can be predicted and the mode of operation can be optimized, even before the first prototype has been built. Moreover, the time required for the development of the printing machine can be dramatically decreased as the control system and the mechanical design can be carried out simultaneously.

5. Simulation of the printout

Even if the simulations of ink droplets and machine vibrations are very helpful, it is often quite difficult to imagine, what impact a certain oscillation mode or parameter, such as the printing velocity, will have on the graphical result of the printed media. To get a visual impression, the print results can be simulated as well.

As input, any image in a supported format can be used. For this example a black test-picture is used, which will be printed with CMYK. Figure 10 shows the original test picture.

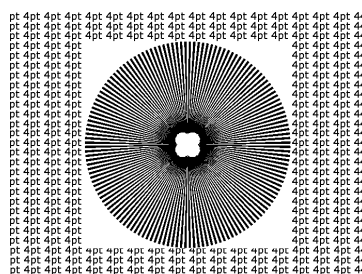


Figure 10: Original test picture

The print head's behaviour can be considered by defining the shape and size of the dots, as well as the geometrical configuration of the nozzles. Therewith, the theoretically achievable printout with an ideal print head and without any vibrations, but with respect to the resolution of the print head, can be computed. This result is shown on the left of Figure 12.

The next step is to compute the impact of the machine vibrations on the test picture. Therefore, data of the printing machine simulation or from measurements can be used. Each dot of the picture is distorted with matrix computation according to the displacements due to vibration in X, Y, and ϕ direction of the print head at the time and the position where it is actually printed (shown schematically in Figure 11).

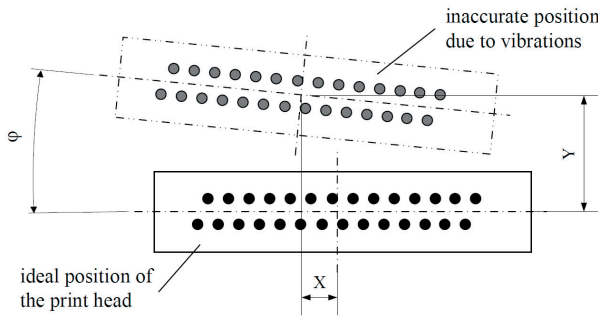


Figure 11:
Distortion of the ideal picture due to vibrations

In Figure 12 on the right, the distortion of the test picture due to vibrations (estimated by measurements) of a printing machine, is shown. The test picture is printed in CMYK. On the images d) and e) in Figure 12, moiré patterns are clearly visible. In Figure 12 f) the deviation of the single droplets can be seen in comparison to the ideal test picture in Figure 12 c). By this visualisation, the impact of the vibrations on the quality of a printed picture can be estimated much better than by pure machine-vibration displacement-diagrams only.

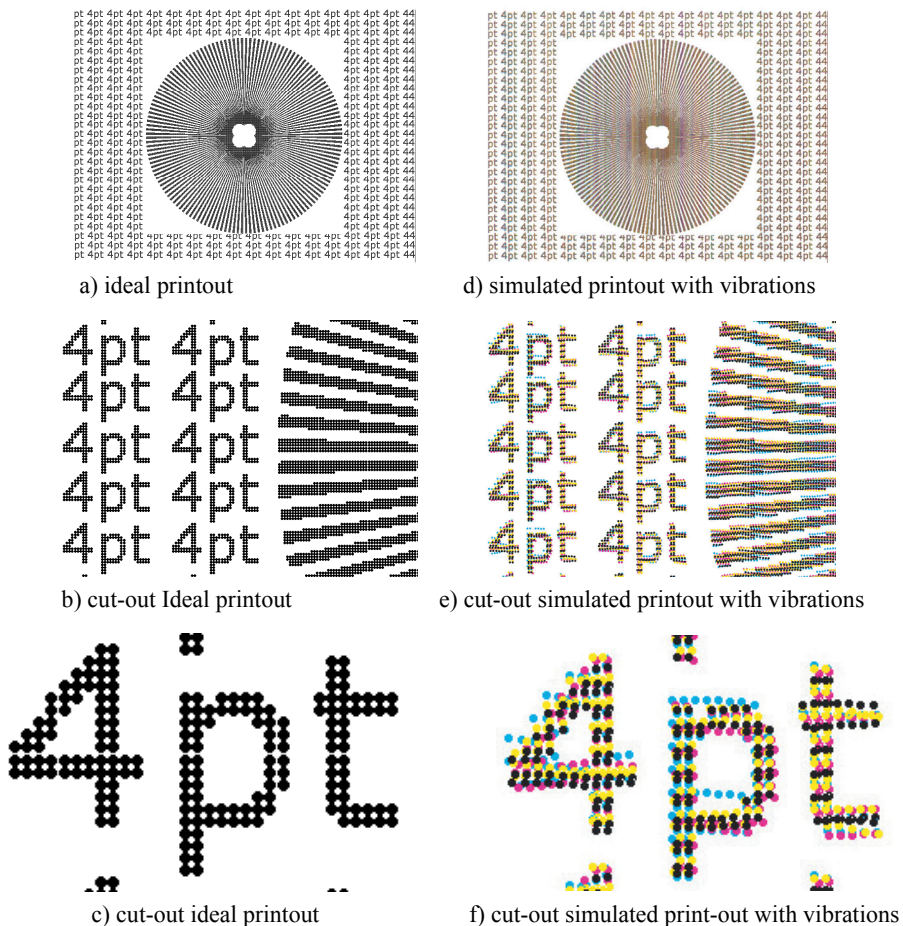


Figure 12: Effects of the vibrations on the printout

If a simulated printout for a specific application is found to be not accurate enough, the simulation will help a lot to find appropriate measures. Thereby a helpful approach is to isolate the impact of a single vibration mode on the printout.

Therefore, only a certain mode, which is expected to cause major problems, is considered to describe the deflection of the structure in the corresponding state space model. In figure 13, the impact of a certain mode on another test picture is visualized.

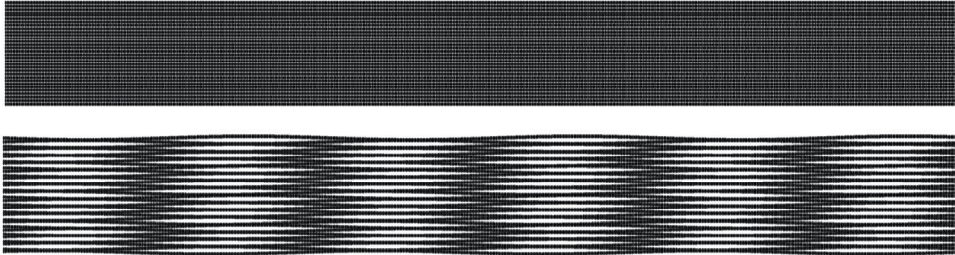


Figure 13: Effects of a single vibration mode on the printout

On the whole, this allows for the distinction between oscillation modes which are harmless and those which need to be eliminated by adjustments of the mechanical structure or by control-algorithms.

6. Experimental validation

Certainly, all the important steps of simulation have to be verified and if possible validated by experiment. This is done using a variety of different measurements. In chapter 3 on the inkjet valve simulation, the validation of the droplet break up is based on high-speed camera recordings. The electromechanical subsystem was validated by comparing the simulation results with measurements of the rise of the current in the coil and the opening time of the valve. The printout simulation was validated by comparison with printed samples.

The structural analysis was verified by comparing different simulation approaches (FEM, Multi Body Simulation and the hybrid flexible multi body simulation) and finally with experimental system-identification on the printing machine and with measurements with acceleration sensors. To present the process of verification and validation in detail would exceed the aim of this paper.

7. Discussion

Simulations are useful for all major components and during the whole designing process. The behaviour of print heads can be modelled and optimized by fully coupled multiphysics simulations. With a model of the machine's mechanical structure which is implemented in a simulation including drive systems and control-algorithms, critical eigenfrequencies can be detected and the vibrations can be minimized by adapting the mechanical structure or the control-algorithms. The printout simulation helps to interpret the impact of the existing vibrations on the final printout's quality.

Furthermore, the benefit of such coupled simulations exists also on another level. Simulation models with interfaces between the different disciplines are a very good basis for an extended discussion between the different engineering fields. Quite often, the agents of the different disciplines are working in isolated atmosphere and thereby knowledge which would be very useful to solve a problem in a neighbouring engineering field gets lost. Complex mechatronic systems have to be regarded as a whole and not only as configurations of different isolated components. A common multidisciplinary model is a good support to achieve a more global view of the systems.

Besides creating complex overall simulations, this approach is also very useful for solving daily problems of inkjet systems. In many cases only a part of the entire simulation-cycle is needed. Some sections of the simulation can be replaced by measurements of existing and proved components, other sections might not be of any interest at all. An existing global concept of simulation is a helpful toolbox, where from the appropriate tools can be selected and coupled according to the needs of the actual problem.

8. Conclusion

This paper presents an approach to simulation aided design of inkjet systems by creating an entirely virtual printing machine. A deeper understanding of the whole printing process can be achieved due to the ability to simulate the entire inkjet system. It is possible to solve a specific problem by simulating an individual setting, if necessary simulations can be coupled. A global approach to simulation with well-defined interfaces and couplings between the different engineering fields increases the interdisciplinary thinking and exchanging of knowledge. In this way, simulations are an efficient and powerful tool to develop and optimize the complex inkjet systems for tomorrow's needs.

Acknowledgements

The section about the simulation of a printing machine is based on the master thesis of Florian Fässler, which he has finished in 2010 at the Institute of Print Technology. The section about the printout simulation is based on the work of Johannes Renner, scientific officer at the Institute of Print Technology. Many thanks for their cooperation.

I owe special thanks to Prof. Fritz Bircher and Dr. Gert Schlegel for the support on editing this paper.

References

- E. Kallenbach, *Elektromagnete*, Vieweg Teubner, Wiesbaden (2007)
- G. Schmitz, M. Pischinger, *Mechatronische Simulation eines EMV-Aktuators*, Fachhochschule Aachen/ FEV Motorentchnik, Aachen, Germany
- M. Hatch, *Vibration Simulation using Matlab and Ansys*, 1584882050th ed. Boca Raton, USA: Chapman&Hall, 2001.
- M. Weck, *Werkzeugmaschinen - Konstruktion und Berechnung*. Heidelberg: Springer, 2006
- O. Thomas, "Strukturmechanische Berechnung und Regelungssimulation von Werkzeugmaschinen mit elektromechanischen Vorschubantrieben," TU München Dissertation ISBN 978-3-8316-0798-3, 2008
- W. Neithardt, "Methodik zur Simulation und Optimierung von Werkzeugmaschinen in der Konzept- und Entwurfsphase auf Basis der Mehrkörpersimulation," Institut für Produktionstechnik Dissertation ISSN 0724-4967 , 2004
- William B. J. Zimmerman, *Multiphysics Modelling with Finite Elements Methods*, World Scientific, Singapore (2008)



Reproducibility of DoD inkjet printing systems

Johannes Renner, Fritz Bircher and Gert Schlegel

Institute of Print Technology / Bern University of Applied Sciences
Pestalozzistrasse 20, CH-3400 Burgdorf, Switzerland

E-mail: johannes.renner@bfh.ch

Abstract

For inkjet printing, the maximal possible accuracy of deposition can be reached with the highest reproducibility of printing and a correction compensating for systematic jetting faults.

In the following article the reproducibility of jetting of a set of industrial print heads in high throw distance and high print speed operation is investigated. Based on the results, methods for the correction of reproducible jetting errors are introduced.

Keywords: inkjet, reproducibility, accuracy enhancement of inkjet printing, throw distance

1. Introduction

If an inkjet process has to meet specific requirements in terms of accuracy and throw distance, the standard way to accomplish these is to make use of components that deliver the required absolute system accuracy without taking the correction of systematic faults, coming from the print head, into account. In the following, the possibility of increasing the throw distance or accuracy of a printing machine by the correction of systematic jetting faults is elucidated.

2. Methods

The local reproducibility of printed dots and average dot position errors of a print system are measured by overprinting a monotonic test pattern multiple times onto coated inkjet paper. As estimation for the local reproducibility errors, the dot gains of the overprinted dots, which are hereafter referred as targets, are utilized. Figure 1 depicts the evaluation of the reproducibility errors in print and cross print direction. The ideal target shape is empirically estimated.

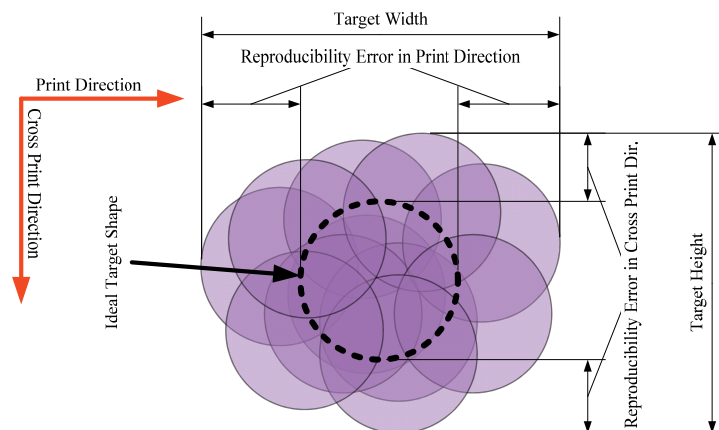


Figure 1: Extract of the test pattern (left) and interpretation of the targets (right)

As there is a deterministic deviation from the position where a drop hits the substrate in average when printing multiple identical samples or overprinting the same pattern multiple times, the total error band of each printed dot may have an average position error. Figure 2 illustrates the evaluation of average position errors. The prediction interval for the position of a single dot may be interpreted as the average position error of the print process at the specific location +/- the reproducibility error.

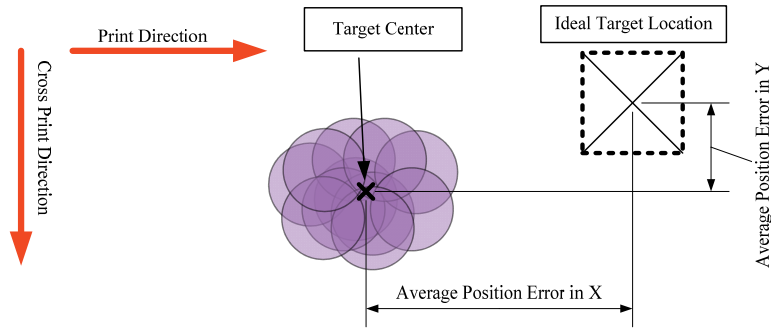


Figure 2: Illustration of the average position error of a single target

Automatic evaluation of the test samples is accomplished with the aid of a precision scanner and the image processing toolbox in Matlab. Thereby hundreds of samples containing each more than 30'000 targets can efficiently be evaluated. On lower throw distances, satellite droplets that are much slower than the main droplets, may hit next to or even over the edges of targets. Therefore a simple correction involving the target area and partially the target shape is used to compensate systematic measurement errors. The algorithm for the evaluation is verified with manual spot measurements. Further measurement errors due to inhomogeneous drop volumes of the printing system are considered small in relation to the magnitude of the total reproducibility faults. Due to the insignificant deviation of the average value and standard deviation in relation to the spot samples, for measurements of the reproducibility errors a total measurement inaccuracy of +/- 5 µm is estimated. Figure 3 depicts extracts of the source and measurement data for the evaluation of errors of monotonic test samples.

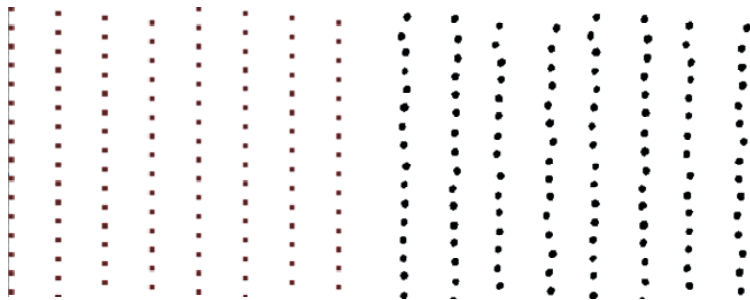


Figure 3: Extract of the test pattern and binary pre-processed measurement data

Manual spot measurements on simple non-monotonic disturbances in the test patterns are taken to estimate the influence of the printed data on the reproducibility and estimate the additional errors to the position offsets and the reproducibility due to crosstalk effects of the print heads. Figure 4 shows a non-monotonic disturbance in a test pattern which is assumed to influence the errors of the neighboured targets in the same line and following it.

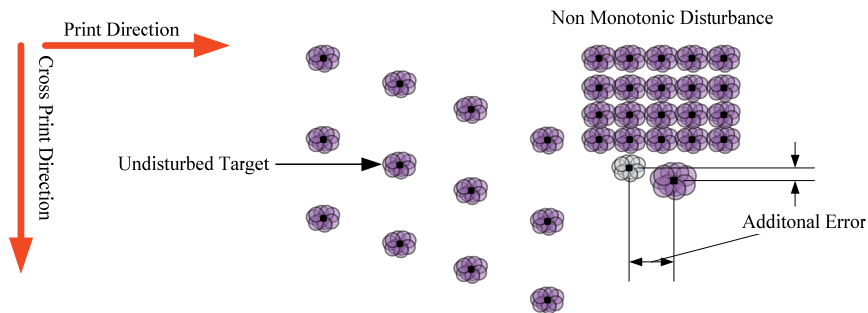


Figure 4: Simple non-monotonic test pattern for the estimation of crosstalk errors

Each overprint is performed in single pass printing operation. Table 1 contains list of the main parameters applied to all the experiments that are the source of the evaluated data depicted under Results.

Table 1: Extract of the main parameters for the printing tests

Parameter	Value	Description
Print heads	KM512 MH	14pl print heads
Print Speed	466 +/- 1 mm/s	
Ink	SunJet UFK Crystal ink	UV curable ink
Ink temperature	35 +/- 1 °C	-
Substrate	Coated Inkjet Paper	-

3. Results

The average position errors of the print system with monotonic test patterns in print and cross print direction seem to be approximately uniformly distributed around zero. In print direction, the empiric range and standard deviation of the average position errors at a throw distance of 5.0 mm is more than three times greater than at 1.5 mm throw distance. Taking the values of the empiric standard deviation of Figure 5 to estimate the 3-sigma boundaries, more than 99.7 % of the average position errors in print direction at 1.5 mm throw distance should be within +/-21 μm or at 5.0 mm throw distance within +/- 72 μm.

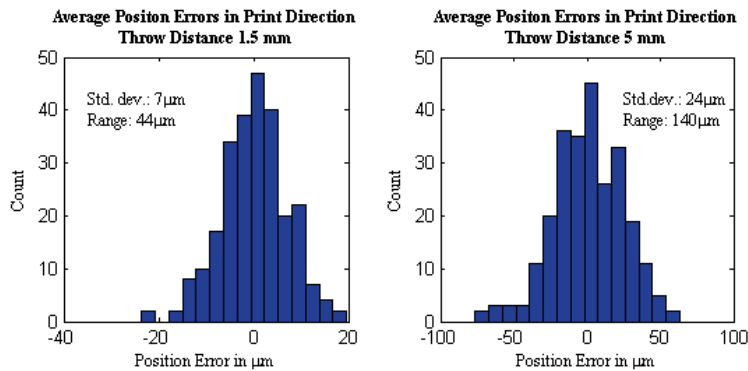


Figure 5: Average target position errors of a monotonic test pattern in Print Direction at 1.5 mm and 5.0 mm throw distance

At 1.5 mm throw distance, the empiric range and standard error of the average position errors are slightly bigger in cross print direction than in print direction. In contrast to the average position errors in print direction, in cross print direction the empiric standard deviation and range have at 5.0 mm throw distance less than twice the magnitude of the values at 1.5 mm throw distance. As estimation for the 3-sigma range out of the values depicted in Figure 6, more than 99.7 % of the average position errors in cross print direction are expected to be less than +/- 33 μm at 1.5 mm throw distance and less than +/- 48 μm at 5.0 mm throw distance.

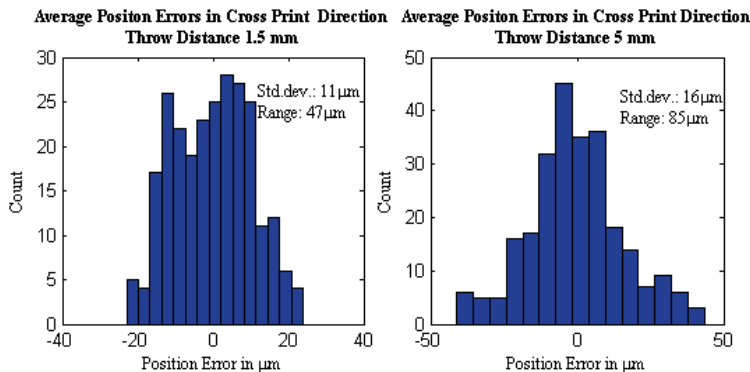


Figure 6: Average target position errors of a monotonic test pattern in cross print direction at 1.5 mm and 5.0 mm Throw Distance

The reproducibility errors in print direction seem to be uniformly distributed as well. The estimated average reproducibility at 1.5 mm throw distance is 18 μm and at 5.0 mm throw distance 27 μm. Therefore the mean reproducibility error at 1.5 mm throw distance is approximately 33 % lower than at 5.0 mm throw distance.

As the values for the empiric standard deviations at 1.5 mm and 5.0 mm throw distance depicted in Figure 7 are approximately identical, the additional error at 5.0 mm throw distance can be expected to be of additive nature.

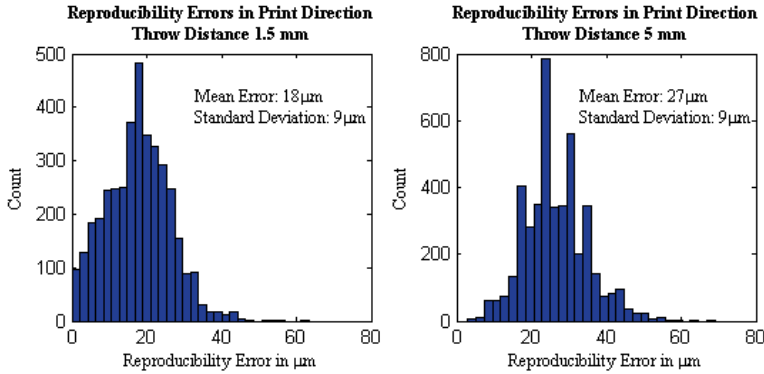


Figure 7: Reproducibility errors in print direction at 1.5 mm and 5.0 mm throw distance

In cross print direction at 1.5 mm throw distance the distribution of the reproducibility errors does not seem to be well uniformly distributed. Comparing the values from the empiric statistics in Figure 8 the relation between the mean error at 5.0 mm and 1.5 mm throw distance is identical to the relation in print direction and expected to be 33 % greater at 5.0 mm throw distance. Considering that the distributions at both throw distances are not well approximated with a normal distribution, the expected values for the reproducibility errors have to be lower than the mean reproducibility errors.

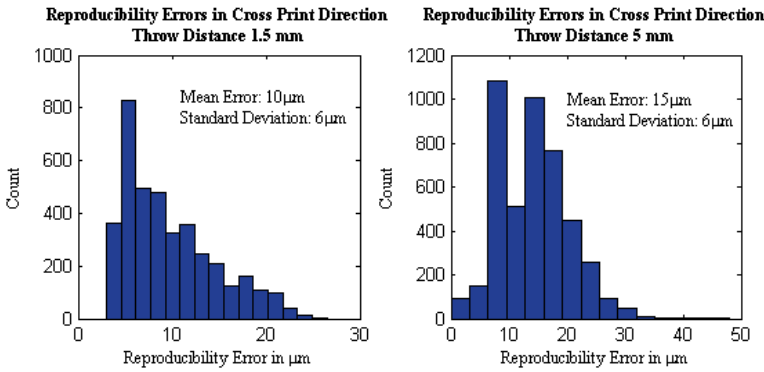


Figure 8: Reproducibility errors in cross print direction at 1.5 mm and 5.0 mm throw distance

Considering influences of the printed data on the reproducibility errors, Figure 9 depicts histograms of additional errors due to non-monotonic disturbances in the printed patterns. As the distributions of the additional errors at 1.5 mm and 5.0 mm throw distance are approximately symmetric around zero, the influence of the printed data is expected to have only a minor or negligible effect on the reproducibility errors.

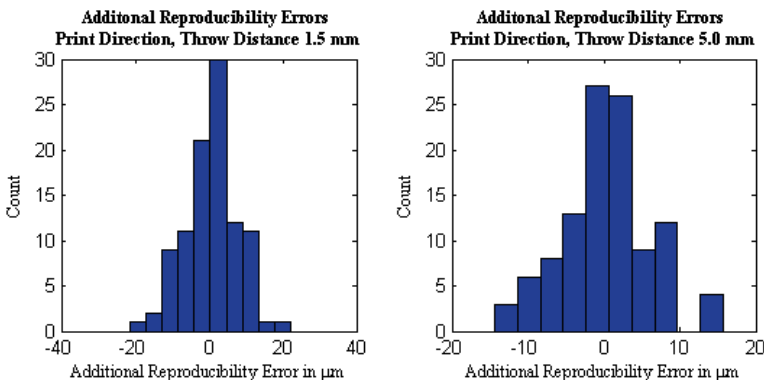


Figure 9: Additional reproducibility errors in print direction due to crosstalk effects of the print head

Similar to the additional reproducibility errors in print direction, in cross print direction the additional reproducibility errors due to a non-monotonic disturbance seems to be negligible as well. The additional errors have about the same magnitude like the dispersions of the reproducibility errors of the targets from one nozzle in a monotonic test pattern.

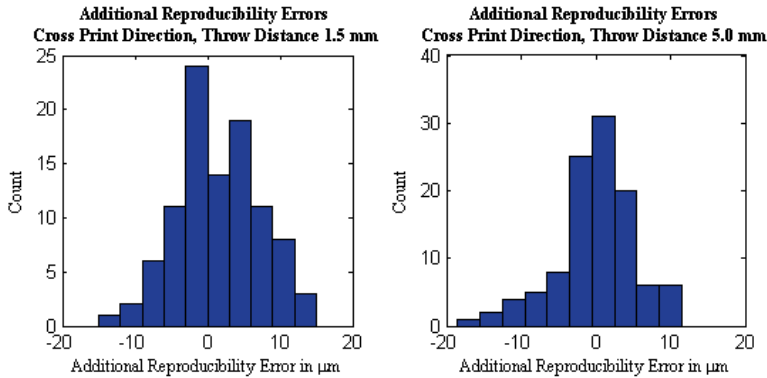


Figure 10: Additional reproducibility errors in cross print direction due to crosstalk effects of the print head

The additional position errors due to the non-monotonic disturbance are negligible at 1.5 mm throw distance and are causing systematic offsets between +50 μm and up to +150 μm at 5.0 mm throw distance. In order to have more detailed results on the influence of crosstalk errors further investigation with a variety of more complex, crosstalk prone printing data is necessary.

The test print at 5.0 mm throw distance with overprinted characters in Figure 11 supports the expectation, that crosstalk has only little influence on the reproducibility errors but causes notable systematic offsets. The overprinted dots of the nozzles have approximately the same size.

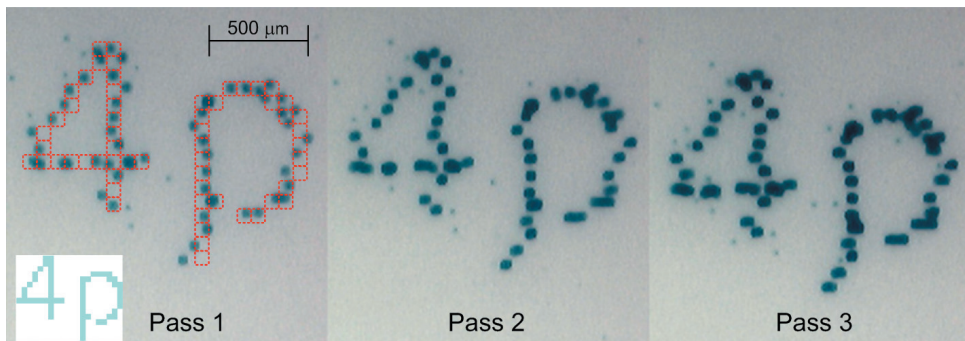


Figure 11: Characters overprinted reproducibly with two passes, printed with 5.0 mm throw distance, source data illustrated in the first pass, printing direction from left to right.

4. Discussion

Even at 1.5 mm throw distance the reproducibility errors are in average about +/- 10 μm in cross print direction. The absolute mechanical accuracy of the printing mechanism during the print is according to the manufacturer +/- 1.25 μm, whereas the reproducibility is assumed to be better by far. For the print direction, the main parts of the reproducibility errors that are related to the print mechanism are the speed variance of the linear drive and reproducibility error of the optical position encoder. At a throw distance of 5.0 mm, an encoder reproducibility of +/- 1 μm and an estimated average drop speed of 3 m/s the sum of these errors is approximately +/- 5 μm. The total average reproducibility error in print direction is about +/- 20 μm. It is therefore obvious, that the notable parts of the reproducibility errors are related to the print heads and imperfect reproducible airflow conditions.

As the variance of the jetting properties of a print head is strongly related to the ink or jetted liquid, it may be worthwhile to find the optimally stable solution. Certain improvements in the base accuracy of the print head with a given ink can be made with fine tuning of the waveforms. According to (McDonald, 2003), with jet

trimming, the variation of the drop speeds between the nozzles of a high accuracy print head could be minimized from +/- 10 % to +/- 2 %. Thereby a more uniform drop speed of all nozzles is achieved, improving the average position errors. Similar to this approach, the waveforms of a print head can also be optimized to deliver a minimum variance of the jetting properties of the nozzles. Likely, this increases the speed variations between nozzles, but also reduces the reproducibility errors.

The part of the reproducibility errors related to the imperfect airflow conditions can be reduced by optimizing the aerodynamic design of the print machine to provide maximum reproducibility of the air currents between the substrates and the print heads during the print.

Considering that the targets have, apart from remaining random reproducibility errors, deterministic average position errors, it is obvious that with an adequate compensation process the overall target errors can be reduced down to the magnitude of the random errors. According to (Scott Bruner and David Xu, 2007) there may be over 250 individual error sources contributing to the overall dot misplacement. These can be seen as static and dynamic mechanical errors and statistical process error sources. By eliminating mechanical error sources (Scott Bruner and David Xu, 2007) could minimize the overall drop misplacement from +/- 10 μm to +/- 2 μm .

As systematic errors in the cross print direction cannot be corrected with a single printhead in a single printing pass, at least a pair of matching print heads or a multipass printing process is required to compensate them. This is also the case in print direction for printheads that have only limited support for sub pixel adjustment of individual jets. Therefore the compensation of systematic errors reduces the possible printing system performance.

Linear systematic errors, like a constant misplacement of a jet in relation to the other jets or misplacement, dependant on the print speed due to static variations in drop speeds, can be compensated accurately with simple measurements on test patterns printed at the desired system configuration and by creating an adequate jet mapping out of the deviations.

Non-linear systematic errors, like cross talk errors, could be compensated to some level with an empirical numeric model for the print head that has to be applied to the printing data. Therefore, again a detailed investigation in the crosstalk behavior of the desired print heads is necessary.

Reproducible but stochastic dot misplacements, like deviations of dots due to turbulent airflow when printing onto non-flat objects, cannot be described systematically. A possibility to compensate them is with an iterative process. Thereby a test pattern is printed and adjusted in multiple steps. The correction for the test pattern has afterwards to be applied on the printing data.

To maintain the additional accuracy achieved by the compensation of systematic faults, it is necessary that time variant errors like aging effects are compensated by measurement and correction in sufficient intervals. As modern print heads have, thousands of nozzles, for the integration of the above mentioned corrections into an industrial process a fast automated measurement and correction process is required.

5. Conclusions

The average reproducibility errors of the test system at 1.5 mm and 5.0 mm throw distance are about twice as big in print direction compared to the cross print direction. The mean reproducibility errors at 1.5 mm throw distance are approximately 33 % lower than at 5.0 mm throw distance. The standard deviations of the reproducibility errors at 1.5 mm and 5.0 mm throw distance are approximately identical.

Spot measurements of samples with simple non-monotonic parts support the assumption that crosstalk errors of the print heads have no remarkable influence on the reproducibility errors but systematically increase the average position errors of dots in print direction at 5.0 mm throw distance up to 150 μm and only insignificantly at 1.5 mm throw distance. In order to conclude these assumptions, further investigation with more complex test patterns is necessary.

The average position errors at 1.5 mm and 5.0 mm throw distance are approximately uniformly distributed around zero. At 5.0 mm throw distance the range of the average position errors is about three times bigger in print direction and twice as big in cross print direction compared to 1.5 mm throw distance.

For monotonic test patterns with the given system configuration at 1.5 mm throw distance, the total 3-sigma range for the deviation of a single target is +/- 48 μm in print direction and +/- 51 μm in cross print direction. At 5.0 mm throw distance, the total 3 - sigma range is +/- 99 μm in print direction and +/- 54 μm in cross print direction.

The maximal possible accuracy of an inkjet printing system may be reached with highest the printing reproducibility and a correction compensating systematic jetting faults. In case of static printing errors on a flat substrate, such a correction may be accomplished with a simple adjustment process. The adjustment requires a measurement of the jetting properties of each nozzle and printing in multiple passes. Far more efforts for compensation of systematic faults are needed if the printing errors are of non-linear but mathematically describable or of only iteratively correctable nature, as it is the case with high speed printing onto non-flat objects. For the integration of such corrections in industrial processes, fast and automated calibration is required.

If a print system of sufficient base accuracy for the specific application exists, the solution may be favorable from the practical point of view, due to the high complexity of the correction process for non-linear but reproducible printing faults.

When reaching physical boundaries of an inkjet process, as it is required in terms of reproducibility for graphics printing of non-flat objects with maximal throw distances and throughputs, there may not be another option but to cope with the strong barrier to implement an automated correction of high complexity. Then the remaining question may be, whether hybrid inkjet printing in combination with a different printing process, could be .

Acknowledgements

Sincere thanks are given to Prof. Fritz Bircher and Dr. Gert Schlegel for the mentoring of this publication.

References

- McDonald, M. (2003). High Precision Jetting and Dispensing Applications Using A Piezoelectric Micropump. *IS&T NIP 19 Conference* (pp. 3-4). New Orleans: Spectra, Inc.
- Scott Bruner and David Xu. (2007). Drop Landing Accuracy Improvements in Inkjet Printed OLED Displays. *Society For Information Display Coference* (pp. 1-2). Long Beach, California: Cambridge Display Technology.



The influence of printing pressure on flexographic print quality

Ákos Borbély and Rozália Szentgyörgyvölgyi

Óbuda University

Doberdó út 6, H-1034 Budapest, Hungary

E-mails: akos.borbely@rkk.uni-obuda.hu; szentgyorgyvolygi.rozsa@rkk.uni-obuda.hu

Abstract

Flexographic printing technology underwent rapid development recently. For a long time the main objective of technological innovation was improvement of print quality. As a result of the development of the past decades achievable quality enabled flexographic printing to become a competitive of offset printing in certain areas of application. A number of recent innovations in flexographic technology are related to setting printing pressure.

Flexographic technology is based on the principles of relief (or letterpress) printing. Inking characteristics are influenced by a number of factors including ink thickness on the printing form, press speed, printing pressure, temperature, printing form and substrate properties. The aim of our research was to broaden our knowledge about the operational characteristics of the technology and its effects on print quality. Our work focuses on flexographic printing characteristics on plastic foil substrates. We investigated the influence of technological parameters (printing pressure, different types of inks and substrates) on the print quality with emphasis on the pressure between the plate cylinder and the substrate on the impression cylinder.

Keywords: flexography, ink transfer, pressure, color measurement

1. Introduction

One of the key printing technologies, which underwent rapid development in the near past is flexography. The fast evolution makes adaptation to this emerging technology quite a burden for most of the printing houses, as they have to print on substrates with very different surface properties using a variety of inks. The primary application is packaging printing, where the most common substrates are plastic films. Other applications include label and hygienic printing, newsprint.

The flexibility of the printing form and low viscosity flexographic inks allow the printing of substrates with surface pattern and non-absorbing plastic foils frequently used in packaging.

For a long time the main objective of technological innovation was improvement of print quality. As a result of the development of the past decades achievable quality enabled flexographic printing to become a competitive of offset printing in certain areas of application. A number of recent innovations in flexographic technology are related to setting printing pressure (Johnson, 2003). In traditional (impact) printing technologies there is physical contact between the printing form and the ink, as well as between the ink and the substrate. Printing happens in the presence of printing pressure (Kipphan, 2000).

2. Objective of the research

Flexographic technology is based on the principles of relief (or letterpress) printing. On the flexible printing form (rubber or photopolymer) printing areas emerge from the plane of the non-printing areas (*Flexography: Principles And Practice, 1999*). Inking characteristics are influenced by a number of factors including ink thickness on the printing form, press speed, printing pressure, temperature, printing form and substrate properties. Ink transfer to the substrate is one of the key parameters during the flexographic printing process (Kajondecha, Hoshino, 2008).

The aim of our research was to broaden our knowledge about the operational characteristics of the technology and its effects on print quality. Our work focuses on flexographic printing characteristics on plastic foil substrates. We investigated the influence of technological parameters (printing pressure, different types of inks and substrates) on the print quality with emphasis on the pressure between the plate cylinder and the substrate on the impression cylinder.

3. Research methods

Flexographic presses usually allow for impression adjustments in precise increments. Variations in impression may occur during normal production, for example settings may sometimes drift out of adjustment during the course of a run due to internal vibrations of the press. In order to explore and characterize the effects of changing the printing pressure on print quality a series of prints were produced with different settings (Johnson, Peter, 2003), (Bohan et al., 2003), (Bould, et al., 2011).

Prints were produced on a Soma Flex Midi 105-8 EG type press using DuPont Cyrel thin (1.44 mm) printing plate with 54 l/cm screen ruling, under typical production conditions. Two types of inks were used for the whole process, ink viscosity was 21 s (DIN4), the applied color sequence was YMCK. Two types substrates were used, BOPP and PET foils with 0.025 mm and 0.012 mm thickness, respectively. Surface tension values of the substrates were measured on the non-printed area of the substrates at different values of impression. Surface tension of the PET foil changed from and 40 to 38 mN/m (dynes/cm) while in case of the BOPP foil it increased from 38 to 40 mN/m. Both substrates were printed in 5 runs with both inks. After the first run the impression was modified within the range of getting visually acceptable images on the test chart. Impression was first set to normal (this usual setting was a company standard based on visual evaluation of the test prints and professional experience), then pressure was gradually altered by increasing and decreasing the gap between the impression cylinder and plate cylinder in steps of 0.03 mm displacement (-0.06 mm, -0.03 mm, 0 mm, +0.03 mm, +0.06 mm). Because the printing form is flexible, a reasonable consequence of the altered pressure is the geometrical deformation of the halftone dots (Figure 1). The degree of deformity can be characterized by the aspect ratio of the minor and major axis of the ellipses modeling the shape of the dot in this case. The average values for the samples shown on Figure 2 were 0.98, 0.90, 0.82 in case of the cyan, and 0.91, 0.86, 0.79 in case the magenta dots. As expected, the circular shape of the dots became gradually elliptical with increasing impression.

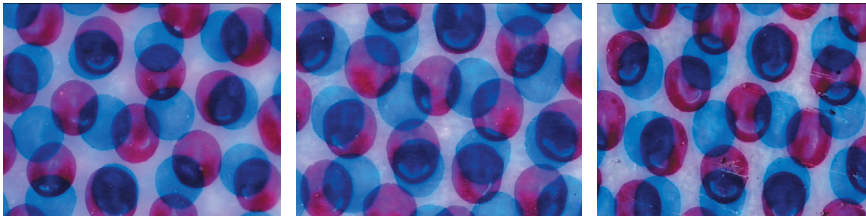


Figure 1: Magnified dot structures of a 40% C +40% M sample printed on BOPP foil using the normal (left), and increased impressions obtained by 0.06 mm (middle) and 0.12 mm (right) displacement of the impression cylinder

In order to explore how changing the impression affects the printed image we constructed a test chart including uniform samples, step wedges for densitometric and colorimetric measurement as well as visual elements for evaluating the overall appearance of the printed image. Colorimetric and tone values were measured by GretagMacbeth SpectroEye spectrophotometer. The visual part of the test chart (Figure 2) was used as an indicator for keeping impression in the range of acceptable print quality.



Figure 2: A photorealistic images of the test chart printed on the BOPP foil with the normal (left) and with increased impression by 0.12 mm displacement of the impression cylinder. The change in the visual quality remains

4. Results and discussion

The visual evaluation of individual test prints obtained at different levels of pressure showed minor differences, mainly in case of elements in machine direction. Apparent changes were observable in tone gradation between prints obtained at different pressure, dot area as well as dot shape of the flexible printing form were primarily affected by variations of impression. Magnified portions of the prints illustrate the gradual dot deformation, as shown previously.

In flexographic printing 20% TVI in the highlight areas can be considered a typical value, the ISO 12647-6 standard allow for values as high as 34%. Changes of TVI curves were also traceable on the histograms of the scanned images on Figure 2. Tone values were increasing together with the printing pressure in the range of midtones (Figure 3) in all cases. In the highlight areas the behavior of the TVI curves did not follow a strict rule, in general we experienced about 10% higher TVI in the case of ink 1 and the BOPP substrate for C, M, Y colors, black process color TVI curves has shown less variation.

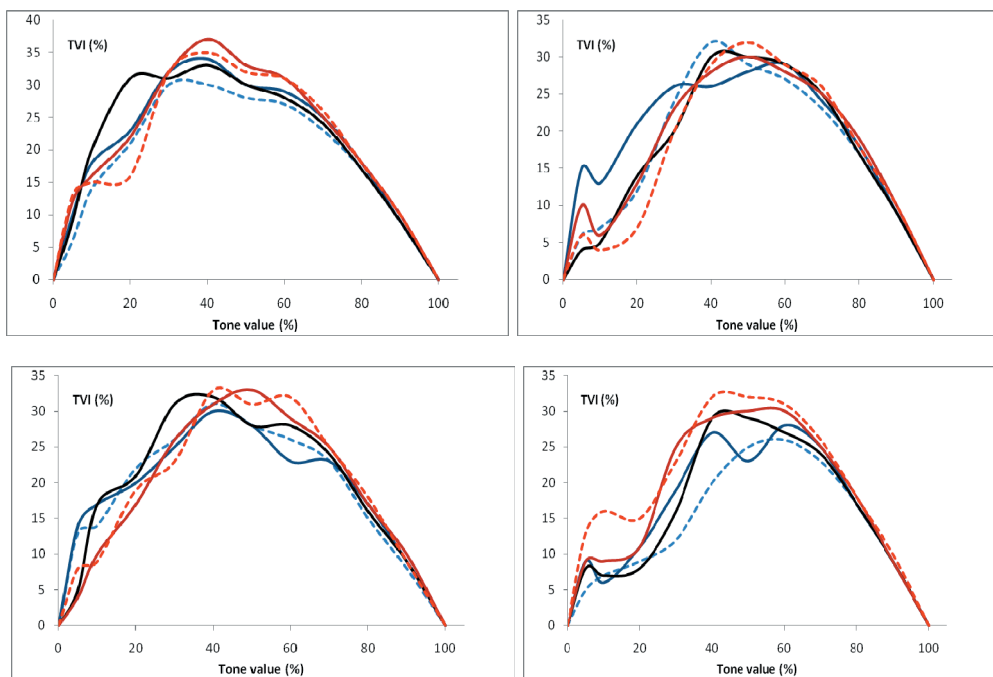
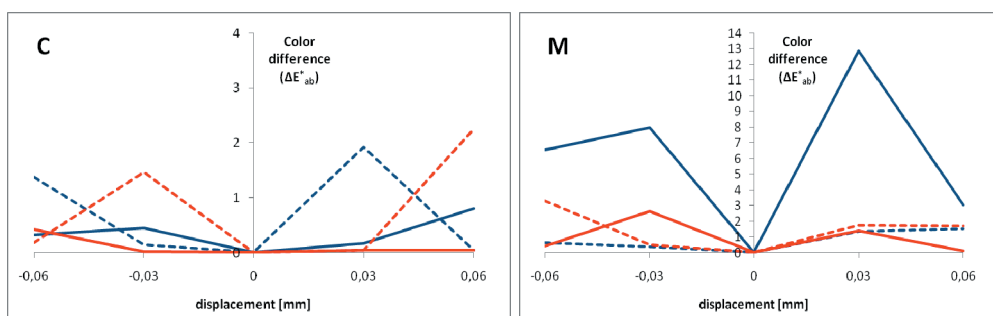


Figure 3: Tone value increase curves of cyan process color at normal (black line), increased (red solid: +0,03 mm dashed: +0,06 mm displacement) and decreased (blue solid: -0,03 mm dashed: -0,06 mm displacement) impression on BOPP (upper row) and PET foil substrates printed using ink 1 (left) and ink 2 (right)

While changes in the TVI curves generate color shifts in the whole tonal range, it is also important to investigate color differences that occur in case of full tones of the process colors as a function of increasing impression (Figure 4). Cyan and yellow colors were producing variations in the range of small color differences, while magenta have produced large shifts in case of ink 1 on BOPP substrate. For the large color differences in case of K the L^* value was responsible dominantly. Densitometric measurements were also performed, variations of chromatic process color densities were well within 10% while in the case of K the highest increase was 20% with increasing impression.



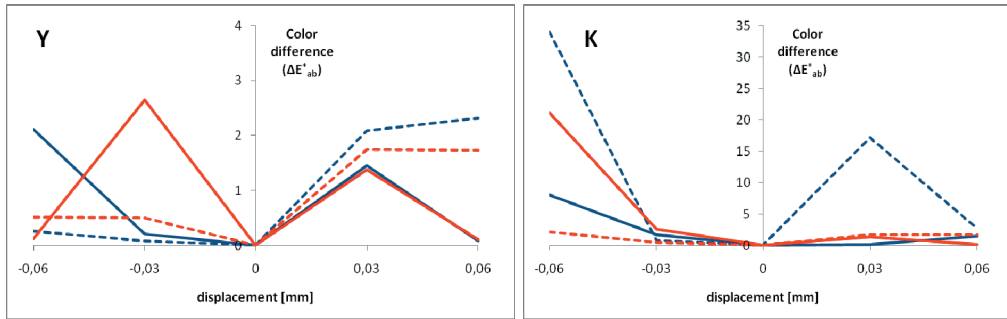


Figure 4: Color differences of solid patches of process colors (C, M, Y, K) at different displacement values. Blue lines correspond to ink 1, red lines represent ink 2, solid lines refer to BOPP and dashed lines refer to PET substrates

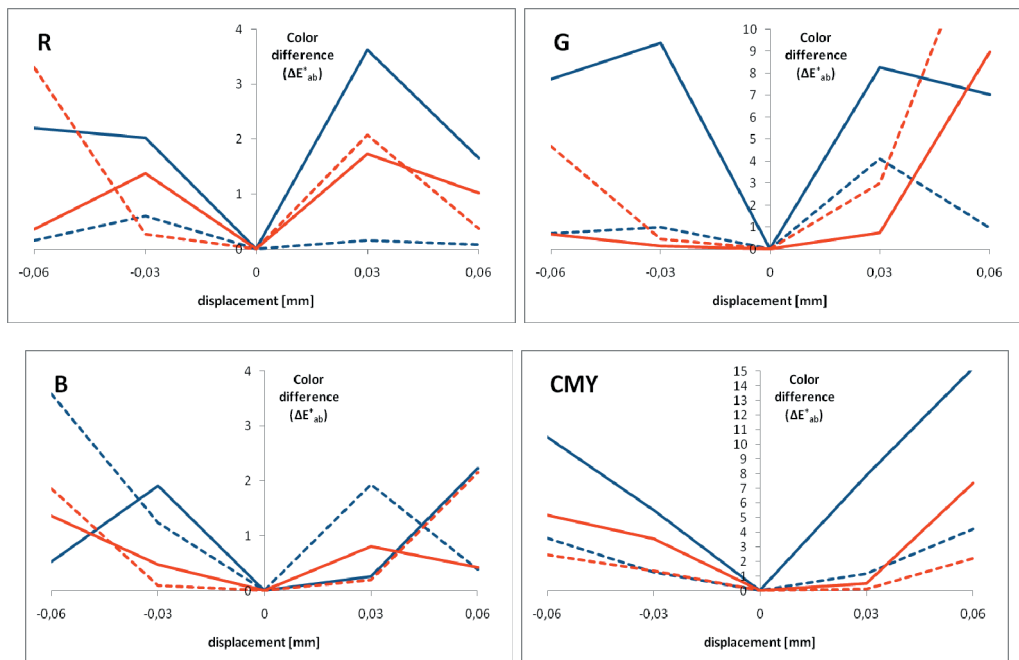


Figure 5: Color differences of solid patches of secondary colors (R, G, B) and a 37% halftone patch of CMY at different displacement values. Blue lines correspond to ink 1, red lines represent ink 2, solid lines refer to BOPP and dashed lines refer to PET substrates

Shifts of process color colorimetric characteristics eventually induce color differences of overprinted dots as well. We investigated secondary colors of printing (R, G, B) together with chromatic grey (CMY). Measurement results of the fulltones of R, G, B and a 37% CMY halftone patch are illustrated in the diagrams of Figure 5. While red and blue show color differences not larger than the chromatic process colors, values of green exceeds this range at larger impression. In case of the CMY halftone patch ink 1 with BOPP substrate produces large differences, like in the case of magenta. The gradual changes of the dot structure of this 37% halftone sample due to the varying impression are revealed on the magnified images of Figures 6-7.

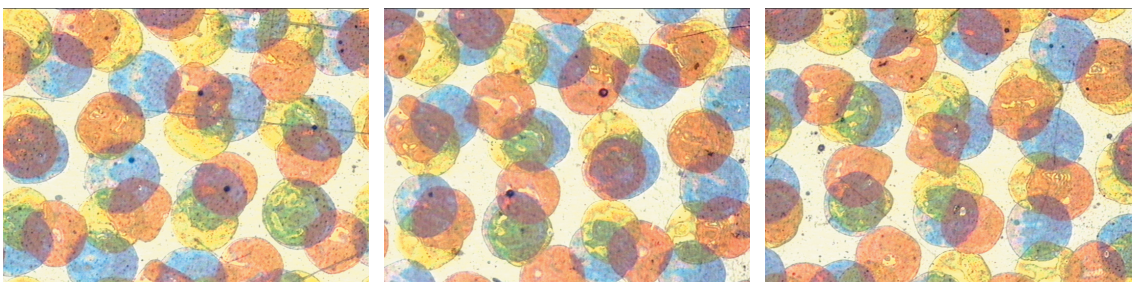


Figure 6: Magnified images of a 37% CMY halftone patch with normal (left), and decreased impression at -0,03 mm (middle) and -0,06 mm (right) displacement

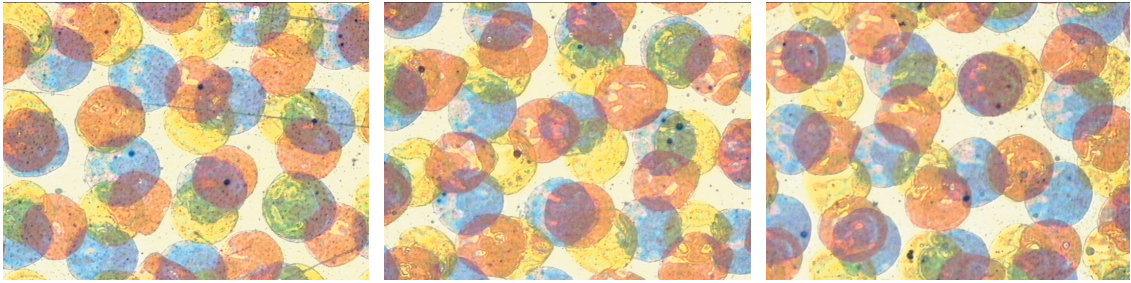


Figure 7: Magnified images of a 37% CMY halftone patch with normal (left), and increased impression at +0,03 mm (middle) and +0,06 mm (right) displacement

The range of reproducible colors (gamut) depends on the printing process and the substrate and other printing materials used. We used a software tool commonly applied in proofing color workflows to visualize and compare the color gamut achievable on the substrates investigated. First, printer profiles were generated using X-Rite EyeOne Pro measurement device and profiling software. A standard CMYK test chart with 323 patches was printed on the substrates of this study, by both printing presses to sample the printable color solid. The profiles were loaded to the gamut visualization tool, which calculated printable gamut in CIELAB color space volume units. Relative printable gamut sizes are shown in Table 1, the largest gamut is taken as reference for every ink-substrate combination. fell within the acceptable range the measured color shifts exceeded standard tolerance values. We experienced changes of the reproducible color gamut within 10%.

Table 1: Relative values of computed printable gamut volumes on BOPP and PET substrates using two types of inks at different impression (displacement values), based on spectral measurements of a CMYK test chart containing 323 halftone patches

Displacement	PET		BOPP	
	Ink 1.	Ink 2.	Ink 1.	Ink 2.
-0,06 mm	0.95	0.90	0.96	0.92
-0,03 mm	0.97	0.96	0.96	0.92
0 mm	0.98	0.97	1.0	0.95
+0,03 mm	1.0	1.0	0.99	0.96
+0,06 mm	0.98	1.0	0.99	1.0

5. Conclusions

Our investigation revealed that changing impression in flexographic printing on foil substrates may appear negligible by visual evaluation and by judging density values only, it has a significant effect on tone and color, the quality of reproduction. Print characteristics on BOPP and PET substrates responded in a different way to the modification of printing pressure. As visual image quality fell within the acceptable range, the measured color shifts exceeded standard tolerance values. Tone values were increasing together with the printing pressure in the range of midtones in all cases. In the highlight areas the behavior of the TVI curves did not follow a strict rule, in general we experienced about 10% higher TVI in the case of ink 1 and the BOPP substrate for C, M, Y colors, black process color TVI curves has shown less variation. Examining color differences we found that, cyan and yellow colors were producing variations in the range of small color differences, while magenta have produced large shifts in case of ink 1 on BOPP substrate. For the large color differences in case of K the L^* value was responsible dominantly. We investigated secondary colors of printing (R, G, B) together with chromatic grey (CMY). While red and blue show color differences not larger than the chromatic process colors, values of green exceeds this range at larger impression. We experience changes in the reproducible color gamut within 10%.

Our intention was to explore how the changes of impression shift colorimetric properties during the reproduction process. Our results may contribute to the optimization factors influencing the quality of products printed by flexographic technology.

Acknowledgements

Special thanks for contribution to Mr Ferenc Várza, chief printer of Pandan Kft.

References

- Bohan M. F. J., Townsend P., Hamblyn S. M., Claypole T. C. and Gethin D. T. (2003): *Evaluation of Pressure in Flexographic Printing*. Published by the Foundation of Flexographic Technical Association, Inc. Printed in the United States of America
- Bould D.C., Hamblyn S.M., Gethin D.T. and Claypole T.C. (2011): *The Effect of Impression pressure and anilox specification on solid and halftone density*.
- <http://www.swansea.ac.uk/printing/research/Published%20papers/Journal/index.htm> (Accessed: 20.06.2011.)
- Flexography: Principles And Practices*. Fifth Edition Published by the Foundation of Flexographic Technical Association, Inc. Printed in the United States of America. Copyright ©1999 by the Flexographic Technical Association, Inc. and the Foundation of Flexographic Technical Association, Inc.
- Johnson, J (2003):. *The Influence of Moisture, Temperature, Pressure Pulse and Substrate on Print Quality in Flexographic Printing*. Karlstad University Studies, ISBN 91-85019-29-1
- Johnson J, Peter R. (2003): *Dinamic Nip Measurements in a Flexographic CI-Printing Press*. Presented at the Technical Association of Graphic Arts Conference, Montereal, Canada, 6-9 April 2003
- Kajondecha P., Hoshino Y (2008): *Halftone Dot Size Variation in Offset, Electrophotographic, and Flexographic Printing and Its Perception*, J Imaging Sci Technol 52(6):060503-7
- Kipphan H. (ed.) (2000). *Handbook of Print Media*, Springer-Verlag, 2000, Berlin 3-540-67326-1

A statistical approach to the modelling of ink transmission on flexo-printed sack paper

Verena Feierer¹, Ulrich Hirn¹, Herwig Friedl², Wolfgang Bauer¹

¹ Institute for Paper, Pulp and Fibre Technology
Kopernikusgasse 24/II, A-8010 Graz, Austria

E-mails: verena.feierer@tugraz.at; ulrich.hirn@tugraz.at; wolfgang.bauer@tugraz.at

² Institute of Statistics
Münzgrabenstraße 11/III, A-8010 Graz; Austria
E-mail: hfriedl@tugraz.at

Abstract

When printing packaging papers in flexo print, deficient ink transmission is a common cause for quality complaints. Which is why this work tries to detect correspondencies between certain paper properties and the failed or successful transfer of the printing ink. In order to describe this dependency, we employ a statistical model available specifically for the handling of binary response variables, the logistic model. Two paper properties, the topography and formation (grammage), as well as the steepness and the curvature of the topography, are considered as explanatory variables for the description of the binary response of successful or failed ink transmission.

The theory to estimate such models is briefly described before a method for the construction of discrete model prognosis masks is presented. Furthermore, different models based on the considered paper properties are fitted and compared with each other via the help of certain characteristic values. A study of different pass band sizes for the filtering of the topography identifies those structures within the paper's surface that are responsible for the occurrence of unprinted areas.

Keywords: ink transmission, flexo print, sack paper, statistical modelling, topography, formation

1. Introduction

Missing ink transmission is a frequent problem when printing packaging papers. In order to gain a better knowledge of the underlying processes, we employ statistical models in our work. These models are based on registered datasets of paper topography and formation and strive to explain the local print reflectance of the sample. As ink transmission is a binary phenomenon, a modelling framework that permits the prediction of a binary target variable had to be developed. The key innovation of the presented work is that we apply a generalized linear model to the problem. This enables us to use *several input variables* at once as predictors for the local ink coverage. Successfully fitted models then allow us to compare the influences of the considered paper properties on the printing process.

Before explaining the underlying statistical model used in our work, we will start with an introduction on the employed materials and the data acquisition. After the outline of the statistical framework, the rest of the paper focuses on several statistical models and their comparisons as well as a more detailed discussion of the filtering of the paper topography.

2. Materials and methods

2.1 Materials

Our study considers sack papers printed in an industrial flexo-printing press. We chose two samples A and B from each of the six sheets, with each sample measuring $5 \times 5 \text{ cm}^2$. A detail of one such sample is given in Figure 1. This detail measures $3 \times 6 \text{ mm}^2$ and will be used throughout the rest of this paper for illustrational purposes instead of the whole, 25 cm^2 large sample. Of the six examined sheets, four were taken from the same basepaper with a grammage of 90 g/m^2 . The other two sheets have a grammage of 70 g/m^2 and once again originate from the same basepaper. Furthermore, the six papers can be separated into two distinct groups according to two different techniques used during the saturation process.

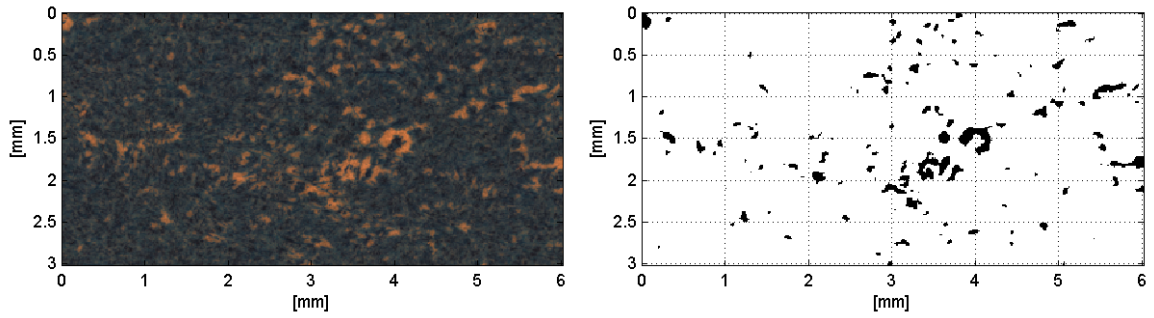


Figure 1: True-colour image and binarized version of a detail of one of the samples. In the binarized image, uncovered areas are shown in black, printed ones in white

Three paper property values have been measured: PPS roughness, Bendtsen and gloss. Their precise values are given in Table 2 in the discussion section. For the moment, it suffices to say that the PPS roughness of the papers ranges from 3.6 up to 6.3 μm , the Bendtsen from 145 to 460 ml/min and the gloss from 7 to 29 %.

In order to ensure a precise matching of the various measurements of paper properties, the area of acquisition was marked with laser holes. Based on those markers, it is possible to exactly allocate the different paper property maps.

2.2 Acquisition of local paper property maps

Print reflectance and surface topography are simultaneously measured using an Infinite Focus System (Wanske et al., 2008) with a resolution of 12.8 μm per pixel. The print reflectance image in Figure 1, right, is binarized so that it only carries information on whether an observation has been successfully printed or not. This is achieved using a semi-automatic image analysis algorithm (Donoser et al., 2006) which yields a binary map that will be used as response in the subsequent statistical models.

The two paper properties shown in Figure 2, topography and formation, are acquired in order to be used as explanatory variables in the statistical model. Local grammage is measured via the employment of beta radiography with a resolution of 50 μm per pixel.

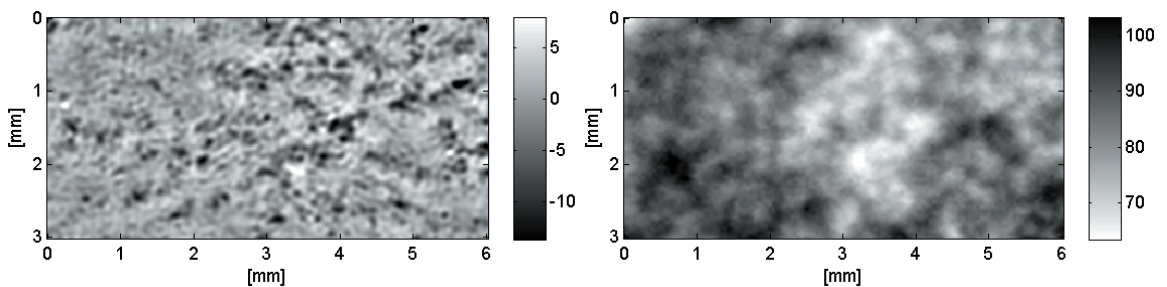


Figure 2: The two paper properties topography (left) and formation (right) that will be considered as predictors in the statistical model. The topography has been filtered with a band pass filter erasing structures smaller than 100 and larger than 3200 μm

Finally, the paper property maps are resized so that all of them have a resolution of 15 μm per pixel. Those rescaled maps are then registered based on holes applied to the paper as registration marks. Thus, we obtain a data set that for every single observation features its (filtered) topography and formation values as well as the binary response for the successful or failed ink transmission.

Theoretically speaking, even more paper properties could be included into this dataset that will later on be used for the statistical model. Two such additional predictors we inspected in our studies are the first- and second-order derivatives of the topography map. These considerations are based on the idea that the steepness of the slopes (gradient) as well as the curvature of the topography structures (laplace) might carry additional, relevant information with regard to the successful transmission of ink. Maps showing these derivatives from the same detail as above can be found in Figure 3.

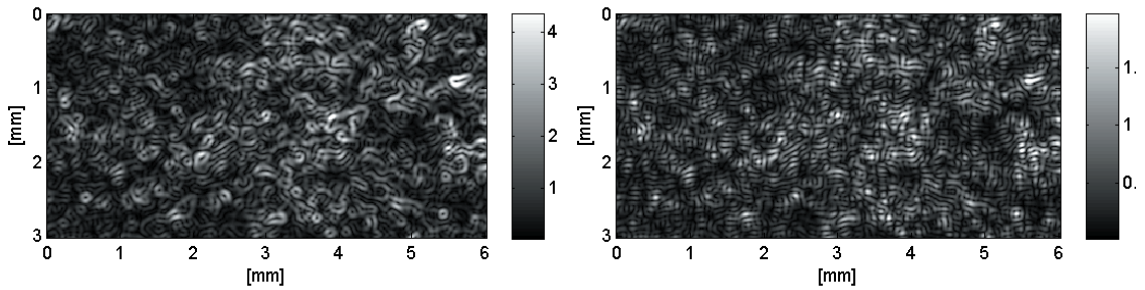


Figure 3: Derivatives of first and second order of the topography map, giving the steepness of the slopes (left) and the curvature (right)

2.3 Statistical modelling

Our aim in fitting a statistical model is to describe the occurrence of uncovered areas in printing. Due to the binary nature of the response, a generalized linear model (GLM) as first introduced by (Nelder & Wedderburn, 1972) needs to be applied. As opposed to a linear regression model, a generalized linear model allows the consideration of non-normally distributed responses.

In a linear regression model, the aim is to describe the mean μ of the response y as a linear combination of the p explanatory variables x_1, \dots, x_p via the relation

$$\mu = \beta_0 + \beta_1 x_1 + \dots + \beta_p x_p \quad [1]$$

for the unknown coefficients $\beta_0, \beta_1, \dots, \beta_p$. One of the crucial assumptions in a linear regression model is that the response variable y has to be normally distributed.

In our case however, the response is a binary variable that tells us whether an observation has been successfully printed or not. This certainly violates the assumption of an underlying normal distribution. Our binary response can be assumed to originate from a binomial distribution, which can be modelled using a GLM. This is achieved by considering a linear combination η of the explanatory variables

$$\eta = \beta_0 + \beta_1 x_1 + \dots + \beta_p x_p \quad [2]$$

as in the case of a linear regression model. But instead of linking this linear predictor directly to the mean μ of the response y , GLMs employ a so-called link-function

$$g(\mu) = \eta \quad [3]$$

for the description of the relationship between the linear predictor η and the mean μ of the response y . In the case of a linear regression model, the link function $g(\mu)$ is the identity. This yields the well-known relation given in equation (1).

As already stated our response y follows a binomial distribution. The special GLM required to fit such a binomially distributed response is known as a logistic regression model. The most convenient choice of link function g for such a model would be the logit-link, defined as

$$\log\left(\frac{\pi}{1-\pi}\right) = \eta \quad [4]$$

where π , the probability for success, equals the mean of a standardized binomially distributed response y . Rewriting formula (4) as

$$\pi = \frac{\exp(\eta)}{1 + \exp(\eta)} \quad [5]$$

better clarifies the need for a link function. The linear predictor η , the sum $\beta_0 + \beta_1 x_1 + \dots + \beta_p x_p$ for p explanatory variables, can in theory yield any real number. But the logistic model works with probabilities π

that are restricted to the unit interval, something a straightforward linear model cannot achieve. Only via the employment of a link function $g: \mathbb{R} \rightarrow [0, 1]$ can the linear predictor η be mapped into the unit interval where the discussion of probabilities is valid.

When a logistic regression model has been successfully estimated, the resulting parameter estimators $\hat{\beta}_0, \dots, \hat{\beta}_p$ allow the identification of important as well as unimportant predictors of a model. As in the case of linear regression models, a $\hat{\beta}_j$ sufficiently distinct from 0 signifies that the corresponding linear predictor x_j does influence the response y .

Furthermore, one can compute the expected probability for successful ink transfer for every single observation based on the parameter estimates $\hat{\beta}_j$ and the numerical values of the predictor variables x_j . The map of the predicted probabilities for successful ink transfer of the detail shown in figures 1 to 3, based on both the topography and the formation map can be found in Figure 4.

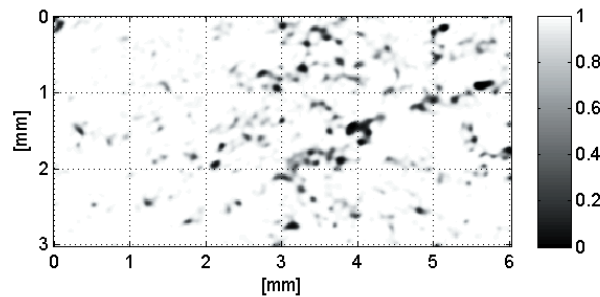


Figure 4: Map of the predicted probabilities for successful ink transmission

These continuous predictions can in a second step be discretized in order to allow a direct comparison with reality. This is achieved by defining all observations with predicted probabilities smaller than a certain threshold value from within the unit interval as unprinted. All observations with predicted probabilities larger than the threshold are categorized as successfully printed areas. Of course, two kinds of errors have to be taken into account when discretizing a continuous prediction: some truly unprinted areas will falsely be taken as printed whereas other, successfully printed regions will incorrectly be identified as unprinted. By defining the threshold in such a way that the same percentage of observations as in the original image will be unprinted in the model prediction, a prediction with minimal number of false alarms as well as missed unprinted areas can be given.

Two measures that give the congruity between the truly unprinted areas and the as unprinted predicted regions can be computed. The so-called sensitivity is defined as the probability that a truly unprinted observation can be identified as such. The second measure, the precision, gives the probability that an as unprinted predicted observation has not been successfully printed in reality as well. These measures are the same ones (Barros & Johansson, 2006) used in their work and can be computed based on comparisons between reality and model prediction as shown in Table 1.

Table 1: The four different cases that arise from a comparison between reality and discretized model fit

		reality	
		unprinted	printed
model	unprinted	negative hit	false alarm
	printed	miss	positive hit

Both sensitivity and precision are conditional probabilities and are computed via the formulas:

$$\text{sensitivity} = P(\text{unprinted predicted} | \text{truly unprinted}) = \frac{\# \text{ negative hits}}{\text{negative hits} + \# \text{ misses}} \quad [6]$$

and

$$\text{precision} = P(\text{truly unprinted} | \text{unprinted predicted}) = \frac{\# \text{ negative hits}}{\# \text{ negative hits} + \# \text{ false alarms}} \quad [7]$$

The models considered in this work differ with respect to the usage of various explanatory variables, especially differently filtered topography maps. It is this simultaneous consideration of topography and formation that as such has never before been considered in the context of ink transmission. In order to compare the discretized predictions of all the considered models, we use the sensitivity and precision values as introduced above.

3. Results

3.1 Various models

From a successfully fitted model, it is possible to compute discrete model predictions such that the proportion of unprinted observations is preserved. Starting with the model that uses only the paper's formation for its prediction shows that formation alone cannot reproduce the real situation at all. The corresponding sensitivity and precision values of only 0.15 underline that observation.

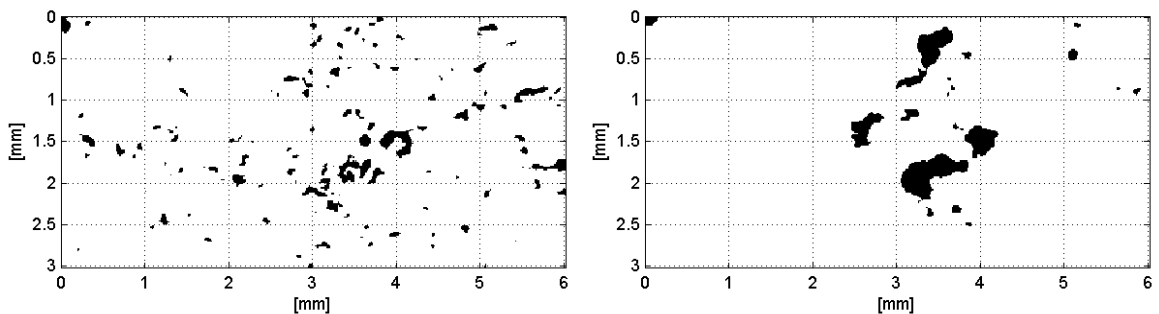


Figure 5: Binarized map of the true-colour image (right) and discretized model estimation based only on the formation of the sample (left)

A model that employs a specifically filtered topography map as explanatory variable can mirror the real situation much better. The resulting discretized model prediction based on the topography filtered with the 100 to 3200 μm pass band is given in Figure 6 (left). A thorough discussion on the size of the pass band can be found in section 3.2. In comparison with the true segmentation mask, the model prediction based on the filtered topography map gives a much better portrayal than the model based on the formation. Most of the more prominent unprinted areas are present in the model prediction and their correspondence with reality lies at 55 %. Next, the discretized model prediction in Figure 6 (right) shows the situation if a model is fitted with both the filtered topography and the formation map. In comparison to a model based only on the topography, the additional information of the formation slightly ameliorates the prediction. Very small-sized, as unprinted predicted spots that have dotted truly successfully printed regions in a topography-only model are now absent from the prediction and therefore allow for a better portrayal of reality. Both sensitivity and precision as well as the pseudo R^2 , a coefficient of determination not unlike the R^2 used in linear regression, are better than in the two models based on only one predictor. We conclude that the additional information introduced by the formation of the sample allows the separation of the considered area into more critical and less critical zones when it comes to ink transfer. In terms of sensitivity and precision, the probability for correctly identifying an unprinted region now lies at 57 %.

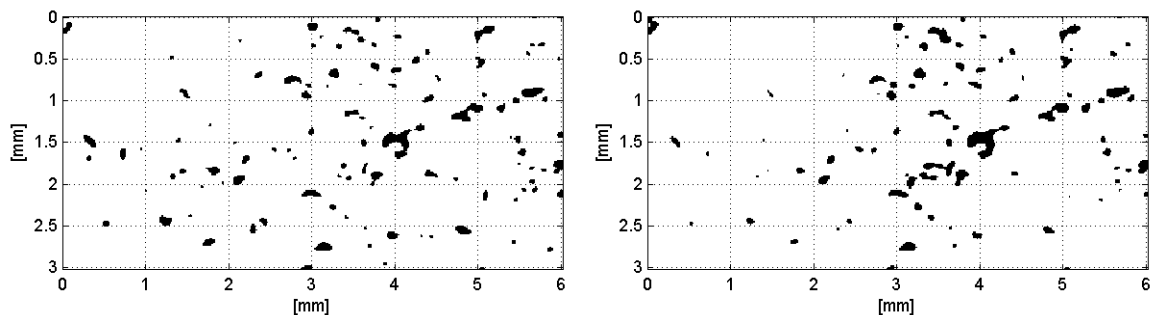


Figure 6: Discretized model predictions for a model based only on the filtered topography map (left, filter band 100 - 3200 μm) and a model based on both the filtered topography map (100 - 3200 μm pass band) and the formation map (right)

Furthermore, we consider models that employ not only a filtered topography and a formation map as predictors, but maps of the first- and second-order derivations of the topography map as well. Figure 7 shows the discretized prediction of such a model as well as the comparison of its pseudo R^2 , precision and sensitivity values with the simpler models introduced above. A simple visual comparison of the binary model prediction in Figure 6 (right), originating from a model based on topography and formation and the binarized map shown in Figure 7 (left) shows that the additional information impairs the prediction.

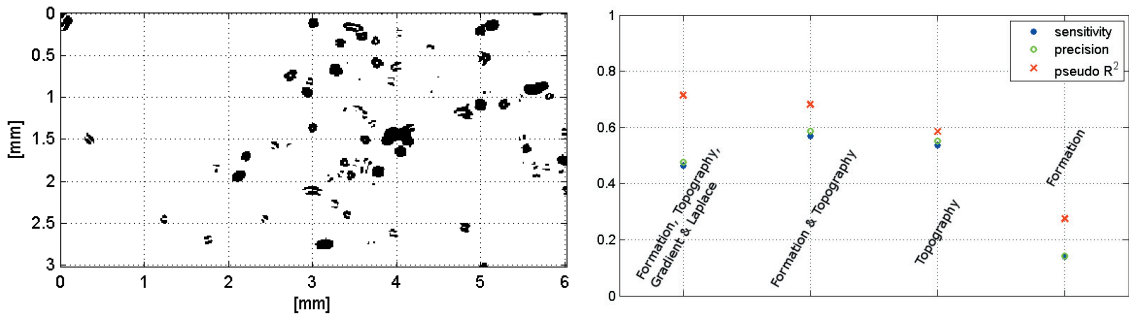


Figure 7: Discretized model prediction of the model based on filtered topography (100 - 3200 μm), formation, first-, and second-order derivations (left) as well as a comparison of its characteristic values with the ones of the three other, simpler models discussed above

This observation can be backed up by the precision and the sensitivity values as well. Where the model based on topography and formation had a sensitivity and precision of 0.57, the new model's values have decreased to 0.46.

As already argued before, a model based only on the formation is a poor copy of reality. The plot in Figure 7 (right) underlines this statement via the poor sensitivity, precision and pseudo R^2 values of said model. A model that uses only the topography of the sample gives a better picture, although a combination of both predictors is even better. If we add the gradient and laplacian map of the sample to such a model, the pseudo R^2 value does no longer improve significantly. Sensitivity and precision, which are based on the discretized image shown in Figure 7 (left) even worsen compared to the simpler model that uses only the formation and topography maps. Based on the characteristic values of these models and the discretized model prediction, we conclude that even though the more complex model is based on four instead of two explanatory variables, it cannot yield better model predictions than the simpler model which uses only the two explanatory variables filtered topography and formation.

3.2 Bandpass filtering of the topography

Now that the gradient and formation maps of a sample's topography have been ruled out as predictor variables, it remains to motivate our choice of the pass band for the filtering of the topography map. The size of the pass band, 100 - 3200 μm , originates from a comparison of various discretized model predictions based on different pass band sizes for the filtering of their topography maps. In order to compare the different models, we use the already mentioned characteristic values pseudo R^2 , precision and sensitivity of each model. A plot summarizing these characteristic values for different models based on relatively small pass bands is given in Figure 8 (left).

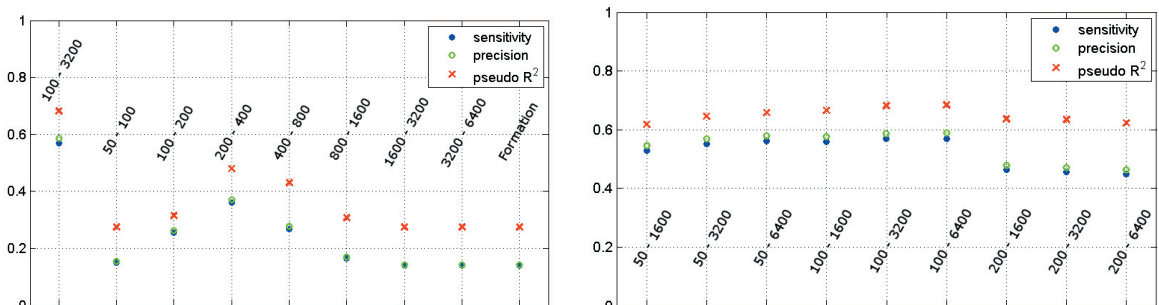


Figure 8: Comparisons of the characteristic values sensitivity and pseudo R^2 of various models. Each model is based on a specifically filtered topography map; the labels give the applied band pass filter for each model

A comparison of the characteristic values shows that pass band filters of 50 - 100 μm , 100 - 200 μm , 800 - 1600 μm and 1600 - 3200 μm structure size yield models that are not better than a model based on the formation alone (rightmost values in Figure 8, left). Only the 200 - 400 μm pass band gives better modelling results than a formation-only model. But the larger pass band that preserves structures between 100 and 3200 μm in size does perform better than any of the other models (leftmost values). Since this comparison shows that the critical structures lie within a larger pass band, a second comparison of model results based on topographies filtered with various broader pass bands was considered. The resulting characteristic values of the models are collected in Figure 8 (right).

The first three pairs of characteristic values are based on pass bands that only delete structures smaller than 50 μm . A comparison of these with the next three pairs of characteristic values shows a slight increase in both pseudo R^2 and sensitivity for increasing filter size. A distinct decrease in both values can be observed for filters that delete all structures smaller than 200 μm (three rightmost pairs). Compared with the 100 to 3200 μm pass band, the 100 to 6400 μm pass band can achieve approximately the same characteristic values, but at the cost of more, obviously redundant information. Based on these observations we deduced that the structures within the topography that are the most responsible for the occurrence of unprinted areas measure between 100 and 3200 μm .

4. Discussion

All the observations and comparisons given under section 3 can be conducted for the large samples described in Section 2 as well. For the remainder of this paper, we will refrain from showing visualizations of our results due to the sheer size of these images. Instead, we will focus our attention on the pseudo R^2 and sensitivity values of the samples as listed in Table 2 along with some information on the different papers. Both PPS and Bendtsen give information on the roughness of the paper, acquired via two different measurement techniques. Higher values indicate a rougher surface in both cases.

The barplot in Figure 9 shows the sensitivity values of the eleven considered models. The value for sample 101 (A) is missing because its model estimation did not converge. The sensitivity, which gives the probability that an as unprinted recognized area truly is unprinted, here ranges from 0.3 to 0.6. In other words, models based on both the filtered topography and formation can explain between 30 and 60 % of the unprinted areas.

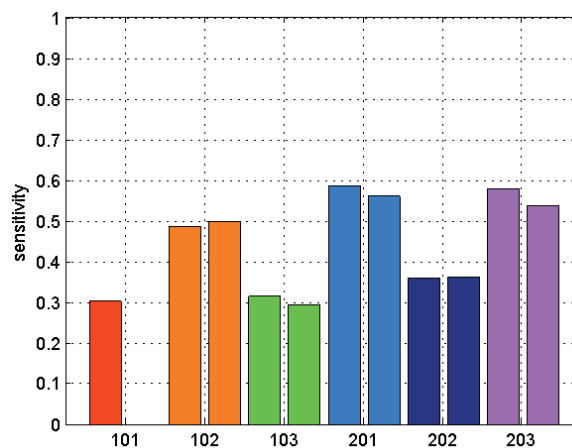


Figure 9: Barplot showing the sensitivity values of the topography and formation based models of the papers

Based on realizations from psychophysicists Weber and Fechner (Roeckelein, 1998) who state a logarithmic connectedness between a stimulus and its sensory impression, we define the print quality as the logarithm of the fraction of the number of observations and the number of unprinted observations. A higher number signifies better printability as the second term in the formula becomes smaller. The samples observed during these studies cover the whole range from very bad (e.g. paper 203) to really good print quality (c.f. paper 101).

$$\text{print quality} = \log(\text{all observations}) - \log(\text{unprinted observations})$$

Table 2: Some properties of the six considered papers with their respective standard errors in brackets as well as pseudo R^2 , sensitivity and precision of the models. The second lines give the values for samples (B) of the papers

Paper	101	102	103	201	202	203
Weight [g/m ²]	90	90	70	90	70	90
PPS [μm]	3.61 (0.1)	4.62 (0.08)	5.46 (0.06)	5.16 (0.11)	6.19 (0.08)	6.26 (0.11)
Bendtsen [ml/min]	225 (35)	350 (85)	460 (50)	145 (30)	355 (70)	440 (60)
Gloss [%]	28.9 (0.8)	19.8 (0.4)	15.2 (0.4)	11.8 (1.4)	7 (0.9)	7.1 (0.7)
Print quality	7.28	6.32	5.16	4.35	4.51	3.31
sample (B)	6.93	5.63	4.74	3.31	5.11	3.20
Pseudo R^2 [0-1]	0.14	0.61	0.34	0.68	0.39	0.60
sample (B)	-	0.57	0.21	0.58	0.43	0.54
Sensitivity [%]	0.29	0.48	0.33	0.57	0.36	0.56
sample (B)	-	0.49	0.21	0.56	0.36	0.53
Precision [%]	0.30	0.49	0.32	0.59	0.36	0.58
sample (B)	-	0.50	0.29	0.56	0.36	0.54

As can be deduced from the values in Table 2, the pseudo R^2 values range from 0.14 for a paper of very good printability up to almost 0.7, this one for a paper of very poor print quality. The sensitivity values of the eleven models (the model estimation for sample 101 (B) did not converge) lie in the interval between 0.3 and 0.6. Figure 10 shows scatter plots of the print quality against the pseudo R^2 value (left) and the against the sensitivity of the models. Based on the present data, a slight increase in the performance of the models for papers with an inferior print quality can be observed.

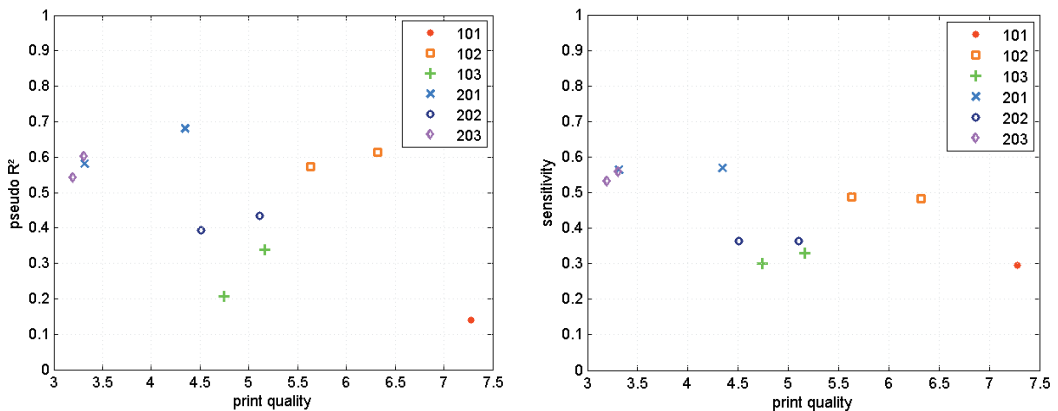


Figure 10: Scatterplots showing the print quality and sensitivity values of the 12 papers against the pseudo R^2

5. Conclusions

Generalized linear models introduce a powerful statistical tool for binary response problems like ink coverage.

Comparisons have shown that the best model fit for the problem of ink transmission considering flexo-printed sack papers can be achieved with a model that uses a band pass filtered topography map with a pass band of 100 to 3200 μm as well as information about the local grammage (i.e. the formation) of the sample. The resulting band pass filter size allows a direct interpretation as it unveils that the for the printing process important topography structures measure between 100 and 3200 μm . The model with both topography and formation allows for a better prognosis than a model that employs only local topography, thus confirming the influence of local grammage on the resulting print. Additional information from first- and second-order derivatives of the topography map which represent the steepness (gradient) and the curvature (laplacian) of the slopes do not increase the quality of the model's prediction.

It is worth mentioning that the introduced models are in no way restricted to the modelling of successful or failed ink transmission in flexo print. A logistic regression model can be applied to other binary print phenomena (e.g. missing dots in rotogravure) as well.

References

- Barros, G. G., & Johansson, P.-A. (2006). Prediction of UnCovered Area occurrence in flexography based on topography - A feasibility study. *Nordic Pulp and Paper Research Journal*, 21 (2), pp. 172-179.
- Donoser, M., Bischof, H., & Wiltsche, M. (2006). Color Blob Segmentation by MSER Analysis. *Proceedings of International Conference on Image Processing (ICIP)*, (pp. 757-760).
- Nelder, J. A., & Wedderburn, R. W. (1972). Generalized linear models. *Journal of the Royal Statistical Society*, A, pp. 370-384.
- Roeckelein, J. E. (1998). *Dictionary of theories, laws, and concepts in psychology*. Greenwood Press.
- Wanske, M., Großmann, H., & Scherer, S. (2008). Messtechnische Bewertung von Tissue Produkten mit dem optischen Messsystem InfiniteFocus (in german). *Wochenblatt der Papierfabrikation*, 36, pp. 473-477.



Influence and interaction phenomena of screen printing machine settings on surface roughness

Ingmar Petersen¹, Gunter Hübner¹, Tim C. Claypole² and Eifion Jewell²

¹ Institut für Angewandte Forschung, Hochschule der Medien
Nobelstr. 10, D-70569 Stuttgart, Germany
Email: petersen@hdm-stuttgart.de

² Welsh Centre for Printing and Coating, School of Engineering, Swansea University
Singleton Park, Swansea, SA2 8PP, United Kingdom
Email: t.c.claypole@swansea.ac.uk

Abstract

The surface quality of screen printed products is getting more and more important in the functional printing market. This paper is focussing on this topic. Different factors of influence on the screen printed surface are analysed via the focus variation measurement system. The results are evaluated using different surface roughness parameters varied by the design of experiment method. The conclusion will give an idea of significant factors of the screen printing machine to support a plane printed surface.

Keywords: screen printing, surface metrology, focus variation, design of experiments.

1. Introduction

Screen printing of fine line structures is a field where intense R&D is being undertaken nowadays. Applications like Photovoltaic, Sensor Systems or Circuitry are focusing on this in general. Reasons are the more and more important question of miniaturization as well as increasing the degree of efficiency. As the screen printing process is very flexible in terms of layout and printed thickness variation the printing of larger structures or even huge areas has become important as well. Famous examples in this field are EL-lamps and OLED displays.

As the screen printing process is based on a tensioned mesh where the ink is pushed through the subsequent ink splitting process itself leaves more or less strong marks (Figure 1) in the printed surface. The surface roughness of the screen printed layers influences its functionality substantially. Concerning Polymer Thick Film conductors Gilileo claims that about 2 - 3 μm is acceptable as well as 20 % thickness deviation (Gil1996). Lee et al. criticize the non-uniformity emission of a screen printed OLED due to its surface topography (Lee2008). In the field of high frequency technology Meinel et al. complain that the surface of a conductor is hilly. If the skin depth sinks at high frequencies below the surface roughness, the current must cover a longer way (Mei1977). A similar proposition is given by Jakubowska et al. in combination with a surface roughness parameter as it is claimed that for low loss transmission the RMS surface roughness should be small compared with the skin depth (Jak200).

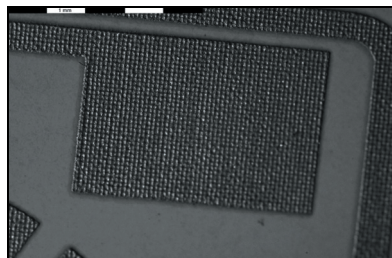


Figure 1: Typical screen printing marks, also known as “mesh marking”

Numerous researches have been undertaken to increase the ink deposit thickness while maintaining a minimum line width of fine structures. Many influences of the mesh and the stencil have been observed. However, the work presented here focuses on printing of comparably large structures where the stencil of the

screen printing form does not have any influence (Figure 2) on the printing result except in the vicinity of the edge of the stencil. It is claimed that this effect starts with a structure width of $w > 1.5 \text{ mm}$ (Sef 2008).

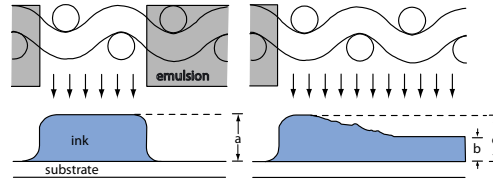


Figure 2: Influence of the stencil on printed ink deposit. The printed layer becomes thinner (b) the farther it is away from the structuring stencil. The stencil or EOM causes a thicker shoulder (c). If the squeegee is not able to push down the mesh directly upon the surface of the substrate (a) a higher ink deposit can be observed

During literature research the factors displayed in Figure 3 were determined as having an impact on print quality (Rie, 1988; Pan, 1998; Fox, 1997, and 1997, Hor, 1974; Hun, 1999; Par, 1991; Cao, 2007 and Abb, 1991). This work further contributes to evaluate the influence of the screen printing machine settings on the resulting surface roughness of large areas. Two extensive Design of Experiments (DoE) were carried out to analyze main as well as interaction effects.

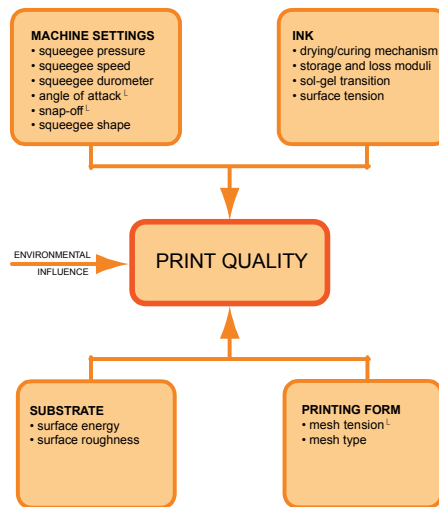


Figure 3: Important factors influencing the print quality

2. Methods

A comprehensive full factorial 2^5 design with 32 runs (Table 1) as initial screening method was carried out. As resulting effects the surface roughness parameter S_k , S_{vk} and S_{pk} as well as the dried ink thickness were analyzed using the statistical software package Minitab R15. The squeegee shape was not included herein as the used straight edge profile is an industrial standard for most applications.

Table 1: Chosen factors and their levels for the basic DoE

Design of Experiment - Basic			
Factor	Factor Name	Level 1 Low (-)	Level 2 High (+)
A	Squeegee Pressure	1.0 bar	4.5 bar
B	Squeegee Speed	40 mm/s	180 mm/s
C	Snap-Off	1 mm	5 mm
D	Angle of Attack	65°	80°
E	Squeegee durometer	65° Shore A	85° Shore A

With the first DoE two factors with highest impact on all response variables were found, the snap-off and the squeegee speed. As these two significant factors face the counterforce mesh tension this one was included in 3 levels in a response surface design with 75 runs (Table 2).

Table 2: Chosen factors and their levels for the advanced DoE.

Design of Experiment - Advanced						
Factor	Factor Name	Level 1	Level 2	Level 3	Level 4	Level 5
A	Squeegee Speed	40 mm/s	75 mm/s	110 mm/s	145 mm/s	180 mm/s
B	Snap-Off	1 mm	2 mm	3 mm	4 mm	5 mm
C	Mesh Tension	10 N/cm	17.5 N/cm	25 N/cm		

To avoid solvent-based effects on the drying behaviour (volume reduction) and on rheology over lifetime the UV-ink Marabu UVSW Ultraswitch was used. It is self-evident that the time between the printing process and the curing has to be constant for all trials. Due to handling conditions it is 6 sec. The chosen substrate was an opaque, white PET film (Melinex type 329 - 175 μm). It was heat stabilized at 145° C to avoid shrinking behaviour and to support flatness during the printing and measuring process. All prints were carried out with the semi-automatic screen printing machine EKRA X1 which enables easy and accurate changes in factor settings during the DoE. The screen printing form was tensioned with Sefar PET 1000 PW 120 - 34 mesh and the emulsion used was Kiwo SR-X. As mentioned above, the emulsion does not have any influence at all but is necessary to structure measuring patterns. The squeegee material was RKS MonoFlex based on polyurethane. The surface roughness was measured on five solid tone squares using the Focus Variation (Figure 4) incorporated in the Alicona microscope.

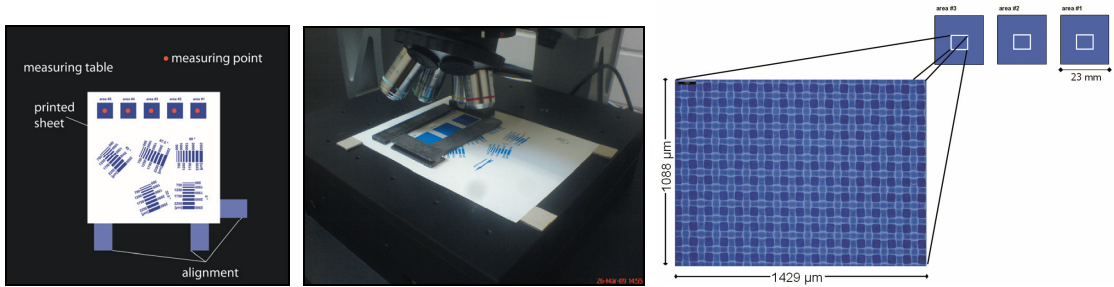


Figure 4: Alicona measurement setup and resulting field of view

The analyzed area was 1088 x 1429 μm . Therefore the chosen magnification collected a maximum of 13 x 17 wires of the chosen 120 - 34 mesh type. The whole field of view included 192 - 221 wire crossings. To abbreviate measurement duration a vertical resolution of 200 nm was chosen. Alicona offers a powerful software solution to process the generated 3D data. Numerous profile and area analysis methods are available. All roughness parameters were derived from the primary data model. The approach for describing the surface topography is based on the Abbott-Firestone Curve (Figure 5). It leads to the probability density of the discrete measured z-values which is transformed into the cumulative probability density function.

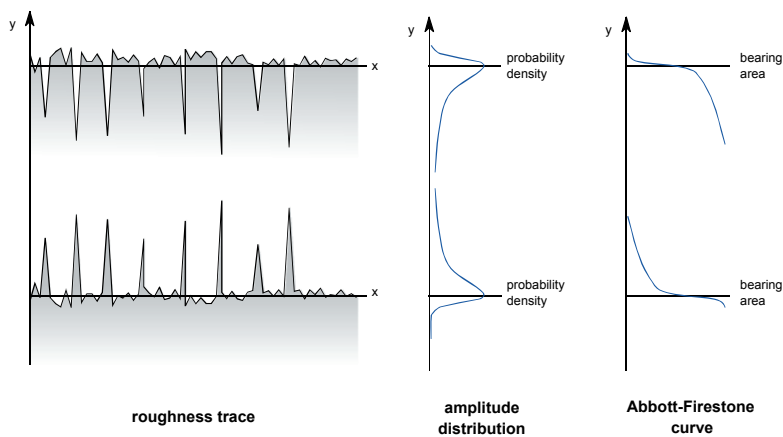


Figure 5: Abbott-Firestone Curve (Wik, 2011)

To get meaningful topographical values from the Bearing Area Curve it is assigned to areas (Figure 6) by a best fit straight line, providing results for the three parameters Spk (Reduced peak height), Sk (Core roughness depth) and Sv_k (Reduced valley height).

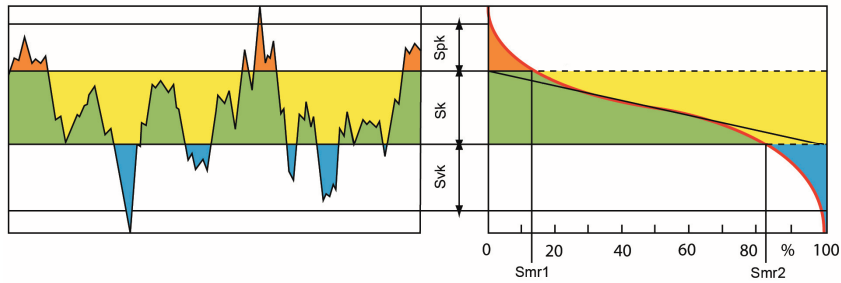


Figure 6: Surface roughness parameters derived from the Bearing Area Curve (BAC)

As the transferred ink volume and therefore the resulting ink thickness is assumed to have a major impact on the final surface properties the dried ink thickness was measured. To achieve the most accurate data the resulting ink thickness was derived from the profile analysis (Figure 7) of a comparatively wide line pattern of 2.5 mm. Taking into account that the patterning stencil has influence on the edge thickness, just a constant centre range was analyzed via double height steps method. It is expected that this region shows similar print behaviour compared to huge areas where the roughness is measured. The profile width consists of 999 separate line analyses which are averaged to one major profile.

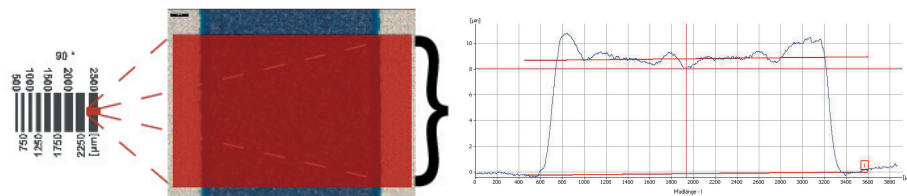


Figure 7: Ink thickness measurement workflow

3. Results - basic DoE

The measurements were analyzed using Analysis of Variance (ANOVA). Additional plots of residuals vs. predicted and residual vs. experiment sequences showed valid independence assumptions. Main effects (Figure 8) and interaction plots (Figure 9) for the above mentioned roughness parameters and thickness have been plotted.

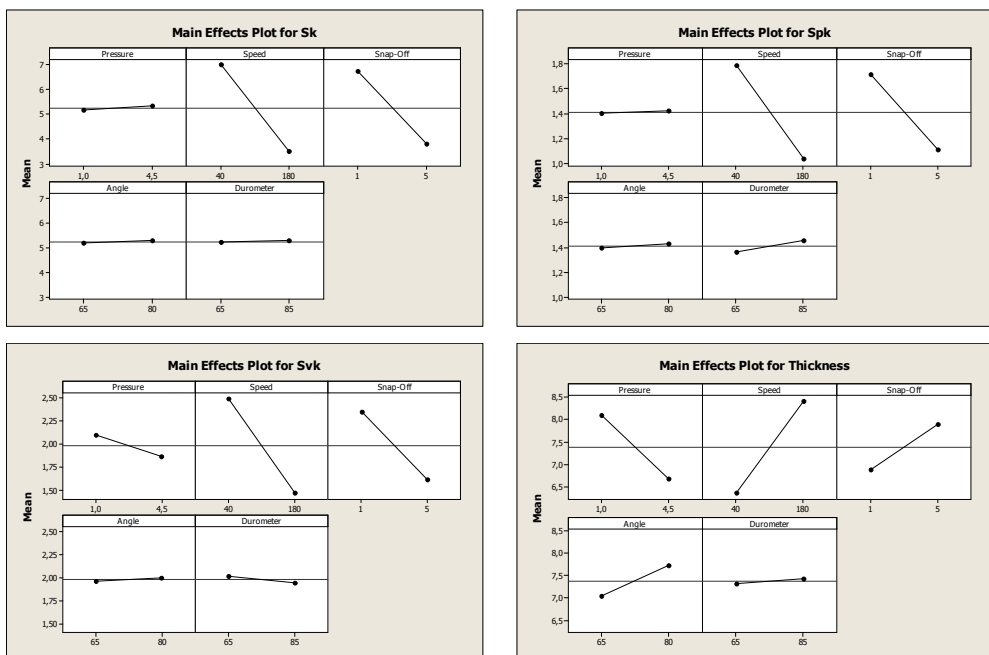


Figure 8: Main effect plots for basic DoE

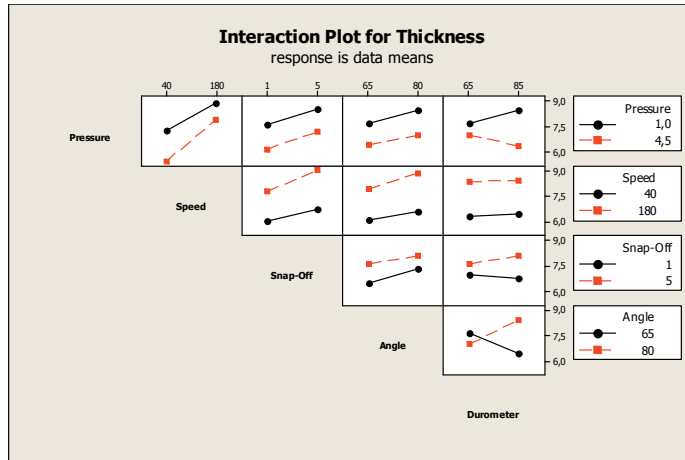


Figure 9: Interaction Plot for basic DoE - response thickness

The statistical significance was tested via the p-values test. A statistical significant effect at the 95 % confidence level is given if the p-value is smaller than 0.05. All significant main and interaction effects for the data means are displayed in Table 3.

Table 3: Significant effects and model quality for basic DoE

		Response is mean data	Sk	Spk	Svk	Thickness
Terms	main effect	A: Pressure	sig.			sig.
		B: Speed	sig.	sig.	sig.	sig.
		C: Snap-Off	sig.	sig.	sig.	sig.
		D: Angle of Attack				sig.
		E: Durometer		sig.		
	2-way interaction	AB				sig.
		AC				
		AD	sig.		sig.	
		AE	sig.	sig.		sig.
		BC	sig.	sig.		
		BD	sig.	sig.		
		BE		sig.		
		CD	sig.			
		CE				
		DE				sig.
	3-way interaction	ABC				
		ABD	sig.			
		ABE				sig.
		ACD				
		ACE				
ADE		sig.			sig.	
BCD						
BCE						
BDE	sig.	sig.	sig.			
CDE				sig.		
Model	R ²	99.64%	97.06%	83,36%	95.79%	

The overall model quality - except for Svk - is very high as the coefficient of determination R² exceeds 90 %. All surface roughness parameters are significantly influenced by squeegee speed and snap-off. Some responses show additional significant main effects, but evaluating structures and significance levels (p-value and t-value) in detail it was found that - by far - squeegee speed and snap-off have the highest impact among all factors. For all other significant main effects p-values are very close to the (critical) significance level ($\alpha = 0.05$). Furthermore some significant interaction effects could be identified. Pressure/Durometer (AE) and Speed/Angle of Attack (BD) are significant 2-way interactions for the better part of roughness parameters. Speed/Angle of Attack/Durometer (BDE) is a significant 3-way interaction for all response variables. Beside these just a few other interaction effects are slightly significant in the analysis of roughness parameters.

Focusing on thickness the significant factors are more complex. Figure 10 shows the impact of different terms (main effects and interactions) using the Pareto Chart.

As it could be seen from Figure 10 the ink thickness is significantly influenced by the four factors A: pressure, B: squeegee speed, C: snap-off and D: angle of attack. Just squeegee durometer (E) itself does not have a significant main effect, but plays an important interaction part together with pressure and angle of attack (terms DE and ADE).

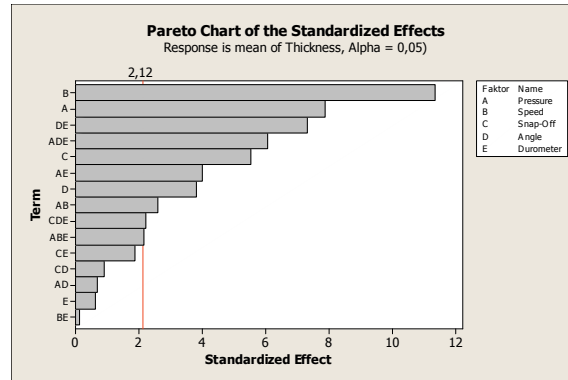


Figure 10: Pareto Chart of standardized effects for basic DoE - response thickness

4. Results - advanced DoE

During the basic DoE squeegee speed and snap-off were identified as the factors which have the highest impact on surface roughness. As the snap-off is responsible for the release behaviour of the mesh out of the deposited ink the factor mesh tension - which acts as a counterforce - had to be involved in an additional DoE. By using more than two levels for each factor a more detailed modelling of the responses is possible and more complex structures like quadratic terms could be additionally evaluated.

Test conditions have been similar to the basic DoE. Additionally squeegee durometer (75 ° Shore A), angle of attack (75 °) and squeegee pressure (1.0 bar) hold constant.

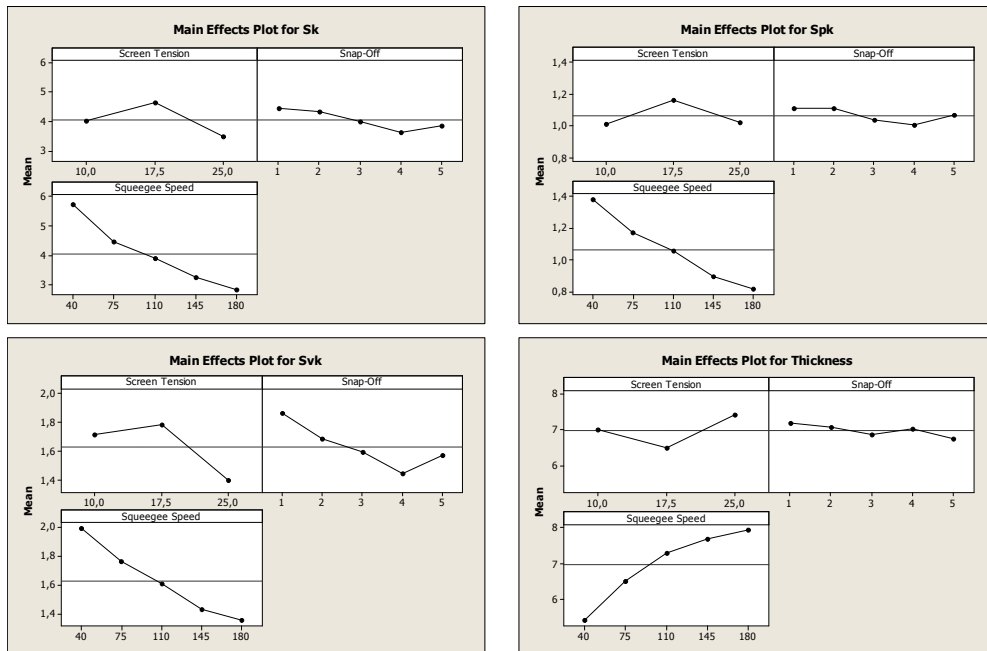


Figure 11: Main effect plots for the advanced DoE

The surface roughness parameter Sk, Svk and Spk show almost similar progressions (Figure 11). Squeegee speed is the factor with highest impact on Sk, Svk and Spk showing a continuous curve progression. The valley components are affected by snap-off and look consistent up to 4 mm. A phenomenon can be found for the factor mesh tension. Sk, Svk and Spk have highest values for medium tension and smaller results for extreme settings of tension. Thickness proves this parabolic progression in the inverse way. Concerning thickness we found the inverse behaviour of squeegee speed for all three surface roughness parameters.

Compared to the basic DoE the model quality is reduced (Table 4). Surprisingly the interaction Snap-Off/Squeegee Speed (AB) does not show the same impact like in the previous investigation. The impact

strength of Snap-off is reduced in general. As displayed in Figure 12 and 13 the dependency between a thicker ink layer and a more even surface could be confirmed.

Table 4: Significant effects and model quality for advanced DoE

Response is mean data		Sk	Spk	Svk	Thickness	
Terms	main	A: Speed	sig.	sig.	sig.	sig.
		B: Snap-Off	sig.	sig.	sig.	sig.
		C: Mesh tension	sig.		sig.	sig.
	2-way	AA	sig.	sig.	sig.	sig.
		BB			sig.	
		CC	sig.	sig.	sig.	sig.
		AB				
		AC				
		BC				
	3-way	ABC				
Model	R ²	84,22%	82,58%	83,72%	85,45%	

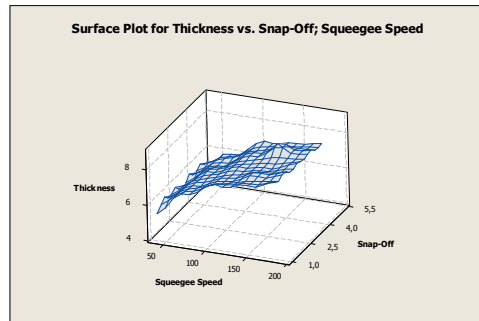
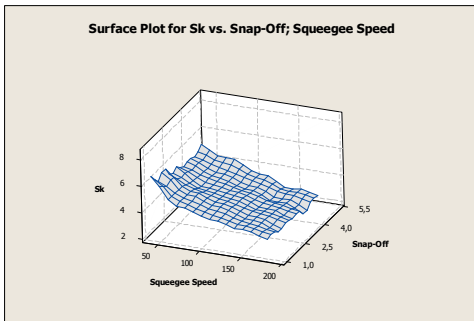


Figure 12: Surface response model for the advanced DoE - responses Sk and thickness

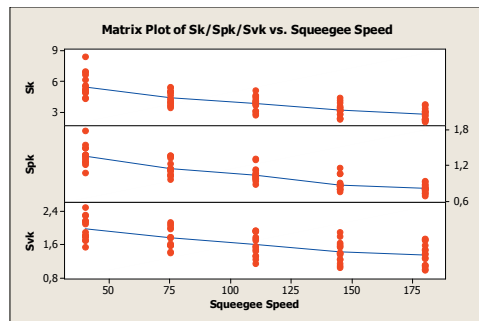
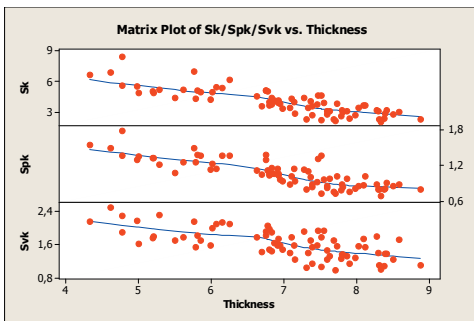


Figure 13: Matrix plots for Sk/Spk/Svk vs. thickness vs. squeegee speed

5. Discussion and conclusion

Squeegee speed and snap-off were determined as the factors with highest impact on the surface roughness of a screen printed area. However, the impact strength of snap-off could not be found in both experiments. Additional confirmation trails have to be carried out.

The physical interpretation for the significance of squeegee speed and snap-off may be the mesh release behaviour after it has been pushed down on the substrate by the squeegee. The higher the snap-off the higher is the release velocity of the mesh. Interacting with the squeegee speed the contact phase - also known as ink trail - is minimized. Furthermore a higher squeegee speed forces higher shear rates in the ink during the injection phase. In case of a shear thinning behaviour this may support a longer levelling time (the ink likely has time for levelling as long as the Loss Modulus G'' stays higher than the Storage Modulus G') of the ink after deposition. Rheological examinations are in progress.

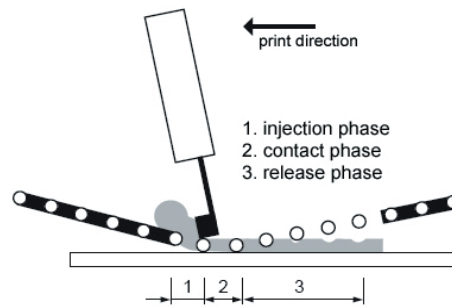


Figure 14: Screen printing phases defined by Riemer [RIE1988]

To understand more about the different phases of the screen printing process (Figure 14) and their influence on surface roughness the printed ink layer thickness has been involved into the examinations. An accurate thickness measuring method was undertaken using the Focus Variation Method. The results have been cross-correlated with different surface parameters to check the hypothesis of increased surface roughness caused by decreased, transferred ink volume. This could be confirmed but ink thickness showed a more complex impact structure compared to all three surface roughness parameters.

Acknowledgments

We would like to thank the following companies for their support: EKRA, Marabu, Sefar, RKS and Hirschmann Car Communication.

References

- (ABB1991) ABBOTT, S. How to be a great screen printer. MacDermid Autotype Ltd. (2008)
- (AND1997) ANDERSON, J. An investigation into the physical aspects of the screen printing process. PhD Thesis. University of Wales Swansea. (1997)
- (CAO2007) CAO ET AL. Optimization of Screen Printing Process. Nanjing Electronics Device Institute. (2007)
- (FOX1997) FOX, I. Ink flow within the screen-printing process. PhD Thesis. University of Wales Swansea. (2002)
- (GIL1996) GILLES, K. Polymer Thick Film. Van Nostrand Reinhold (1996).
- (HOR1974) HORWOOD, R. Towards a better understanding of screen print thickness control. *Electrocomponent Science and Technology*. Vol. 1 pp. 129-136 (1974)
- (HUN1999) HUNT, D. Understanding the mechanism. The essence of process control. *SGIA Journal*. 3rd Quarter (1999)
- (JAK2006) JAKUBOWSKA ET AL. Technology and Performance of Millimetre-Wave Multilayer Components. *Journal of Materials Science*. volume 17 number 2 (2006)
- (LEE2008) LEE ET AL. Single-layer organic-light-emitting devices fabricated by screen printing method. *Korean Journal of Chemical Engineering*. volume 25 number 1 (2008).
- [MEI1977] MEINEL ET AL. Optimisation of thin and thick film technology ... volume 4. Gordon and Breach Science Publishers Ltd. (1977).
- [PAN1998] PAN ET AL. Screen Printing Process Design of Experiments for Fine Line Printing of Thick Film Ceramic Substrates. *Proceedings of the International Symposium on Microelectronics*. San Diego. (1998)
- (PAR1991) PARIKH ET AL. SPC end setup control analysis for screen printed thick films. *Components, Hybrids, and Manufacturing Technology*. volume 14 number 3 (1991)
- (RIE1988) RIEMER, D. Ein Beitrag zur Untersuchung der physikalischen-technischen Grundlagen des Siebdruckverfahrens. Dissertation. TU Berlin. (1988)
- (SEF2008) SEFAR AG. Siebdruckhandbuch. (2008)
- (WIK2011) http://en.wikipedia.org/wiki/Abbott-Firestone_curve

The new technology of perfect binding with vibratory milling heads and investigations of durability of adhesive bonded books

Georgij Petriaszwili, Yuriy Pyryev

Division of Printing Technologies
Institute of Mechanics and Printing, Warsaw University of Technology
Konwiktorska str. 2, PL-00-217 Warsaw, Poland
E-mails: j.petriaszwili@wip.pw.edu.pl; y.pyryev@wip.pw.edu.pl

Abstract

On quality and durability of books, produced by the Perfect Binding method, the great influence has the mechanical operation of cutting away the spine of book blocks. This is realized by the multi-stage milling heads witch treated the spine surface before causing on glue layer. Considerable forces of milling reduce the production speed of bookbinding lines, the quality of processing that in the total, diminishes durability of the books. Investigations shows, that application of vibratory cutting in book spine milling processing allows considerably reduce the cutting force in the book spine processing.

Nowadays it is believed that the main method of book testing which enables to receive the more repeatable test values is Pull Test. Book testing machines, which are known on the market, differed between each other which influences the value of a final result. Therefore, the elaboration of theoretical foundations and standard testing parameters of bindings has a significant meaning. This paper suggests an improved mathematical model for calculating the tensions in the adhesive layer spine during the opening of the book and testing durability of binding.

Keywords: adhesive binding, vibratory spine milling processing, tensions in adhesive layer, durability of books

1. Introduction

Nowadays the adhesive binding technology of book blocks, with total sheared folds (*Perfect Binding*) is currently the most widely used binding technology in the printing industry. For the reader, except for the contents of purchased book a considerable meaning has a graphic design and quality of binding. The worst that can happen to a book lover it is when purchased copy practically falling apart in hands. Practice proves that the adhesive book binding durability to a great extent depends on the mechanical processing of book blocks by milling. The purpose of milling is completely shearing of signature folds and preparation edge of a sheets for a good connection with the adhesive layer. The effectiveness of the spine process depends on the parameters of cutting tools, geometry of used knives and angle of the cutting edge of the book block spine. This is realized by the multi-stage milling heads witch treated the spine surface before causing on glue layer. Considerable forces of milling reduce the production speed of bookbinding lines, the quality of processing, that in the total, diminishes durability of the books. All this tells about the necessity of search of new, alternative methods of milling.

Also important is to develop a theoretical basis of tension analysis occurring in the adhesive layer of book.

2. Vibratory milling method

2.1. Background

In the field of modern cutting technology, the attention should be paid research works on the vibratory method of cutting different materials. The results indicate that vibration cutting is an effective method to reduce the size of the burden of technology, what allows significantly intensify the processing operations.

Influence of vibration on the kinematics of cutting processes is manifested in the variability of the size and direction of cutting velocity vector, which leads to fluctuations in the values of kinematics angles of cut of the cutting tool during processing of materials. It is known, that the force of paper stacks trimming F_{okr} is dependent inter alia on the angle of trimming, and it shall be calculated from the formula (Komarow, Petriaszwili, 1989):

$$F_{okr} = K_o \alpha_{okr}^\gamma \quad [1]$$

where: K_o - generalized coefficient, taking into account parameters of process of cutting, α_{okr} - angle of cutting, γ - an empiric coefficient is taking into account influencing of angle of cutting on cutting force.

At the traditional method of cutting the real angle of cutting (α_{okr}) is determined by the angle of sharpening (α_o) and by the angle of motion φ cutting instruments (Mordowin B. M., 1962). Variable the actual knife trimming angle (Figure 1) taking into account the vibration can be determined from the formula:

$$\alpha_{okr} = \arctg \left(\operatorname{tg} \alpha_o \cdot \frac{V_y}{V_{okr}} \right) \quad [2]$$

where: V_y - the vertical component of the speed of the book feeding, V_x - horizontal component of the speed, V_{okr} - speed of trimming.

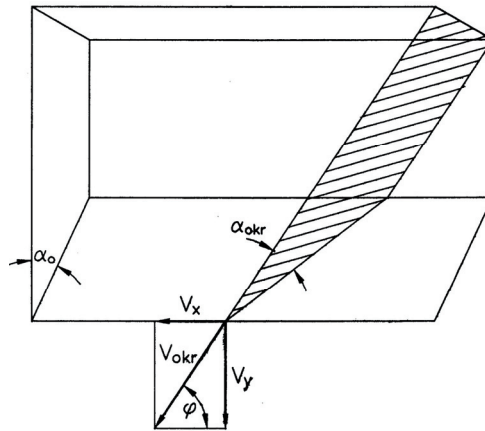


Figure 1: Calculated schema of the transformation of actual cutting angle α_{okr}
 V_y - the vertical and V_x - horizontal components of the speed of the book feeding

The results of vibration trimming of the book blocks (Petriaszwili, 2006) showed a significant reduction in the angles of trimming in proper selection of the direction, amplitude and frequency of transmitted vibrations. For this reason, it is useful to analyze the kinematic process of vibratory milling of books together with optimization of parameters of transmitted vibration.

2.2. Schemes of vibratory milling systems

Analysis of the kinematics of vibratory milling was carried out for three different directions to give a flat vibrations cutting knives: a longitudinal vibration - Figure 2a, cross - Figure 2b and wheeled - Figure 2c.

Consider the diagrams of transmitted vibrations for the flat knife. Velocity vector of trimming V_{okr} can be determined by dependency below:

$$V_{okr} = V_p + V_w \quad [3]$$

where: V_p - speed of feeding blocks, V_w - velocity vector of vibrations.

Velocity of vibration can be determined as:

$$V_w = \frac{dy}{dt} = A\omega \cos \omega t \quad [4]$$

where: $y = A \sin \omega t$ - deflection of the knife vibration, A - amplitude of vibration, $\omega = 2\pi f$ - frequency of vibration, t - time.

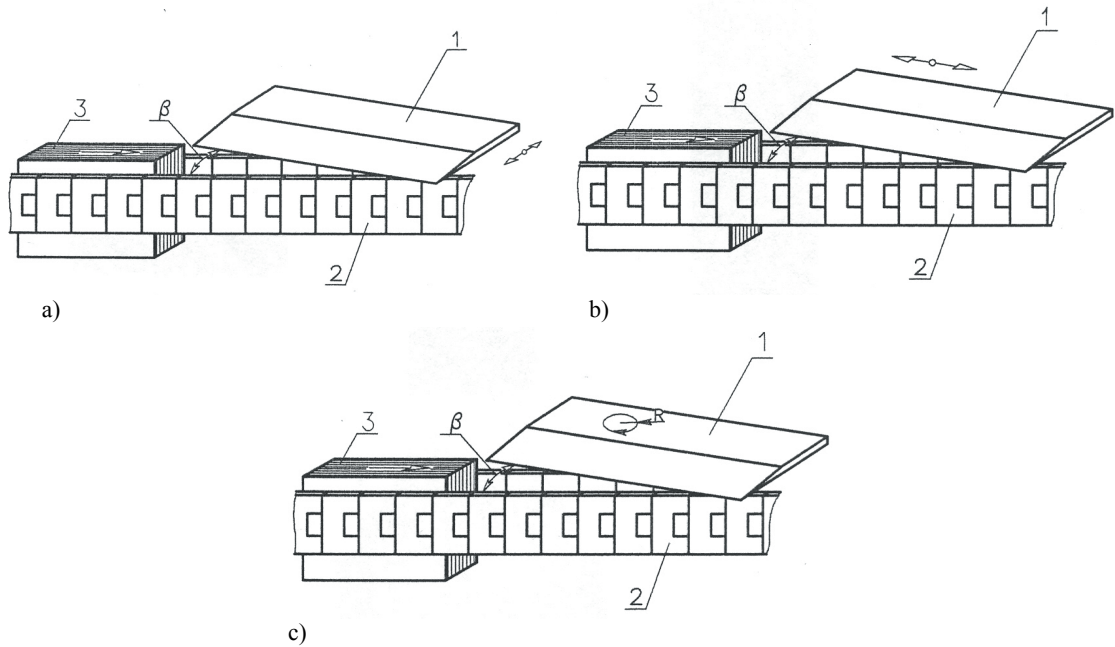


Figure 2: Schemes of vibratory cutting heads (Patent RP. Nr 177365, 1995)
 a - longitudinal vibrations, b - cross vibrations, c - wheeled vibrations,
 1 - knife, 2 - transporter, 3 - book block, β - mounting knife angle

2.3. Analytical research

When set the flat knife at an angle β (Figure 2a) the actual trimming angle α_{okr} with longitudinal vibrations is equal to:

$$\alpha_{okr} = \arctg \left[\operatorname{tg} \alpha_o \left(1 + \frac{A\omega}{V_y} \cos \omega t \right) \operatorname{tg} \beta \sin \gamma \right] \quad [5]$$

In this setting of vibrating knife can be distinguish two basic characteristics of the cutting:

- intermittent cutting, when the knife comes out in a specific phase of the cycle of contact with the book block;
- constant cutting, when the trimming angles change, but the knife is still in contact with the paper

The moment of knife output from the contact with the spine occurs in the phase of vibration ωt_1 in which $V_{okr} = 0$ and is defined as:

$$\omega t_1 = \arccos \left(- \frac{V_y}{A\omega} \right) \quad [6]$$

Moment of the next entry of the knife in the book block is in the phase of vibration ωt_2 , which is determined from the equation:

$$\sin \omega t_2 + \frac{V_y t_2}{A} = \sin \omega t_1 + \frac{V_y t_1}{A} \quad [7]$$

Kinematics of shear folds with the cross vibrations significantly different from the kinematics of the longitudinal vibrations. Characteristically during the trimming knife is always in contact with the paper for an arbitrary set of vibration knives parameters. In the process of vibrating cutting shearing force changes from maximum to minimum value with the fact, that with increasing amplitude and vibration frequency is further reduced shearing forces.

The trimming angle with this method (Figure 2b) is calculated as follows:

[8]

$$\alpha_{okr} = \arctg \frac{\operatorname{tg} \alpha_o}{\sqrt{1 + \left(\operatorname{ctg} \beta + \frac{A\omega}{V_y} \cos \omega t \right)^2}}$$

Studies on impact of angle of the vibrating knife (Figure 2b) showed that the angles $\beta > 10^\circ$ the character of value changes for the trimming angles α_{okr} is close to direction of the knife settings to the feed blocks ($\beta = 90^\circ$). For more attention deserve the angle size range of the knives setting $\beta = 1 \div 5^\circ$, as in this case the maximum values of the trimming angles not reaching the knife blade angles. Noteworthy is examining the kinematics of diagonally adjusted knife with circular movements of the blade (Figure 2c). The above-described study of kinematics of vibratory trimming with broadcasting vibrations in one direction have shown the advantages and disadvantages of each cutting method. Trimming with longitudinal vibrations (Figure 2a) is characterized by interruptions in the cycle of cutting, and the angle is usually the same as the angle of the knife blade. While at cross vibrations of the knife (Figure 2b), the angle trimming value change in the cycle from minimum to maximum. Trimming force will also vary from minimum to maximum value and diminishes with decreasing angle of the knife. Wheeled movements allow of the knife to combine the advantages of schemes examined above: cutting is done with minimum values of the trimming angle however, when the trimming angle has to increase, the knife turning away from the block and then cut into only when the angle of trimming will be again minimal. This type of cut will significantly reduce the mean of the trimming force.

In Figure 3 is shown graphs of changes in the trimming angle α_{okr} at various sizes of the knife angle β . As can be seen from the charts, with a reduction of the angle β , a cutting process from continuous to intermittently, with smaller angles settings of the knife correspond to smaller cutting angles. Research shows that by reducing the knife angle β the process of cutting from the constant contact of the blade with a paper goes into interrupted process.

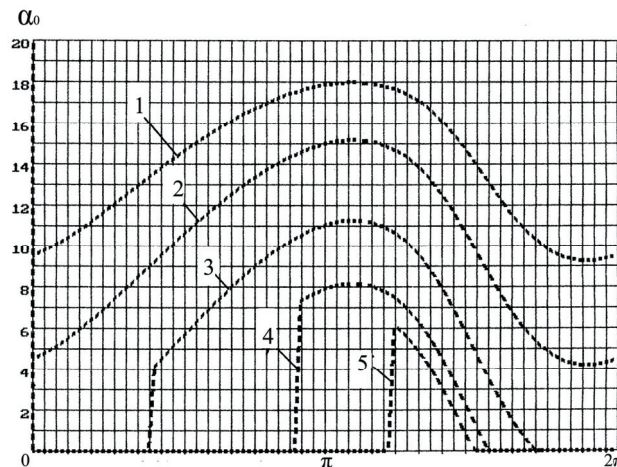


Figure 3: Influence of the knife angle adjustment on changes of character of the actual trimming angle in a cycle of the knife vibrations
 1 - $\beta = 45^\circ$, 2 - $\beta = 30^\circ$, 3 - $\beta = 15^\circ$, 4 - $\beta = 5^\circ$, 5 - $\beta = 1^\circ$

The application of alternative vibration technology can result in the considerable reduction, in cycle of oscillation, angles of cutting, and consequently, to the decline of milling forces of cutting away the signature folds of the book blocks.

3. Mathematical modeling of the tearing out a sheet from an adhesive layer process of book spine (Pull Test)

3.1. Background

There are two main methods used in practice to test the adhesive binding: Pull-test and Flex-test (Liebau, Heinze, 2008). Nowadays it is believed that the main method of book testing which enables to receive the

more repeatable test values is Pull test. There are some book testing machines on the market designed for Pull testing method. Unfortunately, these machines are differed between each other in a way of carrying out of measurement, which influences the value of a final result. Testing devices of various producers are characterized by different binding mounting conditions and tearing out the sheets, what greatly contributes to the defective evaluation of binding strength (Petriaszwili, 2006). All these causes the different results of Pull test of the same bindings. Therefore, the elaboration of theoretical foundations and standard testing parameters of bindings has a significant meaning. The aim of this study is to develop a mathematical model of Pulling out a sheet from an adhesive book spine and survey on the influence of various parameters on the books strength.

3.2. Model of an adhesive sheets connection

The schema of binding of paper sheets in an adhesive layer is shown in Figure 4. During testing the strength of the book, the opening angle of paper sheets $2\theta_0$ situated on both sides of pulled out sheet with a force P is given. The greatest tensions are formed in an adhesive layer between the sheets (Petriaszwili, Pyryev 2007). The topic for investigation in this study are two adhesive layers between two paper sheets of book, that are in contact with the sheet, on which the pulling out force P operates (Figure 5).

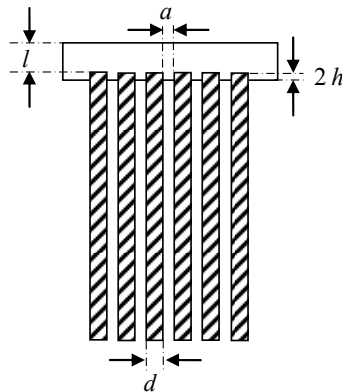


Figure 4: Scheme of an adhesive sheets connection
 d - thickness of the paper sheet, l - thickness of an adhesive layer on the book spine,
 a - distance between the sheets, $2h$ - thickness of an adhesive layer between the paper sheets

It is considered that the adhesive layer have dimensions $a \times b \times 2h$, where b - height of the book spine and are based on the elastic adhesive substrate of a thickness l . It is assumed that the load $q(x)$ acting from the adhesive substrate is proportional to the bending plate $w(x)$ (Winkler's model) and equal to $q(x) = -kw(x)$ (Pisarenko, 1986).

We will focus attention on defining the tension filed, which occurs during usage of a book, namely while the book is opened with angle of $2\theta_0$ and with applied force P . Due to the symmetry of the issue, only one layer and a pulled out sheet were considered (Figure 6). In the considerate model it was assumed that the paper is a stiff material and the glue is a homogeneous isotropic elastic material with mechanical properties: E - Young's modulus, ν - Poisson's ratio.

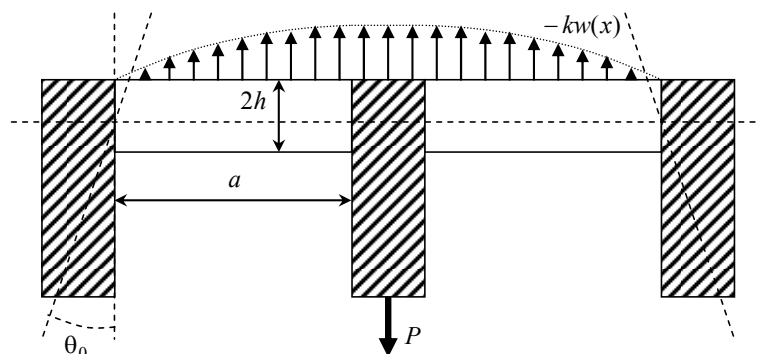


Figure 5:
 Scheme of a model of pulling out a sheet

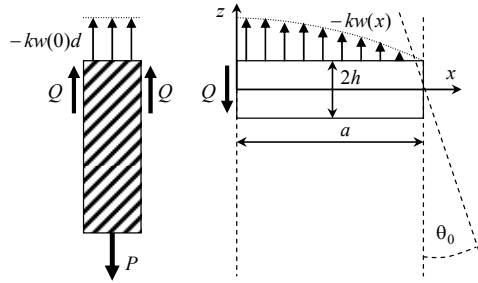


Figure 6: Analytical scheme of pulling out a paper sheet

Differential equation of flexion of an adhesive layer on an elastic substrate in the form of arching of an elongated rectangular plate $w(x)$ (deflection along the arc) has a form (Pisarenko G, 1986):

$$\frac{d^4 w(x)}{dx^4} + 4\alpha^4 w(x) = 0 \tag{8}$$

where: $4\alpha^4 = k/D$, $D = 2Eh^3/3(1-\nu^2)$ - cylindrical rigidity of a plate.

Considered problem comes down to mitigation of the equation (8) with boundary conditions:

$$w(x)|_{x=a} = 0, \quad -\frac{dw(x)}{dx}|_{x=a} = -\theta_0, \tag{9}$$

$$-\frac{dw(x)}{dx}|_{x=0} = 0, \quad -D\frac{d^3 w(x)}{dx^3}|_{x=0} = Q, \tag{10}$$

where the shearing force Q is connected to the pulling out force P with sheet equation of equilibrium (Figure 6):

$$P = 2Q - kw(0)d \tag{11}$$

3.3. Analytical research methods

The general solution of equation (8) is written down as

$$w(x) = B_1 W_1(x) + B_2 W_2(x) + B_3 W_3(x) + B_4 W_4(x), \tag{12}$$

where particular solutions of the equation were introduced

$$W_1(x) = \cosh(\alpha x) \cos(\alpha x), \tag{13}$$

$$W_2(x) = \frac{1}{2\alpha} (\cosh(\alpha x) \sin(\alpha x) + \sinh(\alpha x) \cos(\alpha x)), \tag{14}$$

$$W_3(x) = \frac{1}{2\alpha^2} \sinh(\alpha x) \sin(\alpha x), \tag{15}$$

$$W_4(x) = \frac{1}{4\alpha^3} (\cosh(\alpha x) \sin(\alpha x) - \sinh(\alpha x) \cos(\alpha x)), \tag{16}$$

The four unknowns B_1, B_2, B_3, B_4 are founded by using the four boundary conditions (9), (10).

The final solution of an examined issue has following form

$$w(x) = + \frac{(-PZ_1(\alpha a) - 2D\theta_0 W_3(a))W_1(x)}{dkZ_1(\alpha a) + 2DZ(\alpha a)} + \frac{(PZ_2(\alpha a) + 2D\theta_0 W_1(a) - dk\theta_0 W_4(a))W_3(x)}{dkZ_1(\alpha a) + 2DZ(\alpha a)} - \frac{(PZ(\alpha a) - dk\theta_0 W_3(a))W_4(x)}{dkZ_1(\alpha a) + 2DZ(\alpha a)} \tag{17}$$

where:

$$Z(\alpha a) = \frac{\sin(2\alpha a) + \sinh(2\alpha a)}{4\alpha}, \quad [18]$$

$$Z_1(\alpha a) = \frac{\cos(2\alpha a) + \cosh(2\alpha a) - 2}{16\alpha^4}, \quad [19]$$

$$Z_2(\alpha a) = \frac{\cos(2\alpha a) - \cosh(2\alpha a)}{8\alpha^2}. \quad [20]$$

A shearing force is presented in the form:

$$\begin{aligned} Q(x) = & -D \frac{4\alpha^4(-PZ_1(\alpha a) - 2D\theta_0W_3(a))W_2(x)}{dkZ_1(\alpha a) + 2DZ(\alpha a)} + \\ & + D \frac{4\alpha^4(PZ_2(\alpha a) + 2D\theta_0W_1(a) - dk\theta_0W_4(a))W_4(x)}{dkZ_1(\alpha a) + 2DZ(\alpha a)} - \\ & - D \frac{(PZ(\alpha a) - dk\theta_0W_3(a))W_1(x)}{dkZ_1(\alpha a) + 2DZ(\alpha a)} \end{aligned} \quad [21]$$

Normal tensions ($\sigma_y = \nu\sigma_x$) and tangential cross-section of the adhesive layer is calculated by the formulas

$$\sigma_x(x) = \frac{3z}{2h^3} M_x(x), \quad \sigma_{xz}(x) = \frac{3Q(x)}{4h^3} [h^2 - z^2] \quad [22]$$

where the bending moment has the form:

$$\begin{aligned} M_x(x) = & + D \frac{4\alpha^4(-PZ_1(\alpha a) - 2D\theta_0W_3(a))W_3(x)}{dkZ_1(\alpha a) + 2DZ(\alpha a)} - \\ & - D \frac{(PZ_2(\alpha a) + 2D\theta_0W_1(a) - dk\theta_0W_4(a))W_1(x)}{dkZ_1(\alpha a) + 2DZ(\alpha a)} + \\ & + D \frac{(PZ(\alpha a) - dk\theta_0W_3(a))W_2(x)}{dkZ_1(\alpha a) + 2DZ(\alpha a)} \end{aligned} \quad [23]$$

According to accepted models the normal tension $\sigma_z = -k\omega(0)$ created in a layer of adhesive binding in place of contact with the pulled sheet of paper

$$\sigma_z = -k \frac{-PZ_1(\alpha a) - 2D\theta_0W_3(a)}{dkZ_1(\alpha a) + 2DZ(\alpha a)} \quad [24]$$

In this study a theory of the biggest energy of exclusively figural strain has been used (*Huber - Mises - Hency* energetic strain theory).

$$\sqrt{\sigma_x^2 + \sigma_y^2 - \sigma_x\sigma_y + 3\sigma_{xz}^2} \leq [\sigma], \quad [25]$$

where $[\sigma]$ - acceptable tension.

For the calculation of tensions in dimensionless form, the dimensionless coordinates will be introduced:

$$\xi = x/a, \quad 0 < \xi < 1, \quad \zeta = z/a, \quad -H < \zeta < H \quad [26]$$

and the dimensionless functions and parameters:

$$w(\xi) = \frac{w(\xi a)}{a}, \quad m_x(\xi) = \frac{M_x(\xi a)}{Da^{-1}}, \quad q(\xi) = \frac{Q(\xi a)}{Da^{-2}}, \quad [27]$$

$$\Lambda = \alpha a, \quad \delta = \frac{d}{a}, \quad H = \frac{h}{a}, \quad q = \frac{Qa^2}{D}, \quad p = \frac{Pa^2}{2D}. \quad [28]$$

$$\sigma_* = (1 - \nu^2)[\sigma]/E, \quad \sigma_k = (1 - \nu^2)\sigma_z/E. \quad [29]$$

Dimensionless mitigation of the problem has the form:

$$w(\xi) = -pw_p(\xi) - \theta_0 w_\theta(\xi) \quad [30]$$

where:

$$w_p(\xi) = \left(Z_1^* w_1(\xi) - Z_2^* w_3(\xi) + Z^* w_4(\xi) \right) / z^* \quad [31]$$

$$w_\theta(\xi) = \left\{ w_3^* w_1(\xi) - w_1^* w_3(\xi) + 2\delta\Lambda^4 (w_4^* w_3(\xi) - w_3^* w_4(\xi)) \right\} / z^* \quad [32]$$

$$w_1(\xi) = \cosh(\Lambda\xi) \cos(\Lambda\xi), \quad [33]$$

$$w_2(\xi) = \frac{1}{2\Lambda} (\cosh(\Lambda\xi) \sin(\Lambda\xi) + \sinh(\Lambda\xi) \cos(\Lambda\xi)), \quad [34]$$

$$w_3(\xi) = \frac{1}{2\Lambda^2} \sinh(\Lambda\xi) \sin(\Lambda\xi), \quad [35]$$

$$w_4(\xi) = \frac{1}{4\Lambda^3} (\cosh(\Lambda\xi) \sin(\Lambda\xi) - \sinh(\Lambda\xi) \cos(\Lambda\xi)) \quad [36]$$

$$w_1^* = \cosh(\Lambda) \cos(\Lambda), \quad [37]$$

$$w_2^* = \frac{1}{2\Lambda} (\cosh(\Lambda) \sin(\Lambda) + \sinh(\Lambda) \cos(\Lambda)), \quad [38]$$

$$w_3^* = \frac{1}{2\Lambda^2} \sinh(\Lambda) \sin(\Lambda), \quad [39]$$

$$w_4^* = \frac{1}{4\Lambda^3} (\cosh(\Lambda) \sin(\Lambda) - \sinh(\Lambda) \cos(\Lambda)), \quad [40]$$

$$z^* = 2\delta\Lambda^4 Z_1^* + Z^*, \quad [41]$$

$$Z^* = \frac{1}{4\Lambda} (\sinh(2\Lambda) + \sin(2\Lambda)), \quad [42]$$

$$Z_1^* = \frac{1}{16\Lambda^4} (\cosh(2\Lambda) + \cos(2\Lambda) - 2), \quad [43]$$

$$Z_2^* = \frac{1}{8\Lambda^2} (\cosh(2\Lambda) - \cos(2\Lambda)) \quad [44]$$

Therefore a non dimensional tension being created in an adhesive layer of a book spine in a point of contact with a sheet being pulled out is:

$$\sigma^* = -\frac{8}{3} \Lambda^4 H^3 \frac{-pZ_1^* - \theta_0 w_3^*}{z^*}, \quad [45]$$

Condition durability according to the adopted hypothesis of Huber will take the dimensionless form

$$\sigma_i = \sqrt{(1 - \nu + \nu^2) \zeta^2 m_x^2(\xi) + \frac{3}{4} (H^2 - \zeta^2)^2 q^2(\xi)}, \quad [46]$$

where: $q(\xi) = d^3 w(\xi) / d\xi^3$, $m_x(\xi) = -d^2 w(\xi) / d\xi^2$.

Condition (46) in the dangerous points located on the surface gives the possibility to determine the allowable tearing out force

$$p_{\max} = \frac{\theta_0 B + \sqrt{AX^2 + \theta_0^2 (B^2 - AC)}}{A}, \quad [47]$$

where:

$$A = A_m^2 \nu_1 \zeta^2 + A_q^2 \frac{3}{4} H \zeta, \quad \nu_1 = 1 - \nu + \nu^2, \quad [48]$$

$$B = A_m B_m \nu_1 \zeta^2 + A_q B_q \frac{3}{4} H \zeta, \quad H \zeta = (H^2 - \zeta^2)^2, \quad [49]$$

$$C = B_m^2 v_1 \zeta^2 + B_q^2 \frac{3}{4} H \zeta, \quad X = z^* \sigma_*, \quad A_m = -Z_2^*, \tag{50}$$

$$B_m = -2\delta\Lambda^4 w_4^* + w_1^*, \quad A_q = -Z^*, \quad B_q = -2\delta\Lambda^4 w_3^*. \tag{51}$$

When $\theta_0 = 0$, the allowable force takes maximum value

$$p_{\max} = \frac{X}{\sqrt{A}}, \tag{52}$$

Condition durability in adhesive layer in place of the book spine in contact with pulled sheet of paper according to the adopted hypothesis of Huber gives a limit on the tearing force

$$p \leq \frac{3X}{8\Lambda^4 H^3 Z_1^*} - \theta_0 \frac{w_3^*}{Z_1^*}, \tag{53}$$

Figure 7 represent the theoretical graph on how dimensionless pulling force of the sheet from the adhesive layer of book spine depends on the opening angle of the book sheets.

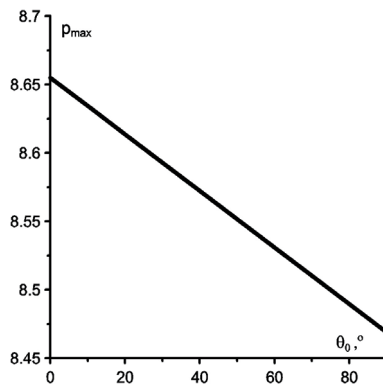


Figure 7: Dependency between dimensionless force tearing the sheet p_{\max} from the adhesive layer p_{\max} spine and the opening angle of the book sheets θ_0

3.4. Experimental results

To perform experimental Martini Tester’s device was used with a modernized system of mounting bindings. The upgraded construction of the measuring table allowed for testing of tearing sheets with the opening book angles $\alpha = 60^\circ, 80^\circ, 100^\circ, 120^\circ, 140^\circ, 160^\circ$ and 180° (Figure 8 a).

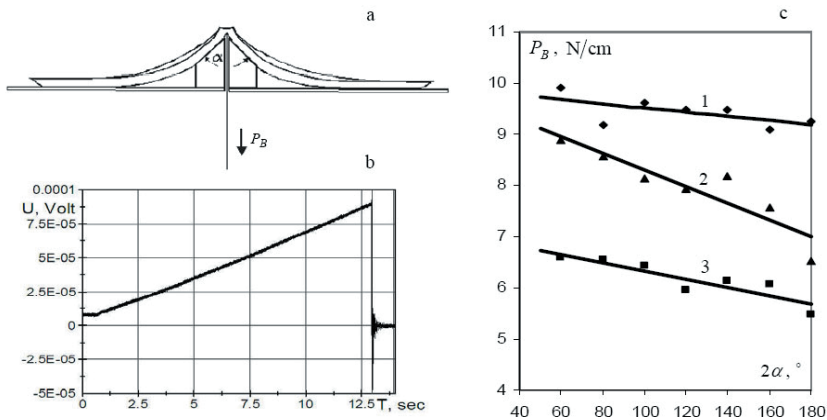


Figure 8: Influence of the book opening angle on an adhesive durability connection with the Pull Test method

- a - scheme of mounting binding with various opening angle α , P_B - the force tearing the sheet;
- b - oscillogram of computer registration sheet tearing force from the book spine, c - experimental results 1,2,3 - independent testing series of the books

In order to register the course of tearing cards from the back of book, the measuring system of the testing apparatus was equipped with sensors attached to the computerized measuring system. In Figure 8 b was shown a typical oscillogram of computer registration tearing force sheet from the spine of the binding. The tests were made in three independent testing series. In each series, the durability of 140 book made of different types of paper and sealed with *hot melt* glue were tested. As can be seen from chart (Figure 8 c), the book opening angle has a significant impact on the evaluation outcome of the strength of glued book. Obtained experimental results allow the consideration of the effects the book opening angle on the outcome of the evaluation in strength tests on different machines book testing. The results of experimental confirm the conclusions from theoretical research results evaluation of the durability of bindings.

4. Conclusions

The conducted researches allowed choose the kinematics parameters of processes of vibratory cutting away the signatures folds of the book blocks. It was shown, that intermittent cutting, when the knife comes out in a specific phase of the cycle of contact with the book block, is most preferable to realization of processes of vibratory milling.

This study proposed an improved mathematical model for the calculations of tensions generated in the book spine adhesive layer on which the pulling out force operates during testing the durability of the book. Taking into account the impact of the book opening angle on the pulling out force it is therefore possible to assess the durability of books, when different test devices were used.

References

- Komarow S., Petriaszwili G. (1989), *Dynamische Untersuchung des Vibrations-schneidens von Papier*. Maschinenbautechnik, 11 (38), p. 503-506.
- Liebau D., Heinze I. (2008), *Industrielle Buchbinderei*. Verlag Beruf + Schule, Itzehoe.
- Mordowin B. M. (1962), *Buchbindereimaschinen I*. VEB Verlag Technik, Berlin.
- Petriaszwili G. (2006) *Investigation of book block fold cutting equipment exploiting vibration cutting technique*. Proc. 6th International Conf. Vibroengineering. Kaunas, p. 84-86.
- Petriaszwili G. (2006), *Testing the bookbinding and facilities of creating the European standard*. Proc. International Conf. Printing technology SPb'06, St. Petersburg, p. 109-111.
- Petriaszwili G., Borowski P., Poliudow A., Kołomijec A. (1995), *Sposób obróbki grzbietów wkładów*. Patent RP. Nr 177365.
- Petriaszwili G., Pyryev Y. (2007), *An analysis of the tensions in adhesive layer during books operational use*. VIII Polygraficky seminar. Pardubice, p. 193-197.
- Pisarenko G, Agaew W., Kwitka A., Popkow W., Umanskij E. (1986), *Soprotiwlenie materialow*, Wyšča škola, Kiew.



2

Printing materials



The role of substrate structure in liquid transfer during heatset offset printing

*Carl-Mikael Tåg*¹, *Maunu Toiviainen*², *Mikko Juuti*², *Cathy Ridgway*³, *Patrick A. C. Gane*^{4,5}

¹ Forest Pilot Center Oy, FIN-21200 Raisio, Finland
E-mail: mikael.tag@fpc.fi

² VTT Technical Research Centre of Finland
PO Box 1199, FIN-70211 Kuopio, Finland,
E-mail: maunu.toiviainen@vtt.fi; mikko.juuti@vtt.fi

³ Omya Development AG, CH-4665 Oftringen, Switzerland
E-mail: cathy.ridgway@omya.com

⁴ School of Chemical Technology
Department of Forest Products Technology, Aalto University
P.O. Box 16300, FIN-00076 Aalto, Finland

⁵ Head of Research and Development
Omya Development AG, CH-4665 Oftringen, Switzerland
E-mail: patrick.gane@omya.com

Abstract

Fountain solution transfer to coated papers in a heatset printing process has been evaluated online. The porous coatings, applied as single coating onto a fine paper substrate, were calendered under different conditions to establish a range of porosities and pore structures whilst keeping the formulation, and hence the surface chemistry, constant. The transfer of fount to the papers was analysed from unprinted areas (non-image) and cyan printed areas at six different positions along the printing line, namely between each printing unit and after the dryer section, using near infrared absorption reflectometry. In this way, real time analysis of the amount of fountain solution (defined as water content) transferred to the paper per printing unit as a function of physical paper surface characteristics has been achieved. The role of printing speed and fountain solution dosage level on water uptake by the various coated paper substrates has been investigated. It was concluded that the higher the speed, the less the surface roughness becomes compressed and shorter is the time for the liquid to respond in respect to permeation and capillary uptake, resulting in less liquid transfer. It was also concluded that the image-area of the print functions as a stronger liquid carrier and at the same time hinders the evaporation of the liquid within the internal structure of the paper

Keywords: fountain solution, porous coatings, liquid carrier

1. Introduction

Liquid and moisture transport in porous media play an important role in a wide variety of processes. The liquid transport in a printing press, including both absorptive and permeative uptake, as well as evaporative mechanisms, has an effect on process stability/runnability, drying energy efficiency and optimisation, and may also impact on environmental concerns considering the effectiveness of recovery of volatile organic compounds used in the printing process. In a nip application process, such as printing, the absorption is driven by wetting forces internal to the structure, whereas permeation is pressure flow driven either by an external force or acting as a resistance against bulk flow once absorption has started.

The paper is wetted in the printing process by a film of fountain solution applied from the printing plate via the rubber blanket to the paper. The fountain solution acts to repel ink from the regions on the printing plate where no image is present. It is important that the fountain solution rapidly penetrates into the paper structure, or is otherwise removed from the surface of the paper, in order not to interfere with the ink from the subsequent colour units, known as ink repellence (Kipphan, 2001). The fountain solution is transferred to the paper in the printing nip and the resulting penetration is highly dependent on paper properties, such as, surface chemistry, surface roughness and pore structure. Adjustment of the fountain solution circulation rate,

flow rate and composition for various paper grades/surfaces, and the concentration adjustment during a press run, are all steered by the fountain solution picked up by the ink and the paper, and equilibrium is established determined by the print quality and press runnability. The effect of the ratio of the moisture content in the image area, namely that transported together with the ink film and/or applied at other colour stations in their respective non-image areas, to the respective non-image area is very important, especially when the image area is dominant and unbalanced in respect to area distribution on the overall printed sheet.

In this study, a technique described earlier, which samples directly the moisture content and its variation in the offset printing process at multiple locations is used (Tåg et al., 2010). The in-line noncontact measurements are facilitated by several near infrared (NIR) diffuse reflectance probes which are connected to both the light source and the spectrometer with optical fibres. Using a spectrograph, the polychromatic radiation from a single detection fibre is dispersed into a full spectrum in the wavelength range 1 000 - 2 100 nm. Presented in this work are some of the factors controlling how the paper surface and bulk characteristics affect liquid transfer in the individual printing units. The NIR measurement data illustrate the changes in moisture content as the paper is passing through the printing nips and dryer, respectively, and the analysis of the mechanisms involved highlight the roles of the contacting surfaces and the relative water carrier properties of the non-image and image areas.

2. Methods

2.1 Coating trials

The coating trials were performed at the Forest Pilot Center Oy, Raisio, Finland with the Valmet OptiConcept, Opticoat Jet application. A fine narrow particle size distribution ground calcium carbonate, having 75 wt-% of particles finer than 1 μm (nfGCC), CC75 (Covercarb 75, Omya AG, Baslerstrasse 42, CH-4665 Oftringen, Switzerland), was used as coating pigment. The Parker Print Surf (PPS 1.0, ISO 8791-4) roughness for the basepaper was 4.85 μm . The applied coat weight was 12.5 + 12.5 g m^{-2} as a (two side coating) single coat. 11 parts of styrene acrylic latex based on 100 parts pigment by weight (Acronal 504 D is a product name of BASF, Ludwigshafen, Germany) was used as binder. The solids content for the nfGCC colour was 66.2 %. Due to the decision to eliminate thickener from the formulation, so as to obviate the undesirable complicating factor of coating colour flocculation, the coater speed was set to 600 m min^{-1} in order to obtain the desired coat weight.

2.2 Calendering trials

After the coating, the reel was calendered over a series of pressures to achieve a range of different roughness levels and porosities. The target moisture content in the coating trials was 4.5 % for the case of retained uncalendered paper and 5.5 % when passing through the calender, resulting in a comparable target moisture content of 4.5 %. The calendering of the papers was performed with an Optiload calender (Metso Paper Oy). The paper web passed 4 + 4 nips (two calender stacks) with polymer and steel thermo rolls. The calendering conditions, and resulting surface gloss and roughness, can be found in Table 1.

Table 1: Trial point information

Trial points*	Line load Stack 1	Line load Stack 2	Online gloss 1 st calender stack	Online gloss 2 nd calender stack	PPS
	/kNm ⁻¹	/kNm ⁻¹	/%	/%	/μm
nfGCC coatings					
Uncalendered nfGCC	-	-	-	-	2.19
20 kNm ⁻¹	20	20	42	43	0.95
500 kNm ⁻¹	500	500	70	69	0.43

* For all calendered trial points, roll temperatures and speed were kept constant: 80 °C and 500 m min^{-1} , respectively

2.3 Printing trials

The printing trials were performed at the Forest Pilot Center Oy, Raisio, Finland, on a Heidelberg Web-8 heatset web offset printing machine with five over five printing units, i.e. with application potential for 5 colours applied to both sides of the paper. The printing plates used were Kodak Gold (Didp Gold - positive plates), together with Reeves Vulcan Alto Plus printing blankets from Trelleborg AB, Trelleborg Sweden. The press room conditions were held constant, maintained at 50 % RH (relative humidity) and temperature,

$T = 23\text{ }^{\circ}\text{C}$. The width of the paper web was 500 mm. The measurements were performed from both unprinted areas (non-image) and cyan printed areas, i.e. areas where only fountain solution was applied to the paper and areas where fountain solution was applied under and/or on top of the cyan ink layer according to the normal offset printing procedure. A schematic picture of the setup is presented in Figure 1.

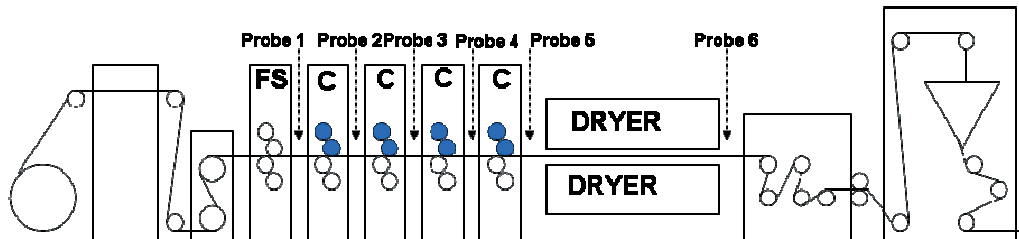


Figure 1: Printing machine and measurement probe setup

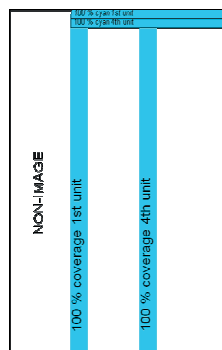


Figure 2: Printing layout. The size of the printed form area was $500 \times 630\text{ mm}^2$

2.4 Mercury intrusion porosimetry

Mercury intrusion porosimetry measurements were performed on a Micromeritics Autopore IV porosimeter using the technique described by Ridgway and Gane (Ridgway, 2003b). In the data analysis, the obtained intrusion values were corrected using a spreadsheet-based program Pore Comp (Environmental and Fluid Modelling Group, University of Plymouth, UK) to correct for mercury compressibility and penetrometer expansion effects (Gane et al., 1996).

2.5 Permeability measurements

A coated paper substrate permeability is obtained using hexadecane by pre-saturating the compacted paper layered sample and applying an external pressure to a liquid head (also hexadecane), and measuring the flow rate through the sample. More details of the measurement setup can be found in (Ridgway et al., 2003a).

2.6 Near-infrared measurement setup

The multipoint NIR instrument utilised in this work is designed to perform diffuse reflectance measurements over the full NIR wavelength range simultaneously at multiple locations. It consists of a halogen lamp as light source and an NIR spectral camera (SWIR Spectral Camera, Specim Ltd., Oulu, Finland) as spectrometer as well as several customised diffuse reflectance probes with fibre-optic illumination and detection. The angle of incident of the probe beam in relation to the normal of the paper was 20° . The vibration of the paper web in the z -direction was allowed to be maximally $\pm 5\text{ mm}$. The measurement probes were mounted into six positions in the printing process, i.e. between each printing unit and after the dryer section (Figure 1). A more detailed description of the NIR device can be found in (Täg et al., 2010).

The moisture profiles were estimated as the area of the NIR absorption peak for water manifest between the wavelengths $1\ 900 - 2\ 000\text{ nm}$. Conventionally, the linearity of measured spectral data is enhanced by subjecting them to the $\log(1/R)$ transform, where the reflectance at the wavelength λ is given by:

$$R(\lambda) = \frac{I(\lambda) - D(\lambda)}{W(\lambda) - D(\lambda)} \quad [1]$$

in which the numerator in Equation [1] consists of the raw signal $I(\lambda)$ corrected for the instrumental dark current $D(\lambda)$, whereas the denominator contains the instrumental response, i.e. the white reference $W(\lambda)$ after dark-correction. The white reference was measured with the non-absorbing material Teflon[®], which has high white scatter with no absorption bands in the NIR wavelengths. The instrumental response was measured using the white reflectance standard (Gigahertz-Optik, Germany) at the beginning and at the end of the trial day, and the dark current was measured hourly. The integration time of the detector was set to 7 ms, and the frame rate was 100 Hz.

2.6.1 Calibration setup and measurements

To obtain quantitative moisture profiles for the experiments performed on the printing press, the measured NIR data should be related to absolute moisture values. The calibration measurements were conducted using the commonly known loss-on-drying method, so that the sample NIR spectrum and weight were measured simultaneously, and subsequently expressed as:

$$\text{Moisture}(\%) = 100 \times \frac{m_{\text{wet}} - m_{\text{dry}}}{m_{\text{wet}}} \quad [2]$$

where m_{wet} is the weight of wet paper, at each stage of drying, and m_{dry} is its dry weight.

To mitigate the effect of measurement error, the loss-on-drying measurement was repeated five times with different samples of the same paper. A more detailed description of the calibration setup can be found in (Tåg et al., 2010).

3. Results and discussion

Multipoint online moisture determination in real-time was obtained via six different locations along the printing line, namely between each printing unit and after the dryer for both non-image and cyan printed areas, to form a moisture profile as a function of time and position. The effect of printing speed and fountain solution volume on the water uptake by the paper was investigated in combination with the drying capability of the press in respect to paper total moisture.

The porosimetry peak to the right in Figure 3, at larger pore diameters, represents the basepaper/coating basepaper interaction pore structure giving the paper its absorption volume capacity properties. These larger connected pores also control the permeability properties of the paper. The smaller peaks to the left represent the coating pore structure and give the paper its surface capillary-driven absorption rate properties. Maintaining constant surface chemistry and applying different calendering conditions enabled a series of coated papers with a defined range of porosity and permeability. The basepaper peak reduces in both volume and pore diameter as the calendering conditions are increased in pressure, in that the structure becomes denser with higher calendering conditions. The coating structure peak is also affected by the calendering conditions, both in terms of total pore volume and pore diameter.

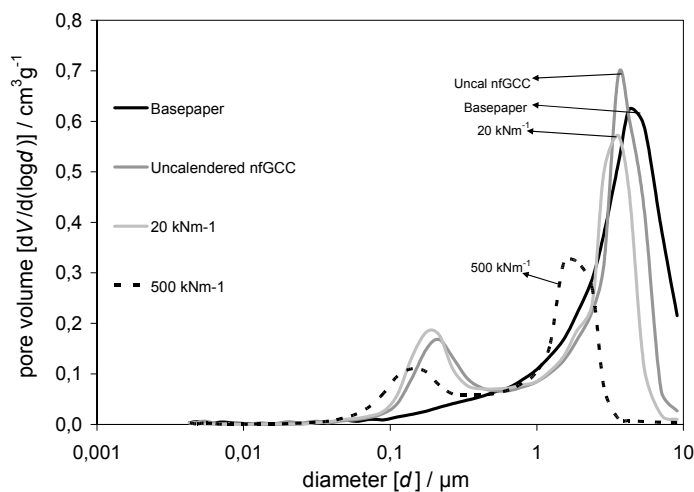


Figure 3: Pore size distribution of the paper samples showing the basepaper and the coating layer-basepaper peaks

In Figure 4, the liquid permeability results are presented in respect to the Darcy permeability factor (Darcy, 1856). The permeability is controlled by the larger connected pores in the structure. For flow in the z-direction, i.e. perpendicular to the plane of the paper, the basepaper displays the highest permeability in the layered structure in contrast to when the coating has been applied. Nonetheless, amongst coatings generally, the nfGCC coating has relatively high permeability, and thus can respond rapidly to the increase in fountain solution volume on the paper surface, letting the nip pressure to some extent force the liquid in. The different calendering levels of the nfGCC coated paper present a decreasing permeability as a function of increasing linear load in the calendering nips. The larger peaks of the porosimetry differential curves follow also this trend.

The differences in wetting are very significant when evaluating a printing process where the liquid is applied under contact conditions, depending on the relationship between liquid volume and the surface rugosity (nip voidage), especially considering rough/matt papers at low delivery volumes of fountain solution. Roughness determines whether a thin film of fountain solution fills the blanket-coating gap. If not filled, then only capillarity can act. If filled, then capillarity and permeability (response to external pressure) can act together, though the more permeable coating has the lower capillary force, normally, as the pores are either larger and/or more uniform and/or more connected. By way of contrast, for a highly viscous paste-like liquid, such as an offset ink, the penetration and spreading are determined by the rheological properties rather than by the surface tension, which does not have such a strong influence on the wetting dynamics under pressure.

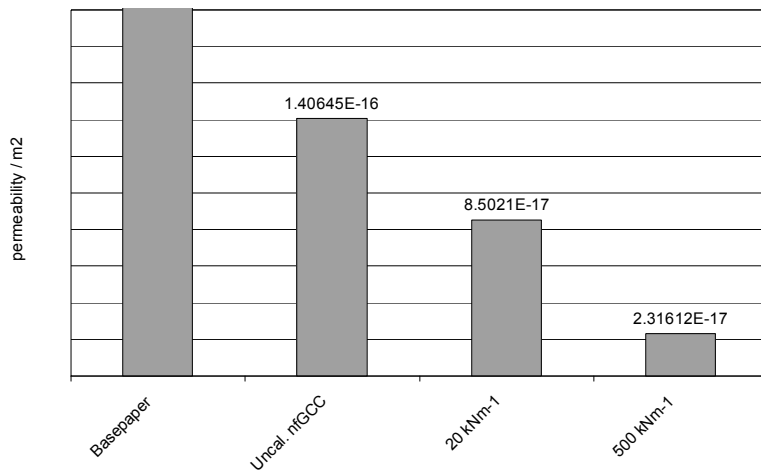


Figure 4: Liquid permeability results

3.1 Dynamic liquid transfer in printing

In Figure 5, the amount of fountain solution transferred to the uncalendered nfGCC coated paper is studied as a function of printing speed.

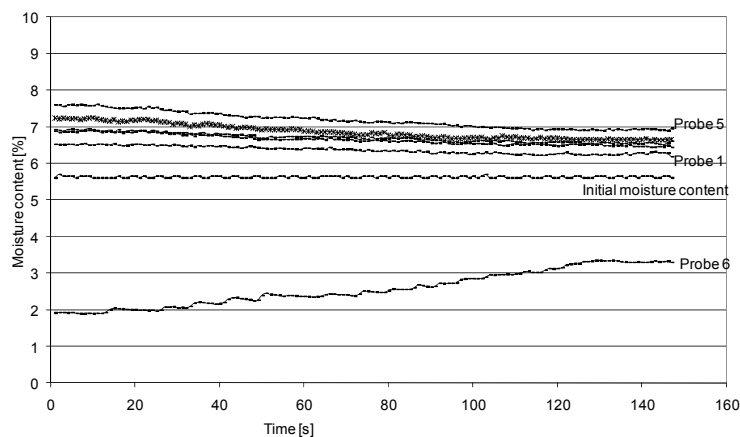


Figure 5: Changes in liquid water pick-up by paper as a function of printing speed spread over time. The coated paper was kept uncalendered. The printing speed was 13000 rph (2.5 ms^{-1}) in the beginning of the trial point and 40000 rph (7.0 ms^{-1}) at the end with continuous speed change of the fountain solution delivery to the printing plate

As the printing speed is increased, the machine automatically compensates the delivery of the fountain solution volume linearly. However, as the printing speed increases, less fountain solution is seen to be transferred to the paper. The permeable structure of the nfGCC can be expected not to hinder greatly the pressure-driven flow. We may conclude, therefore, that the reduced transfer is probably related to the rough surface acting to reduce the print nip pressure by increasing the non-contact volume together with the reduced residence time in the printing nip. It is also seen that, as the printing speed increases, the drying efficiency of the paper in the heated oven is decreasing.

The higher the speed, the less is the compression of the surface roughness relating to the viscoelastic nature of paper, and the less time there is for the liquid to respond in contact to capillary forces. The results indicate clearly that the surface void roughness in the first printing nip is of great importance. This void roughness means low pickup despite the high permeability at the surface at the first unit (Probe 1) despite the permeable coating structure. To illustrate this we can consider now the results shown in Figure 6, in which the dosage of fountain solution was adjusted from a minimum value to its maximum at a given printing speed. The results indicate that, initially at lower fountain solution delivery volumes the nfGCC coating takes up fountain solution during printing by capillarity. As the dosage level is increased, the amount of fount transferred to paper increases linearly. The strongest inclination is seen for Probe 5. This supports the hypothesis mentioned above, in that the volume of liquid must be equal to, or exceed, the blanket-coating contact volume before significant pressure-driven permeation can occur. The nfGCC coating is permeable, and so once the fountain solution volume becomes sufficient the response to uptake is determined finally by permeability.

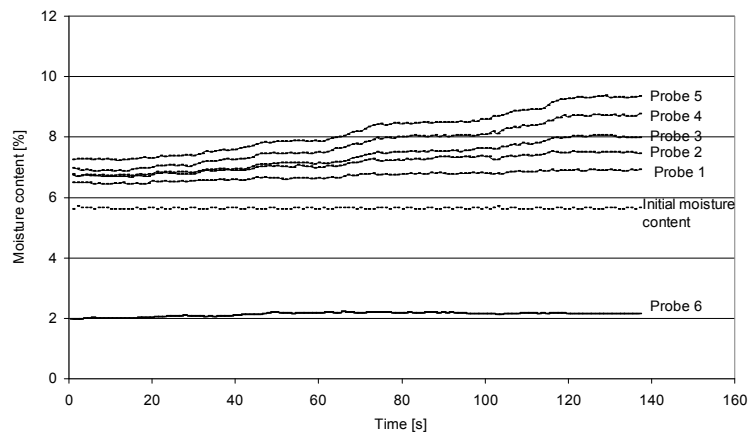


Figure 6: Liquid pick-up (fountain solution) by coated paper as a function of fountain solution dosage at constant speed. The dosage level of fountain solution was changed from minimum to maximum. The coated paper was kept uncalendered. The printing speed was 18000 rph (3.0 ms^{-1})

In Figure 7, the results from printing at the various paper trial points with different calendering levels of the coatings are presented.

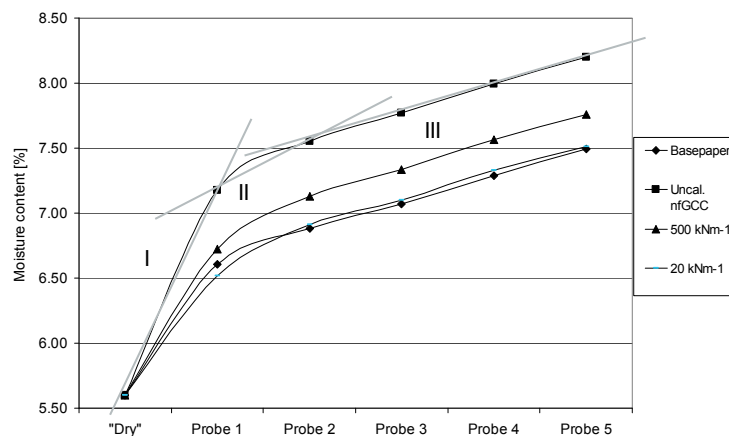


Figure 7: Liquid uptake (fountain solution) by coated paper. The paper coating consists of 100 parts nfGCC pigment and 11 parts latex applied as a single coat (12.5 gm^{-2} per side). The printing speed was 18 000 rph (3 ms^{-1})

For Probe 1 the liquid uptake is lower for the calendered samples compared to the uncalendered sample. The liquid uptake increases as a function of paper passing further printing units. These findings conclude that the mechanism of liquid transfer in subsequent units is controlled by splitting of the liquid film and whatever permeation is able to occur as a function of permeability, which necessarily for calendered coated papers is very low.

The liquid water uptake by the paper as a function of printing units passed (Figure 7) can thus be divided into three regions. In the first region (I), the paper is initially wetted and strong capillary forces act to imbibe the liquid inside the paper leaving the surface void volume essentially empty until it enters the second unit. In the second region (II), the paper structure is partly filled with liquid and surface saturation takes place such that after the second unit further transport inside the paper takes place but then the liquid volume compared to the surface void volume becomes equalized when entering the third unit. In region (III), the linear trend for the last three printing units indicates a saturated surface which takes up more liquid directly via permeation and film splitting. At surface saturation, a “calendered equivalent plane” is created. The transition between region (II) and region (III) is bound to be less distinct, but by definition has to exist simply in terms of mass balance. Thus, for smooth surfaces, or sufficient fountain solution, the solution is drawn into the coating after the nip to a point where the surface menisci balance, or excess remains, respectively, i.e. they are level with the surface or a film remains, depending on the coating capacity and absorption rate. This makes then the “saturated equivalent plane” so that the subsequent dynamics on a relatively non-permeable surface are that of film split followed only by capillarity until the next planar contact, and so on (see Figure 8). Thus, subsequent units on a rough surface behave the same as a calendered surface, in the case where permeability is low, with the water transforming the surface into an aquaplane, i.e. the liquid fills the surface voids between the particles/surface roughness and saturates the surface structure.

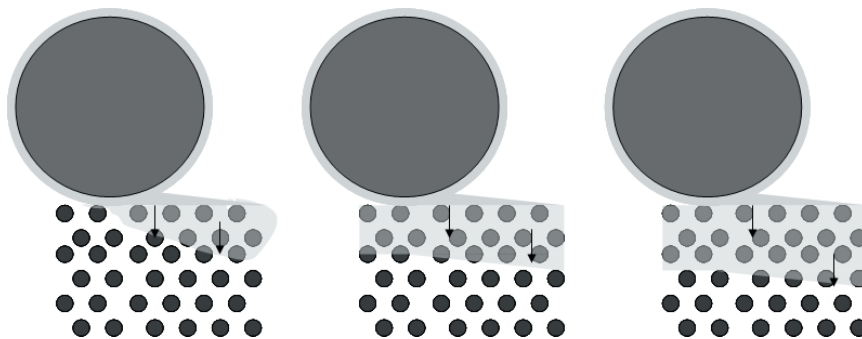


Figure 8: Fountain solution transfer to coated paper surface when surface saturation can occur. First unit is surface roughness dependent, and at subsequent units further capillary transport inside the paper occurs together with film splitting at the blanket roller-paper coating interface

Figure 8 shows the effects during fountain solution application schematically as follows:

- a) the surface voids are progressively filled at the first unit according to the surface roughness conditions, and capillarity is initiated. Then,
- b) the capillarity acts to absorb liquid to the level of the surface profile between units, and
- c) the subsequent units deliver according to film split dynamics a fixed amount of fountain solution, provided permeability is low, and each time this gets absorbed by capillarity to create menisci at the surface profile level provided coating pore volume capacity is sufficient and the volume of fountain solution is not excessive in relation to the capillarity present.

Deviation from this model can occur at step c) if the surface is highly permeable, such that pressure penetration, developed in the case where an excessively high volume of fountain solution is delivered to the surface, will cause additional pressure permeation to occur in the nip.

In Figure 8, we note that there will be a fixed difference between the sequential probes that is independent of calendering, i.e. only the first unit delivers more on an uncalendered sheet and then progressively less on the increasingly calendered sheets. In general, saturation is considered to be a bulk property and depending on the penetration depth of a liquid. The basepaper acts effectively as an infinite sink such that the coating pore volume and structure dominate provided the basepaper coverage is high. Poor coverage would mean that the

basepaper plays a greater role. Thus, it needs to be understood that in this study saturation refers to the saturation near the surface of the porous material. These surface-limited saturation criteria assume an infinite capacity in the coating layer. However, in case of high fount dosage and high printing speed, it is possible that the liquid distribution and the liquid flow is interfered with, so that liquid accumulation or liquid “pools” will arise if the permeability is low, i.e. a liquid layer builds up between the rubber blanket and the paper. As described, the rubber blanket roller further transports the ink and fountain solution not attached to the paper and this might cause problems or even become impossible to handle - an effect similar to aquaplaning. The fount which is not utilised will build up on the respective rollers and on the plate, resulting in streaking and uneven ink distribution, which is beyond the control of the printer, defined by Gane as aquapiling (Gane et al., 2007). The flow resistance of liquid escaping an advancing cylinder generates pressure. The pressure might lift the cylinder in a similar manner to aquaplaning. The nip pressure driven permeation transport thus becomes insensitive due to the liquid saturated surface. The pore space is too small to be invaded by the nip pressure and/or the permeability is too low, i.e. the surface pore volume containing liquid is effectively hydraulically isolated because of the lubrication effect under aquaplaning. The hydraulic isolation is even more pronounced on smoother calendered surfaces. Samples with different pigment particle sizes and pore structure may, therefore, have similar water saturation but require the nip pressure to act without aquaplaning to reach the complete saturation point.

3.2 Image versus non-image areas

Some speculations of the role of incident NIR penetration and the measured absorbance band are relevant concerning the two scenarios, namely moisture determination of printed and non-image area. When fountain solution is added to the surface and some penetrates into the substrate, the absorbance in the coating layer increases. When a pure ink layer is applied, it is assumed to be that the surface reflectance is at its maximum when the ink is liquid (wet) and somewhat lower when dry. When fount is applied first followed by ink, the high surface reflectance concentrates the NIR penetration within the surface sub-layers only, where the moisture is concentrated. The penetration depth might change in the case of a wet ink surface compared to a non-image surface, but this needs further investigation and is at this stage only an assumption. The porosity of the substrate and the coating pigment particle size should, however, have a stronger influence on the penetration depth than the ink layer itself. The measurements showed that the sample which was the most heavily calendered, scatters the least back to the detector as a result of the tight packing structure. Hence, the amount of solid-air interfaces in the matrix is reduced, due to the nature of the thermal plasticity of the binder, causing less diffuse reflectance and an increase in specular reflectance. The increase in specular reflection is also seen because the surface of the sheet becomes more planar.

Figure 9 presents the determination of the moisture content of non-image and cyan printed paper. Cyan ink was applied from two printing units, on separate patch areas. This results in the situation that fountain solution is applied under the ink layer and on top of the ink layer depending on the studied printing unit.

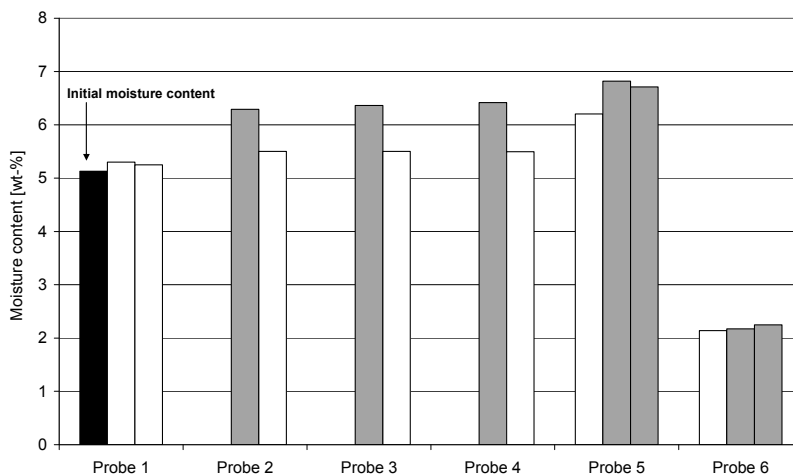


Figure 9: Moisture content of paper as a function of printing nips passed. The initial moisture content (black bar) was determined with Probe 1 when running plain paper through the machine. White bars indicate measurement from a non-image area and grey bars from a cyan area, respectively. The speed of the printing machine was 18 000 rph (3.5 ms^{-1}) and the web temperature in the dryer was $130 \text{ }^\circ\text{C}$

As an example:

Probe 2 measured a cyan patch on top of a layer of fount, i.e. one layer of fount was applied under the ink from the first unit.

Probe 5 measured a cyan patch on top of four layers of fount after the fifth unit.

Probe 5 after being moved also measured a cyan patch where cyan was applied from the second unit, meaning one fount layer under the ink, then three layers of fount on top of the ink.

Again, very logically, an increase in moisture content is observed as the paper passes the printing nips. But also another interesting observation can be made. A strong increase in moisture content of the paper is seen at the probe where the ink layer is applied. This indicates that the ink carries a lot of emulsified fount which increases the moisture content significantly. When the fountain solution is applied on top of an ink layer, the possibility is that the liquid is not able to penetrate through the ink layer, but is squeezed to the sides/edge between ink and non-image area or continues further with the rubber roller as a result of reticulation.

All trial points have the same moisture level after the dryer. This indicates that the combination of drying temperature and printing speed is in balance. An unbalanced drying profile causes stress gradients in the paper sheet which might be observed as a waving feature of the printed paper (Kipphan, 2001).

Considering liquid transport to non-image areas and liquid carriage by printing ink, it was found that the studied areas contain a different amount of moisture, with this ink type and this specific substrate, the inked areas carrying a higher level of moisture. The variations in moisture content can be related to the paper properties (how much liquid a paper can take up) and the ink closing the surface and preventing the moisture from evaporating. As the two areas run into the dryer, an imbalance in the paper occurs during drying, which causes a stronger shrinkage in the non-image areas. Figure 10 presents the moisture contents of printed and non-image paper directly after the drying section. The results clearly show that the printed areas of the web dry slower, resulting in higher moisture content. The ink layer seals the surface, preventing or slowing down the evaporation of the internal paper moisture (partly existing from the manufacturing process and partly transferred in the printing process under the ink). This imbalance in moisture content is further supported by a mixed proportion of surface drying temperature, and machine speed if varied. The heavily inked areas may even cause blisters as the moisture vaporising force increases as the vapour tries to escape out from the structure (Kipphan, 2001).

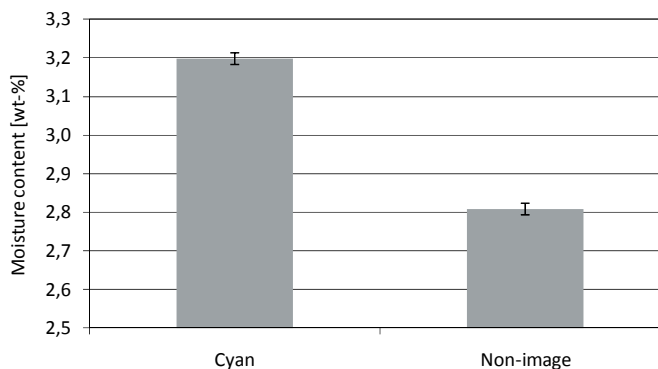


Figure 10: Effect of drying on moisture content in the cyan printed and non-image areas. The measurement probe was scanning after the dryer. The speed of the printing machine was 13 000 rph (2.5 ms^{-1}) and the web temperature in the dryer was $120 \text{ }^{\circ}\text{C}$

4. Conclusions

The amount of fountain solution transferred to coated paper has been determined from multiple locations and in real time by means of NIR reflectance spectroscopy. This novel analysis provides a means of defining the pore structure characteristics of a coated paper surface and bulk in order to obtain optimal press performance in terms of preventing liquid water interference in offset printing. Comparing image and non-image areas clearly demonstrates the imbalance in moisture content that can result during drying, and which can lead to dimensional instability of the paper due to uneven shrinkage behaviour.

In respect to fountain solution uptake, it can be concluded that the first unit delivers fountain solution proportional to surface roughness, provided the volume of fountain solution is not excessive such that pressure penetration would be initiated when the permeability of the coating is high, or the amount of fountain solution is so small as to be independent of volume filling, and the subsequent units deliver fountain solution according to film split only, in the case where permeability is limiting. The controlling factors have been determined to be,

- (i) the volume of fountain solution delivered in the printing nip in relation to the surface contact coating voidage, i.e. roughness,
- (ii) the capillarity of the coating and its ability to remove fountain solution from the surface,
- (iii) the permeability of the coating once sufficient surface film continuity is reached either in relation to fountain solution volume applied or the smoothness of the sheet, and
- (iv) the capacity in respect to pore volume of the coating.

It has been possible, therefore, to deduce the coating structure conditions prevailing that lead to either a dominance of capillarity, permeability or film split, each controlled by the fine pore fraction $< 0.1 \mu\text{m}$, the pore connectivity and uniformity of size and coating pore capacity (permeability and saturation), respectively.

Acknowledgements

Forest Pilot Center Oy (www.fpc.fi) is thanked for the printing trial time at the heatset printer. Omya Development AG is acknowledged for the funding of the project.

References

- Darcy, H., (1856), *Les Fontaines Publiques de la Ville de Dijon*, Dalmont, Paris.
- Gane, P.A.C., Kettle, J.P., Matthews, G. P., Ridgway C.J., (1996), *Void Space Structure of Compressible Polymer Spheres and Consolidated Calcium Carbonate Paper-Coating Formulations*, *Ind. Eng. Chem. Res.* 35 1753.
- Gane, P.A.C., Ridgway, C.J., Burri, P., Arnold, M., Kagerer, K.-H., Madden, B., Ristolainen, M., Purontaus, J., (2007), *Aquapiling: Coated Substrate-Related Influences on Reverse Piling from a One-Side Single Colour Image in Multicolour Offset Printing*. *Advances in Printing and Media Technology, Vol. XXXIV*, Eds. N. Enlund & M. Lovreček, Acta Graphica Publishers, Zagreb, 31-48.
- Kipphan, H., (2001), *Handbook of print media - Technologies and production methods*, Springer-Verlag Berlin Heidelberg New York, 2001.
- Ridgway, C.J., Schoelkopf, J., Gane, P.A.C., (2003a), *A new method for measuring the liquid permeability of coated and uncoated papers and boards*. *Nordic Pulp and Paper Res. J.*, 18 379.
- Ridgway, C.J., Gane, P.A.C., (2003b), *Bulk density measurement and coating porosity calculation for coated paper samples*, *Nordic Pulp and Paper Res. J.*, 18 24.
- Tåg, C.-M., Toiviainen, M., Juuti, M., Gane, P.A.C., (2001), *Dynamic analysis of temporal moisture profiles in heatset printing studied with near-infrared spectroscopy*. *Meas. Sci. Technol.* 2010 21 11

The effect of coating pore structure and geometry on the drying efficiency of heatset web-offset ink solvent

*Philip M. Gerstner*¹, *Hai Zhang*¹, *Patrick A. C. Gane*^{1,2}

¹ Aalto University, School of Chemical Technology
Department of Forest Products Technology
P.O. Box 16300, FIN-00076 Aalto, Finland
E-mail: firstname.lastname@aalto.fi

² Omya Development AG
CH-4665 Oftringen, Switzerland
E-mail: patrick.gane@omya.com

Abstract

This work examines the effect of coating pore structure on the evaporation behaviour of mineral oil - a typical ink solvent. Two different kinds of coating pigments are compared, the first one being a standard ground calcium carbonate (GCC), the second one a highly porous modified calcium carbonate (MCC) with fine intraparticle pores, as might be used in offset and inkjet coatings, respectively. The aim is to identify relevant pore structure parameters of the corresponding systems and their effect on the drying rate.

Two internal stages of drying were identified for both structures: a rising drying rate period and a falling rate period as temperature is increased. In the rising rate period, the effect of film flow was of particular relevance for the case of GCC based structures: binder, filling the pore structure, decreases the internal surface detail of geometry and thus reduces the film flow tendency, progressively depressing the drying rate. At the onset of the falling rate period the liquid phase is in the form of disconnected liquid clusters. Therefore, the diffusion resistance becomes a dominant factor in determining the drying rate during this latter period. Because of the high permeability of MCC systems the evaporation rate proved to be largely unsusceptible to the binder concentration. However, the GCC pigment systems, because of their lower permeability, exhibited an extended peak of the drying rate as a result of the increasing diffusion resistance with increasing binder content.

Keywords: coating structure, capillary vapourisation, film flow, heatset printing

1. Introduction

Drying of porous media is one of the most common operations found in a variety of industries, such as construction, mineral processing, ceramics, food, agriculture and pharmaceuticals. Today, continuously rising energy prices and more stringent environmental requirements, in combination with a raised awareness of carbon emission, demand more attention than ever to be given to the issue of energy efficiency in drying operations. In heatset web-offset about 30-50% of the total energy is used for process heating and cooling, while the efficiency of the actual drying is estimated to be in the order of merely 1-2% (PrintCity, 2008; Frank, 1996). Similar demands are emerging in the drying of inkjet inks from within porous structures, as speeds of printing using this digital technique are increasing. In this work, the effect of the paper coating pore structure on the evaporation behaviour of mineral oil, a typical ink solvent, is investigated. Through the analysis of weight loss under controlled drying conditions, this study attempts to correlate the relevant pore structure parameters with drying rate and thus tries to identify ways to improve the drying efficiency from the perspective of a coated paper.

2. Materials and methods

2.1 Coating structures

Two different kinds of coating pigments are compared, while using the same latex binder material in various amounts. The first pigment is a standard ground calcium carbonate¹ (GCC), the other one a modified calcium

¹Hydrocarb 60, Omya AG

carbonate¹ (MCC). Since the MCC pigment is engineered for enhanced absorption rate and volume capacity, as used, for example, in coated media surfaces for the emerging high speed inkjet print engines, it forms a distinctly different coating structure compared to the GCC pigment. The different nature of the two types of pigment is illustrated in Figure 1.

Compared to GCC, the “egg” shaped MCC pigments (Ridgway et al., 2004) have small internal voids and on the surfaces, creating a structure with fine intraparticle pores. The binder chosen for both systems is a styrene acrylic-based polymer latex² (SA), since it displays a low level of interaction with ink oil (Rousu et al., 2002). Table 1 summarises the particle size data of the pigments and the latex used.

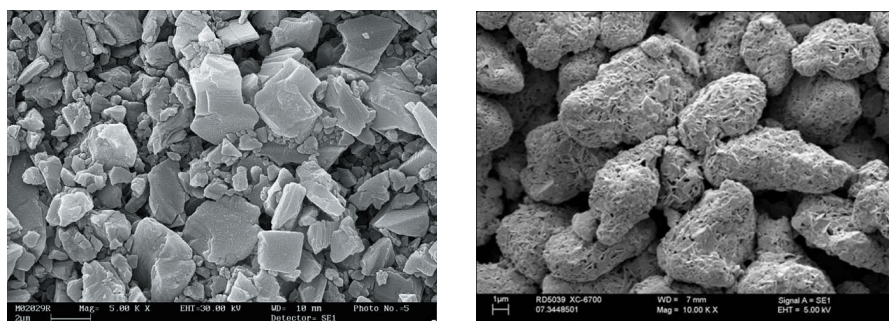


Figure 1: Left: SEM image of GCC (scale bar 2 μm) (Vidal et al. 2008). SEM image of MCC (scale bar 1 μm) (Gerstner and Gane, 2009). The dark regions on the pigment surface indicate access to intraparticle pores

Table 1: Particle size properties of GCC and MCC pigments and SA latex binder systems

	GCC ¹	MCC [*]
Latex		
Dosages [pph]	0, 4, 6, 8, 12	6, 8, 12, 20
Particle size [μm]	0.2	0.2
Pigment		
PSD [w/w%]		
< 5 μm	93	
< 2 μm	60	
< 1 μm	40	
d_{50} (weight median)	1.6	5.1

¹ Particle size determined by Sedigraph (Micromeritics)

^{*} Particle size determined by SEM

2.2 Thermogravimetry

For the pore size characterisation with mercury porosimetry as well as for thermogravimetric analysis (TGA), macroscopic tablets of the coating formulations were used as the basic material. They were formed following the method of Ridgway et al. (2004) in which the coating slurry was dewatered by an applied overpressure. In order to get small samples of uniform size, a core-drill was used to section a smaller pellet from each tablet, as was previously applied by Gerstner et al. (2010). Subsequently, the pellets were immersed to saturation in a mineral oil³, as found in typical offset ink formulations.

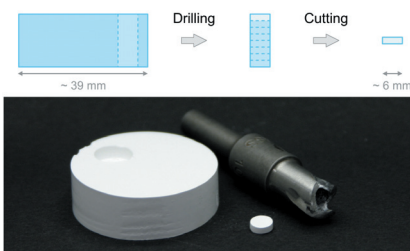


Figure 2: Core-drilling of a pigment tablet to create small, uniform pellets for the use in the TGA furnace (Veikkolainen, 2009)

¹ MCC 564, Omya AG

² Acronal S360D, BASF AG

³ PKWF 4/7, Haltermann Products

The TGA measurement was carried out with a Mettler Toledo TGA/SDTA851°. The pellets were saturated with mineral oil by contacting the lower surface with a liquid reservoir, ensuring no airlock formed, and allowing wicking to progress until no further absorption occurred. The saturated pellets were measured as soon as they were taken out of the mineral oil to avoid weight loss. No action was taken to remove the excess oil adhering to the exterior, but some drops of oil were removed by gently shaking the sample. This should be improved in future studies to avoid the complication of the first stage TGA - observed weight loss region - this will be discussed further in the results section. Based on the findings of a previous study (Gerstner et al., 2010), in which retardation of evaporation was seen according to binder level, the emphasis here is put on the evaporation of the mineral oil occurring in the temperature range of 50-250 °C. A relatively slow heating rate of 0.5 °Cmin⁻¹ was used to avoid a temperature gradient developing within the sample.

2.3 Porosimetry

Each (unsaturated) tablet material was also characterised by mercury porosimetry for both porosity and pore size distribution using a Micromeritics Autopore IV mercury porosimeter. The maximum applied pressure of mercury was 414 MPa, equivalent to a Laplace throat diameter of 0.004 µm. The mercury intrusion measurements were corrected for the compression of mercury, expansion of the penetrometer and, where appropriate, the compression of the solid phase of the sample using the equation of Gane et al. (1996):

$$V_{\text{int}} = V_{\text{obs}} - \delta V_{\text{blank}} + \left[0.175 \left(V_{\text{bulk}}^1 \right) \log(1 + P/1820) \right] - V_{\text{bulk}}^1 \left(1 - \phi^1 \right) \left(1 - \exp \left[\frac{(P^1 - P)}{M_{\text{ss}}} \right] \right) \quad [1]$$

where: V_{int} is the volume intruded into the sample,
 V_{obs} is the observed volume of intrusion,
 V_{blank} is the volume of mercury used in the blank experiment,
 V_{bulk}^1 is the bulk volume of the sample at 1 atm pressure,
 P is the pressure and
 M_{ss} the bulk modulus of the solid sample.

2.4 Liquid permeability

For an additional comparison in respect to the permeation properties for liquid and vapour, the liquid permeability of the different pore structures, formed by the GCC and MCC pigments, was measured adopting the method of Ridgway et al. (2003). In this method, a portion of the pigment tablet, formed by grinding into a cube (edge length ca. 10 mm), is embedded round its edges in resin. The embedded material is saturated with hexadecane, which does not interact with the binders used in the coating structure. The saturated sample block is then placed in a pressure cell. Gas over-pressure pushes excess hexadecane through the sample and an electronic microbalance records the permeated liquid mass flow rate. For the given density of the hexadecane, the volume flow rate of the hexadecane through the sample block can be used in the Darcy equation to determine the permeability κ :

$$\frac{dV(t)}{dt} = \frac{-\kappa A \Delta p}{\eta l} \quad [2]$$

where: V is the volume of permeated hexadecane,
 A is the cross-sectional permeable area,
 Δp the applied pressure difference,
 η the viscosity of the hexadecane and
 l the sample block thickness.

3. Results and discussion

3.1 Porosity and pore size distribution

Figure 3 shows the pore size distributions for the GCC structures. It can be observed that as the binder addition increases the pore volume first increases then decreases, reaching a maximum porosity of 28.06 % at 6 pph of binder. Since the GCC pigment has a broad particle size distribution (see Table 1), the addition of binder tends to affect the packing by firstly interacting colloiddally with the carbonate at low binder doses,

thus creating larger pores by disruption (Ridgway and Gane, 2007). The pore size distribution of the GCC also shows that as the binder addition increases further the average remaining finer pores gradually fill, such that the amount of fine pores in the range of 0.01 - 0.1 μm decreases.

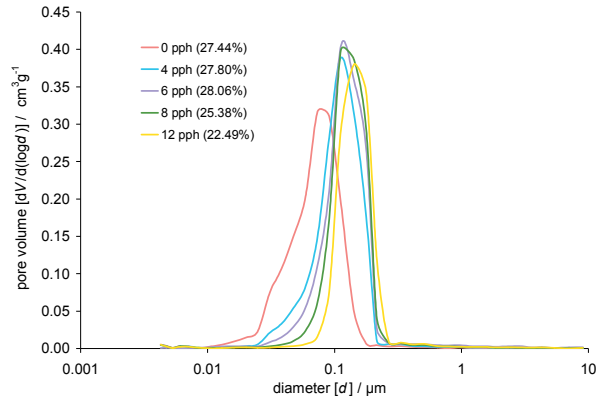


Figure 3: Pore size distributions for GCC based samples. The porosities are given in the legend

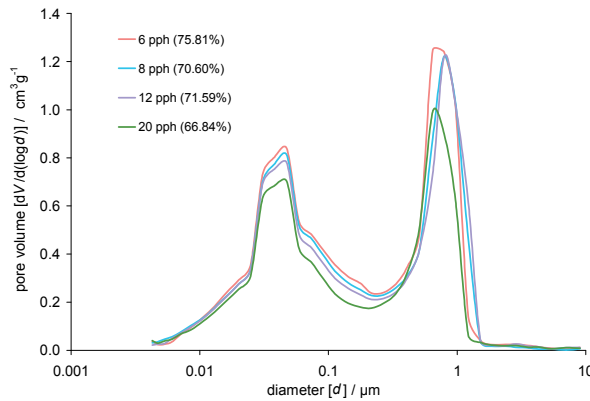


Figure 4: Pore size distributions for the MCC based samples. The porosities are given in the legend

The pore size distributions of the MCC systems, shown in Figure 4, illustrate that the samples not only have much larger porosities compared to the GCC based samples (area under the curves), but also that the distributions are bimodal, distinguishing discretely between intraparticle and interparticle pore space. The addition of binder decreases the pore volume by filling the pores, or their access, in the whole range of the distribution, including the close proximity pathways between contacting particles, which in turn control connectivity, and thus permeability, of the network pore structure.

Keeping in mind the different pore structures of the GCC and MCC systems, one can now proceed to discuss the results of the thermogravimetric measurements.

3.2 Thermogravimetry

Figure 5 and Figure 6 show the differential curves of the normalised weight loss for the thermogravimetric measurements (DTG) of the GCC samples and the MCC samples, respectively, i.e. the effective drying rate for a given temperature. The evaporation behaviour observed for both systems can be divided into three periods associated with evaporation, in turn, from:

External surfaces:

1. Drying of excess liquid

Internal surfaces and pores:

2. Rising rate period with a maximum drying rate
3. Falling rate period

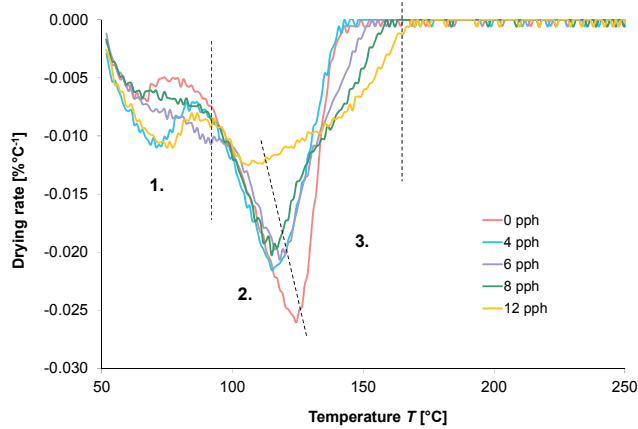


Figure 5: DTG curves for drying of mineral oil from the GCC pellets

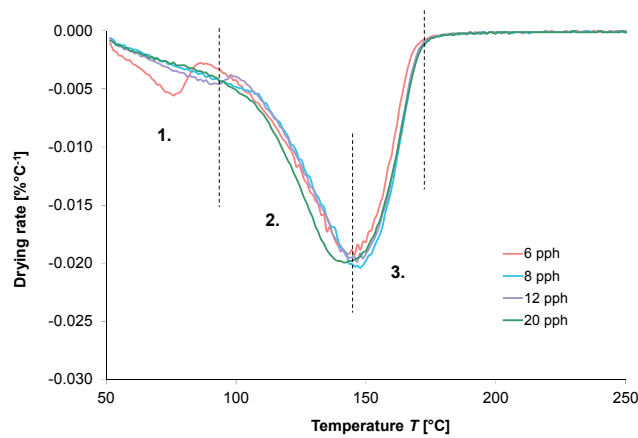


Figure 6: DTG curves for drying of mineral oil from the MCC pellets

3.2.1 External surfaces

In order to compare the drying rate associated with the internal oil evaporation mechanism, and not the external excess oil left after removal from the reservoir, we must further normalise the curves to the start point of the internal evaporation, and set this point to 100 % occurring at the relevant temperature, i.e. at the point where all external oil has been removed. However, this task becomes challenging for the following reasons: firstly, due to the constraints of sample preparation, there are some defects on the external surface of the pellets, i.e. randomly distributed peaks and valleys, and, as a result of this, the amount of excess liquid varies a lot and the drying of external oil completes at different points on the weight loss against temperature curve: secondly, because some drops of external oil are dripped from the sample, the first drying peak becomes unclear in respect to original sample weight, and this also adds difficulty in separating the peaks, and therefore it is impossible to draw a uniform starting point representing loss of internal fluid for all the curves. Nonetheless, a comparison is possible if the drying experiment is performed under isothermal conditions, e.g. heating at 150 or 200 °C constantly for the entire drying process. In such a way the effect of temperature can be isolated and the evaporation of internal oil could be compared in terms of %min⁻¹ once the data for the external oil are removed.

Since we only focus on the general trends between the samples, the slight difference in the starting point representing the transition from loss of external to internal oil will be ignored in the following discussion, and the emphasis will be put on the evaporation from internal surfaces.

3.2.2 Internal surfaces

While the MCC structures exhibit very little difference in the evaporation rates at the different binder levels, the GCC samples show that higher binder contents decrease the maximum drying rates, and also shift the maximum to a lower temperature. This is consistent with previous observations by Gerstner et al. (2010). It was concluded that the effect of binder is not related to a direct interaction of the binder phase and the

mineral oil, but rather to structural phenomena within the sample. The following discussion goes on to analyse separately the likely mechanisms potentially governing the evaporation of the liquid, initially taking place during the rising rate period.

3.2.3 Rising rate period

According to the classical theory for drying of hygroscopic material (Anilkumar et al., 1987), when a liquid saturated porous medium is subjected to thermal drying, two processes occur simultaneously: 1. evaporation of the liquid on the surface; 2. diffusion of the internal liquid to the surface of the porous medium and then subsequent evaporation following again process 1. The drying rate is governed by the rate at which the two processes proceed. A number of factors that may affect the evaporation of surface liquid include temperature, surrounding atmosphere, area of exposed surface and pressure. For the internal transport process, the migration of liquid from within the porous medium occurs through one or any combinations of the following mechanisms: diffusion, capillary flow, and internal pressures caused by shrinkage during drying (Ridgway and Gane, 2007).

Since the temperature and surrounding atmosphere are kept constant in the controlled conditions of the TGA furnace and, on the macroscopic scale, the area of exposed surface is defined by the geometry of the sample pellet, the impact of vapour pressure on drying needs to be studied: the liquid contained within a porous medium exerts a vapour pressure of its own, which is determined by the size of the pores. When liquids are confined in fine pores, present in both the GCC and MCC structures, this so called *Kelvin Effect* can be of significance in determining the evaporation behaviour of the liquid (Melrose, 1989; Aharoni, 1998; Goworek et al., 1995). As the pores get smaller the vapour pressure able to be exerted by the confined liquid will become lower, i.e. as the binder addition increases, the relative amount of fine pores first reduces and then increases again as originally larger pores become filled by binder, correspondingly a slower followed by a faster drying rate would be expected if meniscus confinement was the dominating factor. However, in fact, we do not observe this behaviour on the DTG curves (Figure 5), so the Kelvin effect, associated purely with pore geometrical confinement, can be neglected in this case of relatively high pore connectivity.

Furthermore, capillary forces can cause the preferential advance of liquid in the “corners” of the irregular pore geometry, a phenomenon called *film flow*. For the case of non-cylindrical capillary tubes, a liquid film preceding the bulk meniscus in the tube can form if the relation of $\theta \leq \theta_c$ is satisfied, in which θ is the contact angle that the bulk meniscus forms with the wall of the tube, and θ_c is the critical angle based on the pore geometry (Prat, 2007):

$$\theta_c = \frac{180}{N} \quad [3]$$

where N is the number of sides of the cross section of a capillary tube, e.g. for the case of a triangular, square and hexagonal cross-section, N equals 3, 4 and 6, respectively. When N gets large enough, a tube can be approximated to a circular cylinder, such that the critical contact angle would become very low, i.e. it is impossible to induce any film flow within a cylindrical tube. Prat (2007) showed that, for a given contact angle, the drying time decreases with the decrease of number of sides in the pore, i.e. a triangular pore (three sides) would dry faster than pores of higher polygonal degrees. The GCC pigment has, compared to MCC, relatively sharp edges and rough surfaces (see Figure 1), therefore, the effect of the latex in filling (Al-Turaif and Lepoutre, 2000) the geometrical “corners” of the GCC pore structure can reduce the film flow ability of the liquid and thus reduce the drying rate. This situation is illustrated schematically in Figure 7.

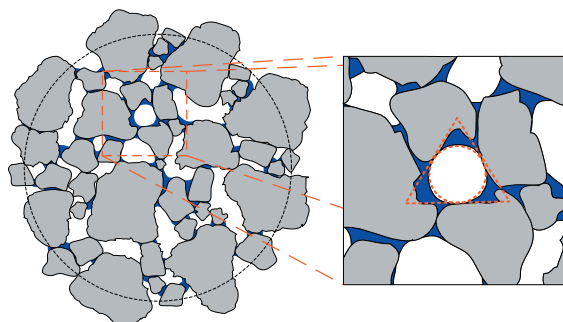


Figure 7: Schematic illustration of a GCC pigment (grey) and binder (blue) structure. Magnified: filling and smoothing of an originally “triangular” pore geometry by binder

In contrast, the MCC pore structure is already close to the situation of polygonal tubes and the addition of binder cannot increase the number of sides significantly. This is consistent with the drying rate curves as shown in Figure 6, in which the MCC pellets with different binder concentrations do not distinguish themselves from each other, and the slight discrepancy may be attributed to the local variation of wettability. The effect of film flow can be supported in respect to differences in the drying of a saturated pellet, which is a real porous medium rather than a single capillary tube.

3.2.4 Falling rate period

Another trend can be observed in Figure 5: as the binder addition increases the peaks of drying rate become extended along the temperature axis, implying that the mineral oil interacts more and more strongly with the structures. To study the possibility of readsorption of mineral oil in this temperature regime, the temperature was held constant at 130 °C for a sufficiently long time (5 h). The results show that all of the mineral oil can be desorbed under such conditions, indicating that the temperature in the falling rate period is high enough to avoid the occurrence of readsorption. Furthermore, the trend of an extended drying rate peak does not appear for the case of MCC pellets (Figure 6). This contrast in behaviour suggests that the factors that may trigger the observed interaction are therefore likely to have a different origin for the two structures.

Bray and Prat (1999) analysed the drying of a porous medium by simulation of the phase distribution in a three dimensional capillary network. They illustrated how the gas phase invades the liquid phase and breaks it down into smaller liquid clusters. There comes a point when the number of liquid clusters increases dramatically and most of the liquid evaporates. The ending of this stage is marked by a moment, namely main cluster disconnection (MCD), at which there is no liquid cluster that is large enough to span the whole network anymore, and the liquid phase only exists in the form of disconnected liquid clusters. This corresponds to the onset of the falling rate period in Figure 5 and Figure 6. At this point, the liquid saturation becomes relatively low, the effect of film flow gets relatively weak due to the development of fully dried regions, and the liquid-gas interfaces start to recede into the centre of the porous medium. Correspondingly, the mineral oil vapour needs to travel out of the porous medium through a tortuous path, and, hence, the diffusion resistance will dominate during this period. Thus, on the basis of drying rate curves, we can predict that the vapour diffusivity within the GCC pellets drops with the increase of binder addition, whereas the addition of binder cannot markedly affect the diffusivity throughout the MCC pellets. The decrease of vapour diffusivity with respect to binder addition generally follows a similar trend as the liquid permeability (Gane and Ridgway, 2009).

Figure 3 shows the measured liquid permeabilities for the GCC system with two different binder levels and compares them to the permeability of the MCC system. It is clear that the general level of permeability is much higher for the MCC (ca. 25 times higher), even at a binder content of 8 pph, and thus a small change in the permeability of that system does not affect the vapour diffusion resistance to an extent that would affect the drying rate in the falling period. However, since the permeabilities of the GCC system are considerably lower, the difference in binder content here affects the diffusion resistance. In fact, the tablet formation itself is a typical process that reflects liquid permeability and that can be described by Darcy's law. In the process of tablet formation, the dewatering time strongly depends on the characteristic packing of the pigment particles, as well as the binder concentration. Table 2 summarises the formation time of the GCC tablets of comparable size, implying that the filtration rate decreases considerably as the binder addition increases. In contrast, the formation time of the MCC tablets persists around 1.5 min regardless of the binder addition.

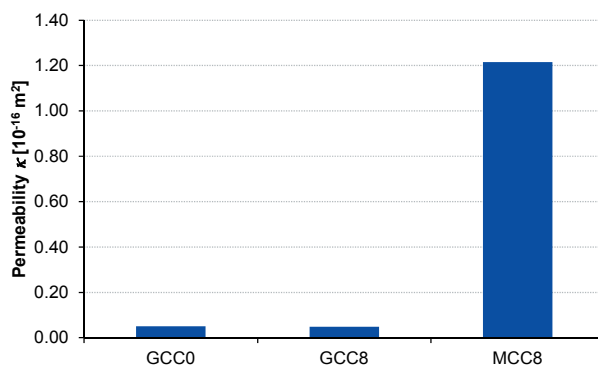


Figure 8: Comparison of the liquid permeability of GCC and MCC tablets

Table 2: The forming time of the GCC tablets as a function of binder addition (Gerstner et al., 2009)

Latex content, pph	Forming time
0	40 min
8	100 min
12	180 min
20	24 h

4. Conclusions

The dynamic drying rates for mineral oil saturated ground calcium carbonate (GCC) and modified calcium carbonate (MCC) coating structures were examined as a function of temperature and for various levels of binder dosage. Two internal stages of drying were identified for both structures: a rising drying rate period and a falling rate period as a function of temperature. In the rising rate period, the effect of film flow, being a major internal mass transport mechanism, has been identified to be of particular relevance for the case of GCC based structures: as the binder addition initially increases the detail of pore geometry, but then progressively fills the surface roughness of pigments and fine pores, such that connectivity is reduced, and thus the drying rate is progressively depressed. Due to the strong intraparticle capillarity of the MCC, film flow within the interparticle structure, which is of larger size than in the case of GCC, is seen to be minimal. At the onset of the falling rate period, the main cluster disconnection (MCD) is reached. Since the liquid phase is in the form of disconnected liquid clusters, it was shown that diffusion resistance becomes a dominant factor in determining the drying rate during this period. While the MCC systems showed a generally high permeability, and thus the evaporation rate proved to be largely unsusceptible to slight changes in the vapour diffusion resistance caused by binder concentration, the GCC pigment systems, because of their lower permeability, exhibited an extended peak of the drying rate as a result of the increasing diffusion resistance with increasing binder content.

Acknowledgments

The authors would like to thank Dr. Cathy J. Ridgway and Pascale Poffet of Omya Development AG, Oftringen, Switzerland, for their assistance in the thermogravimetric measurements. The financial support of TEKES, the Finnish Funding Agency for Technology and Innovation, is gratefully acknowledged. This work was completed as part of the project "Thermal Effects and Online Sensing" (THEOS).

References

- Aharoni, C. (1998), Adsorption and condensation in pores, *Langmuir*, 14:3339-3342
- Al-Turaif, H., Lepoutre, P., (2000), Evolution of surface structure and chemistry of pigmented coatings during drying. *Prog Org Coat*, 38:43-52
- Bray, Y.L., Prat, M., (1999), Three-dimensional pore network simulation of drying in capillary porous media. *Int J Heat Mass Tran*, 42:4207-4224
- Frank, E., (1996), Trocknung im Rollenoffset: Neue technologische und ökologische Erkenntnisse, *Dtsch. Drucker*, 32(25):w2-w10
- Gane P.A.C. and Ridgway C.J., (2009), Moisture pickup in Calcium Carbonate Coating Structures: role of surface and pore structure geometry, *Nord Pulp Paper Res J*, 24(3):298-308
- Gane, P.A.C., Kettle, J.P., Matthews, G.P. and Ridgway, C.J., (1996), Void space structure of compressible polymer spheres and consolidated calcium carbonate paper-coating formulations, *Ind Eng Chem Res*, 35(5):1753-1764
- Gerstner, P., and Gane, P.A.C., (2009), Considerations for thermally engineered coated printing papers: focus on electrophotography, *J Pulp Paper Sci*, 35(3-4):108-117
- Gerstner, P., Paltakari, J., Gane, P.A.C. (2009), Measurement and modelling of heat transfer in paper coating structures. *J Mater Sci*, 44(2):483-491
- Gerstner, P., Veikkolainen, S. and Gane, P.A.C., (2010), Effective thermal conductivity of liquid saturated coatings and their liquid vaporisation behaviour. *Proceedings of the 11th TAPPI Advanced Coating Fundamentals Symposium*, Munich, Germany, 2010, Tappi Press, GA., pp. 174-194
- Goworek, J., Stefaniak, W. and Dabrowski, A., (1995), Porosity of solids by temperature programmed desorption of liquids - various heating programs, *Thermochimica Acta*, 259:87-94

- Melrose, J.C. (1989), Applicability of the Kelvin equation to vapor/liquid systems in porous media, *Langmuir*, 5:290-293
- Mujumdar, A.S., (1987), Drying of solids: principles, classification, and selection of dryers. Handbook of Industrial Drying. Ed. Arun S. Mujumdar. Marcel Dekker, Inc. New York, pp. 3-46
- Prat, M., (2007), On the influence of pore shape, contact angle and film flows on drying of capillary porous media, *Int J Heat Mass Tran*, 50:1455-1468
- PrintCity, (2008), Online, cited 04.05.2010. PrintCity Sustainability, Energy and Efficiency Report. Available online: http://www.printcity.de/index.php?site_id=196
- Ridgway, C.J., Gane, P.A.C. and Schölkopf, J., (2004), Modified Calcium Carbonate Coatings with Rapid Absorption and Extensive Liquid Uptake Capacity, *Colloids Surf. A*, 236(1-3):91-102
- Ridgway, C.J., Gane, P.A.C., (2007), Effect of latex and pigment volume concentrations on suspension and consolidated particle packing and coating strength, *J Pulp Paper Sci*, 33(2):71-78
- Ridgway, C.J., Schoelkopf, J., Gane, P.A.C., (2003), A new method for measuring the liquid permeability of coated and uncoated papers and boards, *Nord Pulp Paper Res J*, 18(4):377-381
- Rousu, S., Lindström, M., Gane, P.A.C., Pfau, A., Schädler V., Wirth, T., Eklund, D., (2002), Influence of latex-oil interaction on offset ink setting and ink oil distribution in coated paper, *Journal of Graphic Technology*, 1(2):45-56
- Veikkolainen, S., (2009), Considerations for the design of thermally engineered coatings. Master's Thesis. Helsinki University of Technology, Espoo, Finland
- Vidal, D., Ridgway, C.J., Pianet, G., Schoelkopf, J., Roy, R., Bertrand, F., (2008), Effect of particle size distribution and packing compression on fluid permeability: a comparison of experiments and Monte-Carlo/Lattice-Boltzmann simulations, *Comp Chem Eng*, 33(1):256-266



Nanoscale single and multilayer adsorption of polyelectrolytes to pulp fibers

Praveen Chandak^{1,2}, Levente Csoka¹, George Grozdits^{3*}

¹ Department of Pulp and Paper Technology, IIT
Roorkee, Uttarakhand
Saharanpur Campus, IN-247667, India
E-mail: chandak.praveen@gmail.com

² Institute of Wood and Paper Technology
University of West Hungary
Bajcsy Zs. E. u. 4., H-9400 Sopron, Hungary
E-mail: lcsoka@fmk.nyme.hu

³ Department of Forestry, Louisiana Tech University
P.O. Box 10138, Ruston 71272 LA, USA
E-mail: grozdits@latech.edu

* correspondence to: Levente Csoka, lcsoka@fmk.nyme.hu

Abstract

The paper and printing industry faces the challenges of meeting the changing demands for paper and paper based products. Advances in the electronic media changed the paper needs and affected the paper markets. The news print market started to shrink, while the office printing paper and packaging increased. Printing paper product requirement also changed due to more and more global marketing and the improvements of graphic art and subsequent printing. The new printing industry requires tighter paper structures with smoother surfaces.

Poly (diallyl dimethyl ammonium chloride) (PDDA) was used to modify the surface of cotton linter fibers by using the monolayer coating of PDDA polyelectrolyte on the fibers surface. Hand sheets were prepared using the polyelectrolyte treated fibres mixing them with untreated linter fibres in different weight ratio. The sheets strength were evaluated using tensile strength.

Adsorption of Titanium Dioxide (TiO₂) and absorbance of PDDA on the fibers in the solution was measured using the UV Spectrophotometer and Beer Lambert Law. It was shown that the polyelectrolyte treatment increases the strength and double folding of the paper as the weight percentage of the PDDA treated fibers is increased from 0% to 40% and the adsorption of TiO₂ on the sheet also increased. It was also shown that the PDDA treated pulp loses more water in a certain time interval and works as a retention aid for adsorption of TiO₂ during the paper sheet formation and change the surface charge to positive. Digital printing technique - copier machine, ink-jet and laser printing - were used to show the advantages of positively charged fiber surface during printing.

Keywords: layer-by-layer nanocoating, retention, digital printing, surface charge

1. Objective

The main objective of this research paper is to understand the mechanism of the LbL surface treatment of linter fibers and enhanced toner attract on positively charged fiber surface and the functionalized fibers, which will lead eventually to the possibility to increase retention of organic clays and inorganic toner particles of such systems.

2. Introduction

Many types of paper, such as packaging paper grades, are limited by their dry strength properties and printing paper grades are necessary to be surface coated for better surface properties and ink sorption.

The worldwide importance of electronic print processes is constantly increasing. Multi-color ink jet technology is growing, especially for the home and office markets (Williams, 2001). A large and growing consumer

market for ink jet has developed in packaging, publication, and specialty areas. The quality of ink jet printing is influenced by the printers in use, as well as by the physio-chemical properties of printing ink and print substrate.

In IJ printers, ink is forced under pressure through a small nozzle or array of nozzles onto paper where image is formed by means of computer control (Anczurowski et al., 1986). There are two basic methods of propelling ink drops: continuous and impulse. In continuous IJ printing (Corso, 1986), ink is ejected from a single orifice or nozzle under modest pressure and projected through a charging tunnel where the ink droplets are given a positive or negative electric charge. Impulse systems (Watson, 1997) operate on a drop on demand basis, i.e. ink droplets are fired by a drop generator as and when required. The drop generation can be either piezo-electric or thermal.

On the other hand, in packaging paper grades, the existing paper physics theories state that the fiber strength and the strength of joints between individual fibers are the most important factors determining the tensile strength properties of paper (Bristow et al. 1986). In general terms, the strength properties of weak sheets of low density are limited by the fiber-fiber joint strength, while those of strong sheets of high density are more limited by fiber strength (Page 1969). However, it is possible to pull out intact fibers from both strong and weak papers, indicating that the weak link in any paper is the fiber-fiber joint (Davison, 1972).

When paper is formed, wood fibers are brought into close contact with each other by capillary forces as water is removed during drying and pressing. In this process, electrostatic interaction between the fibers has been shown to influence the number and strength of the fiber-fiber joints created in the paper. Reduced electrostatic interaction between carboxymethylated rayon fibers reduces the joint strength, though overall sheet strength is increased (Torgnysdotter and Wågberg 2004). In addition, the ability of the fiber surfaces to adjust to each other in forming a large contact area is largely determined by the mechanical properties of the fiber surface layers and the fiber flexibility, i.e., the wet elastic properties of the fiber surface in the transverse direction (Nilsson et al. 2001, Emerton and Kenley 1957, Paavilainen, 1993).

In conventional papermaking, beating is more or less always used to prepare a more flexible fiber and hence a stronger sheet. The mechanical properties of paper can be further improved by adding dry strength agents, typically cationically charged polyelectrolytes. The polyelectrolytes used can differ in terms of chemical structure and physical properties, making it difficult to clarify the exact reasons for the increase in paper strength. However, over the years research into paper strength and strength additives has significantly improved our understanding of the molecular mechanisms underlying the action of dry strength additives, and most such findings have been well covered in recent reviews (Davison, 1980; Pelton 2004, Lindström et al. 2005). In the literature, different types of molecular mechanisms are presented as the forces holding the fibers in a sheet together, forces such as hydrogen bonding, Van Der Waals interaction, and covalent bonding. Such chemical interactions require that the fibers come into close contact with each other, as explained by the interdiffusion theory suggested by McKenzie (McKenzie, 1984).

This theory suggests that polymer segments adsorbed onto fiber surfaces will mix/diffuse into each other as the fibers are forced into contact with each other during sheet formation, thus allowing for the creation of strong adhesion between fibers. This theory was further supported by Pelton et al., who showed that polyelectrolytes adsorbed onto the fiber surfaces must be compatible in order to create strong joints between the fibers (Pelton et al., 2000).

Researches done in this field states that there is an increase in tensile strength (Zhiguo et al. 2006, Eriksson et al. 2006, Agarwal et al. 2006) but its application in industry is difficult because of the following factors: a) It has been done at very lower consistency which is not very economical and b) It is done Layer by Layer which is difficult to apply in an Industry.

So in this current research we have performed monolayer treatment on the cotton linter fibers (Cotton linters were used as the pulp in this investigation for several reasons. First, cotton linters are similar to wood pulp in that they both basically consist of cellulosic fibers which develop a similar surface upon refining. Second, unlike wood fibers, cotton linters are almost free of hemicelluloses and lignin which could interfere with polymer Adsorption) (Proxmire, 1988) using Poly(diallyldimethylammonium chloride) (PDDA) which is more economical than the other polyelectrolytes used before for such a research and we also measured the absorbance using UV Spectrometer of PDDA and TiO₂ on the fibers and the effect on strength properties of the sheet with and without using surface agents and TiO₂.

2. Materials and research methods

This work uses the layer-by-layer (LbL) nanoassembly techniques and on the results of modification of lignocellulose fibers, which made stronger dry and wet strength paper, increased positive surface charge and paper recyclability. The LbL assembly is a nanofabrication technique, which has been used to produce multilayered films with nanometer precision through alternate adsorption of oppositely charged components, improving the fiber surface properties mainly for better bonding (Zhiguo et al., 2006; Safouane et al., 2005, Agarwal et al. 2006 and 2009, Wistrand 2007).

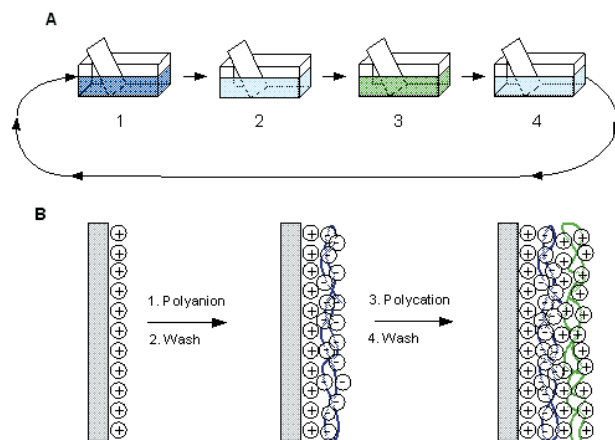


Figure 1. Schematic representation of the LbL process based on the alternate adsorption of oppositely charged macromolecules or colloids (here polycations and polyanions) as proposed originally by G. Decher in 1997 (Science, 1997, 27, 1232)

Systematic modification of fiber external surfaces and their lumen can be demonstrated by using layer-by-layer (LbL) nanoassemblies via alternate adsorption of positive and negative polyelectrolytes. It can be attested by confocal laser scanning microscopy that both external surface of the fibers and the internal surface of their lumen are coated after the alternate adsorption of polyelectrolyte films, with 5-25 nm in thickness depending on molecular composition of the LbL multilayers. Typically, a polycation monolayer or 3-4 polycation/polyanion bilayer coating can be used. Polyelectrolytes with medium and high molecular weight do not enter into the delignified fiber cell walls but form a continuous coating with increased deposition over fiber wall openings. LbL assembly can successfully be applied to beaten and unbeaten pulp fibers; therefore, it provides a unifying fiber property development for papermaking. In the best case scenario of 1:1 mixture of positively and negatively charged LbL-treated pulp, the paper dry tensile strength can be doubled. The wet strength can be improved by 30% with nano-olycations (poly(amidamin) with epichlorohydrin) and carboxymethyl cellulose (CMC). Anionic polythiophene (PEDOT-PSS) in alternation with polycations results in conductivity of $5 \times 10^{-3} \text{ Scm}^{-1}$ for unbeaten and 10 Scm^{-1} for beaten softwood fibers and was further increased up to 20 Scm^{-1} by sandwiching a multilayer of conductive co-polymer PEDOT-PSS with CNT-PSS through a polycation (PEI) interlayer. Fiber conductivity is proportional to the number of deposited PEDOT-PSS monolayers. Iron nanoparticles can magnetize fibers. Fibers can also be coated with organized multilayers of nanoclays (TiO_2 , SiO_2 , and tubule halloysite) with controlled loading and these processes can be connected with commercial paper technology. An environmentally friendly process offered by LbL nanoassembly may provide important development to the relevant paper processing industry and to the improvement of the different type of paper products (Zhiguo et al 2006, Agarwal et al. 2006).

2.1 Fiber treatment

The fibers used in this study were dried, cotton (Linter) fibers from Buckeye Paper, USA. The fibers were kept in water for a few hours and were defibrated in a disintegrator for 30 000 revolutions according to a standard method, ISO (International Standardization Organization) 5263-1:1997. And then the beating of fibers was performed using Laboratory Valley Beater until a °SR of 35 was achieved.

Linter pulp was treated with PDDA in a fiber water suspension and was stirred continuously. The fiber concentration during the experiment was 1 wt % and 2 wt % i.e. the treatment was performed at 1% and 2% consistency. Polyelectrolyte concentration was also varied from 1 mg/gm to 20 mg/gm fiber for an adsorption time of 15 min in water at pH 7. After filtering off the excess polyelectrolyte using a Buchner funnel, the fil-

ter cake formed was mixed with untreated fibres in different weight ratios from 0% to 40%. After mixing them in different weight ratios the fiber suspension was treated with Sizing agent 5 wt % and TiO_2 10 wt % of fiber.

2.2 Sheet preparation

After the adsorption of polyelectrolyte and TiO_2 , hand sheets with a grammage of 100 g/m^2 were made on HAAGE-sheet former according to the standard DIN EN ISO (International Organization for Standardization) 5269-2 method, using rapid Kothen sheet preparation equipment (Paper Testing Instruments (PTI), Pettenbach, Austria). Sheets were formed after vigorous agitation of the fiber suspension. The sheets were dried at 93°C under a pressure of 93 kPa for 7-8 min. Industrial scale PDDA treated paper was prepared as described here, but using only 30% PDDA treated fibers.

2.3 Paper testing

Dry tensile testing to determine stress-strain curves for paper strips was conducted according to the SCAN (Scandinavian Standards for Pulp and Paper Manufacturer)-P 67:93 standard (listed in the SIS Catalog of Swedish Standards). The grammage, thickness, and density of the sheets were evaluated using appropriate equipments. Paper strength can be expressed in several ways, the tensile index being commonly used. The tensile index is the force at break per unit width and unit grammage.

2.4 Adsorption of TiO_2 and PDDA on fibers

PDDA with high molecular weight was purchased from Aldrich. PDDA was delivered as 20 wt % in aqueous solution. TiO_2 used was purchased from Kemira Pigment, Finland and the Sizing agents were bought from BASF Chemicals. TiO_2 was delivered in powdered form and Sizing agent was provided in solution as liquid.

Absorption of PDDA on the fibers was determined using S2000 UV/Vis Spectrophotometer. The concentration of PDDA in the solution before and after the treatment was calculated using Beer-Lambert Law. And similarly for TiO_2 the absorbance of the solution was observed before and after the sheet formation and the concentration was determined using Beer-Lambert Law.

2.5 Water drainage rate of pulp

For calculating the rate of drainage of water for pulp with different weight ratios of treated and untreated fibers, a pulp solution with 3gm of fibers (with the required weight ratios) and 1 liter was prepared. The drainage time was simply observed with a manually operated timer and the time for drainage of same amount of water from different solution was observed.

2.6 Printing tests

In this project we used the paper made by PDDA treated fiber (30% by weight) and untreated fiber for printing the same, standard black pictures using different inks and printers. We used IGT and oil based inks in two different printing machines: HP Officejet 6000 printer and Sharp AR-M 160 copier machine and the images of different samples were captured using DPM 100 Digital Microscope. The images were studied using software IrfanView and differences were observed. The testing papers were made in laboratory as well as using paper machine. Laboratory sheets were made from industrial grinded fibers and the shape was round type whereas industrial paper was cut to A/4 size. Fonts and simple standard test objects were printed and copied to papers to analyze differences.

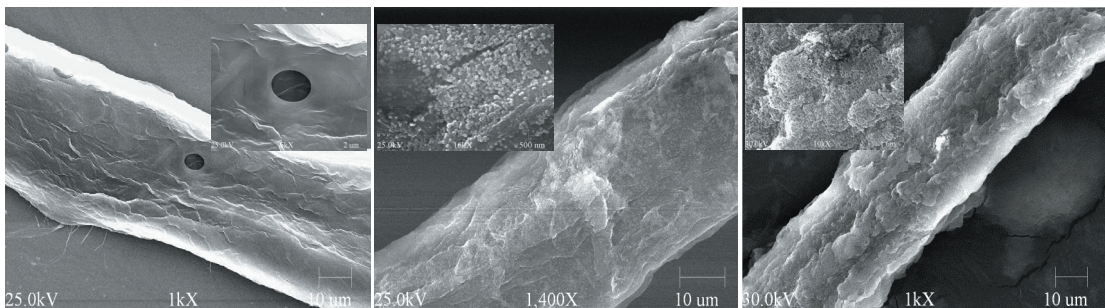


Figure 2: Scanning electron microscopy images of untreated pulp fiber and LbL assembled fiber-(PDDA/SiO₂)₂, fiber-(PDDA/SiO₂)₂ (Grozdzits and Lvov 2007)

3. Results and discussion

3.1 Strength properties

PDDA was used for making a coating of cationic polyelectrolyte on the fibers surface. The concentration of the polyelectrolyte in the fiber water solution at 1% consistency was varied from 1mg/gm of fiber upto 20 mg/gm of fiber by weight. The ratio of treated to untreated fiber was kept 50% by weight. And it was found that polyelectrolyte concentration of 1.5-2 mg/gm of fiber had the optimum effect on the tensile strength of paper sheets i.e. for concentration higher than 2 mg/gm of fiber the strength of sheets formed from the solution didn't show any increase in the tensile strength. Table 1 summarizes the results of varied concentration of PDDA and the tensile index of the paper sheet. Figure 3 shows the graphical representation for Table 1.

Table 1: Optimized adsorption of PDDA

Amount of PDDA during the treatment in mg/gm of fiber	Tensile Index in Nm/gm
0	26.87
1	29.84
1.5	31.3
2	30.78
5	30.21
10	30.04
20	30.17

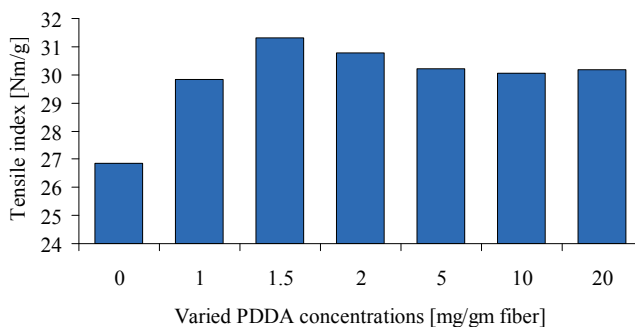


Figure 3: Changes of tensile index

After the optimum concentration for the treatment was determined all the fibers were treated with a polyelectrolyte amount of 1.5 mg/gm of fiber at 1% and 2% consistency. When the treatment was performed at 2% consistency it showed a decrease in the tensile strength as expected as it PDDA requires more surface area to adsorb properly and as we increase the consistency of the solution the surface area of the fiber becomes less and less as the solution is getting dense resulting in poor adsorption of polyelectrolyte on the fibers surface and thereby less increase in the strength of the paper. The consistency was kept 1% after this throughout the experiment and it wasn't performed at lower consistency as it becomes highly unlikely to be used at an industry.

Once the consistency for polyelectrolyte treatment and amount of polyelectrolyte was fixed i.e. 1% consistency and 1.5 mg PDDA/ gm of fiber, the weight ratio of treated fiber was varied from 0-50 % in the hand sheets and the tensile index of the hand sheets were measured. The results obtained are shown in Table 2 and Figure 4.

Table 2: Tensile index changes of treated papers

% Treated Fibers	Tensile Index in Nm/gm
0	26.87
10	29.89
20	30.77
30	32.14
40	31.52
50	31.3

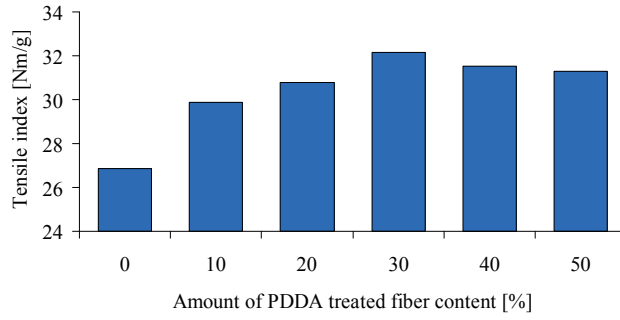


Figure 4: Different handsheet compositions

It was found that the tensile index of the sheets shows an increase of 19.6 % for 30% by weight treated fibers and there is a slight decrease in the same as we go on increasing the percentage of polyelectrolyte treated fiber.

Later on hand sheets were made from the treated fibers with the use of Titanium Dioxide and sizing agent at 10% and 5% by weight respectively. And the tensile indexes of these sheets were also measured and following data was obtained:

Table 3: Tensile index with TiO₂ adsorption

% Treated Fibers	Tensile Index in Nm/gm
0	26.98
10	30.45
20	31.06
30	33.61
40	32.17
50	31.77

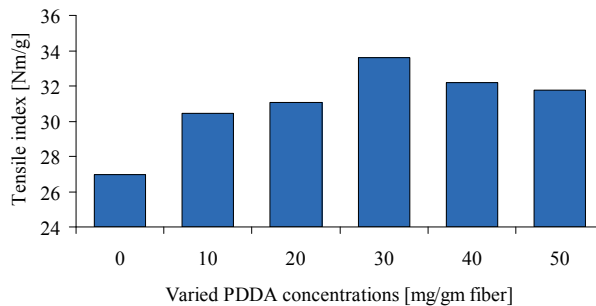


Figure 5: Tensile indexes with TiO₂ and sizing agent

The observed tensile index was found 24.6 % higher than the plain handsheet made from the same raw materials with TiO₂ and sizing agent. Other properties were also measured like SCT Index, Bending Stiffness, Bulk but there was no significant improvement detected in these areas. LbL treatment using PDDA-PSS-PDDA using 1.5 mg/gm of fiber for both the polyelectrolyte at 1% consistency upto two layers didn't show any further increase in the properties either. The absorbance of PDDA at 1.5 mg/gm of fiber in 1 % consistency was found to be 83.33% i.e. the decrease in the concentration of PDDA after the treatment of fibers.

3.2 Effect on retention of titanium dioxide

After the polyelectrolyte treatment of fibers using PDDA at 1.5 mg/gm of fiber and mixing them in desired weight ratios Titanium Dioxide was added at 10% by weight to the fiber water suspension and was mixed thoroughly. Then the solution was used for sheet preparation and the sample of drained water from the sheet was collected and was used to determine the concentration of Titanium Dioxide in the drainage water using UV/Vis Spectrophotometer and Beer Lambert Law. The retention of Titanium Dioxide was determined as the concentration before was same for all solutions i.e. 60 mg/L. Table 4 shows the concentration of Titanium Dioxide in the drained water.

Table 4: Retention of TiO_2

% Treated Fibers	Concentration of TiO_2 in mg/L
0	31.7
10	27.3
20	26.4
30	25.2
40	24.9
50	24.2

The results above clearly indicates that as the amount of treated fibers is increased the retention of TiO_2 on the sheet increases. It is because PDDA is a cationic polyelectrolyte and TiO_2 is slightly negatively charged so PDDA helps in increasing the retention of TiO_2 on the sheet.

3.3 Effect on water drainage

PDDA treated pulp with 1.5 mg/gm of fiber at 1% consistency was mixed with untreated pulp in a wt % of 0-50 and a total of 3gm of sample was prepared. This sample was mixed with 1 liter of water to make a fiber water solution. Than this solution was poured on a Schopler Reigler instrument with one side of the instrument completely blocked such that all the water was allowed to flow through one pipe and the time for 200 ml, 300 ml and 400 ml of water from different sample was observed and the total amount of water drained was also noted. The results have been summarized in the Table 5 and Figure 6.

Table 5: Water drainage values

% Treated Fiber	Time for Drainage of 200 ml	300 ml	400 ml	Total Amount of water lost at the end in ml
0	10.67	24.43	47.96	745
10	9.35	22.16	44.55	816
20	9.08	21.8	42.63	847
30	8.76	21.52	41.18	856
40	8.48	21.08	40.29	874
50	8.41	20.79	40.67	898

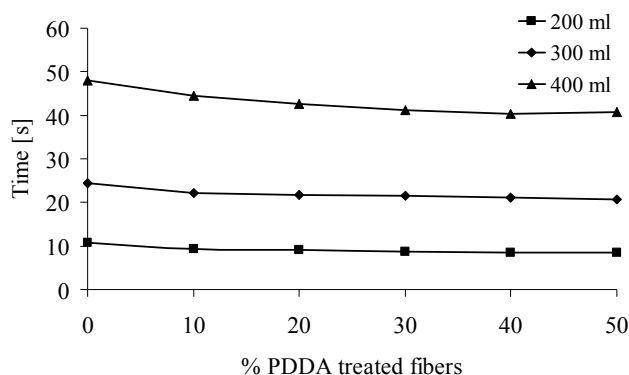


Figure 6: Water drainage values in different % treated fiber mats

It is observed that as we go on increasing the amount of PDDA treated fiber in the solution the time decreases and total amount of water in the end is more, showing that PDDA treated pulp loses water more easily. The reason for this can be as the pulp is treated with polyelectrolyte it covers the hydroxyl groups of cellulose which causes less hydrogen bonding and thereby resulting in more easy removal of water. This means that other than increasing the strength properties of paper ad retention of additives it also can help in saving a lot of energy when used in a commercial way i.e. in an industry.

3.4. Effect on ink sorption

It was found that IGT ink can penetrate and color the fibers better when treated paper is used as compared to that when paper made by untreated fibers is used. It also shows that in copier printing the images have better sharpness and brightness when printed on treated paper as it has charged fibers which enhances the ink particles, so the ink particle density is less which can be helpful in lowering the ink consumption during printing.

It was concluded that paper made from PDDA treated fiber has better affinity towards ink particles than the control paper, which means better binding and lower particle density which means lower ink consumption.

A gray scale histogram from the untreated paper indicates, that pixel distribution is wider and the peak is lower (index=187, 6.7% pixels related to that peak, higher index number correlates with white, lower index values are black ones). The lower peak contain 9400 pixels (0.5% of the whole picture). For a printed PDDA treated paper that distribution shows narrower histogram peaks and a higher one (index=197, 6.4% pixels related to that peak).

The lower peak contain 15900 pixels (0.8%).

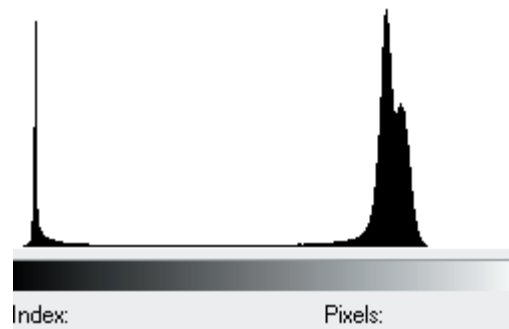


Figure 7: Grey level histogram for an untreated printed paper sample

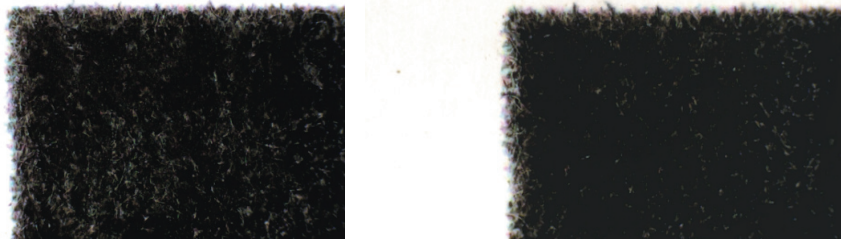


Figure 8: Examples of untreated (left) and PDDA treated (right) paper prints

Conclusion

It was clearly shown that the cationic polyelectrolyte nano scale PDDA is adsorbed by cotton linter fibers (zeta potential -12 at pH 7) and helps in increasing the strength of the paper by improving fiber-fiber bonding, increases the retention of TiO_2 (as it is slightly negatively charged) during the sheet formation and toner particles after digital printing. The adsorption of PDDA by the fibers decreases as the consistency of the fibers is changed from 1% to 2% showing that PDDA requires greater surface area for better adsorption on fibers surface. It is also found that the PDDA treated fibers loses water more readily than the untreated fibers, which can be helpful in saving a lot of energy in its industrial use.

References

- Williams, Ch., (2001) *Printing Ink Technology*, 1st ed., Pira International, Leatherhead, UK, p. 94
- Bristow, A.; Kolseth, P., (1986), *Paper Structure and Properties*; Dekker: New York
- Page, D. H., (1969), *Tappi*, 52 (4), 674
- Davison, R. W., (1972), *Weak link in paper dry strength*, *Tappi*, 55 (4), 567
- Torgnysdotter, A.; Wågberg, L., (2004), *Nord. Pulp Pap. Res. J.* 19 (4), 440
- Nilsson, B.; Wågberg, L.; Gray, D., (2001), *Conformability of wet pulp fibers at small length scales*, 12th *Fundamental Research Symposium*, Oxford, U.K.
- Emerton, H. W., (1957), *Fundamentals of the Beating Process. The Theory of the Development in Pulps of Papermaking Characteristics by Mechanical Treatment: British Paper and Board Industry Research Association: Kenley, U.K.*

- Paavilainen, L., (1993), *Conformability flexibility and collapsibility of sulfate pulp fibers. Pap. Puu*, 75 (9-10), 689.
- Davison, R. W., (1980), *Theory of dry strength development. Dry Strength Addit.1*
- Pelton, R., (2004), *On the design of polymers for increased paper dry strengths A review. Appita J.* 57 (3), 181.
- Lindstrom, T.; Wågberg, L.; Larsson, T., (2005), *On the nature of joint strength in papers A review of dry and wet strength resins used in paper manufacturing. 13th Fundamental Research Symposium, Cambridge, U.K.*
- McKenzie, A. W., (1984), *The structure and properties of paper. Part XXI: The diffusion theory of adhesion applied to interfiber bonding. Appita J.* 37 (7), 580.
- Pelton, R.; Zhang, J.; Wågberg, L.; Rudolf, M., (2000), *The role of surface polymer compatibility in the formation of fiber/fiber bonds in paper. Nord.Pulp Pap. Res. J.* 15 (5), 400.
- Zhiguo, Z.; John, M.; Rajneek, K.; Yi, S.; Tatsiana, S.; George, G.; Lvov, Y., (2006), *Layer-by-layer nanocoating of lignocellulose fibers for enhanced paper properties. J. Nanosci. Nanotechnol.*, 6, 624.
- Eriksson, M.; Torgnysdotter, A.; Wågberg, L., (2006), *Surface modification of Wood Fibers Using the Polyelectrolyte Multilayer Technique: Effects on Fiber Joint and Paper Strength Properties. Ind. Eng. Chem. Res.* 45, 5279.
- Agarwal, M.; Lvov, Y. (2006), *Varahramyan, K. Conductive wood microfibrils for smart paper through layer-by-layer nanocoating, Nanotechnology* 17,5319.
- Proxmir, P., (1988), *The Influence of Aluminum Salts on the Retention of Titanium Dioxide When Using Cationic Polyelectrolyte as a Retention Aid. The Institute of Paper Chemistry, Dissertation*
- Safouane, M., Miller, R., Möhwald, H., (2005), *Surface viscoelastic properties of floating polyelectrolyte multilayers films: a capillary wave study, J. Colloid Interface Sci.*, 292, 86-92
- Wistrand, I.; Lingstrom, R.; Wågberg, L., (2007), *Preparation of electrically conducting cellulose fibres utilizing polyelectrolyte multilayers of poly(3,4-ethylenedioxythiophene):poly(styrene sulphonate) and poly(allyl amine) • Review article European Polymer Journal, Volume 43, Issue 10, 4075-4091*
- Agarwal, M.; Lvov, Y. (2009), *Conductive paper from lignocellulose wood microfibrils coated with a nanocomposite of carbon nanotubes and conductive polymers, Nanotechnology* 20, 215602



The influence of UV coating application on printed cardboard surface properties and colourimetric values

Igor Karlović¹, Erzsebet Novotny², Ivana Tomić¹, Dragoljub Novaković¹

¹ Faculty of Technical Sciences, Department of Graphic Engineering and Design
Trg Dositeja Obradovića 6, SRB-21000 Novi Sad, Serbia
E-mails: karlovic@uns.ac.rs; tomic@uns.ac.rs; novakd@uns.ac.rs

² State printing house, Halom u. 5, H-1102 Budapest, Hungary
E-mail: novotny@any.hu

Abstract

With the application of the widely used UV coatings as an surface enhancement materials which affect the optical properties of coated surfaces and final appearance of the printed product we can change the surface topography of the original surface like the printed paper. The UV coating after the curing process forms the final surface of the coated print which greatly influences the scattering and absorption of the incoming light. These changes of the surface properties can cause a change in colour appearance and thus yield unexpected results in quality control. The application of different amounts of the same UV coatings can lead to different surface properties due to the applied amount and rheological behavior of the coatings during the forming the final coated layer over the printed samples. By using contemporary surface investigation methodology the AFM and SEM microscopes we have obtained surface roughness data and measured the scattering light and calculated the colourimetric values. We have investigated the influence of three different amounts of UV glossy and matte overprint coatings on the measured reflectance curves and colour difference values of offset printed cardboard samples.

Keywords: UV coating, surface roughness, reflectance, colour difference

1. Introduction

These type of surface characterization and data handling can also give us additional information about possible surface effects which can be related to other process parameters like drying, sheet handling.

To obtain more predictable results it is necessary to investigate the influence of these coatings in different amounts on the colourimetric results which can lead to better colour prediction and more efficient production in terms of coating quantity application. Obtaining the empirical data there is a possibility to make a computer prediction of the final colour appearance dependent on the coating amount which would make the screen stencil selection more convenient.

2. Theoretical part

The total colour appearance of any object is the combination of its chromatic attributes (colour defined through lightness, saturation and tone) and its geometrical attributes (gloss, translucency, texture and shape) inside the surrounding in which the object is observed or measured. With the application of liquid dispersions and coatings changes in the microstructure and surface topography of the ink paper system is changed. The leveling, smoothing and the creation of other surface effects has a direct influence on the direction and the amount of the reflected light. The amount of scattering light depends on the wavelength of the light, the angle of incidence and the surface roughness. For a slightly rough surface, most of the light is still reflected in the specular direction, but as roughness increases, the scattering becomes greater, until at some point the light is scattered diffusely in all directions. For some materials, scattering of light transmitted into the bulk will also be significant - this property is important in paints and coated paper for example, and contributes to the perceived brightness of the material. (Surfoptic, 2007). Measuring the specific surface roughness parameters the process of the surface forming of coated samples can be defined, and by defining the physical properties of the formed surface its influence on the geometrical and colourimetric values can be obtained. Research of the coated surfaces on the total colour appearance or other chromatic components were done in (De La Rie ER. 1987), (Berns, de la Rie, 2003) and (Simonot and Elias, 2004) and (Novaković et al, 2009). A paper by (Elias et al., 2006) investigated the correlation between the reflected light, molecular weight of coatings and

surface roughness on the coating substrate interface. In all these papers the changes of the CIE tristimulus values of the coated samples were observed. All these paper mainly focused on surface coated with one amount of the coatings. In the graphic arts industry there is a flexible possibility to change the applied amount and thus produce different surfaces with different light scattering. One of the most popular technique is by screen stencil as an additional surface treatment step in the print production workflow. The amount of the coating transfer on the printing substrate is defined by the horizontal and vertical movement as well the pressure of the rubber squeegee which adheres to the stencil and forces the coating through. Because of the different used materials and weaving methods there can be a considerable difference in the transferred coating amount. The total transferred coating amount is influenced by the thread thickness on the surface of the printed samples minus the volume of the threads on that surface. The transferred amount is also of course influenced by the coating viscosity (Satas & Tracton, 2001).

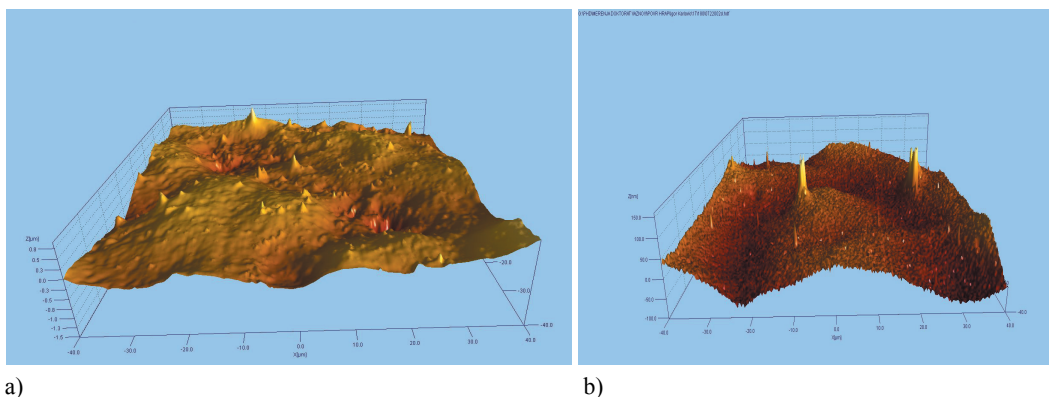
3. Methods and materials

We have investigated the influence of three different amounts of UV glossy and matte overprint coatings on the measured reflectance curves and colour difference values of offset printed cardboard samples. The cardboard samples were printed on the Casino Classic 320g/m² glossy surfaced cardboard. The samples were printed on a Heidelberg Speedmaster SM 52 four colour offset machine using the standard inking values of the ISO 12647-2:2004 ISO norm and other process parameters. After the printing the samples were offline coated with the semi automatic SPS Rhemus screen coater. We have used UV printing inks and different amount of coatings on the printed samples were achieved using three different screen stencils of 180 threads/cm, 150 threads/cm and 120 threads/cm thread count. By using these different screens we have measured the applied coating quantities in g/m². The used commercial UV glossy coatings by UNICO 946 series was dried using the recommended standard for the 120W UV lamp, and the matte version of the coating was also accordingly dried. The measured and calculated averaged transfer of the UV glossy coating to the surface of the printed sheets was 7,92 g/m² for the 180 threads/cm stencil, 11,31 g/m² for the 150 threads/cm stencil and 14,96 g/m² for the 120 threads/cm stencil. For the matte UV coatings the yielded transferred coating amount was 10,92 g/m² for the 180 threads/cm stencil, 10,948 g/m² for the 150 threads/cm stencil and 17,48 g/m² for the 120 threads/cm stencil. The differences in the transferred amounts are in direct connection with the threading density and physical and chemical properties of the used coatings and the properties of the particles in the coatings.

4. Results

The cardboard samples were analyzed with AFM Veeco CP-II and SEM JEOL 646OLV microscopes to obtain surface topography and ISO roughness values and surface properties, which were evaluated in the correlation with the measured colorimetric values. The samples on the coated and non coated samples on the AFM were done on 6 sample positions in x and y direction on 80x80 µm² surface. After the surface scanning we have use Image Metrology SPIP software package to analyze the data and make a graphical representation of the scanned surfaces. In Figure 1 we can see the images of the glossy coated and non coated surfaces scanned with AFM microscopes.

As we can observe from Figure 1 the roughest surface is the non coated cardboard sample, while the coated samples exhibit surface smoothing with very small valley scattered through the surface area. To obtain more



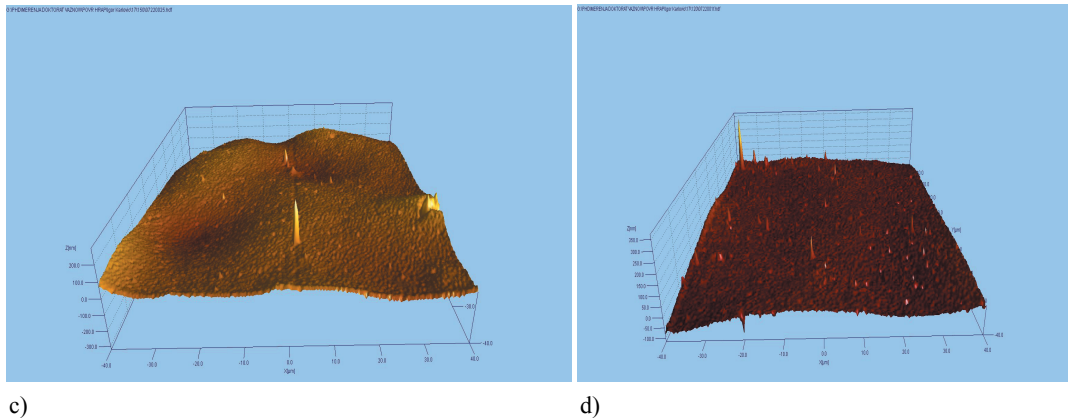


Figure 1: a) Cardboard sample with ink no coating; b) glossy coating 180 threads/cm; c) glossy coating 150 threads/cm; d) glossy coating 120 threads/cm

precise data we have calculated the S_a roughness average, S_q root mean square roughness and S_{sk} surface skewness and S_{ku} surface kurtosis which comply to the ISO/DIS 25178-2 and ASME B46.1 standards and surface roughness terminology. The average roughness S_a parameter for the printed surface without the coating was 169.273nm which plummeted to 35.86 nm after the application of the smallest amount and to 21.49 nm and 13.27 nm with the application of the coating with the 120 threads/cm stencil. The data for all parameters of non coated and glossy coated samples is presented in Table 1.

Table 1: Surface roughness parameters for the glossy coated samples

Sample	S_a roughness average (nm)	S_q root mean square roughness (nm)	S_{sk} surface skewness	S_{ku} surface kurtosis
No coating	169.273	242.52	0.52	9.53
180 threads/cm	35.855	46.17	0.34	4.31
150 threads/cm	21.4927	29.13	-0.26	6.143
120 threads/cm	13.269	17.64	0.16	14.1

The skewness (S_{sk}) of the topographical height distribution S_{sk} is a measure of the asymmetry of surface deviations from the mean plane, and it can be used to effectively to describe the shape of the topography height distribution. For a Gaussian surface which has a symmetrical shape for the surface height distribution, the skewness is zero. For an asymmetric distribution of surface heights, the skewness may be negative if the distribution has a longer tail at the lower side of the mean plane or positive if the distribution has a longer tail at the upper side of the mean plane. The S_{ku} describes the shape of topographical height distribution, i.e., the “peakedness” of the surface topography and this parameter characterizes the spread of the height distribution. A Gaussian surface has a kurtosis value of 3. On the other hand, a centrally distributed surface has a kurtosis value larger than 3, whereas the kurtosis of a widely spread distribution is smaller than 3. By a combination of the skewness and the kurtosis, it is possible to identify surfaces which have a relatively flat tops and deep valleys. As we can see from the data the surface skewness is almost always positive except for the 150 threads/cm samples. The S_{ku} kurtosis value is always positive and largest for the biggest amount of coating applied and smallest for the least amount of glossy coating applied. To gain additional visual understanding of the coating formation and changes in the surface topography we have imaged the surfaces with SEM microscopy and some of the samples are presented in Figure 2.

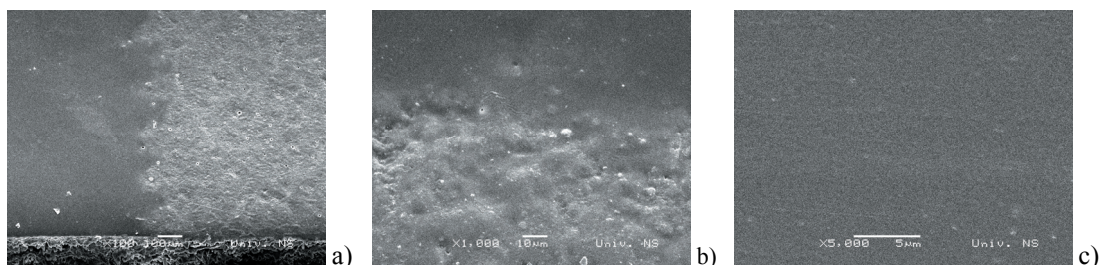


Figure 2: a) The borderline of UV ink and the cardboard; b) The borderline of UV ink and the cardboard coated with 180 thread/cm; c) Print coated with 180 thread/cm stencil

With matte coatings the surface roughness had rise to 263.95 nm after the first amount which lead to rougher surface then the printed sample with no coating and to 247.06 nm with the next amount and 213.02 nm with the highest amount of matte UV coating. All the measured and calculated data for the matte coated samples is presented in Table 2 and the AFM surface images are presented in Figure 3.

Table 2: Surface roughness parameters for the matte coated samples

Sample	S _a roughness average (nm)	S _q root mean square roughness (nm)	S _{sk} surface skewness	S _{ku} surface kurtosis
No coating	169.273	242.52	0.52	9.53
180 threads/cm	263.947	348.662	0.6859	5.6147
150 threads/cm	247.0605	322.583	0.4420	4.3211
120 threads/cm	213.019	276.366	0.5114	4.3825

As we can observe after the initial rise of the surface roughness with the application of the smallest amount of the coating there is a decline in surface roughness with the application of larger amounts of UV matte coating, while the UV glossy coating shows a throughout linear decline in average surface roughness with the additional coating amount applied. The surface skewness showed all positive values while the surface kurtosis showed a decline from the non coated sample but similar values for all coated samples, and overall smaller values then for the glossy coated samples.

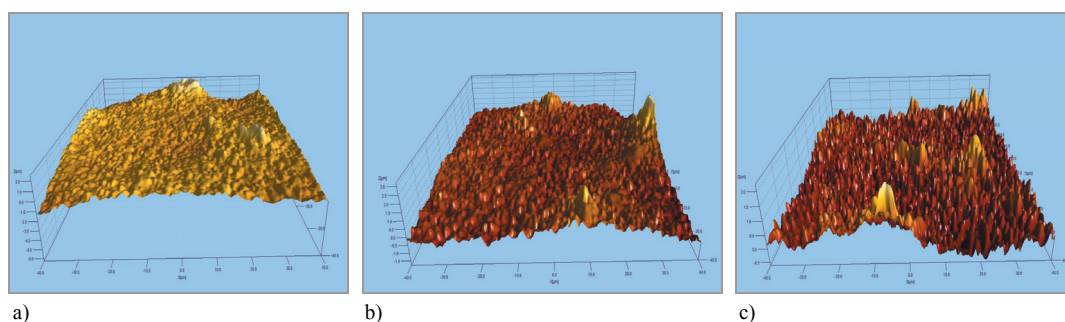


Figure 3: a) Cardboard sample with matte coating 180 threads/cm b) matte coating 150 threads/cm and c) matte coating 120 threads/cm

The results from the SEM pictures also showed differences in the changed surfaces of the print samples. The images of the matte coated samples is presented in Figure 4.

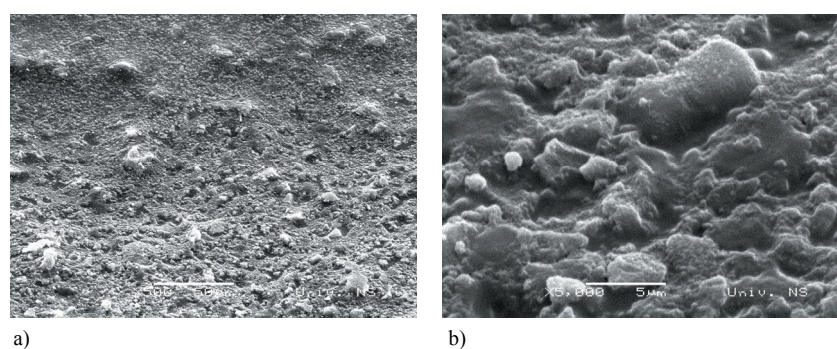


Figure 4: SEM images of the a) matte coating applied with the 180 thread/cm stencil b) 5000x magnification of the matte coated surface

As we can observe from Figures 4. on the borderline and on top of the UV ink the matte coating is containing larger particles (which cause the rougher surface and diffuse scattering of the light).

The colourimetric properties of the coated and non coated samples was evaluated with an $0^0/45^0$ spectrophotometer Techkon SpectroDens (D_{50} and 2^0 standard observer) and the appropriate colourimetric values, CIE ΔE colour difference values were calculated. The results are presented in Figure 5.

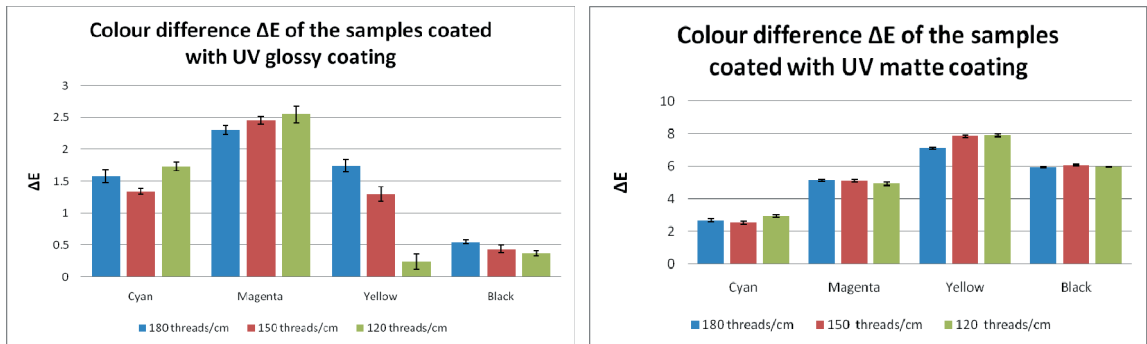


Figure 5: The colour difference values for the glossy and matte coated samples

The measured colour differences for the glossy coated samples was very small values with maximum around 2.5 and many of the samples were almost unnoticeable in human sensitivity terms (under $\Delta E < 1$) while the matte coated samples showed somewhat larger differences averaged between 2.51 to 7.88 which is noticeable even to the untrained eye. In colourimetric terms the glossy samples had darker more saturated values with the addition of coating while the matte coating changed the colour values to lighter less saturated. Separating by ink colours magenta has the largest differences for the glossy coated samples and black the smallest values, while for the matte coated samples the yellow and the black had larger values then the magenta and cyan ink. Cyan was in range of small differences while the other colours had noticeable colour difference above 4. The results are very dependable on the measurement geometry, and one of the factors influencing the differences in glossy and matte coated measured values are due to the directional geometry of the colour measuring instrument. These results indicate that for the colour rendering effect the smallest amount and the largest amount of glossy UV coating yield almost the same results and for matte coating more attention needs to be provided in the proofing process because of the larger changes especially in lightness terms.

5. Conclusions

At the end we made and calculated correlations and got for the linear approximation $r = 0.79$ for the average coating amount and average colour difference and $r = -0.95$ for the colour difference and surface roughness. We can observe that there is no high linear correlation between applied coating amount and colour difference, while on the other hand there is a linear decline in colour difference with the reduction in surface roughness. For the matte coatings these coefficients were $r = 0.89$ for the colour difference and coating amount (higher colour difference with higher coating amount) and $r = 0.84$ for the correlation of the surface roughness and colour difference. These results are highly influenced by the used measurement geometry because coated samples exert the larger reflection in the specular direction which is often defined as specular gloss. Nevertheless because gloss is hard to define because of the large influence of the direction of the surface elements it is also necessary to make additional colour quality control for the printed sheets. In the future we shall make an additional multiangle measurement of the samples to gain extended colour measurement data on this topic and to see the ratio of the specular and diffuse reflection on these kind of samples.

Acknowledgements

This work was supported by the Serbian Ministry of Science and Technological Development, Grant No.: 35027 "The development of software model for improvement of knowledge and production in graphic arts industry".

This work was supported by the Vojvodinian Secretariat for Science and Technological Development and authors want also to thank the Federation of Hungarian Printers and Paper Makers.

References

- Berns R.S., de la Rie E.R. (2003) The Effect of the Refractive Index of a Varnish on the Appearance of Oil Paintings, *Studies in Conservation*, 48 (4), pp 251-262
- Berns, R.S., de la Rie, R. (2003) Exploring the optical properties of picture varnishes using image techniques. *Studies in Conservation*, 48, pp. 73-82

Elias M., E. de la Rie R, Delaney J., Charron E., Morales M. K. (2006) Modification of the surface state of rough substrates by two different varnishes and influence on the reflected light, *Optics Communications*, Volume 266, Issue 2, 15 October 2006, Pages 586-591

Simonot L., Elias M. (2004) Color change due to a varnish layer, *Color Research and application*, 29 (3), pp.196 - 204

Satas D., Tracton A.A. (2001) *Coatings technology handbook*, Marcel Decker, New York

Surfoptic (2007) *Reflectometry Technical Paper No. 2*, Surfoptic, Accessed at www.surfoptic.com/TP2%20Imaging%20Reflectometer%20Theory.pdf (06.06.2011)

Novaković D., Karlović I., Gojo M., Agić D. (2009) Utjecaj površinskog oplemenjivanja otiska na kolorimetrijske i vizualne karakteristike. *Tekstil*. 58 (8), pp. 384-392

Extending the use of fibre based substrates using novel surface treatment methods: case studies

*Vesa Kunnari*¹, *Annaleena Kokko*¹, *Tomi Erho*¹, *Timo Kaljunen*¹,
*Thea Sipiläinen-Malm*¹, *Mikko Keränen*²

¹ VTT Technical Research Centre of Finland, Biologinkuja 7, FIN-02044 Espoo, Finland

Emails: vesa.kunnari@vtt.fi; annaleena.kokko@vtt.fi; tomi.erho@vtt.fi; timo.kaljunen@vtt.fi;
thea.sipilainen-malm@vtt.fi

² VTT Technical Research Centre of Finland, Kaitoväylä 1, FIN-90571 Oulu, Finland

E-mail: mikko.keranen@vtt.fi

Abstract

Consumer trends and the business environment as a whole are changing with a continuously faster pace. Introducing new innovative and sustainable products are the key for success. Development of new bio-materials enables the development of novel sustainable products for packaging and printed media.

This paper presents three different cases where novel pilot scale surface treatment line has been used successfully to demonstrate three pre-commercial applications beyond traditional paper process concepts. The first application was based on replacement of traditional pigments in coatings by a thermoplastic starch pigment to create a smooth surface for printed electronics. The second application was based on an oxidizing reaction between an enzyme and a substrate to produce a colour reaction. The third application concentrated on tailoring paper surface properties using thin starch based coating layer so that the same base paper could be used for offset or rotogravure printing depending on the end use.

Keywords: surface treatment, printed electronics, enzyme, colour reaction, tailored surfaces

1. Introduction

VTT's novel pilot scale surface treatment line has successfully demonstrated three new pre-commercial applications that could be referred to as printed intelligence. Printed intelligence can be defined as components and systems which extend the functions of printed matter beyond traditional visually interpreted textual and graphical communications and perform actions as a part of functional products or information systems.

Creating bioactive functionality and printed intelligence on paper by printing and coating is already possible and some simple demonstrative examples such as new detection methods, integration of electronics and optics onto large area substrates have been created already. These applications are aimed to replace more expensive products or are more sustainable for low value end uses (Pelton, 2009). Bioactive paper can be defined as paper-like products, cardboard, fabrics and their combinations, etc., with active recognition and/or functional material capabilities (Aikio, 2006).

Pilot equipment used for creation of pre-competitive demos has the acronym SUTCO shortened from surface treatment concept. The line consists of 16 individual components that can be connected as desired and can be set up according to the research needs. The main benefits of the surface treatment concept are low cost, low coating material demand and wide range of suitable substrates including plastics, paper and carton board.

The case study demos described in the following show some general principles how the flexibility of the pilot line may be used to generate tailored, functional surfaces for similar type cases in the future.

To ensure sufficient printability and conductivity a low surface roughness is desired in creating base for printed electronics on paper. The first case study presents the development work and results acquired to create smoother base for printed electronics by replacing a traditional coating pigment by a thermoplastic starch pigment in coating colour. Thermoplastic starch was plasticized after coating in the calendar nip at elevated nip pressure and high surface temperature of calendar rolls. Conductive patterns were printed successfully on thermoplastic starch coated paper surface using silver containing conductive ink in a lab scale rotogravure press.

Development work and results from creation of bioactive functionalities on a fiber based web in the form of a simple biosensor are presented in the second case study. An enzyme - substrate solution combination was created using known and commercially available enzymes and substrate solution and applying them on fibre based, commercially available base paper. The enzyme causes an oxidation reaction in the substrate solution which is seen as colour change. The enzyme was applied as a fine mist using spray-application followed by careful drying to avoid the inactivation of the applied enzyme. Substrate solution added on to the enzyme coated base causes an immediate local colour reaction. This technique enables small regions of large area of fiber web to be cut out and each small piece can be used to create a fast reacting biosensor.

In the third case study tailored paper surface properties were created using thin layers of about 0.5 gm⁻² of modified starch based coatings [Kataja, 2006]. The application was made using flexo-type coating or spray coating. The coating layer influenced water spreading and absorption of water based inks. For solvent based and oil based printing inks the absorption could be delayed and spreading restricted.

2. Materials and methods

2.1 First case study: smoother surface for printed electronics

A precoated wood-free fine paper with a basis weight of 65 gm⁻² was used as a base material for the surface treatments applied on the pilot line.

The reference material chosen for the smoothness measurements was chosen to be a product called LumiFlex. It had previously been shown to be suitable for simple printed electronics application as printing substrate while printing a conductive ink in VTT's own research studies. LumiFlex is a semi-gloss, one-side coated paper designed for heavier basis weight flexible packaging applications with high printing side smoothness (Kataja, 2006) The smoothness levels are presented in table III.

Three different surface coating materials were selected based on the resulting smoothness that they generated. A platy Capim-type fine kaolin pigment sourced from Brazil was an obvious pigment choice. A Flexo-varnish used for protection of printed surface and to enhance appearance of magazines and quality packages was the second chosen coating. The Flexo-varnish primer was first added and followed by top coat varnish. The third chosen surface coating was based on a thermoplastic starch pigment developed, patented (Peltonen et al, 2008) and successfully used as a coating colour pigment (Saari et al., 2006). No pre-treatments or multiple different coatings for the same trial point were used in order to create a smooth surface. The thermoplastic starch is a coating colour pigment originally developed by a joint research effort by VTT, University of Helsinki and University of Joensuu. The pigment is a starch based, thermoplastic and may be considered as a bio-based replacement for mineral filler and coating pigments. The starch pigment can be made for example from chemically cleaved potato starch. The non-water soluble starch derivatives are dissolved in an organic solvent mixture. Water is added to this mixture to dilute it, a milky-like particle dispersion is spontaneously formed. Particle size distribution can be varied by the dilution process, dilution speed and concentration of starch polymer solution. The organic solvent is removed after dilution by evaporation under controlled conditions which depend on the solvents used (Saari et al., 2005).

The starch pigment can be made as a non-dried pigment or as spray-dried pigment after precipitation. For practical storage and transportation reasons it is more feasible to use the dried quality starch. Dispersion of the spray dried starch pigment requires slightly more attention than dispersion of optimized mineral pigments. The spray dried pigment is light and therefore dusts easily. Mixing during disintegration should be done with slower than average rotation speeds while the slurry is prone to foaming if too high mixing speed is used. The dried starch pigment was dispersed to 30% solids content in the trials (Saari et al., 2005).

Coating colour formulation for thermoplastic starch pigment and kaolin based coating colours are shown in Table 1.

Table 1: Formulation of thermoplastic starch and kaolin based coating colours. The dry solids content of the thermoplastic starch based colour was 30 %. The dry solids content of the kaolin based colour was 45 %

Coating colour component	Parts
Thermoplastic starch or Kaolin	100
Latex	12
Thickener	0.8
Dispersing agent	0.1

No lubricant or optical brightening agents were added in the coating colours in order to generate as simple as possible coating colours. Optical properties were not the scope of the case studies.

A soft bar coating method was developed in order to achieve a high coating amount in single coating pass and also to eliminate the problem of an orange peel pattern occurring while coating viscous coatings using flexo-type roll coating.

The coating colour amount that can be applied on a web using flexo-type roll coating becomes smaller with every pass and it may require excessive number of passes to reach coating amount needed to create coating layers of over 10 gm⁻².

The soft bar coating was designed utilizing available in house materials and is based on a grooved rod backed up by a flexible element. The grooved rod is loaded against the soft backing roll and the volume of the grooves determines the coating amount on the web. The rod was placed on existing element on the coating equipment. The rod is at preset in a stationary configuration. The technique is similar to industrial rod coating (Carney, 2009). Principle of soft bar coating and developed equipment are shown below.

1. Coating reservoir/tray
2. Flexible edge doctors; placed only on web edges
3. Counter roll
4. Fixed pre-doctor
5. Coating bar/loaded soft bar
6. Softening/cushioning element
7. Doctor-cleaning of excess coating from counter roll

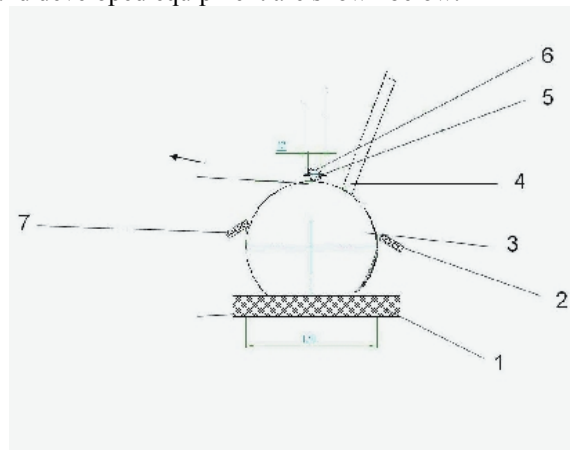


Figure 1: Illustration of the soft bar coating station structure

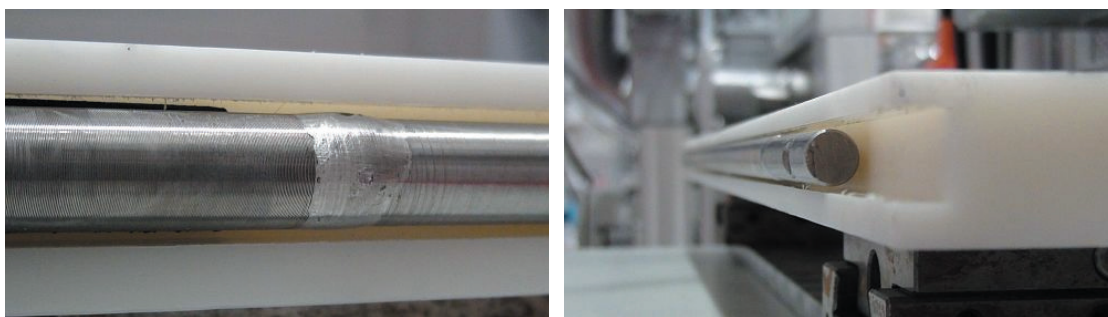


Figure 2: Rod and softening element placed under the rod.

After coating, the paper webs were calendered in a single, hard-soft nip laboratory calendar. The calendar conditions were specified for each coating using elevated nip pressure and when possible high surface temperature of calendar rolls. Flexo-varnish coating showed signs of adhesion and sticking under calendar roll surface temperatures of 100 °C so that it was calendered using unheated rolls.

The calendaring conditions are presented in table 2.

Table 2: Calendaring conditions

Coating based on	Thermoplastic starch	Kaolin	Flexo-varnish
Nip pressure, kN/m	150	150	150
Roll surface temperature, °C	140 - 150	150	25
Number of passes	3	3	3

After coating, the webs were printed. “Pico lab-scale gravure printing machine” was used to print the conductive ink and a predetermined test pattern. The test pattern consisted of three similar pattern having different cell volumes. Conductivity was measured as resistance, using a common multimeter. The resistances were measured for each coated web from selected straight line patterns using same distance for resistance meter pens. The printed pattern is shown in Figure 3.

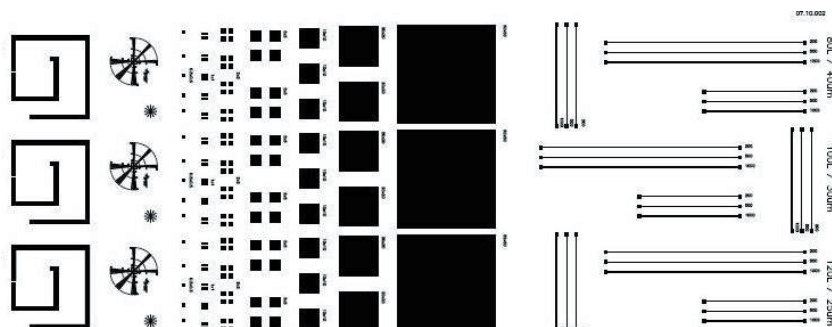


Figure 3: Printed pattern used in case study

The resistances were measured from the line patterns, shown above, by placing multimeter measuring tips in the squares in the end of each straight line. This ensured that measuring distance was equal for each trial point.

2.2 Second case study: enzyme-based bioactive functionalities on paper web

Enzyme, substrate solution raw materials and base paper materials were commercially available and purchased from known suppliers. In this context substrate means the solution that is added on the enzyme coated surface and changes colour. Due to the confidential nature of the case study the name and type of substrate solution or the name, type and the amount of enzyme used cannot be specified.

The enzyme was applied with a spray application on to a uncoated lwc-base type base paper to create a colour reaction. AVAC A4 high shear rate viscometer was utilized to provide the necessary pressure for the enzyme-solution to be added on to a moving web as spray mist. A single spray-nozzle was located in a position with appropriate fume removal to prevent misting of the enzyme solution. The spray pattern of the nozzle was wide enough to cover the width of the 500 mm when placed at an appropriate distance above the moving web. To prevent the blockage of the nozzle the enzyme solution was filtered through a smaller mesh size screen than the spray-nozzle opening size prior to spraying.

During drying of the enzyme solution, moderate temperatures, typically 40-50 °C, were used on the drying section to prevent the inactivation of enzyme during drying.

2.3 Third case study: Tailored paper surface properties

Tailored surface properties were created using modified starches which were processed from native potato starch or hydrolyzed potato starch and amylase rich maize starch as raw material. Modified starches producing most promising results used in this case study were hydroxypropylated and acetylated starch (PA_PO) and starch octenyl succinate (P_OSA). The polymers were self organizing (SOS) type. For example the starch can be modified by attaching octenylsuccinate-units on the base-starch polymer chain. The behaviour of anionic character hydrophilic starch polymer changes as the attached hydrophobic units might be able to open the starch agglomerate. As the starch chain opens the hydrophilic part is able to settle on hydrophilic paper surface and the hydrophobic part (e.g P_OSA) stays upwards altering paper surface to more hydrophobic character.

The paper substrates used was an uncoated lwc-type paper with hydrophilic and hydrophobic surface properties before application of starch based coatings.

The thin coatings were applied using flexo-type coating. The capacity of the anilox rollers was varied to coat the target amount of starches having different dry solids consistency on to the paper surface. The amount of modified starch coated on the web were between 0.5 - 1.0 gm-2 (dry coating). After coating the papers were calendered in laboratory calendar using 130 kN/m nip pressure, 62 °C roll surface temperature. The residence time in nip was 22 ms. The coated paper were tested using IGT gravure printing testing equipment.

3. Results

3.1 First case study: smoother surface for printed electronics

It was possible to print conductive patterns for all coated webs after calendaring. The conductivity of the pattern was related to smoothness of the printed surface.

Generally the smoother the paper surface, the lower the resistance of the conductive pattern. As a reference for conductivity measurements a biaxially-oriented polyester film plastic called Lumirror was used (Toray, 2011). Lumirror is a proven, valid base substrate for printing electronics. The thickness, Bendtsen roughness, roughness values from Veeco optical profiler measurements (Veeco, 2008) and resistances are shown in Table 3.

Table 3: The thickness, Bendtsen roughness, Ra roughness values from Veeco measurements and resistances of different trial points

	Thickness, μm	Bendtsen roughness, ml/min	Roughness Ra, μm	Resistance, Ω Area 3
Thermoplastic starch	64 ± 2	0	1,96	117 ± 1
Kaolin	60 ± 2	0	1,42	125 ± 2
Flexo-varnish	70 ± 1	10 ± 1	1,57	324 ± 10
LumiFlex Ref	95 ± 2	13 ± 1	1,96	-
Lumirror Ref	-	-	-	70 ± 1

The kaolin based coating colour and thermoplastic starch based coating colour samples have the lowest electrical resistances. Although it is still about 30% greater compared to the printed Lumirror reference. Flexo-varnish coated samples had clearly the highest resistances as the samples were rougher as a consequence of their inability to tolerate calendaring using elevated nip pressure.

The flexo-varnish coating could not tolerate high temperatures so it was calendered using room temperature calendaring rolls. Despite this more gentle treatment with unheated calendar rolls, after calendaring some minor small scale cracking was observed in flexo-varnish coated samples which contributed to increased resistance. To minimize resistance as smooth as possible surface is desired.

Obviously also interpreted from the results was the fact that when ink amount on the coated surface is higher, the electrical resistance is lower. The resistances correspond to cell depth in used for a gravure roll which defines the ink amount.

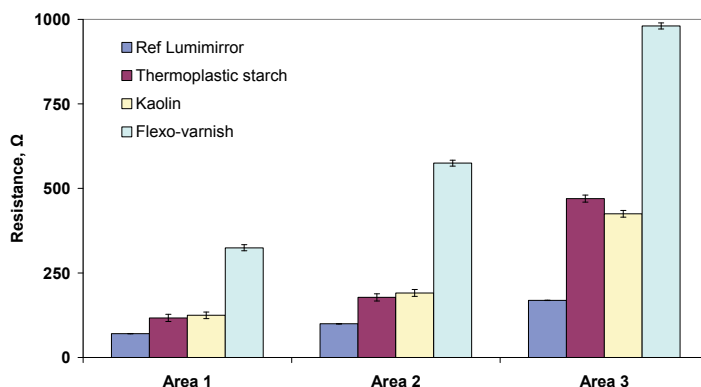


Figure 4: The resistances of different trial points as printed line width was 1000 μm . Gravure cell capacity increased from area 3 to area 1

3.2 Second case study: enzyme-based bioactive functionalities on paper web

Application of substrate solution on an enzyme coated web created a colour reaction on lwc-type base web successfully, which proves the enzyme stayed active during the process of spraying and drying. Based on these trials, the application technique developed during this case study has later been used in other similar application for slightly modified purposes.

To create a colour reaction the enzyme has to remain active during the drying section on the paper or printing machine. The enzyme has to possess also high enough activity on the paper web which can be altered by mixing different amount of enzyme to carrier solution. The carrier solution was water in these trials. Also the substrate solution needs certain high enough specified concentration that a rapid and constant colour reaction can be created. Due to confidential nature of the case study the name and type of substrate solution or name, type or amount of enzyme used cannot be specified.

After substrate solution is added selectively on an enzyme coated web a colour reaction is seen already 5 seconds after application. The intensity reaches a maximum in 10 seconds time. The reference point compared to enzyme coated web immediately after application of substrate solution and 10 seconds after application is shown in figures 5-6.



Figure 5: The reference point compared to enzyme coated web immediately after application of substrate solution

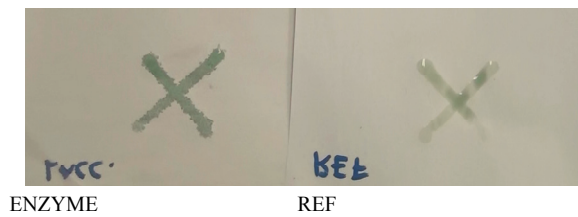


Figure 6: The reference point compared to enzyme coated web 10 seconds after application of substrate solution

The colour reaction could be utilized for example in tickets. The enzyme could be printed on ticket and at the event a printed pattern could be revealed using substrate solution. Mass production identification techniques or to verify the authenticity of a product could be other applications.

3.3 Third case study: Tailored paper surface properties

By applying a small amount of modified starch on paper surface it was possible to change and tailor the paper surface properties.

The print density clearly improved and print through decreased when using polymers which decreased air permeability. This might be result of good film forming properties or pore blocking of paper structure. The contact angle measurements could support the principle where the starch polymer organizes on hydrophilic paper surface and the surface to become more hydrophobic. The contact angle results will be published in a separate paper.

Table 4: Print density, print through, change in air permeability and contact angles for water for modified starches

	Print density	Print through	Change in air permeability, %
LWC Base	1.90	0.35	0
Water-Ref 20 gm-2	1.65	0.32	9
P_OSA3-1 0.4 gm-2	1.31	0.27	-25
P_OSA3-1 0.8 gm-2	1.38	0.24	-62
PA_PO5-6 0.4 gm-2	1.27	0.30	-13
PA_PO5-6 0.8 gm-2	1.43	0.25	-32

The best gravure printing results were received with hydroxypropylated and acetylated starch (PA_PO) and starch octenyl succinate (P_OSA) treated papers.

Figure 9. shows how the thin starch coating layer appears on printed paper when coated with similar type polymer as PA_PO and P_OSA. The print through is clearly better in the trial point where modified starch

polymer has been added. Also the print density is much better. These changes are also visible to the naked eye and not only for laboratory equipment.

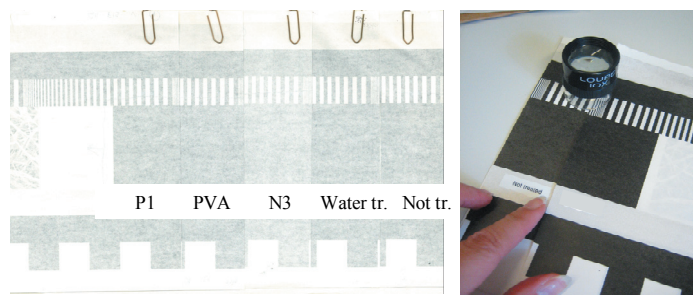


Figure 7: Test pieces showing decrease of print through and enhancement in print density after tailoring of surface properties

Additional measurements from water and oil spreading clearly showed that both can be affected by application of thin modified starch layers to give better print quality.

4. Conclusions

In the first case study a new coating method was developed and implemented successfully. The calendered product was sufficiently smooth to print conductive patterns. The surface roughness was not as low as the surface roughness of plastic. Trials attempting to create smoother base for printed electronics will continue at pilot scale.

The second case study proved a simple concept of a relative cheap solution to create bioactive surfaces. By combining knowledge from biotechnology a simple biosensor was successfully implemented using pilot surface treatment environment.

Trials made during third case study showed that by applying a small amount of starch based coatings on paper webs the surface properties of paper can be affected and changed in the desired direction. The printing properties such as print through and density can be significantly enhanced. Also printing colour behaviour for water based, oil based and solvent based on paper surface can be affected. The tailoring of paper surface enables printing of same base paper using e.g. offset or gravure printing. The same base paper becomes suitable for several end products.

The surface treatment concept pilot line was successfully used to create demonstrative products of printed intelligence in the applications described in this paper. The modifications necessary were implemented for successful surface treatment. The surface treatment concept line opens new possibilities for new products and processes for forest industry and converters.

Acknowledgements

This work was done at VTT Technical Research Centre of Finland. The work done by technical laboratory staff and mechanical work of machine shop at VTT contributed significantly to the successful implementation of the case studies presented. Authors would like also like to thank the following companies that provided equipment and materials used in the case studies: Coatema Coating Machinery GmbH, UPM-Kymmene, Toray, Imerys, AB Enzymes and Sun Chemicals.

References

- Aikio, S., et Al, (2006), *Bioactive paper and fibre products patent and literary survey*, VTT Working Paper 51, VTT Technical Research Centre of Finland, Oulu, Finland.
- Carney, B., (2009), *Coater Backing Roll Information*, Tappi PaperCon, May-June 2009, St Louis.
- Kataja, K., (2006), *Tailoring paper printability with small amount of polymers or with plasma treatment*, Cost E32, September 2006, Ljubljana.

LumiFlex, (2011), <http://www.storaenso.com/products/packaging/packaging-papers/flexible-packaging-papers/Pages/lumiflex.aspx>

Pelton, R., (2009), *Bioactive paper provides a low-cost platform for diagnostics*, *Trends in Analytical Chemistry*, Vol 28, No. 8, 925-942.

Peltonen, S., Mikkonen, H., Qvintus, P., Varjos, P., Kataja, K., (2008), *Pigment and filler and method of manufacturing it*, *WO 2005030844*, 1-49.

Saari, J., Kataja, K., Qvintus, P., Mikkonen, H., Joyce, M., (2006), *Organic Starch Based Pigments in Paper Coatings*, TAPPI Advanced Coating Fundamentals Symposium, 8-10.2.2006, Turku, Finland.

Saari, J., Kataja, K., Qvintus, P., Mikkonen, H., Joyce, M., (2005), *Coating Trials Results with Non-Mineral Starch Based Pigments*, Tappi Coating Conference and Exhibit, 17-20.4.2005, Toronto.

Toray, (2011), http://www.toray.com/business/products/ict/electronics/ele_003.html.

Veeco optical profilers, (2008), <http://www.optics.arizona.edu/opti696/Sp%202008/TermPapers/VEECO.pdf>

Improving the light fastness of sublimation transfer printed polyester substrate

Imadeddine Afara, Philip Urban, Edgar Dörsam

Technische Universität Darmstadt
Institute of Printing Science and Technology
Magdalenenstr. 2, D-64289 Darmstadt, Germany
E-mails: afara@idd.tu-darmstadt.de, urban@idd.tu-darmstadt.de, doersam@idd.tu-darmstadt.de

Abstract

In this paper we are investigating methods to improve the light fastness of sublimable colorants printed on a polyester substrate. A combination of UV-Absorber (UVA) and Hindered amine light stabilizer (HALS) is applied directly as post-treatment to the printed polyester substrate. The influence of the colorants concentration (C%), transfer-temperature (T_{trans}), transfer-time (t_{trans}) and the combination of the UVA/HALS is investigated in this work. Distinct combinations of these influencing factors are found for that the light fastness of printed fabric is improved significantly in terms of ΔE^*_{ab} colour difference. The light fastness of all CMYK inks is improved significantly (50-70 %)

Keywords : light fastness, sublimation transfer printing, polyester substrate, UV-absorber and HALS

1. Introduction

The Reducing of the pollutions to protect the environment is a relevant subject, especially where the environment laws and regulations are severe. Therefore, we are working to develop a printing Method that is environment friendly and able to meet the claimed requirements (an excellent light fastness). Many methods are available to print polyester based textiles. Some of these methods such as screen printing or digital printing, which are described as direct printing methods, are able to provide a satisfied light fastness. However a washing stage is necessary to remove the unfixed colorants.

Sublimation transfer printing which is described as an indirect method, enable to print the polyester based textile without using a washing stage. Unfortunately a printed substrate due to this method offers a poor light fastness (Afara, 2008).

In this paper we investigate methods to improve the light fastness of sublimable colorants printed on a polyester based textiles. These colorants are organic dyes that are usually based on Azo or Anthraquinone groups. They are very damageable by absorb the rays of incident light in the UV-VIS range (320-780 nm). The smaller the wavelength, the higher is the energy of radiation. Therefore the energy that is absorbed by the colorant is able to activate the reaction sites of the colorant's molecules, which can lead to internal conversion of the colorant's molecules or to destroy it. This phenomenon is expressed as colour fading duo to light exposure.

The light fastness, which describes the colour's stability against the light, is related to its absorption ability in UV-VIS range. Therefore some of these colorants undergo change in the colour shade, while others undergo a change only in the lightness (Figure 1).

The majority of previous studies investigated two ways to protect a dyed synthetic fibre against the UV-VIS radiation:

- The first one is the chemical conversion of the colorant's molecule: Kim et al. reported that the disperse dyes, which possess a Phenylindole group as a coupling compound, exhibit an excellent resistance to light (Kim, 2001) H. Freeman et al. included integrated a built-in UV-stabilizer in a commercial product. The light fastness was improved but the selection of the UV-stabilizer group as well as the integration location in the molecule remains critical (Freeman, 2004).

US-patent U.S 7,125,443 B2 (Lee, 2006) describes the improvement of the light fastness of conventional colorants in building a chemical bond between the colorant molecule and the group of the UV-stabilizer (Lee, 2006). H. Maradiya et al. reported that the colorant that is based on an N, N-

dialkylanilines and 2, 6-dibromo-4-nitroaniline possesses an excellent light fastness (Maradiya, 2001; Maradiya, 2002).

- The second one is by applying an additive: Maerov et al. reported that more groups of UV-light stabilizer based on Benzophenone are able to protect the colorant against radiation. This additive was applied by a dying process (Maerv, 1961). Reutsch et al. investigated how UV-Absorber diffuses into the fibre. He observed that different UVA diffuse differently (peripheral und cross-sectional) in the fibre and that the distribution of the UV-Absorber has a large influence on the light fastness of colorant and fibre (Ruetsch, 1996). Rich et al. reported that the application of UV-absorber in the dye bath to protect a dyed nylon substrate against the radiation was not successful (Rich, 1993). Crews et al. tried to apply the additive in a post-treatment, which was not successful as well (Crews, 1990). Afshari et al. applied the additive by a pretreatment and a post-treatment process. He reported that the direct application to a dyed substrate in the dye bath was unsuitable because the dye was desorbed (Afshari, 2005).

Practically, there are no sublimely colorants that are able to offer the light fastness that meets our requirements. Therefore we investigated in this work the possibility to apply a special mixture of different additives either as post- or pretreatment that is able to protect the colorant against the light.



Figure 1: Colour fading of sublimely colorants printed on polyester based textiles, which is exposed to light included a high amount of UV-radiation

2. Methods

In our experiments we tested the influence of different additives as well as transfer conditions (transfer-temperature (T_{trans}), transfer-time (t_{trans}) and the concentration of the colorant (C %)) on the light fastness of the final textile print. Figure 2 shows the experimental setup.

The substrate is a special technical fabric designed for the automotive industry. The colorants in **CMYK** developed for rotogravure printing were supplied as water-based ink-concentrates. The ink formulation is performed by the Institute of Printing Science and Technology. The investigated additives were:

- UVA-1, UVA-2
- HALS-1, HALS-2

The paper is supplied in different grammage from two different paper manufacturers.

We investigate two ways of applying the additives to the substrate: pretreatment and post-treatment. In the following text we will describe the whole procedure including the pre- and post-treatment steps. Please note that pre- and post-treatment are applied exclusively.

The mirror-inverted motive is printed by the IGT G1 05 laboratory rotogravure printing press on paper (see Figure 2, block 1). Then the printed paper is dried at room temperature and humidity for more than 24 h.

Pretreatment (optional)

In the case of pretreatment, the additives were placed and fixated on the polyester substrate *before* the transfer step. For this purpose a two-step approach is used: In the first step, a layer of UV-Absorber is applied to the fibre following a thermal fixation.

In the second step, a layer of light stabilizer is applied on it and fixed thermally as well. In this work we fixated the additives utilizing the Baier Geba 6 transfer press. The transfer of the colorants from paper to the fibre substrate is performed under defined conditions using the Baier Geba 6 transfer press (Figure 2, block 2).

Post-treatment (optional)

In the case of post-treatment, the additives were placed and fixated on the polyester substrate *after* the transfer step. The procedure is similar as explained in the pretreatment step.

A Xenon tester (SUNTEST XLS+ from ATLAS Material Testing Technology) with an air-cooled 1700-Watt Xenon arc lamp is used to simulate the fading of colorants under natural daylight and daylight filtered by a window glass (see Figure 2, block 3). The filter system of the Xenon tester consists of two filters:

- A cut-off filter at approximately 320 nm is used to simulate the sun light exposure behind 3 mm thick window glass (Figure 3),
- A basic filter based on quartz glass with IR-reflective coating is used to ensure low **black standard temperature (BST)** values in the test chamber by reducing the heat radiation

The exposure conditions were as follows:

- **Black standard temperature (BST):** 100°C
- **Chamber temperature (CHT):** 45-50°C
- The **relative humidity** in the test chamber (RH): 10%
- The **irradiation intensity** is controlled in the range of 300-400 nm: $I_{rr300-400nm}$ is 60 w/m²

The light fastness of the colorant printed on the polyester based textile is evaluated using the CIELAB colour difference ΔE_{ab}^* (formula (1)).

Calculation of colour difference:

$$\Delta E_{ab}^* = \sqrt{(\Delta L^*)^2 + (\Delta a^*)^2 + (\Delta b^*)^2} \quad [1]$$

$$\Delta L^* = L_1^* - L_2^*, \quad \Delta a^* = a_1^* - a_2^*, \quad \Delta b^* = b_1^* - b_2^*$$

$$(L_1^*, a_1^*, b_1^*) = \text{color before exposure}$$

$$(L_2^*, a_2^*, b_2^*) = \text{color after exposure}$$

The colour difference of a sample-set is measured before the exposure (R_{befor}) and after the exposure (R_{after}) using the *Konica Minolta CM 2600d* spectrophotometer (Figure 2, block 4). The settings of the instrument were selected as follows:

- Measuring geometry: spherical geometry (d/8°)
- Illumination: D65, Observer: 10°, Gloss: the measurements were performed without gloss (modus SCE)
- UV component: cut-off at 400nm, Measuring aperture is 11mm

The average of three measurements on different positions is calculated.

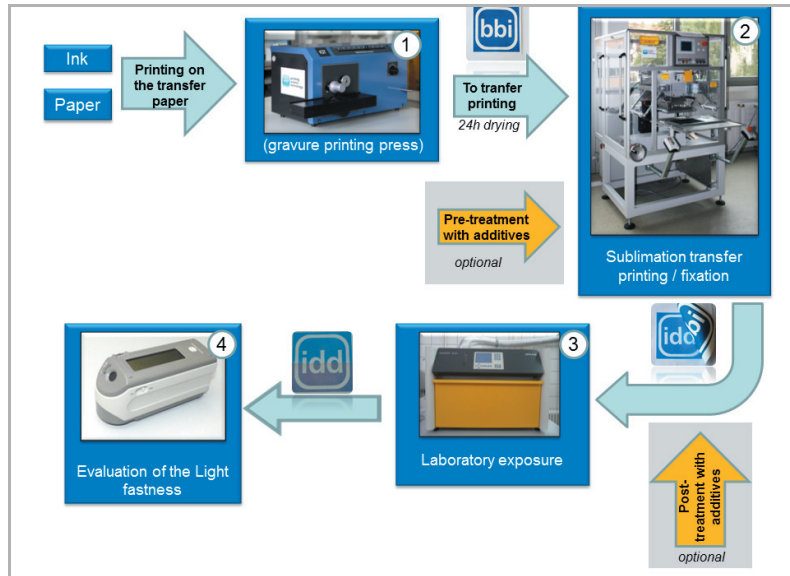


Figure 2: The workflow of the experiments

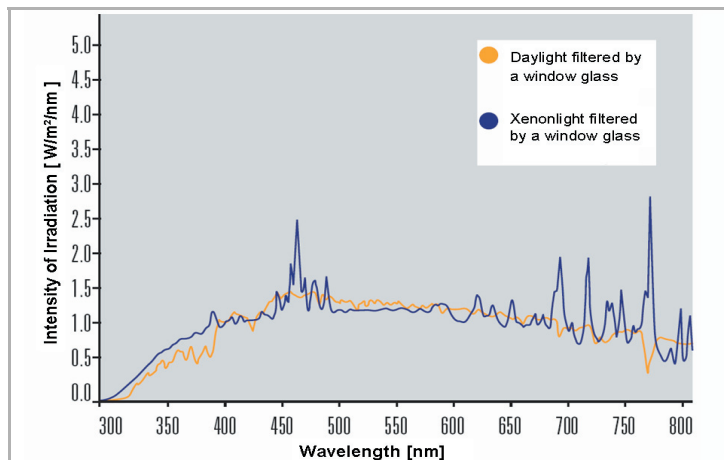


Figure 3: Xenon light compared to daylight both filtered by a window glass [Atlas-mts, 2010]

In sublimation transfer printing, the colorant diffuses in the structure of the polymer and builds no layer on the substrate’s surface. Therefore, the deeper is the colour’s shade the greater is the amount of the colorant on the substrate. We used the reflectance [%] to describe this amount of colorant. Please take care that this relation ship [reflectance vs. colorant’s amount] isn’t linear.

Calculation of the reflectance [%]

$$\text{Reflectance} [\%] = \sqrt{\frac{1}{n} \sum_{i=1}^n (R_1^i - R_2^i)^2} \tag{2}$$

R_1, R_2 : are the spectrums of the colorant

3.Results and discussion

Manufacturers of sublimation inks usually recommend defined conditions (t_{trans}, T_{trans}) for transferring the motive to achieve high print quality and to keep costs low. The influence of these conditions on the light fastness properties of the printed substrate depends on the special application of the product. Constrained to the requirements of our industrial partner we analyzed the process parameters to enhance the light fastness of printed polyester substrates. For this purpose, we investigated which conditions ($C\%, t_{trans}, T_{trans}$ and additive combination) result in the best light fastness.

What colorant concentration can offer the best light fastness?

Giles et al. reported for a dying process that the light fastness of anomalous dyes is not monotonically related with the concentration of colorants. He observed that the light fastness increases to a maximum with increasing concentration in the dye bath. By further increasing the concentration the light fastness decreases to a minimum, and rises again (Giles, 1998).

Under the experimental conditions we observed that the light fastness (described with the ΔE^*_{ab}) of sublimely colorants increases with increasing concentration (Figure 4).

Particularly, we found under the test conditions that the amount of transferred colorants increases with increasing colorant concentration of the stock ink (Figure 4 - decrease of the reflectance [%]). The reason is that the transport of the colorant is a diffusion process that is related to the initial concentration.

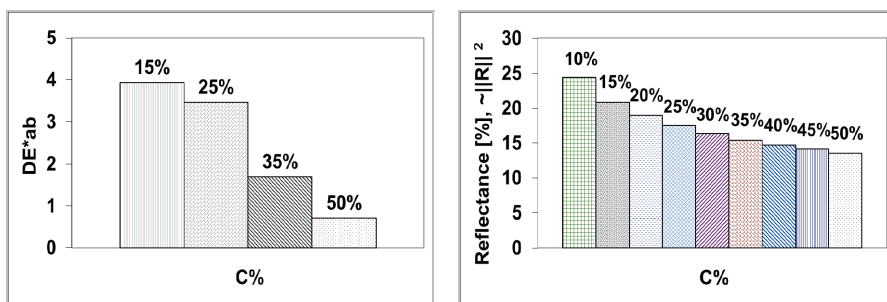


Figure 4: Influence of the colorant's concentration C% on the colour difference of the printed polyester (left) and on the reflectance (right). [F-1 black, t_{trans} : t_3 s, T_{trans} : T_3 °C, filtered by a window glass, Dosage: 34500 kJ/m^2]

Under heat supply of the transfer press the colorants sublime into the air gap between the transfer paper and the fibre and then penetrate into the polyester mass. These diffusion processes are depended on the physical and chemical properties of the polyester and the colorants. Giles et al. reported that the deeper a dye penetrates into the substrate structure, the less accessible is it to air and moisture and therefore the less liable to fade (Giles, 1998). In textile dyeing the dye is forced to penetrate deeper into the substrate by longer dyeing duration or higher dyeing temperature. We believe that for printing applications the correct adjustment of the printing parameters (the printing speed, the pressure of the impression roll, the depth and size of the gravure cylinder's cells, transfer-temperature and transfer-time) might enhance the light fastness. This raises the question:

What transfer-time and temperature may offer the best light fastness?

When the transfer-temperature (T_{trans}) or transfer-time (t_{trans}) increases, more thermal energy will be supplied from the transfer plate. The diffusion rate which is depended on the colorant concentration, temperature and duration of the transfer process will be accelerated. That means that the amount of the transferred colorant on the fibre is larger (Figure 5). We believe that the colorants are diffused deeper into the substrate, because the reflectance value and the colour fading that is described by ΔE^*_{ab} , decrease significantly (Figure 6).

The selection of the investigated parameters (T_{trans} , t_{trans} and C%) has economical and technical aspects. Depending on the requirements on the product and cost the optimal parameters ($T_{um, op}$, $t_{um, op}$ and C_{op} %) should be selected.

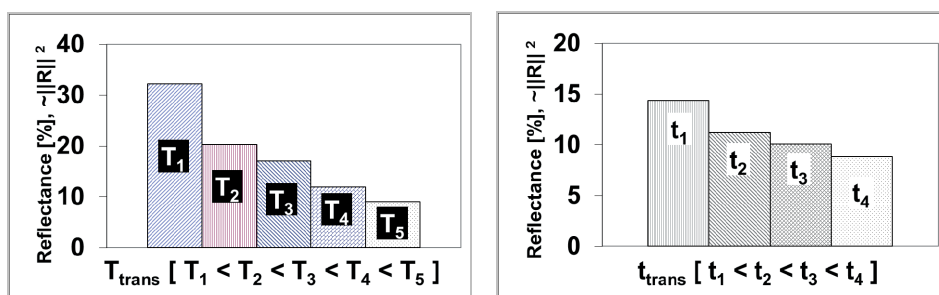


Figure 5: Influence of the transfer-time t_{trans} (left) and temperature T_{trans} (right) on the reflectance shown for the unexposed substrate

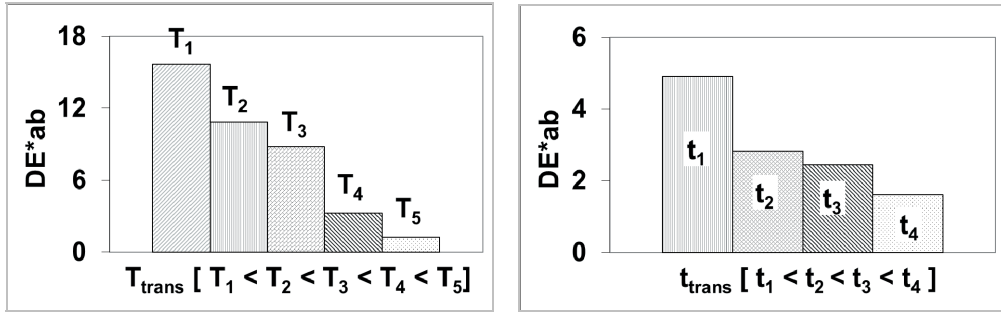


Figure 6: Influence of the transfer-time t_{trans} (left) and temperature T_{tran} (right) on the colour difference between the unexposed and exposed printed polyester substrate.

Which combination of UVA / HALS is required?

As expected, a combination of the UVA and HALS is required to enhance the light fastness of colorants (Table 1). Due to a chemical conversion of the UVA-molecule, the energy of the incident photons is absorbed. This energy is disposed in harmless form by a reordering of the UVA-molecule.

The energy that is not absorbed by the UVA-molecule causes free radicals that accelerate the fading of the colorant. The HALS-molecules scavenge these free radicals and convert them in harmless form. Since UVAs and HALS's are not 100% stable against the incident radiation their protective effect vanishes over the time. The different UVA's possess different absorption abilities in UV-range. Therefore they exhibit different protective effects (Table 1).

Table 1: Influence of the applied additive on the light fastness ΔE^*_{ab} of the printed fiber

[t_{trans} : t_3 s, T_{trans} : T_3 °C, daylight filter with UVmax, irradiation duration: 140h]

Colour Additive	$\Delta E^*_{ab_Black}$	$\Delta E^*_{ab_Magenta}$	$\Delta E^*_{ab_Cyan}$	$\Delta E^*_{ab_Yellow}$
Original	3,43	10,92	8,61	11,18
UVA-1 + HALS-1	1,33	2,92	2,04	2,9
UVA-1 + HALS-2	1,67	2,93	2,24	2,21
UVA-2 + HALS-2	1,23	4,15	2,63	5,01

As mentioned in the introduction other authors apply the additives in a pretreatment or post-treatment step, or added them directly to the dyeing bath. This raises the question:

Where to apply the additives?

In the present work, we investigate how the combination of additives should be applied to increase the light fastness. We observed in our experiments that a post-treatment is able to improve the light fastness better than the pretreatment (Figure 7). The colorant will be partially resublimed during the post-treatment stage. This is not a disadvantage because only the improperly fixed dyes will be re-sublimed.

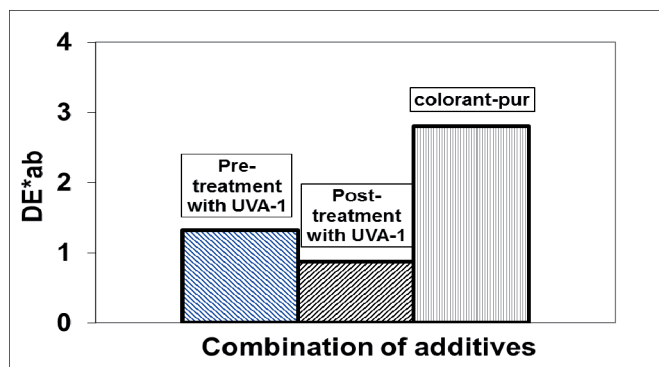


Figure 7: Influence of the treatment stage on the light fastness(the colour difference between the unexposed and exposed printed polyester substrate). [F-I-black, t_{trans} : t_3 s, T_{trans} : T_3 °C, daylight filter with UV_{max} , irradiation duration: 140h]

4. Conclusion

In this work we have investigated the influence of distinct parameters of sublimation transfer printing on the light fastness of sublimely colorants printed on a polyester substrate.

The following results were obtained:

1. The light fastness (expressed in ΔE_{ab}^*) of a sublimely colorant is a function of the colorants concentration, transfer-time and the transfer temperature.
2. The light fastness of these colorants is enhanced up to 50-70% by applying the correct combination of the additives and optimizing the colorant's concentration, transfer-time and temperature.
3. Post-treatment improves the light fastness more than pretreatment.
4. The re-sublimation of the colorant during the thermal post-treatment is not a disadvantage.

In future work we will investigate how a mixture of additives and colorants will affect the light fastness of the printed substrate. In case this is successful, the post-treatment can be omitted and the colorants are not re-sublimated.

Acknowledgments

This work is financially supported by the Arbeitsgemeinschaft industrieller Forschungsvereinigungen "Otto von Guericke" e. V. (AiF). The authors thank Mr. Grumbach, Mr. Lawrenz, Mr. Euler and Mr. Kurmakaev for experimental assistance. In addition, we thank the following companies for donating their products: Sensient Technologies Corporation, BASF, Clariant, Huntsman, Sun Chemical and Carl Stahl.

References

- Afara, 2008, Verfahren und Maßnahmen zur Verbesserung der Lichtehtheit im Textildruck, Masterarbeit, Institut für Druckmaschinen und Druckverfahren, Technische Universität Darmstadt
- Afshari, 2005, the Study of Effect of a UV-Absorber in the Dyeing of Polyester with disperse Dyes, *Vlákna a textil* 12/2
- Atlas-mts, Spezifikationen des SUNTEST XLS+, Atlas Material Testing Solution, www.atlas-mts.de
- Crews, D. Clarck, 1990, Evaluating UV Absorbers and Antioxidants for Topical Treatment of Upholstery Fabrics, *Textile Research Journal*
- Freeman, N. Berthelon, L. Edwards, 2004, Studies towards Lightfast Automotive Dyes for Polyester, *JTATM* Vol.3, and Issue.4
- Giles, 1998, Anomalous Light fastness in Disperse-Dyed Systems and its Significance in Studies of Fading Mechanism, *Textile Research Journal* 38: 467
- Hering, R. Martin, M. Stohrer, 2007, Physik für Ingenieure 10 Auflage, Springer Verlag
- Kim, E. Park, 2001, Relation between Chemical Structure of Yellow Disperse Dyes and their Light fastness, *Fibres and Polymers* Vol.2, No.3
- Lee, 2006, United States Patent, US 7.125.443 B2
- Maerov, H. Kobsa, 1961, Light fastness Studies of Basic Dyes on Acid Modified "Dacron" Polyester fibre, *Textile Research Journal*
- Maradiya, V. Patel, 2001, Dyeing of hydrophobic fabrics with disperse dyes, *J.Serb.Chem.Soc* 66(6)367–376
- Maradiya, V. Patel, 2002, Disperse Dyes based on 2-Aminothiazole derivatives for Polyester, *Bulletin of the Chemists and Technologists of Macedonia*, Vol. 21, No. 1
- Rich, P. Crews, 1993, Influence of Shade Depth on the Effectiveness of Selected Ultraviolet Absorbers in Reducing Fading, *Textile Research Journal* 63, and No.4
- Ruetsch, 1996, UV stabilization of PET fibre, *Textile Research Journal* 66(4)



Impacts on the impression of printed effect pigments

Martin Haas¹, Edgar Dörsam¹, Evgeny Kurmakaev¹, Thorsten Euler¹,
Martin Schmitt-Lewen², Immanuel Fergen², Joachim Sonnenschein²

¹ Technische Universität Darmstadt
Institute of Printing Science and Technology
Magdalenenstr. 2, D-64289 Darmstadt, Germany

E-mails: haas@idd.tu-darmstadt.de; doersam@idd.tu-darmstadt.de;
kurmakaev@idd.tu-darmstadt.de; euler@idd.tu-darmstadt.de

² Heidelberger Druckmaschinen AG
Kurfuersten-Anlage 52-60, D-69115 Heidelberg, Germany

E-mails: martin.schmitt-lewen@heidelberg.com; immanuel.fergen@heidelberg.com;
joachim.sonnenschein@heidelberg.com

Abstract

Effect pigments are more and more used to upvalue printed products in finishing processes. The main effect of these pigments is their changing color impression (color shift) depending on the viewing and illumination angle based on the physical effect of interference. Also higher gloss and sparkling effects can be achieved. While effect pigments of the first generation reflect color changes from a certain color to transparent, further developed pigments (second generation) allow changes from one to another color. The relative high pigment prices compared to those of common varnishes makes it interesting to use a highly effective printing process with a maximal utilization of the desired effects. In fact pigment manufacturer give considerations for the application of effect pigments by different printing processes. Nevertheless a general impact of print parameters to the effects caused by effect pigments has not been reported. Furthermore in printing praxis measurement systems for a quality control of the effects are rarely used. Printed products including effect pigments are often evaluated visually by the operators and customers.

The impacts of several print and material parameters on the impression of printed effect pigments are shown and discussed intensively. Based on the results of a systematic printing trial, general considerations for the operator to optimize the effects regarding customer-related issues like enhanced print quality and economic aspects are presented.

Keywords: effect pigments, print parameters, design of experiments, print quality

1. Introduction

Special effect pigments are more and more used for high-quality printing products. The main effect of these pigments is their changing color impression (color shift) depending on the viewing and illumination angle based on the physical effect of thin layer interference (Pfaff and Reynders, 1999; Maile et al., 2005). Also higher gloss and sparkling effects can be achieved. The geometry dependent interference effect of the pigments occurs due to the optical path difference caused by the thin titanium dioxide (TiO₂) layers covering the thin mica or silica flakes. For an interference effect, the optical path length the light has to pass within the material is important. Using the same material for the thin layers (refractive index of TiO₂: $n_{\text{TiO}_2} = 2,7$), the color impression of the effect pigments depends on their thickness (see Figure 1).

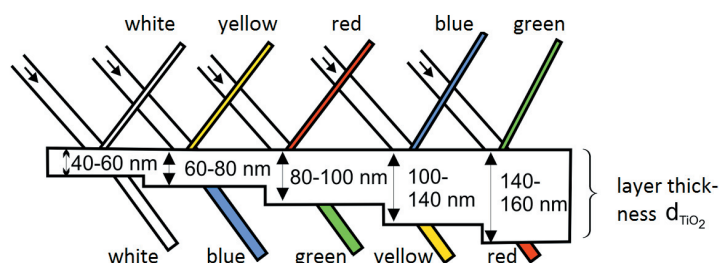


Figure 1: Layer thickness of titanium dioxide defines the interference effect color (Maisch, 1991; Hupp, 2008)

While effect pigments of the first generation reflect color changes from a certain color to transparent (Maisch, 1991), second generation pigments allow changes from one to another color (Pfaff, 2007). Table 1 shows the pigments and their properties, which were used for this study.

Table 1: Properties of the used effect pigment types (Merck, 2007f; Merck, 2007g; Merck, 2007h; Merck, 2007i)

Pigment Type	Compounding	Pigment Size
Iriodin® 211 Rutil Feinrot	Mica + SnO ₂ + TiO ₂	5 µm – 25 µm
Iriodin® 7215 Ultra Rot	Mica + SnO ₂ + TiO ₂ + SiO ₂	10 µm – 60 µm
Colorstream® T10-02Arctic Fire	Silica Flakes + SnO ₂ + TiO ₂	5 µm – 50 µm
Miraval® 5321 Scenic Copper	Potassium-Aluminium-Borosilicate + SnO ₂ + TiO ₂ + SiO ₂	10 µm – 100 µm

The Iriodin pigments, with a color shift from red to transparent, belong to the first, the Colorstream and Miraval pigments to the second generation effect pigments. While the Colorstream pigments offer a color shift from red to green, the Miraval pigments advance sparkling effects. The comparably high pigment prices (up to 500 €/kg) make it interesting to use a highly effective printing process with a maximal utilization of the desired effects. In fact, pigment manufacturers give considerations for the application of effect pigments by different printing processes (Merck, 2007; Merck, 2007a; Merck, 2007b; Merck, 2007c; Merck, 2007d; Merck, 2007e). Nevertheless, a general impact of print parameters like printing speed, anilox volume, halftoning and pigment concentration to the effects has not been reported.

One impact of these effects corresponds to the orientation of the pigments. It is evident that the drying conditions and the leveling time until the drying influence the effects of the pigments. For optimal effects the pigments have to be orientated parallel to the substrate and surface, not agglomerated and well dispersed [Bühne et al., 2008]. Within relatively thick films (> 200 µm), e.g. for car finishing, the application method of the pigmented lacquer has the greatest influence on the pigment orientation (Pfaff, 2007).

Due to the forces in the nip, in printed layers the pigments are lying parallel to the substrate right after their application. To avoid a disorientation, a quick drying is recommended (Pfaff, 2007; Bühne et al., 2008). Contrariwise disoriented pigments which align themselves after a while, because of solvent evaporation and subsequent shrinking of the coating layer, is also reported (Maile et al., 2005).

In Figure 2 the effect pigment *Iriodin 7215 Ultra Rot* from *Merck KGaA* is printed upon a black underprint. Although the layer looks homogeneous for the human eye, a certain pigment distribution is apparent. It is evident that the pigment orientation and its concentration must influence their effects. For a quality control of the described effects measurement systems are rarely used in the printing industry (Cramer and Gabel, 2001). Printed products including effect pigments are often evaluated visually by the operators and customers.

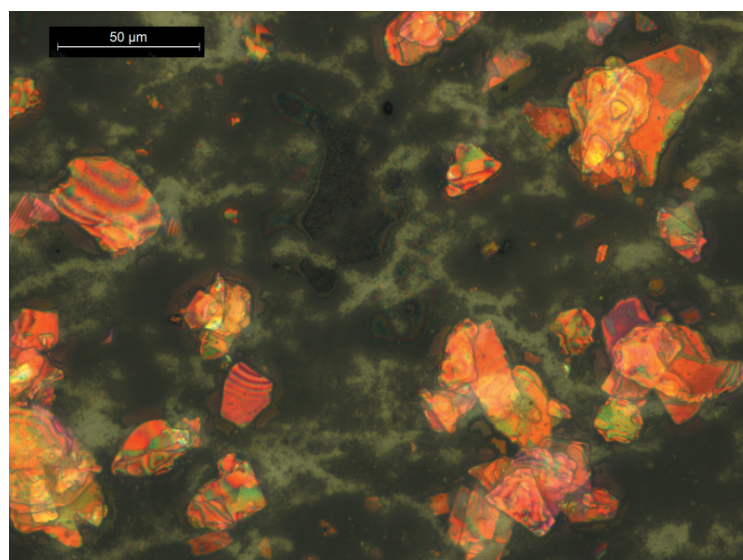


Figure 2: Flexo printed effect pigment *Iriodin 7215 Ultra Red* form *Merck KGaA* upon black ink

2. Intention

The impacts of several printing and material parameters on the impression of printed effect pigments are shown and discussed intensively. Based on the results of a systematic printing trial, using Design of Experiment (DoE) methods, general considerations for the operator to optimize the effects are presented. These include customer-related issues like enhanced print quality (Pfaff and Rathschlag, 2002) and economic aspects.

3. Methods

Therefore, in this work the effect impression of different printed effect pigments was split up into the following effects: color shift, gloss and sparkling. Since our work is focused on the first two effects, we used two quality measurement methods for quantifying. With the multi-angle spectrophotometer *Multi FX10* from *Datacolor* the color shift (ASTM, 2006) and with the reflectometer *Vipgloss-1* from *FAG* the gloss effect were measured. The data of the reflectometer could be taken directly as a value for the *gloss* of the printed samples. For the color shift - as proved by Hupp (Hupp, 2006; Hupp, 2008) - the ΔE^*_{ab} value was calculated out of two different viewing and illumination positions (see Figure 3) of the measurement results (Equation 1). L^* , a^* and b^* are the coordinates of the CIELAB color space. They are measured with the multi-angle spectrophotometer.

$$\Delta E^*_{ab} = \sqrt{(L^*_{45^\circ/90^\circ} - L^*_{45^\circ/120^\circ})^2 + (a^*_{45^\circ/90^\circ} - a^*_{45^\circ/120^\circ})^2 + (b^*_{45^\circ/90^\circ} - b^*_{45^\circ/120^\circ})^2} \quad [1]$$

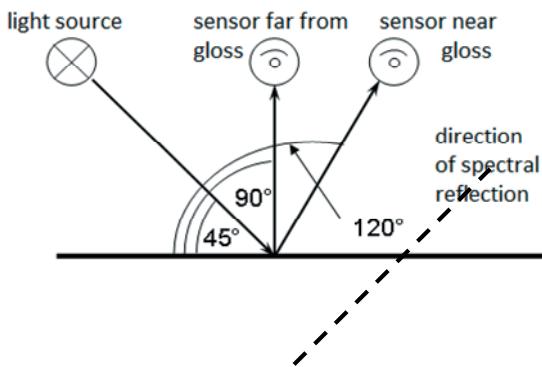


Figure 3:
Angle setting for calculation of the ΔE^*_{ab} value
(light source = illumination angle 45° , sensor = viewing angle 90° and 120°)

The quality control of these effects is practically arranged by subjective means, varying by the illumination and viewing conditions (Döring, 1993). To proof sufficient correlation simple appearance matching tests for the gloss and color shift effect were arranged. For example the color shift of flexographic printed samples was eyed up in an own built cabin under the same viewing and illumination angles as the measured ones. We compared the achieved results with the measured and calculated data. As the visual impressions matched quite well, an assured measurement certainty was given. After that the main printing test was planned with a DoE software to achieve optimal results out of a practicable amount of printed samples. The trial was configured to be printed with the flexographic unit of the adapted web fed printing machine *Gallus RCS 330-HD* (Figure 4) varying the printing parameters of Table 2. All pigments used are from *Merck KGaA*. As substrates Maxi Satin - a matt coated paper - and an OPP foil (oriented polypropylene) were used. The three different positions of the dryers are shown in Figure 4. Every dryer consists of a hot air drying unit and two IR-lamps. Both dryers stood next to each other for every printing trial.

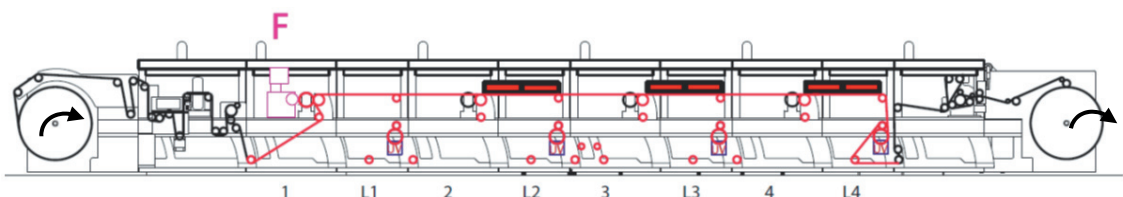


Figure 4: Print setup of the *Gallus RCS 330-HD* for the effect pigment layer. *F* points on flexography. The web trial and the different hot air/IR dryer positions (in *L2*, *L3* and *L4*) are shown

Table 2: Varying print parameters for each printing trail. Samples with theoretical anilox volumes of 13 cm³/m², 19 cm³/m² and 25 cm³/m² due to a banded anilox roll and halftoning areas of 50 %, 70 % and 100 % due to the printing plate (figure 6) are produced

Substrate	Pigment Type	Pigment Concentration	Dryer 1 (Hot Air)	Dryer 2 (Hot Air)	IR-Lamps Dryer 1	IR-Lamps Dryer 2	Position of Dryers	Printing Speed [m/min]
OPP	Colorstream Arctic Fire	10 %	on	on	0	0	L2	20
Maxi Satin	Miraval Scenic Copper	20 %	off	off	1	1	L3	30
	Iriodin Ultra Rot	30 %			2	2	L4	50
	Iriodin Rutil Feinrot							

The last two mentioned parameters must not be considered for the amount of printing trails, as the halftoning areas are part of the printing plate in every section of the banded anilox roll (see Figure 5). Multiplying all other parameter factors, as usual for general full factorial design, more than 7.700 printing trials would be necessary. As in printing very often a great amount of parameters can be modified, the use of DoE turned out to be a wise tool in this field of research.

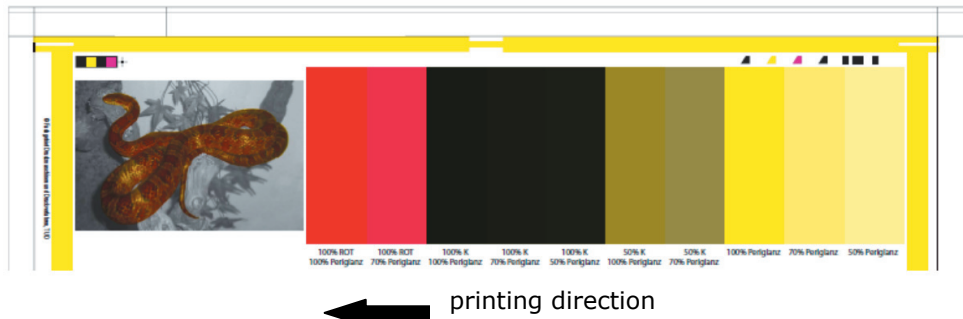


Figure 5: Layout of the printing plate for every band of the anilox roll: red and black - first layer printed with offset, yellow - effect pigment layer printed with flexography

DoE can be divided into the stages: planning, execution of the test and analysis (Figure 6), in which the planning has the greatest importance. Once having considered insufficiently some parameters, interactions, disturbances or ambient conditions within the planning stage, those can only be included afterwards by extra trials. After having accomplished all printing trials, a regression model can be created with the measurement results. All parameters are divided into command, influencing and disturbance variables. A further classification grades the variables into continuous or discrete ones. The disturbance variables are to be kept constant or controlled metrologically. The command variables have to be measurable. They are the variables which should be optimized in order to satisfy the customer interests. For a measurement of the command variables in an appropriate way a measurement certainty has to be given. With a system analysis, the expected impacts of the influencing variables on the command variables are displayed in form of mathematical functions. The same is realized within the influencing variables itself in a cross-impact matrix. The number of trials rises depending on the amount and type of the expected impacts on the command variables and cross-impacts of the influencing variables. An adequate software calculates the amount and type of the trials, which are necessary to ascertain the regression coefficients of the command variables. The type of trials is chosen by the software considering the principles of balance, collinearity and randomization out of the full factorial design and finally display a fractional factorial design.

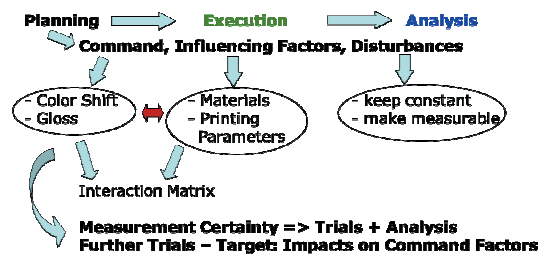


Figure 6: Approach of DoE for printed effect pigments

For this study the DoE software *Cornerstone* was used. Preliminary printing trials showed little cross-impacts of the influencing variables concerning the ΔE^*_{ab} values. Cross-impacts take place between the pigment type and concentration, anilox volume and substrate and anilox volume and pigment type. Concerning the gloss we noticed that only the anilox volume and the pigment concentration showed small cross-impacts.

To avoid blocking caused by insufficient drying, the maximum printing speed was reduced to 50 m/min. All pigments were dispersed in a water based lacquer. The OPP foil was corona pretreated before the application of the effect pigment layer. A protective lacquer, as often used in industrial practice, was not overprinted as it would affect the color shift and gloss effect. Each sample without a colored first layer in Figure 5 was measured three times concerning the color shift effect and nine times regarding the gloss effect. For the analysis, the arithmetic mean was used. All in all 495 different printing samples have been measured and the impact of the parameters on the color shift and gloss effect was evaluated.

4. Results

Comparing Iridoin (1st generation) with Colorstream (2nd generation) pigments, the last show a generally higher color shift. Concerning the gloss effect, a great impact of the substrate and a possibly applied lacquer was verified. Matte uncoated papers reach much higher gloss gain by printed effect pigments as natural glossy papers. The thicker the printed effect pigment layer, the bigger is the gloss effect.

Regarding the samples printed during the DoE trials, the measurement uncertainty increased with decreasing homogenous printed effect pigment layers. Analysis of visual high quality printing products showed good accordance of different printed samples with the same parameter settings. Based on the measurement results, a linear regression for all influencing factors was possible. Figure 7 shows the influences on the command variable color shift. Pigment type, anilox volume and area coverage have the greatest impact on the color shift effect. Among the pigments, the Colorstream pigment Arctic Fire with its color shift from green to red provides the highest ΔE^*_{ab} values. 22 out of 30 printed samples with the highest ΔE^*_{ab} values had been printed with the highest anilox volumes and 27 out of 40 with a total area coverage. Hot air drying seems to advance the color shift effect in contrast to a drying with IR-lamps. The substrate had almost no impact. The greatest negative impact on this effect has the time until drying. This correlates with the decreasing effect due to higher printing speed in the studies in (Pfaff, 2007; Bühne et al., 2008).

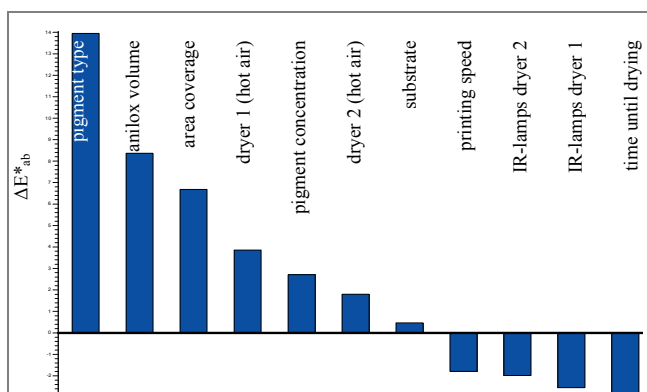


Figure 7:
Impact of the influencing factors
on the color shift

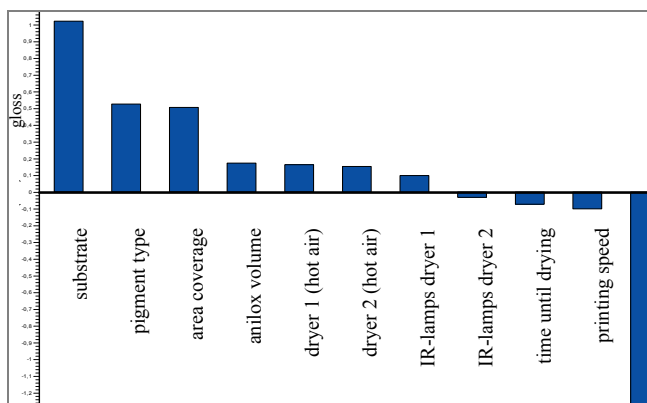


Figure 8:
Impact of the influencing factors
on the gloss values

In Figure 8 the influences on the gloss effect are visible. The greatest impact on the gloss effect has the pigment concentration followed by the substrate. With an increasing pigment concentration the gloss effect decreases. The gloss values of the samples printed on OPP-foil are higher compared to the samples printed on paper. As the absolute values of the unprinted substrates differ in the same way, this result is comprehensible. Pigment type and area coverage have a similar impact on the gloss effect. The Miraval pigments, generating the highest sparkling effect, also offer the highest impact on the gloss, followed by the Colorstream and Iriodin pigments.

5. Discussion

With the achievements generated in Section 4, general considerations for the operator, customer-related issues like enhanced print quality (Pfaff and Rathschlag, 2002) and economic aspects are possible. All advices depend on the customer requests. Does the customer for example rate both effects - the color shift and the gloss effect - in the same way, the following suggestions to increase these command variables can be given:

To get a better color shift effect, the pigment type is essential. It is better to use more expensive but high effective pigments (2nd generation) and decrease their concentration than using lower effective ones with a higher concentration. Concerning the gloss effect, the choice of the right substrate is important if an overprint with a brilliant varnish is missing. Amongst others a low pigment concentration favors the gloss effect, as the pigments are more easily able to align themselves parallel to the substrate.

6. Conclusion

With the results of the main printing trial, conclusions about the importance of the varied parameters concerning the color shift and gloss effect could be given. Recommendations for the production process were possible considering economic aspects as well as the print quality. Nevertheless, all results cannot be transferred to other pigment types or printing machines as the interaction of the printing and material parameters are not extensively examined. However the results can contribute to an effective production using interference effect pigments.

7. Outlook

Due to a systematic printing trial opportunities for efficient and enhanced printing processes of effect pigments optimizing their color shift and gloss effect have been shown. Now the results have to be proved in field tests with different printing machines and over larger printing periods to gain relevance for industrial print products. Such printing trials are planned together with the *Heidelberger Druckmaschinen AG*. Within these printing trials the development of the halftoning areas will be especially observed, as the printing plate might be clogged with pigments after longer printing periods. Apart from that further work will be investigated to quantify the negative impact on the color shift effect due to the time until drying caused by evaporation and pigment orientation.

Acknowledgments

The authors thank Mr. Andreas Becker (*Merck KGaA*) for supporting this study.

References

- ASTM (2006). *ASTM WK 1164: Standard Practice for Multiangle Color Measurement of Interference Pigments. Revision 16.0.*
- Bühne, S., Woocker, A. and Linzmaier, A. (2008). *Orientierung von Effektpigmenten*, Farbe und Lack. 11-2008, 114. Jahrgang: 34-39.
- Cramer, W.R. and Gabel, P.W. (2001). *Measuring Special Effects*. Paint & Coatings Industry: 36-43.
- Döring, G. (1993). *Correlation between Visually and Instrumentally Estimated Colour Differences of Metallics*. Die Farbe. 39. Jahrgang: 177-186.

- Hupp, H. (2006). *Measuring printed special-effect colours - First Experiences with the MultiFX10 spectrophotometer*. 33th Iarigai Conference
- Hupp, H. (2008). *Qualitäts- und Prozesskontrolle gedruckter Interferenzeffektfarben erster Generation*. Institut für Druckmaschinen und Druckverfahren. Darmstadt, Technische Universität Darmstadt.
- Maile, F. J., Pfaff, G. and Reynders, P. (2005). "Effect pigments--past, present and future." *Progress in Organic Coatings* 54(3): 150-163.
- Maisch, R; Weigand, M. (1991). *Perlglanzpigmente. Bibliothek der Technik, Landsberg/Lech, Moderne Industrie*.
- Merck (2007). *Effektpigmente für die Druckindustrie - vom Design zum Druck*. Darmstadt, Merck.
- Merck (2007a). *Effect Pigments - Colorcard Flexo Printing*. Darmstadt, Merck.
- Merck (2007b). *Effect Pigments - Colorcard Offset Coating*. Darmstadt, Merck.
- Merck (2007c). *Effect Pigments - Colorcard Gravure Printing*. Darmstadt, Merck.
- Merck (2007d). *Effect Pigments - Colorcard Offset Printing*. Darmstadt, Merck.
- Merck (2007e). *Effect Pigments - Colorcard Screen Printing*. Darmstadt, Merck.
- Merck (2007f). *Sicherheitsdatenblatt Iriodin 211 Rutil Feinrot*. Darmstadt, Merck.
- Merck (2007g). *Sicherheitsdatenblatt - Iriodin 7215 Ultra Rot*. Darmstadt, Merck.
- Merck (2007h). *Sicherheitsdatenblatt - Colorstream T10-02 Arctic Fire*. Darmstadt, Merck.
- Merck (2007i). *Sicherheitsdatenblatt - Miraval 5321 Scenic Copper*. Darmstadt, Merck.
- Pfaff, G. (2007). *Spezielle Effektpigmente. Hannover, Vincentz*.
- Pfaff, G. and Rathschlag, T. (2002). *New Design Possibilities with Special Effect Pigments in Printing Inks*. *Paint India*. (4/2002) 65.
- Pfaff, G. and Reynders, P. (1999). "Angle-dependent optical effects deriving from submicron structures of films and pigments." *Chemical Reviews* 99(7): 1963-1981.



Screen printing with effective printing inks

*Raša Urbas*¹, *Jana Rozman*¹, *Marta Klanjšek Gunde*²

¹University of Ljubljana, Faculty of Natural Sciences and Engineering

Snežniška 5, SI-1000 Ljubljana, Slovenia

E-mails: rasa.urbas@ntf.uni-lj.si; jana.rozman@ntf.uni-lj.si

²National Institute of Chemistry

Hajdrihova 19, SI-1000 Ljubljana, Slovenia

E-mail: marta.k.gunde@ki.si

Abstract

The quality of prints prepared by screen printing depends on relationship between mesh geometry and pigment particles which are transferred through the mesh. Relatively simple relationships are valid for conventional inks which have uniform distribution of nearly round-shaped pigments. In such circumstances the fineness of the screen, its thickness and degree of opening determine printing properties.

The rather simple situation could change considerably if the ink contains flaky-shaped pigments. If flaky-shaped pigments are used in printing ink, the printing process should support the parallel orientation. The simple rules for conventional inks are not valid for inks with flaky pigments. Our research is devoted to get the connections between the mesh properties and print quality for such printing inks.

Three different pigments were applied, two bright conductive and one interference pigment, with different lateral sizes, ranging from 59 up to 110 μm . They were applied in printing base in 5% and 20% mass concentration. The prepared printing inks were screen-printed on two papers, Biogloss and Biomatt. Two mesh densities were applied, 27 and 61 threads/cm. The quality of prints was analyzed by scanning electron- and optical microscope, optical profilometer and \angle geometry. The angle-dependent effects were judged colorimetry in 8 visually.

It was found that higher density of meshes gives thinner layers, larger angle-dependent effects and sharp edges of prints. Larger concentration of flakes gives rise to higher disorder of flakes and poor angle-dependent effects. Wet on wet printing causes large deterioration of orientation. Smooth substrate surfaces support better orientation of flakes. The research on influence of these parameters on functional properties is going on.

Keywords: screen printing, effect pigments, flakes, angle-dependent optical effects

1. Introduction

With increasing and unifying of the global market manufacturers and the owners of trademarks find it harder and harder to catch the attention of costumers. Due to that reason more and more graphic designers are searching for the way of presenting their products with the help of packaging design and through commercial information.

Beside the use of different types and colours of paper, paperboard or foils, printing with special effect pigments represents one type of solution. With different effects of printing substrate, printing processes, printing inks and effect pigments, a product which will fully correspond to original graphic solution could be printed.

The quality of prints prepared by screen printing depends on the relationship between mesh geometry and pigment particles which are transferred through the mesh. Relatively simple relationships are valid for conventional inks which have uniform distribution of nearly round-shaped pigments. In such circumstances the fineness of the screen, its thickness and degree of opening determine printing properties¹. This rather simple situation could change considerably if the ink contains flaky-shaped pigments with different transparency, surface finish and lateral dimensions (2-6). Such pigments are commercially available for various applications such as decorative, protective and security applications (2, 3). In addition, there are also novel platelet-shaped bright conductive pigments available that offer new applications in electromagnetic shielding and antistatic applications (5). The quality of such application depends strongly on orientation of these flakes in the final coating layer. The highly preferred orientation is parallel to the substrate. Such sample exhibits the highest possible angular dependent appearance.

However, simple rules of conventional ink applications are not valid for inks with flaky pigments. It is supposed that the geometrical properties of the applied mesh prevail among several factors that might influence on the orientation of flaky pigments during printing and drying processes. Our research aspires therefore to find the connections between the mesh properties and print quality for such printing inks.

2. Materials and research methods

Three different pigments were applied into printing base (Thermo-Jet[®] 950): two bright conductive (Minatec[®] 51 CM, Minatec[®] 60 CM (Merck) and one interference pigment (Iriodin[®] 9225 Rutil Perlblau WR (Merck)).

Interference pigments are consisted of mica core material (with low refraction index) and a layer of metallic oxide (TiO₂) (with high refractive index). Different thickness of applied metallic oxide enables varying colour shades of pigment while refractive index of mentioned metallic oxide influences the glitter (with higher refractive index higher glitter is achieved). With interference on the thin layer colours which are very intense appear and they change with the angle of observation (7).

Bright conductive pigments consist of layer-substrate structure of substrate (mica) coated with a layer of conductive inorganic metallic oxide (Sb-doped tin dioxide). Conductivity is achieved by suitable doping of Sb into the thin oxide lattice. The mixture of spheres and platelet shapes is beneficial in the formation of conductive pathway by imparting a particle-to-particle network within the coating layer.

Selected effective pigments (Minatec[®] 51 CM, Minatec[®] 60 CM and Iriodin[®]) differed in their lateral sizes which ranged from 59 up to 110 µm. Effective pigments were applied in printing base (Termo-Jet[®] 950 (Proell KG) in 5 wt.% and 20 wt.% mass concentration. For achieving the suitable rheological properties inks had to be diluted with universal diluent for screen printing CMA (Kemis Plus) (8).

Prepared printing inks were screen-printed on two papers, Biogloss and Biomatt (150 g/m²). Both selected papers were coated, one with matt coating and the other with glossy.

When choosing the proper mesh density the lateral size of pigments had to be considered. Pigments have to be at least 30% smaller than the mesh opening otherwise the particles could be/stay trapped between the mesh threads during printing. Lateral size of used pigments (their biggest particles) was measured with Scanning Electron Microscope (SEM) JEOL JMS 6060LV. Differences in lateral sizes are presented in Figure 1.

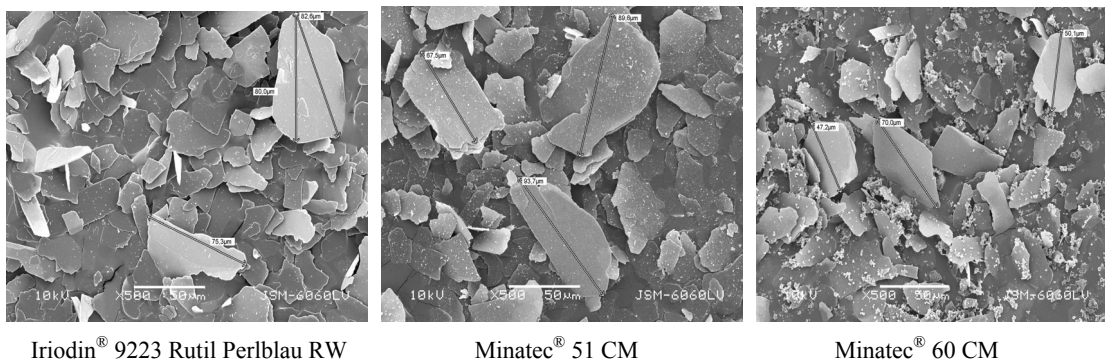


Figure 1: Lateral size of bright conductive (Minatec[®] 51 CM, Minatec[®] 60 CM (Merck) and interference pigment (Iriodin[®] 9225 Rutil Perlblau WR (Merck))

According to measurements of pigment lateral sizes two screen printing meshes in plane weave were used:

- a. mesh with density 27 threads/cm, yarn diameter 120 µm and mesh opening 249 µm
- b. mesh with density 61 threads/cm, yarn diameter 64 µm and mesh opening 90 µm.

For the determination of connections between the mesh properties and print quality for effective printing inks the printing form of lines with different thickness was composed. The quality of prints was analysed with different techniques: scanning electron and optical microscope, optical profilometer and colorimetry in 8°/D

geometry. The angle-dependent effects were ascertained visually. Parameters of final coating layer (printing effective inks) thickness, paper and printed coating roughness, optical properties and calorimetric values were measured and the analyse of printed surface was performed/executed.

Thickness and roughness of final coating layer (printing inks) and paper substrate was measured by optical profilometer (Form Talysurf Series 2 (Taylor - Hobson)).

The quality of printed samples were analysed by means of these results.

3. Results

Scanning electron microscope technique enabled only the determination of ink layer thickness on Biogloss paper due to the fact that the sharp border between the paper surface and printed ink coatings was not possible on Biomatt paper because of the ink penetration into its interior. Thickness of printed inks was therefore measured only on Biogloss paper (Figure 2).

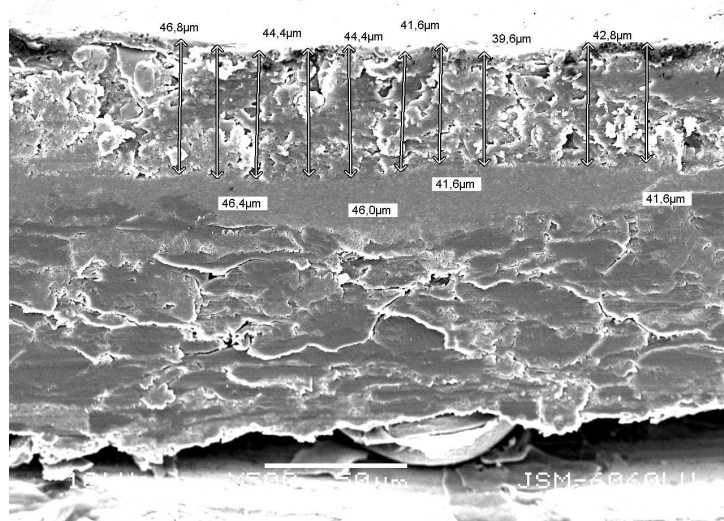


Figure 2: Thickness of ink coating measured by SEM

Measurements of ink coating thickness performed by profilometer showed that the greatest influence on thickness of printing inks could be contributed to screen printing meshes. Denser meshes gave thinner coatings of printing inks. It was established that the pigment lateral size also affects the thickness of applied ink coatings. The smaller are the pigment particles the more of them can penetrate trough the screen printing mesh and therefore higher thicknesses of printing ink coatings can be achieved. Research also showed that increase of pigment's concentration contributes to thicker ink coatings (Table 1, Figure 3). Beside mentioned results analyses also showed that printing on Biomatt substrate gave thicker ink coatings which could be attributed to poorer parallel orientation of flaky pigments during printing and drying processes.

Table 1: Values of measured ink coatings thickness.

Substrate	Mass conc. [%]	Mesh [threads/cm]	Thickness of ink coatings [μm]		
			Iriodin [®] 9223 Rutil Perlblau RW	Minatec [®] 51 CM	Minatec [®] 60 CM
Biogloss	5	27	13.4	9.5	15.8
		61	7.5	7.8	6.8
	20	27	14.5	12.6	16.4
		61	7.8	9.1	8.6
Biomatt	5	27	13.9	13.2	16.4
		61	10.0	8.2	8.6
	20	27	16.1	13.6	17.1
		61	7.5	9.5	11.1

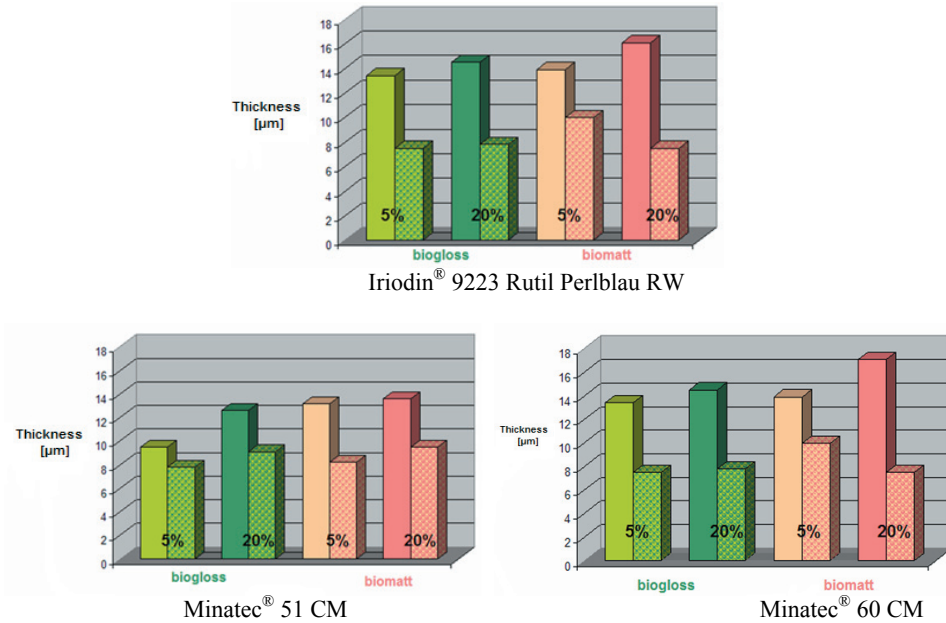


Figure 3: Thickness of printed ink coatings in μm (coloured columns represent prints printed with mesh densities of 27 threads/cm and dashed columns with densities of 61 threads/cm)

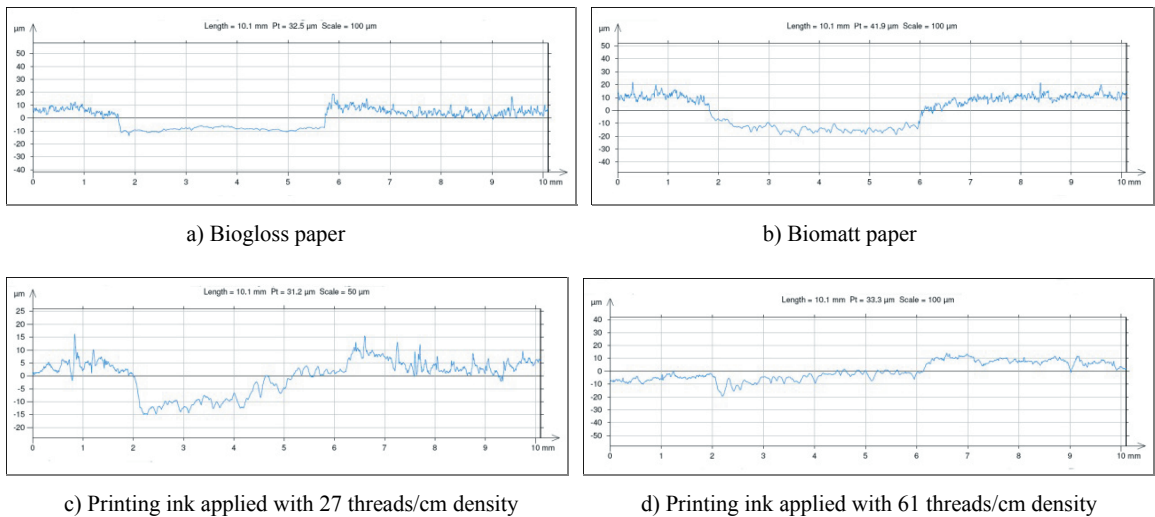


Figure 4a-4d: Roughness of printed surface with Iridodin® 9223 Rutil Perlblau RW pigment

Roughness of printing material and printed inks was measured by a profilometer. It was expressed as R_a , the arithmetic mean of the absolute differences of the surface profile from the mean line within long enough sampling length. Results showed that the values of measured printed ink coatings thickness, printed under the same conditions (same mesh density and the same concentration of the pigment) on the Biomatt paper were higher than on Biogloss (Figure 4a-4d) due to higher roughness of Biomatt paper.

Surfaces of prints printed with the meshes of lower densities were rougher than in the case of higher mesh densities. The later was more distinctive in the profiles of prints with higher (20 wt.%) concentration.

Measurements of light reflection were made with UV/VIS spectrophotometer Lambda 800 (PerkinElmer®) in the area of wavelength from 250 to 900 nm, in 5 nm step. L^* , a^* , b^* values were calculated from the measured reflectance spectra (Figure 5a-5b). Measurements and calculations showed that meshes with higher densities give higher colour saturation and that higher concentration of pigment contributes to lower lightness L^* and higher chroma values (Table 2). Bigger colour differences between the samples are contributed to higher concentration of the pigment printed on the same paper substrate trough different mesh densities of screens.

Table 2: Colour values $L^*a^*b^*$ of used pigments

Pigment	Substrate	Mass conc.	Mesh [threads/cm]	L^*	C^*	a^*	b^*
Iriodin® 9223 Rutil Perlblau RW	Biogloss	5	27	91.62	1.65	-1.60	0.43
			61	92.06	0.38	-0.37	-0.10
		20	27	89.09	1.68	-1.56	0.54
			61	90.46	1.05	-0.93	-0.40
	Biomatt	5	27	91.04	0.79	-0.66	0.42
			61	93.76	0.33	-0.33	-0.01
		20	27	87.48	1.48	-1.39	0.52
			61	91.00	1.00	-1.05	-0.04
Minatec® 51 CM	Biogloss	5	27	91.51	0.88	-0.45	0.76
			61	92.96	0.46	-0.29	0.37
		20	27	89.27	3.24	-1.28	2.97
			61	91.12	1.69	-0.78	1.50
	Biomatt	5	27	90.93	0.96	-0.35	0.90
			61	93.73	0.50	-0.20	0.46
		20	27	90.31	3.17	-1.16	2.95
			61	92.21	1.85	-0.74	1.70
Minatec® 60 CM	Biogloss	5	27	91.04	0.98	0.66	0.72
			61	92.78	0.60	0.32	0.50
		20	27	85.85	4.52	-2.40	3.83
			61	90.23	1.50	-1.01	1.11
	Biomatt	5	27	91.68	1.20	-0.66	0.90
			61	93.86	0.57	-0.29	0.49
		20	27	86.05	3.98	2.27	3.27
			61	90.56	2.08	1.25	1.60

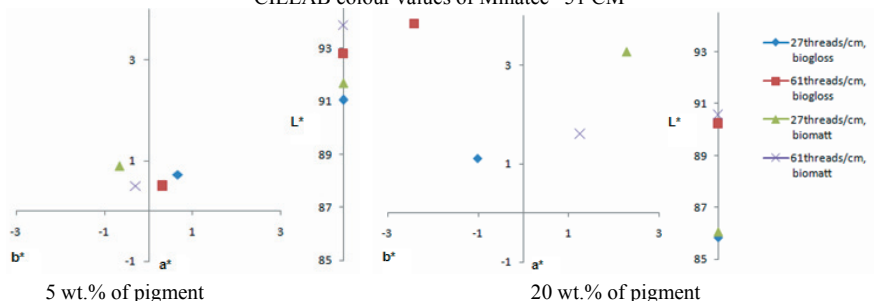
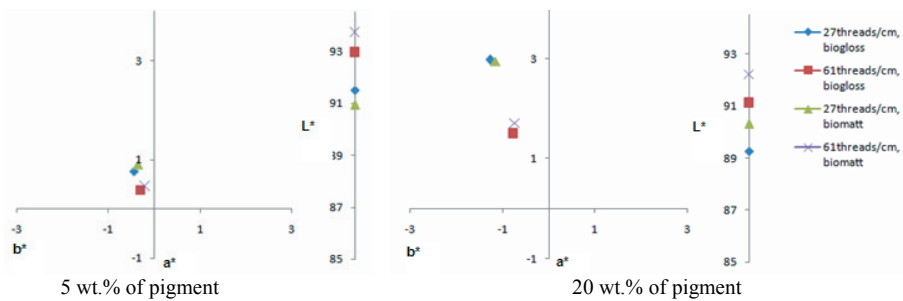
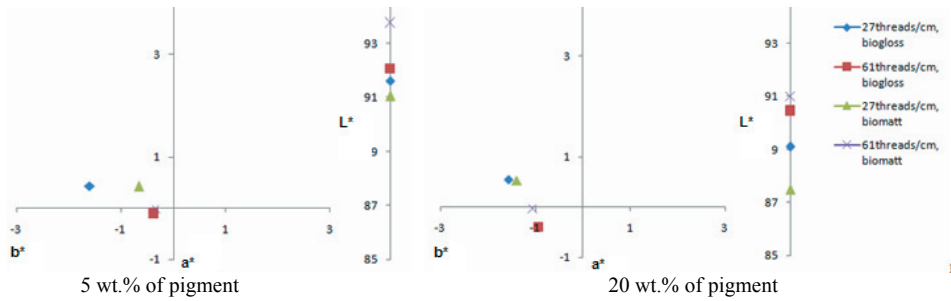


Figure 5a-5b: CIELAB colour values of prints with selected pigments

Picture analysis of printed surfaces as well as the surfaces of papers was made with optical microscope Leica EZ4D in 20x magnification (Figure 6a-6d).

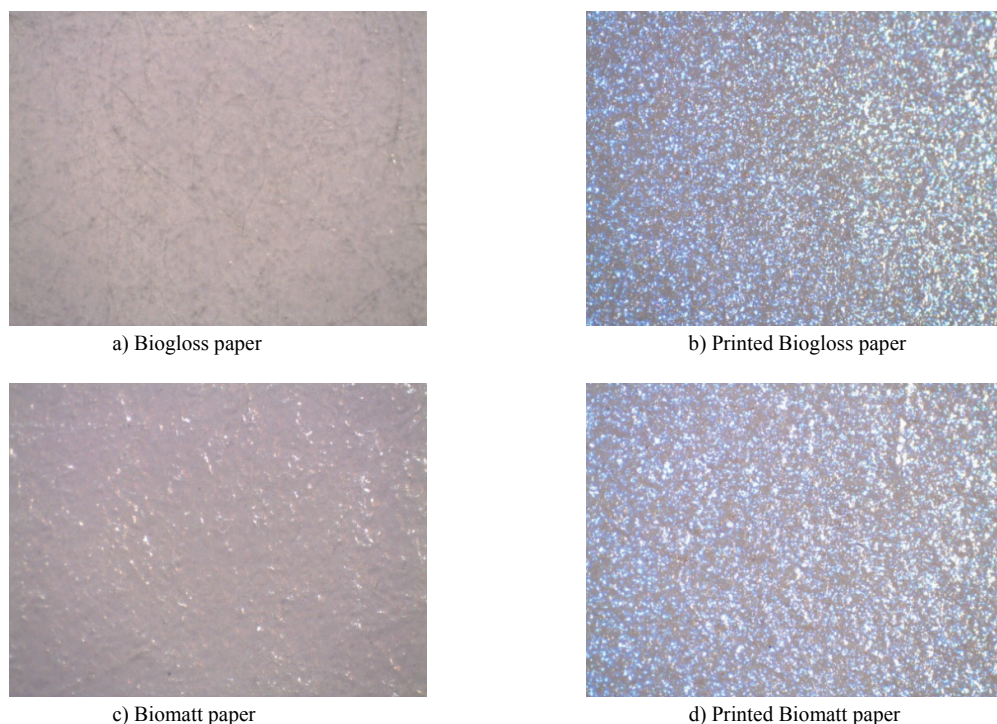


Figure 6a-6d: Microscopic images of paper with and without applied printing ink Iriodin[®] 9223 Rutil PerlblauRW

Structure of printing material indeed affects the angle-dependent effects of prints that are most distinctive on prints made on coated materials where their surface is smooth and has higher gloss. The effect is smaller on prints made on uncoated papers where pigment particles due to higher surface roughness differently orientate on the fibres of the paper.

The colour of printed samples is affected by the smoothness of the applied paper - especially when we print with transparent pigments - because the visual effect of pigments depends on the transmission of the light through the pigment, refraction and the reflection of light on interfaces between layers and the reflection of the light on the paper substrate. Prints are more intensive in colour if transparent pigments are printed on black substrate than printed on white surface base.

4. Conclusions

Research showed that the highest effect on ink coating thickness could be contributed to screen printing meshes. Meshes with higher densities give thinner printed layers and stronger angle-dependent effects. It was established that pigment particle size also effects on ink coating thickness. Smaller pigment the particle sizes more of them can penetrate through printing mesh which results in higher measured values of ink coating thickness. Beside mentioned, higher weight concentration of pigment causes larger disorder of printed layer structure. Such samples can show very poor angular-dependent effects, as a consequence of poor orientations of effect pigments. Sets of pigment particles appeared on prints printed with lower density meshes and higher used concentration in printing inks.

It was established that for the printing of effect pigments it is necessary to use substrates (papers) with smooth surfaces because they do not cause higher disorder in orientation of flakes and as a consequence a poor angle-dependent appearance. Mentioned fact is more evident in profiles of prints where mass concentration of pigment was higher (20 wt.%).

Our results also showed that wet on wet printing in two transitions practically has no effect on L*a*b* values but causes the deterioration of angle-dependent appearance of prints. Research showed that higher mesh

densities gave more saturated colours. Higher pigment mass concentration contributes to lower lightness and higher chroma. Higher mass concentration also gave bigger colour differences between the samples printed on the same substrate with different mesh densities. All used pigments were colourless and partly transparent (Minatec[®] 60 CM at least) which indicates the smallest changes in lightness in dependence of pigment concentration. The most probable cause for this is the presence of spheres which cause light scattering in the printed layer.

Angle dependant visual effects are most distinctive on prints made on coated substrates, where the surface is smoothest and has highest gloss. Effects are smaller on uncoated substrates where pigment particles due to the roughness of the surface tend to orientate differently on the fibres of the paper.

Visual evaluation showed that the prints made with Iriodin[®] 9223 Rutil PerlblauRW changed lightness and the blue colour shade in dependence of the observation angle. The effect was more distinguished on prints printed with higher mesh densities (thinner layers of the prints) on coated substrates with higher mass concentration of the pigment. Although high concentration caused clustering of the pigment for which printed thin lines weren't consistent. Prints made with Minatec[®] 51 CM printed with meshes of lower densities weren't sharp and the effect of the mesh could be seen. Angle dependant visual effect was most distinctive in prints made with lower mass concentration. Research showed that prints with Minatec[®] 60 CM pigments made with meshes of lower densities and 20 % mass concentration were due to thicker deposit of the printing ink and to high pigment part very rough and without gloss. Entirely different visual effect was obtained using higher mesh densities where surface of prints made on coated substrate (due to thinner layer of printed ink) was smoother and glossier.

Therefore some general conclusions of the research could be made:

- meshes with higher densities give thinner layers of printing ink, higher angle-dependant effects and sharper edges of printed lines;
- higher mass concentration of added pigment causes higher disorder of the structure. Clusters of pigments occur on prints made with lower mesh densities and higher mass concentration of the pigment. Therefore thin lines in prints are usually not consistent and angle-dependant effects are not distinctive;
- for printing with effective pigments it is necessary to use smooth surfaces because they do not cause disorder of flakes and lower angle-dependant effect;
- increase of printing squeegee passes (wet on wet technique) practically has no effect on L*a*b* colour values and actually causes deterioration of angle-dependant effects.

Additional research on influences of some parameters on functional properties is still in process.

References

- (1) KIPPHAN, H. Handbook of Print Media. Heidelberg, Berlin : Springer, 2001.
- (2) PFAFF, G., REYNDERS, P. Angle-dependent optical effects deriving from submicron structures of films and pigments. Chemical Reviews, 1999, vol. 99, pp. 193-1981.
- (3) ARGOITIA, A. Diffractive pigments help document security. European Coating Journal, 2004, vol. 11, pp. 32-35.
- (4) BARLE, N. Coatings in coating applications. Interdisciplinarity of color, Part II, Slovenian colorists association, 2003, pp. 307-312.
- (5) VOGT, R., NEUGEBAUER, E., PFAFF, G., STAHLLECKER, O. Bright conductive pigments with layers. European Coating Journal, 1997, vol. 7-8, pp. 706-708.
- (6) KLANJŠEK GUNDE, M. Angle-dependent phenomenon. Interdisciplinarity of color, Part II, Slovenian colorists association, 2001, pp. 246-248.
- (7) CRAMER, W.R. Description and Characterization of Interference Pigments. <http://web.ua.es/es/gvc/documentos/docs/cramer/cramer5.pdf>
- (8) Minatec[®] 60M - bright conductive pigments (Product information). <http://85.238.144.18/pigments/brochures/Minatec%2060CM.pdf>



Pore structural changes in inkjet coatings by the inclusion of binders and additives

Cathy J. Ridgway¹, Vesa Kukkamö² and Patrick A. C. Gane³

¹ Omya Development AG,
CH-4665 Oftringen, Switzerland
E-mail: forename.surname@omya.com

² Omya International AG,
CH-4665 Oftringen, Switzerland
E-mail: forename.surname@omya.com

³ Aalto University, School of Chemical Technology
Department of Forest Products Technology
P.O. Box 16300, FIN-00076 Aalto, Finland

Abstract

This study considers pore volume loss in inkjet coating structures when using various binders and polymer additives. Starch is shown to prevent access to the crucially absorbing pores, and is non-absorbing. Polyvinyl alcohol (PVOH) absorbs up to ~30 % of its own weight of water, but acts to limit the absorption rate by reducing it to that of the interpolymer matrix diffusivity. PVOH also reduces the volume according to the binder filling internal pore space. Latex particulate binder can be used to allow continued access to the nanopore region by choosing the right glass transition temperature, T_g , and chemistry of the synthetic polymer. Similarly, the permeability can be maintained to a large extent.

Water fastness requires that the coating be cationic, when considering anionic ink dyes. The added cationic polymer, such as PolyDadmac, itself reduces the available pore volume by distributing itself on the pigment surfaces and within pores. Linking pore volume loss to increased feathering and bleeding supports the need to reconsider the use of water soluble polymers and binders, and indicates that coating formulation optimisation, when using cost-effective porous pigments in inkjet coatings, points to the minimising of charge conversion requirements and the development of improved particulate binders.

Keywords: inkjet coatings, speciality inkjet pigments, formulating for inkjet coating, cationising, soluble binders

1. Introduction

In a range of printing methods, including traditional offset and flexography, and the rapidly emerging high-speed digital methods, such as inkjet, liquids are required to wet the print medium surface either differentially, as in offset, or uniformly, as in flexography and inkjet. In the case of pigment coated papers and boards, absorption of liquid is also an integral part of the ink setting and drying process. The rate and volume of liquid absorption is dependent on the porous network structure of the coating layer established via coating pigment particle packing in the presence of binders, for example starch, polyvinyl alcohol (PVOH) or latex. The time scale of absorption falls under the description of network pore structure imbibition theory (Ridgway et al. 2006, Schoelkopf et al. 2000a, Schoelkopf et al. 2000b) and the chemical nature of the surface encountered by the liquid, together with diffusion effects (Rousu et al. 2001, 2002). The printing process manifests time scales of phenomena from nanoseconds through milliseconds up to minutes and hours depending on ink and coating chemistry. For the absorption of the ink diluent/solvent the coating structure should have enough capacity to hold the fluid and also have rapid absorption speeds to enable fast ink setting.

Inkjet technology is identified as a strong driver for change in the printed paper market. Traditionally, inkjet receiving surfaces, with their need for high volume and rapid liquid absorption capacity, meant that speciality papers arose with these properties as the main design criteria. To achieve the necessary porous structures, coating pigments such as precipitated or fumed silica were used, sometimes together with superabsorbing polymers. The formation of a liquid receiver layer based on such pigments, together with a glossy superabsorbing top layer, lies behind the successful development of photographic quality inkjet

papers, for example. The emergence of cost competitive print engines is, however, changing the market perspective toward technologies that challenge the traditional offset production quality, in terms of both speed and, eventually, cost. The ability to reduce inventory is a major factor underpinning these developments. To meet the cost-effectiveness challenge, it is recognized that the cost of coating pigment specialities for such grades needs to be reduced, and silica is seen as being progressively unable to meet this value requirement. Therefore, speciality designed inkjet coatings today increasingly employ the use of alternative highly porous pigments.

The development of calcium carbonate grades for inkjet coatings, either PCC or GCC-based, has seen big progress in recent years. An example of such a porous pigment, developing a discretely bimodal pore structure controlling permeability via the interparticle pores and capillarity via the intraparticle pores, is modified calcium carbonate (Ridgway et al. 2006). Similar structures also exist in respect to precipitated calcium carbonate. These designed structures provide for high absorption volume and fast absorption rate, but depend on the availability of the pores to perform this action by absorbing the liquid vehicle of the ink. Blockage of pore entries or reduction of pore connectivity can reduce the effectiveness of the potential capillary force and/or the permeability of the coating, respectively. Though primarily with the aim of entering the new cost-effective inkjet printing grades, the technology is advancing at such a pace that it is likely that designs may soon appear to challenge even the highest cost specialities. Clearly, however, the high absorptive performance of silica sets a major technical hurdle to be reached, and the solution lies not only in coating pigment design, but also in formulation design, which requires change from the traditional silica-containing formulation recipes. Principally this change is required to allow calcium carbonate pigments to perform in respect to the demands on pore volume and pore size distribution.

In coating colours, besides the pigments with their particle packing characteristics and internal pore structure, there is also the binder to consider. By changing binder amount or binder type the inkjet ink penetration can be influenced. First of all, the binder amount should be sufficient that the coating colour has an adequate adhesion to the paper surface and cohesion within the coating layer such that dusting problems are minimal. The surface strength is not needed at such high levels as in traditional offset printing, but nonetheless dust generation is critical, as it could lead to blockage or damage of the inkjet nozzles, and so diminish the print quality and reduce the lifetime of expensive print engine components. In coating colours for inkjet papers, polyvinyl alcohol (PVOH) is a very commonly used binder, and it has a high capability to bind pigments. It is also a very hydrophilic binder, and exhibits swelling on contact with water (Chapman, 1997; Hara, 2006; Pinto and Nicholas 1997). Pinto and Nicholas showed in their study that ink diffusion is unrestrained by PVOH, and the colorant concentration profile is uniform in a PVOH layer as shown by time-of-flight secondary ion mass spectrometry (TOF-SIMS) analysis. Recently, the binder type has been shown to have an effect on the inkjet ink print density and bleeding development, (Nilsson and Fogden, 2008, Svanholm et al., 2006).

Soluble binders, despite their role in some cases of also being absorptive - polyvinyl alcohol (PVOH), for example - nonetheless deplete the available pore volume, as their swelling potential is less than the potential availability of empty pore space. Lamminmaki et al. (2009) showed that PVOH binder affects both the pore structure and its ability to take up liquid by diffusion. PVOH swells during the diffusion process. Although the volume of liquid imbibition related to PVOH swelling can be small at low binder levels it acts to dominate the ink interaction with the pigment surface and the fine pore structure as binder levels increase. Mercury porosimetry results (Lamminmaki et al., 2009) indicated that PVOH binder can go into or cap (film over the entry) the intra-particle as well as the connecting pores, and exists around the larger inter-particle pores as Boisvert and Guyard (2003) and Wedin et al. (2006) assumed in their studies. At sufficiently high levels, any interaction of the binder with the liquid phase of the ink becomes important, not only in the structural modification of pore volume but in the diffusion of liquid through the polymer network, effecting swelling in the case of PVOH.

The work reported here addresses the loss of pore volume question and illustrates how the future application of inkjet coatings needs a further developed formulating strategy to assist in delivering the required inkjet substrate surface properties. To illustrate the effects, the pore structures of compressed inkjet designed calcium carbonate coating pigments, as well as coatings on aluminium foil, are compared, and their combination with various amounts of soluble polymer and particulate binders, respectively, are studied to determine the impact on pore volume loss and hence print performance in the demanding inkjet field.

2. Materials and methods

2.1 Coating pigments

The pigments used are modified calcium carbonates (MCC) of two different particle size ranges, nMCC and bMCC, with narrow and broad particle size distribution, as might be used in the emerging new generation of inkjet coatings for Transpromo grades and high speed applications, respectively, and a coarse ground calcium carbonate (cGCC) (Hydrocarb 60 ME, Omya AG, CH-4665 Oftringen, Switzerland). The particle size distributions for these pigments can be seen in Figure 1. In addition, a laboratory made MCC, having high pore volume and extremely narrow particle size is used to exemplify more clearly the impact of binder addition (Figure 2).

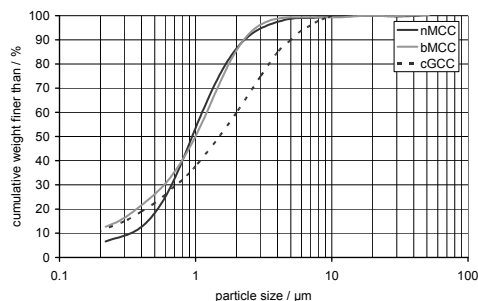


Figure 1: Particle size highdistributions of bMCC, nMCC and cGCC

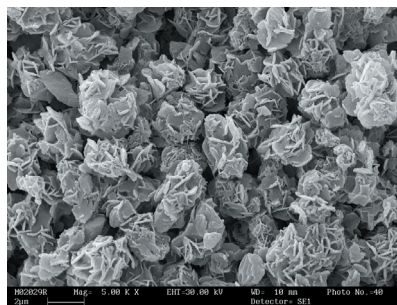


Figure 2: An example of a laboratory made pore volume modified calcium carbonate (MCC)

For illustrative particulate binders, two latices were used: a vinyl acetate (PVAc) (Latexia PVAc, CHP 104, CH Polymers OY, Finland), having T_g 30 °C and styrene acrylic (SA) (Acronal S360D, BASF, Ludwigshafen, Germany), having T_g 5 °C. The effects of soluble binders, starch (Raisamyl 21451, Chemigate OY, Finland) and PVOH (PVOH 88 % (Partly hydrolyzed) BP-05, CCP, Taiwan) and cationic polymer (PolyDadmac) (Alcofix 169, BASF, Ludwigshafen, Germany) on the pore structure are also investigated.

The coating structures formed using the nMCC and bMCC together with the soluble binders mimic as closely as possible a real world inkjet paper coatings.

2.2 Porous sample formation

Tablet press

Tablet structures, consolidated from coating colours with cationic polymer or latex, were formed by applying a constant pressure (15 bar) to the suspension/slurry for ~ 3 hours such that water is released by filtration through a fine 0.025 μm filter membrane (Millipore VSWP04700) resulting in a compacted tablet of the pigment, (Ridgway et al., 2004). Samples with and without cationic polymer were formed and tablets with and without latex were formed. The tablets have dimensions of ~ 4 cm diameter with a thickness of 1.5 - 2.0 cm, which can be divided and fashioned into suitable sample configurations for subsequent analysis. The tablets were removed from the apparatus and dried in an oven at 60 °C for 24 hours (Ridgway et al., 2004).

Coatings on aluminium foil

In the case of coating colours containing PVOH and/or starch, the dewatering of tablets becomes extremely long, and so coatings were made on an impermeable foil substrate. The use of the substrate also provides similarity with real coatings due to the unconstrained thin layer shrinkage properties occurring in the presence of soluble binders, but by using foil any basepaper influences on coating holdout, binder migration etc. were excluded.

Mercury porosimetry

A portion of each tablet of approximately 0.7 g (0.3 cm³), or a strip (20 cm x 1.5 cm) of coated foil, was characterised by mercury porosimetry for both porosity and pore size distribution using a Micromeritics Autopore IV mercury porosimeter. The maximum applied pressure of mercury was 414 MPa, equivalent to a Laplace throat diameter of 4 nm.

Mercury porosimetry utilises the intrusion of a non-wetting liquid (mercury) under pressure to reveal a representative pore diameter via the Young-Laplace diameter-pressure relationship. In network structures, frequently large pores are accessed only by a narrower entrance channel or capillary. The volume associated with the larger pore, however, is recorded as volume associated with the finer entry geometry as the mercury is forced first through this smaller dimension at a given pressure associated with that dimension. This effect is known as “pore shielding”. By taking the first derivative of the cumulative intrusion curves the pore size distributions based on equivalent Laplace diameter, inevitably including pore-shielding, are revealed. The data were corrected using Pore-Comp for mercury and penetrometer effects and also for sample compression (Gane et al., 1996).

3. Results

3.1 Modified calcium carbonate (MCC) and coarse GCC (cGCC)

Effect of Particulate Binder Addition

The example of a discretely bimodal pore structure, controlling permeability via the interparticle pores and capillarity via the intraparticle pores, is provided by modified calcium carbonate (Ridgway et al., 2004). Similar structures also exist in respect to precipitated calcium carbonate. These designed structures provide for high absorption volume and fast absorption rate, but depend on the availability of the pores to perform this action by absorbing the liquid vehicle of the ink. It was shown previously (Ridgway and Gane, 2002) that within a porous structure it is the smaller voids that supply the necessary driving force for absorption to take place. It was also shown that a structure also needs larger voids to act as local supply reservoirs for fluid if this driving force is to continue unhindered by lack of liquid volume. Furthermore, the interconnectivity of the larger voids define the permeability of the network, i.e. the structure also needs to be connected with a high permeability so that the fluid can flow through to the larger pores (reservoirs) and hence to the smaller pores to promote the faster absorption rate defined by the high capillarity of the discrete finer pores. The interpretation of the separability of the intrusion curves to classify these two parameters, of absorption driving force and liquid delivery limitation, is only possible if the driving force exists in a network structure discrete from that of the bulk structure determining the permeability, (Ridgway et al., 2004). Tablets were made both with and without latex (12 parts by weight of SA latex based on 100 parts of pigment) using a laboratory made high pore volume example of this type of pigment to illustrate the effects more clearly, Figure 2, and also from the cGCC.

SA latex is used as an example of a virtually inert, liquid-polymer non-interacting, particulate binder. It is not being used here as a recommendation but as an illustration of the beneficial physical role a particulate binder could have in contrast to the limiting effect of soluble binders. The concept is to provide such illustration to encourage the development of more suitable binder systems based on particulates for the inkjet market.

The mercury intrusion curves for the laboratory made MCC with and without latex are shown in Figure 3a, and compared with the cGCC. The corresponding pore size distributions of these samples are shown in Figure 3b.

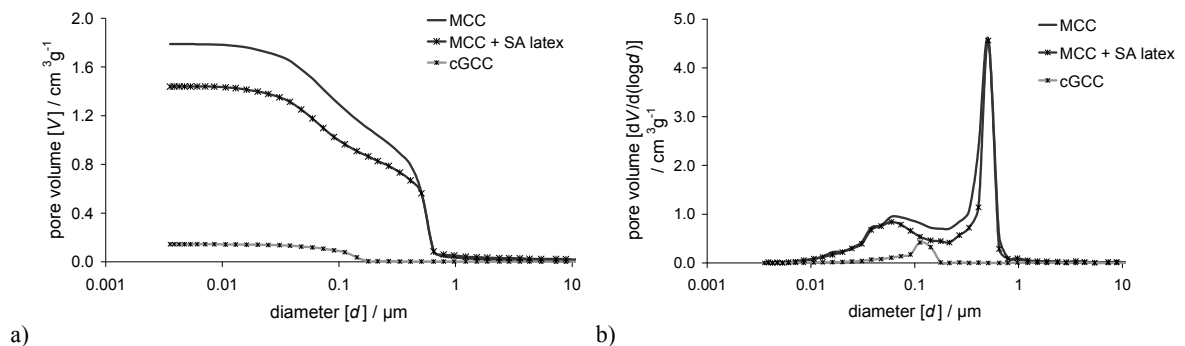


Figure 3: a) Mercury intrusion curves of tablets of laboratory made MCC with and without the addition of SA latex (12 parts), compared with cGCC; b) Pore size distribution of tablets of laboratory made MCC with and without the addition of latex (12 parts), latex (12 parts), compared with cGCC

The mercury intrusion curves for the laboratory made MCC samples show how much more pore volume can be achieved using this pigment compared with a standard coarse GCC (cGCC). The addition of latex reduces the total intruded volume but this volume is still much greater than that of the cGCC.

The pore size distribution curve for the standard cGCC shows that in comparison to the MCC there are very much fewer small pores and therefore this structure has a relatively low capillary driving force for absorption. The laboratory made MCC sample, in comparison, has a significantly greater number of fine pores together with a high permeability (larger pore diameter at the point of inflection of the intrusion curve) and therefore a high liquid delivery rate with the higher number of fine pores providing the driving force. These data show that the combination of fine pore size regions and the permeability of the whole are acting as separable parameters in discrete network structures (Ridgway et al., 2004).

The clearly defined bimodal distribution of MCC is maintained with the addition of the latex with a more pronounced separation between the two pore size distributions when the latex is present in the structures. The dip in the pore size distribution at 0.1 - 0.2 μm corresponds with the void filling action of the monosize latex. A similar analysis can be made for idealised light scattering, where, in such systems, the differentiation between the two size distributions would be even more pronounced with the separation occurring at 0.2 μm .

3.2 Loss of pore volume as a function of additive(s)

Cationic polymer addition

Cationised surfaces are required to provide water fastness when using anionic dye-based inkjet inks. Two different inkjet pigments, nMCC and bMCC, were analysed with the addition of 7 parts per 100 parts by weight of pigment of PolyDadmac, a cationic polymer. Figure 4a shows the mercury intrusion curves for the different tablet samples made from the cationised slurries.

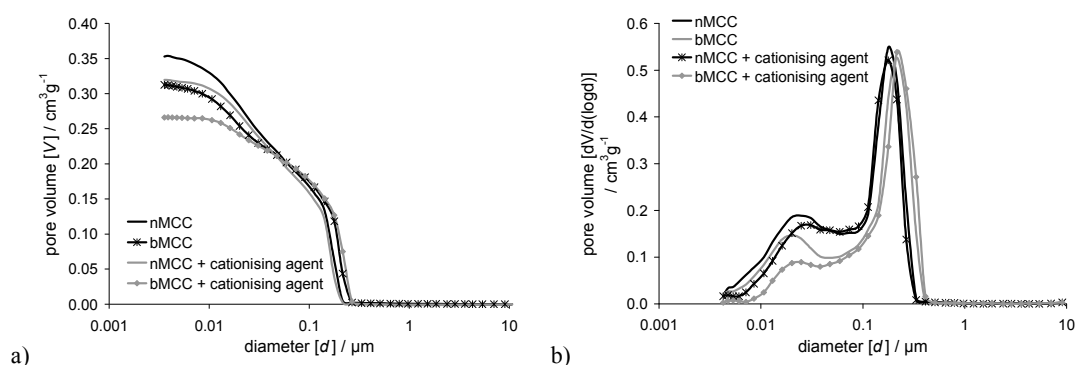


Figure 4: a) Mercury intrusion curves of the tablet samples; b) Pore size distributions of the tablet samples effect of cationic polymer addition on pore size distribution

The bMCC is seen to have less pore volume than the nMCC, as would be expected from the difference in breadth of the particle size distributions. Furthermore, and very importantly, the effect of the cationising agent is seen to lower the total intruded volume for both sample types, especially in the important fine pore region, which is needed for capillarity. The porosity values and the intruded volume into the samples are summarised in Table 1, in the case where 7 pph cationising polymer has been added.

Table 1: Total intruded volume into the samples, showing the reduction due to added cationic polymer

Sample	Total specific intruded volume / cm ³ g ⁻¹	porosity /%
nMCC	0.353 ± 0.004	47.5 ± 1 %
bMCC	0.313 ± 0.003	44.7 ± 1 %
nMCC + cationising agent	0.320 ± 0.003	44.5 ± 1 %
bMCC + cationising agent	0.266 ± 0.003	40.0 ± 1 %

By taking the first derivative of the cumulative intrusion curves the pore size distributions based on equivalent Laplace diameter, inevitably including pore-shielding, are revealed. This is shown in Figure 4b.

All samples have a large peak in the pore size distribution representing the interparticle pore volume as was shown in general for MCC (Ridgway *et al.*, 2004). This peak falls at $0.18\ \mu\text{m}$ for the nMCC samples and at $0.22\ \mu\text{m}$ for the bMCC samples. The smaller peak at finer diameters represents the intraparticle pore volume. These peaks fall at $0.02\ \mu\text{m}$ for the original samples with more pore volume attributable to these pores for sample nMCC, as seen by the curve lying above that for bMCC. The nMCC also has more pore volume attributable to the pore diameter range between the two peaks, which is related to the connectivity of the packed structure in the case of the discretely bimodal pore size distributions.

Once cationically “flipped” by the addition of the polymer, both samples lose some significant proportion of the high capillarity pore volume. This loss is slightly greater for bMCC. The use of PolyDadamac cationising polymer, therefore, additionally reduces this fine pore-related pore volume. Polymer addition, therefore, to cationise anionic pigments will deteriorate performance in respect to absorption rate and absorption volume. A move to pigmented inks (rather than anionic dye-based inks) should be welcomed, as it would allow more cost-effective coating pigments to be used by retaining more of the original pore volume delivered from the pigment manufacture.

Effect of PVOH and starch addition on loss of pore volume

PVOH absorbs up to $\sim 30\%$ of its own weight of water, but if present in pores acts also to limit the absorption rate by reducing it to the interpolymer matrix diffusivity, and reduces the volume according to the loss of pore space by the presence of the swelling PVOH. The role of PVOH in MCC coatings has been studied in more detail by Lamminmäki *et al.* (2009) who studied the action of PVOH as a swelling binder in the coating layer structure, combining these findings with the role of porosity and pore diameters in the inkjet setting process. This work showed how the PVOH coatings operate in defining the print quality formation of dye-based inks in high speed inkjet printing.

In this current study, we combine PVOH and starch as a mixed binder system. The cationic sample was pre-cationised using 5 parts PolyDadamac, as described in the previous section, and is labelled bMCCc. Two coated foil samples were prepared. The coatings were formulated from the inkjet pigment types bMCC and bMCCc plus 2.5 parts PVOH and 2.5 parts starch. To illustrate also the similarity between tablets and coated substrates, Figure 5a shows the mercury intrusion curves for the coated foil samples exemplifying, again, the impact first of all of cationising, but now in the presence of PVOH and starch and as a coating on foil. As can be seen, the effects are similarly displayed as a loss by cationising and an overall greater loss of pore volume induced by the presence of PVOH and starch binder - compare Tables 1 and 2. The volume differences are due to the increased restriction on compaction occurring in the films.

Differences between the coated foil samples at the larger diameters $> 1\ \mu\text{m}$ were seen due to the sample preparation technique, i.e. as the mercury intrudes between the scrolls of the foil, and where the coating may have poor adhesion to the foil. This region of the curve does not contribute any relevant pore structure information in respect to the coating structure and for this reason the data have been truncated at $1\ \mu\text{m}$. This means that the total porosity cannot be evaluated, rather the relative porosity in those pores with an equivalent Laplace diameter $< 1\ \mu\text{m}$ is derivable by direct comparison of the truncated curves. To comment further on the total porosity would require detailed normalisation using oil absorption techniques (Ridgway and Gane, 2003).

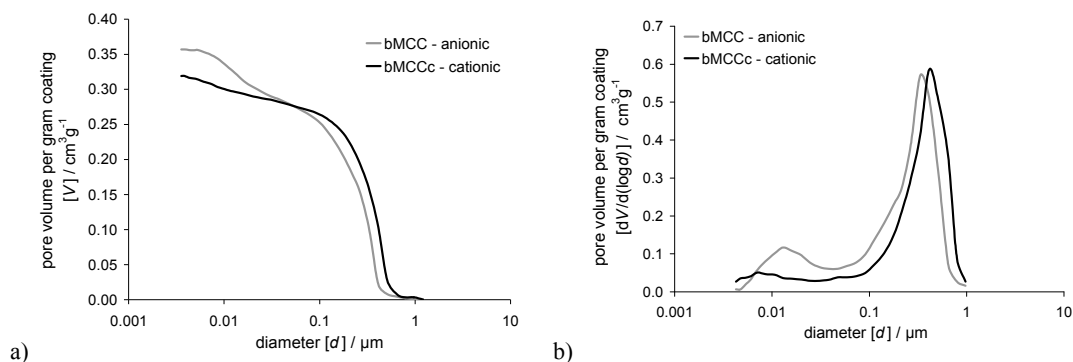


Figure 5: a) Mercury intrusion curves of the coated foil samples, containing both PVOH and starch binders, showing the truncated at $1\ \mu\text{m}$, showing the impact of cationising; b) Pore size distribution of the coated foil samples effect of cationising. The loss of pore volume by the use of PVOH and starch can be seen by comparing with Figure 4b

The total intruded volumes into the samples over the diameter range 0.004 - 1 μm are summarised in Table 2.

Table 2: Total intruded specific volume into the coated foil samples, showing the reduction even in thin films when adding cationic polymer to the mix, in this case also in the presence of PVOH and starch.

Sample	Total specific intruded specific volume / cm^3g^{-1}
bMCC + PVOH + starch	0.357 ± 0.004
bMCCc + PVOH + starch	0.319 ± 0.003

By taking the first derivative of the cumulative intrusion curve the pore size distributions based on equivalent Laplace diameter, inevitably including pore-shielding, are revealed. This is shown in Figure 5b.

Both samples show a main peak at larger pore diameters representing the inter particle pore structure. These peaks fall at 0.33 μm and 0.41 μm for anionic and cationic samples, respectively. Both samples show a smaller peak at finer pore diameters representing the intra particle pore structure. The anionic sample has this peak at 0.013 μm , whereas the cationic sample has a similar but much smaller fine pore volume contribution over the diameter range 0.004 - 0.100 μm . There is a slight peak at 0.007 μm .

We can see from these data, that the cationising has two effects when considered in binder containing thin film coatings. First of all the dispersing quality is not as good as the anionic. This can be seen from the slightly larger pore size of the interparticle structure, indicating some agglomerates/flocculation. Additionally, the nanopores needed for high capillarity are reduced in number, and thus volume. This is due to the cationic polymer used to cationise partly filling the pores.

Latex Addition to Formulations with PVOH and Starch Additives

Three coated foil samples were prepared. The coatings were formulated from the pigment bMCC plus 2.5 parts PVOH, 2.5 parts starch and 5 parts PolyDadmac. The addition of polyvinyl acetate latex (PVAc) was made at two levels, 5 and 10 parts, and compared to a sample without latex. The truncated mercury intrusion curves are shown in Figure 6a.

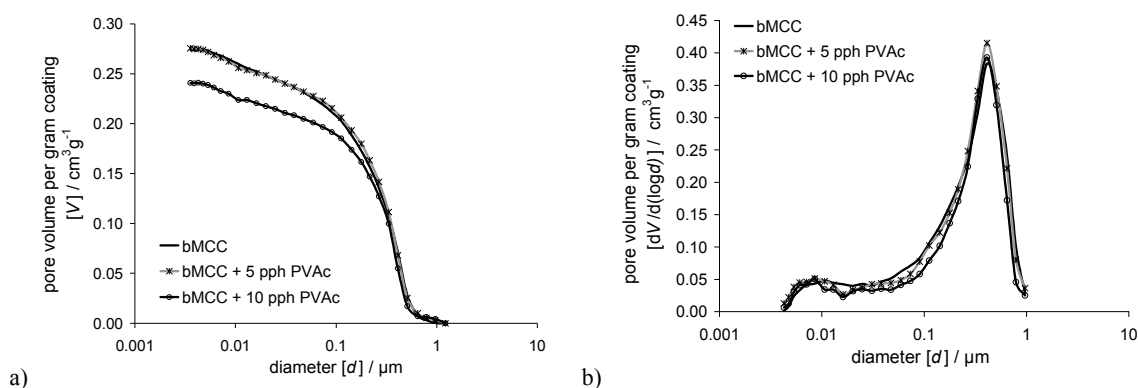


Figure 6: a) Mercury intrusion curves of the coated foil samples truncated at 1 μm , showing the effect of adding particulate PVAc latex to a formulation containing PVOH and starch; b) Pore size distribution of the coated foil samples, illustrating the loss of mid-range and larger pores when particulate latex is added at higher dose in the presence of PVOH and starch

Interestingly, the addition of 5 pph PVAc as a particulate binder has little to no effect on pore volume, whereas 10 pph addition then induces a much lower total intruded volume. The total intruded specific volumes into the samples over the diameter range 0.004 - 1 μm are summarised in Table 3.

Table 3: Total intruded volume into the coated foil samples showing the effect of progressive PVAc latex addition into a formulation containing PVOH and starch

Sample	Total specific intruded volume / cm^3g^{-1}
0 pph PVAc	0.274 ± 0.003
5 pph PVAc	0.276 ± 0.003
10 pph PVAc	0.241 ± 0.002

By taking the first derivative of the cumulative intrusion curve the pore size distributions based on equivalent Laplace diameter, inevitably including pore-shielding, are revealed. This is shown in Figure 6b.

All samples in Figure 6b show a main peak in the distribution at 0.41 μm representing the inter particle pore structure. The sample with 5 pph particulate PVAc binder has the highest pore volume attributable to these pores. Thus, we can conclude that the permeability is maintained or even increased a little (Ridgway *et al.*, 2004). This effect of adding a level of latex below ~ 8 parts has been demonstrated previously by Ridgway and Gane (2007), and is indicative of the disruptive colloidal interference effect when adding latex to a carbonate-based formulation - an effect deriving from depletion flocculation. The next largest peak is shown by the sample containing only the soluble binders without latex addition, and the smallest by the structure with 10 pph particulate PVAc. The sample with 10 pph PVAc has a narrower peak, representing the progressive closure of the interconnecting pores.

In respect to the mid-range (connectivity) pores, the sample without additional latex has the highest pore volume attributable to the pores between pore diameters 0.02 - 0.09 μm , whereas adding latex, especially at the higher dose level, reduces connectivity and so can be expected to reduce permeability.

All samples show a broad peak between pore diameters 0.005 - 0.050 μm representing fine pore volume contributions. It is shown that starch is particularly disadvantageous as it not only prevents access, when film formed, to the crucially absorbing pores, but is itself effectively non-absorbing. It is also shown that latex particulate binder can be used to allow continued access to the nanopore region within the porous pigment particles, and by choosing the right glass transition temperature, T_g , and chemistry of the synthetic polymer, the permeability can also be maintained to a large extent, provided the added level is not too high, (Ridgway *et al.*, 2004, Ridgway and Gane, 2007).

Therefore, latex, at least as part of the binder mix has benefits over all-soluble binder formulations as it does not block pores. The disadvantage today, however, is the as yet somewhat limited choice of latex binders available that are cationically stable.

3.3 Pore structure overview

Table 4 summarises the pigments and additives used in the sample preparation, and links the combinations with the porosimetry data: displayed are the specific pore volume, and the inter and intra particle pore diameters, to give an overview of the pore structure changes.

Table 4: Overview of the pore structure parameters

	total specific intruded volume cm^3g^{-1}	interparticle pore diameter peak μm	interparticle specific pore volume cm^3g^{-1}	intraparticle pore diameter peak μm	intraparticle specific pore volume cm^3g^{-1}
Figure 3a & b (tablets)					
cGCC	0.144	0.110	0.140	-	-
MCC	1.788	0.500	1.028	0.060	0.760
MCC + SA latex	1.440	0.500	0.808	0.060	0.632
Figure 4a & b (tablets)					
nMCC	0.353	0.180	0.201	0.025	0.152
bMCC	0.313	0.220	0.221	0.020	0.092
nMCC + cationising agent	0.320	0.180	0.194	0.025	0.126
bMCC + cationising agent	0.266	0.220	0.219	0.020	0.047
Figure 5a & b (foil)					
bMCC	0.183	0.330	0.146	0.013	0.037
bMCCc	0.157	0.410	0.139	0.007	0.018
Figure 6a & b (foil)					
bMCC	0.274	0.410	0.240	0.007	0.034
bMCC + 5 pph PVAc	0.276	0.410	0.240	0.007	0.036
bMCC + 10 pph PVAc	0.241	0.410	0.211	0.007	0.030

3.4 Implications for printability

Changes in the coating formulations will lead to changes in the printing quality. One of the tests used to characterise print quality is the level of colour-to-colour bleed, an example of which is shown below in Figure 7.

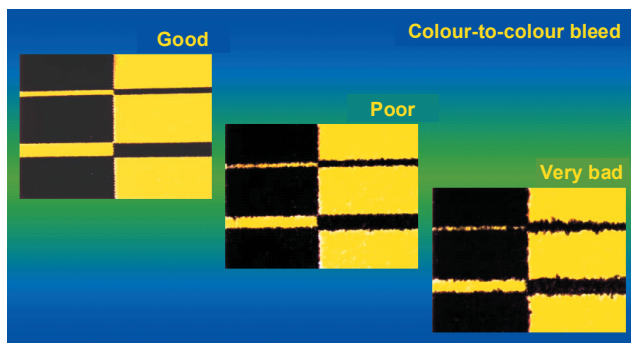


Figure 7: Colour-to-colour bleeding example

The changes in the formulations that we have discussed in this study may not lead to effects as large as that illustrated as “very bad” in Figure 7, but reducing the additive amounts by 1-2 parts can already improve the print quality toward that of “good”. More notably, if polymer additives for cationising could be eliminated, which is expected as inkjet inks move toward pigmented formulations in the emerging generation of presses, and soluble binders further reduced, being eventually replaced by particulate binder, one would anticipate additional significant cost savings as pore volume could be better retained. As a result, the expensive porous coating pigment component could in turn be reduced whilst maintaining constant pore volume. It is thus seen as a significant step forward to be able to reduce the amount of soluble polymers required in the coating formulation.

4. Conclusions

All polymer additives, especially water soluble ones, in some way reduce the pore volume of speciality calcium carbonate inkjet pigment structures, with particular emphasis on the loss of fine high capillarity pores; especially low molecular weight, water soluble ones.

Because of the requirements of anionic dye-based inks for water fastness, coatings need to be cationised. This is typically achieved by “flipping” anionically dispersed formulations using a cationic polymer, such as PolyDadmac. Even if cationically dispersed pigments are considered, most other coating colour components, if stabilised particulates, also require cationising to become compatible in the dispersion. Inevitably either adsorbed or free cationic polymer will be on the high surface area walls of the fine pores or will migrate to the fine pore regions during the drying process, respectively. This effect impacts on the absorption efficiency due to lost pore volume and lost capillarity.

Soluble binders can be considered either water absorbing, such as PVOH, or relatively insoluble (starch). In both cases, they too act to reduce available pore volume. Even in the case of absorbing/swelling binders, the efficiency of absorption is reduced to that of the interpolymer diffusion in the binder matrix, and the volume is reduced despite its absorbency.

The use of particulate binder, such as PVAc latex, on the other hand preserves to a large extent the total pore volume, and even permeability of the structure can be preserved when used at low to moderate dose levels. Higher dose rates lead to a loss of permeability, but the capillarity is nonetheless retained. A disadvantage of currently available particulate binders nonetheless remains, insofar that, if cationising of the latex or the whole formulation is still required, the stability of the dispersion is compromised, and, once again, the capillarity is reduced.

References

- Boisvert, J.-P. and Guyard, A., (2003), "Influence of Structural Properties of Nanoporous Silica-Polymer Materials on Ink Absorption", *Nordic Pulp and Paper Research Journal*, 18(2), 210-216.
- Chapman, D. M., (1997), "Coating Structure Effects on Ink-Jet Print Quality", *Coating Conference*, , 73-93.
- Gane, P. A. C., Kettle, J. P., Matthews, G. Peter and Ridgway, C. J., (1996), "Void Space Structure of Compressible Polymer Spheres and Consolidated Calcium Carbonate Paper-Coating Formulations", *Industrial and Engineering Chemistry Research*, 35(5), 1753-1764.

- Hara, K., (2006), "Speciality PVOH in Ink Jet Coating Formulations", *Paper Technology*, 47(3), 27-30.
- Lamminmäki, T., Kettle, J. P., Puukko, P., Gane, P. A. C. and Ridgway, C. J., (2009), "Inkjet Print Quality: The Role of Polyvinyl Alcohol in Speciality CaCO₃ Coatings", *Journal of Pulp and Paper Science*, 35(3-4), 137-147.
- Nilsson, H. and Fogden, A., (2008), "Inkjet Print Quality on Model Paper Coatings", *Appita Journal*, 61(2), 120-127.
- Pinto, J. and Nicholas, M., (1997), "SIMS Studies of Ink Jet Media", *Proceedings of IS&T's NIP 13: International Conference of Digital Printing Technology*, Seattle
- Ridgway, C. J. and Gane, P. A. C., (2002), "Dynamic Absorption into Simulated Porous Structures", *Colloids and Surfaces A: Physicochemical and Engineering Aspects*, 206(1-3), 217-239.
- Ridgway, C. J. and Gane, P. A. C., (2003), "Bulk Density Measurement and Coating Porosity Calculation for Coated Paper Samples", *Nordic Pulp and Paper Research Journal*, 18(1), 24-31.
- Ridgway, C. J. and Gane, P. A. C., (2007), "Effect of Latex and Pigment Volume Concentrations on Suspension and Consolidated Particle Packing and Coating Structure", *Journal of Pulp and Paper Science*, 33(2), 71-78.
- Ridgway, C. J., Gane, P. A. C. and Schoelkopf, J., (2004), "Modified Calcium Carbonate Coatings with Rapid Absorption and Extensive Liquid Uptake Capacity", *Colloids and Surfaces A*, 236(1-3), 91-102.
- Ridgway, C. J., Gane, P. A. C. and Schoelkopf, J., (2006), "Achieving Rapid Absorption and Extensive Liquid Uptake Capacity in Porous Structures by Decoupling Capillarity and Permeability: Nanoporous Modified Calcium Carbonate", *Transport in Porous Media*, 63(2), 239-259.
- Rousu, S. M., Gane, P. A. C., Spielmann, D. C. and Eklund, D., (2001), "Separation of Off-Set Ink Components During Absorption into Pigment Coating Structures", *Nordic Pulp and Paper Research Journal*, 15(5), 527-535.
- Rousu, S. M., Lindström, M., Gane, P. A. C., Pfau, A., Schädler, V., Wirth, T. and Eklund, D., (2002), "Influence of Latex-Oil Interaction on Offset Ink Setting and Ink Oil Distribution in Coated Paper", *Journal of Graphic Technology*, 1(2), 45-56.
- Schoelkopf, J., Gane, P. A. C., Ridgway, C. J. and Matthews, G. P., (2000a), "Influence of Inertia on Liquid Absorption into Paper Coating Structures", *Nordic Pulp and Paper Research Journal*, 15(5), 422-430.
- Schoelkopf, J., Ridgway, C. J., Gane, P. A. C., Matthews, G. P. and Spielmann, D. C., (2000b), "Measurement and Network Modeling of Liquid Permeation into Compacted Mineral Blocks", *Journal of Colloid and Interface Science*, 227(1), 119-131.
- Svanholm, E., Wedin, P., Ström, G., and Fogden, A., (2006), "Colorant Migration in Mesoporous Inkjet Receptive Coatings", *9th Advanced Coating Fundamentals Symposium*, TAPPI, Atlanta.
- Wedin, P., Svanholm, E., Alberius, P. C. A. and Fogden, A., (2006), "Surfactant-Templated Mesoporous Silica as a Pigment in Inkjet Paper Coatings", *Journal of Pulp and Paper Science*, 32(1), 32-37.

Influence of flexographic inks on optical density of full tone fields and contrast in printing on the biodegradable films

Joanna Izdebska, Halina Podsiadło

Warsaw University of Technology, Faculty of Production Engineering,
Institute of Mechanics and Printing, Department of Printing Technology
Konwiktorska 2, PL-00-217 Warsaw, Poland

E-mails: j.izdebska@wip.pw.edu.pl; h.podsiadlo@wip.pw.edu.pl

Abstract

Biodegradable films were printed with commercial flexographic inks: water-based and solvent based with different resins. Six biodegradable, compostable films which are the samples of three kinds of such materials were selected; 3 based on cellulose, 2 PLA and 1 starch blends. The optical density of full tone and halftone fields were measured and relative printing contrast were calculated. Some properties of inks tests as well as adhesive and scratching tests of printed films were submitted in the paper. The influence of inks on optical density and contrast, main quality parameters are discussed. Flexographic inks for printing of available on the market biodegradable films enable to obtain, on proper selection of ink and kind of printing base, copies of good quality.

Keywords: flexographic inks, optical density, relative printing contrast, biodegradable film

1. Introduction

The European market of packages is continuing to change and develop. The materials dominating in Europe in the production of packages are: paper and cardboard (38%) and plastics (31%) (Tuka, 2009). The highest percent consumption of plastics is observed in the package industry, mostly in the production of food packages. Among the most important groups of plastics currently used for the manufacture of packages, the following should be mentioned: polyethylene (PE), polypropylene (PP), polyvinyl chloride (PVC), polystyrene (PS), polyesters (PET), polyamides (PA). All of them are possible to be replaced by biodegradable polymers such as polylactid (PLA), starch and starch blends, cellulose, polyhydroxyalkanoates (PHA), etc. (Rudnik, 2008). The name of biodegradable materials is given to polymeric plastics that can undergo biodegradation or biological decomposition or are made of renewable raw materials. They become degraded within the time of several months to several years depends on the condition, where the traditional synthetic, petroleum-based plastics need hundreds or thousands years. Nowadays biodegradable materials based on PLA, starch blends, cellulose are the most important on the market of such materials (IntertechPira, 2010).

In addition to the primary functions of packaging (protection of the product, facilitation of portioning, providing of information on the packaged object) a modern package must also play advertising, promotion and environment friendly roles. This is explanation why the print quality is so important now. An increasing interest in ecological aspects of both the products and their packaging is observed in all European country. The tendency of limiting the harmful effect on natural environment is observed in both the producers of materials searching for new technologies capable of reducing the amount of waste materials, use of renewable sources for production of materials (for example in production of biodegradable polymers) or replacing some components by other ones, more friendly for the natural environment, and in new designs of printing and packaging-forming machines. The biodegradable materials due to they degradable properties seem to be the future materials special for packaging where the time of products life is very short. Nowadays they represent less than 1% of the total market of plastics, but a significant increase is anticipated (Shen, 2009; Nampoothiri, 2010).

Such printing technologies as flexography, gravure and rarely offset and digital printing which are referred to printing on traditional plastic films could be used also to biodegradable ones. The paper shows the results of studies on the influence of commercial flexographic inks on optical density of full tone fields and contrast in prints made by flexographic printing technique. Optical density is one of the parameters which determine the copies quality. It is a measure of colour saturation of printing ink used. The optical density of ink-coated fields depends i.a. on pigment concentration in the ink and on ink layer thickness on the print (Kipphan, 2001). For

flexography printing there is no unequivocal values of optical density on full tone fields. The values for black ink which are quote in literature are: 1,4 (Czech, 1993), 1,33÷1,47 (FFTA, 2003), 1,4÷1,5 (Czichon, 2006) or 1,2÷1,9 (Stępień, 2007). Other parameters that characterized the print can be derived by means of density measurement, for example: relative printing contrast or trapping (ink acceptance). Contrast can be calculate from the measured values of the ink density in the full tone and the ink density in the halftone screen (it is preferable to measure this value in 70%, 75% or 80%) (Kipphan, 2001; Czichon, 2006).

2. Experimental

2.1. Materials

Biodegradable films of various producers, based on three kinds of polymers, differing in structure and properties, were used as the object of investigation. The materials were the following biodegradable, compostable films: cellulose based, PLA and starch blends (see Table 1).

Table 1: Characteristics of biodegradable films

	Film 1	Film 2	Film 3	Film 4	Film 5	Film 6
Kind of polymer	cellulose	cellulose	cellulose	PLA	PLA + AAC	starch blends
Producer	Innovia Films	Innovia Films	Innovia Films	Sidaplax	BASF	Novamont
Name of product	NatureFlex 23 NVS	NatureFlex 23 NVR	NatureFlex 23 NK	Earthfirst PLA (BCP)	Ecovio L BX 8145	Mater-Bi
Thickness [μm]	23,3	23,3	23,6	20	21	23
Gloss	very high	very high	very high	very high	high	very low
Utility to welding	+	+	+	+	+	+
Barrier to oxygen	very high	very high	very high	very high	high	very high
Barrier to humidity	poor	middle	very high	poor	middle	poor

Water-based inks (also referred to as water dilutable inks) and solvents flexographic inks were used in the research. Ecology regulations give favour to water-based inks, the consumption of which on the market of packages is expected to increase, accordance the solvent-based are more suitable to printing films. According to standard EN 13432 both kind of inks are suitable for printing biodegradable films when the concentration of each component in the final packaging is limited to 1% and the total concentration of all components is less then 5% of dry weight of the final product, and not include dangerous substrates (EN 13432, 2000).

The printing process was carried out with the use of water dilutable black printing ink based on styrene-acrylic resin and 3 organic-solvent dilutable black inks based on different kinds of resins and one solvent-based black ink which is certificate by AIB-Vincotte as biodegradable (see Table 2). All inks have declaration of producers to utility at printing food packaging.

Table 2: Characteristics of printing inks

	Ink 1	Ink 2	Ink 3	Ink 4	Ink 5
Kind of resin	styrene-acrylic	PA	PU/NC	NC/PU	NC/PU
Biodegradable, compostable according to EN 13432	-	-	-	-	+
Producer	Chespa	WFFG	WFFG	WFFG	Flint Group
Name of product	Process	Urania	Wifester	Wiflex	FlexiPrint MV

2.2. Methods

The studies comprised the inks tests, and preparation of copies and their research. Adhesive and scratching tests were done. Optical density of full tone and 80% tone fields were measured and the relative contrast values were calculated.

Inks tests

Physicochemical properties of flexographic inks, like generally all printing inks, determine printing process and future properties of the copies. Main of them such as viscosity and grind grade were studied before the printing process. The inks were also subjected to visual observation and dry mass contents were determined. The visual observation conforming to the standard enabled to check the presence of surface scum, homogeneity, colour, and form of the products. The viscosity was determined at $23\pm 0,5^{\circ}\text{C}$ with the use of a Ford cup of outflow orifice diameter 4 mm according to ISO standard (ISO 2431, 1999). The grind grade was tested according to properly ISO standard (ISO 1524, 2002). A drier-balance Santorius MA 30 was used as analyzer of liquid products. The analyses of dry mass were conducted for $1\pm 0,02$ g of inks at temperature $110\text{-}120^{\circ}\text{C}$ until the constant mass.

Printing process

The prints on the biodegradable package films tested were made with the use of Flexiproof 100 device using a flexographic technique, involving printing plate prepared by digital laser-photochemical method, from photopolymer plate Nyloflex® FAH produced by BASF. The Flexiproof device is comparable to a single-color printing press. Testing take place at a constant speed 60 m/min. Pressure between anilox roller and plate cylinder was 98 units, and between plate cylinder and impression cylinder was 61 units. Flexible photopolymer printing plate on size 260x90 mm with thickness value of 1,7 mm was used for printing. The screen frequency of plate was 36 l/cm (91 lpi). The plate was mounted on the print cylinder using the soft tesa plate mounting tape with thickness 0,5 mm. Anilox roller cell counts used for printing were: 200,6 l/cm (509,6 lpi). The ambient condition were: temperature $21,5\pm 2,5^{\circ}\text{C}$, RH $42\pm 2\%$.

Copies tests

Adhesion tests using tests tape according the standard (ISO 4624, 2004) and scratch resistance (Rentzhog, 2006) were performed before laboratory printing. The scratch resistance was described with 5 level grade where 1 is the best and means there was no changes in the appearance of copy and 5 means the ink in place of scratching was removed from the copy. The grades from 1 to 3 showed the scratch resistance was acceptable. The adhesion was evaluated with 3 level grades and the grades 1 and 2 were recognized as satisfactory.

Optical density of printed full tone and 80% halftone fields were measured by means of Spectro Eye spectrofotometer (Gretag Macbeth). Densitometric measurements were performed in reflective light after placing printed films on the Matchprint Proofing Paper used as a white standard. The measurements conditions were: physical filter - polarizing, white standard - paper, illumination - D50, observation angel - 2° , density standard - DIN. The reported results are the average of ten measurements in case of solid field. The relevant printing contrast was calculated according the formula (1).

$$K = \frac{D_V - D_R}{D_v} \cdot 100 \% \quad [1]$$

where: K - relative printing contrast [%],
 D_V - optical density in the solid,
 D_R - optical density in the halftone.

3. Results

The collected results of adhesive and scratching tests and measured properties of inks are arranged in Table 3.

The best results in the adhesive test were obtained by all studied inks in printing on Film 1, Film 2, Film 3 and Film 4. In case of Film 6 adhesive is lower for water-based ink (Ink 1). The worst adhesive property has Film 5 for all inks. Also totally not acceptable adhesion is recognized for Film 5.

The highest resistant for scratching have Ink 1 printed on Film 2, Film 3 and Film 6, and Ink 3 and Ink 4 printed on Film 1, Film 2 and Film 4. The worst results were achieved for the inks with PA resin (Ink 2) and biodegradable one (Ink 5) (see Table 3).

Table 3: Inks tests results

		Ink 1	Ink 2	Ink 3	Ink 4	Ink 5
Viscosity [s]		18	20	20	20	20
Grind grade [μm]		2 \pm 1	2 \pm 1	1 \pm 1	1 \pm 1	2 \pm 1
Dry mass [%]		48,04 \pm 1,09	29,10 \pm 1,06	21,16 \pm 1,44	21,11 \pm 1,00	25,20 \pm 1,44
Scratch resistance	Film 1	2	4	1	1	4
	Film 2	1	3	1	1	2
	Film 3	1	5	5	4	5
	Film 4	2	4	1	1	4
	Film 5	4	4	2	4	-
	Film 6	1	2	1	3	-
Adhesion	Film 1	1	1	1	1	1
	Film 2	1	1	1	1	1
	Film 3	1	1	1	1	1
	Film 4	1	1	1	1	1
	Film 5	3	2	2	2	-
	Film 6	2	1	1	1	-

Measurement of the optical density of full tone depended on the kind of ink and film are displayed in Figures 1÷5. A comparison of these figures show that water dilutable ink (Ink 1) exhibits higher optical density, compared to solvent-based inks. The result of that are differences in pigment concentrations between inks. The values of dry mass of Ink 1 is almost double-times higher than for the rest of the inks. The lowest values of optical density of full tone were obtained for all inks in case of Film 2. Irrespective of the kind of film the most similar values of density were received with biodegradable ink.

Measurements of the optical density in full tone fields printed on Film 1, Film 3, Film 4 and Film 6 with solvent-based inks were approximated to each one. Ink 4 allowed receiving a few or several percent higher values of optical density then Ink 3 and Ink 2. The ink based on NC/PU resin compared to PU/NC one, with the same ink adhesion to the printing base, give opportunity to receive the copies of quality parameters more similar to that described in literature and a little bit worse scratching resistance.

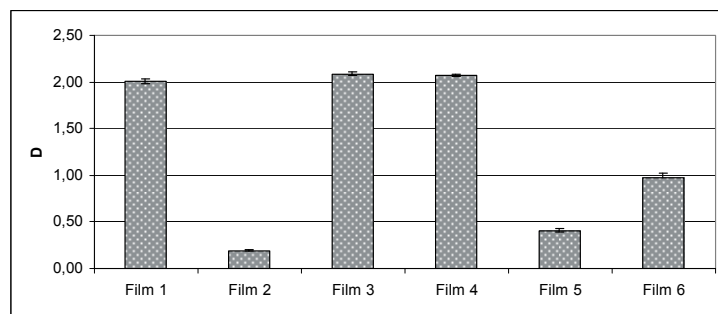


Figure 1: Optical density of full tone printed using Ink 1

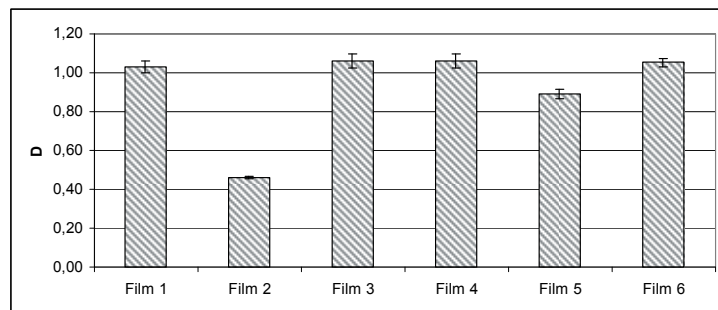


Figure 2: Optical density of full tone printed using Ink 2

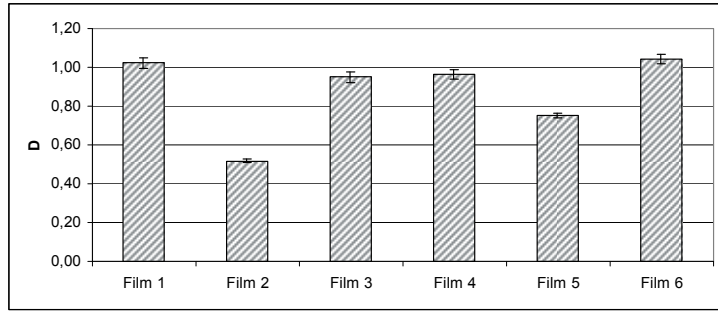


Figure 3: Optical density of full tone printed using Ink 3

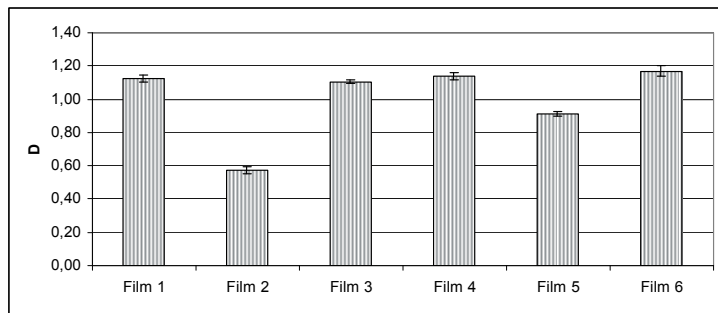


Figure 4: Optical density of full tone printed using Ink 4

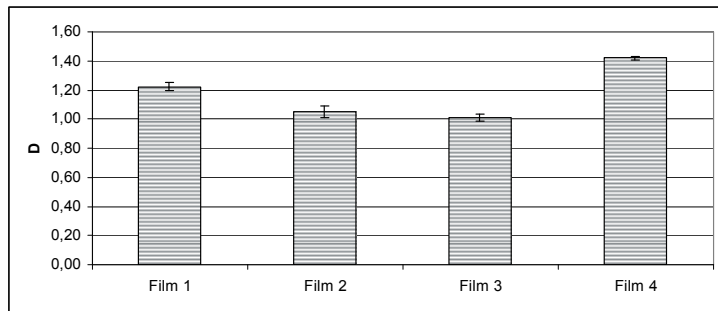


Figure 5: Optical density of full tone printed using Ink 5

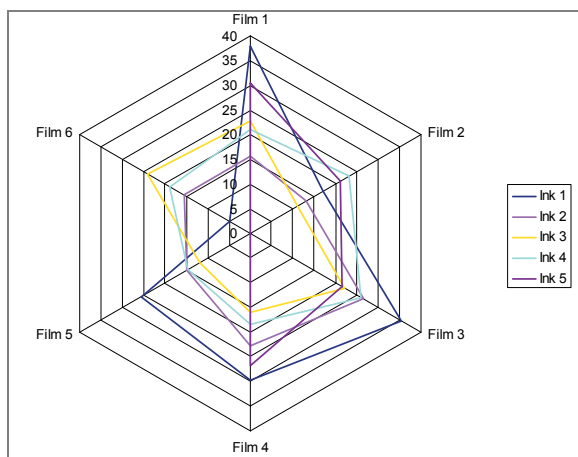


Figure 6: Relevant printing contrast depended on kinds of ink and film

The results of contrast are parallel to optical density of full tone. Figure 6 shows the values of relevant contrast depended on kinds of ink and film. Copies printed with water-based ink (Ink 1) on Film 1 and Film 3 have the highest contrast values. Contrast above 25 for copies printed with Ink 1 is noted also on Film 4 and Film 5. In addition biodegradable ink allowed to receive a good quality of printing with contrast values from 21 to 30 units. Relatively good effects were obtained also for another ink based on NC/PU resin - Ink 4.

4. Discussion

Czech et al. wrote the maximum value of the full tone density in the copies depends on inks and printing materials (Czech, 1993). The results of experimental tests show the biodegradable films used as printing materials have in this case bigger influence than the kind of inks. The type of ink, water- or solvent-based, is very relevant, but the kind of resin and the composition of ink determined the results only in small range.

Water dilutable ink because of the higher pigmentation needs another printing parameters than solvent-based ink. The copies printed on the films which are well wetting by water dilutable inks (Film 1, Film 2 and Film 4) achieve too high values of optical density, compared to announce in literature (see Figure 1). The data has indicated that a lot of inks had been transferred to the film. However, for these three films, respectively it is to be supposed changes in the printing process such as: harder printing plate, other anilox roller cell counts would allow to achieve very good quality of the copies with this one water-based ink.

The other one very important parameter outside the pigmentation, which has an influence on optical density of copies, is transfer of ink to printing base. It depends on wettability of substrates and spreading of inks on flexographic printing units. In case of Film 2 printing with the used inks except Ink 6 in ambient conditions near the standard temperature and humidity do not allow to achieve copies of high quality. The results have shown that there were problem with wettability of Film 2. Such difficulty was found also in case of Film 5, but in smaller range. The Film 2 according to recommendation about printing some cellulose films with temperature of the base about 80°C (Czichon, 2008) would allow to achieve good results. However, other cellulose biodegradable films used in the research are well printability in typical ambient condition. The same of course apply for the rest of tested biodegradable films.

Film 5 needs more carefully choice of the ink to the printing base than other used films. The quite good results gave printing with Ink 2 and Ink 4. Some changes in printing process such as modification of ink (improvement of scratch resistance) and the corona activation of film surface before the printing could get better quality of the copies, acceptable in the production process. However, the activation of film surface is used in case of almost all traditional plastics film to receive good quality, it has been emphasized in first step of development of biodegradable materials that in printing on that kind of films it is not necessary. Nowadays some producers of biodegradable films mention to dose the corona activation before printing what reduce the problems with wetting the base and give better quality of copies. In case of Film 5 it is able that activation of film is necessary to achieve high quality of printing. However, the rest of tested films could be printed successfully without changes of surface free energy.

Czichon value of relevant contrast $K(80)$ equal 40% treated like the optimal (Czichon, 2006). According to the another publication (FFTA, 2003) values of $K(70)$ should be higher than 15%. On the copies which we can treat like good quality according the optical density analyses the data have shown that the values of contrast was not so high as 40%, but was a lot of higher than 15%. It is important to realized that the optical density in 70% halftone is lower than this value measured in 80% halftone, what means that $K(70)$ should have higher value than $K(80)$. Because of that the received results can be assumed like satisfactory.

5. Conclusions

Experimental tests and analysis of the results obtained enable to state that the biodegradable films available on the market and intended for production packages differ in the values of optical density for the same kind of ink and differ for each of inks. In printing biodegradable films with water-based inks the optical density of full tone are generally higher what can be caused by higher pigmentation of this ink. Flexographic water-based as solvent inks for printing of biodegradable films enable to obtain, on proper selection of ink and kind of printing base, copies of good quality - with proper optical density and relevant printing contrast values, as well as good adhesion of ink to film. The maintenance of adhesion-cohesion equilibrium is necessary to achieve high quality print, what was shown on the printed films. Even small modifications in the ink composition (the same kind of resin, differ additives) can lead to changes in the optical density of the biodegradable films printed.

References

- Czech G. (ed.), (1993), *Technologia fleksograficzna zagadnienia standaryzacji (Standardization problems in flexography print processes)*, COBRPP, Warsaw.
- Czichon H., Czichon M., (2006), *Formy fleksodrukowe (Flexographic plates)*, OWPW, Warsaw.
- Czichon H., Czichon M., (2008), *Folie chlorowinylowe, celulozowe i biorozkładalne jako podłoża drukowe*, Świat Druku 3, 70-73.
- EN 13432:2000 *Packaging – Requirements for packaging recoverable through composting and biodegradation – Test scheme and evaluation criteria for the final acceptance of packaging*.
- FFTA (ed.), (2003), *Flexographic image reproduction. Specification and tolerances. 3rd edition*, FFTA, USA.
- IntertechPira: *PHA and bio-derived PE to Drive Bioplastic Packaging Market to 2020*, <http://www.intertechpira.com/pha-and-bio-derived-pe-to-drive-bioplastic-packaging-market-to-2020.aspx>, Accessed 13 December 2010.
- ISO 1524:2000 *Paints, varnishes and printing inks. Determination of fineness of grind*.
- ISO 2431:1993 *Paints and varnishes. Determination of flow time by use of flow cups*.
- ISO 4624:2002 *Paints and varnishes. Pull-off test for adhesion*.
- Kipphan H. (ed.), (2001) *Handbook of Print Media*, Springer, Heidelberg.
- Nampoothiri K. M., Nair N. R., John R. P., (2010), *An overview of the recent developments in polylactide (PLA) research*, *Bioresource Technol.* 101, 8493-8501.
- Rentzhog M., Fogden A., (2006), *Print quality and resistance for water-based flexography on polymer-coated boards: Dependence on ink formulation and substrate pretreatment*, *Progress in Organic Coatings* 57, 183-194.
- Rudnik E., (2008), *Compostable polymer materials*, Elsevier, New York.
- Shen L., Haufe J., Patel M., (2009), *Product overview and market projection of emerging biobased plastics*, *PRO-BIP, Utrecht*.
- Stępień K., Khadzhynova S., Leks-Stępień J., (2007) *Czynniki wpływające na przenoszenie farby we fleksografii (Parameters influenced to ink transfer in flexography)*, *Opakowanie* 3, 7-11.
- Tuka A. (ed.), (2009), *The packaging industry and market in Poland*, *Polish Chamber of Packaging, Vidart, Warsaw*.

Appendix - abbreviations and their meaning

- AAC - aromatic-aliphatic copolymers
NC - nitrocellulose
PA - polyamide
PLA - polylactide
PU - polyurethane
K(70) - relevant printing contrast calculated with optical density in 70% halftone
K(80) - relevant printing contrast calculated with optical density in 80% halftone



Evaluation of image segmentation algorithms for folded substrate analysis

Magdolna Apró¹, Dragoljub Novaković¹, Pál Szabolcs²

University of Novi Sad, Faculty of Technical Sciences
Trg Dositeja Obradovića 6, SRB-21000 Novi Sad, Serbia

¹Department of Graphic Engineering and Design

E-mail: apro@uns.ac.rs; novakd@uns.ac.rs

²Department of Computing and Automatics

E-mail: pal.szabolcs@gmail.com

Abstract

This paper presents an analysis of segmentation algorithms in respect to their accuracy to detect failures (cracked surfaces) on folded substrates. For this purpose an initial set of 24 algorithms was chosen in a way to cover a wide range of segmentation algorithm types. The analysis was performed in two steps. The first step was a rough, visual comparison and served as an initial filter to reduce the number of potential algorithms. The four best performing algorithms were then further analysed in the second step, using objective measures like: misclassification error, modified Hausdorff distance, positive and negative false detection.

Besides the segmentation algorithms, a basic analysis of colour spaces and smoothing pre-filters was performed, too. Best results were derived by the Maximum Entropy algorithm.

Keywords: image segmentation, folding, quality assessment

1. Introduction

The folding process has a great impact on the visual appearance of printed products as well as on their mechanical behaviour. During the folding process, printed or non-printed substrates, like paper or paperboard, are exposed to high tensile stresses on the outer side and compression stresses on the inner side of the folding line. These stresses can lead to coating cracks, which decrease the expected aesthetic feature and what is more, if there are more serious surface damages like bursting open of the substrate surfaces and material breaking, the products can completely lose their functionality. The phenomena of surface damaging in the folding process, its experimental and numerical analysis, are subject of several papers published in the last 40 years which are summarized by Barbier (Barbier, 2004). There are many factors that influence surface cracking. Some of them are related to the paper manufacturing technology, others to the printing and converting processes. Several reports and papers have indicated that proper adjustment of folding machines plays an important role in real production conditions (Eklund, 2002; Gidlöf, 2004). In order to maintain high production efficiency and quality, a permanent process control is necessary. The most frequently used folding quality assessment method is based on visual control by experts. Since, this method has a subjective nature, the obtained results are not always repeatable, they heavily depend on the controller's experience and the method can be very time-consuming. To overcome these problems, an objective quality estimation method is needed. Like in other fields of industry, computer vision based quality control can be applied. The basic solution of objective folding quality assessment (OFQA) was presented in previous papers of the authors, which was also based on the visual evaluation, using image processing algorithms in combination with neural network (Apró, 2009). The presented algorithm obtained objective quality measures of SAPPI evaluation scale (Sappi, 2006), which were in good correlation with subjective grades. However, further work was necessary to additionally improve and fine-tune the method's accuracy.

During the development and improvement process, which included a complete revision of some parts of the algorithm, the image segmentation was identified as the first most critical step. Since most of the model output variables depend on an accurate segmentation (cracked surface estimation, crack distribution and size), it has the greatest influence on the method's accuracy.

In order to find the best image segmentation method, an additional investigation was done, which results are presented in this paper.

2. Methods

2.1 Test samples

For development of OFQA algorithm, a test form was developed, based on the experimental test form from (Eklund, 2002) and (Gidlöf, 2004). The test form included test fields for printing quality assurance and for analysing the folding behaviours. The region used for folding test includes five different colour areas and a blank area in order to cover different situations from real production process. With CMYK notation the printed areas were: C 50%, K 50%, K 100%, C 40% + M 40% + Y 50% + K 20%, C 80% + M 80% + Y 80% + K 80% (see Figure 1).

The test form was printed on KBA Performa 74 offset machine with process colours (Sun Chemical). The samples were made from uncoated, glossy- and matte-coated paper (FEDRIGONI) with basic weight of 100 g/m², 140/150 g/m² and 170 g/m². 50 samples of each paper grade were prepared in machine and cross direction on the Perfecta 76 high-speed cutting machine and were folded on the Horizon AFC544AKT folding machine (only one buckle folding unit used). The experiment was performed 48 hours after printing at standard conditions (temperature of 22 °C, relative humidity of 55%).

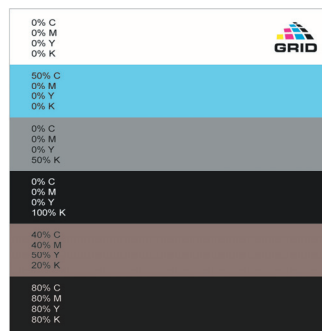


Figure 1: Test form for the folding quality evaluation

The folded and gathered samples were digitalized with three different methods: commercial digital camera (Canon A520), flatbed scanner (Canon, CanoScan 5600F, sRGB IEC61966-2.1) and digital microscope (Veho VMS-001 USB microscope, magnification of 200X). For this investigation a subset of 12 images have been selected from the base set, covering all three digitalisation methods and four different surface textures. These surface textures present a particular challenge to automated segmentation: halftone cyan (Figure 2a) and black (Figure 2b), solid-tone black (Figure 2c) and the CMYK halftone pattern, known as rosette pattern (Figure 2d).

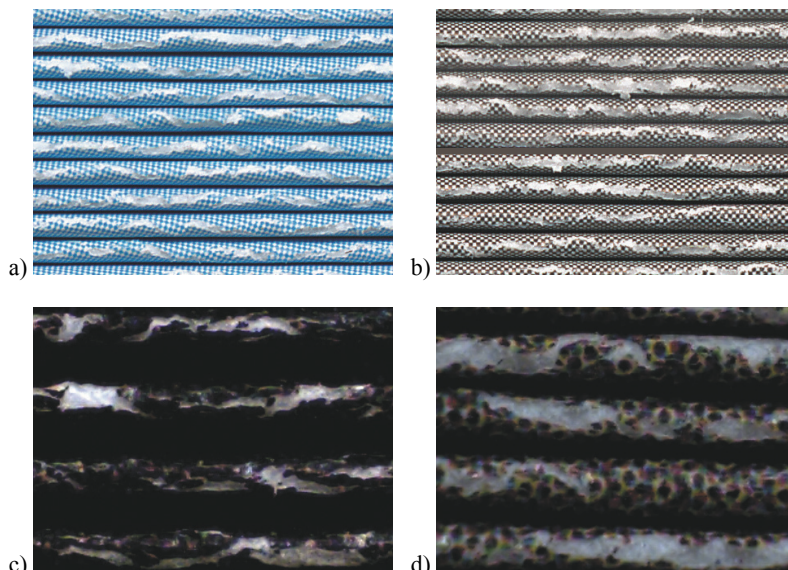


Figure 2: Examples of selected images with 50% cyan (a), 50% black (b), 100% black (c) and CMYK rosette pattern (d)

In addition, 4 images were added to the evaluation subset, presenting perfect folds without surface cracking (Figure 3), since this type of surface is also demanding for segmentation.

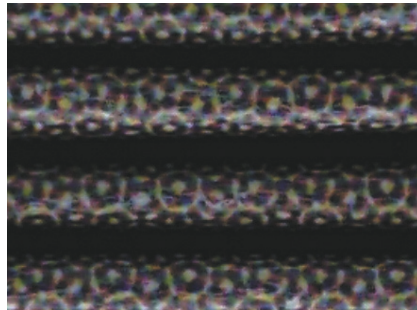


Figure 3: Example of folded paper without damages (cracking)

2.2 Image segmentation

Image segmentation is the process of separating or grouping an image into different parts (Marsh, 2004). It is the first and most important step in every image recognition application and even though it is not a new field of investigation it remains a complex problem to tackle. Early segmentation algorithms were based on grey-level segmentation, but with the increase of available processing power (faster PCs, embedded platforms) colour image processing gained popularity. The problem of introducing colour image analysis is with the exponential growth of possible data points. A simple three-channel image with 8 bit colour depth has a colour space of more than 16 million points, compared to a plane greyscale image analysis, where the colour space has just 256 elements (supposing 8 bit greyscale values) the necessary computational effort is orders of magnitude higher. For this reason and for simplicity reasons, greyscale image segmentation algorithms were analyzed for the problem at hand.

Segmentation algorithms can be roughly grouped into global and local thresholding methods. However, a more comprehensive and accurate categorisation is given by Sezgin (Sezgin, 2004), where 6 different groups of algorithms are recognized. For this research, 24 algorithms were chosen in a way to cover most of these groups and they are presented in Table 1. Since, the final algorithm should work autonomously and with a wide range of samples, only algorithms with auto-detected thresholds were considered.

Table 1: Overview of selected segmentation algorithms and algorithm groups

Group of methods	Chosen algorithms	Short description
Histogram shape based methods	Huang, Intermodes, Mean, Minimum, Triangle, Percentile	the peaks, valleys and curvatures of the smoothed histogram are analyzed
Clustering based methods	IsoData, Minimum Error, Otsu, K-means	the grey-level samples are clustered into two parts as background and foreground, or alternately they are modelled as a mixture of two Gaussians
Entropy based methods	Li, Maximum Entropy, Renyi Entropy, Shangbhag, Yen.	the entropy of the foreground and background regions, the cross-entropy between the original and binarized image, etc. are used to segment the image
Object attribute based methods	Moments	search a measure of similarity between the grey-level and the binarized images, such as fuzzy shape similarity, edge coincidence, etc.
Spatial methods	RATS	higher-order probability distribution and/or correlation between pixels are analysed
Local thresholding methods	Bernsen, Mean, Median, MidGray, Niblack, Sauvola	adapt the threshold value on each pixel to the local image characteristics rather than use a single, global threshold

For the evaluation platform, a widely used and well-supported program, ImageJ has been chosen. The selected algorithms can be found as basic processing tools in the program or can be installed as a plug-in.

In order to determine the performance of particular algorithms reference (ground truth) images were needed. These were generated by hand segmenting every sample image, marking just the cracked surfaces as foreground objects (see example on Figure 4).

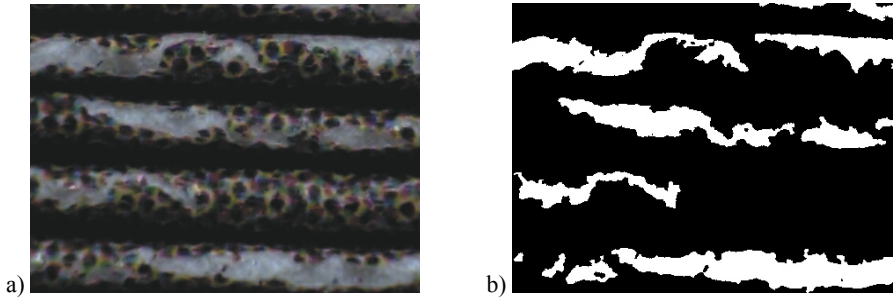


Figure 4: Example of original (a) and its hand-segmented pair (b)

Since the algorithms work on greyscale images, the sample images (originally in RGB colour space) needed to be transformed to get their lightness component. RGB colour space is not best suited for image analysis tasks, because the components are highly correlated and the distance measure between two colours is not according to subjective opinion (Cheng, 2001). For this reason the two widely used colour spaces, HSL and CIE Lab, were analysed as possible colour formats for the task. Both are non-linear transforms, separate the colour information of an image from its lightness information and have better capabilities to represent the colours of human perception (Cheng, 2001). For this investigation the lightness information of the two colour spaces were used as the greyscale representation.

Textures and uneven highlighting can compromise the results of automatic segmentation. In this case, both factors were present, on one side due to the half-tone screen and rosette patterns (representing a complex texture), on the other side, uneven surfaces (due to folding lines) make an optimal highlighting very difficult, which in most samples could not be achieved. These difficulties caused false positive detections since on one side the cracked area and the non-printed area of paper surface were having the same colour (luminance), but on the other side poorly highlighted crack lines were hardly distinguishable. Applying smoothing filters as a pre-filter step can reduce this problem by removing redundant details and noise from the input image. For this reason three different filters were tested and evaluated: the Gaussian, Mean and Kuwahara filters.

2.3 Experiment

The evaluation was done in two phases. In the first phase, the algorithms were roughly evaluated, comparing their outputs visually. As a result of the first phase, a sub-set of algorithms were selected, which performed the best from the initially selected group. These algorithms were then further evaluated in the second phase, deriving their objective performance measures for each test image. The selected objective measures are described in the following.

Misclassification error (ME), which reflects the percentage of background pixels wrongly assigned to foreground, and conversely, foreground pixels assigned to background. For the two class segmentation problem, ME can be simply expressed as:

$$ME = 1 - \frac{|B_o \cap B_T| + |F_o \cap F_T|}{|B_o| + |F_o|}, \quad [1]$$

where B_o and F_o denote the background and foreground of the ground truth image, B_T and F_T denote the background and foreground areas of the tested image, and $|\cdot|$ is the cardinality of the set. ME varies from 0 for a perfectly classified image to 1 for a completely wrongly binarized image (Sezgin, 2004).

The Hausdorff distance can be used to assess the shape similarity of the thresholded regions to the ground-truth shapes. Since the maximum distance is sensitive to outliers, shape distortion can be measured via the average of the *Modified Hausdorff distances* (MHD) over all objects, which can be defined as:

$$MDH(F_o, F_T) = \frac{1}{|F_o|} \sum_{f_o \in F_o} d(f_o, F_T), \quad [2]$$

where $d(f_o, F_T)$ denotes the minimal Euclidean distance of a pixel in the thresholded image from any pixel in the ground-truth image, $|F_o|$ is the number of foreground pixels in the ground-truth image. Notice that, since an upper bound for the Hausdorff distance cannot be established, the MHD metric could not be normalized to

the interval (0, 1) (Sezgin, 2004). Also, it should be noted that the MHD can not tell too much about quality on its own, it could be rather used together with ME, where this measure would decide which of the results is best when the two MEs are close to each other.

Positive false detection (PFD) is the proportion of background pixels wrongly assigned to the foreground object. Normalization can be done using the number of foreground pixels or the overall number of pixels in the ground-truth image. In this paper, normalization was done using the number of foreground pixels.

Negative false detection (NFD) is the proportion of foreground pixels wrongly assigned to the background. Normalization was performed in the same manner as for the PFD.

As a derived measure the NFD – PFD ratio is defined, too. It serves as an auxiliary measure to make the balancedness of false detection values easy to read. It is defined as:

$$\text{NFD - PFD ratio} = \begin{cases} \frac{PFD}{NFD}, & \text{if } PFD \geq NFD \\ \frac{NFD}{PFD}, & \text{else} \end{cases} \quad [3]$$

This measure has a minimum in 1, which is also its optimum, desired value. The choice of measures was guided by the attempt to optimise the following criterion: automated segmentation results should be matching the ground truth as close as possible, preferably 100%, but if there are some mismatches, the misclassified pixels should be as close as possible to the desired foreground object. Since some measures of the OFQA are using the ratio of foreground and background pixels it is also preferable to have balanced number of false positive and false negative detections, which would in this case give a good estimate of the real measure.

Not only the number of algorithms was narrowed after the first phase of testing, but other factors, like colour space and the choice of the smoothing pre-filter were fixed, too. This helped to keep the amount of data to process in a manageable range. Evaluation of these side factors was done in a simplified manner (only by subjective, visual comparison) since they should not compromise particular algorithms but rather improve the performance of all algorithms (however this could be the subject of further investigation).

3. Results and discussion

After the first phase of the investigation the four best performing algorithms were selected for further investigation in the second phase. These algorithms were from the global thresholding group of algorithms: Minimum, Maximum Entropy, Renyi Entropy and Huang methods. The local thresholding algorithms did not prove to be of better performance for the whole sample range (despite the expectations before testing), just for some single cases, therefore they were not considered for further examination. A possible explanation for their poor performance can be found in high spatial complexity of the test samples which made it impossible for local thresholding to distinguish between surface patterns and real cracks.

The results of the first phase also showed that segmentation based on HSL lightness information is more successful (Figure 5a), that that based on CIE Lab colour space (Figure 5b). The HSL colour space based images produced less noisy binarized images and had less false positive detections, therefore the HSL colour space was used in further steps of the investigation.

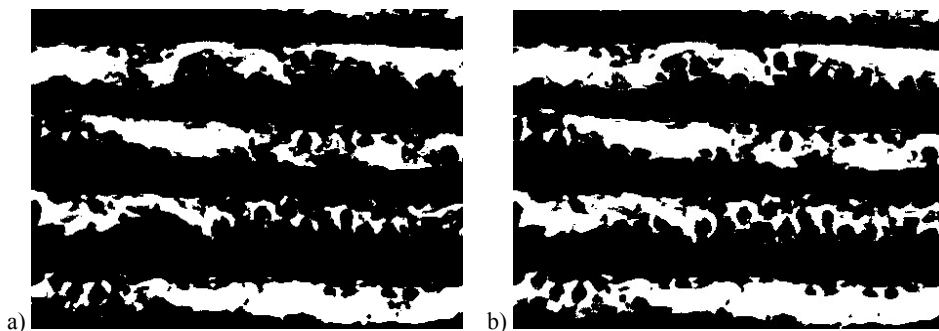


Figure 5: Comparison of HSL (a) and CIE Lab (b) based segmentation

During this evaluation (first phase) three different smoothing filters were analysed: Gaussian, Mean and Kuwahara filters. Best results were derived using the Mean filter in most of the cases, in some specific pattern and colour combinations, the Kuwahara filter showed good result also, although the improvement of adequate segmentation was modest. As for the used colour space, the smoothing filter was also fixed after the first phase and the choice was the Mean filter.

The second phase of the investigation, was performed with a reduced parameter set (one colour space and smoothing filter and 4 segmentation algorithms), but with objective measures. As mentioned in the previous chapter, ME, MHD, PFD and NFD were derived. The ME results are shown in Table 2.

Table 2: Misclassification error of particular algorithms over the whole test set

File name	Huang	Renyi	Minimum	Maximum Entropy
Test image 1	0.072418	0.594383	0.67166	0.594383
Test image 2	0.218408	0.109296	0.145511	0.063509
Test image 3	0.41113	0.223333	0.458219	0.223333
Test image 4	0.268641	0.079438	0.166353	0.081743
Test image 5	0.622369	0.208899	0.61647	0.268463
Test image 6	0.258325	0.085476	0.121843	0.08329
Test image 7	0.495637	0.397154	0.523738	0.379428
Test image 8	0.447247	0.393672	0.487824	0.389253
Test image 9	0.38099	0.569384	0.656467	0.545916
Test image 10	0.523362	0.56852	0.587554	0.56363
Test image 11	0.325813	0.092093	0.222844	0.093034
Test image 12	0.350615	0.140864	0.307446	0.154755
Test image 13	0.167239	0.066367	0.114964	0.043694
Test image 14	0.281955	0.281955	0.284506	0.331961
Test image 15	0.402413	0.331912	0.278154	0.266139
AVG	0.348437467	0.276183067	0.376236867	0.272168733

According to the ME measure, two algorithms, the Maximum Entropy and Renyi Entropy, performed better than the remaining two (best performance for a particular image is given in bold letters). Although Huang method performed significantly better on two test images (test image 1 and 9) the overall performance of the Maximum Entropy and Renyi methods was almost in all other cases superior. However, their performance was very similar (only 0.004 difference between the two average values) hence other measures needed to be consulted to tell the best. These additional measures were the MHD and the ratio of NFD and PFD which are given in Table 3 and Table 4, respectively, for those images which had similar ME values.

Table 3: MHD measure of Maximum Entropy and Renyi algorithms for some test images of interest together with ME and PFD to help interpret the results

File name	Misclassification error		Modified Hausdorff distance		PFD	
	Renyi	Max. Entropy	Renyi	Max. Entropy	Renyi	Max. Entropy
Test image 2	0.109296	0.063509	1.024365	1.30028	0.001597	0.092515
Test image 4	0.079438	0.081743	15.066588	14.871598	0.147478	0.214391
Test image 6	0.085476	0.083290	1.164125	1.210582	0.083903	0.104331
Test image 7	0.397154	0.379428	8.325566	8.282748	3.086195	2.943015
Test image 8	0.393672	0.389253	6.554903	6.537661	1.984381	1.959677
Test image 9	0.569384	0.545916	6.455211	6.3852	2.779713	2.664666
Test image 11	0.092093	0.093034	5.449015	5.426666	0.231543	0.256777
Test image 12	0.140864	0.154755	5.161102	5.255056	0.449810	0.572214
Test image 13	0.066367	0.043694	1.063936	1.115893	0.019647	0.116210
Test image 14	0.281955	0.331961	6.253087	6.327061	2.065047	2.528167

Test images 1 and 3 were not analysed further because the two algorithms gave identical results. Test images 5, 10 and 15 were not considered because they are samples without cracks, hence the MHD and the NFD – PFD ratio cannot be defined for them.

Table 4: NFD-PFD ratio of Maximum Entropy and Renyi algorithms for some test images of interest together with PFD and NFD to help interpret the results

File name	NFD-PFD ratio		PFD		NFD	
	Renyi	Max. Entropy	Renyi	Max. Entropy	Renyi	Max. Entropy
Test image 2	454.441	3.570	0.001597	0.092515	0.725978	0.330263
Test image 4	1.400	1.430	0.147478	0.214391	0.206532	0.149889
Test image 6	4.492	3.304	0.083903	0.104331	0.376883	0.344674
Test image 7	122.033	99.437	3.086195	2.943015	0.025290	0.029597
Test image 8	72.336	66.315	1.984381	1.959677	0.027433	0.029551
Test image 9	-	-	2.779713	2.664666	0	0.000480
Test image 11	1.164	1.029	0.231543	0.256777	0.269585	0.249474
Test image 12	1.257	1.816	0.449810	0.572214	0.357836	0.315081
Test image 13	22.054	1.566	0.019647	0.116210	0.433290	0.181988
Test image 14	19.380	88.481	2.065047	2.528167	0.106553	0.028573

The analysis of particular images is given in the following.

Maximum Entropy performed better with test images 2, 6, 7, 8, 9, 11 and 13. For test images 2, 6 and 13 it had lower ME and despite the higher MHD the NFD-PFD ratio is much more suitable for our needs. For test image 7, 8 and 9 every measure, ME, MHD and NFD-PFD ratio (despite test image 9, where this measure is not meaningful) is in favour of Maximum Entropy. For test image 11 despite the ME measure, the other two measures are clearly in favour of Maximum.

Renyi method showed better performance with test images 4, 12 and 14. For test image 4 the ME and the NFD-PFD ratio are in its favour and for test images 12 and 14 all measures are better with Renyi.

Based on these results, the Maximum Entropy algorithm proved to be best suited for the optimization criteria set in Methods section, hence it will be used as the segmentation algorithm of OFQA.

However, it should be noted, that on two sample images with cyan halftone pattern (test image 1 and 9) the Huang algorithm performed well, while the other algorithms over detected the cracked areas. This could be explained by the histogram characteristics of these pictures. Since Huang method is histogram shape based and test picture 1 (and 9 too) has clear and significant peaks (see Figure 7), which is better suited for this algorithm. While Maximum Entropy set the threshold value to 110, which is just before the two significant peaks in the histogram, the Huang method set it between them, at the value of 175. However, clear and significant peaks are usually rare and the performance of the Huang method for example on test picture 11, which has an almost monotonic, decreasing histogram (see Figure 8), is rather poor in comparison with Maximum or Renyi Entropy. Huang method set the threshold to 52, at a local saddle in the histogram, while Maximum Entropy set it at 110, clearly favouring the bright pixels.

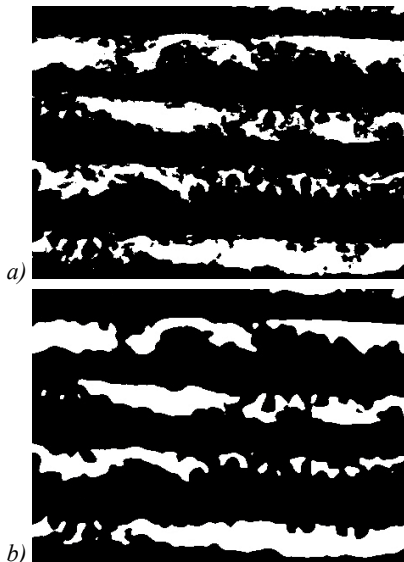


Figure 6:
Examples of segmentation by Maximum Entropy without (a) and with (b) the applied Mean smoothing filter

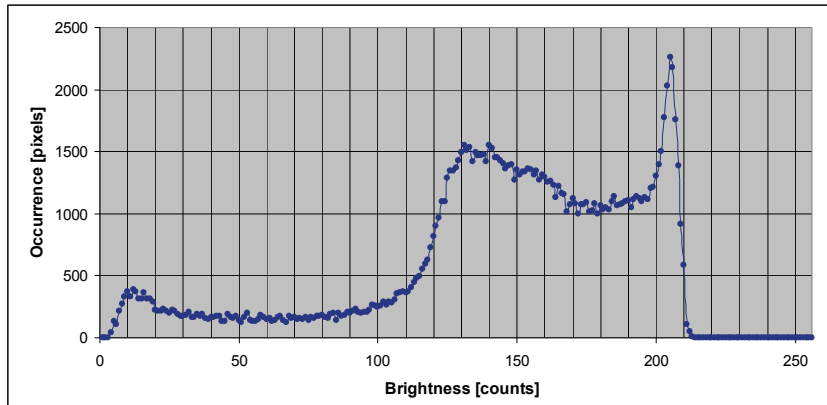


Figure 7: Histogram of test image 1

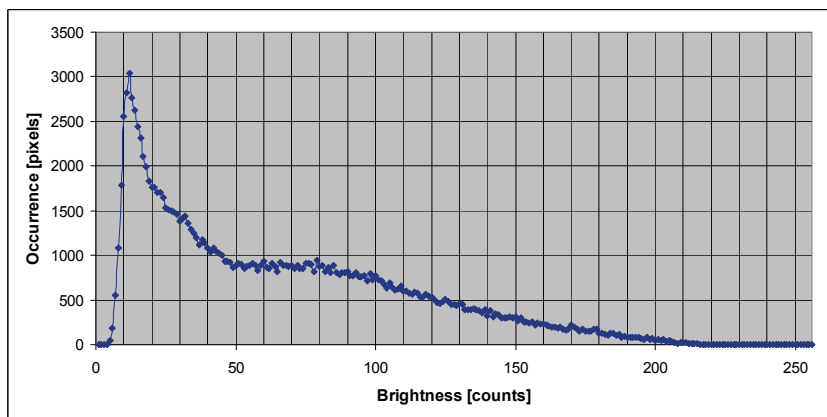


Figure 8: Histogram of test image 11

4. Conclusions

In this paper an analysis of segmentation algorithms is presented in respect to their accuracy to detect crack lines on folded substrates. The analysis was done in two steps, where the first included a number of different algorithms, smoothing pre-filters, colour spaces. Assessment of performance was done visually, and based on these first results a smaller subset of algorithms was selected, which performed the best. These algorithms were then thoroughly tested and compared by objective measures. The results showed that the Maximum Entropy algorithm had the best performances, according to the criteria set at the start of the investigation. Other conclusions were also made, which included the choice of colour space to use as the source of lightness information. According to the first phase of investigation the HSL colour space was found to perform better than the CIE Lab space (resulting segmented images had less noise and hence less over-detection (PFD)). However, this analysis was not thorough enough, hence another, dedicated investigation should search this field, since the impact of colour space on the segmentation quality can be significant. Besides the colour space the smoothing pre-filter was also invariant for the second phase of investigation. The Mean filter was selected from the starting set because it's good performance and computational efficiency. However, the improvement of segmentation quality by applying a smoothing pre-filter is rather modest. It helps to eliminate the salt-and-pepper type of noises from the resulting images and helps to smooth the edges of regions.

Since the nature of the problem foretells a three-colour detection problem (colour of the shadow, of the print surface and that of the base paper at cracks) a multi-threshold solution to the problem should be also considered. However, this is not a strait forward choice since some substrates are printed solid-black or almost without shadows. For this reason, the investigation should be continued and extended to search for solutions containing more complex decision criteria or maybe some kind of soft computing. Also the colour information should be considered, instead of just the lightness information, in order to improve segmentation performances.

Acknowledgements

This work was supported by the Serbian Ministry of Science and Technological Development, Grant No.:35027 "The development of software model for improvement of knowledge and production in graphic arts industry"

References

- Anon. (2006), Folding and creasing, Sappi's Technical brochures, 2nd, revised edition, Available from: <http://www.sappi.com/NR/rdonlyres/F3F8F3B0-89B8-4528-9684-7D40C7A5817A/0/FoldingandCreasing.pdf> (accessed: 04. 2008.)
- Apro, M., Novaković, D., Pal, Sz., (2009), Investigation of optimal parameter set of the objective quality estimate of folded paper, IXth Seminar in Graphic Arts, Pardubice, Czech Republic, pp: 99-104, ISBN: 978-80-7395-200-6
- Barbier, C., (2004), On Folding of Coated Papers, Doctoral Thesis no. 56, Royal Institute of Technology, Department of Solid Mechanics, Stockholm, Sweden, Available from: http://www.t2f.nu/s2p2/S2P2_MS_9%20.pdf (accessed: 04. 2008.)
- Cheng, H., Jiang, X., Sun, Y., Wang, J. (2001), Color image segmentation: advances and prospects, Pattern Recognition, Vol. 34, No. 12, pp: 2259-2281.
- Eklund, J., Österberg, B., Eriksson, L., Eindenvall L., (2002), Finishing of digital prints – a failure mapping, IS&T NIP 18 San Diego, California, USA, pp: 712-715, Available from: www.t2f.nu/t2frapp_f_56.pdf (accessed: 05. 2008)
- Gidlöf, V., Granås, J., Dahlström M., (2004), Functionality in Digital Packaging Printing, TAGA conference 2004, San Antonio, Texas, USA, Available from: http://www.t2f.nu/t2frapp_f_140.pdf (accessed: 05.2008.)
- Marsh, M. (2004), A Literature Review of Image Segmentation Techniques and Matting for the Purpose of Implementing Grab-Cut.pdf, Available from: <http://citeseerx.ist.psu.edu/viewdoc/download?doi=10.1.1.103.1334&rep=rep1&type=pdf> (accessed: 04. 2011.)
- Sezgin, M., Sankur, B, (2004), Survey over image thresholding techniques and quantitative performance evaluation, Journal of Electronic Imaging, Vol. 13, No. 1, pp: 146-165





3

*Special
printing applications*

Inkjet printed electronics at UAB-CNM: technology and design flow developments

*Eloi Ramon*¹, *Francesc Vila*², *Elkin Gonzalo Diaz*¹, *Jofre Pallarès*²
Lluís Terés^{1,2}, *Jordi Carrabina*¹

¹ CAIAC - Universitat Autònoma de Barcelona
Campus UAB Bellaterra, Edifici Q, E-08193 Cerdanyola del Vallès, Barcelona (Spain)
E-mail: name.surname@uab.cat

² IMB-CNM (CSIC)
Campus UAB Bellaterra, 08193 E-Cerdanyola del Vallès, Barcelona (Spain)
E-mail: name.surname@imb-cnm.csic.es

Abstract

Our main goal is to propose methodologies & tools for designing and printing electronic devices using inkjet printing technology. Printed-electronics emerging technologies are far from being mature enough; thus, lots of efforts have to be done to reach stable working technologies. In these sense current developments requires in depth knowledge about related inkjet printing machinery, functional inks, substrates and their interactions.

In this work we discuss the benefit of developing fabrication technology and a design methodology together with a set of tools for building reliable and precise inkjet printed flexible and organic systems. Different printed devices and test structures has been studied and analyzed. Printed passive and active components are crucial for the development of low cost, flexible and printed systems.

Regarding the design methodology and related flows and tools we have also studied and defined how to move the well-known Technology & Design Kit (TDK) concept from silicon based to printed based microelectronics. Once the design flow has been identified we are selecting CAD tools and developing the TDK concept. Specific backend tools to transfer the design resulting drawings or layouts into the specific technology set (printer+inks+substrates) have been developed to make specific technology compensations and adjustments.

Keywords: FOLAE, EDA tools, IJPE, technology & design kit, electronic devices characterization

1. Introduction to printed electronics

Printed Electronics (PE) is a new concept in electronics manufacturing which introduces new challenges in applications, design, technology, processes and materials concerning conventional electronic and micro-electronic technology. Organic and inorganic inks with electronic properties as conductors, semi-conductors or dielectrics can be printed using techniques such as offset, flexography or inkjet, over large surfaces not constrained by current microelectronic wafer dimensions, so we are facing the foundations of an emerging and challenging technology that could potentially revolutionize flexible, large area and organic electronics fabrication (ObN, 2010).

1.1 Inkjet printed electronics

Inkjet printed electronics (IJPE) can be considered the main printing technique in the research environment nowadays, due to its combination of low-cost equipment, process flexibility, and low material consumption (Tob, 2011). Inkjet systems are designed to construct devices and circuits drop by drop, which would lead to a new paradigm in electronics fabrication. These drops vary from pL to a few μL , while the minimum feature resolution is in the range of μm . Although we can find several promising works showing the fabrication of transistors and basic analog and digital cells (Sub, 2005), (Man, 2008), IJPE technology is still in its early development stage and several big challenges remain, such as printer head clogging, undesired satellite drops or low ink viscosity leading to coffee stain effects (Yin, 2010).

In recent years an increasing interest in direct-write fabrication methods has emerged, with the aim of developing low cost and large area electronics fabrication techniques. Micro-fabrication of electronic and mechanical structures is typically a time-consuming and expensive process because of the complicated optical lithography system. The Drop-On-Demand (DoD) inkjet technique is an attractive approach (Wan,

2004) as it enables data driven patterning, and a process that is low cost, non-contact, low temperature, flexible and has a very low material waste. Inkjet printing is therefore one of the most promising printing technologies for Flexible Organic and Large Area Electronics (FOLAE). Some technical attributes of inkjet make it best suited for mass customization, small batch size and simple and disposable circuitry. Inkjet is becoming an enabling technology for on-demand production in printed electronics, electronic design flexibility and rapid design testing.

In a DoD inkjet printing system, a nozzle ejects functional material droplets that take a ballistic trajectory from the print head down to a certain position on the substrate. Neighbor droplets overlap each other and form patterns that could be used either as an active device layer or as a mask for subsequent process steps. Figure 1 shows a sequence example of an envisioned ink jetted transistor fabrication roll-to-roll (R2R) process.

All these considerations make DoD inkjet printing method a truly promising technology to take into account for FOLAE and other solution-based materials deposition usage. An inkjet platform consists of 3 key elements: print head, ink and substrate. In order for the system to work properly, each one must be totally adapted to the others. Print head-ink and ink-substrate compatibility is required. In the first case, print head-ink, there are different techniques to generate droplets, but currently the most popular is the piezoelectric one because it applies no thermal load to the organic inks compared with the bubble inkjet technique (Yin, 2010).

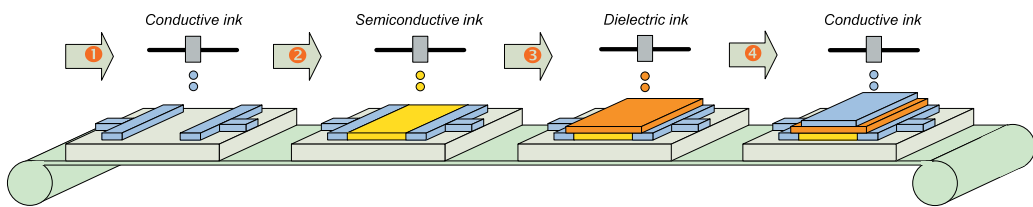


Figure 1: Different stages of DoD inkjet print heads in R2R equipment are proposed to eject different functional materials to build a complete electronic system in an integrated process

When a drop of ink reaches the substrate, the balance between the absorption of the ink and the evaporation of the solvents determines the final spot shape and consequently, the surface homogeneity. Deposited spot morphology can be as a donut-like shape known as a “coffee-ring” effect (Hua, 2002) or result in a spot of near circular horizontal profile.

The printing materials consist of a solute dissolved or dispersed in a solvent formulated as ink. In PE, the various roles of active materials lead to different constraints on technology. Recent works (Str, 2009), (Sol, 2008), (Kan, 2010) demonstrated the need for improved control of the behavior of inkjet-printed lines and shapes. By characterizing and understanding the conditions that lead to different printed line morphologies, electronic devices performance and yield can be improved; thereby the various aspects of ink-substrate interactions must be revisited for printed electronics.

Furthermore, since substrates such as paper tend to swell and shrink during the printing and drying process, the deposition of a new layer on top of another one can modify the expected layer geometries. Layer registration is another key challenge to be faced.

The inkjet printing setup used in the present study is based on a Fujifilm Dimatix DMP2831 printer. It uses one user-fillable piezo-based ink jet print cartridge with 16 nozzles, able to eject 1pl or 10pl drops. It is able to jet a wide range of fluids with a variable jetting resolution and also integrates a cleaning cartridge station and vision tools. The substrate vacuum plate is temperature controllable. The DoD printing was undertaken in a 10.000-class standard laboratory environment. In this work, the lab inkjet printer platform has been used as the path from printing technology to devices.

1.2 Designing IJPE devices and circuits

Once an IJPE fabrication process is set-up, a design flow must be formalized in order to produce circuits and systems composed of previously tested and characterized devices, out of a design process composed of a set of design automation tools oriented to increase the design and fabrication productivity and reliability.

Design methodology depends directly of the technology evolution and process formalization. To allow cost effective design and inkjet manufacturing of printed electronics systems, the impact of substrates, device structures and printing process must be taken in account during the design process. However, previous know-

ledge from conventional printing and silicon microelectronics is still applicable while the various aspects of ink and media interactions must be revisited for inkjet printed electronics. Furthermore, since substrates such as paper tend to swell and shrink during the printing and drying process, the deposition of a new layer on top of another can modify the expected layer geometries, what has to be taken into account as a kind of mechanical design rules (MRC) similar to existing geometric or electrical ones. Such MRC shall also address the performance variations of operational circuits when bended.

While inkjet technologists usually have poor knowledge of circuit issues, circuit designers usually have poor knowledge of IJPE fabrication process. This means that methodology and tools are needed to abstract unnecessary technology details and providing an easier and more effective interaction between both sides.

1.3 IJPE at CNM-UAB

IMB-CNM (CSIC) and UAB started IJPE research few years ago coming from classical silicon-based microelectronic technologies background out of different factors: flexible printed circuits board (PCB) technologies, were appearing as commodities to give more freedom and flexibility for electronic system designers; evolution of RF technologies (from RFID to NFC and beyond) requested hybrid solutions of silicon on top of printed antennas; there were promising complementary technologies such as touch sensors, OLEDs or photovoltaics that can be better integrated in electronic solutions from a fabrication point of view.

With this idea in mind, and taking profit of our past experience in setting up design kits for different technologies (i.e. CNM CMOS processes) we started bridging the gap between design and technology concerning both Electronic Design Automation (EDA) tools for design automation and fabricating and characterizing structures in order to obtain device models (see Figure 2).

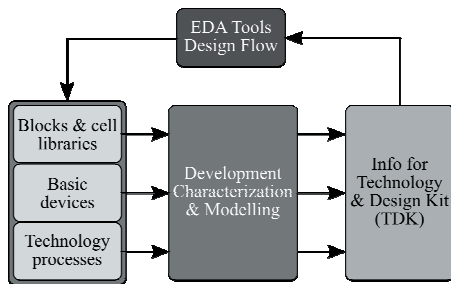


Figure 2:
Detail of the link between EDA tools and characterization in order to build a set of processes, devices and libraries to be integrated in a TDK

This work addresses two complementary topics, the IJPE technology development and characterization and the PE design flow definition, development and application. This way we intend to link technology and applications by means of: 1) process development, stabilization and characterization; 2) devices and cells development and characterization; and 3) Technology & Design Kit (TDK) development and integration into EDA tools design flow. Figure 2 shows interactions among those different issues. For our research, a lab inkjet printer platform is used as the path from printing technology to devices and final systems on different flexible substrates as PET, PEN, Kapton™ (PI) and paper. The printed ink response will be analyzed to obtain physical design rules in order to develop the passive and active devices required to design and manufacture electronic systems.

Our proposal is based on our previous experience of the silicon integrated circuit (IC) foundry model, and the idea of the process design kit as the nexus between design and technology. The aim of this work is, therefore, transfer this model to the IJPE process. Although our focus is on inkjet printing, many topics of this discussion could be extended to a wide range of printing technologies.

2. Inkjet technology processes development and characterization

A key aspect to address the process characterization is the precise control of geometries and printed patterns. This is the first step for a further characterization of other aspects like materials or device behaviors. A concise description of process characteristics have been done through process characterization to get the quantitative relation between designed patterns and printed dimensions.

Some of these representative effects of inkjet-printed features are reviewed in the Figure 3. The discrete drop nature of inkjet-printed shapes creates waviness line behaviors (scalloped) as shown in Figure 3a and a stacked dot surface morphology as shown in Figure 3b due to consecutive ink spots. Both phenomena signi-

ificantly affect electrical devices requirements. Also, the balance between drop size, drop spacing and substrate interaction can create a bulging effect in lines as shown in Figure 3c modifying the expected interconnection wire morphology.

Stacked coin and uniform type are the more interesting print types for printed electronics. Their suitability depends on the final application. For example, in wiring interconnections, the stacked coin type is preferred, as its predictable behavior is very useful and its possible irregular surface, due to a strong coffee ring effect, is not that critical. In other situations, like transistor (where a smooth edge is required for drain/source electrodes) or gate dielectric (where regular surface is required), a uniform type is better. Printing layer-by-layer is also a key challenge as it directly affects device and system performance through the design rules formulation and device repeatability. The interaction between consecutive deposited layers of different active materials is shown in Figure 3d. Deposited active materials absorption mechanism is strongly substrate dependant. So, when active materials are printed on prior deposited layers, expected line or shape morphologies can be different.

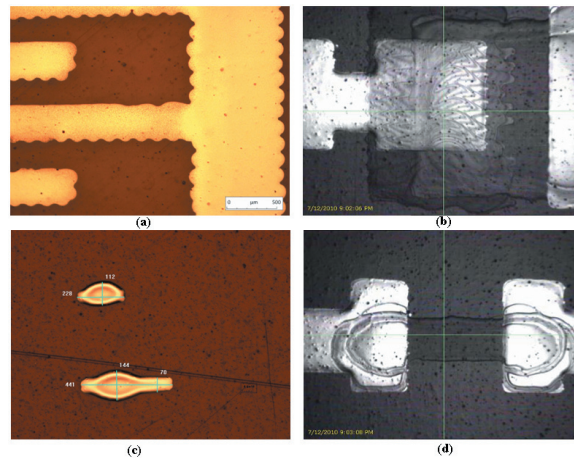


Figure 3 a) to d): Different printing effects

2.1 Devices Development and Characterization

The materials used in this work have been electrically characterized in order to use their characteristics for further devices development (i.e. electrical conductivity in conductive inks or dielectric constant in capacitor or crossover structures). Different test vehicles and analysis methods have been used (some of them adapted from the microelectronic world) for this purpose.

2.1.1 The conductive track case

The ink used for this experiment was Sunchemical's Silver ink U5603 (commercially known as Suntronic Jettable Silver). This ink is a silver nanoparticle solution and 20% of its weight consists of silver particles. Inorganic inks are composed of a combination of nanoparticles, solvents and binders in a given proportion. Solvents evaporate when ink is jetted and contacts substrate. Inorganic particles deposited have a thick layer of binders helping melting during low-temperature curing process. Low curing temperatures don't create an inter-metallic melt, binders act as a conductive adhesive creating a particle melting with a strong union between them (Figure 4 left).

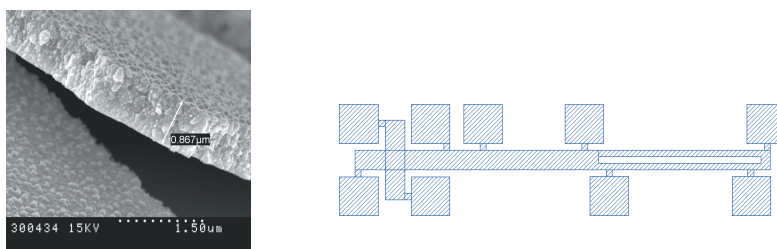


Figure 4: Left: SEM images of Silver nanoparticle; Right: Split-Cross Bridge Resistor test vehicle

A first set of structures to analyze conductivity in simple patterns vs curing temperature and time was printed on a commercial kapton™ substrate (75μm thick) using various numbers of layers and curing parameters.

Results show that curing time is not a key factor after 30 min in oven. A range of temperatures between 150 and 200°C gives good results in conductivity. A lower melting point is a key factor as it increases the number of substrates useful to print. A temperature around 160°C is acceptable for paper and plastic low-cost substrates.

A test vehicle (Figure 4 right) with 5x5 mm pads and 200µm width tracks was printed using first 1 layer and then 2 consecutive deposited layers and 20µm drop spacing. Initially, a Van der Pauw measurement method (Van, 1958) was used to ascertain conductivity in large surfaces. A thickness of 860nm for 1 layer and 1.4µm for 2 layers and a conductivity of $6.8 \cdot 10^6$ S/m \pm 1% were measured. Alternatively, the Greek Cross Bridge Technique (Bue, 1986) was used to calculate R_{\square} and conductivity in tracks. A measured R_{\square} of 138mΩ/sq for 1 layer (630nm thick) and 70mΩ/sq for 2 layers (1060nm thick) was obtained giving us a conductivity of $1.25 \cdot 10^7$ S/m \pm 10%, 5 times less than the bulk silver conductivity.

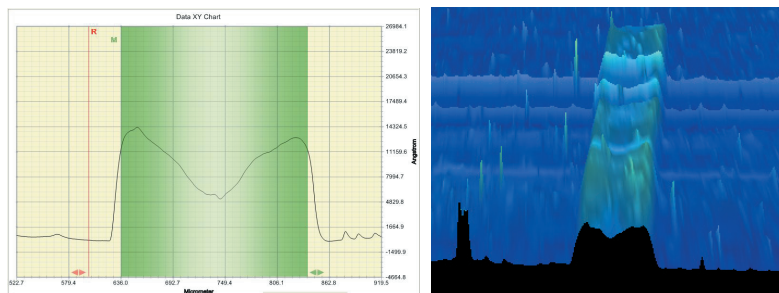


Figure 5: Cross-section and 3D image of a conductive track

We consider that differences between Van der Pauw and Cross Bridge techniques are because of the difficulty in printing homogeneous 200 µm lines and measuring them. Section in 200 µm lines is not uniform. Figure 5 shows a section of a printed track with 2 layers where the non-homogeneous track surface can be observed. Also, the cross-section is not constant throughout the whole printed track, making it difficult to obtain a correct characterization and conductivity parameter. The cross-section should be measured in the whole track to detect the minimum section that matches the electrical conductivity obtained. Wider tracks compensate these differences better, going closer to Van der Pauw obtained measurements.

The usage of this test structures improve the manufacturing task, because it allows the monitoring of the printing process. These structures enable a fast measure of: conductivity, thickness, line width and other properties of printed layers. Experiments with test structures were performed and results show that some of them are usable for this technology after some changes to take into account printing phenomena.

I.e. a 3D view of the Cross-Bridge Resonator reveals that the Greek cross is not uniform (Figure 6). Printed angles and intersections present two main defects that were detected with mechanical profilometer: The coffee ring effect, and the attraction between droplets, which is reflected in movement of ink toward places with previous deposited ink.

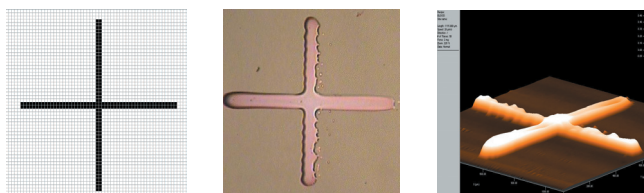


Figure 6: Greek cross shape to be printed; printed structure and 3D profile (printing direction from left to right)

2.1.2 Passive devices

Other passive devices as resistors and capacitors have been printed using PEDOT:PSS (Clevios P Jet HC from HC Starck) as a resistive material and poly(4-vinyl phenol) (PVP) as a dielectric. Figure 7 shows some of these printed devices.

Printed resistors tolerance for some scenarios of manufacturing is reported. The best scenario for printing resistors achieved a square resistance of 473 Ω with tolerance of \pm 20%, which is interesting in comparison with standard diffused resistors (integrated resistors). A similar technology of Integrated Circuit Poly-silicon resistors generally have sheet resistance tolerances ranging from \pm 15% to \pm 20%.

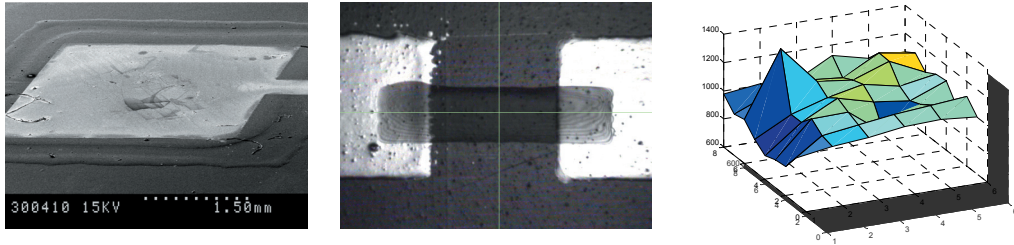


Figure 7: Inkjet printed devices: a) capacitor; b) resistor; c) resistor values chart

Printed capacitors tolerance for different designs and sizes was estimated. The best design for capacitance tolerance (out of 40 design structures fabricated), achieved a capacity per area of $10\mu\text{F}/\text{m}^2$ with tolerance of $\pm 28\%$, which is interesting in comparison with standard integrated capacitors. The corresponding poly-silicon capacitors generally have tolerance ranging from $\pm 30\%$ to $\pm 40\%$.

3. Design flow and tools for inkjet printing

In order to fill the gap between the designer and the fabrication processes, a design flow and a set of backend tools specifically for PE must be defined.

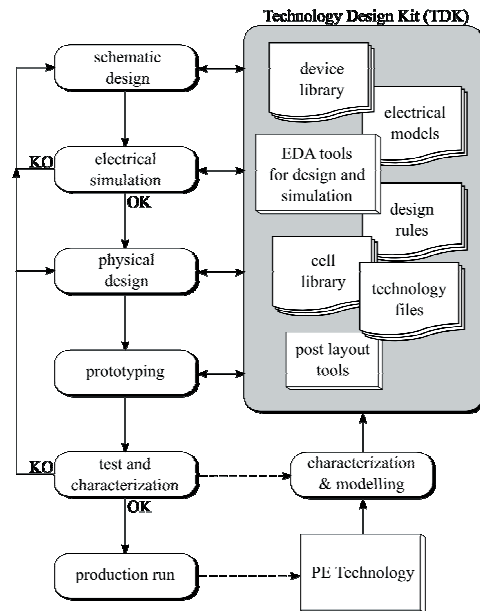


Figure 8:
Proposed design, development and
characterization flow, showing TDK
information needed for each level

3.1 Schematic to layout design flow

Figure 8 shows the proposed design flow, which is basically derived from the silicon technology one. Due to the very high Non-Recurring Engineering (NRE) cost, the integrated circuit designer must spend main efforts in the electronic circuit design - schematics and electrical pre/post-layout simulation loop - in order to ensure with the maximum degree of confidence that the produced design will meet the specifications. On the other hand, thanks mainly to the lower costs and faster fabrication process, the PE designer can relax the efforts on the initial simulation steps and take a straighter route from the design to prototyping, testing several prototypes before production run.

The proposed design flow is oriented to circuit design but it is also useful while characterizing the technology. Characterization output will improve the TDK. On the test and characterization step, information can be extracted to model the technology (device models and design rules) in the TDK, for the process customization on EDA tools that designers will use in the design process.

3.2 Physical design flow

Design methodology depends directly on the technology evolution. Although PE circuit design will have the important heritage of the silicon technology knowledge, the adaptation to the technology limitations, material evolution and printing processes is required.

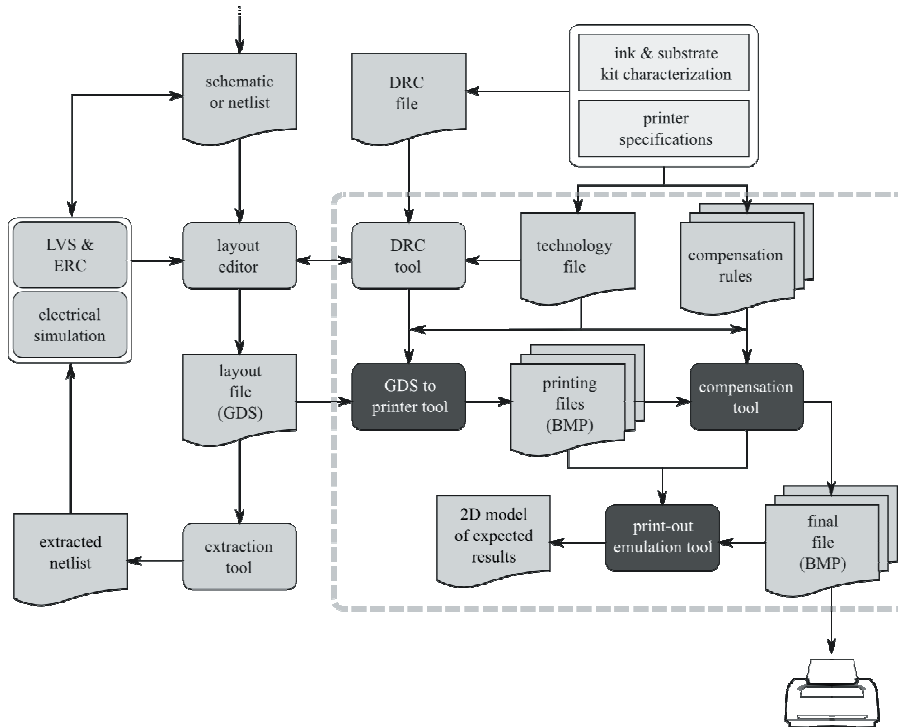


Figure 9: Physical design flow including a set of backend processes enclosed in a dashed line. The proposed EDA tool component fills the functions marked with a dark background color

Along with the definition of a specific design flow for PE, the needed geometrical-layout tools and backend processes have been identified and depicted inside physical design flow on Figure 9. Basically, the layout design phase starts from the schematic or electrical netlist, from where the designer creates the layout GDS file that is extracted and verified using Layout Versus Schematic tools (LVS) and the electrical simulation of the extracted netlist. The Design Rule Checking (DRC) tool aids to properly build those geometries and avoid layout design rules violations. The GDS to printer tool generates a file ready to be interpreted by the inkjet printer by using the vectorial description of the layout and the specific technology parameters of each fabrication process. We have added an additional compensation tool, which processes these BMP files in order to minimize undesired printing effects described in previous sections. Although there are a lot of similarities with the traditional silicon-based microelectronics (Cle, 2000), some specific processes and tools (dark boxes in Figure 9) will need important changes to be useful for IJPE. The proposed EDA tool component described on next section fulfills some of these functions.

3.3 Backend processing

In addition to the definition of a design flow specifically adapted to IJPE, a novel EDA tool component has been created. This tool covers a subset of backend processes as depicted on Figure 9. It takes a layout file describing the design to be printed and a set of technology files and compensation rules extracted from technology characterization and produces one bitmap file for each layer. This bitmap can be directly used by the printer to produce devices and circuits.

In order to be able to automate the whole process, the changes on printer parameters have to be minimized. To achieve this, the printer always works at maximum resolution; meaning the minimum spacing between ejected drops. Once the printer is configured this way, different ink concentration is achieved by filling the shapes with patterns which are more or less dense depending on the layer region.

In addition to enable a more fine-grained control over the total amount of ink that is deposited, printing at maximum resolution and using patterns is useful to compensate the final design and prevent possible device failures (i.e. resolving some effects due to ink-substrate interactions, as explained on section 2).

An example of two different patterns is shown in Figure 10. These patterns are defined (in technology files) as matrixes that produce geometries sketched as grey-scale figures representing the final ink amount and distribution that will be deposited on each case.

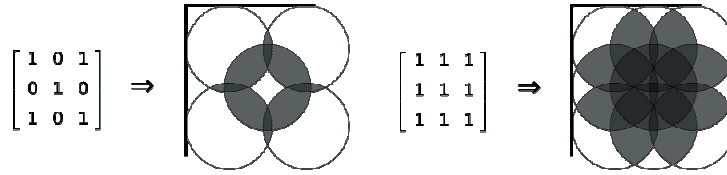


Figure 10: Different pattern examples and the resulting filled shape

As a result, the tool is able to compensate the design according to the geometry and set of layers present on a given region. This compensation will use the rules and parameters obtained by characterization. Regions are obtained by applying Boolean operations between layers (Hal, 2004). At every region, the technology file gives the estimated drop size and the corresponding pattern that will be used. For instance, Thus, if a dielectric layer lies crosses first on top of the substrate and then on a conductor layer, these will be two different regions with different ink jet properties. To assure that final printed dimensions are as accurate as possible (according to the designed layout) the region is shrunk by a factor of the drop radius (Aic, 1995) (Cac, 2010). Shrinking ensures that drops closer to the layer boundary will remain inside the shape.

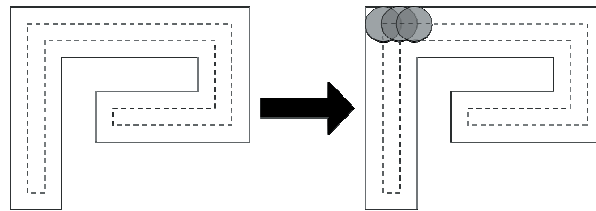


Figure 11: Process from the shape shrinking to drop placement. The solid line shows the original shape, the dashed line shows the shrunk shape. There are some example drops placed showing the final result

Figure 11 illustrates the procedures done by our tool automatically. The original shape, drawn with a solid line is shrunk by a factor of the drop radius resulting on the shape defined by the dashed line (consistent with printer resolution). Droplet eject points will be placed along this dashed line. Drop spacing (taken from technology file according to the region) will optimally fill the generated shape. In depth explanation of the proposed tool algorithms and compensations can be found on (Vil, 2011) and (Vil, 2010).

4. Summary and conclusions

UAB as a university and CNM as a research centre are deeply involved in the development of flexible organic and large area electronics fabricated with printing technologies, with focus in inkjet printing. Both, UAB and CNM, come from the inorganic silicon microelectronics discipline were both have been evolving according the Moore's law since the early 80s. UAB and CNM are being concentrated in the preliminary steps towards building a technology development and design methodology consistent with current printed electronics processes. This nowadays requires some basic technology and design flow developments build around the Technology and Design Kit (TDK) concept to be able to use Electronic Design Automation (EDA) tools. Several scientific publications and one open source tool have already been produced (Diaz, 2010) (Muj, 2010) (Muj, 2011) (Ram, 2010) (Vil, 2011) (Vil2, 2011).

Concerning IJPE Technology, processes and printed devices, our activities are focused to improve devices performance and yield through the control of the behavior of inkjet-printed lines and shapes. The results from such activities are:

- Techniques and test vehicles have been refined to improve electrical characterization of the materials and devices.
- Passive and active devices have been developed using inkjet printing on flexible substrates.
- Repeatability and tolerance characteristics have been analyzed in order to the give rules to the design automation tool that will increase yield and performance.

Concerning design methodologies, flows and tools, our activities follow a bottom-up approach looking for a top-down application design approach once design kits will be ready to customize current EDA tools. Specifically the results from such activities are:

- Identification of different abstraction levels for the design flow (from cell-based design down to handmade drawings) and TDK for IJPE incremental development proposal.
- Technology files definition and its basic customization over specific CAD tools to allow layout editing capabilities.
- Backend post-layout tools to allow basic design rules checkers and move layouts to specific printer formats while applying technology (printer+inks+substrate) specific operations and compensations.

A key point for such current and future achievements relies in our approach of addressing concurrently both technology and EDA tool developments. We believe that this strategy will allow rapid application design when PE technologies reach high transistor count (thousands of them per foil) as expected for the coming years.

Acknowledgements

This work was partly supported by the Spanish Ministry MITYC project TSI-020110-2009-360, the Spanish Ministry MICINN project TEC2008-03835/TEC, the Grant GICSERV 2009 & 2010 from ICTS-CNM (CSIC), the Catalan Government Grant Agency Ref. 2009SGR700 and VALFUS08-2-0001 and the FlexNet (FP7-ICT 2010-2012) “Network of Excellence for building up Knowledge for improved Systems Integration for Flexible Organic and Large-Area Electronics (FOLAE) and its exploitation” under grant agreement n° 247745. We want to acknowledge the Technological Centre CETEMMSA for the samples of the dielectric ink developed by them.

References

- Francesc Vila and Jofre Pallarès and Lluís Terés, (2011), *Layout to Bitmap: A layout design compensator and bitmap converter for Printed Electronics, LOPE-C Proceedings.*
- Buehler, M.G. and Hershey, C.W. (1986), *The split-cross-bridge resistor for measuring the sheet resistance, linewidth, and line spacing of conducting layers, IEEE Transactions on Electron Devices, 1572-1579.*
- Byung Ju Kang and Je Hoon Oh, (2010), *Geometrical characterization of inkjet-printed conductive lines of nanosilver suspensions on a polymer substrate, Thin Solid Films, 518, 2890-2896.*
- Carver A. Mead. Linn. A. Conway, (1980), *Introduction to VLSI Systems. Addison-Wesley Pub.*
- Dan Clein, (2000), *CMOS IC Layout: Concepts, Methodologies and Tools.*
- Dan Halperin, (2004), *Handbook of Discrete and Computational Geometry, chapter 24, 529-562.*
- Dan Soltman and Vivek Subramanian, (2008), *Inkjet-printed line morphologies and temperature control of the coffee ring effect, Langmuir 24, 2224-2231.*
- Daniel Tobjörk and Ronald Österbacka, (2011), *Paper Electronics, Advanced Materials, XX, 1-27.*
- Elkin G. Diaz, (2010), *Characterization of Inkjet Printed Devices and Test Structures MSc Thesis*
- Eloi Ramon. (2010) *Design of Printed Organic HF Rectification Structures in RFID Front-ends. MSc Thesis.*
- Fernando Cacciola, (2010), *2D straight skeleton and polygon offsetting, In CGAL User and Reference Manual. CGAL Editorial Board.*
- Francesc Vila, (2010), *Layout to Bitmap: A Printed Electronics EDA Tool Component, MSc Thesis.*
- Hua Hu and, Ronald G. Larson, (2002), *Evaporation of a Sessile Droplet on a Substrate, J.Phys.Chem. 106, 1334-1344.*
- Jonathan Stringer and Brian Derby, (2009), *Formation and stability of lines produced by inkjet printing, J.Eur.Ceram.Soc. 29, 913-918.*
- Jordi Mujal et al. (2011), *Methodology and Tools for Inkjet Process Abstraction for the Design of Flexible and Organic Electronics, International Journal of High Speed Electronics and Systems (IJHSES) (In press).*
- Jordi Mujal, (2009), *Technology Characterization Oriented to Printed Electronics Design: Touch Panel Case. MSc Thesis.*
- Jordi Mujal, Eloi Ramon, Elkin Diaz, Jordi Carrabina, Alvaro Calleja, Ricardo Martinez and Lluís Terés, (2010), *Inkjet printed antennas for NFC systems, Proc. Of 17th IEEE Int. Conf. on Electronics, Circuits and Systems, 1220-1223.*
- L. Van der Pauw (1958), *A method of measuring the resistivity and Hall coefficient on lamellae of arbitrary shape, Philips Technical Review, vol. 20, no. 8, pp. 220-224, 1958.*

Oswin Aichholzer, Franz Aurenhammer, David Alberts and Bernd Gärtner, (1995), *A novel type of skeleton for polygon*. *Journal of Universal Computer Science*, Vol..1, No. 12, 752-761.

Richard Mannerbro et al., (2008), *Inkjet printed electrochemical organic electronics*, *Synthetic Metals*, No. 158, 556-560.

Vivek Subramanian et al. (2005), *Printed Organic Transistors for Ultra-Low-cost RFID Applications*, *IEEE Transactions on Components and Packaging Technologies*, Vol. 28, No. 4, 742-747.

Yan Wang, Jeffrey Bokor and Arthur Lee, (2004), *Maskless Lithography Using Drop-On-Demand Inkjet Printing Method*, in *VIII Proc. of International Society for Optical Engineering*, Bellingham.

ZhouPing Yin et al., (2010), *Inkjet printing for flexible electronics: Materials, processes and equipments*. *Chinese Science Bulletin*, Vol. 55, No. 30, 3383-3407.

Links

[CEA, 2011] http://ec.europa.eu/information_society/events/cf/bud11/document.cfm?doc_id=17650

[COS, 2010] <http://www.project-cosmic.eu>

[OPD, 2011] <http://opdk.umn.edu/>

[Pho, 2011] <http://www.phoenixbv.com/product.php?prdgrpID=3&submenu=2>

[POL, 2010] <http://www.polaricproject.eu>.

[Vil, 2010] Francesc Vila, (2010), *Layout to Bitmap: A Printed Electronics EDA Tool Component*, *Master's Thesis*, http://www.cnm.es/~fvila2/downloads/msc_thesis.pdf.

[Vil, 2011] Francesc Vila, *Layout2Bitmap open-source tool*, <http://cnminfo.cnm.es/~fvila2/l2b.html>

Electrical and print quality of flat-plate capacitor screen-printed on paper

*Marta Klanjšek Gunde*¹, *Marijan Maček*², *Maša Žvegljč*¹, *Tadeja Muck*³, *Tjaša Vidmar*³,
*Janja Plevnjak*³, *Nina Hauptman*¹, *Raša Urbas*³, *Gorazd Golob*³, *Marica Starešinič*³

¹National Institute of Chemistry

Hajdrihova 19, SI-1000 Ljubljana, Slovenia

E-mails: marta.k.gunde@ki.si, masa.zvegljic@ki.si, nina.hauptman@ki.si

²University of Ljubljana, Faculty of Electrical Engineering

Tržaška 25, SI-1000 Ljubljana, Slovenia

E-mails: marijan.macek@fe.uni-lj.si

³University of Ljubljana, Faculty of Natural Sciences and Engineering

Snežniška 5, SI-1000 Ljubljana, Slovenia

E-mails: tadeja.muck@ntf.uni-lj.si; tyasa.vidmar@gmail.com; janja.plevnjak@gmail.com;

rasa.urbas@ntf.uni-lj.si; gorazd.golob@ntf.uni-lj.si; marica.staresinic@ntf.uni-lj.si

Abstract

Flat-plate capacitors were screen-printed on two paper substrates, the one which is used for conventional printing and another one with nanoporous hydrophilic coating which was developed for printed electronics applications. The thermally drying silver-based electrically conductive ink was applied for conductive plates and the UV-curable dielectric ink for the interlayer. The capacitors were printed in three sizes with single- and double-printed dielectric layer. The conditions for good print- and electrical quality were determined other than those recommended by the producer. The print quality of the top electrode and of the entire final product depends on the UV curing energy applied for dielectric layer. The effect is more pronounced when the capacitors were printed on conventional paper and less on the more smooth paper dedicated for printed electronics. The serial capacity of printed capacitors with double-printed dielectric layers appears to be independent on UV curing dose. However, the print quality of corresponding structures retains almost all dependence observed in structures with single-printed dielectric.

Keywords: printed electronics, conductive ink, dielectric ink, ultraviolet curing, capacitor

1. Introduction

Printing of electronic systems on common flexible substrates such as paper, plastic, and textile using standard printing processes is expected to provide low-cost electronic systems suitable for integration on smart packaging (1). Simplified structures are required for this purpose which could be printed by the lowest possible number of printing inks. The whole production must be feasible at low enough price, which was estimated to be below 0.2 € per piece (2).

Printing of a flat-plate capacitor requires electrically conductive and dielectric functional inks which must be printable one over another so that the multilayered structure with good stacking geometry, well defined interlayer and suitable electrical properties could be obtained. However, achieving optimal electric properties may require preparation conditions that could be unusual for a paper substrate.

The methods which are usually applied in graphic industry to test the quality of prints are not necessarily applicable for printed electronics where the visual assessment may not coincide with electrical functionality. Therefore, some other methods should apply.

The ability of paper-based materials to serve as substrate for printed electronics structures is of considerable importance to reach feasible application in smart packaging (1). The special properties of paper-based substrates originate in non-homogeneous paper structure and different surface properties which influences the functionality of the overprinted layer. This layer represents the base material for the next layer and so forth. Printing of homogeneously thick continuous layers and overprinting them one over another is not necessary in conventional graphic applications where appropriate dots of basic colours are applied and mixing occurs in visual system.

The purpose of our research was to analyze three-layered structure of capacitors printed on paper substrate using two commercially available screen printing inks. Silver-based conductive ink was used for bottom and top electrode and dielectric ink for the dielectric interlayer. Drying and curing conditions were varied for each layer. The quality of prints and their electrical properties were analyzed in dependence on printing conditions. The stability of paper substrate to these conditions was also tested. Two paper-based substrates were applied, Pe:smart type 2, which is dedicated for printed electronics, and Biomatt, which is suitable for conventional printing.

2. Materials and methods

Two commercially available inks were applied. The Electrodag PM-470 (Acheson, Netherlands) is silver-based electrically conductive screen printable ink, specifically designed for printing RFID antennae onto paper and polyester film. The producer recommends drying for minimum 15 minutes at 120°C (3). The second ink was screen printable, UV-curable dielectric ink, designed for insulating and protective coating in the production of low voltage circuitry on polyester and polycarbonate film. It has 100% solid content with urethane-acrylate binder and magnesium silicate pigments. The ink has translucent green colour, dielectric constant 5.09 and dielectric strength 2400 V (AC). It is recommended to be cured at UV energy level of 500 - 700 mJ/cm² (4).

Two different paper substrates were used, Pe:smart paper type 2, which is dedicated for printed electronics, and Biomatt, which is suitable for conventional printing. Pe:smart paper type 2 is produced by Felix Schoeller Service GmbH & Co.KG, Germany. The raw paper is both-side coated where the front surface has additional hydrophilic nanoporous coating. It is highly white paper, 205 µm thick, 200 g/m². The Biomatt is white paper, 140 µm thick, 150 g/m², produced by Paprinica Vevče, Slovenia).

The three print forms (Figure 1) contain all necessary shapes for three flat-plate capacitors: bottom and top electrode, dielectric interlayer between them and all electrical contacts for LCR measurements. Three capacitors were printed, C1 (20x20 mm²), C2 (10x10 mm²) and C3 (5x5 mm²). Two SEFAR® high-modulus monofilament polyester plain weave meshes were applied; 62/64Y (open area 30.1 %, theoretical ink volume 30.4 cm³/m²) for conductive layers and 120/34Y (open area 29.6 %, theoretical ink volume 16.3 cm³/m²) for dielectric layers. The squeegee with hardness 75 °Sh was applied for printing. Special attention was paid to appropriate settlements of the three layers. The capacitors were with single- and double printed dielectric layers. Each layer was dried before overprinting.

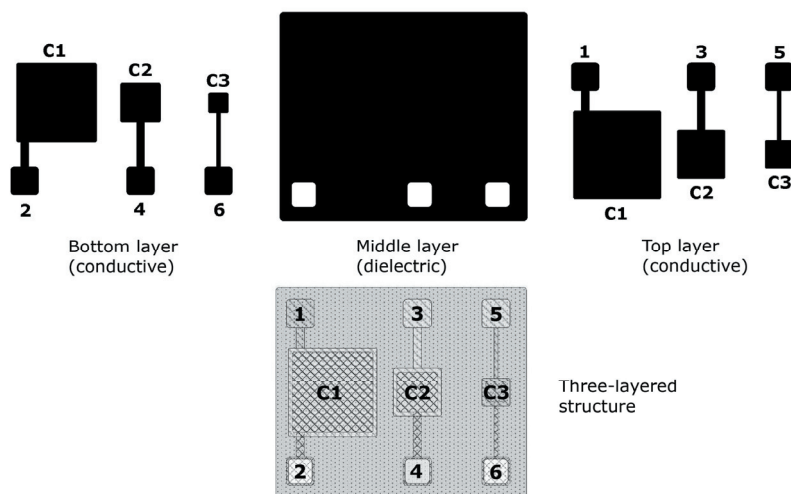


Figure 1: The three print forms applied for printing three flat-plate capacitors C1, C2 and C3

The conductivity of conductive layers depends on several printing parameters (5). Following our previous research, the highest conductivity of printed shapes is obtained if prints are first air-dried for 5 minutes and then passed IR drying channel ten times at 200 °C; therefore the curing process takes together approximately 7.5 minutes at 200 °C. UV curing energy applied to cure dielectric layer was varied from 450 to 4200 mJ/cm².

It was accomplished by several successive crossings of UV Dryer Aktiprint L 10-1 (Technigraf Germany) equipped with air-cooled medium pressure mercury lamp with power density 120 W/cm. The UV dose was controlled by UV integrator (Technigraf Germany).

The topology of surfaces was evaluated by profilometer Hand-held Roughness Tester TR200 (ISO 4287) and roughness by Bendtsen air permeability tester (ISO 8791-2:1990). The Cobb water absorbency (ISO 535:1991) was applied to express the amount of water pick-up per unit surface area of applied papers. The surfaces of samples were analysed by Field-Emission Scanning electron Microscope (Karl Zeiss Supra 35 VP), equipped with Energy-dispersive X-ray elemental characterisation unit (SEM-EDS). The surface coatings were analysed additionally by the infrared attenuated total reflectance (IR-ATR) measurements. For this purpose the FT-IR spectrophotometer Bruker IFS 66/S equipped with Golden Gate Mk II ATR accessory with diamond top-plate and KRS-5 lenses was applied.

The stability of paper substrates were analysed by the help of colour difference (calculated in CIELAB colour space) caused by exposure of papers to the required drying and curing conditions. For this purpose the II (Gretag Macbeth) measurements were applied.

Electrical properties of printed capacitors were measured by Agilent 4284A precision LCR meter at 1 MHz. Capacity and serial resistance (model Cs-Rs) were measured on square shaped capacitors C1, C2 and C3 (see Figure 1). From the known surface areas and perimeters of used structures the defect density was also estimated in terms of UV curing energy and paper substrate.

3. Results and discussion

The SEM micrographs of Pe:smart and Biomatt papers are shown in Figure 2. The results of elemental analysis are depicted in Figure 3 and IR-ATR spectra in Figure 4. The SEM micrographs show completely different size and shapes of pigments applied in surface coatings of both papers. Combined information of SEM-EDS and IR-ATR methods show that the particles on Pe:smart, most likely, are nano-sized γ - Al_2O_3 or γ - AlOOH nanorods (6,7,8). These could be regarded as nano-sized analogues to the alumina trihydrate ($\text{Al}(\text{OH})_3$), a platy-shaped bright pigment which is frequently applied in coatings for papers (9). The Ca, appearing in elemental analysis, could be the CaCO_3 pigment constituting the basic coating under the thin hydrophilic nanoporous coating. This was confirmed by the analysis of the rear side, where the GCC (ground calcium carbonate: calcite, CaCO_3 with small amount of MgCO_3) was confirmed. We suppose that the basic coating is the same on both sides. The Biomatt surface coating consists of mixture of GCC and kaolin clay ($\text{Al}_2\text{O}_3 \cdot 2\text{SiO}_2 \cdot 2\text{H}_2\text{O}$).

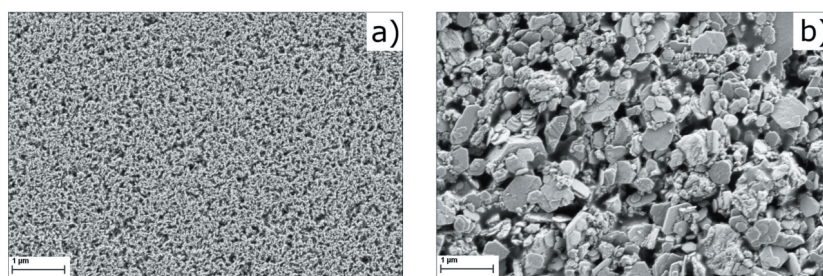


Figure 2: SEM micrographs of the applied paper substrates: Pe:smart (a) and Biomatt (b).

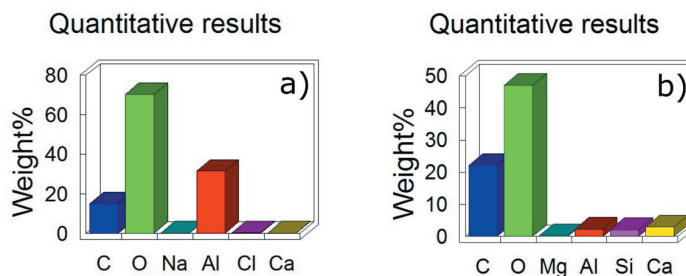


Figure 3: Results of SEM-EDS analysis for Pe:smart (a) and Biomatt (b) surfaces

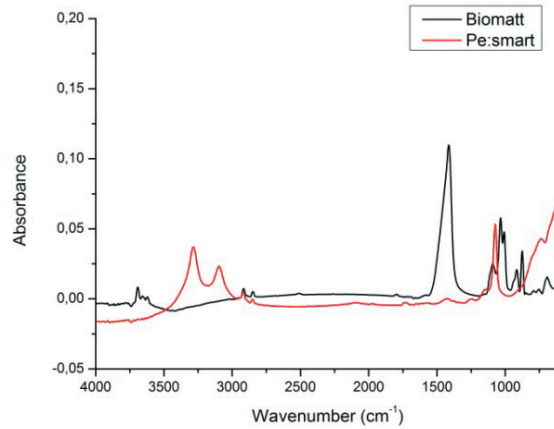


Figure 4: IR-ATR spectra of Pe:smart and Biomatt paper surfaces

The pigment particles on Biomatt surface are up to 1 μm large and the surface is not smooth (not calendered). Opposite, the particles in the coating on Pe:smart paper are extremely tinny and uniform, therefore produce very smooth and homogeneous surface. These are the basic reasons for the very different surface roughness (mean height of surface irregularities, R_a , profilometer result), water absorptiveness (Cobb), and surface smoothness (air leak - Bendtsen method). These results are collected in Table 1. The R_a of the Pe:smart surface is over 4-times lower than of the Biomatt. The Bendtsen method shows smaller difference in smoothness. The Pe:smart paper has twice as large water absorptiveness than the Biomatt paper.

Table 1: Surface properties of the applied papers: mean height of surface roughness (R_a), surface smoothness (Bendtsen) and water absorptiveness (Cobb_{60})

Paper	R_a (μm)	Bendtsen (mL/min)	Cobb_{60} (g/m^2)
Pe:smart	0.63	10	14.9
Biomatt	2.60	5	7.3

The colour difference caused on paper surface by crossing the IR drying channel in dependence on its temperature is shown on Figure 5. This analysis confirms that both applied papers are stable up to 200 $^{\circ}\text{C}$. At higher temperatures a rapid increase of colour difference was obtained, giving evidence of thermal decay.

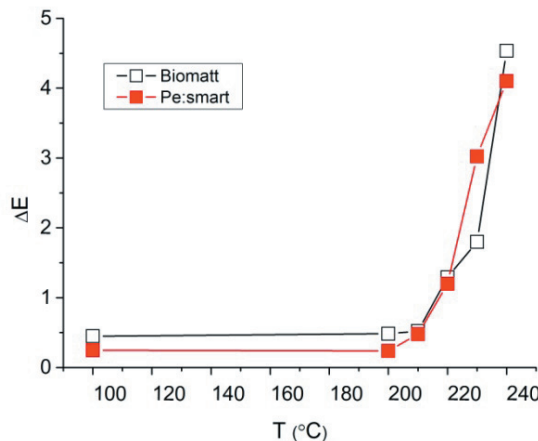


Figure 5: CIELAB colour change on Pe:smart and Biomatt papers as a function of temperature

The dielectric layer, printed over the conductive layer, seems to be cured sufficiently already at UV energy of 450 mJ/cm^2 : it becomes dry, has an acceptable adhesion and appropriate surface touch. However, the print quality of the conductive layer which was printed over such dielectric layer (in our case for the top electrode)

depends strongly on the curing energy applied for the dielectric layer. The wet top conductive layer looked well; however, several surface wrinkles appeared after thermal drying. They are most heavily pronounced at the lowest curing energy and disappeared when it was above 1500 mJ/cm^2 (Figure 6). The effect is somewhat smaller on Pe:smart paper, but it is still clearly observable by naked eye. It appears that dielectric layer with smaller curing energy prevents the top layer to be dried efficiently. The details of this phenomenon are not known yet.

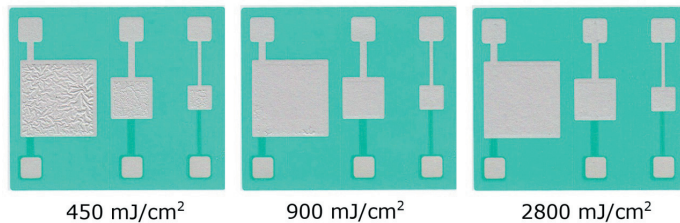


Figure 6: Scanned prints of the three printed capacitors obtained when UV curing energy of 450, 900 and 2800 mJ/cm^2 was applied to dielectric layer. See wrinkles on the surface of top conductive layer. The Biomatt paper was applied here

The serial capacity C_s of the three capacitors as a function of UV curing energy applied for the dielectric layer is shown in Figure 7. If the dielectric layer is single-printed, the C_s increases with curing energy and becomes constant above 1500 mJ/cm^2 . This phenomenon corresponds well with acceptable appearance of corresponding prints (see Figure 6). It could be understood by dependence of dielectric constant ϵ on curing energy that may occur below 1500 mJ/cm^2 . Such effect would show that ϵ reaches its proper value somewhat below this UV dose. Further research is needed to understand the intrinsic material phenomenon. However, in capacitors with double-printed dielectric layer the phenomenon did not appear (Figure 7).

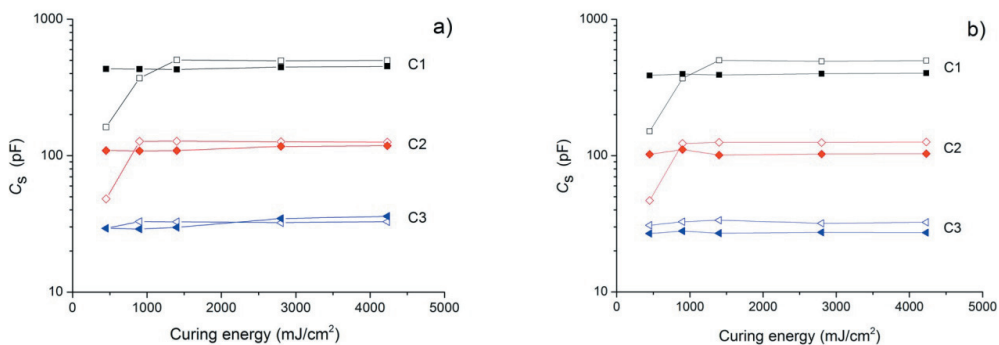


Figure 7: Serial capacity of the three capacitors, C1, C2 and C3 as a function of UV curing energy applied for single-printed (open signs) and double-printed dielectric layer (full signs). The capacitors were printed on Pe:smart (a) and Biomatt paper substrates (b)

The electrical defects, i.e. shorts between bottom and top capacitor electrodes were very frequently created in capacitors with single-printed dielectric layer. They are generated mostly (about 95%) in the bulk of the capacitor and rarely (5%) on the edges. Defect density is 0.13 def/cm^2 for structures printed on the Pe:smart paper to and 0.35 def/cm^2 on the Biomatt paper. In capacitors with double-printed dielectric layer almost no defects were observed. It is very likely that this could be explained by some non-continuous points in dielectric layer which appear on arbitrary places of each individual dielectric layer. By overprinting the additional dielectric layer, such points appear on different places and are therefore covered; this prevents the electrical shorts between bottom and top electrodes. Deeper understanding of all these phenomena requires more extensive research.

4. Conclusions

Good print quality and acceptable electrical properties of screen-printed flat-plate capacitors requires high temperature drying for silver-based conductive ink and heavy UV curing conditions for dielectric ink. Temperature stable and minimum electrical resistivity was obtained if each conductive layer was dried at $200 \text{ }^\circ\text{C}$, the highest temperature the substrate can withstand. This temperature is much higher than $120 \text{ }^\circ\text{C}$ which is recommended by the producer.

The capacitance of flat-plate capacitor with single-printed dielectric layer increases with UV curing doses and becomes stable when it approaches 1500 mJ/cm². This effect correspond well with acceptable print quality of three-layered print: the top layer without surface wrinkles was formed only when the underling layer was cured to almost 1500 mJ/cm². This is almost threefold of the recommended UV dose. The observed dependence of electrical properties on curing conditions could be connected with intrinsic material changes. All capacitors with single-printed dielectric layer have rather high density of electrical defects. These effects are somewhat less pronounced when the flat-plate capacitors were printed on the smooth hydrophilic nanoporous Pe:smart paper than they are on the rough Biomatt paper.

The capacitance becomes practically independent on UV curing energy if the dielectric layer was double-printed. The second dielectric layer prevents formation of electrical defects; most likely, possible electrical shorts are covered by ink which isolates bottom and top electrodes at these defect places and forms better capacitor. However, the print quality still retains some imperfections, which is revealed by surface wrinkles of the top layer; the effect is smaller than in capacitors with single-printed dielectric layer.

The smooth hydrophilic nanoporous paper, dedicated to printed electronics appears somewhat better than the rough paper used for conventional printing. However, the differences are not as large as one could expect. The possible reason could be the size of functional particles in conductive ink applied in our study. They are much larger than pores in both papers, so all conductive particles remain within layer after drying in both applied papers.

The observed unusual phenomena in printed capacitors, which depend on intrinsic material properties of dielectric layer, have to be analysed in further details.

Acknowledgements

The authors acknowledge the financial support from the state budget by the Slovenian Research Agency (project No. J2-9455). Maša Žvegljč acknowledges the Slovenian Research Agency for young researchers support.

References

- (1) J. Kerry and P. Butler, (2008), *Smart packaging technologies for fast moving consumer goods*. Chichester : John Wiley & Sons, cop.
- (2) M. Berggren, D. Nilsson, N.D. Robinson, (2007), *Organic materials for printed Electronics*. *Nature Materials* 6, 3-5.
- (3) Electrodag® PM-470 Silver based PTF ink, Product data sheet, Acheson Industries (Europe) Ltd., GB 03/05-ED PM-470.
- (4) Electrodag® 452SS Ultraviolet Curable Dielectric Coating, Product data sheet, Acheson Colloides Company, Port Huron, MI, 08-364-RV901.
- (5) M. Žvegljč, V. Demšar, R. Urbas, N. Hauptman, M. Maček, M. Klanjšek Gunde, (2009), *Electrical resistivity of screen printed conductive lines*. *Advances in printing and media technology*. Vol. 36. Darmstadt: Media and Graphic Arts Industries, 421-427.
- (6) H.S. Potdar, Ki-Won Jun, Jong Wook Bae, Seung-Mood Kim, Yun-Jo Lee, (2007), *Synthesis of nano-sized porous γ -alumina powder via a precipitation/digestion route*. *Applied catalysis A: general* 321, 109-116.
- (7) K. M. Parida, A. C. Pradhan, J. Das, N. Sahu, (2009), *Synthesis and Characterization of nano-sized porous gamma-alumina by control precipitation method*. *Materials Chemistry and Physics* 113, 244-248.
- (8) Hongwei Hou, Yi Xie, Quing Yang, Qixun Guo, Chedroug Tan, (2005), *Preparation and characzerization of γ -AlOOH nanotubes and nanorods*. *Nanotechnology* 16, 741-745.
- (9) Pigment Coating & Surface Sizing of Paper, Papermaking Science & Technology Series, Volume 11, Edited by Esa Lehtinen, Finnish Paper Engineers' Association & TAPPI, (2005), ISBN: 952-5216-11-X.

Characterisation of catalyst layers for fuel cell printed by flexography

Chloé Bois¹, Anne Blayo¹, Rémi Vincent², Christine Nayoze², Didier Chaussy¹

¹ Grenoble Institute of Technology

461 Rue de la papeterie, BP 65, F-38402 St Martin d'Hères Cedex France

E-mail : chloe.bois@lgp2.grenoble-inp.fr

² CEA, LITEN

Laboratoire des composants piles à combustible, électrolyse et modélisation (LCPEM)

17 rue des Martyrs, F-38054 Grenoble Cedex 9, France

E-mails: remi.vincent@cea.fr; christine.nayoze@cea.fr

Abstract

Optical techniques of printing characterisations are tested to be implemented as a characterisation of functional layers, referred to as catalyst layers, where electrochemical reactions take place in Proton Exchange Membrane Fuel Cells. While optical density techniques poorly discriminated the types of ink used and the ink loading transferred by superimposition of 1 to 5 layers, reflectance spectra measurements succeed in differentiating (i) inks formulated with carbon adsorbed platinum or carbon powder without platinum and (ii) ink loadings higher than 0.062 mg.cm⁻². In addition, printing defects of marbling and lacks of ink can also be evaluated by reflectance measurements. Owing to its validation as a characterisation technique, it is successfully used to evaluate the ability of platinum-free ink layers to cover three ink layers with platinum. Confirmed by SEM observation, the reflectance does not highlight mixing phenomena between layers during their manufacturing by superimposition. However, it confirms the presence of printing defects on ink layers with a low ink loading.

Keywords: proton exchange membrane fuel cell, flexography, catalyst layer, spectrophotometric characterisation

1. Introduction

1.1 The objective of the research

Fuel cells were discovered in the nineteenth century and have been the core of numerous research programs ever since. At the end of the twentieth century, the interest for Proton Exchange Membrane Fuel Cells (PEMFC) grew, especially for portative and transport applications. These fuel cells are composed of a stack of Membrane Electrode Assemblies (MEA's). MEA's are multilayered materials where two electrodes are separated by an electrolytic membrane. The electrodes are composed of a Gas Diffusion Layer (GDL) and a catalyst layer. The catalyst layer contains functional elements (platinum catalyst, proton and electron conductors). MEA's are fed with reactive gases (oxygen and hydrogen) and electrochemical reactions take place in the catalyst layers following the equations [1] in anode and [2] in cathode



The products of these reactions are water and heat as described in equation [3].

The catalyst layers of the fuel cell are commonly manufactured by coating or spraying techniques (1-3). One major concern of fuel cell manufacturing is the cost of platinum catalysts. It tends to limit fuel cell use growth. In this context, printing processes can be considered as alternative techniques of catalyst layer production (4). Non continuous techniques such as screen printing and ink jet have already been investigated (5-7).

This study deals with the potential of flexography on catalyst layer manufacturing. The interest of flexography has been demonstrated in photovoltaic applications where layer with functional components are printed (8). This deposition technique consists in a doctor blade depositing the ink on a special cylinder

called an Anilox. The Anilox is micro-engraved, and the cells that cover its surface are filled by the ink. The blade removes the ink excess at the surface of the Anilox, thus, at each turn, the same amount of ink is contained by the Anilox. This volume of ink is the major characteristic of the Anilox. It is described in volume of ink that can be contained by one square meter of developed Anilox surface ($\text{cm}^3 \cdot \text{m}^{-2}$). The Anilox transfers the ink on a printing form. In flexography, this form, called a cliché, is polymeric and the information that has to be printed is in relief. The ink deposited by the Anilox on the relief patterns of the cliché is then transferred onto the substrate in the nip zone formed by the printing cylinder and the cylinder on which the cliché is glued. Similarly to other printing processes, the flexography process has been turning aside from its original application and now allows transferring functional inks. In fuel cell manufacturing by printing processes, the catalyst layer is manufactured by flexography, transferring a functional ink (the catalyst ink) that contains platinum onto a GDL, considered as a printing substrate.

The catalyst layer characterisation is commonly performed by either single cell performance tests or half cell tests. These characterisations require the use of specific equipments and take several hours (4).

It is therefore crucial to characterise the print quality of the catalyst layers at each step of the flexography manufacturing, before the electrochemical tests. As the print quality is commonly quantified by optical measurements, the relevance of two techniques is investigated: optical density and reflectance spectrum measurements.

2. Materials and methods

2.1 Materials

2.1.1 Inks

Two water-based inks for catalyst layers were formulated to fulfil process and fuel cell requirements. Water, already used in running MEA, was chosen as the vehicle of the catalyst ink solvent. It limits potential pollutants use that could damage electrochemical properties of the membrane electrode assembly. Furthermore, it is compatible with the flexography process and reduces volatile organic component use. Some functional elements may enter into the inks formulation.

- Nafion® PFSA ionomers dispersion (DuPont TM, Wilmington, USA) that allows the protons conductivity
- and
- Vulcan XC-72R carbon nanoparticles (Cabot Corporation, Alpharetta, USA) that confer the electrical conductivity to the electrode
- or
- Carbon-supported catalyst (46 % w/w platinum on Vulcan XC-72R; Tanaka) that allow the electrical conductivity as well as catalyse the electrochemical reactions [1] and [2].

The I_{33} ink contains by carbon-supported catalysts, and there is 33 % w/w of platinum in the ink dry content. The I_0 ink contains platinum-free carbon nanoparticles. Both inks have the same carbon content in volume.

2.1.2 Substrates

Gas Diffusion Layers are non-woven substrates made of carbon fibres network and polytetrafluoroethylene (PTFE), a highly hydrophobic polymer. The carbon network assures the electron conductivity, and the PTFE handles the water management, and a specific porous structure leads to water, and reactive gas diffusion. The GDL used in this study is a SGL 24 BC (SGL Group, Wiesbaden, Germany). It has been characterised as a classic printing substrate. The GDL has a thickness of $247.6 \pm 2.6 \mu\text{m}$, a specific weight of $101.7 \pm 2.0 \text{ g} \cdot \text{m}^{-2}$, and a weight per volume of $410.7 \pm 12.5 \text{ kg} \cdot \text{m}^{-3}$. It is composed of two layers:

- A carbon fibres network with polytetrafluoroethylene polymer named the macroporous layer, in contact gas feeders,
- A microporous layer composed of carbon nanoparticles and a polytetrafluoroethylene polymer.

The presence of polytetrafluoroethylene confers the microporous layer surface a highly hydrophobic character that is known to limit its affinity with water-based inks.

2.2 Research methods

2.2.1 Deposition methods

Printing is performed with a Flexiproof, a sheet-fed laboratory proofing device for flexography (Testing Machines Inc. TMI, New Castle, USA). This device recreates the ink transfer of a flexography system.

The ink transfer is controlled by adjusting the pressure between the form cylinder and the Anilox, and the pressure between the form cylinder and the printing cylinder. The cliché pattern is a solid. Catalyst inks are deposited at a constant speed of 25 m.mn^{-1} by Anilox cylinders of 4 and $13 \text{ cm}^3.\text{m}^{-2}$. On each sample, a variable number of layers of inks I_0 and I_{33} are transferred (from 1 to 5 layers).

2.2.2 Characterisation methods

Catalyst layer samples printed with the Flexiproof are firstly characterised by their ink loading (mg.cm^{-2}). It represents the weight of dry ink transferred onto the substrate per unit of surface. It is given by the difference of the masses of the substrate before and after the ink transfer and the ink drying. This parameter is commonly used in fuel cell fields to describe the amount of functional particles (platinum for example) in a catalyst layer (9).

Observations with Environmental Scanning Electron Microscopy (ESEM) on a Quanta 200 FEI device (Everhart-Thornley Detector) (FEI, Hillsboro, USA) lead to characterise the morphology of the catalyst layer deposited (5). Pictures are acquired using BackScattered Electrons detection (BSE). It consists of high energy electron beams that are reflected out of the sample detection volume. The particularity is that the heavy elements backscatter the incident electrons more strongly than the light elements. Therefore, elements with a high atomic number (Z) appear brighter on the image. The platinum element has an atomic number equal to 78 when the other elements existing in the inks, catalyst and gas diffusion layers have a lower atomic number, namely: carbon ($Z=6$), oxygen ($Z=8$), fluorine ($Z=9$) and sulphur ($Z=16$). Hence it allows a contrast of the platinum elements (6) that enters in the composition of the I33 ink. For given settings, the brighter a picture is, the more platinum elements can be detected by the device.

Further characterisation techniques of the printing quality are then performed using optical tests whose relevance is investigated in this paper. The optical density was measured using a GretagMac Beth, DC 19C densitometer (X-rite, Grand Rapids, USA). The principle of an optical density measurement is explained hereafter. When an incident light with an intensity equal to I_0 illuminates the surface of a material, the light can be either reflected in the specular direction or adsorbed, transmitted or reflected back (retrodiffused) after multiple scattering phenomena (multiple reflection and/or refraction phenomena due to the interaction of light with the material). The retrodiffused part (intensity I_R) is used to define the optical density OD , given as follows as a function of the light wavelength λ :

$$OD(\lambda) = -\log\left(\frac{I_R(\lambda)}{I_0(\lambda)}\right) \quad [4]$$

The lower the retrodiffused part of the incident light intensity, the higher the optical density and the darker the surface appears. In this study, as deposited inks contain carbon powder particles that are opaque, an increased optical density will indicate an increased thickness of the deposited ink layer.

The measure of reflectance spectra of the printed samples were performed with an i1 Pro (X-Rite, Grand Rapids, USA). Reflectance spectrum quantifies the ratio between I_R and I_0 for a range of wavelength between 350 and 730 nm.

For each transfer number, five samples are printed. The results presented in this paper are the average of five measures performed on each of the five samples with constant printing parameters.

3. Results and discussion

3.1 Multilayer protocole

Catalyst layer manufacturing by flexography aims to transfer a precise quantity of functional ink on a specific substrate. The ink quantity is a significant parameter since the catalyst layers are defined by their quantity of platinum by unit of surface (mg.cm^{-2}) referred as a loading. The ink quantity deposited by two Anilox cylin-

ders that differs by their volumes was characterised by increasing the number of superimposed ink layers (Figure 1). Catalyst layers are indeed made by superimposing several ink layers without any drying between each ink transfer.

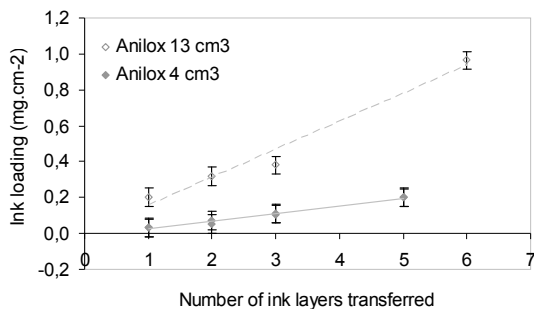


Figure 1: Ink loading as a function of the number of ink transferred onto SGL by two Anilox cylinders

For each Anilox cylinder, ink loadings increase following the number of ink layers transferred. The amount of ink deposited at each transfer is equal to 0.035 ± 0.05 and 0.16 ± 0.03 mg.cm⁻² for Anilox cylinders of 4 and 13 cm³ respectively. At each transfer, the use of the 13 cm³ Anilox leads to the deposition of more than four times more ink loading onto the substrate.

The electrochemical properties of catalyst layers made by such a multilayer protocol have already been investigated (10). However, the control of the ink loading requires the mass of the substrate to be precisely measured before and after its printing. This is difficult to implement in the case of a continuous roll-to-roll process.

3.2 Relevance of characterisation of catalyst layers by optical measurements

Optical measurements are currently used in printing field to adjust process parameters. Their potential for characterisation of functional deposits obtained by printing has to be highlighted.

3.2.1 Relevance of characterisation of catalyst layers by optical density measurements

Optical density is tested as a characterisation measure on samples of catalyst layers manufactured by flexography. The investigation is focused on

- the influence of the platinum amount in the ink on the optical density
- the influence of the number of ink layers superimposed

The results are described in Figure 2.

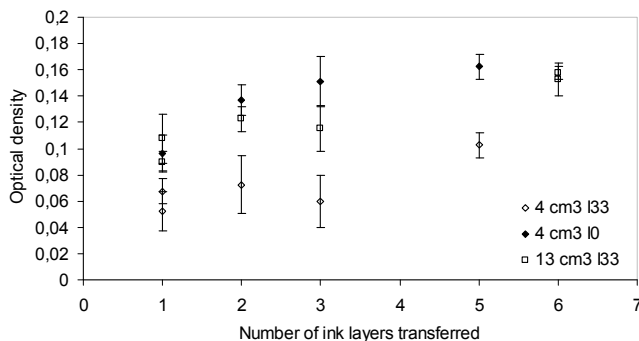


Figure 2: Optical densities in black of catalyst layers samples made by multilayer protocol

Considering the samples manufactured with the Anilox cylinder that has a volume equal to 4 cm³, and for each number of superimposed layers, the optical density allows the discrimination the I₀ and I₃₃ inks (respectively 0.05 ± 0.01 and 0.10 ± 0.01 at one layer transferred).

As expected, the optical densities values of the samples made using the 13 cm³ Anilox are higher than the one obtained with the 4 cm³ Anilox.

However, it appears that the optical densities of samples made with the I_{33} ink show poor variations as a function of the number of ink layers superimposed. For example, catalyst layers made with the 4 cm^3 Anilox by the superimposition of 1, 2, 3 and 5 layers have optical densities respectively equal to 0.05 ± 0.01 , 0.07 ± 0.02 , 0.06 ± 0.02 and 0.10 ± 0.01 . Similarly, catalyst layers made using the 13 cm^3 Anilox have optical densities that are equal to 0.10 ± 0.01 , 0.12 ± 0.01 and 0.11 ± 0.02 for superimposition of 1, 2 and 3 layers.

The optical density allows to discriminate :

- both types of ink tested: with or without platinum, at the same ink loading
- large variations of ink loadings, such as the difference of loadings induced by the use of 13 or 4 cm^3

Anilox cylinders, with the same ink.

Nevertheless, sample with unknown parameters, such as the presence of platinum in the ink, the Anilox volume use, or the number of ink layers cannot be determined with this technique.

3.2.2 Relevance of characterisation of catalyst layers by reflectance spectrum measurement

The characterisation of catalyst layers by reflectance spectra measurements is performed on

- samples that have the same ink loading, but different platinum amounts
- samples with the same platinum amount in the ink, but different loadings

Reflectance spectra of samples manufactured by deposition of three ink layers with an Anilox cylinder of 4 cm^3 are presented in Figure 3.

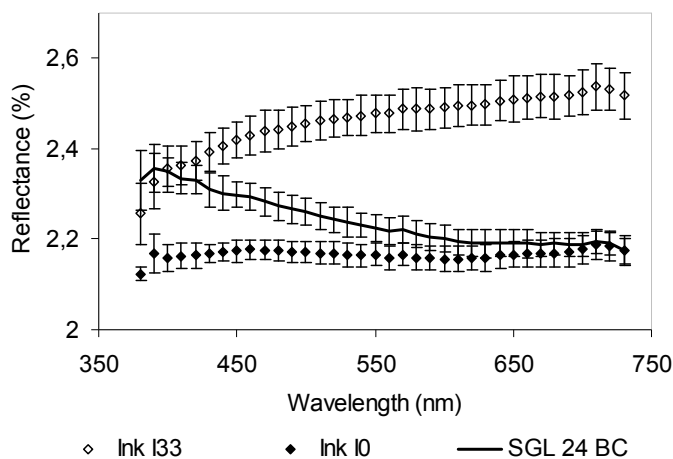


Figure 3: Reflectance spectra of one layer of the platinum-free ink I_0 and the one that contains platinum I_{33} printed onto the substrate and the reflectance spectrum of the substrate SGL 24 BC

The reflectance spectrum of the superimposed layers made with platinum-free ink I_0 has lower reflectance values than the three superimposed layers made with platinum I_{33} ink as a function of the wavelength ranging from 350 to 730 nm. That means that the carbon nanoparticles appear darker than the one with adsorbed platinum, confirming the optical density values of these samples discussed in the previous part.

Moreover, the curve shapes differ depending on the platinum presence. It also may be used to indicate the type of ink transferred onto the SGL substrate. This is additional information that could be collected from reflectance spectrum measurements.

The influence of the ink loading of samples manufactured with the I_{33} ink on the reflectance spectra is detailed in Figure 4.

For wavelengths ranging from 420 to 730 nm, the reflectance values decrease with the increasing of the ink loading deposited onto the SGL 24 BC. The values of reflectance for wavelengths equal to 450, 550, 650 and 730 nm are plotted as a function of the ink loading in Figure 5.

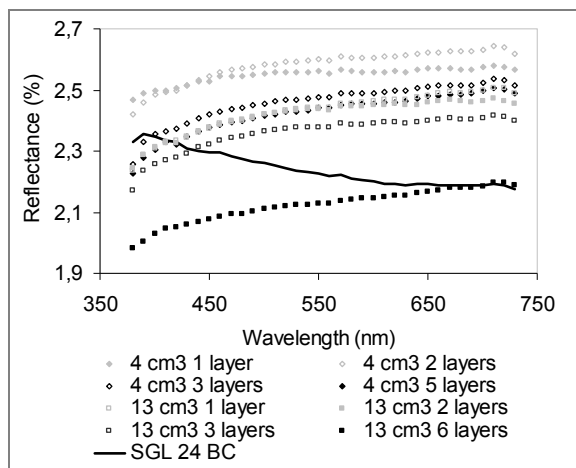


Figure 4: Reflectance spectra of samples made with I33 ink

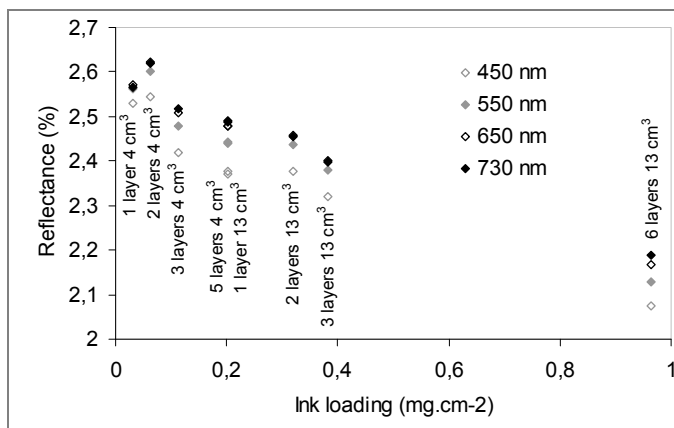


Figure 5: Reflectance value as a function of the samples ink loadings

For each wavelength, the general trend of the curves of reflectance as a function of the ink loading confirms the previous conclusion. However, it appears that the two first samples with loadings equal to 0.032 and 0.062 mg.cm^{-2} do not follow the decreasing trend as a function of the ink loading. The reflectance of samples with low ink loadings might be the limitation of the reflectance characterisation. This limitation of discrimination between samples with different ink loading is twice lower those observe for optical density measurement. Indeed, optical density cannot differentiate the three first samples with loading equal to 0.032 , 0.062 and 0.112 mg.cm^{-2} .

Two samples have similar ink loadings, the first is made by the superimposition of 5 layers with a 4 cm^3 Anilox ($0,201 \text{ mg.cm}^{-2}$) and the second is made by the deposition of 1 layer with a 13 cm^3 Anilox ($0,203 \text{ mg.cm}^{-2}$). Their reflectance values at 450 nm are equal to 2.42 ± 0.04 and 2.37 ± 0.03 respectively. Hence, it confirms the correlation between ink loading and reflectance value, whatever the protocol of ink deposition.

Looking back at Figure 4, at wavelengths lower than 420 nm , the order of the reflectance values does not decrease with the increasing of the sample ink loadings. The samples made by the deposition of one layer with the 4 and 13 cm^3 Anilox cylinders have lower reflectance value than their counterpart made by the superimposition of two layers. A previous study (10) has described printing defects appearing when the first layer of ink is transferred onto the SGL 24 BC. Figure 6 represents a picture of the deposition of one layer of I₃₃ ink with Anilox cylinders of 4 and 13 cm^3 volumes.



Figure 6:
Surface views of (1) ink-free substrate (SGL 24 BC), (2) substrate with one layer of ink and (3) two layers of ink

Patterning occurs with a marbling appearance. This defect is a typical well known printing problem, indicating a lack of affinity between the ink and the surface and was expected during the deposition of a water based ink onto a substrate with such a high hydrophobic behaviour. Thus, the ink film splitting in the nip is not favourable to ink transfer and the ink is only partially transferred. This leads to an inhomogeneous ink layer. The lack of ink of a sample made by the deposition of one only layer with a 4 cm^3 Anilox is estimated at $60 \pm 10\%$ of the sample surface, while a one layer sample made with a 13 cm^3 Anilox has a surface fraction of substrate non-covered by any ink is estimated at $30 \pm 5\%$.

Consequently, the reflectance spectra presented in Figure 4 of samples made by one layer are impacted by the substrate surface. However, when a second layer is superimposed, the fraction of substrate directly visible clearly decreases. Manufacturing catalyst layers by superimposing several ink layers leads to print quality amelioration.

The reflectance spectrum measure may be used to highlight the presence of printing defects that impact the uniformity of catalyst layers which then in turn may degrade the electrochemical properties of the catalyst layer in running fuel cell.

3.3 Use of reflectance spectra to characterise the superimposition of layers with different platinum amounts

Reflectance spectra measurement allows discriminating with accuracy the two inks studied in this paper. Consequently, this technique is used to understand the impacts of the multilayer protocol on the structure of the catalyst layer manufactured by flexography. Tests are performed to observe where the components of one ink layer are located after superimposition of several ink layers.

Three layers of I_{33} ink are transferred onto SGL 24 BC samples. Then, without any drying, layers of I_0 ink are superimposed as described in Figure 7.

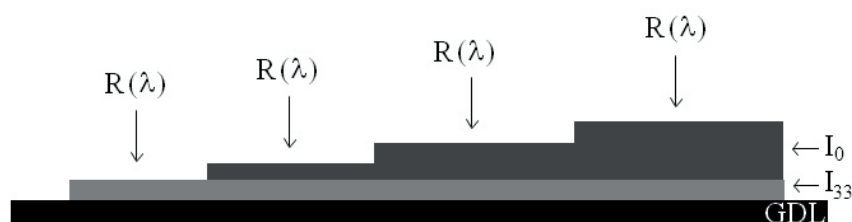


Figure 7: Superimposition of I_0 and I_{33} ink

SEM observations and reflectance measures aim to follow the location evolution of the carbon adsorbed platinum particles in the entire catalyst layer. First, surface views of the Figure 8 are taken in the exact same settings from samples:

- (1) Printed by three layers of I_{33} ink, this sample is a surface view brightness reference of layers containing platinum,
- (2-4) Printed by three layers of I_{33} ink covered by n layer(s) of ink I_0 , with n equal to 1, 2 and 3,
- (5) Printed by three layers of ink I_0 , this sample is a surface view brightness reference of layers without platinum.

Figure 8 presents one surface view of the observation panel of the samples described above. The reflectance values at 450 nm of the stacks are presented in Figure 9.

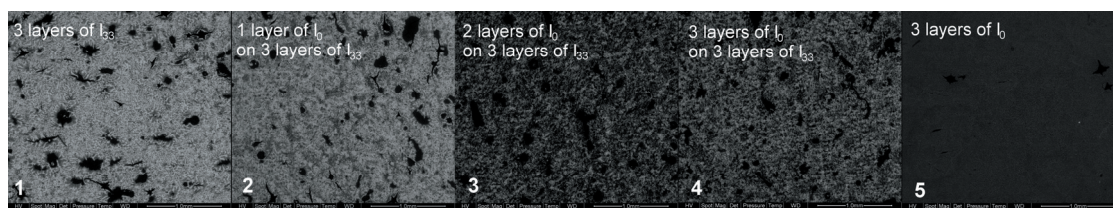


Figure 8: Surface views of printed samples: (1) three layers of ink with platinum I_{33} , on which are transferred (2) one (3) two and (4) three layers of ink I_0 , and (5) three layers of ink I_0 directly deposited on the substrate

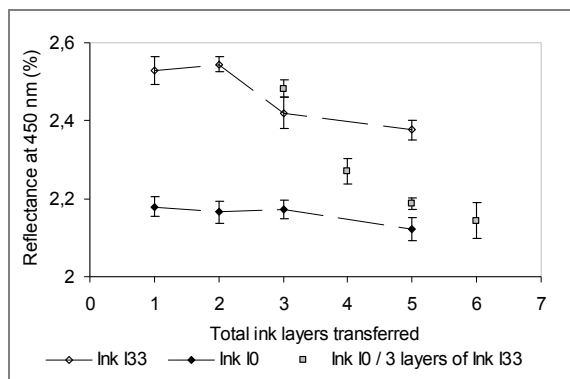


Figure 9: Reflectance of catalyst layer samples at 450 nm deposited on GDL as a function of the number of total ink layers transferred onto the substrate

The reflectance values at 450 nm and the surface views of the samples present the same trends : the more layers of I_0 ink are superimposed onto the three layers of I_{33} ink,

- the more the brightness of the ESEM pictures diminishes,
- and the more the reflectance values at 450 nm move from the reflectance values of layers only made by the I_{33} ink toward the reflectance of those only made by layers of I_0 ink.

However, the ink covering is not completely performed. Consequently, a sample (4) fracture cross view is presented in Figure 10.

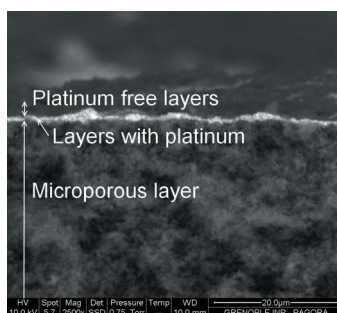


Figure 10: Cross view of a three layered platinum ink sample covered by three layers platinum-free ink

The layers of I_0 ink clearly covered the under layers, made with the I_{33} ink. No mixing between the layers with different compositions is highlighted.

4. Conclusion

The demonstration of the relevance of the flexography process for manufacture catalyst layers of fuel cells had been previously achieved [10]. The transfer of inks for catalyst layers is possible with a multilayer protocol that allows controlling the platinum loading deposited onto a GDL. A characterisation technique has been successfully tested on catalyst layers. Reflectance measurement is able to discriminate (i) catalyst layers with same ink loading and different platinum amounts, as well as (ii) catalyst layers made with several ink layers.

Reflectance is used to assess the superimposition quality of ink layers that contain platinum or not. Further studies will look into the possibility of reflectance spectrum measurements to discriminate platinum quantity, not only by the superimposition of ink layers with the same amount of platinum, but also by changing the platinum amount in the ink. In addition, spectroscopy characterisation is planned to be tested in order to evaluate the catalyst layer electrochemical properties, as a complement or even a replacement of electrochemical tests.

The validation of the reflectance measurement technique leads to confirm that the flexography allows the superimposition of layers with different platinum contents without ink layers mixing.

The use of a 4 cm³ Anilox cylinder creates a number of printing defects, marbling or lacks of ink on the substrate. Future studies will detail the influence on the Anilox volume on the printing defects and layers mixing of catalyst layers made by superimposition.

References

- (1) S. Martin, P.L. Garcia-Ybarra, J.L. Castillo, *Electrospray deposition of catalyst layers with ultra-low Pt loadings for PEM fuel cells cathodes*, *Journal of Power Sources* 195 (2010) 2443-2449
- (2) R. Sitanggang et al., *Fabrication of gas diffusion layer based on x-y robotic spraying technique for proton exchange membrane fuel cell application*, *Energy Conversion and Management* 50 (2009) 1419-1425
- (3) M. Chaparro et al., *Properties of Catalyst Layers for PEMFC Electrodes Prepared by Electrospray Deposition*, *Journal of The Electrochemical Society*, 157 (2010) 7 B993 B999
- (4) B. Wang, *Recent development of non-platinum catalysts for oxygen reduction reaction screen printing*, *Journal of Power Sources* 152 (2005) 1-15
- (5) B. Andrade et al., *Fabrication of High Precision PEMFC Membrane Electrode Assemblies by Sieve Printing Method*, *Journal of Fuel Cell Science and Technology* 6 (2009)
- (6) R. Hansch, M. R. R. Chowdhury, N. H. Menzler, *Screen printing of sol-gel-derived electrolytes for solid oxide fuel cell (SOFC) application*, *Ceramics International* 35 (2009) 803-811
- (7) S. Towne et al., *Fabrication of polymer electrolyte membrane fuel cell MEAs utilizing inkjet print technology*, *Journal of Power Sources* 171 (2007) 575-584
- (8) T. Mäkela et al., *Continuous roll to roll nanoimprinting of inherently conducting polyaniline*, *Microelectronic Engineering* 84 (2007) 877-879
- (9) G. Sasikumar, J.W. Ihm, H. Ryu, *Dependence of optimum Nafion content in catalyst layer on platinum loading*, *Journal of Power Sources* 132 (2004) 11-17
- (10) C. Bois et al., *Fundamentals and Developments of Fuel Cells*, 2011 January, Grenoble: World Trade Center, 2011, 41-42 p.



Gravure printing of thick film electrodes for PEM fuel cell production

Frank Siegel¹, Albert Kohl², Eugen Enns², Wolfgang Deger², Holger Dziallas²,
Andreas Willert³, Reinhard R. Baumann³

¹ Chemnitz University of Technology
Institute for Print and Media Technology
Digital Printing and Imaging
Reichenhainer Str. 70, D-09126 Chemnitz, Germany
E-mail: frank.siegel@mb.tu-chemnitz.de

² SolviCore GmbH & Co. KG,
Rodenbacher Chaussee 4, D-63457 Hanau-Wolfgang, Germany

³ Fraunhofer Institute for Electronic Nano Systems ENAS,
Department Printed Functionalities, D-09126 Chemnitz, Germany

Abstract

A major environmental friendly alternative to traditional fossil fuels based power sources are Proton-Exchange-Membrane Fuel Cells (PEMFCs) converting hydrogen and oxygen into water by yielding an electric current. The electrochemically active component of these fuel cells, the membrane electrode assembly (MEA), has been manufactured following mainly batch process workflows or slow film creation technologies. This paper presents recent results on combining the benefits of gravure printing and gravure coating to achieve thick material layers for the fabrication of catalytic electrodes for the MEAs of Proton-Exchange-Membrane Fuel Cells (PEMFCs).

Keywords: gravure printing, layer thickness, fuel cell, PEMFC, functional printing, membrane electrode assembly (MEA)

1. Introduction

A major environmental friendly alternative to traditional fossil fuels based power sources are Proton-Exchange-Membrane Fuel Cells (PEMFCs) converting hydrogen and oxygen into water by yielding an electric current. The electrochemically active component of these fuel cells, the membrane electrode assembly (MEA), has been manufactured following mainly batch process workflows or slow film creation technologies.

Various methods for MEA manufacturing have been published over time: rolling powder (Bey, 1998), dispersion spraying (Ral, 1997), screen printing (Zaf, 2004) of thick films on decal substrates or directly on the Proton Exchange Membrane, and sputtering (Lit, 2004). Recently inkjet printing routes have been described to deposit the catalyst layer on different substrates (Edw, 2006; Tay, 2007; Tow, 2007; Mer, 2010). However, the productivity of flat-bed printing and inkjet techniques is low compared to industrial printing technologies like gravure printing. To grow the availability of fuel cells for a broad variety of applications the industrial production of MEAs has to be established.

The employment of continuous production techniques based on web-fed machinery should definitely contribute to a strong reduction of the manufacturing costs of MEAs (Tsu, 2004) and therefore support the widespread utilization of these promising, alternative energy sources.

Gravure printing is a highly productive and efficient web based production technique commonly used for printing of high quality magazines and packaging on different substrates with run lengths beyond 300.000 prints. Nevertheless gravure printing has an enormous potential to satisfy the demands of functional printing and this technology is already widely used in coating applications by modifications of the gravure process itself.

This paper presents recent results on combining the benefits of gravure printing and gravure coating to achieve thick material layers for the fabrication of catalytic electrodes for the MEAs of Proton-Exchange-Membrane Fuel Cells (PEMFCs).

2. Research strategy

The basis of the research is a highly efficient and productive roll-to-roll gravure printing process on flexible substrates. To identify tasks of the work, certain production requirements have been defined. The electrodes should have a defined thickness of 5 to 10 μm and it should be possible to print on substrates with low surface energies in case of detaching the electrode (so called Decal method).

The key aspects of the production process parameters are:

- high throughput (i.e. m^2/h)
- scalability (i.e. different geometrical areas)
- no individualization but layout flexibility (i.e. electrode designs)
- high reliability (i.e. functional layers)
- high robustness (i.e. a reliable process parameter regime)

The quality requirements for the printed layers are in particular:

- electrode quality (i.e. number of defects, geometric size of defects, roughness of layer surface, edge sharpness of printed areas)

Solving these tasks requires a research strategy, which is set out in Figure 1. Most of the experiments were done with Model-Inks printed on PET film to evaluate the variation of line screens and the influence of the ink rheology.

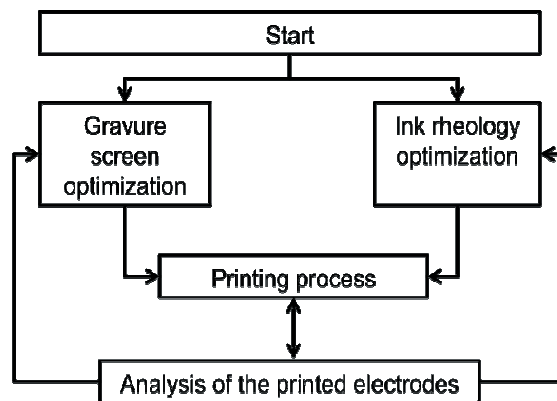


Figure 1: Scheme of the research strategy and relations

The work is focused on ink rheology optimization and gravure screen development towards a maximized dipping volume. The results were also described in a patent (Sie, 2010).

3. Ink rheology

The rheology of the ink has a significant effect on the printing process itself and its process window. Further it determines the results regarding the layer quality, defects, thickness and layer waviness. The main parameters for determining the ink properties are the flow curve and the yield point of the inks. If the yield point is too high the printed layer will show a big waviness and a large amount of defects caused by bad leveling characteristics. These ink characteristics are strongly dependent on the amount of binder (Pha, 2009), the solid content and the type of pigment, which is dispersed. In this investigation several different model-ink formulations were used for most of the experiments to get closer to an ideal rheology. Two different model-inks and their influence onto the printed layer quality will be discussed.

To characterize both model-inks the Linear-Viscoelastic range (LVE range) and the flow curves were measured. The LVE range gives an account of the ideal viscous (loss modulus G'') and ideal elastic parts (storage modulus G') of dispersions. Figure 2 shows the diagrams of the LVE range and the flow curves.

Model-ink I has both a high storage and loss modulus of nearly the same value but the storage modulus prevail. For this reason a yield point of around 20.000 Pa could be identified. So Model-Ink I will have a

slower leveling characteristics as the adjusted model-ink II. This model-ink has no yield point in the Linear-Viscoelastic range due to a higher loss modulus than the storage modulus and the elastic part is breaking down under shear stress.

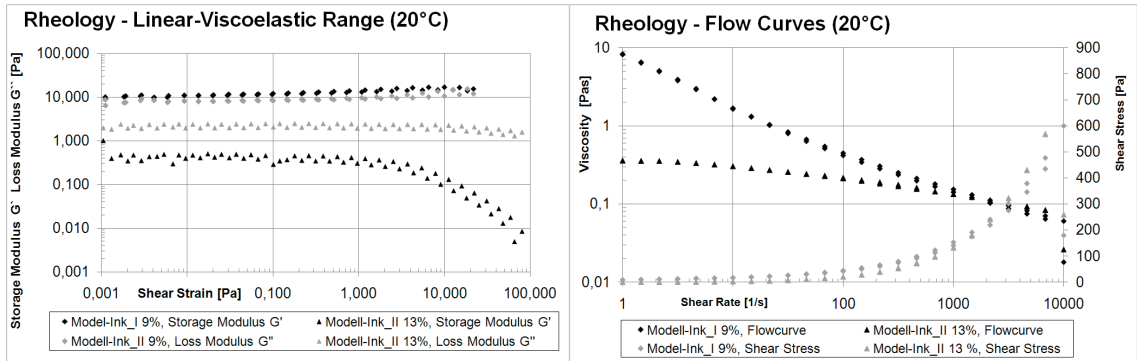


Figure 2: Rheological characteristics of the applied Model-Inks, Linear-Viscoelastic range and flow curves

Furthermore, the flow curve of model-ink I is typical shear-thinning. It has an initial viscosity of around 10.000 mPas (@ 1 1/s and 20 C) and under shear-stress 140 mPas (@ 1.000 1/s and 20 C). Model-ink II has less shear-thinning characteristics with a viscosity of around 130 mPas (@ 1.000 1/s and 20°C). Under stress both model-inks are almost comparable but after shearing the leveling quality for model-ink I will be insufficient caused by the distinct elastic part (storage modulus). The rheology of inks is influencing the whole printing process, from inking the cylinder to the printing step and the grade of leveling on the substrate afterwards.

4. Screening - maximizing the dipping volume of the printing cylinder

Conventional graphic arts screens for the gravure printing process are designed and built for the reproduction of defined dots for grey level simulation, color impression. It is indeed possible and popular to use conventional electro-mechanically engraved screens for functional printing. Table 1 shows an overview of the employed electro-mechanically engraved screens and their typical dimensions and dipping volumes. But for manufacturing thick electrodes with the presented purpose graphic arts screens with dipping volumes of up to 16 ml/m² at 48 L/cm are not sufficient.

Table 1: Graphic arts screens electro-mechanically engraved and their dimensions

Screen Ruling	48 L/cm	70 L/cm	90 L/cm
Dipping Volume	~16 ml/m ²	~9 ml/m ²	~6 ml/m ²
Layer thickness model-ink II	0,8 µm	0,6 µm	0,4 µm

For basic experiments the screens shown in Table 1 shown screens were used to print the lower-viscous model-ink II achieving layer thicknesses of less than 1 µm. To enable a one impression printing process the amount of ink dipped by the printing cylinder has to be much higher to obtain an adequate film thickness. After drying, the film thickness shall be approximately 5 to 10 µm.

The approach of this work is to use a gravure cylinder employing a hybrid line screen with etched structure depths between 150 μm and 180 μm , a very low resolution down to 7 L/cm and a variation of the screen at the edges to achieve straight and sharp edges of the printed areas. In general two different types of line screens are achieved: Closed line screens, with continuous walls containing the etched grooves and open line screens with interrupted walls. Figure 3 shows the classification in closed and open screens as well as selected strategies for edge adjustments and a micrograph of an open line screen with a screen ruling of 7 L/cm.

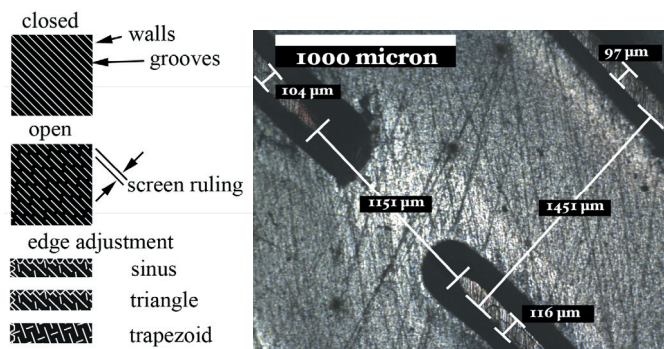


Figure 3: Improved line screens for printing electrodes, strategies for edge adjustment and micrograph of an open line screen

The employed line screens have much larger dimensions with a wall width of around 106 μm , a groove width of more than 1400 μm (7 L/cm), wall interruptions of around 1100 μm and etch depths of around 160 μm are much larger than the dimensions of electro-mechanically engraved screens (compare table 1). The number of walls per area is minimized to maximize the dipping volume, but having enough support for blading the cylinder during the inking process resulting in dipping volumes of 115 ml/m².

5. Analysis of the printed electrodes

Gravure printing is a highly efficient production technique; therefore there is a need of fast inline (or at least in-situ) measurement methods to observe the printed layer quality with regard to layer thickness and layer defects. During the investigations of this work a semi-automated characterization strategy was developed to analyze the printed electrodes with respect to counting the amount of defects and their size. First, the printed electrodes were digitized by means of the conventional web inspection system Drello V7000 with a resolution of 18 μm per pixel at the highest zoom position and backlight, capturing the missing material sections. Second, the digitized sections were analyzed by a program, counting defects and measuring the geometric defect area. For first tests the free software Image J was used. But research objective is an automated inline approach with adequate fast commercial software.

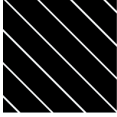
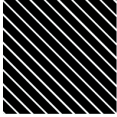
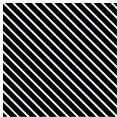
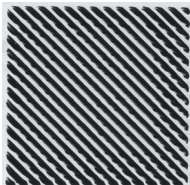
Further layer characterization like layer thickness of the printed electrodes was done with a tactile mechanical profilometry. Optical methods are only partially successful due to the high optical densities of the carbon-based inks. The results and their interpretation are discussed in detail in the following section.

6. Results and conclusions

Both Model-Inks were printed with four different line screens (closed and open, different screen rulings) at a speed of 0.6 m/min on PET film. Table 2 gives an overview of the applied screens and the printing results. The size of an electrode is 20x20 mm². There is a significant difference of the resulted layer quality between Model-Ink I (high viscous, high yield point) and Model-Ink II (medium viscous, no yield point). First some comments about Model-Ink I. It was shown, that the ink has insufficient leveling characteristics, the grooves were printed but there is no flooding of the walls. The edge sharpness is low caused by shifting the ink during the doctoring process and the low resolution of the screen. Applying the open line screen seems to be an approach to overcome partly the leveling problems.

However, Model-Ink II is showing a very good layer quality instead. It should be noted; the screen ruling influences the waviness of the edges of the electrodes, like the known saw-tooth effect. Approaches to overcome these effects are shown in Figure 3.

Table 2: Printing results and the applied line screens (printed electrodes with a size of 20x20 mm²)

Type of screen	Screen dimensions	Model-Ink I	Model-Ink II
	closed 3 L/cm ~140 ml/m ²		
	closed 7 L/cm ~115 ml/m ²		
	closed 10 L/cm ~95 ml/m ²		
	open 7 L/cm ~125 ml/m ²		

Quantitatively, after digitizing the samples, defects were counted and surveyed by image analysis and a histogram was created. For an easy readable visualization Figure 4 applying a bubble-histogram was developed. The larger the extent of a bubble the larger the amount of defects classified to the size of the defect in mm². Additionally, the total defect area in percentage is noted and the used screen parameters.

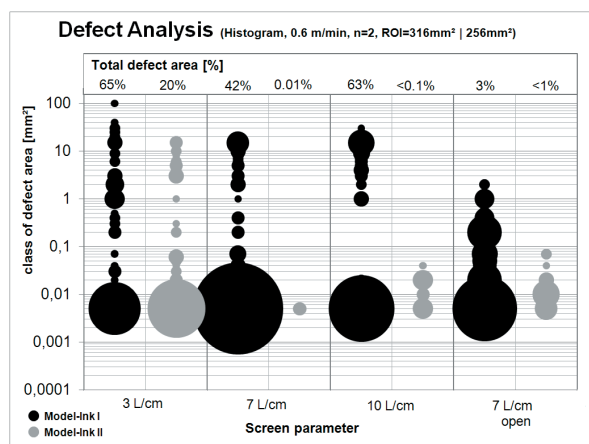


Figure 4: Defect Analysis: Bubble-histogram and mean total defect area in percentage, printing speed 0.6 m/min, ROI=316 mm² and 256 mm

Figure 4 shows that the defect minimum is at 7 L/cm both closed and open line screen for Model-Ink I and II. In particular, the effect of utilizing an open line screen is significant for Model-Ink I caused by a better allocation of the ink. However, the optimized Model-Ink II has a very good performance from 7 L/cm up to 10 L/cm, closed and opened line screens at a low process speed of 0.6 m/min. For the screen at 3 L/cm large effects with sizes between 0.1 and 10 mm² should be noted. On this account such low screen rulings are not expedient for further experiments.

Finally, the layer thickness was measured for the best results, Model-Ink II and open as well as closed 7 L/cm line screens. The goal of achieving layer thicknesses of around 10 μm was not reached but at least albeit was possible to manufacture electrodes with a mean thickness of 5 μm by means of a one impression gravure printing technique. This is more than five times applying a 48 L/cm graphic arts screen with the same Model-Ink II.

The printing results fulfill the demands for using the industrial gravure printing technology for the manufacturing of electrodes for fuel cell applications with layer thicknesses of around 5 μm . A novel approach of hybrid line screens with dipping volumes up to 125 ml/m² is used for printing the electrodes within one impression. The main result presented in this paper is the definition of the line screen parameters to achieve less dead volume caused by walls and maximized dipping volume by etching depths up to 160 μm . The results for higher printing speeds to evaluate the productivity of the whole process are published in (Sie. 2010) with following findings: open line screens are more sufficient with regard to layer quality at higher printing speeds. But in general the main challenge is to fill the grooves right on time at printing speeds from 18 to 60 m/min. Thereby, the layer quality and thickness is decreasing during increasing speed.

In conclusion, the researched screens are also a general benefit for other applications where there is a need of structured thick material layers on flexible substrates, mainly for active materials like functional layers for electrochemical devices or sensors. Gravure printing is able to complement rotary screen printing in the lower film thickness range utilizing a lower viscosity range like it is common for rotary screen printing. But applying novel gravure screens with maximized dipping volumes causes an adoption of the whole printing process, combining ideas of gravure coating and printing.

References

- (Bey, 1998) D. Bevers, et. al. (1998), *Innovative production procedure for low cost electrodes and electrode / membrane structures*, *Int. J. Hydrogen Energy*, Vol. 23, No. 1, 57-63, 1998
- (Ral, 1997) T. R. Ralph, et. al. (1997), *Low Cost Electrodes for Proton Exchange Membrane Fuel Cells*, *Journal of Electrochemical Society*, Vol. 144, No. 11, 3845-3857
- (Zaf, 2004) R. Zaffou, et. al. (2004), *A Study Of Screen-Printing Processing Conditions in Making Membrane Electrode Assemblies for PEM Fuel Cells*, *Proceedings of The 205th Meeting of The Electrochemical Society*, 310
- (Lit, 2004) S. Litster, et. al. (2004), *PEM fuel cell electrodes*, *Journal of Power Sources*, No. 130, 61-76
- (Edw, 2006) Edwards, et. al. (2006), *Roll-to-roll Manufacturing of Electronic and Optical Materials*, Patent Publication, Cabot Corporation, WO 2007106699
- (Tay, 2007) A. Taylor, et.al. (2007), *Inkjet printing of carbon supported platinum 3-D catalyst layers for use in fuel cells*, *Journal of Power Sources*, No. 171, 101-106
- (Tow, 2007) S. Towne, et.al. (2007), *Fabrication of polymer electrolyte membrane fuel cell MEAs utilizing inkjet print technology*, *Journal of Power Sources*, No. 171, 575-584
- (Mer, 2010) A.-G. Mercier, et. al. (2010), *Inkjet printing of catalyst layers used in fuel cells membrane electrode assemblies*, *Proceedings of Advances in Printing and Media Technologies, 37th International Research Conference*
- (Tsu, 2004) H. Tsuchiya, et. al. (2004), *Mass production cost of PEM fuel cell by learning curve*, *International Journal of Hydrogen Energy*, Vol. 29, 985-990
- (Sie, 2010) F. Siegel, et. al. (2010), *Method for producing catalyst layers for fuel cells*, Patent Publication, SolviCore GmbH & Co. KG, WO 2010136204
- (Pha, 2009) J. W. Phair, et. al. (2009), *Leveling and thixotropic characteristics of concentrated zirconia inks for screen-printing*, *Rheol Acta*, No. 48, 121-133
- (Sie, 2011) F. Siegel, et. al. (2011), *Thick Film Gravure Printing Process for the Production of Catalyst Layers*, *Proceedings of Large-area and Organic Printed Electronics Convention, LOPE-C 2011*

UHF RFID antenna printing on offset paper substrate using inkjet and screen-printing technologies

Markus J. Müller, Susana Otero, Vicente de Gracia

AIDO, Technological Institute of Optics, Colour and Imaging, Valencia, Spain

E-mail: mjohannes@aido.es

Abstract

The demand from the world leaders in retail business has made RFID (Radio Frequency Identification) increasingly popular for product tracking applications. As noted in Wall Street Journal, RFID “will be in every product imaginable”, and will replace barcodes and magnetic strips.

This situation has been driving both product manufacturers and packaging suppliers to be ready for RFID implementation. While RFID technology was being developed to satisfy its rapidly growing market, the application cost turned to be a serious problem. The responsibility for RFID tagging application would, sooner or later, be shifted to packaging suppliers because of its complication and additional cost. Packaging manufacturers should be aware. Once being asked by customers for RFID, an efficient way was to provide it with an affordable cost at a minimal price. At the moment, many technologies have been studied to overcome the cost barriers. One among them was “printed RFID” technology.

Conductive ink would allow packaging printers to print RFID-antenna directly on the packaging substrates and attaching microchips in-line. RFID integration into packaging would significantly reduce the cost of RFID implementation in mass production because it would eliminate the needs for labels and the manual “slapping” (attaching) process.

The goal of this research is basically to study the performance of inkjet- and screen-printed RFID-antennas on fibre based packaging substrate and to work out processing parameters to improve the performance of the antennas just by set up different printing or process parameters.

Keywords: printed electronics, RFID antenna, inkjet printing, screen printing, nano silver ink, sintering process

1. Introduction

The demand from the world leaders in retail business has made RFID (Radio Frequency Identification) increasingly popular for product tracking applications. As noted in Wall Street Journal, RFID “will be in every product imaginable”, and will replace barcodes and magnetic strips (Delaney, K. J., Wall Street Journal, 2001).

This situation has been driving both product manufacturers and packaging suppliers to be ready for RFID implementation. While RFID technology was being developed to satisfy its rapidly growing market, the application cost turned has become to be a serious problem. The responsibility for RFID tagging application would, sooner or later, be shifted to packaging suppliers because of its complication and additional cost. Packaging manufacturers should be aware. Once being asked by customers for RFID, an efficient way was to provide it with an affordable cost at a minimal price. At the moment, many technologies have been studied to overcome the cost barriers. One among them was “printed RFID” technology.

Conductive ink would allow packaging printers to print RFID-antenna directly on the packaging substrates and attaching microchips in-line. RFID integration into packaging would significantly reduce the cost of RFID implementation in mass production because it would eliminate the need for labels and the manual “slapping” (attaching) process.

The goal of this research is to study the performance of inkjet- and screen-printed UHF-RFID-antennas on fibre based packaging substrate. Further it should be shown, if changing printing parameters will change as well the performance of the printed antennas. Comparisons are made with conventional aluminium etched RFID-antennas. Passive UHF spectrum RFID systems archive read ranges longer than one minute and thereby they are defined as long-range systems. These systems operate at the UHF centre frequencies of 866 MHz (Europe), 915 MHz (Americas), and 956 MHz (Asia and Australia).

2. Research methods

The RFID-UHF TE14 THINPROPELLER passive tagging antenna was printed on 300g/m² Creator Silk Coated Carton from TORRAS PAPEL. This antenna is not specially designed for printing production on fibre based substrates. However, as the performance of conventional aluminium etched antennas is known a comparison could be made between silver ink printed antennas and aluminium etched antennas. Both inkjet and screen printing were used.



Figure 1: Antenna TE14 THINPROPELLER

2.1 Screen printing process

For the screen printing process NOR-COTE UV curable conductive Silver thick film paste ELG 210 was used. The difficulty in UV curable conductive silver inks is that silver reflect UV energy and conductive fillers do not allow UV energy to pass through them to reach all of the polymer binder in a conductive ink. To obtain a complete crosslinking by UV energy in a conductive ink, the only way to do this is by using dual cure chemistry, where the UV energy starts a reaction to cure the surface of the ink and give partial curing to the top part of the ink layer. Once this is done, another chemical reaction starts that keeps the polymer crosslinking through the entire cross section. The used UV paste is therefore a two part system. The viscosity of the paste is between 70,000 and 100,000 cp at 25°C.

The screen printer used for the experiments is an Alraun P760 flatbed semi-automatic screen printer with a dual squeegee print head. Screen printing parameters were altered in order to achieve an even coverage of ink over the entire image. These included the used mesh as Sefar[®] high-modules monofilament polyester plain wave mesh 120/30Y and the squeegee hardness of 75°Shore next to snap-off distance and adequate print speed.

Once printing was concluded, the printed samples were cured with an Aktiprint UV Mini dryer at curing energies recommended by the ink manufacturer in order to bond and fix the ink onto the substrate. Even under the best curing conditions, UV conductive pastes still are not as mechanically strong, solvent and heat resistant, or electrically conductive as traditional solvent, water or epoxy based conductive inks.

2.2 Inkjet printing process

In the second stage the same antenna-design was printed on DIMATIX Inkjet Materials Printer DMP 2831 using the solvent based silver nano-particle inkjet ink Sunjet EMD5603. This ink is suitable for printing conductive lines and features in printed electronics as RFID antennas. The silver content of the ink is about 20% and the viscosity is about 10 - 13 cps at 25°C. After printing, the ink was thermally sintered in laboratory convection oven at 200°C for 30 min. The same fibre-based substrate was used for both the screen printing and inkjet printing processes.

To produce a closed printed layer, the Drop Space (DS) respectively the grid size of 25 microns was applied to the printed points. Further there has been printed different samples with different Drop Space (DS), which describes the distance between two drops of inks and therefore the quantity of ink applied. If the Drop Space gets bigger, less ink will be jetted. It has been realized print samples with DS10 (respectively 10µm), DS15, DS20 and DS25.

Finally there were five different of RFID-antennas printed during the project.

Table 1: Printed RFID-antennas

RFID-Antenna	Printing Method	Parameter
RFID-Antenna 1	Inkjet-Printing	Drop Space 10
RFID-Antenna 2	Inkjet-Printing	Drop Space 15
RFID-Antenna 3	Inkjet-Printing	Drop Space 20
RFID-Antenna 4	Inkjet-Printing	Drop Space 25
RFID-Antenna 5	Screen-Printing	1-pass-print

2.3 Characterization of the printed antennas

The characterization of the printed antenna includes measuring the printed thickness, visual inspection of the edge sharpness and all relevant parameters to consider in the analysis and validation of printed antennas used in inlays under the standard UHF Generation2.

The thickness and the profile of the lines are measured with a Leica DCM 3D optical profilometer. The advantage of Micro optical measurement technology fulfils two important requirements of metrology: non-destructive measurement combined with high accuracy. The measuring range starts from a few nanometres to several millimetres. The visual inspection has been realized with a Microscope Scopeman MSX-500 Di with 180% augmentation.

The antennas were printed with silver inks. Every metal component has a resistance that limits the intrinsic ability of electrons and hence the current to flow through the material. The formula that defines the resistance value depending on the characteristics of the metal used and the geometry of the antenna is:

$$R = \rho \frac{L_{\text{eff}}}{A_{\text{eff}}} \quad [1]$$

Where ρ is the resistivity of conductive material, the L_{eff} is the effective length of the antenna and A_{eff} is the effective area of the antenna. These values depend on the material used for printing the antenna and its geometry. UHF RFID antennas for the guidance value of a good antenna design should not exceed $0,5\Omega$.

Another important parameter for RFID antennas is the electrical impedance, which describes a measure of opposition to alternating current (AC). Further it was also measured the distance of the RFID-Tag and a Reader when a chip was applied to the antenna. The performance was measured in real field with a conventional RFID reader and compares the values with the reference tags (etched conventional aluminium antennas on polyester substrate).

3. Results and discussion

3.1 Printed layer thickness and visual inspection

The profiles of the printed inkjet- and screen-printed antennas were measured by profilometer. As the five antennas were printed in different printing methods and parameters (Table 1), the thickness of the cured ink is different as well.

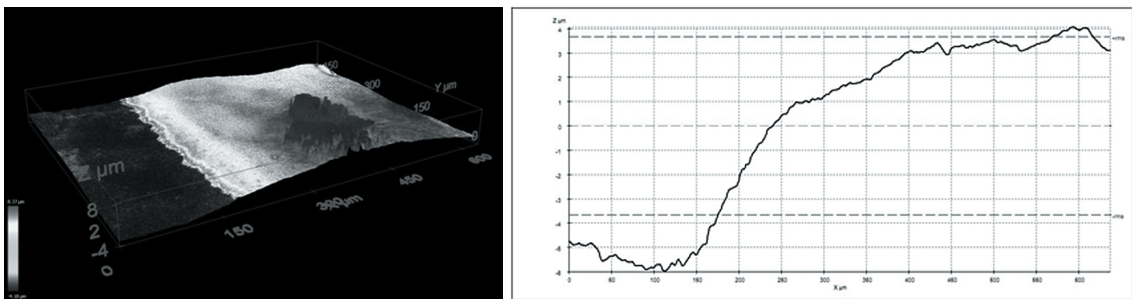


Figure 2: The profile of the inkjet-printed antenna with DS10

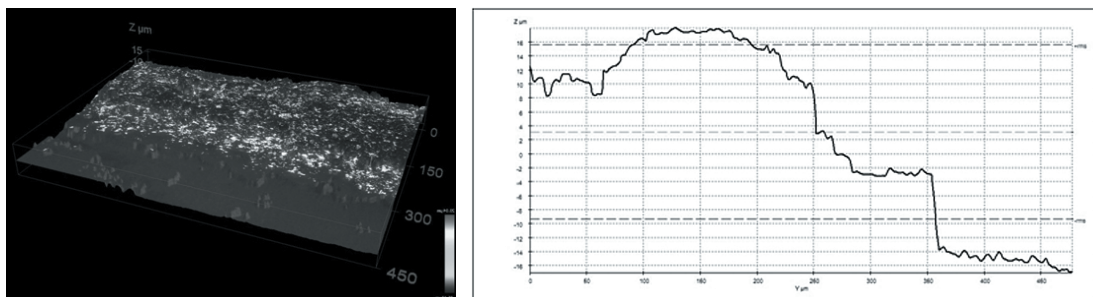
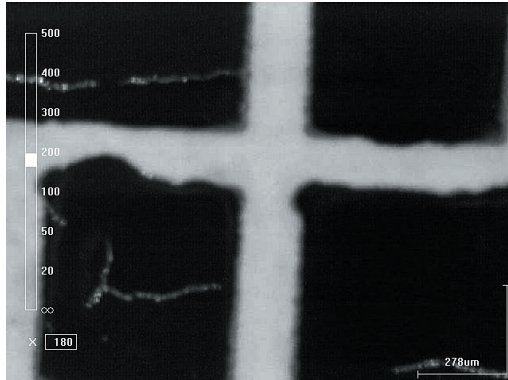


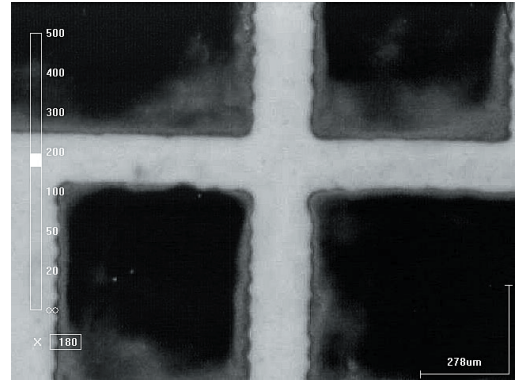
Figure 3: The profile of the screen-printed antenna on the same substrate

The results of all printed antennas are shown in Table 2. As smaller drop space in inkjet printing as higher layer thickness are achieved. However small drop space means higher nano silver ink application which results in our research at Drop Space 10 in worsening the edge sharpness because the substrate wasn't able to absorb that quantity of ink applied at the Drop Space of 10µm.

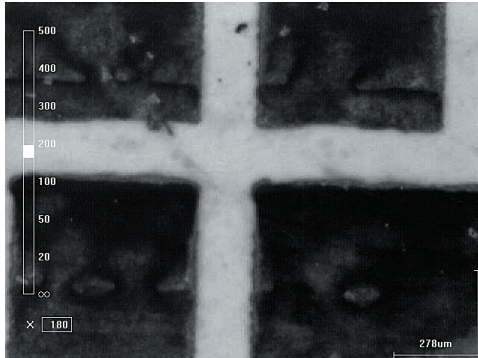
Visual Inspection by Microscope Scopeman MSX-500 Di with 180% augmentation



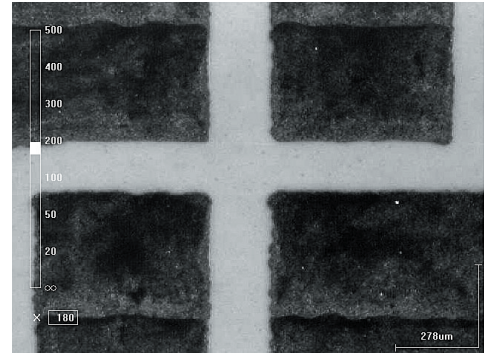
Inkjet-printed with Drop-Space DS 10



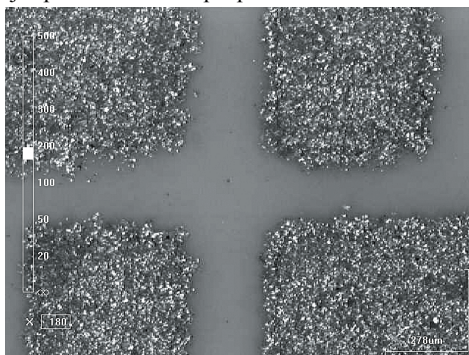
Inkjet-printed with Drop-Space DS 15



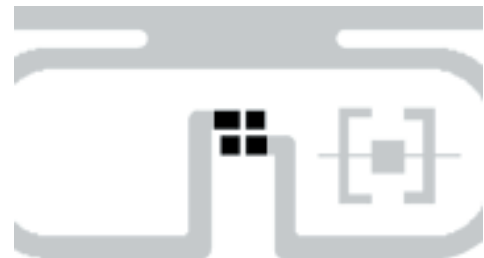
Inkjet-printed with Drop-Space DS 20



Inkjet-printed with Drop-Space DS 25



Screen-printed sample



The augmentation shows actually the darker part of the RFID UHF antenna TE14.

Figure 4: Visual inspection of the edges of the inkjet- and screen-printed antennas

The part of the antenna which is showed enlarged is actually the part where later on the Chip will be mounted. Therefore the edge sharpness is especially very important in that part of the antenna.

It could be observed, that the surface of the screen-printed and the inkjet-printed samples are quite different. The inkjet-printed samples have a more uniform surface. In terms of edge sharpness get inkjet-printing better results than screen-printing. Very important in inkjet-printing is the right parameters in Drop-Spacing. If the Drop-Space is really small, more ink is applied. As we see in the picture of DS10, so much ink is applied that the paper couldn't absorb all the ink. The edge-sharpness of the printed sample with Drop-Space DS 20 has the best printing resolution.

Table 2: Results from the characterization of the printed RFID-antennas

RFID-Antenna	Printed Layer Thickness	Visual Inspection
RFID-Antenna 1 - Inkjet-printed DS10	8 μ m	Bad
RFID-Antenna 2 - Inkjet-printed DS15	6 μ m	Good
RFID-Antenna 3 - Inkjet-printed DS20	5 μ m	Best
RFID-Antenna 4 - Inkjet-printed DS25	4 μ m	Good
RFID-Antenna 5 - Screen -printed	32 μ m	Good

3.2 Relevant Parameters of printed antennas under the standard UHF Generation2

RFID chips were attached on the printed antennas manually using a two-part silver epoxy conductive adhesive. The attached chip is a Monza[®] 4 UHF Gen 2 RFID Tag Chip.

Reference Parameters: TE14 THINPROPELLER			
Frequency	866 MHz	915 MHz	956 MHz
Impedance of the antenna	25 + j175 Ω	43 + j185 Ω	45 + j180 Ω
Impedance of the inlay	613 - j880 Ω	310 - j435 Ω	614 - j880 Ω
Phase of the inlay	- 4,3 ^o	- 8,8 ^o	- 6,9 ^o
SWR of the inlay	36	18	16
Resistance between terminals	0,5 Ω		
Reading distance	> 500 cm		

Table 3

Reference Parameters: TE14 THINPROPELLER (Inkjet-printed, DS10)			
Frequency	866 MHz	915 MHz	956 MHz
Impedance of the antenna	42 + j143 Ω	65 + j155 Ω	55 + j143 Ω
Impedance of the inlay	488 - j260 Ω	282 - j227 Ω	490 - j267 Ω
Phase of the inlay	- 2,3 ^o	- 4,0 ^o	- 6,0 ^o
SWR of the inlay	9	8	8
Resistance between terminals	34,1 Ω		
Reading distance	Ca. 210 cm		

Table 4

Reference Parameters: TE14 THINPROPELLER (Inkjet-printed, DS15)			
Frequency	866 MHz	915 MHz	956 MHz
Impedance of the antenna	37 + j159 Ω	58 + j175 Ω	64 + j174 Ω
Impedance of the inlay	403 - j207 Ω	265 - j435 Ω	410 - j211 Ω
Phase of the inlay	- 2,8 ^o	- 4,8 ^o	- 7,0 ^o
SWR of the inlay	9	8	8
Resistance between terminals	35,9 Ω		
Reading distance	Ca. 270 cm		

Table 5

Reference Parameters: TE14 THINPROPELLER (Inkjet-printed, DS20)			
Frequency	866 MHz	915 MHz	956 MHz
Impedance of the antenna	48 + j137 Ω	68 + j122 Ω	58 + j120 Ω
Impedance of the inlay	388 - j198 Ω	255 - j412 Ω	400 - j200 Ω
Phase of the inlay	- 2,0 ^o	- 4,2 ^o	- 6,9 ^o
SWR of the inlay	8	7	7
Resistance between terminals	42,5 Ω		
Reading distance	Ca. 120 cm		

Table 6

Reference Parameters: TE14 THINPROPELLER (Inkjet-printed, DS25)			
Frequency	866 MHz	915 MHz	956 MHz
Impedance of the antenna	55 + j125 Ω	70 + j111 Ω	63 + j105 Ω
Impedance of the inlay	372- j180 Ω	243 - j408 Ω	388 - j192 Ω
Phase of the inlay	- 1,7 ^o	- 3,8 ^o	- 6,3 ^o
SWR of the inlay	8	7	7
Resistance between terminals	48,4 Ω		
Reading distance	Ca. 90 cm		

Table 7

Table 8

Reference Parameters: TE14 THINPROPELLER (Screen-printed)			
Frequency	866 MHz	915 MHz	956 MHz
Impedance of the antenna	$38 + j164 \Omega$	$40 + j162 \Omega$	$36 + j172 \Omega$
Impedance of the inlay	$528 - j100 \Omega$	$400 - j190 \Omega$	$350 - j220 \Omega$
Phase of the inlay	$-3,0^{\circ}$	$-5,1^{\circ}$	$-7,8^{\circ}$
SWR of the inlay	10	9	9
Resistance between terminals	27,8 Ω		
Reading distance	Ca. 330 cm		

Please note: The reference values are provided from the manufacturer of the aluminium etched RFID antennas. These antennas are on polyester substrate. Polyester has completely different dielectric properties as it paper has, so both types of antennas are not really comparable. However the comparison should only show, if it's possible to print RFID antennas on normal fibre-based packaging substrate.

It must also be considered that some read errors may also be conditioned by problems in the insertion of the chip onto the antennas, as this has been done manually and is therefore very prone to errors.

4. Conclusions

The sensitivity of the tag depends on the frequency, and the feedback signal depends on the transmitted power. Both parameters are an important basis for describing the performance of passive UHF RFID tags. The data measured with these procedures are valid to compare the printed RFID-antennas with the reference parameter from the etched aluminium RFID-antennas.

In general terms, consistent with the comparative features of printed RFID-antennas with the conventional aluminium RFID-antennas, we can infer that:

- ✧ Screen-printing might an appropriate printing method for printing UHF RFID antennas on fibre-based substrates. Screen printing achieves high printed layer thickness. The edge-sharpness is another important criterion and seems to be good enough for UHF RFID antennas.

A great advantage is the possibility to cure the used ink NOR-COTE silver UV ink with UV light as the UV curing process is relatively simple, fast and well-known in the graphic printing industry. As well is UV drying much more substrate friendly than thermal sintering. Unless the UV silver ink doesn't archive high electrically conductive as traditional solvent, water or epoxy based conductive inks we could print RFID-antennas which archived 330 cm of reading distance between lector and RFID-tag. The aluminium etched antennas which are used as reference archive more than 500 cm.

Since UV inks contain little or no solvent, there is a lot of interest in using it because of lack of VOCs (volatile organic compounds). Either reducing VOCs or eliminating the need to report those both have appeal. The reduction of VOCs has an appealing environment effect. Unless the use of UV inks on packaging is still an issue, especially in using on food-packaging. So silver UV inks are could be neither used on food-packaging.

- ✧ Inkjet printing is another appropriate printing method to print UHF RFID antennas on fibre-based substrates. It must be kept in mind, that an appropriate layer thickness and edge sharpness must be archived. The best archived reading distance was 270 cm.

In terms of Processing, it is obvious that the time for thermal Sintering of nano Silver ink for inkjet-printing is the bottleneck in the production process, as Sintering times of 30 min. would increase the cost of the production and also the production time. Packaging printing of fibre-based container is basically a sheetfed-offset printed domain, so each sheet must transport into an oven. A handling or automation system doesn't exist for it yet. Even if packaging would be printed on ROLL-TO-ROLL, the necessary way which the web has to go in an oven must be 900 meters (0.5 m/s at 30 min).

As well as the substrate changing appearance during the thermal sintering process (colour changing to yellowish and shrinking) the process can also damage or change the printed offset graphic. An effective Colour-Management-System is not possible if in the process workflow includes a thermal Sintering process. There is an urgent need to search for alternative sintering methods. Photonic sintering seems to be the most interesting and forward-looking method next to NIR-sintering and microwave sintering among others

Acknowledgements

This research work is the result of the ELECTROPRINT research project and is funded by the Institute for Small and Medium Industry of the Generalitat Valenciana (IMPIVA) and co-financed by the European Regional Development Fund (FEDER).

Special thanks goes to Yuresky Rojas Rincón from Tag Ingenieros en Alicante for the measurements of the RFID-antennas.

References

- Delaney, K.J. (2002, Sep). Beyond bar codes: Radio ID tags may soon be placed in every product imaginable. Wall Street Journal (Europe), R.3.
- Merilampi S., Ukkonen L., Sydänheimo L., Ruuskannen P., Kivikoski M.; (October 2007), Analysis of Silver Ink Bow-Tie RFID Tag Antennas Printed on Paper Substrates. International Journal of Antennas and Propagation.
- Li, Yang; Rida, A.; Vyas, R.; Tentzeris, M.M.; Georgia Institute of Technology, Atlanta (Dec. 2007), RFID Tag and RF Structures on a Paper Substrate using Inkjet-Printing Technology
- Siden, J.; Nilsson, H.-E.; Mid-Sweden University, Sundsvall (June 2007), Line width limitations of flexographic-screen- and inkjet-printed RFID antennas



Optimization of aperture size and distance in the insulating mask of a five layer vertical stack forming a fully printed thermoelectric generator

Andreas Willfahrt, Gunter Hübner

Institute for Applied Research, Media University Stuttgart
Nobelstrasse 10, D-70569 Stuttgart, Germany

E-mails: willfahrt@hdm-stuttgart.de; huebner@hdm-stuttgart.de

Abstract

Printed thermoelectric generators (TEG) combine the advantages of screen printing with the uncomplicated assembly and reliability of thermoelectric devices. Successively printed layers on top of each other are needed for a completed device in a vertical stack setup. One of the challenging layers is the insulating mask which provides cavities for the thermoelectric legs. By governing the thickness of this insulating mask the overall thickness of the TEG is determined, too. The spatial separation is a necessity for reasonable energy conversion efficiency.

Keywords: Thermoelectric generators (TEG), insulating mask, energy conversion

1. Introduction

1.1 General

Thermoelectric generators (TEG) convert thermal energy directly into electricity. This effect is called Seebeck effect. The inversion of the Seebeck effect is called Peltier effect and is used in thermoelectric coolers (TEC). Due to thermal diffusion in electrically conductive materials there is a charge separation of the majority charge carriers. This effect occurs when a temperature gradient is applied along the electrical conductor, depicted in Figure 1, thermal diffusion.

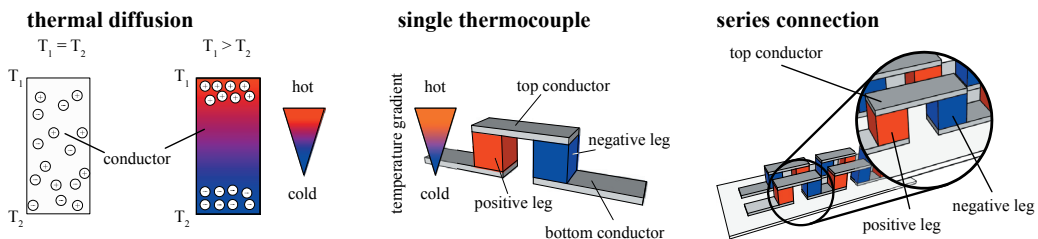


Figure 1: Principle of the Seebeck effect (left), a single thermocouple and a series connection of five thermocouples.

The Seebeck coefficient is a material constant. The higher the Seebeck coefficient, the higher the generated thermoelectric voltage. If two dissimilar materials are electrically connected forming a thermocouple (TC) a higher thermoelectric voltage will be generated. When connecting several to thousands of TCs electrically in series, the overall generated voltage will be proportional to the number of TCs, see Figure 1.

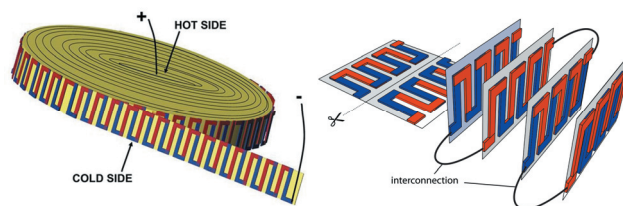


Figure 2: Coplanar printed thermoelectric generators as reported by (Weber et al., 2006) and (Glatz et al., 2006)

Two different approaches to printed TEGs are discussed in the scientific community: the coplanar combination of both thermoelectric materials lying in the same geometric plane, as depicted in Figure 2, and the 3D or vertical combination of the thermoelectric materials connected via electrical conductors, shown in Figure 1. Printing planar TEGs is discussed by (Weber et al., 2006; Wüsten, 2008; Duby et al., 2005) and

(Glatz, 2008) amongst others. The difficulty with coplanar compositions is to provide a good thermal contact of the heat source and heat sink to the TEGs warm and cold side. If both thermoelectric legs are printed on the substrate, the substrate has to be coiled-up or stacked like shown in Figure 2 in order to bring the cold and warm side in good contact with the heat sink and source respectively.

The situation is different with a vertical setup - as reported in (Böttner et al., 2004; Strasser et al., 2003) and (Koplow et al., 2008) - since the structures are deposited in x- and y-axis whereas the temperature gradient is maintained across the height of the thermoelectric legs. Therefore, the height of the thermoelectric materials is very important. In the authors' opinion a vertical setup similar to the conventional production of thermogenerators and thermoelectric coolers is to prefer over the coplanar setup.

Five layer setup of a fully printed thermoelectric generator

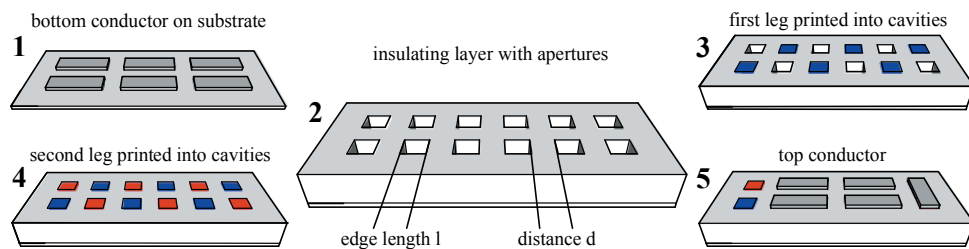


Figure 3: Fully printed thermoelectric generator in a five layer setup. 1) bottom conductor 2) insulating layer with apertures (cavities) 3&4) thermoelectric materials printed in cavities 5) top conductor

In this paper the authors discuss the optimization of the insulating layer of fully printed thermoelectric generators (TEG) comprising of five functional layers. These layers are subsequently printed on PET film in order to provide a flexible TEG. Printed in large scale these TEGs could, for instance, convert industrially generated waste heat. Printing technology may help to reduce the costs of TEGs drastically due to the uncomplicated production process and high throughput.

1.2 Seebeck effect

The Seebeck effect - found by physicist Thomas Johann Seebeck in 1821 - describes the direct conversion of a temperature gradient into electrical energy. If two dissimilar conductors experience different temperatures in their junctions, a thermoelectric voltage is generated. The thermopower or Seebeck coefficient describes the maximum thermoelectric voltage a material provides (common units are mV/K or $\mu\text{V/K}$). Since the Seebeck coefficient S of one material is subtracted from the other (1), the deployed materials must have different signs to achieve a reasonable thermoelectric voltage U_{th} per Kelvin (temperature gradient). Thus, p- and n-type materials with positive (holes) and negative (electrons) majority charge carriers respectively are used to maximize the calculated thermoelectric voltage.

$$U_{th} = (S_1 - S_2)\Delta T \quad [1]$$

The best known thermoelectric material in the range of room temperature is p- and n-doped Bi_2Te_3 . Unfortunately, there is no printing ink consisting of Bi_2Te_3 particles commercially available. In (Weber et al., 2006) the authors report about problems with oxidation of Bi in self-made ink formulated for screen printing. Hence, this investigation deals only with commercially available inks or simple self made compositions. In this case Nickel and PEDOT:PSS were chosen as materials to start from. In the authors' opinions the results will be easily adoptable to other ink formulations for materials with higher thermoelectric power which may be developed in the future.

The approach for fully printed TEGs chosen here is the vertical setup, illustrated in Figure 3. The bottom and top layer of such a fully printed vertical thermoelectric generator must supply best possible electrical conduction between the legs of the thermoelectric materials; hence, silver ink is used. The insulating layer is printed on top of the bottom silver conductor. The apertures in this layer provide the cavities for the thermoelectric materials which are printed into the cavities in two subsequent print runs. The printed top conductors complete the TEG, see Figure 3.

The insulating mask provides two major benefits: it determines the overall thickness of the printed thermoelectric device and it helps to separate the warm and the cold side to maintain the temperature gradient.

(Koplow et al., 2008) reported a similar composition using molds for structuring cavities for the thermoelectric materials to be filled in. According to Glatz et al. (Glatz et al., 2006) the height of the thermoelectric legs should be around 150 μm if Bi_2Te_3 is deployed. Since this material is not available as printing ink, 150 μm are considered as lower limit.

1.3 Aperture base area and height of the cavity

According to Ohm's law (2) the thermoelectric voltage U_{TEG} has to be high and the total resistance R_{total} of the thermoelectric generator must be low to achieve a good thermopower P_{TEG} (3).

$$I_{\text{TEG}} = \frac{U_{\text{TEG}}}{R_{\text{total}}} \quad [2]$$

$$P_{\text{TEG}} = U_{\text{TEG}} \cdot I_{\text{TEG}} \quad [3]$$

Thermoelectric materials with very different Seebeck coefficients generate a high thermoelectric voltage, see (1). To achieve a low R_{total} the leg dimensions have to be matched to the material properties of the thermoelectric materials. A poor electrical conductor needs a different base area than a good electrical conductor, since R_{total} is determined by

$$R_{\text{total}} = 3 \cdot R_{\text{conductor}} + 2 \cdot R_{\text{contact1}} + 2 \cdot R_{\text{contact2}} + R_{\text{leg1}} + R_{\text{leg2}} \quad [4]$$

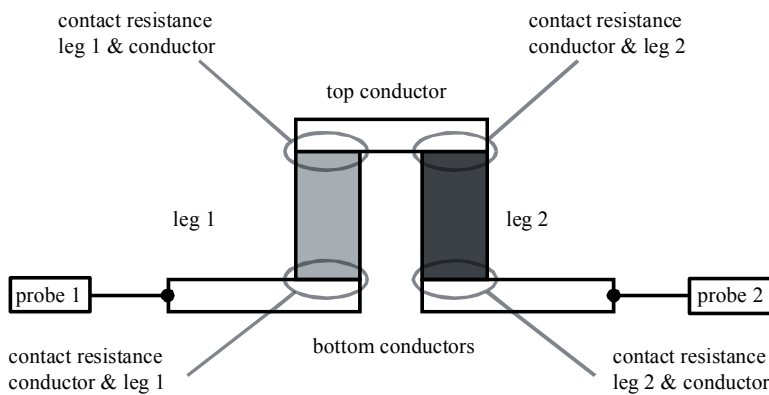


Figure 4: The total resistance of a single thermocouple is determined by a series connection of the volume resistivities and contact resistances between the different materials

The total resistance comprises of the resistance of the top and bottom conductor ($R_{\text{conductor}}$) the contact resistance between bottom/top conductor and leg1 (R_{contact1}), the contact resistance between bottom/top conductor and leg2 (R_{contact2}) and the resistance of top leg1 (R_{leg1}) and leg2 (R_{leg2}). In Figure 4 the contact resistance is illustrated.

R_{total} is mostly governed by the base area of the apertures and the height of the cavities in the insulating mask, since the resistance of the silver conductor is negligible small compared to the resistance of the thermoelectric legs (Ni and PEDOT:PSS). The contact resistance is determined by the deposition process and the material properties of Ni, Ag and PEDOT:PSS. Thus, it is only possible to affect the contact resistance indirectly.

An obvious way to affect the resistance is by altering the thermoelectric legs geometry. According to the definition of the Volume Resistivity

$$R_{\text{vol}} = \rho \cdot \frac{h}{A} \quad [5]$$

the resistance is determined by the material constant ρ (= specific resistance), the height of the thermoelectric leg h and the base area A . The base area is determined by the aperture shape, e.g. the radius of the circle or the edge length of the square and the height is determined by the thickness of the insulating layer. Since the thickness also determines the stability of the temperature gradient, only the aperture base area can be modified in order to alter the electrical resistance.

With reducing the base area, the resistance will rise et vice versa. Since the authors' intention is to find an optimized power output P_{TEG} the best correlation between the number of single thermocouples per area and the aperture geometry must be found.

The aspect ratio between the height h and the aperture edge length l needs to be optimized, depending on the distance d . It is possible to generate thicker ink films by means of several print runs, but it is advisable to optimize the amount of ink that is transferred by one print stroke. Otherwise, the complexity of the production process will increase. In order to optimize the insulating layer the first step is to examine the ink deposition depending on the aperture distance (grid distance).

2. Methods

Initial tests were carried out establishing the preparation of thick film stencils for a high ink deposition on the substrate. In a full factorial design of experiments (DOE) the most affecting parameters were found. The screen mesh, the stencil thickness and the squeegee geometry were identified as the main factors influencing ink deposition.

Furthermore, initial tests were conducted finding an appropriate ink for the insulating layer. Assuming that all polymer based inks show the same magnitude of electrical and thermal insulation, the printability and the height of the ink layer printed with one screen printing stroke was crucial. Beside the ink layer thickness the usage and printability plays an important role.

Table 1: Initial tests with insulating materials and the achieved ink layer thickness printed on glass substrate

32-100 screen mesh, dry ink layer thickness on substrate, one print stroke			
Printperfekt EX-TS	550 μm		
Polystyrene	370 μm		
SunChemical CFSN 6052	200 μm		
77-48 screen mesh, SunChemical CFSN 6052			
Printed layers	1x	5x	10x
Height	27 μm	77 μm	122 μm

Table 2: Initial tests with insulating materials and the achieved ink layer thickness printed on PET plastic film

54-64 screen mesh, dry ink layer thickness on substrate, one layer	
SunChemical CFSN 6052	20 μm
Manoukian Argon TEXIPLAST 5000	30 μm

The SunChemical CFSN 6052 dielectric UV ink is designed for printing over conductive tracks to form a protective insulating layer (SunChemical, 2009). The water based Printperfekt EX-TS puff ink is designed for relief printing in textile screen printing as well as the plastisol ink Manoukian Argon TEXIPLAST 5000. The thickest ink layer was obtained with the printperfekt EX-TS puff printing ink (see Table 1). This ink needs a special thermal treatment after being printed. The ink puffs up (foams) during drying at 140°C to 150°C. This process is quite unpredictable and not convenient for the insulating layer. The self made polystyrene ink established an ink layer thickness of around 370 microns. Since no additives were used in the polystyrene ink foaming occurred. Normally, foaming is a unwanted negative property of inks. But since the entrapped air in the dry ink layer acts like a thermal resistance, this effect is positive for the printed insulating layer. Although this ink was discarded since it was very tacky and tended to block the stencil rapidly. The SunChemical CFSN 6052 UV curable ink achieved a smaller ink film thickness (200 microns), but printability and curing were very good. The results are predictable and due to the UV curing it is feasible to print in several runs very quickly.

The plastisol ink Manoukian Argon TEXIPLAST 5000 also showed good results. With the first print stroke the plastisol ink established a thicker ink film on the substrate than the UV ink, see Table 2. When several layers are subsequently printed the ink deposition of both materials are almost equal. The plastisol ink needs 2 to 4 minutes drying at 140 to 150°C. The curing time could be reduced by deploying a so called flash curing unit, "this is a powerful heater suspended a few inches above the print which, when activated, raises the print to the gelation temperature in a matter of seconds." (Sericol, 2011).

The flash cured ink layers need to be tempered afterwards for achieving good adhesion to the substrate. This complies with the following printed layers (Ni, PEDOT:PSS, Ag) which require thermal treatment at a minimum of 130°C. Due to the advantage of the really short curing time the UV ink was used for the investigation of the apertures.

2.1 Parameters

The parameter settings for the investigation of the apertures in the insulating mask are shown in Table 3.

Table 3: Machine settings and parameters for the investigation of aperture distance variations

Screen mesh	tension	mesh opening	mesh thickness	achieved EOM
54-64	20,0 N/cm	115 µm	103 µm	19 µm
77-48	20,6 N/cm	77 µm	80 µm	15 µm
90-48	20,0 N/cm	55 µm	78 µm	12 µm
Coating				
Automatic coater Svecia H-41E (Harlacher AG)				
Emulsion	Kiwo Azocol Poly-Plus S-RX			
Coatings	1x print side, 2x squeegee side			
Coating velocity [%]	30			
Exposition				
Vacuum time	130 seconds			
Exposure	130 seconds			
Printing				
Printing ink	SunChemical CFSN6052			
Squeegee	RKS			
Angle	75°			
Hardness Shore A	75			
Print velocity	140 mm/s			
Flooding velocity	120 mm/s			
Squeegee pressure	80 N/mm			
Snap off distance	1.5 mm			

2.2 Aperture distance

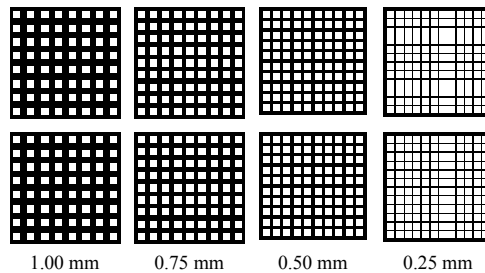


Figure 5: Template for the investigation of the aperture distance. The edge length of the squares is kept constant at 1.00 mm. The white areas represent the apertures in the insulating mask (black). The grid differs in the distance between the apertures (white)

While the base area of the aperture is kept constant, the distance is varied in four steps of 0.25 mm from 0.25 mm to 1.00 mm, as shown in Figure 5. For statistical significance 10 samples were printed and measured with each of the three used screen meshes 54-64, 77-48 and 90-48 (SEFAR PET 1500). The automatic coating machine Svecia H-41E (Harlacher AG) was used with the same process parameters for all screens. The Theimer Montakop ST exposure unit was set at 130 seconds vacuum and 1400 units exposure time. Due to the various mesh parameters, the emulsion over mesh (EOM) differed from screen to screen (see Table 3).

2.3 Microscope profile measurements

Special attention is paid to the determination of the printed structure's heights since in most cases the surface is rugged. There is not only one height that easily can be determined, it is rather a mean value of an arbitrary number of single heights. Different measurement systems were examined to encounter this problem, e.g. a micrometer screw gauge, a magnetic induction handheld device and the Alicona Infinite Focus microscope. The latter was used for generating the profiles shown in Figure 7-10. The analysis software of the microscope allows the measurement of the profile along a path set in the image data, see Figure 6. The path width can be

set between 1 px and 999 px, each representing a single profile. If more than 1 px is set, the profile is a mean profile of the comprised single profiles.

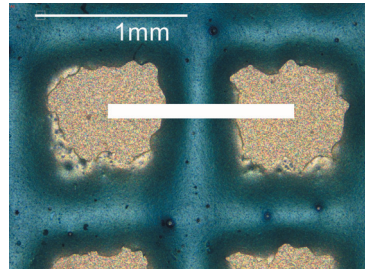


Figure 6: The analysis software generates the profile according to the path set in the image data. The image shows a sample printed with 54-64 screen mesh, grid distance 0.25 mm

The authors chose to average the “plateau” values of the printed structures. The advantage of this method is the elimination of peak values which may distort the approximated profile height. Figure 7 shows the plateau of a sample printed with 54-64 screen mesh and a grid distance of 1.00 mm. The starting point and the endpoint of the plateau was chosen subjectively, thus a systematic error was made. By repetition of the measurement it was found that this systematic error is negligible small.

Comparing the profiles the 0.50 mm and 0.75 mm grids printed with the 54-64 screen mesh (Figure 8) for instance shows the effect of this approach. Visually assessed it seems that the 0.75 mm grid is slightly higher than the profile of the 0.50 mm grid. According to the calculated plateau mean value both profiles have the same height. Since the plateau surface of the 0.50 mm grid profile is more homogenous than the surface of the 0.75 mm grid, this result is plausible.

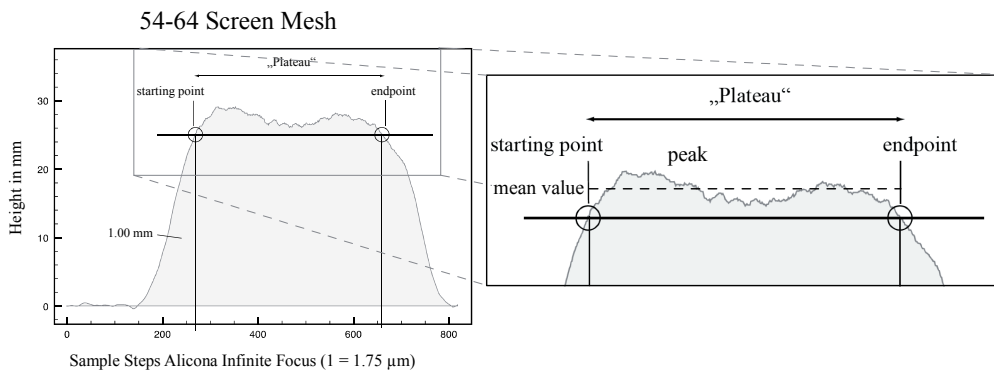


Figure 7: Determination of the profile's height by means of calculating a mean value of the so called plateau

3. Results

3.1 Comparison of mesh types

The mesh mainly governs the ink transfer onto the substrate, since the mesh opening (corresponding to radius r of the pipe) has a greater impact (see (6), radius r to the power of 4) on the ink deposition than the stencil height, as shown by the Hagen-Poiseuille equation

$$\dot{V} = \frac{dV}{dt} = \frac{\pi \cdot r^4 \Delta p}{8 \eta L} \quad [6]$$

with:

- \dot{V} volumetric fluid flow through a pipe
- r radius of the pipe
- L length of the pipe
- η dynamic viscosity of the fluid
- Δp pressure difference between the entrance and the exit of the pipe

For this reason the difference in the EOM is not considered as a severe drawback. A coarser screen mesh provides a higher mesh opening, but the print resolution will suffer from this. In order to find a compromise between ink layer deposition (mesh opening) and the achievable print resolution (mesh count), three mesh types are compared regarding the ink layer thickness and the reduction of the aperture area.

In Figure 8-10 all profiles are plotted against the sample steps of the microscope (1 unit equals 1.75 μm). As expected from the mesh data (Table 3), the screen mesh with the highest mesh opening establishes the thickest ink layer.

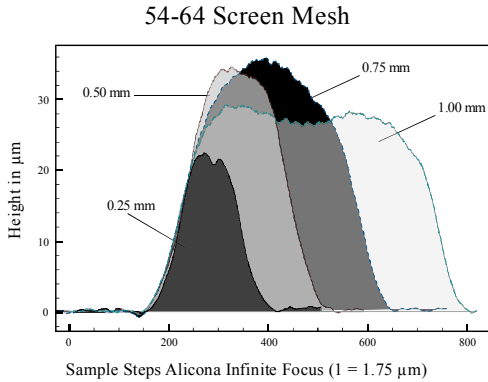


Figure 8

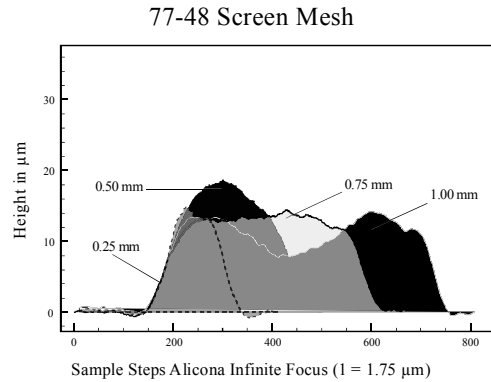


Figure 9

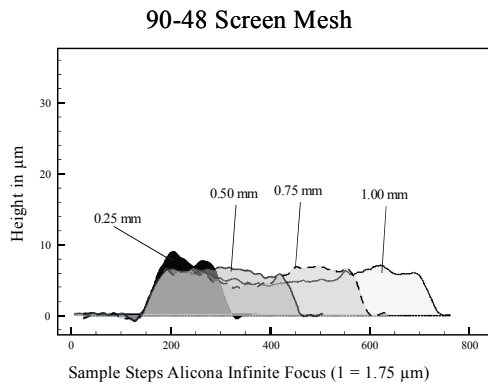


Figure 10

Figures 8, 9 and 10:
The Figures show the influence of the distance between the apertures on the height of the grid

But it is more interesting to compare the impact of the distance between the apertures than opposing the mesh types. At a grid distance of 0.50 and 0.75 respectively, the coarsest screen mesh 54-64 performs best. The lowest ink layer thickness was achieved at a distance of 0.25 mm. In contrary the finest screen mesh 90-48 generated the highest ink layer thickness with the smallest distance of 0.25 mm. The 77-48 achieved the thickest ink layer film at an aperture distance of 0.5 mm. According to the plotted profiles in shown in Figure 8 to 10 and Table 4 respectively, the optimum combination of screen mesh and grid distance can be determined in order to establish a maximum ink deposition. The bold values mark the thickest ink layer achieved with the screen mesh.

Table 4: Ink layer thickness per screen mesh with \bar{h} = thickness mean value (h) and σ = standard deviation

Distance in mm	54-64		77-48		90-48	
	\bar{h} in μm	σ	\bar{h} in μm	σ	\bar{h} in μm	σ
0.25	22.0	3.9	13.8	1.9	7.9	1.3
0.50	33.4	5.0	17.5	2.6	6.4	1.1
0.75	33.4	6.2	13.2	2.6	5.6	1.6
1.00	27.5	5.3	11.1	1.8	5.5	1.2

Apart from the achieved ink layer thickness the reduction of the area of the apertures has to be assessed. Figure 11 shows the reduction of the apertures printed with the different screen meshes and with different

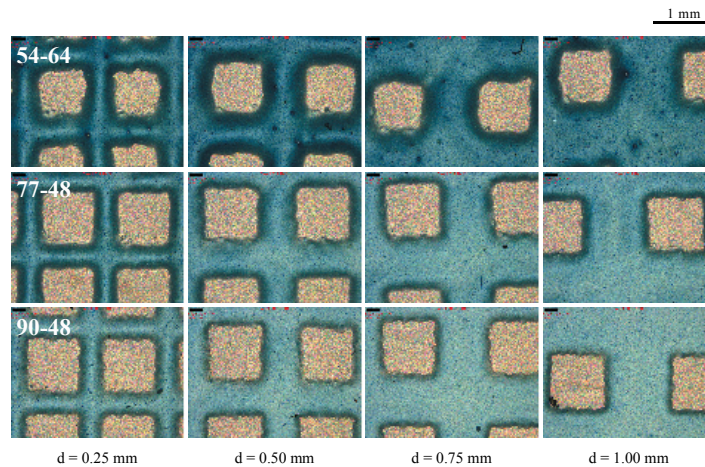


Figure 11: Apertures printed with 54-64 (first row), 77-48 (second row) and 90-48 screen mesh. Grid distance 0.25 mm, 0.50 mm, 0.75 mm and 1.00 mm (from left to right)

grids. On the left hand side the grid with a distance of 0.25 mm is shown. On the right hand side the longest grid distance of 1.00 mm is shown. The most significant reduction of the aperture area was noticed with the coarse mesh 54-64. The grid with 0.25 mm distance only achieved 70% of the nominal area. The other grids yielded almost 80% (0.50 mm = 77%, 0.75 mm and 1.00 mm = 79%, see Figure 12). A tendency can be seen: the finer the mesh, the lower the reduction of the area. According to this the best results were shown by the 90-48 screen mesh (0.25 mm = 89%, 0.50 mm and 0.75 mm = 90%, 1.00 mm = 91%). Additionally, there is a slight trend towards broadening of the grid lines by reducing the grid distance with a coarse mesh. Especially at a distance of 0.25 mm the 54-64 screen mesh suffers from this tendency.

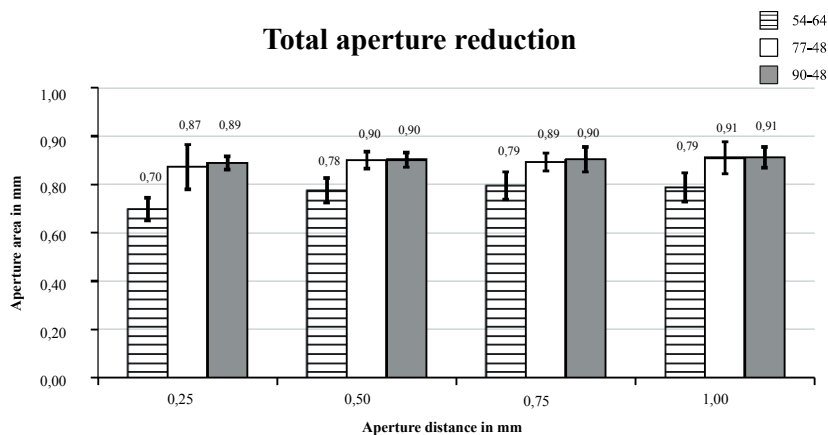


Figure 12: The aperture area printed with different mesh types. The higher the mesh count, the better the approximation of the actual value to the nominal value (1 mm²)

According to the results, a correction factor can be implemented in the data for the template to achieve the intended aperture size in the printed samples, e.g. the data must be multiplied with 1.3 if a 54-64 screen mesh with an aperture distance of 0.25 mm will be deployed.

4. Conclusions

For the optimization of a fully printed thermoelectric generator (TEG) the insulating layer plays a very important role. This layer determines the total height of the TEG and thus, governs the efficiency of a TEG. In this paper the focus is set on the apertures in the insulating layer forming cavities for the thermoelectric legs. The apertures have to meet two contradictory requirements: the aperture area must be large in order to reduce the Resistivity of the thermoelectric materials, but their edge length should be minimized to achieve a high package density. Additionally, the insulating layer has to achieve a reasonable thickness to maintain the temperature gradient between the hot and the cold side.

With all that in mind, the investigation of the apertures is a key to an optimized printed TEG. The information out of the reduction of the grid size (distance between the apertures) gives an indication for choosing the parameters depending on the deployed mesh. The mesh itself in combination with the stencil thickness governs the ink layer thickness. In order to achieve the intended open area (aperture area) in the insulating layer, a correction factor must be established in screen preparation. Due to the investigation of the reduction of the aperture area at defined parameters (screen mesh, grid distance etc.), this correction factor was found. A first step was taken in evaluating the screen printing parameters. Certainly, there is more work to be done, e.g. the impact of the stencil thickness and the grid size on the ink deposition.

Acknowledgements

The research project “printed thermoelements” is funded by Germanys Federal Ministry of Education and Research (BMBF).

The authors would like to thank the following industrial partners for their assistance in providing materials and technical advice in the creation of this work: Heraeus, SunChemical, Kiwo, Ulano, Sefar and DuPont as well as EKRA for providing the printing press.

References

- Böttner, B., Nurnus, J., Gavrikov, A., Kühner, G., Jäggle, M., Künzel, C., Eberhard, D., Plescher, G., Schubert, A., & Schlereth, K.-H. 2004. New thermoelectric components using microsystem technologies. *Journal of Microelectromechanical Systems*, 13(4), 414-420. gelesen 20.07.2009.
- Duby, S., Ramsey, B. J., & Harrison, D. J. 2005. Printed thick-film thermocouple sensors. *Electronics Letters*, 41(6), 312-314.
- Glatz, W. 2008. *Development of flexible micro thermoelectric generators*. Ph.D. thesis, ETH Zürich.
- Glatz, W., Muntwyler, S., & Hierold, C. 2006. Optimization and fabrication of thick flexible polymer based micro thermoelectric generator. *Sensors and Actuators A: Physical*, 132(2), 337 - 345. The 19th European Conference on Solid-State Transducers.
- Koplow, M., Chen, A., Steingart, D., Wright, P. K., & Evans, J. W. 2008. Thick film thermoelectric energy harvesting systems for biomedical applications. *Pages 322-325 of: Proc. 5th Int. Summer School and Symp. Medical Devices and Biosensors ISSS-MDBS 2008*.
- Sericol Limited. 2011. *Flash Cure Printing of Plastics*. Sericol Limited, Pysons Road, Broadstairs, Kent CT10 2LE, England.
- Strasser, M., Aigner, R., Lauterbach, C., Sturm, T. F., Franosh, M., & Wachutka, G. 2003. Micromachined CMOS thermoelectric generators as on-chip power supply. *Pages 45-48 of: Proc. TRANSDUCERS, Solid-State Sensors, Actuators and Microsystems, 12th Int. Conf*, vol. 1.
- Technical Information Leaflet, SunTronic Dielectric 680 (CFSN6052), http://coates.com/File/Library/Photovoltaics/SOLSYS_CFSN6052_CFSN6057-UV-Dielectric.pdf
- Weber, J., Potje-Kamloth, K., Haase, F., Detemple, P., Völklein, F., & Doll, T. 2006. Coin-size coiled-up polymer foil thermoelectric power generator for wearable electronics. *Sensors and Actuators A: Physical*, 132(2), 325 - 330. The 19th European - Conference on Solid-State Transducers.
- Wüsten, J. and Potje-Kamloth, K. 2008. Organic thermogenerators for energy autarkic systems on flexible substrates. *Journal of Physics D: Applied Physics*, 41(13), 135113.



Smart-printed-pack - intelligent packaging container attached with opening detector and paper-based electroluminescent indicator lamp

Vicente de Gracia¹, Susana Otero¹, Nuria Herranz², Markus J. Müller¹, Juan Diaz²

¹ AIDO, Technological Institute of Optics, Colour and Imaging, Valencia, Spain

E-mail: mjohannes@aido.es

² ITENE, Technological Institute of Packaging, Transport and Logistics Research, Valencia, Spain

Abstract

Smart Packaging is a term which has become increasingly important in the last few years. While previously, the only purpose of packaging was product protection and advertising, nowadays it has changed and packaging is becoming increasingly more functional.

AIDO and ITENE are collaborating together in a research project called "SMART-PRINTED-PACK" that has the aim to develop a carton package equipped with sensor which detects if the packaging has previously been opened. The packaging contains an electroluminescent lamp (EL lamp), which illuminates if the packaging is opened once. All components of the package as EL lamp, conducting lines and sensors are realized by printed technologies.

Keywords: smart packaging, printed electronics, opening detector, paper-based electroluminescent lamp

1. Introduction

Smart Packaging is a term which has become increasingly important in the last few years. While previously, the only purpose of packaging was product protection and advertising, nowadays it has changed and packaging is becoming increasingly more functional.

Heidelberger Druckmaschinen AG, the biggest printing press manufacturer worldwide for offset sheet fed printing presses asked in their publication "White paper Packaging, October 2008", "What does the packaging market need?" The answer is basically two trends in packaging sector; one is the trend in design and material to strengthen and enhance their brand image. The other big trend is **Smart packaging** with all kinds of additional functions which is currently enjoying rapid growth. Smart Packaging refers to additional functions such as RFID-technology, Game Cards, and various types of printed sensor. Applications like this would sooner or later be applied to packaging or on other printing products (Heidelberg, 2008).

AIDO and ITENE are collaborating together in a research project called "SMART-PRINTED-PACK" that has the aim to develop a carton package equipped with sensor which detects if the packaging has previously been opened. The packaging contains an electroluminescent lamp (EL lamp), which illuminates if the packaging is opened once. All components of the package as EL lamp, conducting lines and sensors are realized by printed technologies.

2. Research methods

2.1 Development of a printed conductive sensor to attach on packaging for features such as opening-detector or anti-counterfeit

This visible sensor consists basically of printed conductive areas on different parts of the packaging box. One printed part of the sensor is located in the flap and the other inside of the packaging box. If the box is closed, there is electrical connection between the contacts and this acts as an opening detector. The idea is that if the packaging gets opened once, the sensors are interrupted and a light through a printed EL lamp lights up. That means that the printed circuit must be controlled by a programmed microcontroller which is placed on the packaging. The microcontroller is always powered through a micro-battery, and when the controller detects that a driver pin increases the electrical resistance (box gets opened), the microcontrollers put the electrical flow through other printed conductive lines, which are connected with the EL lamp.

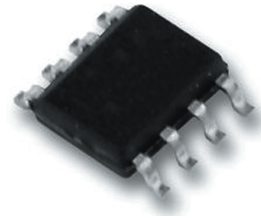


Figure 1:
Microchip used in this project -
PIC12F675-E/SN. - IC, Microcontroller, 8BIT

To create this printed contact sensor it was necessary to study the different conductive inks for different printing processes as inkjet-printing and screen-printing. It is quite important to achieve high conductive values to ensure the correct functionality of the sensor. Good adhesion of the conductive ink on the used substrate is also very important. The substrate used in the project is a Creator Silk Coated Carton from TORRAS PAPEL with 300g/m².

2.2 Development of a paper-based electroluminescent lamp (EL lamp) to print on packaging boxes

Electroluminescent lamps on ITO pre-coated PET Foils are actually state-of-the-art. ITO stands for Indium Tin Oxide and is a transparent conductive material. The approach in this project is to print the EL lamp on fibre-based packaging substrate without using the conductive ITO layer. EL lamps on ITO pre-coated PET Foils are built-up in different layers which consists of conductive layers of silver inks, emission layer of phosphor ink and dielectric layers and finally an encapsulation, which could be a polyester film or an ink which acts as protection layer, to protect and isolate the EL lamp.

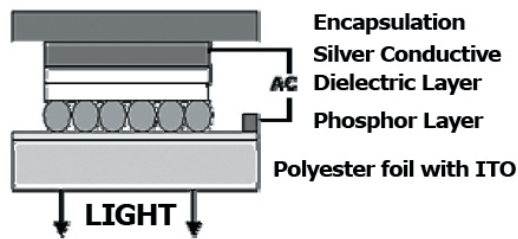


Figure 2: ITO Film standard El lamp construction

To print an EL-lamp on fibre-based packaging substrate two challenges need to be solved. The first one will be the protection respectively the encapsulation of the EL lamp on both sides, as the fibre-based substrate doesn't have the same barrier properties as a PET-foil has. The encapsulation of the lamp will be realised with encapsulation inks which are applied by screen-printing. The whole EL lamp will therefore be fully printed and will not need further processing. The other challenge will be the reverse printing order to built-up a fibre-based EL-lamp compared to a PET-foil EL lamp. These inks are only available for screen printing. So the sheets are printed before with the graphical publicity print on offset-sheet-fed printing presses. The inks used for the EL lamps are UV inks and are easily cured with a normal UV-dryer typically used in printing companies and do not need further processing. Therefore, the printed sheets won't be exposed to further temperature stress.

2.3 Printed electronics integration into conventional electronics

The whole electronic system for the opening detector in this demonstration packaging cannot be realized only with printed components. In this step the conventional electronics, such as the microcontroller and different electrical resistor components must be implemented into the printed circuit which connects these components with the printed sensor on the packaging substrate.

Conventional solder technology is one of the most common methods used to connect electrical components with electrical conductors. Basically it uses a tin alloy as a connecting element to solder the conductive elements. Melting the tin alloy requires temperatures up to 400° C, and therefore this technology is not suitable to solder electrical components on a fibre-based packaging substrate.

A suitable technology to connect electrical components is via ECA (Electrically conductive adhesives). ECA are primarily polymer matrices with a filling of conductive particles. The polymer resins provide the physical and mechanical properties such as adhesion, mechanical strength and impact resistance, while filling electrically conductive metal particles.

ECA adhesives have many advantages over welding technology, such as better response to the environment, mild processing conditions, few processing steps and precision in the interconnection of small connectors. However, they are limited in certain specific applications because they show some limitations as a relatively low electrical conductivity, the loss of conductivity with time and/or humidity, to carry the current limitations and limited impact resistance (C.P. Wong et al., 2010, Springer).

There are different groups of ECA adhesives such as anisotropic conductive adhesives (ACA) and anisotropic conductive film (ACF). Another interesting group are isotropic conductive adhesives (ICA) which is a group of ECA adhesives. They are composed of polymer resin and conductive fillers, and are characterized by being able to drive in three dimensions. They form an adhesive matrix to form the mechanical bond for the connections and set conductive filler particles.

3. Results and discussion

3.1 Development of a printed conductive sensor to attach on packaging for features as opening-detector or anti-counterfeit

Finally the screen printing process has been chosen to print this sensor due to the fact that with screen printing it is possible to get high ink thickness, which means high conductive values. The NOR-COTE UV silver ink ELG 216 is a good choice because of the easy curing method with UV light to avoid sintering methods by printing nano silver printing inks. In general, all sintering methods are not substrate-friendly and therefore not suitable for fibre-based packaging substrate.

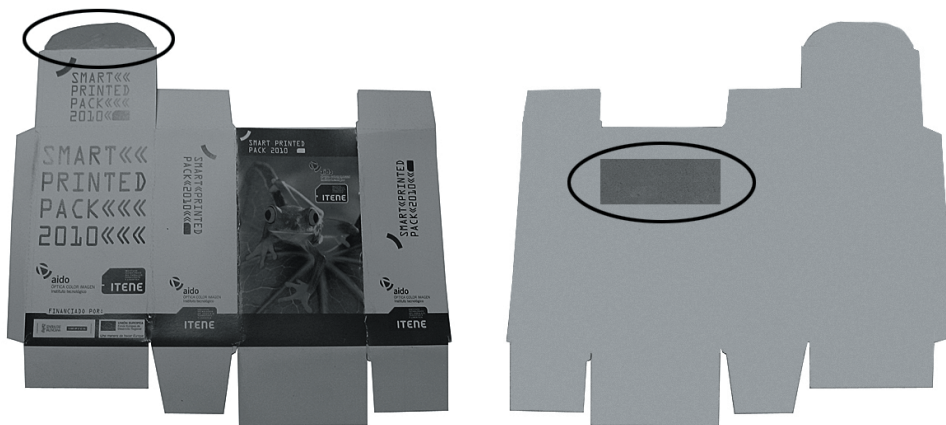
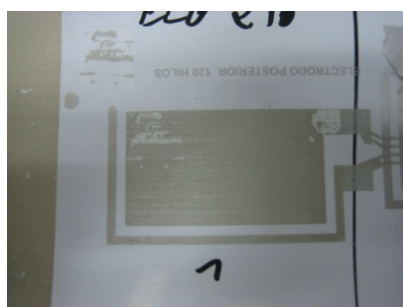


Figure 3: Demonstration packaging with the printed conductive sensors. If the packaging box is folded and closed, the both marked fields are touching acts as an open-detector sensor

Good adhesion is very important for this kind of contact sensor. The used screen printing ink NOR-COTE ELG 216 is basically designed to get good adhesion on polyester substrates or on ITO. The qualification of the adhesion of the conductive silver ink on the substrate is made through a “tape-test”.



NOR-COTE ELG 216
Printed over carton
varnish



NOR-COTE ELG 216
Printed over pre-printed carton with ELG 141

Figure 4: Results of the screen-print ink NOR-COTE 216 after the tape-test

The tape test is a method for evaluating the adhesion of a cured coating or ink on a substrate. Pressure-sensitive adhesive as TESA type 4104 or Scotch tape No. 650 is applied to an area of the coating which is sometimes cross-hatched with scratched lines. Adhesion is considered to be adequate if no coating is pulled off by the tape when it is removed.

The ink was printed directly on used Creator Silk Coated Carton and also on the same substrate but with a pre-printed UV varnish ELG 141 from the same ink supplier.

According to the tape-test, better adhesion is achieved by pre-printing a NOR-COTE ELG 141 varnish instead of printing the UV silver ink directly on the Creator Silk Coated Carton. The NOR-COTE ELG 141 acts also as first and last printed layer to protect and isolate the EL lamp.

3.2 Development of a paper-based electroluminescent lamp (EL lamp) to print on packaging boxes

The EL lamp has been printed on Creator Silk Coated Carton with 300g/m² using reverse layer construction as the EL lamps fabricated with ITO polyester foil. The inks used to print the EL lamp were from NOR-COTE. To avoid ITO a Transparent Conductive ink was used to build the cathode layer.

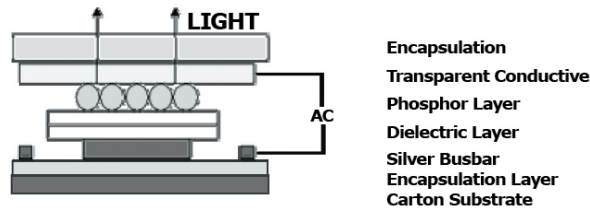


Figure 5: EL lamp layer construction using transparent conductive ink over carton substrate

The lifetime of EL lamps on carton substrate is usually an issue, even if the packaging’s lifetime is normally not more than six months. The reverse constructed EL lamp is fully functional; however there are some issues on the lamp’s life-time because encapsulation ink which is printed as first and last layer on the carton substrate do not have the same WTVR barrier properties (water vapour transmission rate) as polyester foil has.

3.3 Printed electronics integration into conventional electronics

The final decision for the technology to connect the electrical elements has been Isotropic Conductive Adhesives (ICA) due their low temperature processing. In comparison to solder technology, they are more suitable to use for fibre-based packaging substrates. The following table compares the technology of solder with tin/lead and Isotropic Conductive Adhesives (ICA).

Table 1

Characteristics	Solder with tin/lead	Adhesives ICA
Volume Resistivity	0,000015Ωcm	0,00035Ωcm
Union R	10-15mW	< 25mW
Thermal Conductivity	30 W/m-deg K	3.5 W/m deg K
Maximum cutting force	2200 psi	2000 psi
Finest lines of combination	300µm	< 150-200µm
Minimum temperature processing	215°C	< 150-170°C
Environmental impact	Negative	Reduced
Thermal fatigue	Yes	Minimal

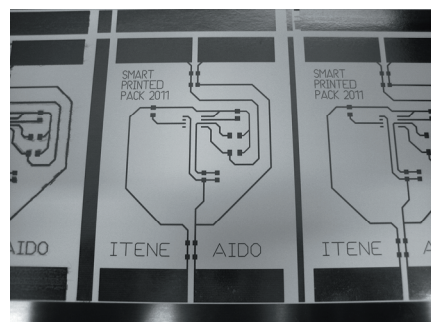


Figure 6: Printed conductive lines on Creator Silk Coated Carton where the electrical components need to be applied

3.4 Results of smart-printed-pack

The final result of the research project Smart-Printed-Pack of AIDO and ITENE is a packaging box as a demonstrator attached with a printed contact opening-detector and a printed EL lamp to give a signal if the box is opened once. The system is controlled by a microcontroller which is applied with ICA adhesives on the printed conductor lines.

Followed functions were realised by printing technologies:

- ◆ Printed sensor for opening detection: The sensor is easy to realize and apply on the packaging substrate;
- ◆ Printed EL lamp on fibre-based packaging.

The novelty offered by this project is its focus on smart packaging and therefore fibre-based substrates for printed electronics as paper-based electroluminescent lamps and paper-based sensors.



Figure 7:
Demonstration packaging. The printed EL lamp is applied on the eyes of the frog

4. Conclusions

Printed Electronics opens new markets and opportunities for many sectors. The packaging sector may be one of the sectors that benefit most from the printed organic electronics. New features such as sensors, circuits, and electroluminescent devices can be applied on packaging substrates in an easy and economic way by printing technologies.

As already mentioned it is possible to add functionalities onto a packaging box by printing technologies. However, there are still many issues left, mainly in process optimization as how would be the packaging production workflow in future with value-added as RFID, EL-lamps and so on. In which stage of the production workflow would chips and other electronic devices be integrated and can printers do all this work or would that be outsourced into another specialized companies? The cost of the conductive inks and the processing of sintering also still have issues. Smart-Printed-Pack still utilises conventional electronics. The challenge in further projects will be the substitution of conventional electronics to printed electronics.

Acknowledgements

This research work has been in collaboration between AIDO, Technological Institute of Optics, Colour and Imaging and ITENE, Technological Institute of Packaging, Transport and Logistics Research and is funded by the Institute for Small and Medium Industry of the Generalitat Valenciana (IMPIVA) and cofinanced by the European Regional Development Fund (FEDER).

References

- http://www.heidelberg.com/www/html/en/binaries/files/press_lounge/archive/basic_press_texts/whitepaper_packaging_pdf
- C.P. Wong, Yi Li, and K.-s. Moon, Nano-conductive adhesives for nano-electronics interconnection. 2010: Springer.



Printability of thermochromic offset inks and their interactions with dampening solution

Ondrej Panák¹, Bohumil Jašůrek¹, Jan Vališ¹, Marie Kaplanová¹, Marta Klanjšek Gunde²

¹ Department of Graphic Arts and Photophysics, University of Pardubice
Studentská 95, CZ-532 10 Pardubice, Czech Republic

E-mail: ondrej.panak@upce.cz

² National Institute of Chemistry
Hajdrihova 19, SI-1000 Ljubljana, Slovenia

Abstract

The paper focuses on the interaction of TC offset inks with dampening solutions and how influences the composition of dampening solution behaviour, functionality and ability of TC inks to be transferred in offset printing process. Two thermochromic inks were used in the study (red CTI, and blue SICPA). Studied inks exhibited a very large tendency to built emulsion with high fraction of dampening solution. The rheological parameters are highly influenced by emulsification. The tack of both the inks is not much influenced by emulsification and it is lower than the tack of conventional CMYK inks. The compositions of dampening solutions did not influence the colour or thermochromic functionality of thermochromic inks. For preparing printing master a 48 lpc screening is recommended.

Keywords: thermochromic, offset, functionality

1. Introduction

Thermochromic (TC) offset inks contain a special pigments that become discoloured while heated. Basic component of pigment is a mixture containing a solvent (a relatively low melting hydrophobic compound), a developer and a dye. When solvent is in the solid state, the dye compound has stronger interactions with developer. The dye experiences more polar environment and becomes coloured. The dye-developer interactions become weaker when the solvent melts and consequently the dye become colourless. The melting point of a solvent determines the temperature region where the colour change occurs. It is then usually denoted as an activation temperature of TC ink. The thermochromic system is encapsulated in a polymeric envelope, usually a melamine formaldehyde resin or epoxy resin. In this form of spherical particles of about micrometer diameters (1-15 μm) it can be incorporated into a binder to produce TC ink (1-4).

During the printing process, the emulsification of dampening solution in an ink occurs. The stability of this emulsion is an important parameter for high quality prints (5). Rheological parameters of TC offset inks significantly differ from rheological properties of conventional offset inks (6). Rheological properties of TC ink are influenced by type of a binding system, size of a pigment (several micrometers), shape of the pigment (spherical particles) and its concentration. However, the rheological behaviour of TC inks in printing machine is also influenced by small droplets of dampening solution emulsified in the ink (7). Therefore it is expected, that the emulsion (ink/dampening solution) would have different tack and rheological parameters comparing to non-emulsified inks.

The TC offset inks result in pastel colours. The TC pigment is sensitive to polarity of its close environment. Therefore dampening solution without alcohol or even distilled water is recommended (4, 8). However modification of water surface tension is needed by adding some additives.

This paper focuses on the interaction of TC offset inks with dampening solutions. The aim of the paper is to determine, whether the composition of dampening solution significantly influences behaviour, functionality and ability of TC inks to be transferred in offset printing process. Other objective is to find significant limitation which could further influence the product design and functionality described in literature (9, 10). Presented work continues in previously published results on properties of TC offset inks investigated by authors (6, 11, 12, 13).

2. Experimental material and methods

Two TC offset inks were used in this study: blue ink produced by SICPA with activation temperature 27 °C and red ink produced by CTI (Chromatic Technologies) with activation temperature 31 °C. Special testing pattern was printed by Man Roland R505 printing press, and these prints will be marked in following text as “commercial prints”. The pattern consisted of areas with range of tone values, areas of lines with different thickness, star target, target with letters of Helvetica font with different body size, and areas with overprints. Printing masters were prepared using 68 lpc and 48 lpc screening. Dampening solution used in the printing press contained 4 % of IPA (Isopropyl alcohol) and 3.5 % of fountain solution Substifix AF (Michael Huber GmbH).

The prints were performed at maximum possible dosed amount of thermochromic inks (upper end of the tolerance interval). A Glossy coated paper (200 g/m²) and uncoated paper (75 g/m²) were used as a printing material. The optical properties of prints were evaluated by spectrophotometer X-Rite 530 and optical microscope.

Additionally, laboratory tests with CTI RED and SICPA BLUE inks were performed. Three dampening solutions were used in emulsification tests. The first was the same as the one used in printing press (contained 3.5 % of Substifix AF and 4% of IPA, marked in following text as IPA 4%), the second was alcohol free (contained 4 % of Dyna Col AC388, PCO Europe B.V. marked as IPA 0%) and the third was modified dampening solution from printing machine with 3.5% of Substifix AF and higher amount of IPA (marked as IPA 8%).

The emulsification tests were done by Duke Ink Water Emulsification Tester Model D-10 (HDuke Enterprises, USA), where fifty millilitres of dampening solution were stirred in fifty grams of an ink and after 1 minute a water pick-up was measured (the speed of stirring was 90 rotations of stirring tool per minute). This is in following test denoted as a cycle. The amount of water pick-up and time needed to attain saturated emulsion were observed.

The tack of emulsified and non-emulsified inks was measured by Tackmaster-92 (Kershaw Instrumentation) at rotating speed 1200 rpm in the time interval of 10 minutes. Consequently the rheological parameters were obtained by rotational rheometer RV1 HAAKE with a cone-plate measuring system (titanium cone with radius 20 mm and angle 1° was used). Both tests were performed at 32 °C. All emulsions and non-emulsified inks (CTI RED, SICPA BLUE) were printed on glossy coated paper (200 g/m²) by laboratory printing device IGT C1. The printing speed was 0.3 m/s and the printing force was set to 250 N.

3. Results and discussions

3.1 Evaluation of commercial prints

Tone values of target fields on prints prepared with theoretical tone values (A_{teor}) in interval 10-100 % with 10% steps were measured by spectrophotometer X-Rite (2° observer, D50) on 10 randomly selected sheets from 250 sheets run length. Effective tone values (A_{eff}) were computed from the reflectance spectra using Murray-Davies equation (14):

$$A_{eff} = \frac{R_W - R_A}{R_W - R_S} \cdot 100 \quad [1]$$

where R_W is a reflectance of white paper, R_A is reflectance of measured area with specific theoretical tone value, and R_S is reflectance of solid area (tone value 100 %). Mean values and range for each area measured are presented in Figure 1 (for coated paper) and in Figure 2 (for uncoated paper). At 68 lpc screening CTI RED ink exhibits different dot gain than SICPA BLUE ink.

It can be observed, that at 48 lpc the change in tone value is very small. Also the range of measured values is much smaller than in case of 68 lpc screening. It can be thus concluded, that the dot gain is smaller for TC inks at 48 lpc screening in comparison to 68 lpc screening, and thus better in use. The tendency of TC inks to gain the dot size is opposite to conventional inks at 48 lpc screening.

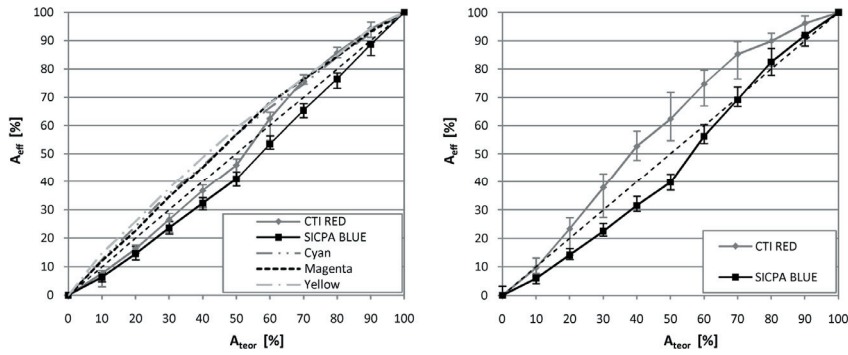


Figure 1: Transfer characteristics of TC inks at 48 lpc (left) and at 68 lpc (right) for coated paper

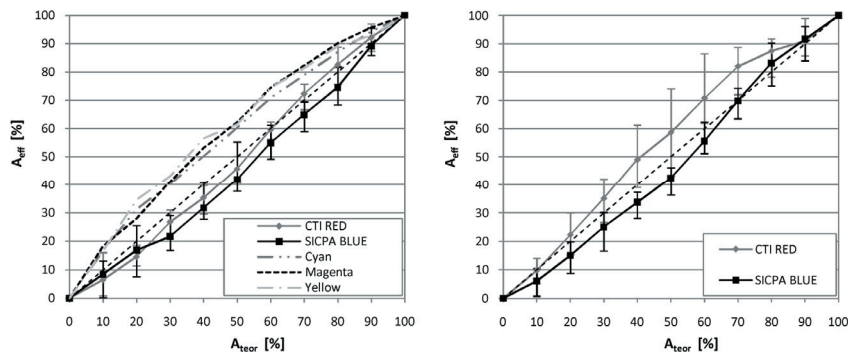


Figure 2: Transfer characteristics of TC inks at 48 lpc (left) and at 68 lpc (right) for uncoated paper

The line resolution for TC inks was observed by optical microscope. The recognition of the highest line frequency was at 16 lines per centimetre (the lines and space between lines had the same width) and the smallest font size clearly reproduced was around 3 points. At the same printing conditions we observed that the line resolution on prints with conventional C, M, Y offset inks was 32 and the font size was 1 point. The reason for lower line resolution of TC inks could be due higher dosage of the ink and a smaller tack, which will be discussed later. Another possible reason is a lower colour contrast due to pastel colour of printed TC inks. The results are similar for both tested screening and both papers.

3.2 Emulsification tests

Results of Duke emulsification test of three types of dampening solutions in TC inks are summarized in Table 1, where are presented numbers of cycles needed for emulsification and volume of the dampening solution that was emulsified after each cycle (expressed as a percentage of the original volume). All 50 ml of all the dampening solutions were emulsified after several cycles. This indicates that the saturated emulsion was not obtained in any case and a higher amount of dampening solution could be probably still emulsified in TC inks. Thus problems with ink optical density and smudging could be expected during longer print runs. Emulsions of CTI RED ink were not stable, small droplets of water could be observed getting out of the emulsion. The increase of the dampening solution dosage in printing press was also observed during commercial prints. These results pointed out a need to control the dosage of dampening solution very carefully. The dampening solution without addition of IPA is more rapidly accepted by both TC inks than emulsions with IPA content.

Table 1: Volume of emulsified dampening solution accepted by TC inks during Duke emulsification test

	Volume of emulsified dampening solution (%)										
Cycle (min)/Sample	1	2	3	4	5	6	7	8	9	10	11
CTI RED IPA 0 %	30	46	60	74	88	98	100	–	–	–	–
SICPA BLUE IPA 0 %	24	44	64	80	87	98	100	–	–	–	–
CTI RED IPA 4 %	30	40	54	66	78	89	98	100	–	–	–
SICPA BLUE IPA 4 %	17	33	45	56	67	75	83.4	89	94	98	100
CTI RED IPA 8 %	23	35	47	62	74	81	87	91	94	97	100
SICPA BLUE IPA 8 %	18	31	45	58	70	80	89	95	98	100	–

3.3 Tack tests

Tack is the force required to split the ink film between two rollers. Tack is an important property in the inking system as well as in the ink/paper interaction and in the ink trapping for multi-colour printing. Figure 3 shows the tack measurement results of two emulsions of TC inks in dependence on time. The tack of the ink was characterised by four parameters: the maximum tack at initial stage (T_1), the time at which the maximum of tack is achieved (t_1), the mean value from the stable middle region (T_2) and the final tack at the end of the test (T_3). Table 2 summarizes results of the tack measurements for non-emulsified and emulsified inks at 32 °C.

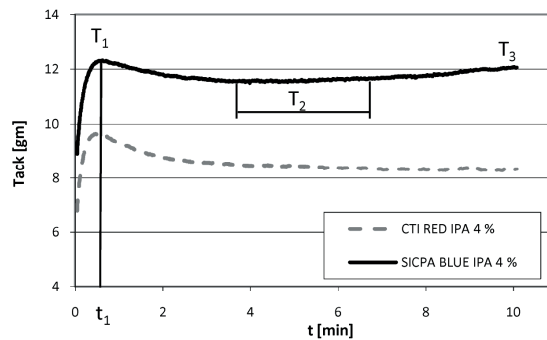


Figure 3: Evaluation of the tack

From Table 2 it is apparent that tested inks have different tack. The tack of red ink from CTI is very low where T_2 and T_3 are between 7.5-8.7 gm. The tack of SICPA BLUE ink is higher than CTI RED (between 11.2-13.5 gm). Another difference between tested inks was their drying process during the test. The CTI RED ink shows almost the same tack in the middle region - T_2 and at the end of test - T_3 (after 10 minutes). It means that this ink does not dry (or very slowly) on the rollers of Tackmaster-92. The SICPA BLUE ink has at the end of the test the tack about 0.5-1 gm higher than in middle region during 10 minutes test. SICPA BLUE ink dried faster than CTI RED. The time dependence of the tack of emulsions with fountain solution Substifix AF with different amount of IPA (4 and 8% of IPA) had a similar course. In case of emulsions with fountain solution Dyna Col AC388 the tack was slightly lower in comparison to Substifix AF.

High tack of inks is generally desirable in offset printing process, but too high tack can result in pulling fibres out of the paper (this negative effect may occur more strongly in dependence on surface properties of papers - coated, uncoated, etc.). Tested inks have low (SICPA BLUE, approximately 8.5 gm) or very low (CTI RED, approximately 11.5 gm) tack which can cause lower sharpness of printed dots. This result was confirmed in chapter 3.1, where CTI RED ink shows lower line resolution than SICPA BLUE. Conventional offset printing inks have tack usually between 12 and 16 gm.

Table 2: Parameters of the tack measurements of non-emulsified and emulsified inks

Tack parameter / Sample	t_1 (s)	T_1 (gm)	T_2 (gm)	T_3 (gm)
CTI RED non-emulsified	30	9.29	7.88	7.59
CTI RED IPA 4 %	28	9.64	8.49	8.32
CTI RED IPA 8%	38	9.55	8.58	8.65
CTI Red IPA 0 %	35	9.17	8.32	8.29
SICPA BLUE non-emulsified	42	13.17	12.51	13.54
SICPA BLUE IPA 4 %	37	12.33	11.64	12.06
SICPA BLUE IPA 8 %	37	12.61	12.00	12.59
SICPA BLUE IPA 0 %	41	11.51	11.21	11.91

3.4 Rheological parameters

Study of the rheological properties of some of the emulsified inks in rheometer with cone/plate geometry was complicated by shear instability of these systems at high shear rates. Measured sample in the gap was not stable due to many interactions of the binder and particles in the system (spherical pigment, drops of emulsified dampening solution). In general the measured emulsified systems had much smaller interval of shear rates, under which the test could be performed. Rheological parameters were computed using Casson equation (15):

$$\sqrt{\tau} = \sqrt{\tau_m} + \sqrt{\eta_c \dot{\gamma}} \quad [2]$$

where τ is shear stress in dependence of shear rate ($\dot{\gamma}$) and τ_m is a Casson yield point, and η_c is a Casson viscosity. Casson yield point describes the transition from the state of the rest to the state of the flow of a liquid and Casson viscosity describes the viscosity at the shear rate limiting to infinity. Table 3 shows calculated parameters of two TC inks studied in this paper. Their parameters ratio (τ_m / η_c) describes the tendency of inks to mist. The higher values indicate the lower tendency of emulsified TC inks to mist. Casson viscosities, which are small for non-emulsified inks are even smaller for emulsified inks.

Table 3: Casson yield point and Casson viscosity of TC inks and theirs emulsions

Visc. par. / Sample	CTI RED			SICPA BLUE		
	τ_m (Pa)	η_c (Pa.s)	τ_m / η_c (s ⁻¹)	τ_m (Pa)	η_c (Pa.s)	τ_m / η_c (s ⁻¹)
Non-emulsified ink	20.72	10.7	1.94	47.15	13.9	3.39
IPA 0 %	–	–	–	383.77	15.8	24.23
IPA 4 %	69.48	4.5	15.39	286.19	7.1	40.13
IPA 8 %	–	–	–	–	–	–

3.5 Laboratory printing tests

The main concern in laboratory prints was to investigate, how different dampening solutions influence the colorimetric parameters of printed layers. During the test each TC ink, and each emulsified ink was dosed to the IGT laboratory device step by step. At each step the printing was performed and weight of transferred ink was measured. Using this process a series of printed samples with increasing amount of transferred ink were obtained. Figure 4 shows a^{*}b^{*} diagram of these series printed on IGT laboratory printing device.

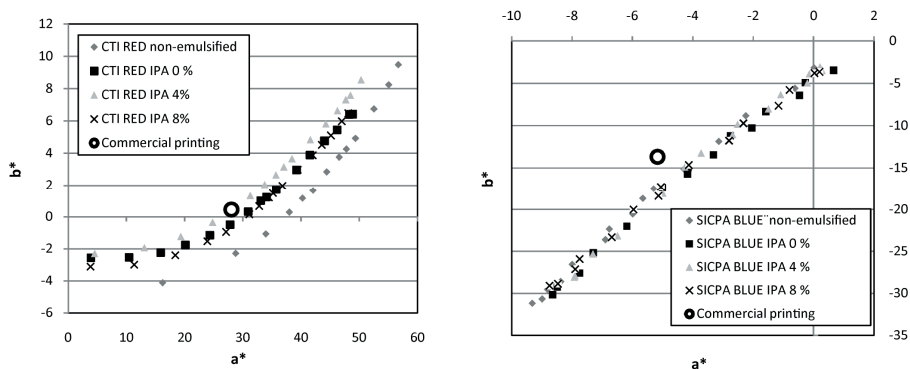


Figure 4: The a^{*}b^{*} diagram of samples printed on IGT laboratory device

It can be seen, that the type of dampening solution does not influence SICPA BLUE ink. The a^{*}b^{*} coordinates of commercial printing, which differ from laboratory prints, could be influenced by the cleaning process of printing press before replacing conventional CMYK inks by TC inks. (ΔE_{ab} is approximately 2.5). Slightly acidic dampening solution influences the colour coordinates of CTI RED inks. The thermochromic functionality was also not influenced by addition of any tested dampening solution. All samples became discoloured when the heating temperature was above the activation temperature.

Consequently the amounts of transferred non-emulsified ink, and emulsified inks, were evaluated with regard to the colour of commercial printing. The evaluation was done by comparing ΔE_{ab} between IGT prints and commercial print (measured on dry ink layer). IGT prints were characterized by the amount of transferred ink. Graphs in Figure 5 illustrate the colour difference in dependence of the ink transfer. The lowest colour difference for CTI RED ink is almost the same for ink transfers around 2.3 g/m² for non-emulsified and emulsified inks. For the SICPA BLUE non-emulsified ink the value is approximately 2.15 g/m² and it is increased by addition of dampening solution to 2.5-2.9 g/m². The difference in the amount of transferred ink is not so different for non-emulsified and emulsified inks. It was expected, that amount of emulsified ink would be much larger to obtain the same colour tint as by non emulsified ink. We attribute this effect to the evaporation of dampening solution. In laboratory prints, the emulsified ink was dosed to the rollers, whereas in printing press the emulsification takes place between the oscillating rollers in touch to the rollers of dampening solution or dampened printing master.

The dosage of TC inks in printing press was set toward higher values than for conventional inks to obtain the maximal colour strength of full area of TC ink. During the printing, a certain amount of dampening solution could be observed in ink ducts. This corresponds with our results of laboratory tests of emulsification. A very high amount of dampening solution is possible to emulsify in TC inks and the emulsion is not stable.

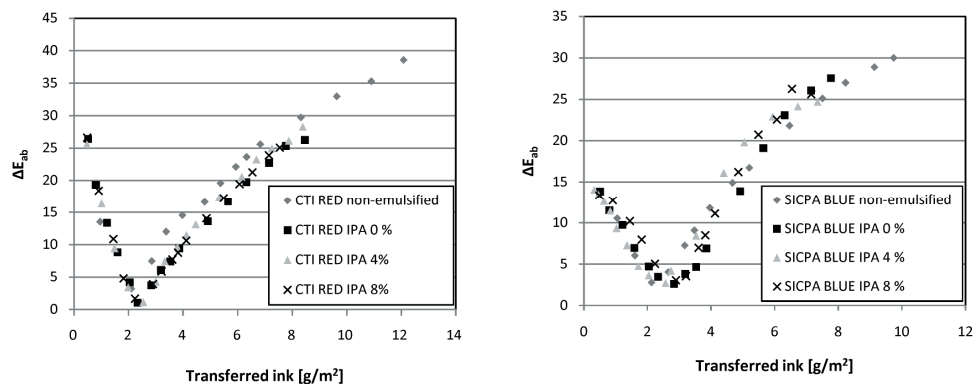


Figure 5: Colour difference in dependence on amount of transferred ink

4. Conclusions

The interactions of TC inks with dampening solutions were investigated. Studied inks exhibited a very large tendency to built emulsion with high fraction of dampening solution. Moreover, the emulsions of dampening solutions and CTI RED ink were not stable. Therefore much effort should be given to control the printing process, especially the amount of dosed dampening solution and the ink. If too much of dampening solution is dosed, smudging could appear during the printing process. The rheological parameters are highly influenced by emulsification in terms of lowering the viscosity and lower tendency to mist. The tack of TC inks is lower than that of conventional inks especially the tack of CTI RED ink. The tack of both the inks is not much influenced by emulsification. The lower tack could negatively influence the sharpness of printed dots or lines; moreover it can negatively influence a trapping of two overprinting ink layers. The compositions of dampening solutions did not influence the colour or thermochromic functionality of the ink layer, even the polar IPA is used in the solution. Therefore no special composition of the solution is needed. However we would recommend performing a test of concrete ink/dampening solution interaction due large variability in commercially available additives. In graphical design it should be taken into account, that letters and thin lines are not very good reproduced by using thermochromic offset inks. We would recommend using fully covered (solid) areas due to the pastel colours of TC offset inks in graphic design images. If some tone values have to be used in the design, 48 lpc is recommended for screening.

Acknowledgements

This work was supported by Ministry of Education, Youth and Sports of Czech Republic research project No. MSM 0021627 501. Special thanks are due to Studio Kozel s.r.o., Czech Republic for performing the commercial prints and enthusiasm to test thermochromic inks in real conditions.

References

- (1) MacLaren D. C., White M. A., (2005), *Design rules for reversible thermochromic mixtures*, Journal of Material Chemistry, Vol 40, pp. 669-676.
- (2) Seeboth A., and Lötzh D., (2008), *Thermochromic phenomena in polymers*, Smithers Rapra Technology Limited, United Kingdom
- (3) Seeboth A., Klukowska A., Ruhmann R., Lotzsch D., (2007), *Thermochromic polymer materials*, Chinese Journal of Polymer Science, Vol 25 (No 2), pp. 123-135.
- (4) Small L. D., Et all (1999), *Thermochromic ink formulations, nail lacquer and methods of use*, US patent no. 5997849
- (5) Kipphan H., (2001), *Handbook of Print Media*, Berlin, Springer Verlag

- (6) Panák O., Kaplanová M., Gunde M. K., Friškovec M., (2010), *Rheological Properties of Thermochromic Offset Inks*, 5th International Symposium on Novelties in Graphics, 27-29 May 2010, Conf. proc. pp. 529-533,
- (7) Coussot P., (2005), *Rheometry of Pastes, Suspensions and Granular Materials*, Wiley, New Jersey
- (8) CTI, *Technical notes: thermochromic offset ink*, (online) (cit. 30.1.2010) available <<http://www.ctiinks.com/images/imagefiles/Offset%20%20Technical%20Sheets/Technical%20Notes%20on%20Thermochromic%20Offset.pdf>>
- (9) Johanson L., (2006), *Creation of Printed Dynamic Images*, PhD thesis, Linköpings Universitet, Norrköping
- (10) Phillips G. K., (2000), *Combining thermochromics and conventional inks to deter document fraud*, Proceedings of SPIE, Vol 3974, pp. 99–104
- (11) Gunde M. K., Friškovec M., R. Kulčar, Hauptman N., Kaplanova M., Panak O., Vesel A., (2011), *Functional properties of the leuco dye-based thermochromic printing inks*, TAGA 63rd Annual Technical Conference, Pittsburgh, March 6-9 2011, Conf. proc.
- (12) Kulcar R., Panák O., Otahalová L., Friškovec M., Kaplanová M., Gunde M. K., (2010), *Dynamic Colour and Appearance of Thermochromic Offset Inks*, 5th International Symposium on Novelties in Graphics, 27-29 May 2010, Conf. proc. pp. 795–800
- (13) Panák O., Hruška J., Kaplanová M., (2010), *Vlastnosti ofsetových termochromných farieb (Properties of thermochromic offset inks)*, Polygrafia Academica 2010, Bratislava 9-10 September 2010, Conf. proc. pp. 795-800
- (14) Green P., Macdonald L.W., (2002), *Colour Engineering: Achieving Device Independent Colour*, West Sussex
- (15) Metzger T. G., (2002), *The Rheology Handbook*, Vincentz Verlag, Hannover



Polymer films with watermark for protected printing production

Alexandr Kondratov, Evgeniy Bablyuk, Marina Dryga, Evgeniya Anokhina

Moscow State University of Printing Arts of Ivan Fedorov
2a, Prianishnikova Street, RU-127550, Moscow, Russian Federation

E-mails: info@mgup.ru; apkrezerv@mail.ru; babliukevgen@mtu-net.ru;
amdicat@yandex.ru; evgeniya_anokhina@list.ru

Abstract

This article is devoted to the new method of protection of labels and other printing products from the falsification, based on using of polymer film with unique optical properties. The reasons of showing up and regularity of the optical and mechanical effects were investigated theoretically and experimentally. The ways of realization of protection method in production of multilayer labels and film package are suggested.

Keywords: polypropylene film structure, protection of pack against falsification, appearing and disappearing, watermark

1. Introduction

One way of solving of task of resistant to the falsification of printing production is using in printing industry printed materials with unique optical and mechanical properties which are producer's "know-how" (Peter Daisler, 2000). This production is protected against copying.

The aims of this investigation are:

- 1). developing of physical basics for new protecting method of printing production (labels, flexible packing) from the forgery by using polymer films with special programmable microstructure and physical properties.
- 2). searching for the optimal combination of the optical and elastic parameters of the polymer films for making label or flexible packing of new type, which is resistant to forgery, and intended for mass consumption goods.

New transparent polymer film material, made of polypropylene, designed for printing protecting tags, multilayer labels and other complicated printing products, is investigated in Moscow State University of Printing Arts of Ivan Fedorov.

It is possible to create special 3-D watermark in volume of polymer material using special technology. Watermark is slightly distinguishable on a gleam, but contrastly appearing in low tension of the film at tensile 5-25% (Alexandr Kondratov, 2010).

2. Methods

Investigation of the elastic properties of the polymer films was carried out by using tensometric devices and testing machines, which allow recording the stretching-elongation diagram in the regimen of constant speed of deformation (stretching) with the 1% accuracy. Study of the optical properties of polypropylene (PP) films and transparence of the watermark was made by photometric measurement in transmitted and in indirect light by using of Tobias TQ+ spectrophotometer.

Screening of the barcode and applying of the PVA varnish layer on the film were carried out on the machine of Argon company.

Modification of the film structure was performed using thermowelder laboratory device HSE-3 of RDM Test Equipment company in the temperature range 120 - 170 °C, under the pressure 20 - 80 psi and treatment time 0.1 - 2 sec.

3. The essence of the proposed method of protection against counterfeit

Previously proposed (Alexandr Kondratov, 2010) design of multilayer adhesive label with detachable label made of new material containing appearing and disappearing "watermark".

The construction of multilayer self-stick protecting label with the tag made of new material watermark. A consumer may check the originality of the label and goods visually by straining flexible label and its fixing in the high-adhesion zone (position 1 or 2 on Figure 1). Watermark in the film's structure, which appears and disappears on the label in tension, may have a form of the narrow stripe, the letter, may have special figure or be producer's logotype. The appearance of the watermark depends on conditions of its obtaining process. It may be a white sign on a transparent background, transparent character on a white background, or these options can transform into each other at different stage of tensile (Figure 1).

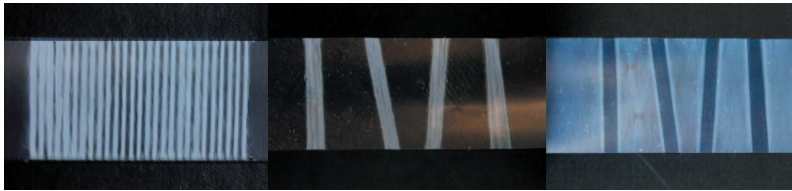


Figure 1: Watermarks, appearing in the film tension (tag of the multilayer label)

One more option: the tag has a shape of bud (flower, leaf) on the narrow stem, which is the stress concentrator. When stretching the label manually, only the stem is deformed, as there is maximum stress in it, i.e. several times higher than the stress in other parts of the tag. During stretching watermark at first appears and then disappears. Two fixation zones of the bud are printed by contrast color and are not covered with the antiadhesive varnish for the precise determination of the value of stretching of the tag of self-stick label (Figure 2).

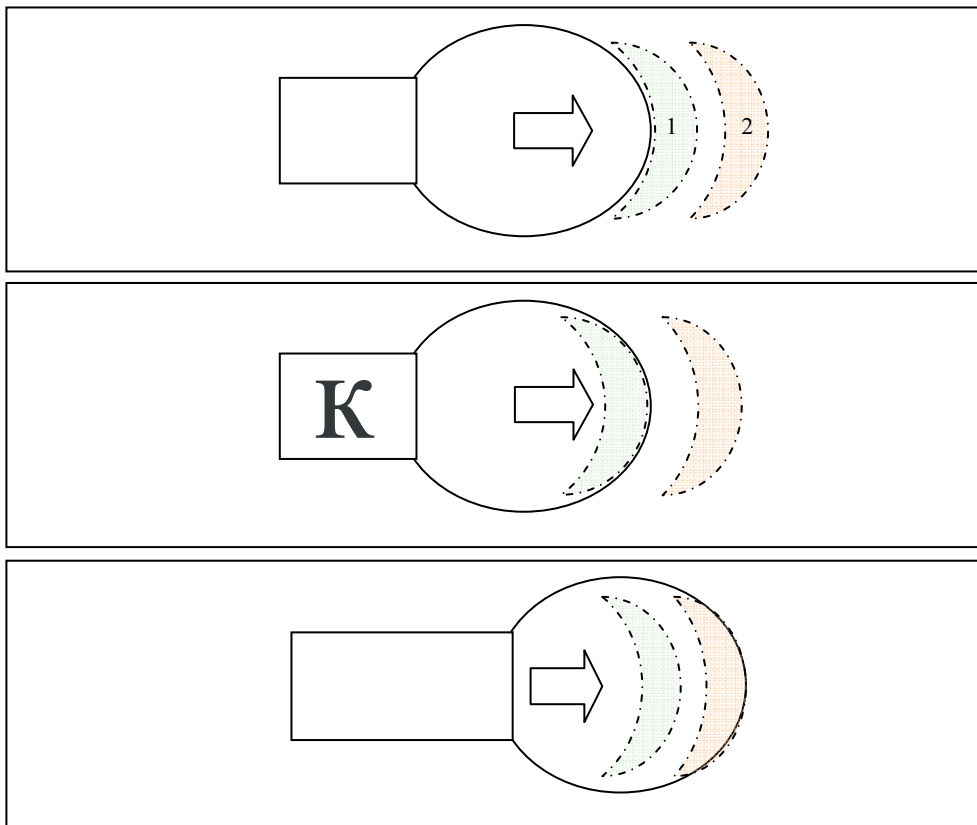


Figure 2: The example of multilayer self-stick label with the flexible tag. Watermark is hidden in the unstrained condition; Watermark appears when the label sticks in the position 1 Watermark disappears when the label sticks in the position 2

4. Mechanical properties of the polymer film

Watermark is a result of local desintegration of the polymer film's structure on the nanosize level. Watermark is formed by nanosized cavities and through-pores, mechanical strength of which differs from mechanical strength of the rest material. It may be formed by: thermal action on the polymer, local ultrasound treatment in combination with the irradiation of film surface by electric charge plasma.

Management of the local polymer's structure loosening in the narrow section is rather difficult if to use isotropic material and usual industrial film of polyolefins, which were subjected orientation stretching when heated in one or two directions.

Satisfying results are achieved when using polyolefin films made by melt extrusion through the slotted jet with the degree of jet stretch 5 - 15 times and cooling on the irrigated steel drum. We used high-density polyethylene and HD-polypropylene with the thickness of $100 \div 200$ microns. Polypropylene film acquires "rigid elastic" properties, i. e. capability to great reversible deformation with high initial modulus when the first tension (Figure 3). Rigid elastic - polymer which has significant reversible deformation even at high elongation besides high tensile modulus, which is between tensile modulus of isotropic (~ 1 MPa) and high-oriented samples (≥ 10 MPa), which brings it closer to the properties of elastomers.

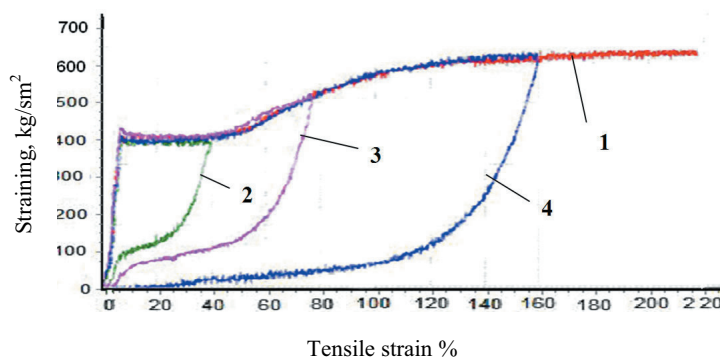


Figure 3: Load-elongation diagram of polypropylene film. 1 - film's stretching before destroying; 2. 3. 4 - tensile elongation up to 40, 75 and 150% with following elastic reduction without load

Load-elongation diagram of polypropylene film (Figure 3) demonstrates "rigid elastic" condition, which allows to use this material for printing deformable parts of the labels, tags and the like packing details. Polypropylene deformation is followed by appearance and then disappearance of milky-white color in the film's sections with "specially reduced rigidity" (Evgeniy Bablyuk, 2010). The initial modulus of polypropylene is $50 \div 130$ MPa, and this modulus is $7 \div 20$ times less at the following stretching, it is 10-20 times less at film's reduction. When the load is removed in any moment when deformation is less than 200%, the sample rapidly recovers its original size practically completely. Elasticity of the material allows its using for making package, originality of which may be checked many times. These unique properties appears under

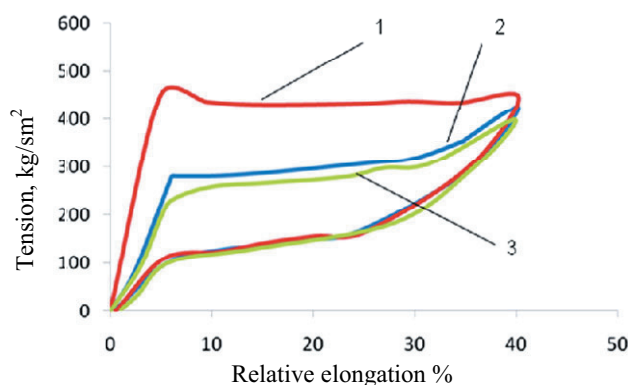


Figure 4: The stretching diagram of hard-elastic PP film up to 40% elongation with following elastic reduction with no load. 1 - first cycle, 2 - second cycle, 3 - third cycle

cycle tension. Effect Patrikeeva-Mullins is characteristic of hard-elastic polypropylene. [Polymer's encyclopedia, 1997] Mechanical properties of any elastomer or film, that has reversible deformation, unevenly change after first tension or contraction. Material becomes softly, and much less effort than in first cycle of tension is required for its tension and whitening in second time and further. This phenomenon is illustrated in the diagram of cyclic stretch of PP, where 1- is the first tension cycle, 2 - is the second cycle.

The third and the following cycles are practically identical (Figure 4). At high speed of tension, which is typically for manual checking of label originality by consumer, material bears more than 100 cycles of tension without significant degradation of properties.

5. Optical properties of polymer film

The basis of the effect of the appearance of a watermark in the films is the effect of local loosening of the structure of semicrystalline polymers during deformation, which was detected and quantitatively described during stretching of ftorlon films in inactive liquid medium (Alexandr Kondratov, 1980; Alexandr Gromov, 1990) using gravimetric of the films method in the drawing process.

It is known that loosening of film's structure during the process of deformation may be localized (in the neck) and delocalized (Alexandr Volynskiy, 1980), i.e. it may occur simultaneously over large areas of the material or immediately over all the polymer body. Both of these extreme cases are well studied, are described in monographs and are fundamental basis for the technology of printed polymer materials with watermarks. For the practical applicability the section of the film, included in the watermark, should have optimal, as a rule, centimeter size, clear, not blurred boundaries; it should highlight by some color or intensity of color on the background of the rest material and it should appear at least once during the film tension.

An attempt of qualitative description of the mechanisms, which determinates the effect of a local "cloud" sections of the polymer film, subjected to tensile strain, was made. It is reasonable to connect the conception of it with the general electromagnetic radiation scattering law of visible range in the mediums, including highly dispersed heterogeneity, the dielectric characteristics of which differ significantly from the characteristics of the dispersion medium - polymer material. In our case, such irregularities are distributed in the film microdefects (pores) that can change its dimensions and shape under the mechanical deformation (stretching) of the film, and restore to original state without this effect. In general, the description of light scattering of the films inhomogeneities can be based on the concept of extinction (dilution) of the light flux in accordance with the well-known law of Bouguer-Lambert-Beer, according to which a thin layer of medium dl dissipates and absorbs light in proportion to the thickness of the layer and to the light flux, passing through the layer. It means that it is true for the scattering

$$dI = -rI dl \quad [1]$$

or in integral form:

$$I = I_0 e^{-rl} \quad [2]$$

where I - luminous flux, l - thickness layer, r - dissipation coefficient

Relations for the absorbing component of the extinction are similar to the relation (1), with one exception, that the exponential dissipation coefficient r changes to the absorption coefficient q . However, since the absorption in the micropores of the material, filled with a medium with a negligible small imaginary part of refractive index, is not important in this paper, it is possible to take into account only the processes associated with the scattering of light. Taking into account the latter condition, the extinction efficiency factor (Q), defined as total energy flow, weakened by a single element of heterogeneity in the material to the total flux of energy, incident on the specified element, considered solely as a factor in the scattering efficiency (Q_s). In the accordance with this assumption, the scattering coefficient of the film, with scattering elements, distributed in it, each fraction of which contains fraction n_i of particles with a cross section of S_i , will take the form

$$r = \sum_{i=1}^{\infty} n_i Q_{s_i} S_i \quad [3]$$

or in integration:

$$r = \int_0^{\infty} S n(d) Q_s dd \quad [4]$$

where d - the characteristic size of the elements

Q_s for spherical cells and, in some approximation, when using the characteristic (equivalent) size of d , for the elements of random shape, takes the following form:

$$Q_s = \frac{8}{3} \alpha^4 \left[\frac{m^2 - 1}{m^2 + 2} \right]^2 \quad [5]$$

where m - refractive index of the element, and the dimensionless parameter α relates the wavelength of incident light λ and the characteristic size (diameter) ratio of d by the relation

$$\alpha = \pi d / \lambda \quad [6]$$

Nonlinear dependence of the efficiency factor of scattering parameter α , in our opinion, is the basis of the effect which is the subject of this paper investigation. A typical dependence Q_s from the specified parameter for transparent dispersed inclusions in transparent dispersion medium for the difference in the values of their refractive indices may support this statement.

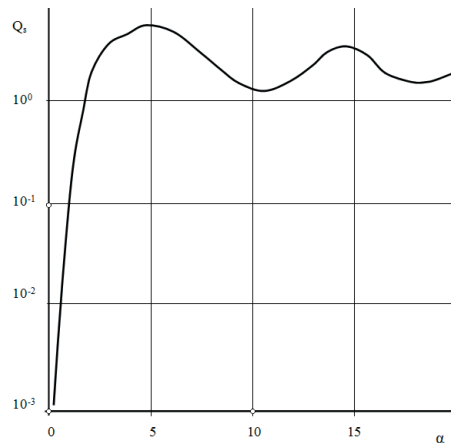


Figure 5: The dependence of the scattering efficiency factor (Q_s) on the parameter α for dispersed phase and dispersion medium with small imaginary parts of refractive index (Kerker M., 1963)

The graph shows that Q_s is very critical to changes of values of the argument, especially for small values of α , with d much smaller than λ . 2-times increasing of the characteristic size of scattering particles in this interval due to film stretching should lead to increasing of efficiency factor of scattering in a 1.5 order of magnitude (16 times), that is in good agreement with the results of experiments with a deformable film, made in this work. Explanation of the "cloud" effect of the film, obviously, might be connected with the fact, that characteristic dimensions of the included pores grow under the tension of the film, and they begin to dissipate the intense light, when they are comparable with the wavelength of the illuminating light (the relative boundary of which can be considered as $\lambda/16$ in accordance with the Rayleigh criterion). And that leads to appearing of the evident white color (by analogy with the fog in the atmosphere). Pores grow under the further deformation and it is followed, figuratively speaking, by "the transformation of white mist in the colorless rain". Relaxation of the film after tensile force removing leads to the opposite process, running with some "hysteresis" effects, that is proved by the dependence, presented in Figure 5.

It is obviously, that statements above determine "blooming" of the deformable film due to scattering of light on the way from the light source to the observer, i. e. "peek-a-boo". But more interesting and practically applicable effect appear when we consider angular dispersion of investigated films. These effects are described by known functions of scattering of Mie theory. The presence of an intense white color of thin polymer film leaves no doubt in multiple interactions between photons and the scattering elements. This fact limits applicability of Bouguer-Lambert-Beer law and makes us to consider mechanism of light scattering of the film with the point of view of radiation transfer. But this theory is not worked out very good (Maikl Kerker, 1963).

6. Variants of applying of polymer films

Authors work out the new constructions of complicated multilayer labels made of nanodispersed film with controlled transparency, methods of protection of printing production from falsification and algorithms of identifications of the originals. For example there is interesting way of protection of label against forgery in which printing of linear element of barcode on transparent film is used. The essence of this method is that linear or two-dimensional barcode, printed on self-adhesive label with the stress concentrator, is deformed specially on prepress stage. The deformation is achieved by reducing of space's width. Deformed barcode is not detected by scanning device.

Reading of such code is possible only when stretching the film in the places of deformation approximately in two times. Surface of the film is closed by rigid cover in proper place. This cover does not allow film to stretch. This is made for localization of stretching in proper place. Film is stretching and whitening strictly locally in the spaces area, which are not covered with rigid varnish. Width of spaces distinguishes proper size in result of local stretching of the film up to 20 - 30%. Herewith bars, printed on the areas, are not stretching. Additional function, which significantly increases level of protection of such labels against forgery is appearing in space area of milky-white color. It has crucial importance because it is known (Electronic resource) that barcode is not read on the transparent film.

Figure 6:
Scheme of barcode's checking



Algorithm of identification process of product using our labels consist of following steps: visual control of transparence of film, mechanical (manual) stretching of label and instrumental control.

Consumer or controller may put an item to the barcode's scanning device, which presents in any sales area, ant may pull the tag in required direction. The aim is checking of product's originality, instruction is printed on the base element of the label. Reading of barcode will prove product's originality. And information on display of scanning device will show to customer necessary information about quality and place of manufacture of goods.

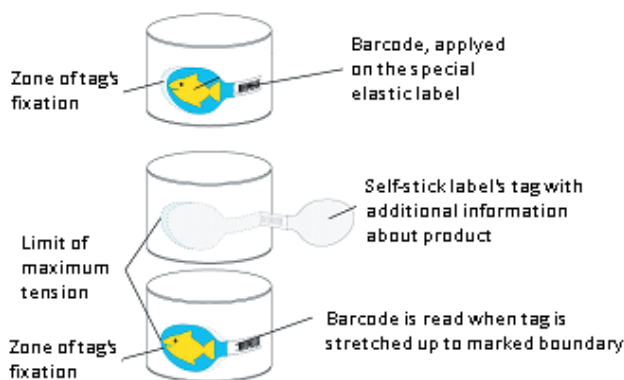


Figure 7: Scheme of checking of product's originality using multilayer label from polymer film with protective-information code printed on it

7. Conclusion

In addition we would like to pay attention of firms which specialize in printing production, protected from falsification, and manufacturers of unique mass consumer goods to the fact that our film is made using low cost polymers. And implementation of these methods of protection against forgery does not require

significant changes in construction of printing and packing equipment. We are ready to continue cooperative researches, developing and patenting printing equipment (for printing of labels). And also developing and patenting additional units of printing machines for applying watermarks on your goods.

References

- Alexandr Gromov, Alexandr Kondratov, (1990), Encapsulation in polymer films, 192 p., Moscow, Chemistry
- Alexandr Kondratov, Marina Dryga, (2010) Polyolefine films with watermarks for protected printing products//University's news. Problems of printing art and publishing industry., № 4, p. 44
- Alexandr Kondratov, Evgeniy Bablyuk, (2010), Multilayer protection label with planar concentrator of stress, Patent RF № 97844 (U1), MPK G09F3/00, published 20.09.
- Alexandr Kondratov, V. Manin, U. Kosarev, (1980), Structural loosening of the amorphous-crystalline polymers under deformation in liquid inactive medium, USSR Academy of Sciences, 1243 p., № 3
- Alexandr Volynskiy, N. Bakeev, (1980), A highly-dispersed oriented state of polymers, Moscow, Chemistry, 192 p.
- Evgeniy Bablyuk, Alexandr Kondratov, A. Erofeeva, Information-protective label, Patent RF № 97843, MPK: G09F, 20.09.2010
- Maikl Kerker, (1963), Electromagnetic Scattering, 213 p., New York.: Pergamon, 1963.- 213p.
- Peter Daisler P., (2000), Labels are against piracy, counterfeiting of well-known producer's goods, Print process. - Heidelberg, Russian version, 4, p. 5-9.
- Bar coding (basic information) - Electronic resource http://markerovka.ru/state/shtrixovoe_kodirovanie.html



Braille dot height impact on the functionality and legibility of the pharmaceutical packaging

*Gorazd Golob*¹, *Bojan Rotar*¹, *Damjan Šulc*²

¹ University of Ljubljana, Faculty of Natural Sciences and Engineering
Aškerčeva 12, SI-1000 Ljubljana, Slovenia
E-mail: gorazd.golob@ntf.uni-lj.si

² Tiskarna Novo mesto, d.d.
Vavpotičeva ulica 19, SI-8001 Novo mesto, Slovenia
E-mail: damjan.sulc@tiskarna-nm.si

Abstract

From October 2005 the EU Directive 2004/27/EC came into force. According to Directive the name of the pharmaceutical product must also be expressed in Braille format on the packaging.

First set of measurements was based on 4 different two-side coated cardboard. We prepare 21 different samples. 18 of them were relief printed on the die-cutting machine by applying different degrees of pressure. The legibility of the names on the pharmaceutical packaging was analyzed with help of nine blind people who have contributed to the successfully completed work. It is evident from the results that the successful reading of the blind is greatly dependent on the height of the dots of Braille.

Second part of the study of the Braille text quality and endurance of embossing tools was based on aluminium matrix and eight different materials for matrix, including steel, brass, plastics (marbafibre) and different photopolymers.

Third part of the study included measurements of Braille text produced in-line tools (Accu-Braille) on folder-gluer, UV ink-jet printed Braille text and UV screen printed on pressure sensitive labels, with analysis of legibility with a group of blind persons with proper skills.

Keywords: Braille, legibility, blind and weak-sighted, embossing, raised printing

1. Introduction

Braille is strongly associated with the blind. Being blind implies that sight is insufficient for reading and Braille gives those people literacy and equality to other people. Taking the varying definitions of blindness into account, it is estimated that 30 million Europeans are blind or partially sighted of whom 1/8 or 3.75 million Europeans are blind. More than 1 million Americans are registered as legally blind.

In the UK, there are some two million people having difficulty seeing, and around one million of these have sufficient sight problems that they could officially register as blind or partially sighted, according to the Royal National Institute of the Blind (RNIB). Somewhere between 10,000 and 20,000 of them use Braille. In Germany there are about 155 000 blind people of whom 15 to 20 % read Braille. There are 3717 members (2005) of Blind and Weak Sighted Association in Slovenia, the number of Braille users is officially unknown but comparable to other countries.

EC Directive 2004/27 requires labeling and information for the partially sighted and the blind to be provided with medicinal products. This includes Braille on the packaging (Article 56a). The European legislation was passed on 31st March 2004, for implementation by 31st October 2005, but the details of how this requirement can be implemented into national legislation have not been promulgated. The first implementation of Braille on food, drinks and pharmaceutical packaging and labels began in 1997 in Europe and USA, so it is not something very new on the market. In September 1997 Universal Braille Dots Inc. submitted a proposal to the Food and Drug Administration in the United States for Braille and large print on the drug labels in USA. We expect that all developed countries will follow the content of EU Directive in their national legislation in near future and that Braille will become widely accepted by food and beverage industry too. The main goal of our work was testing of Braille, embossed or printed on pharmaceutical packaging according to EC Directive and to analyze Braille legibility on pharmaceutical packages and labels.

2. Background

Braille, developed to its full extent in 1825 by young Frenchman Louis Braille, basically consists of a base set-up of 2 dots horizontally and 3 vertically. This gives a total 2^6 dot combinations, 64 in all. As one of the 64 combinations is all zeros - all dots not present -, this is considered as the space rather than a real Braille character (Figure 1).

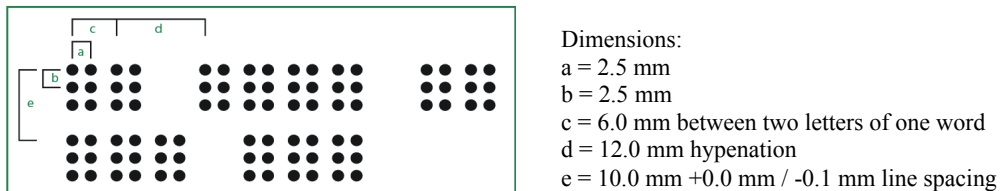


Figure 1: Typical layout of Braille according to the Marbach Medium standard

There are different Braille systems for different European and other languages where the same symbols sometimes have different meanings. For more complex messages a combination of two signs is in use. Capitals, numbers and special characters have initial character first.

The ability to read Braille by sense of touch and transfer the information through the fingers to create understanding, recollection or simple factual recognition requires that the Braille is fully legible, that the user masters the Braille characters and the tactile sense of the blind user is intact.

Braille is typically applied to the packaging through embossing (Figure 2) on the press, die-cutter or even folder-gluer, which is the common process for pharmaceuticals, or with the addition of an ink-jet or screen-printed label. Labels tend to be more robust than embossing, which can be flattened during transport, or fail to achieve sufficient dot height because the board is too thick.

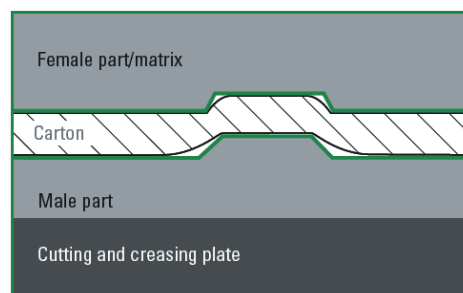


Figure 2: Typical Braille dot formation on die-cutter

There are small differences in symbol dimensions between national Braille systems. To avoid problems the Marbach Medium standard Braille is strongly recommended by EC Directive. The height of the dots is not specified for Marbach Medium standard. It is recommended by EC Directive to use the proposal of The National Council for the Blind of Ireland for the height of the dot 0.5 mm +/- 5 %. It is also recommended to write all names in full (grade 1) Braille, to omit uppercase indicators and to represent the letters A to Z and numbers 1 to 0 in the same way in all countries. Accented characters have to be written in Braille according to the national standard in the country / countries in which such accented characters are parts of the alphabet. Accented characters are typically omitted on pharmaceutical packaging.

Braille dot height in national standards and recommendations (not for packaging) varies from 0.25 mm in Sweden up to 1.0 mm in France. International standard Braille dot height for buildings (i.e. elevators) is from 0.6 to 0.9 mm.

Dot height on pharmaceutical packaging was an object of discussion and research projects of pharmaceutical and packaging industry, their associations and of national and European blind and weak sighted associations. In Great Britain the packaging manufacturers found out that the Braille dot height on pharmaceutical packaging may not be as critical as for Braille books. As a rule, carton-board is embossed to a depth where cracking is not visible to the naked eye. On the basis of tests carried out over several years in different countries, using samples produced by several carton makers, it has been established that a minimum dot

height of 0.12 mm is acceptable for medicinal product identification. This figure has been incorporated into UK Draft for Development Standard DD264:2007. At the CEN Working Group, the 0.12 mm Braille dot height has been challenged by some organizations representing the blind, but no validated evidence has been produced to support the need for a higher Braille dot height. The minimum Braille dot height requirements could be established using a protocol based on a UK pilot study carried out in 2006. A set of medicinal product cartons with varying Braille dot heights from 0.06 to 0.18 mm (in original Harper's text from 0.6 mm to 1.8 mm?) were tested by a group of blind Braille readers of different ages and competences, who were asked if they could identify the product. The results demonstrated correct identification of the medicinal product if the Braille dot height was greater than 0.10 mm. The minimum height of the Braille dots for labels (printed in UV screen-printing) is specified as 0.20 mm in the UK Draft for Development. It is important that the Braille dots are clearly formed. In comparison the Royal National Institute of Blind (RNIB) recommends a minimum height of 0.46 mm. The European Blind Union (EBU) suggests a minimum height of 0.5 mm +/- 0.05 mm.

Study, concluded in 2008 by the University of Birmingham and RNIB in cooperation with other European institutions, was based on legibility investigation and analysis of embossed and printed pharmaceutical packaging. Embossed Braille dot height in the range from 0.06 to 0.23 mm was studied, at height 0.18 mm results were accepted according legibility (67 % of participants definitely recognize text, 27 % probably), but cracking of a board surface was present at this height.

Another difficulty is the measurement method of the height of Braille dots. The use of standard thickness gauge is not suitable because of soft, sensitive dots, the more sophisticated methods are expensive and final evaluation of the results is not always reliable. (Graeme, 2008; Gill, 2006; Goldstein, 2007; Heilbrunn, 2006; Jones, 2005; Makarchuk; Mihelič, 2005; Thompson 2007, West).

3. Experimental

Experimental work has been performed in several steps, including study of the correlation of legibility with dot height, stability of the embossing process and evaluation of the quality of Braille text, printed using different conventional embossing methods, screen printing and ink-jet digital printing techniques.

3.1 Legibility of the embossed Braille text

Table 1: Specification of some technical data of package containing Braille

Sample	Name	Thickness (mm)	Basis weight (g/m ²)	Pressure die-cutter (T)	Braille dot height (mm)
1	Kromopak	0,395	275	38	0,103
2A	Kromopak	0,395	275	38	0,072
2B	Avanta prima	0,450	275	20	0,050
2C	Avanta prima	0,450	275	38	0,088
2D	Avanta prima	0,450	275	43	0,200
3	Kromopak	0,430	300	28	0,121
4	Kromopak	0,395	275	44	0,163
5	Kromopak	0,395	275	46	0,180
6	Kromopak	0,430	300	28	0,093
7	Kromopak	0,395	275	45	0,105
8	Kromopak	0,395	275	46	0,200
9A	Kromopak	0,430	300	18	0,042
9B	Kromopak	0,430	300	38	0,090
9C	Kromopak	0,430	300	47	0,155
9D	Avanta prima	0,485	300	15	0,037
9E	Avanta prima	0,485	300	38	0,087
9F	Avanta prima	0,485	300	47	0,141
10	Avanta prima	0,450	275	30	0,071
11	Package 1				0,128
12	Package 2				0,196
13	Package 3				0,183

For the evaluation of legibility we prepared sample boxes of pharmaceutical packaging, made of different cartons using working punch (nylon) patrix and hard plastic matrix on the die-cutter under different pressure for some samples. We added three commercially available samples, two of them (12, 13) produced using thick UV screen-printed Braille. We measured thickness, roughness, gloss and other parameters of carton-board first (Table 1). On printed and varnished (as usual with water based varnish) boxes we measured Braille dot height using thickness gauge and LM1 laser profile-meter (handheld device using visual measurement option).

Table 2: Numerical presentation of evaluation:

Sample	Persons									Average
	A.P.	A.S.	B.Š.	B.V.	J.N.	M.J.	S.K.	T.J.B.	V.V.	
1	3	1	3	3	3	3	3	3	3	2.8
2A	1	1	1	1	1	1	1	1	1	1.0
2B	1	1	1	1	1	1	1	1	1	1.0
2C	1	3	1	1	3	3	3	3	1	2.1
2D	3	3	3	3	5	5	5	5	3	3.9
3	1	3	1	1	3	3	3	3	3	2.1
4	1	3	1	1	3	5	3	3	1	3.4
5	3	3	3	3	5	3	3	5	3	3.4
6	1	3	1	1	3	1	3	1	1	1.7
7	1	3	1	1	3	3	3	1	1	1.9
8	1	5	1	3	5	5	5	3	3	3.4
9A	1	1	1	1	1	1	1	1	1	1.0
9B	1	3	1	1	3	3	1	1	1	1.7
9C	3	3	3	3	5	5	3	3	3	3.4
9D	1	1	1	1	1	1	1	1	1	1.0
9E	3	3	3	3	3	3	1	3	3	2.8
9F	3	3	3	3	3	5	3	3	3	3.2
10	1	1	1	1	1	1	1	1	1	1.0
11	3	1	3	3	5	3	3	5	3	3.2
12	5	3	5	5	5	3	5	5	5	4.6
13	3	5	5	5	5	5	5	5	5	4.8
Average	2.0	2.5	2.0	2.1	3.2	3.0	2.7	2.7	2.2	

Then we gave our samples to 9 blind people with different Braille skills and competences from the School at Blind and Weak-sight Institute from Ljubljana. They made a short verbal description of the quality of Braille text of each sample, which was recorded and transformed for evaluation into the numbers from 5 (best, perfect legible), 3 (good), to 1 (not legible at all, wrong reading) (Table 2).

3.2 Durability of embossing tools

Second part comprised the study of the Braille text quality and endurance of embossing tools. It was based on aluminium matrix and eight different materials for patrix, including steel, brass, plastics (marbafibre) and different photopolymers. Decreasing Braille dot height using different patrix materials for embossing is presented in Figure 3. Relatively high Braille dots, achieved under optimal setting of the die-cutter and tools, were cracked (Figure 4 and 5) and therefore unacceptable for the customer. Cracked dots give better tactile experience, so dots are more legible compared to the uncracked dots, but damaged surface of the cardboard has negative influence on the confidence of the end-user and general image of the pharmaceutical product and the company.

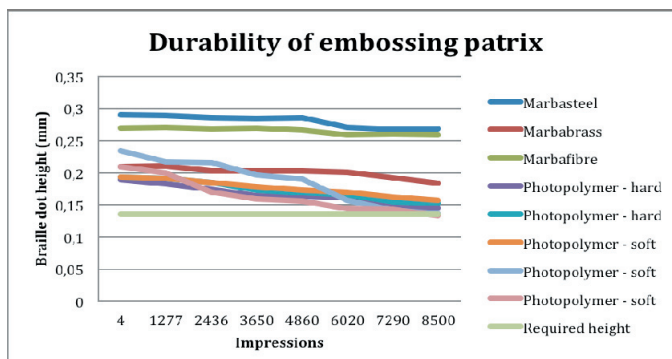


Figure 3: Decreasing Braille dot height caused by low durability of embossing patrix materials

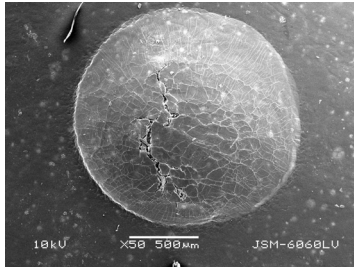


Figure 4: SEM micrograph of slightly cracked Braille dot

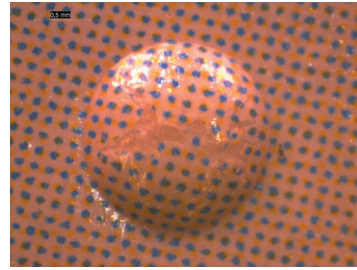


Figure 5: Cracked Braille dot, image taken by optical microscope

3.3 Evaluation of Braille text printed using different techniques

Three sets of samples were prepared for further investigations, using different pressure settings at Accu-Braille unit mounted on Bobst Mistral 80 folder-gluer (Table 3), using InkJet Roland DG LEC-330 UV digital large format printer applying different modulation of Braille dots (Table 4) and UV screen printed samples on pressure adhesive labels (Table 5). Another group of eight persons were included in legibility test, using the same method as in the first investigation of legibility, presented in section 3.1. Braille dot height, measured using digital micrometer are added in Tables 3, 4 and 5. Measurements of transparent UV printed dots performed using PixelProof apparatus were not reliable and were omitted from this paper.

Table 3: Evaluation results of samples, prepared on Bobst Mistral 80 folder-gluer

Sample	Persons									Average	Dot height (mm)
	M.A.	I.T.	I.M.	M.B.	B.Š.	M.S.	A.P.L.	M.M.			
Bobst 1a	1	1	1	1	1	1	1	1	1	1.00	0.136
Bobst 2a	1	1	1	1	1	1	1	1	1	1.00	0.200
Bobst 3a	1		1	1	1	1	1	1	1	1.00	0.146
Bobst 4a	1	1	1	1	1	1	1	1	1	1.00	0.148
Bobst 5a	1	1	1	1	1	1	1	1	1	1.00	0.131
Bobst 6a	1	1	1	1	1	1	1	1	1	1.00	0.149
Bobst 7a	1	1	1	1	1	1	1	1	1	1.00	0.151
Bobst 8a	1	1	1	1	1	1	1	1	1	1.00	0.114
Bobst 9a	1	1	1	1	1	1	1	1	1	1.00	0.159
Bobst 10a	1	1	1	1	3	1	3	1	1	1.25	0.171
Bobst 11a	1	3	1	1	3	3	3	3	3	2.00	0.164
Bobst 12a	3	3	1	1	3	3	3	3	3	2.50	0.200
Bobst 13a	5	3	3	3	3	3	3	3	3	3.25	0.182
Bobst 14a	3	3	3	3	3	3	3	3	3	3.00	0.173
Bobst 15a	5	3	3	3	3	3	3	3	3	3.25	0.184
Bobst 16a	3	5	3	3	3	3	3	5	3	3.50	0.203
Bobst 17a	5	3	3	3	3	3	3	5	3	3.50	0.184
Bobst 18a	3	5	3	3	3	5	3	5	5	3.75	0.232
Bobst 19a	3	3	3	3	5	5	3	5	5	3.75	0.236
Bobst 20a	3	3	3	3	5	5	5	5	5	4.00	0.205
Bobst 21a	5	3	3	3	5	5	5	5	5	4.25	0.222
Average	2.33	2.24	1.86	1.86	2.42	2.42	2.52	2.42			

Samples printed on UV ink-jet printer were modulated using 3 or 5 layers of UV varnish, printed on a basic layer, to achieve proper height. As an option, 3 additional layers have been added for rendering the top surface of a Braille dot. Cracked Braille dot was simulated using printed incision and rough surface with some microdots at the surface of the dot peak (Figure 6).

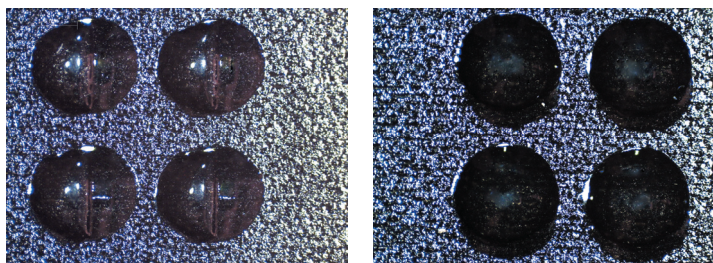


Figure 6: Ink-jet printed Braille dots with incision (left) and microdots (right) on the top

Table 4: Evaluation results of the samples, printed on InkJet Roland DG LEC-330 UV digital printer

Sample	Persons									Dot height (mm)
	M.A.	I.T.	I.M.	M.B.	B.Š.	M.S.	A.P.L.	M.M.	Average	
Roland 3 layers	5	5	3	3	3	3	3	3	3.50	0.250
Roland 5 layers	3	3	5	5	5	5	5	5	4.50	0.420
Roland 5 layers + incision	5	3	3	3	3	5	3	3	3.50	0.350
Roland 5 layers + dots	5	5	5	3	5	3	3	3	4.00	0.350
Average	4.50	4.00	4.00	3.50	4.00	4.00	3.50	3.50		

Table 5: Evaluation results of the samples, printed in UV screen printed technique on pressure sensitive labels

Sample	Persons									Dot height (mm)
	M.A.	I.T.	I.M.	M.B.	B.Š.	M.S.	A.P.L.	M.M.	Average	
Screen 1	3	3	1	3	3	3	3	1	2.50	0.166
Screen 2	3	1	3	3	3	3	5	3	3.00	0.203
Screen 3	3	1	3	3	3	3	3	3	2.75	0.210
Screen 4	3	1	1	3	3	3	3	3	2.5	0.190
Screen 5	3	3	3	3	3	3	3	3	3.00	0.200
Screen 6	1	3	3	5	3	3	3	1	3.38	0.190
Screen 7	3	1	3	3	5	3	3	3	3.38	0.170
Screen 8	3	3	5	3	5	3	3	3	3.50	0.220
Screen 9	5	1	1	3	3	3	3	3	2.80	0.205
Average	3.00	1.89	2.56	3.22	3.44	3.00	3.2	2.56		

During microscopic analysis of the Braille dots, printed using UV screen printing technique, gas bubbles were observed that probably contribute to the dot height (Figure 7).



Figure 7: Gas bubbles in the Braille dot, printed using transparent UV varnish are barely visible

4. Conclusions

The number of samples and involved blind persons with Braille literacy was not high enough to get optimal statistically valid answers and confirmations. It is evident that even blind persons that are not perfect Braille users can use good UV printed or embossed Braille text. During our investigations we found two samples with wrong Braille text, which is unacceptable and life endangering.

It is evident that Braille dot height of 0.12 mm, required by some customers, is the lowest limit for good legible text, best results are expected near 0.20 mm or over Braille dot height. At this dot height, cracking of the carton-board (packaging) surface is present when we use embossing technique. Development and improvement of carton-board is a challenge for substrate manufacturers and packaging producers. Printed Braille text with dot height of about 0.20 mm with smooth, undamaged packaging surface, is better legible compared to embossed Braille text.

Improvements of ink-jet and screen-printed Braille text are in progress. Problems with optical height measurements of printed transparent dots on Pixel Proof device should be solved using new formulation of printing inks or improved system of image analysis.

Further progress of our research work on Braille legibility is expected by optimizing the form of digital printed dots, optimized for blind readers with lower reading skill. It is interesting, that conventional shape of

a Braille dots, printed using ink-jet printing technique were very good legible, however Braille dots with additional features, simulating cracking or roughness of the embossed dots, were confusing even for the experienced blind readers. For general use, traditional embossing methods and materials for pharmaceutical packaging should be improved in the future.

Acknowledgement

Authors acknowledge technical support of the *Grec d.o.o.* Grafično ekološki center, *Lek d.d.* a Sandoz Company from Ljubljana and the *School at Blind and Weak-sight Institute* from Ljubljana for cooperation and support.

References

- Graeme Douglas, Annette Weston, Jennifer Whittaker, Sarah Morley Wilkins, Duncan Robinson: *Braille dot height research: Investigation of Braille Dot Elevation on Pharmaceutical Products: Final Report, 31 January 2008*, University of Birmingham, ISBN: 0704426919 / 9780704426917
- Gill, J.: *Pharmaceutical packaging and labelling for blind and partially sighted people*, Pharmaceutical Technology Europe, Nov 1, 2006
- Goldstein S.: *Packaging News*, 07 June 2007
- Harper, T.: *Touch to communicate*, World Pharmaceutical Frontiers, | www.worldpharmaceuticals.net
- Heilbrunn, J.: *NEWSLETTER No 53 (Chairman)*, EBU Working Group on Pharmaceutical Braille Labelling EBU, December 2006
- Jones, F.: *Compliance Column: Medicine's blind spot*, April 28, 2005, http://www.honeycombconnect.com/printversiondoc.aspx?page=compliance_column&datasource=397&document=5325&hive=12
- Makarchuk, A.: *Braille on pharmaceutical products: Braille information on over the counter drug labels*, Alliance for Equality of Blind Canadians / L'Alliance pour l'Égalité des Personnes Aveugles du Canada (AEBC) – Publications
- Mihelič, B., Čufer, B.: *Podaj mi roko: 85 let organiziranega delovanja slepih in slabovidnih na Slovenskem*, Ljubljana, 2005
- Thompson, A.: *Making an Impression with Braille*, Paperboard Packaging, Jun 1, 2007, <http://www.packaging-online.com/paperboardpackaging/>
- West, R.: *The Value of Braille: Literacy for Blind People Braille*, Authority of the United Kingdom.
- Technical guidelines: Braille in the folding carton production*, Fachverband Faltschachtel-Industrie e.V., August 2005
- The EU Directive relating to pharmaceutical labelling*, http://www.rnib.org.uk/xpedio/groups/public/documents/publicwebsite/public_B2B_pharmaFAQ.hcsp
- Tiresias Scientific and Technological Reports, 2007, http://www.tiresias.org/reports/braille_cell.htm





Evaluating color-difference formulas in LCD-based soft-proofing

Maria Fedutina, Philipp Urban, Edgar Dörsam

Institute of Printing Science and Technology, Technische Universität Darmstadt
Magdalenenstr. 2, D-64289 Darmstadt, Germany

E-mails: fedutina@idd.tu-darmstadt.de; urban@idd.tu-darmstadt.de; doersam@idd.tu-darmstadt.de

Abstract

The prediction performance of three color-difference formulas (CIE76 - Euclidean distance in CIELAB, CIE94 and CIEDE2000) was evaluated on an LCD (Liquid Cristal Display) typically used in soft-proofing applications. For this purpose we conducted an LCD-based visual experiment to analyze perceived color differences around five color centers recommended by the CIE and created a new color-difference dataset. The performance of the color difference formulas to predict these perceived differences was evaluated by the STRESS index, which allows also a statistical analysis whether one formula is significantly better than another. It was found that the CIE94 and CIEDE2000 formulas perform significantly better than CIE76. For default parametric variables ($kL = kC = kH = 1$) the CIEDE2000 formula performs significantly better than the CIE94 formula. If the parametric variables are optimized both formulas perform almost equally. We analyzed the over- and under-fitting behavior of the formulas and could verify the results of other investigations that predicted color differences on typical LCDs are perceived smaller than similar differences on hard-copies.

Keywords: STRESS; color difference; F-test; LCD

1. Introduction

Soft-proofing aims to simulate a printout on a display (Kipphan, 2000). If this simulation is accurate a hard-copy proof can be omitted and costs might be reduced significantly. However, even if we calibrate and characterize a display perfectly and the displayed CIELAB color coordinates are identical to the colors of the hard-copy proof, the question remains whether the displayed reproduction appears equally to the printed one. Please note in this regard that the corresponding colors are only metamers and the broadband spectral stimuli of the hard-copy deviate drastically from the narrowband soft-proof spectra. Furthermore, a much higher luminance level is used for color critical applications to judge hard-copy proofs (see ISO 3664 - viewing condition P1) than in soft-proofing (see ISO 12646).

In this paper we investigate differences of colors shown on a liquid crystal displays (LCD) that almost replaced cathode ray tubes (CRT) in the graphic arts industry. We are especially interested in the following questions:

Are color differences perceived equally on LCDs and on hard-copy prints? Are standardized color difference formulas (*CIE76* - Euclidean distance in CIELAB, *CIE94* (CIE, 1995) and *CIEDE2000* (CIE, 2001) able to predict perceived color differences on typical LCDs? What formula performs best in terms of prediction errors?

To answer these questions we created a suprathreshold color-difference dataset on an LCD commonly used in the graphic arts industry. The experimental setup mimicked the RIT-DuPont experiment (Berns, Alman, Reniff et al., 1991) that was conducted to obtain one of the most reliable color difference datasets. The *CIE94* and *CIEDE2000* formula were partly fitted to the RIT-DuPont data.

We evaluated the performance of color difference formulas to predict our experimental data using a recent measure of disagreement, the Standardized Residual Sum of Squares (STRESS) index (García, Huertas, Melgosa et al., 2007). An F-test applied on STRESS indices of two color difference formulas allows a comparison whether one formula performs significantly better than the other (García, Huertas, Melgosa et al., 2007).

The STRESS index is always in the range of 0 and 100. A larger STRESS index indicates a higher disagreement between predictions and the visual data. The STRESS index vanishes for an errorless prediction. For the RIT-DuPont visual dataset that is based on surface-colors, Melgosa et al. reported STRESS values of approx. 30 for *CIE76*, 20 for *CIE94* and 19 for *CIEDE2000* (Melgosa, Huertas and Berns, 2008).

Finally, we investigated each formula with respect to its over- and under-fitting behavior. Acquiring experimental color difference data is always biased by visual uncertainty. The population's mean color differences are only approximated by the average color differences obtained by a small observer panel, i.e. if we ask different subjects to conduct our experiment we would probably get slightly different results. A color difference formula that performs errorless is likely to over-fit the visual data, i.e. the formula is fitting the visual noise and not the underlying data. Over-fitting can be usually observed for high model complexity such as the *CIEDE2000* formula. If the formula's prediction errors exceed the visual uncertainty then under-fitting is likely. We used a Monte-Carlo-based method recently proposed by Shen and Berns (Shen and Berns, 2009) to detect over- and under-fitting of the investigated formulas.

We start with a brief description of the visual experiment.

2. The experiment

2.1 LCD

The *EIZO ColorEdge 301W* LCD with fluorescence backlight was used in our visual experiment. It allows an exact adjustment of luminance and gamma by means of a hardware calibration. The display was calibrated to a D65 white point with a luminance of 120 cd/m². We used D65 instead of D50 that is typically used for printing applications because the color difference formulas investigated in this paper are optimized for D65. The gamma was set to 2.2. All calibrations were performed with the X-Rite i1 instrument. All stimuli used for the database were measured with the Konica Minolta CS1000 spectroradiometer.

Before starting the experiments we made a detailed characterization of the LCD including:

- Warm-up time,
- Colorimetric stability,
- Calibration performance, and
- Spatial display uniformity.

2.2 Experimental setup

The *method of constant stimuli* (Montag and Wilber, 2003) was used to determine color differences around five color centers that are perceived equally to the difference of two neutral colors, the so called anchor pair colors. For the experiment we chose five color centers recommended by the CIE. These are: CIE Gray, CIE Red, CIE Yellow, CIE Green, and CIE Blue (Fairchild). We investigated 14 directions around each color center (Figure 1). Along each direction five samples were chosen resulting in $14 \times 5 = 70$ test colors for each color center.

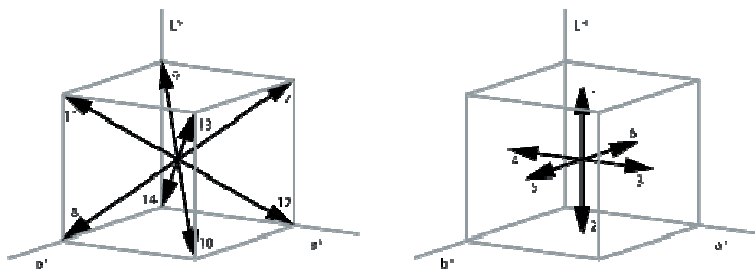


Figure 1: Investigated directions (Berns, Alman, Reniff et al., 1991; Urban, Fedutina and Lissner, 2011)

The software for displaying the stimuli was developed in MATLAB using the Psychophysics Toolbox Version 3 (Psychtoolbox; Brainard, 1997). 31 observers (12 female and 19 male with average age of 33.4 years) with normal color vision according to the Ishihara and Farnsworth D-15 test participated in the experiments.

The stimuli were arranged as shown in Figure 2. The patches covered approximately ten degrees of the visual field. A white border ($(L^*, a^*, b^*) = (100,0,0)$) was displayed simulating the *CIEXYZ* color coordinates of the D65 white point and a luminance of 120 cd/m². The patches were placed on a neutral gray background ($(L^*, a^*, b^*) = (50,0,0)$). The experiment was conducted in a dark black-painted room.

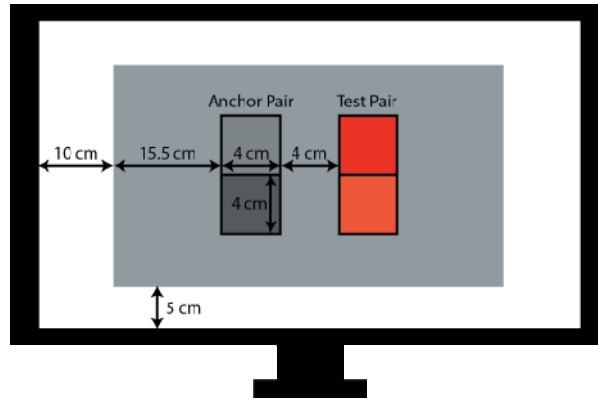


Figure 2: Experimental setup on LCD (Urban, Fedutina and Lissner, 2011)

The observer was asked to select the color pair (test or anchor pair) with the larger apparent color difference. The anchor pair was composed of two neutral gray colors with a color difference of $\Delta V = \Delta E^*_{ab} = \Delta L^* = 2.2$ ($\Delta E^*_{94} = 2.2$, $\Delta E_{00} = 1.97$). Each test pair was composed of a color center and one of the 70 test colors. To avoid memory matching the color positions within the pair and the pairs' positions were switched randomly. After each observer decision a random monochromatic noise was shown for 1.5 seconds before the next patches appeared. A detailed description of the experiment can be found in reference (Urban, Fedutina and Lissner, 2011).

Probit analysis was used to determine a color along each investigated direction with a color difference to the color center that is perceived equally to the anchor pair difference ΔV . These colors were determined as the points where 50 percent of the observers perceived the color difference in the test pair greater than the color difference in the anchor pair. In this paper they are denoted as T50-distances. The dataset was named IDD-LCD (IDD is a German abbreviation for Institute of Printing Science and Technology).

3. Results

3.1 General results

One of the most important results is related to the choice of the anchor pair color. The RIT-DuPont experiment that was performed using surface-based colors for an illuminance level of approx. 2000 lx, which corresponds to a luminance of 636.6 cd/m^2 for a Lambertian white sample. The anchor pair was selected to have a color difference of $\Delta E^*_{ab} = 1.02$. This color difference was clearly visible under the corresponding viewing conditions. In our experiment most observers could not perceive any difference between these anchor pair colors. Therefore, we used an anchor pair with a larger color difference of $\Delta E^*_{ab} = 2.2$. This validates previous observations that differences of colors displayed on an LCD ($120 \text{ cd}/\text{m}^2$) are perceived smaller than differences between similar surface colors shown in a typical viewing booth (2000 lx).

3.2 Color difference formula results

The *CIE94* and *CIEDE2000* equations possess weighting parameters k_L , k_C and k_H that normally are being set to one (Berns, 2000; Luo, Cui and Rigg, 2001; Melgosa, Huertas and Berns, 2008). In this work we optimized these parameters to minimize the disagreement between perceived differences and their predictions (Table 1). This is recommended by the CIE to account for parametric effects such as different viewing conditions. We were surprised to see, that after optimization the parameters for *CIEDE2000* became smaller than one. Sprow et al. obtained parameters greater than one (Sprow, Stamm and Zolliker, 2010).

However, this could be a result of different experimental setups, e.g. the adapting white border as well as the thin black line that surrounded each patch was only used in our experiment.

Table 1: Optimized weighting parameters k_L , k_C and k_H for *CIE94* and *CIEDE2000*

Color-difference equation	k_L	k_C	k_H
CIE94	1.04	0.77	0.69
CIEDE2000	0.92	0.90	0.87

Figure 3 shows ellipsoids fitted to IDD-LCD data for the five color centers (solid ellipses) and iso-distance contours corresponding to the visual difference ΔV for *CIE94* (ellipses with dashed outline) and *CIEDE2000* (ellipses with solid outline). Optimizing the parameters k_L , k_C and k_H mostly improved the prediction performance of the color difference equations as can be seen in Figure 4. Both figures show that the iso-distance contours of the *CIEDE2000* formula in the blue region of the color space consider the special anti-clockwise rotation of the ellipsoids fitted to the visual data.

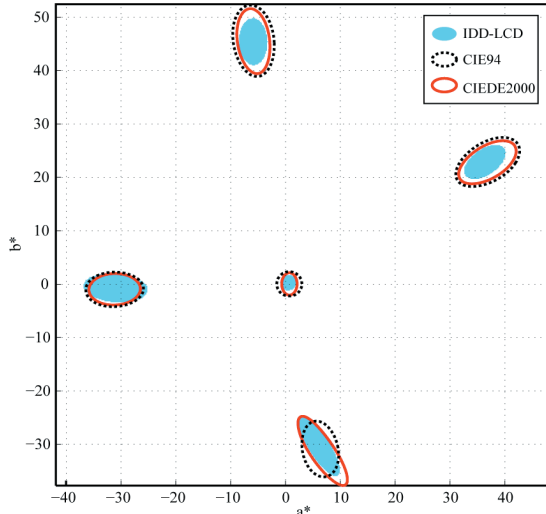


Figure 3: Ellipses fitted on IDD-LCD data and iso-distance contours for *CIE94* and *CIEDE2000* before parameters optimization

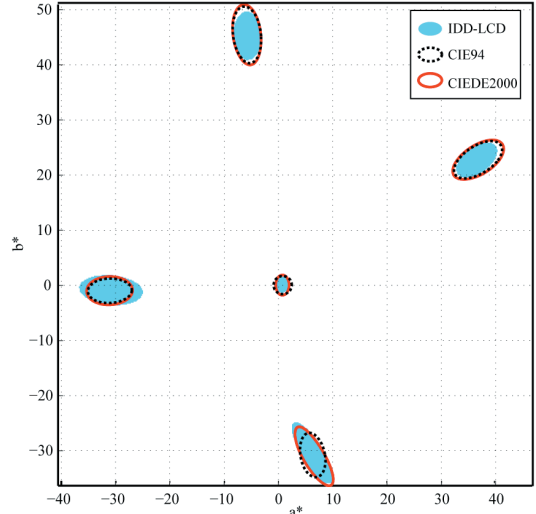


Figure 4: Ellipses fitted on IDD-LCD data and iso-distance contours for *CIE94* and *CIEDE2000* after parameters optimization

3.3 Which formula performs better on an LCD?

To answer this question we calculated STRESS values between each of the investigated color difference formulas and the corresponding visual color differences (Table 1).

The STRESS values of *CIE76* and the non-optimized *CIE94* formula ($k_L = k_C = k_H = 1$) were in the previously reported range. The STRESS value of the non-optimized *CIEDE2000* formula was smaller than expected. A smaller STRESS value indicates a smaller disagreement between the visual data and the formula's prediction.

However, of special interest is the statistical significance of the prediction errors between the color difference formulas that can be calculated by an F-test utilizing their STRESS values. F-tests show that the prediction performance of the *CIE94* and *CIEDE2000* formulas are significantly better than the performance of the *CIE76* formula. According to the F-test the non-optimized *CIEDE2000* formula performs significantly better than the *CIE94* formula.

However, the STRESS value of *CIE94* formula was reduced significantly by the optimization whereas the STRESS value of *CIEDE2000* remains nearly constant. Comparing both STRESS values by the F-test shows no significant differences between the prediction performances of the optimized formulas. (F-test result is located between F-test values F_c and $1/F_c$). Table 3 summarizes the significant differences between the investigated color-difference formulas according to the F-test.

Table 2: STRESS values and F-test results for comparison of performance of color-difference equations

STRESS values				
<i>CIE76</i>	<i>CIE94</i>		<i>CIEDE2000</i>	
	Optimized k	Not optimized k	Optimized k	Not optimized k
31.30	16.83	20.93	15.23	15.33
F-test between <i>CIE94</i> and <i>CIEDE2000</i>				
F-test result	Optimized k		Not optimized k	
	1.22		1.86	
F_c	1.61			
$1/F_c$	0.62			

Table 3: The arrows point to the color-difference formula that performs significantly better according to the F-test

	CIE76	CIE94	CIEDE2000	CIE94 optimized	CIEDE2000 optimized
CIE76		↑	↑	↑	↑
CIE94	←		↑	↑	↑
CIEDE2000	←	←			
CIE94 optimized	←	←			
CIEDE2000 optimized	←	←			

3.4 Do the color difference formulas over- or under-fit the visual data?

A formula’s prediction accuracy is not the only measure of performance. Due to uncertainty of the visual data, average color differences obtained by the visual experiment are usually not the population's average color differences. A formula that accurately predicts such biased color differences are likely to over-fit the data. A formula with large prediction errors under-fits the data.

Recently, Shen and Berns proposed a method to analyze the over- and under-fitting performance of a color difference formula by considering the uncertainty of the visual data (Shen and Berns, 2009). They use a Monte-Carlo approach to calculate a large number of STRESS values between T50-distances and randomized color differences based on the fiducial limits (standard errors). These STRESS values indicate the visual uncertainty of the data (see Table 4, columns 2-5). By calculating F-tests for each of these STRESS values and STRESS values shown in Table 4, columns 6-10, we obtain percentages of significant differences that are used to determine over- and under-fitting (see Table 5). A detailed description of the method would go far beyond the scope of this paper and we refer to the original paper for details [Shen and Berns, 2009].

Table 4: STRESS values measuring the uncertainty of the data set and deviation of the color-difference formulas from visual color difference

Color Center	STRESS values								
	Between the randomized and the T50 visual color differences				Between the color-difference equations and visual color difference of the anchor pair				
	Mean	Max	Min	Std	CIE76	CIE94		CIEDE2000	
						Optimized k	Not optimized k	Optimized k	Not optimized k
Gray	6.84	27.31	1.96	3.27	19.54	12.27	20.16	15.35	15.24
Red	6.28	17.59	1.92	2.12	17.68	8.08	14.34	9.69	10.74
Yellow	7.07	22.79	2.20	2.92	20.52	17.69	24.24	16.86	16.63
Green	4.48	9.79	1.51	1.15	31.91	14.64	13.40	12.93	13.22
Blue	4.79	10.99	1.29	1.28	27.06	18.06	21.05	12.65	12.34

Table 5: Percentage of F-test results. The "larger"/"smaller" columns show the percentages of F-tests for that the formula's STRESS value (based on T50-distances) is significantly larger/smaller than the randomized-difference-based STRESS values describing the uncertainty of the visual data

Color center	Percentage of F-test results for 5000 randomized visual color differences comparing with different color-difference equations (deviation to the T50 visual color differences)									
	CIE76		CIE94				CIEDE2000			
	larger	smaller	Optimized parameters		Not optimized parameters		Optimized parameters		Not optimized parameters	
			larger	smaller	larger	smaller	larger	smaller	larger	smaller
Gray	88.92	0.00	67.66	0.20	89.58	0.00	80.46	0.04	80.46	0.04
Red	94.06	0.00	21.10	0.32	82.52	0.00	40.82	0.02	40.82	0.00
Yellow	91.7	0.00	85.68	0.00	96.22	0.00	83.42	0.00	83.42	0.00
Green	100.00	0.00	99.56	0.00	98.8	0.00	98.20	0.00	98.2	0.00
Blue	100.00	0.00	99.92	0.00	100.00	0.00	95.28	0.00	95.28	0.00

In Table 5, smaller percentages indicate a better performance. Values in bold face show where a color-difference formula under-fits the data at the corresponding color center for a critical value of 99.5% (approx. three standard deviations), i.e. the prediction error of the color difference equation is significantly higher than the uncertainty of the visual data. The critical value was suggested by Shen and Berns (Shen and Berns, 2009). No color-difference formula over-fits the data. As expected, *CIE76* has the worst performance and under-fits the data at two color centers (green and blue). *CIE94*, especially the optimized version, performs much better, but under-fits the data at the same color centers. *CIEDE2000* does not over- or under-fit the data.

4. Conclusions

We can draw the following conclusions:

1. Color differences perceived on typical LCDs appear smaller than surface-based color differences. This is especially important for soft-proofing applications since small color differences that are apparent on hard-copy proofs might be below the just noticeable difference on LCDs.
2. *CIE76* performs significantly worse than *CIE94* and *CIEDE2000*. *CIEDE2000* is significantly better than *CIE94* for the default parameters ($k_L = k_C = k_H = 1$). In case these parameters are optimized *CIE94* and *CIEDE2000* perform similar.
3. None of the three investigated formulas over-fit the visual data. *CIE76* and *CIE94* under-fit the visual data at some color centers. *CIEDE2000* does not under-fit the data independent of parameter optimization.

Acknowledgment

We thank Ingmar Lissner for supplying Matlab code for ellipsoid fitting and plotting. The research was financially supported by the German Research Foundation (Deutsche Forschungsgemeinschaft).

References

- Berns (2000). *Billmeyer and Saltzman principles of color technology*, John Wiley & Sons, Inc.
- Berns, Alman, Reniff, et al. (1991). "Visual Determination of Suprathreshold Color-Difference Tolerances Using Probit Analysis." *COLOR research and application* 16.
- Brainard (1997). "'The psychophysics toolbox'." *Spatial Vision* 10.
- CIE (1995). *CIE Publication No. 116*. "Industrial colour-difference evaluation". Central Bureau of the CIE, Vienna.
- CIE (2001). *CIE Publication No. 14*. "Improvement to industrial colour-difference evaluation". Central Bureau of the CIE, Vienna, 2001.
- Fairchild *CIE TC1-34 Testing Colour-Appearance Models: Guidelines for Coordinated Research*. Munsell Color Science Laboratory Center for Imaging Science Rochester Institute of Technology.
- García, Huertas, Melgosa, et al. (2007). "Measurement of the relationship between perceived and computed color differences." *J. Opt. Soc. Am* 24.
- Kipphan (2000). *Handbuch der Printmedien*. Berlin Heidelberg, Springer-Verlag.
- Luo, Cui and Rigg (2001). "The Development of the CIE 2000 Colour-Difference Formula: CIEDE2000." *COLOR research and application* 26.
- Melgosa, Huertas and Berns (2008). "Performance of recent advanced color-difference formulas using the standardized residual sum of squares index." *Optical Society of America* 25.
- Montag and Wilber (2003). "A Comparison of Constant Stimuli and Gray-Scale Methods of Color Difference Scaling." *COLOR research and application* 28.
- Shen and Berns (2009). "Evaluating Color Difference Equation Performance Incorporating Visual Uncertainty." *COLOR research and application* 34.
- Sprow, Stamm and Zolliker (2010). *Evaluation of Color Differences: Use of LCD monitor*. Color and Imaging Conference, San Antonio, Texas, USA.
- Urban, Fedutina and Lissner (2011). "Analyzing small suprathreshold differences of LCD-generated colors." *Journal of the Optical Society of America Early Posting*.
- Psychtoolbox. Retrieved 21.06.2011, from <http://psychtoolbox.org>.

Colour effect changes at security graphics due to print media and colour sequence

*Erzsébet Novotny*¹, *Rozália Szentgyörgyvölgyi*², *Pál Görgényi-Tóth*³

¹ PNYME/Állami Nyomda Nyrt
Fő utca 6, H-1027 Budapest, Hungary
E-mail: novotny@any.hu

² Óbuda University
Doberdó út 6, H-1034 Budapest, Hungary
E-mail: szentgyorgyvolygyi.rozsa@rkk.uni-obuda.hu

³ Állami Nyomda Nyrt.
Halom utca 5, H-1102 Budapest, Hungary
E-mail: gorgenyi@any.hu

Abstract

At colour reproduction of security graphics, there are often significant colour distortions resulting from the features of design, approval and production processes associated with guilloche patterns. The overall colour effect of the printed product may differ from the approved graphic design or proof as well. The colour effect differences are due to a number of reasons: printing technology, different colorimetric properties of inks and base materials, etc. Changes to the sequence of colours being printed may also lead to deviations in colour.

We realised that most of researches are concerned with the colour management problems of four-colour printing, while the direct-colour line art reproduction has received much less coverage. Because of it our research aimed to determine the extent of colour distortions generated during the security graphics reproduction and identify the reasons for variations in colour effect.

We examined the changes in line thickness and colour of the patterns. We concluded that, in order to get the proper colour effect, the printing order of colours and the vertical or horizontal position of security graphic elements on the sheet must definitely be specified during the design process.

Keywords: security printing, guilloche design, line art reproduction, colour measurement

1. Introduction

Security printing as a means of protecting documents, labels, packages against counterfeiting, forgery, tampering, and other fraudulent is very important nowadays. Protection against counterfeiting consists of various security elements: these elements may be incorporated in the media materials, created using print technology solutions, or produced based on special procedures. Depending on the function of printed matter, security elements visible to the human eyes (Figure 1), as well as ones only visible using simple or complex devices (Figure 2) are both used. A combination of the two results in the appropriate security level of the printed matter. (Prado, 2004) (Warner, Adams, 2005)

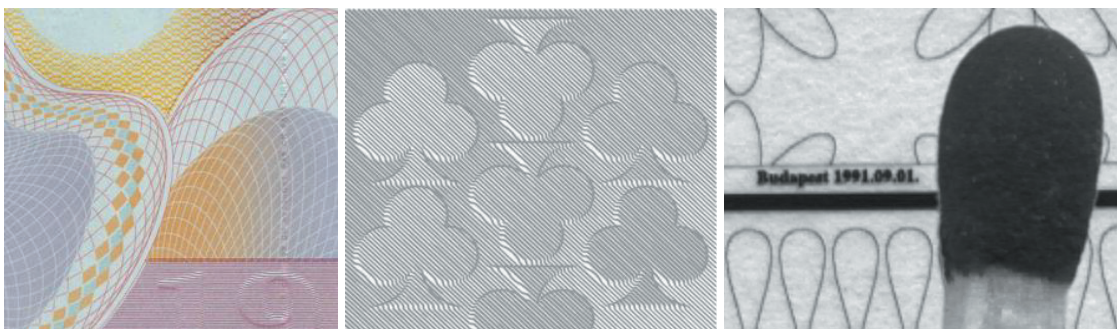


Figure 1: Visible security elements - rainbow print (left), relief (middle), micro-script (right)



Figure 2: Security elements, visible without (left) and then by special illumination (right)

The production of securities sets strict requirements with respect to the entire production process. An important aspect in the design of securities is the aesthetically pleasing appearance of the graphics printed on the security and, at the same time, the use of a layout and technology which make their reproduction difficult. (Eiler, 2007) (Leparmentier, 2007).

Printed matter that is protected against counterfeiting contains, as visual elements, characteristic patterns consisting of a complex system of delicate, thin lines (Figure 3). This is the so-called guilloche pattern, which is special graphics made up of complex shapes and very subtle lines with varying line thickness, which cannot be reproduced in good quality using photocopying or other conventional techniques. The shape and dimensions of mathematically determined, periodic function patterns are today developed using computer-based design software. (Giotto, 2009)

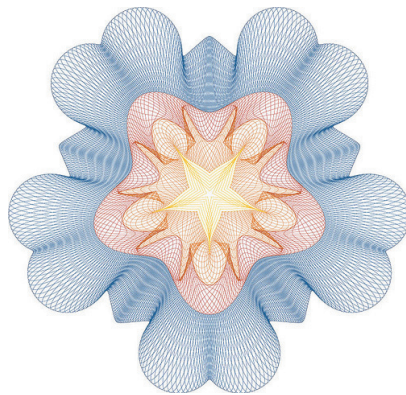


Figure 3: Multicolour Guilloche pattern

Approval of security graphics is also implemented through digital proofs before printing, just like other printed products today. Digital proof procedures do not use these direct colours, which makes the accurate colour reproduction of guilloche patterns more difficult. Although today's proof devices are able to make prints in 12 colours, which results in a significant improvement in terms of the rendition of direct colours, the proof printer must be calibrated to the relevant printing conditions to ensure conformity with the printing process. (ColorAcademy, 2006)

2. The objectives of the research

Technical literature and the majority of printing industry standards are concerned with the colour management problems of four-colour printing, while the issue of colour modifications in case of superimposing line-based graphical objects using direct colours has received much less coverage. (Pekaricova et al., 2009) Because of the lack of research findings on the subject, major problems arise in security printing as well, where the guilloche pattern, one of the visual elements of security prints, is created by printing direct-colour line-based graphical objects next to and on top of one another. There is often significant colour distortion resulting from the peculiarities of the design, approval, printing and possible finishing processes associated with guilloche patterns. The overall colour effect of the finished product may differ from what the customer expected, or from the approved graphic design or proof. In such patterns,

colour effect differences are due to a number of reasons. Some of these are technological issues, e.g. the fact that the digital proof used for design purposes and the printing procedure are based on different principles. The colorimetric properties of inks also vary, and the surface and colorimetric properties of the base materials used may also be different. In addition, changes to the sequence of colours being printed may also lead to deviations in colour. Furthermore at the second or further print runs of securities is also essential to apply the first run's setting because the overall colour effect can be change and it can cause problem with costumers. (Malacara, 2002)

3. Test printing

To review changes in colour effects, we first designed a two-colour guilloche pattern, and then prepared a test form incorporating the guilloche pattern and the field-based version of the same. In order to be able to analyze changes in line thickness, we included in the test form a sequence of five line grids using lines with a thickness of 30, 50, 70, 90, 110 μm and a filling ratio of 10, 25 and 50%. Furthermore, we incorporated also full-tone fields to examine the influence of the order of printed colours.

We made digital proofs based on the test form using an Epson Stylus Pro 7880 proof printer. We prepared the print on six of the materials (offset paper, matt coated paper, Casino Classic card paper, water-marked security paper, PVC core foil, Tyvek foil) that are most commonly used in industrial practice at security printing, which varied widely in terms of their type and printability. We selected colours that are the most frequently used for the production of security prints. We also varied the colour sequence of the patterns during the printing process to know how the colour effect of the lines printed with direct colours on top of one another alters when the colour sequence changes. (Figure 4)

The examined colour pairs were:

P284 Blue - P727 Ocher

P346 Green - P021 Orange

P128 Yellow - P211 Rose

P1785 Red - P429 Grey

The printing process was performed on a Heidelberg Speedmaster SM 52-4+L UV-curing sheet-fed offset press with Schneemann Supra UV inks, and under standard operating conditions.

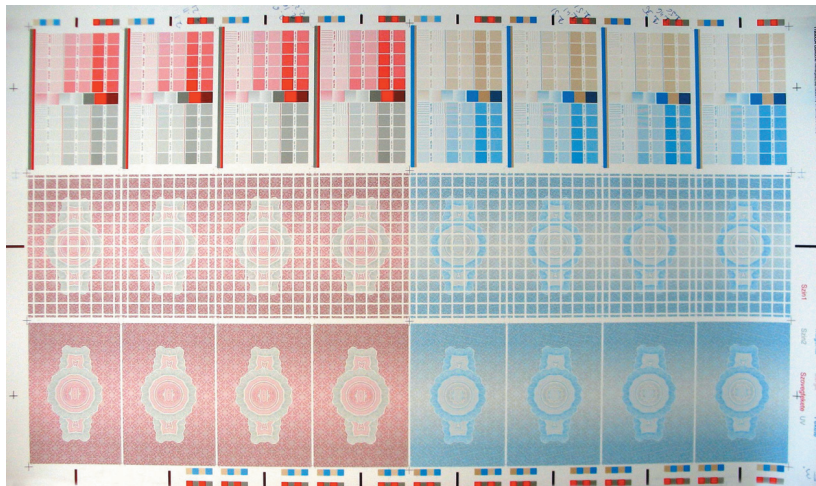


Figure 4: Printed sheet of red-grey and blue-ocher pairs on Casino Classic paper

4. Measurements and evaluation of the results

The prints and proofs were examined not only instrumental measurements, but also visual comparison, the most important aspect for the customer being the conformity of the finished product with the overall effect he deemed acceptable according to his original design and the proof that has been presented to him and approved by him. (Figure 5)

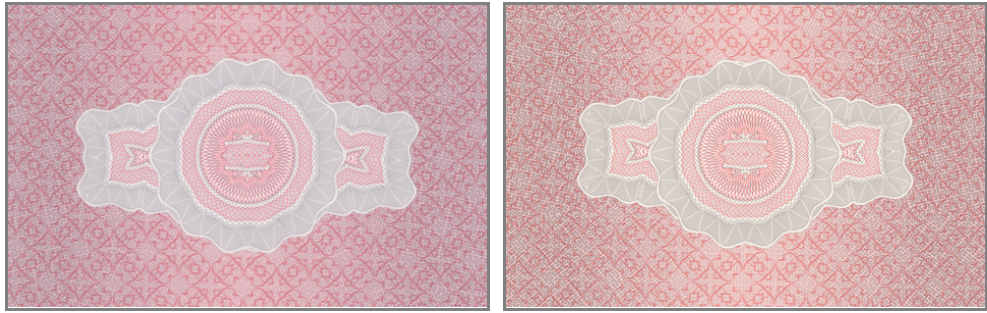


Figure 5: Proof (left) and print on Casino Classic paper (right) of the test guilloche pattern

4.1 Line thickness and filling ratio changes

For examination of the line thickness of guilloche patterns (Figure 6) we used Mitutoyo Absolute Digimatic built-in calliper ruler, and Mitutoyo precision measuring magnifier. Based on our measurements we realised that the line thickness increase depends on the line vertical or horizontal position (to printing run direction) significantly. We observed 20-60 µm increase in thickness at the vertical lines depending on original line thickness and printed media. At the horizontal lines the average value of increase was smaller, 20 µm. The proof also showed a difference to the original value.

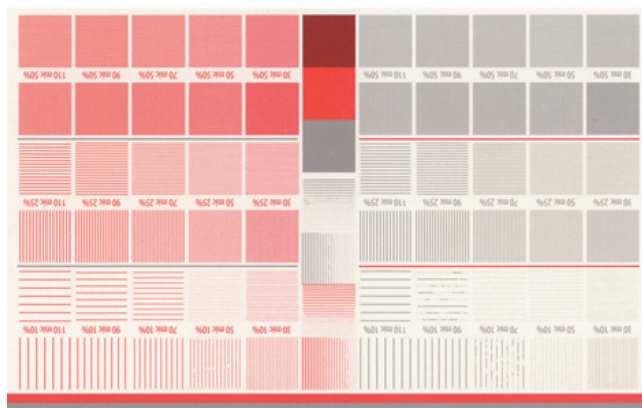


Figure 6: Test chart for lines

The effect of the line thickness increase can be observed at the results of filling ratio examination. The fields of vertical lines differ from fields of horizontal lines in increasing of filling ratio significantly. For example the next diagrams (Figure 7-9) show the results at red colour.

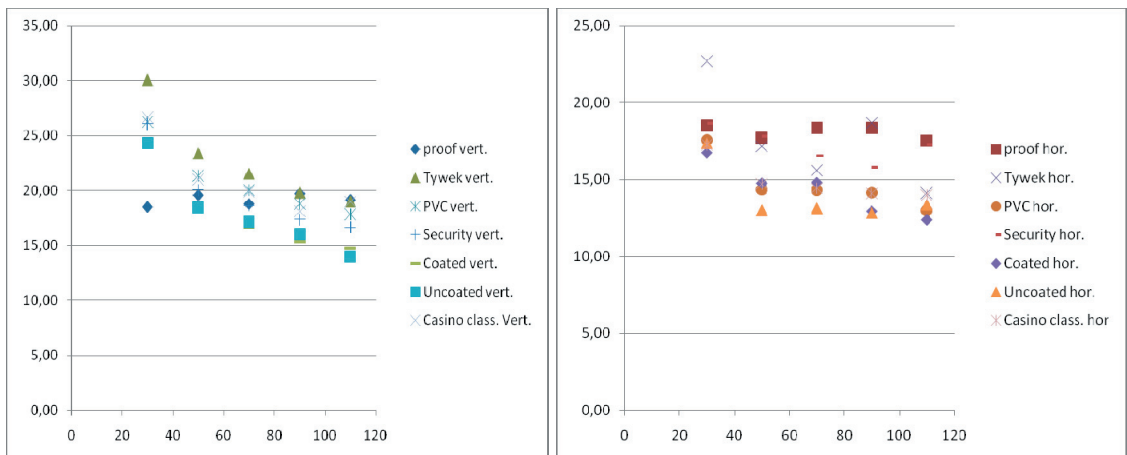


Figure 7: Increase in filling ratio at 10% in the case of different print media and proof (vertical and horizontal lines with thickness of 30, 50, 70, 90, 110 µm)

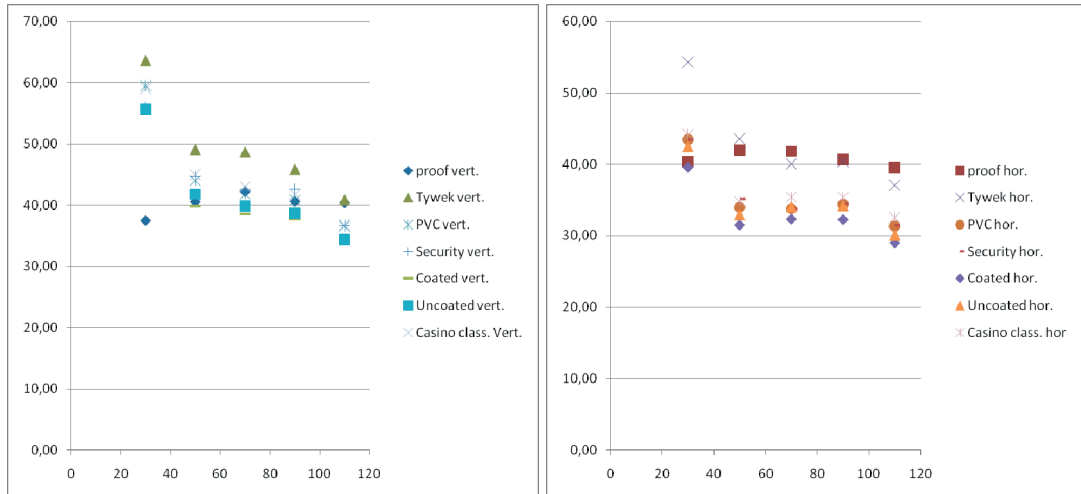


Figure 8: Increase in filling ratio at 25% in the case of different print media and proof (vertical and horizontal lines with thickness of 30, 50, 70, 90, 110 μm)

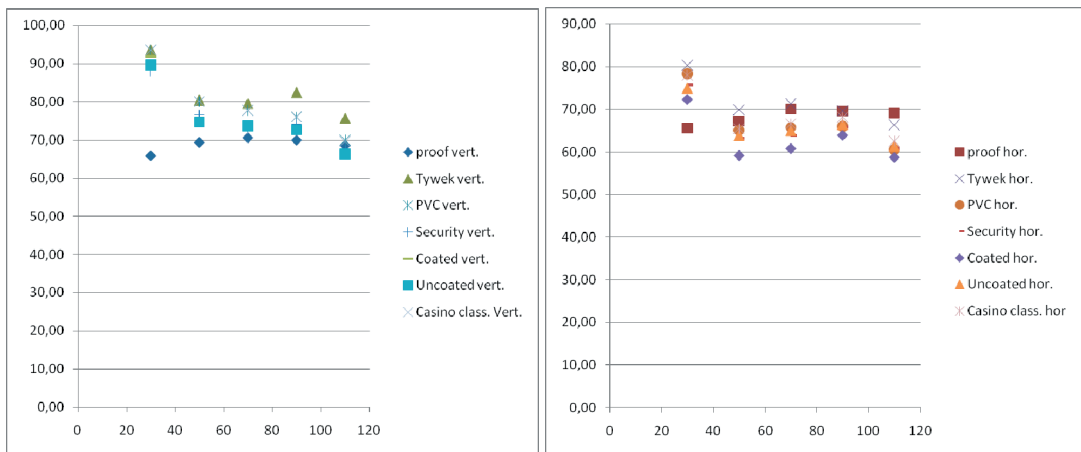


Figure 9: Increase in filling ratio at 50% in the case of different print media and proof (vertical and horizontal lines with thickness of 30, 50, 70, 90, 110 μm)

All in all, the smallest line thickness variation in comparison with the original value was seen with ochre lines, taking into consideration all reviewed colours. The colour showing the largest variation, on the other hand, was green and red.

Based on our analysis of line thickness, and filling ratio changes, we concluded that, from among our base materials, coated paper and security paper were characterized by the lowest amount of line distortion (Figure 10), while the largest differences were seen on Tyvek special plastic foil. On this printing medium, lines with a thickness of 30 μm are intermittent and the thickest. The images, printed on this surfaces, and the PVC core foil are uneven, line edges are wavy (Figure 11).

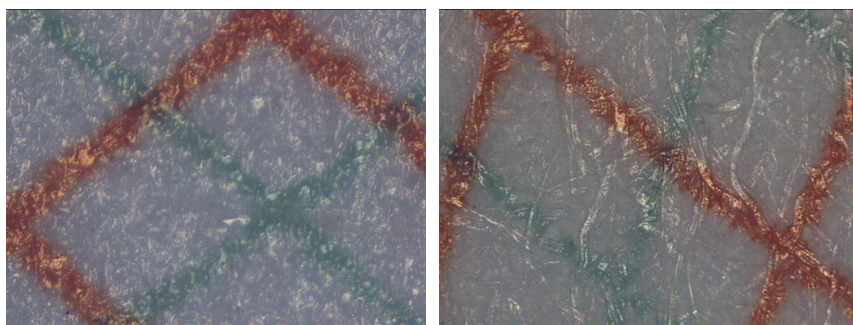


Figure 10: Video-microscopical picture on coated (left) and security (right) paper

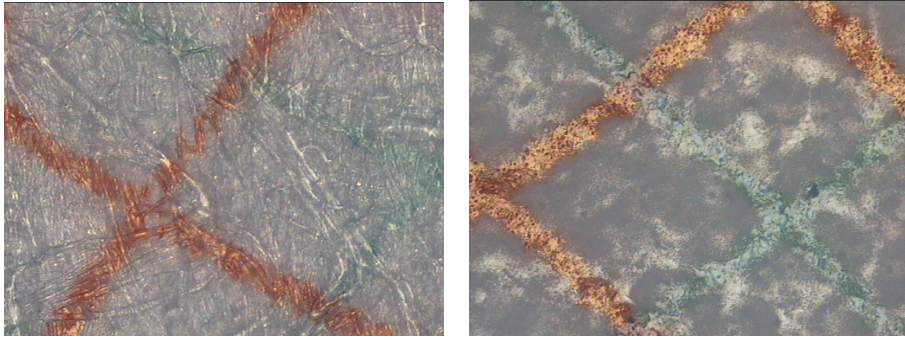


Figure 11: Video-microscopical picture on Tyvek (left) and Casino Classic (right) printing media

4.2 Colour differences

A GretagMacbeth SpectroScan spectrophotometer was used to measure the chromatic stimulus values of printed patterns. We measured fields with a filling ratio of 100%, looking at both direct colours and the L^* , a^* , b^* colour coordinates of superimposed colours. Using the colour coordinates of the digital proof as a reference, we calculated the ΔE^*_{ab} colour difference, and ΔH^*_{ab} values.

Colour effects deviated from the digital proof in both printing rounds, with the largest variations shown by green and red. On the contrary, blue and yellow were characterized by the smallest amount of colour deviation.

The next figures (Figure 12-13) show our results at red-grey colour pairs.

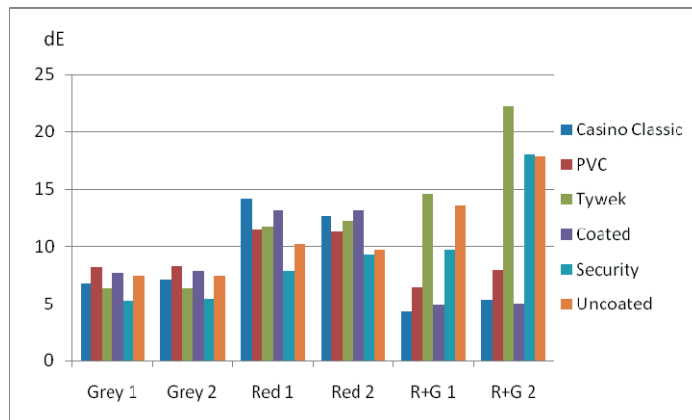


Figure 12: ΔE^*_{ab} difference values between proof and colours printed on examined media (Casino Classic, PVC, Tyvek, coated, security, and uncoated paper) of both printing run at red-grey colours

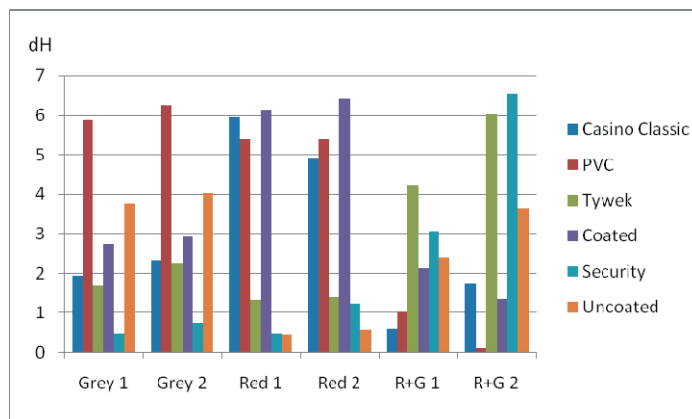


Figure 13: ΔH^*_{ab} difference values between proof and colours printed on examined media (Casino Classic, PVC, Tyvek, coated, security, and uncoated paper) of both printing run at red-grey colours

Examining the ΔE^*_{ab} and ΔH^*_{ab} difference values between superimposed colours of two ink sequences printed on examined media of both printing run we realised that these differences also are the largest at red-grey colours. (Figure 14)

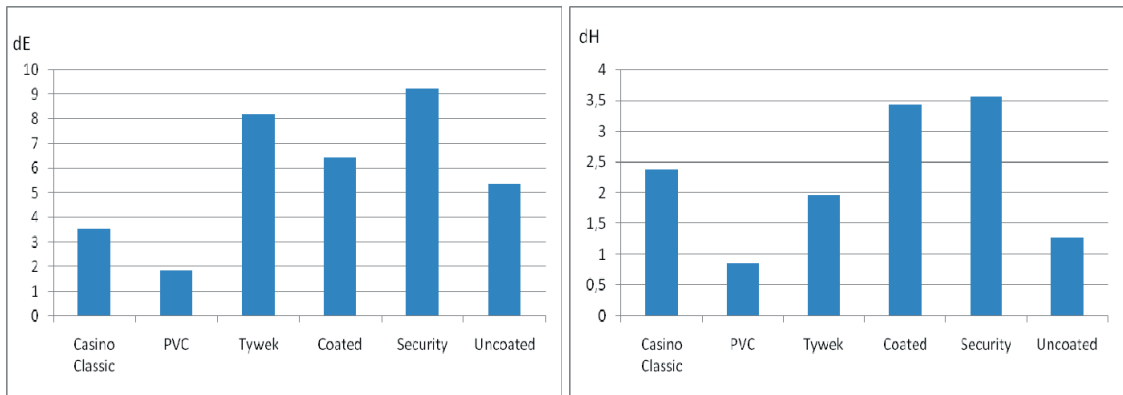


Figure 14: ΔE^*_{ab} and ΔH^*_{ab} difference values between superimposed colours of two ink sequences printed on examined media of both printing run at red-grey colours

When superimposing the colours, colour effect differences decreased to the largest extent as a result of modifying the order of colours for the red-grey and green-orange pairs, as compared to the digital proof. The specified sequence of 30-110 μm thick lines changed in comparison with the proof for all base materials, and thicknesses varied widely. The lines of the image exposed on a CtP plate, as well as the ink collected by the rubber blanket from the plate undergo a long process, and all those processes increase line thickness. Line thicknesses on the proof were not constant either. As a result of all of the above, there is a significant difference between the colour effect perceived on the proof and the prints, depending on the increase in line thickness, the line direction, the colour sequence, and base materials.

5. Conclusion

Because of the guilloche pattern is created by printing direct-colour line-based graphical objects next to and on top of one another there are often significant colour distortions resulting from the special design, approval, printing method.

Examining the changes in line thickness and colour of the patterns, we concluded that, in order to get the proper colour effect, the printing order of colours and the vertical or horizontal position of security graphic elements on the sheet must definitely be specified during the design process. Changes in line thickness, also led to variations in the overall colour effect. Because the customer accepts the proof as a prototype, colour differences and increases in line thickness both need to be kept within certain limits. We can simulate the colour modifying effect of the printing process at proof making. The simulation should be performed for all colours and basic material, frequently ordered by customers. This method results in costs for the printing company but is still less costly than individual proof printing in the press room or the possible consequences of customer complaints.

We gave special importance to this issue as we wish to know to what extent the reproduction process results in colour effect differences. Our findings may contain useful information for the design of guilloche patterns and for the approval of the same.

Acknowledgements

Special thanks to Mr. Eperjesi, Mr Schaffer, Mr. Balas and Mr. Pongracz for contributing in printing and measurements.

References

- Prado, (2006-2009), *Glossary of Security Documents, Security Features and other related technical terms*, http://www.consilium.europa.eu/prado/HU/glossaryPopup.html#_028_1, accessed Jan 10, 2011
- ColorAcademy, (2006), <http://www.coloracademy.co.uk/ColorAcademy%202006/subjects/munsell/page3.htm>, accessed Jan 10, 2011
- Eiler, E., (2007) *A biztonsági nyomtatás*, Magyar Grafika, LI, 7., PNYME, Budapest
HU ISSN 04779-48x
- Malacara, D., (2002) *Color Vision and Colorimetry, Theory and Applications*, SPIE Press, Bellingham, WASHINGTON
- Leparmentier, G., (2007) *Manipulating colors in .NET*.
<http://www.codeproject.com/KB/recipes/colorspace1.aspx>, accessed Jan 10, 2011
- Pekarovicova, A., Chovancova-Lovell, V., Sangmule, S. A., Fleming, P. D., Wu, Y. J., Guillot, B., (2009) *Rotogravure spot color proofing for decorative laminates using SmartColour iVue software*, Advances in Printing and Media Technology, Vol. XXXVI. p. 193-200. IARIGAI, Darmstadt
- Giotto, (2009) *Security Design System*, http://www.pitagora.ch/giotto/Giotto_01_en.html, accessed Jan 10, 2011
- Warner, R. D., Adams, R. M., (2005), *Intoduction to Security Printing*, Books-On-Line, Einnemucca, NV. ISBN 0883623757

Characteristic analysis of the primary color inks in color print

Mahziar Namedanian, Sasan Gooran

Department of Science and Technology
Linköping University, SE-601 74 Norrköping, Sweden
E-mails: mahna@itn.liu.se, sasgo@itn.liu.se

Abstract

Characterization of color inks gives proper insight to the behavior study of inks such as penetration and spread on paper. By sending a light with a wavelength in the reflective wavelength interval of a color ink, the ink becomes totally transparent, and therefore disappears from the paper. In color prints, due to the fact that the color inks are not ideal, it is hard to find a wavelength band at which one color ink completely absorbs the light and the others completely transmit it. In this situation, the color inks, which transmit the light, cannot be thoroughly removed from the paper and their shadow remains. In this paper, in order to separate the shadow, we propose a simple approach based on the reflectance histogram of microscale images captured by a high-resolution camera. By separating the effective dot area of different color inks, it is possible to study the ink behavior once when it is printed individually on the paper and another time when it is printed with other color inks. The result of this study provides useful information to paper and ink manufacturers, and also the graphic art industry.

Keywords: microscale image, reflectance histogram, dot gain, color print

1. Introduction

The characteristics of primary-color inks are far from ideal and estimating the actual behavior of them can be useful for system calibration and quality control in color reproduction. Many of the color prediction models consider that the characteristics of a color ink printed on paper differs from the characteristics of the same ink printed together with another ink (Hersch, 2005), (Emmel, 1999), (Qu, 2011). By separating different primary color inks of a color print from each other, it is possible to study some ink characteristics such as ink spread and penetration of each individual ink in the paper. In the reflective wavelength band of a color ink, the ink transmits the incoming light, and thereby becomes invisible. Moreover, in the absorbing wavelength band of a color ink, the ink absorbs the light, and hence it becomes visible. Previously in (Namedanian, 2011), the authors used this fact to separate two process-color inks from each other. Since the inks are not ideal, it is sometimes impossible to find a wavelength band at which one color ink completely absorbs the light and the other one completely transmits it. Therefore, the effect of the latter ink is not completely removed when sending the light at the absorbing wavelength band of the former ink. In this case, a shadow of the latter ink remains. Due to this fact, using a Spectrophotometer to measure the reflectance of the color patches in different wavelength bands is not a proper approach to study the characteristic of each color ink when printed together with others.

In this paper, we separate color inks from each other by using a high-resolution camera. A minimum search approach is presented to overcome the problem of the remaining shadow by studying the histogram of the captured microscale images. By completely separating the color inks, we are able to study the properties of each primary color ink (CMY) when once printed on paper and another time when printed together with one of the other two inks. Comparing the difference between the properties gives more insight to the characteristics of the color inks in different color printing situations.

The paper is organized as follows: In Section 2, we analyze the color inks behavior with regards to the different wavelength band in the visible spectrum. In Section 3, we present our approach, which separates the effective dot area of each color ink in color print. In Section 4, we study the ink characteristics in different situations, and Section 5 concludes the paper.

2. Analysis of color inks in different wavelength bands

The color inks printed on paper transmit the light in some wavelengths and absorb the rest. This fact indicates that the color ink acts as a filter in the visible wavelength interval (380 nm-730 nm). Therefore, the light wavelengths, which are filtered by the color ink and reflected from the substrate are perceived as color. For

instance, yellow ink perceives yellow, because it absorbs all the wavelengths of visible spectrum except the wavelengths we call yellow (500 nm-730 nm).

In this study, 21 single color patches with different coverage of cyan, magenta and yellow are printed. We have also printed 21 two-color patches for each combination of two primary inks using dot-on-dot strategy. All the patches are halftoned by AM (150lpi, 1200dpi) and printed by commercial offset press (Heidelberg) on coated paper (150 gr/m²). The reference dot area coverage of the patches are (0, 5, 10, ..., 95, 100%). The print density of cyan, magenta, and yellow are 1.62, 1.62, and 1.56, respectively.

Figure 1 shows the reflective wavelength band of the primary (CMY) and secondary (RGB) colors. For two-color patches, by illuminating the light in the reflective wavelength band of one of the two colors, it is possible to neglect the effect of that color and have only the second one. Since the color inks are not ideal, sometimes it is impossible to find an appropriate wavelength in order to separate the two color inks. For example, by looking at the reflectance spectra in Figure 1(c) (the blue patch), we can notice that at 700nm, magenta will disappear but at both 500nm and 550nm (the absorbing wavelengths of magenta) it is not fully possible to separate cyan from magenta. The reason is that at 500nm, although cyan is somewhat transparent, the magenta ink does not completely absorb the light, and at 550nm, the cyan ink also absorbs most of the incoming light. The contrast between cyan and magenta dots is more evident at 500nm, and therefore we use this wavelength band to capture magenta.

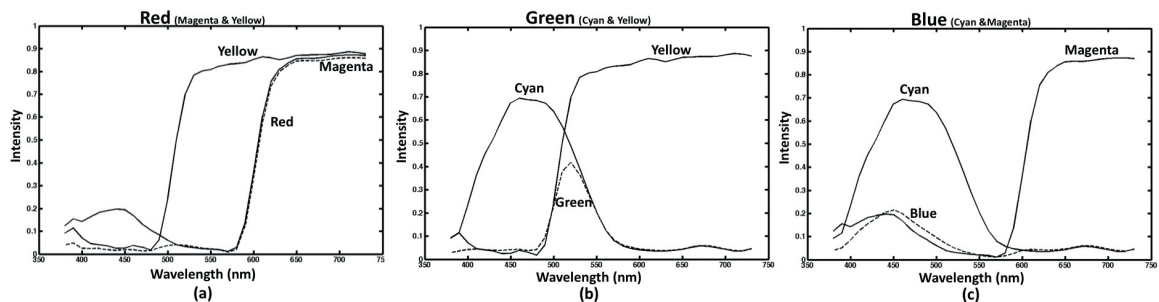


Figure 1: Absorbing and reflective wavelength band of color inks

For analyzing the color inks behavior such as total and physical dot gain (ink spreading), microscale images are captured in different wavelengths. In order to capture the microscale images, we use a high-resolution camera (1.9 μ m/pixel), which is equipped with a set of seven broadband interference filters with center wavelengths band of 400nm, 450nm, 500nm, 550nm, 600nm, 650nm, and 700nm, in addition to the light source (a tungsten halogen lamp). All the interference filters have a bandwidth of 80nm, full width-half maximum (FWHM), except for the filter with 400 nm, having 50 nm FWHM. The filters are located on the color filter wheel. By rotating the filter-wheel it is possible to illuminate the light in a specific wavelength band [see Figure 2 (a) and (b)].

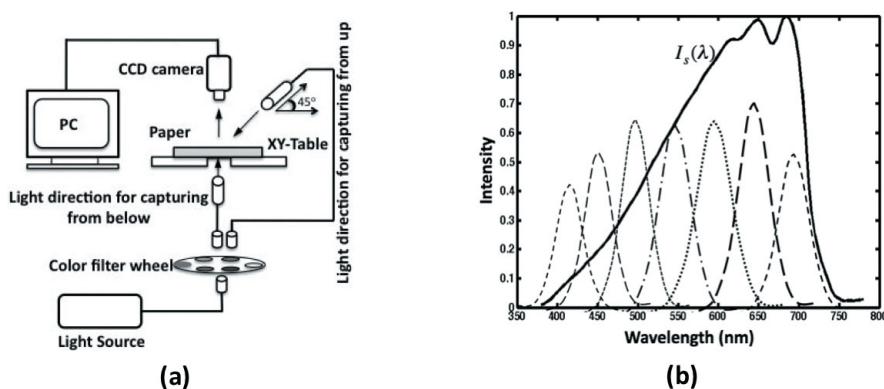


Figure 2: (a) The high-resolution camera setup (b) Transmittances of seven interference-filters

In (Namedanian, 2011), the authors proposed two approaches based on Murray-Davies equation, to obtain the total dot gain by using microscale images and reflectance spectra. In the microscale image approach, an unprinted stripe, and a fulltone stripe, i.e. 100% ink are placed at the side of each halftone patch. By using

these stripes the gray tones of the unprinted paper, I_P , and the full tone coverage, I_i , are computed by taking the average of the pixel values of the unprinted and fulltone stripes, respectively. By using the Murray-Davies model the total dot gain, Δa_{tot} , is given by the difference between the effective $a_{eff}(a_{ref})$ and reference dot area, a_{ref} .

$$a_{eff}(a_{ref}) = \frac{I_{ave}(a_{ref}) - I_P}{I_i - I_P} \quad [1]$$

$$\Delta a_{tot} = a_{eff}(a_{ref}) - a_{ref} \quad [2]$$

In Equation 1, $I_{ave}(a_{ref})$ is the gray tone of the halftoned patch obtained by taking the average of the pixel values of this patch. According to the filter characteristics of color inks, the amount of $I_{ave}(a_{ref})$ is changing in different wavelength bands. Hence, by illuminating the light in different wavelengths, the total dot gain, including both optical and physical dot gain, can be obtained for those specific wavelength bands.

Figure 3(a) shows the microscale image of blue patch (cyan and magenta) under the daylight illumination, which is captured by the high-resolution camera. Figure 3(b) illustrates the same image at 700nm. Here, we can only see the cyan dots, while the magenta dots are completely disappeared. Figure 3(c) shows the captured image at 500nm, and in this figure the magenta dots are evident together with the shadow of cyan dots. This shows that at the absorbing wavelength band of cyan, magenta has no effect, but at the absorbing wavelength band of magenta, cyan has an impact. By impact, we mean that the measurement results show a big total dot gain for magenta at 500nm, which is partly because of cyan's shadow. Notice that the position shift between cyan and magenta in Figure 3(a) is to show the effect of shadow on the total dot gain when there is a register variation in print.

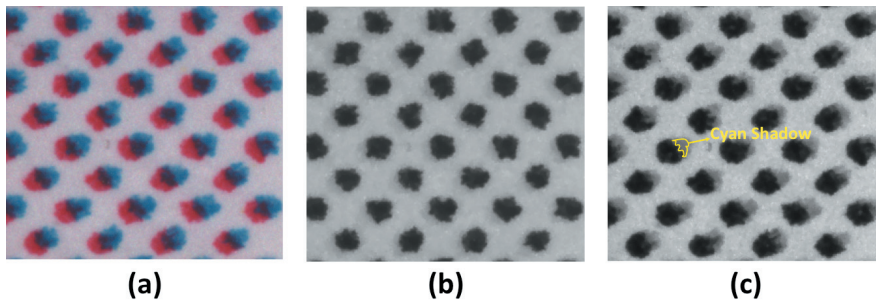


Figure 3: (a) Blue patch (cyan & magenta), (b) Blue at 700nm (only cyan), (c) Blue at 500nm (magenta with the shadow of cyan)

As it can be seen in Figure 3(c) the effect of cyan's shadow has also an impact on $I_{ave}(a_{ref})$. The total dot gain of blue ink at 500nm includes both dot gain of magenta and the cyan's shadow effect (Equation 3), while in 700nm, only the cyan dots can affect the total dot gain (Equation 4). It is obvious that the total dot gain of blue patch at 500nm would become bigger than the total dot gain of blue at 700nm.

$$I_{ave}(blue_500nm) = I_{ave}(magenta) + I_{ave}(cyan_shadow) + I_{ave}(paper) \quad [3]$$

$$I_{ave}(blue_700nm) = I_{ave}(cyan) + I_{ave}(paper) \quad [4]$$

According to the above discussion, it seems logical that in the reflectance spectrum measured by spectrophotometer the color ink's shadow has an impact. In order to compare the shadow effect in the reflectance spectrum and microscale images, the total dot gain of blue patches has been computed by using both reflectance spectrum and microscale images. Figure 4(a) and 4(b) show the total dot gains of blue patches obtained by illuminating the light in two different wavelengths: 500nm (magenta), and 700nm (Cyan). The reflectance values of I_P , I_i , and $I_{ave}(a_{ref})$ are measured by both the spectrophotometer and the high-resolution camera. The total dot gain is obtained for the blue patches at 500nm and 700nm (Equation (1) and (2)). As seen in Figure 4(a) and 4(b) the results are close to each other with maximum difference around 1%. This shows that the shadow of cyan has an impact in the reflectance spectrum measured by spectrophotometer.

Now it can be concluded that using the spectrophotometer to measure color patches is not an appropriate approach to separate the effect of cyan on magenta at some wavelengths.

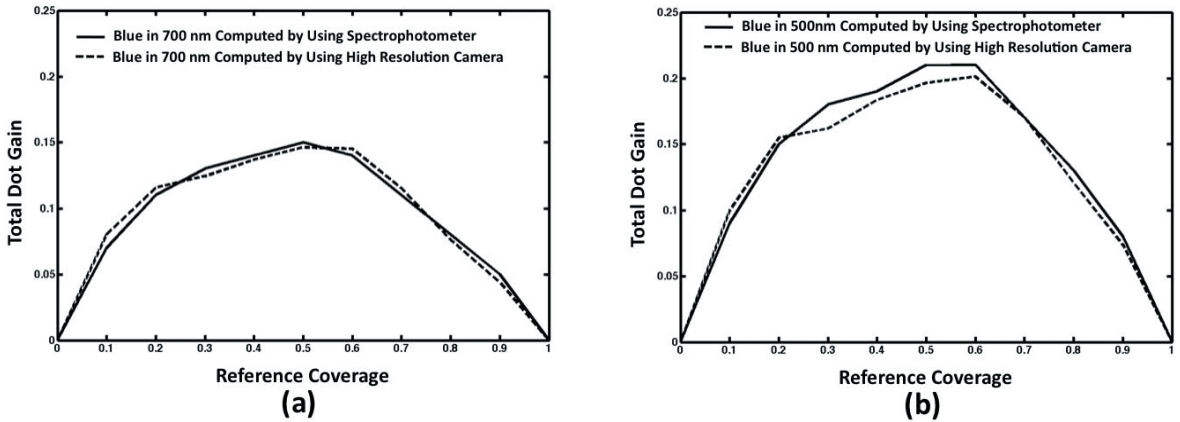


Figure 4: Solid line indicates total dot gain obtained by using spectrophotometer and dashed line total dot gain obtained by using high-resolution camera. (a) Total dot gain of cyan (blue in 700 nm) (b) total dot gain of magenta (blue in 500nm)

3. Omitting the shadow effect

In this paper in order to remove the shadow effect, the reflectance histogram of the captured microscale images has been studied. A histogram indicates how pixel values of the binary image are distributed between 0 and 1. In a bitmap image histogram, there are only two peaks: one for black dots with pixel values equal to zero, and the other one for the white area between dots with pixel values equal to one. In the printed image, as the dots are not fully black, the peak for black dots shifts from zero, corresponding to the dots actual pixel value (Namedanian, 2010). On the other hand, due to the propagation of light in the paper (optical dot gain) the pixel value of paper between dots also reduces from one, and the corresponding peak shifts to the actual pixel value (Hersch, 2005), (Emmel, 2002), (Arney, 1996). The minimum search approach used in this study is based on finding the position in the histogram between the two peaks having the minimum value.

Figure 5(a) shows the reflectance histogram of a blue patch in 500nm. There are three peaks; the first peak corresponds to the magenta dots, the second one to the shadow of cyan, and the third one to the paper between dots. For omitting the shadow effect, we have to find the position on the reflectance histogram between the peaks of magenta and the cyan’s shadow, which has the minimum value.

The minimum point in the histogram indicates the boundary between the magenta dots and the rest of the surface (i.e. paper, optical dot gain and the shadow of cyan).

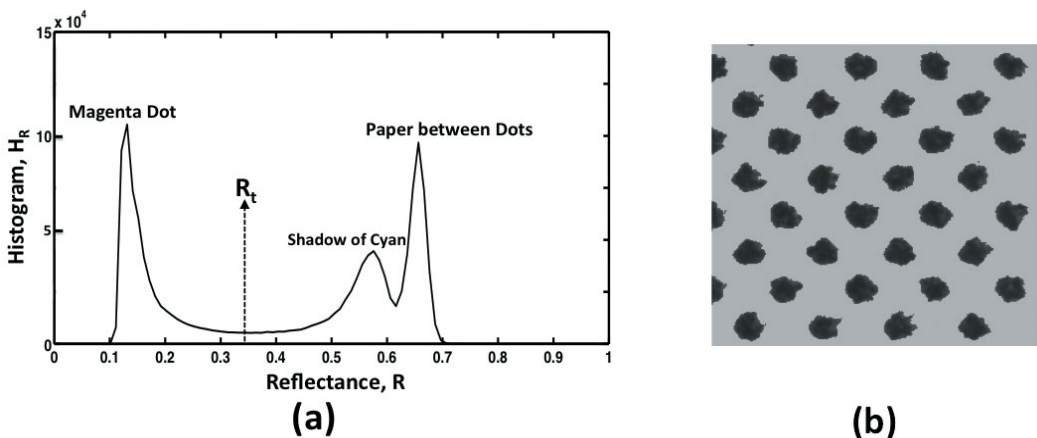


Figure 5: (a) reflectance histogram of blue patch in 500nm (b) magenta dots after removing the cyan’s shadow

In Figure 5(a), the threshold point R_t , which indicates the effective dot area border, is obtained by minimum search approach. Now the fraction of physical dot area (ink spreading) can be computed from the reflectance histogram by using a threshold value R_t as a border between ink and shadow:

$$a_{eff,R} = \frac{\sum_{m=0}^{R_t} H_r(m)}{\sum_{m=0}^1 H_r(m)} \quad [5]$$

In Equation 5, H_r , and R_t denote the reflectance histogram and the threshold between magenta dots and the shadow of the cyan dots, respectively. However, the same equation can be used for other color inks.

The physical dot gain, Δa_{phy} , is computed by Equation 6, where a_{ref} and $a_{eff,R}$ are the reference dot area and the physical dot area of color inks after the print, respectively.

$$\Delta a_{phy} = a_{eff,R} - a_{ref} \quad [6]$$

By finding the threshold point it is possible to graphically illustrate the effective dot area of magenta, on which the cyan's shadow has no impact, (Figure 5(b)). Now by using the proposed approach we are able to separate the color inks from each other and characterize the color inks behavior in color prints.

4. Characterization of color ink

The printed dots normally appear bigger than they are in the bitmap. Several factors can contribute to the increase of the halftone dot area. Different paper types have different ink absorption rates; for instance uncoated papers can absorb more ink than coated ones. Cylinders pressure can squeeze the ink out of its dot shape, and ink viscosity is a contributing factor in coated papers; the higher the viscosity inks the better they can resist the pressure (Sormaz, 2009), (Yang, 2001).

Most of the already proposed approaches separate the physical dot gain of only one-color ink printed on paper (Yang, 2004), (Arney, 1996). Since we have the possibility to separate two color inks, which are printed on top of each other, it would be interesting to investigate how the physical dot gain of each color ink behaves. The two primary color inks are printed using dot-on-dot strategy. The microscale images have been captured by illuminating the light in the absorbing wavelength band of each color ink. In the next step the physical dot gains of each color are computed by using minimum search approach (see Equations 5 and 6).

Figure 6(a) shows the physical dot gain of yellow printed on paper, once together with cyan (green patch) and once with magenta (red patch). It can be seen from the figure that the physical dot gain of yellow is smaller when printed on paper compared to the case when it is printed together with cyan or magenta. Figure 6(b) shows the physical dot gain of cyan printed on paper, together with magenta (blue patch) and yellow (green patch). It is shown that the physical dot gain of cyan is almost the same in all three cases.

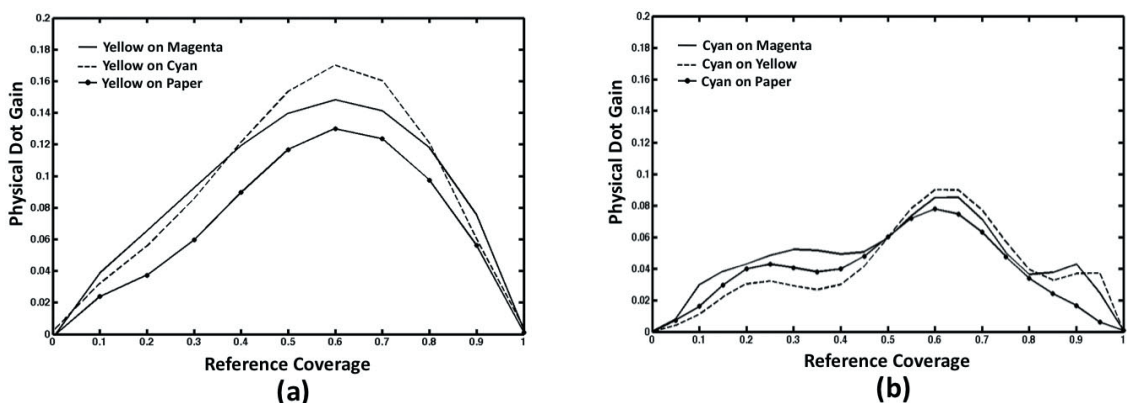


Figure 6: (a) Physical dot gains of yellow (b) Physical dot gains of cyan

By comparing Figure 6(a) and 6(b), we can see that the physical dot gain of yellow is bigger than that of cyan, although the print density of yellow is lower than the two other inks. This shows that the yellow ink is spread more when printed on paper. Unlike cyan and magenta, the yellow ink also spreads more when printed on another ink compared to when it is printed on paper.

5. Conclusions

In this paper we proposed a method to separate the effect of the color inks by using microscale images. This method also provides the possibility to investigate the characteristic of the color inks in different printing situations. The result of this study can help improving the accuracy of the existing color-prediction models. It is also possible to measure the register variation by the proposed method (Gooran, 2011). The approach can also be used in print electronics applications. Since in print electronics materials with different wavelength properties are printed on top of each other, it is possible to separate those layers and detect the possible deficiencies. For example, when a transistor is printed, there are several layers with different wavelength characteristics in the visible wavelength band printed on top of each other. Using our approach and separating the layers can detect the probable invisible disconnection of the lower layers.

Acknowledgements

The industry participants in the PaperOpt project and the Swedish Governmental Agency for Innovation Systems (VINNOVA) are acknowledged by the authors for their financial support.

References

- Arney J. S., Arney C. D., Katsube M., and Engeldrum P. G., (1996), "An MTF analysis of paper," *J. Imaging Sci. Technol.*, 40 (1), 19-25.
- Emmel P., and Hersch R. D., (2002), "Modeling Ink Spreading for Color Prediction," *J. Imaging Sci. Technol.*, Vol. 46, No. 3, 237-246.
- Emmel P., and Hersch R. D., (1999), "A Model for Color Prediction of Halftoned Samples Incorporating Light Scattering and Ink Spreading," *Proceeding of the IS&T/SID 7th Color Imaging Conference*, pp. 173-181.
- Gooran S., Nyström D., Namedanian M., and Hauck Sh., (2011), *Measuring Register Variation and Investigating its Effect on Color Appearance for Different Halftoning*, Proc. TAGA (Technical Association of the Graphic Arts), March 2011, Pittsburgh, PA.
- Hersch R. D., Crete F., (2005) "Improving the Yule-Nielsen modified Neugebauer model by dot surface coverages depending on the ink superposition conditions," *IS&T/SPIE Electronic Imaging Symposium*, SPIE Vol. 5667, pp. 434-445.
- Hersch R. D., Emmel P., Collaud F., and Crete F., (2005), "Spectral reflection and dot surface prediction models for color halftone prints," *J. Electronic. Imaging*, 18 (3), 3300.
- Namedanian M., and Gooran S., (2011), "Characterization of Total Dot Gain by Microscopic Image Analysis," *J. Imaging Sci. Technol.*, 55(4).
- Namedanian M., and Gooran S., (2010), "High Resolution Analysis of Optical and Physical Dot Gain," in TAGA conference proceeding, 48-51.
- Namedanian M., Gooran S., and Nyström D., (2011), "Investigating the Wavelength Dependency of Dot Gain in Color Print," *IS&T/ SPIE, Electronic Imaging Sci. Technol.*, No. 786617.
- Qu Y., and Gooran S., (2011), "A Simple Color Prediction Model based on Multiple Dot Gain curves," *IS&T/ SPIE, Electronic Imaging Sci. Technol.*, No. 786615.
- Sormaz M., Stamm T., Mourad S., and Jenny P., (2009), "Stochastic modelling of light scattering with fluorescence using a Monte Carlo-based multiscale approach," *J. Opt. Soc. Am. A*, 26 (6), 1403-1413.
- Yang L., Lenz R., and Kruse B., (2011) "Light scattering and ink penetration effects on tone reproduction," *J. Opt. Soc. Am. A*, 18 (2), 360-366.
- Yang L., (2004). "A Unified Model of Optical and Physical Dot Gain in Print Color Reproduction," *J. Imaging Sci. Technol.*, Vol. 48, No. 4, 347-353, (2004).

Regression method for predicting the colorimetry of spot colour overprints

Kiran Deshpande, Phil Green

London College of Communication
Elephant and Castle, London SE1 6SB
United Kingdom
E-mail: kiranudeshpande@gmail.com

Abstract

Despite the advancements in ICC colour management, there is still need for predicting the spot colour overprints accurately. Although spot colours can be characterised by using an ICC profile, it is not practical every time to print a profile target and generate an ICC profile for all inks in combination.

We propose a simple mathematical model to predict the spot colour overprints by using power regression. This is a refinement of our previous overprint model, which is based on linear regression. Each spot colour is defined separately by printing the ink step-wedge chart to predict the colour of overprinting solids and halftones. This model was evaluated by printing different combinations of process inks (C, M, Y, K) and two spot colours on three substrates. Model shows good accuracy with average CIEDE2000 values between the measured and predicted overprint colours below 2.5.

This model can be applied in different scenarios, like predicting the colour of 2-inks overprints, multiple-inks (more than 2-inks) overprints and a combination of process inks and spot colour.

Keywords: spot colours, overprint, regression

1. Introduction

Recently there have been some attempts to predict the overprints of spot colours. Viggiano (2008) used various ink trapping equations to predict the overprint colour. Chung (2008) found that the display-to-print match fails completely for spot colour overprints and there is a colour management gap in pre-media software's ability to predict spot colour overprints accurately between display and print.

Spectral printer models can be used to predict the ink combinations of spot colours. These models try to depict the complex interaction between light, paper and ink in order to characterise the conventional printing systems. Some of these models include: Kubelka-Munk model, Yule-Nielsen modified spectral Neugebauer (YNSN) model (Viggiano, 1990), Van De Capelle and Meireson model patented by EskoArtwork (Van De Capelle, 1997), Enhanced Yule-Nielsen modified Neugebauer (EYNSN) model to account for ink spreading in different ink superposition conditions (Hersch, 2004 and 2005). Some of these models require extensive number of inputs and optimisation process. For example, YNSN model requires printing all combinations of primary inks and optimising the Yule-Nielsen factor. For a 6-ink printing system, it needs 64 colour patches. The packaging industry uses a large number of spot colours. It is not practical to print and measure all possible combinations of these inks in order to apply the spectral models. Furthermore, these are relatively complex models and they cannot be easily integrated into the existing standards like ICC profiles and PDF/X.

We proposed a simple numerical method to estimate the spot colour overprints by using linear regression (Deshpande, 2010). Here, the model accuracy is improved by using power regression method. The assumption made in this method is that at each wavelength the reflectance factor of an overprint approximates the product of the reflectance factors of the two inks measured independently. When this reflectance product is modified by using power regression, the approximation is often a good prediction of the actual reflectance. Since CIEXYZ is a linear transform of reflectance, the same approach can be adopted for CIEXYZ tristimulus values.

2. Overprint model

Consider an overprint colour obtained by printing ink on top of another ink. Since each ink reflectance spectrum represents the absorbance of light across the spectrum, the reflectance of an overprint can be

approximated by simply convoluting the two reflectances. We can take a spectral product of the individual inks to predict the spectrum of the overprint colour. The error is typically an underestimate, and occasionally overestimates, of the reflectance.

Scaling the spectrum by a single parameter often gives an acceptable reflectance. Thus, the spectral reflectance product of two inks can be modified numerically by a correction factor. This correction factor depends on colorant opacity, ink sequence and the dot area of the overprint colour.

Figure 1 shows a spectral reflectance curve of the overprint colour, obtained by printing yellow ink on top of magenta. The spectral product of magenta and yellow inks is also shown as a grey curve. It is an underestimate of the real overprint. When we apply a correction factor to this spectral product, the resulting spectrum (dashed curve) is closer to the actual measurement of the overprint colour.

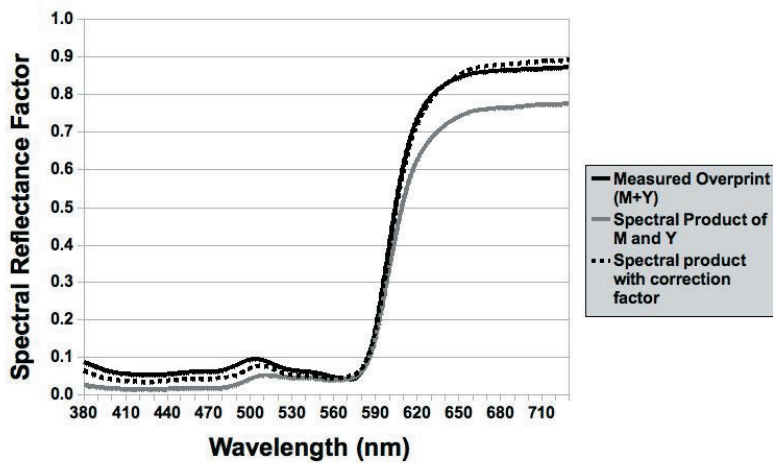


Figure 1: Spectral product of individual inks with correction factor

However, the spectral data is usually not available in PDF and in ICC profiles. Therefore, a trichromatic-based approach (CIEXYZ or CIELAB) is required. Since XYZ is a linear transform of reflectance, the same approach is applicable to XYZ.

Where a spot colour is printed over another colour, the first-printed underlying colour can be considered as a background object and the overprinted spot colour as a foreground object. For example, if we print 40% Spot2 on top of 70% Spot1, then 70% Spot1 is called as a background colour and 40% Spot2 is called as a foreground colour.

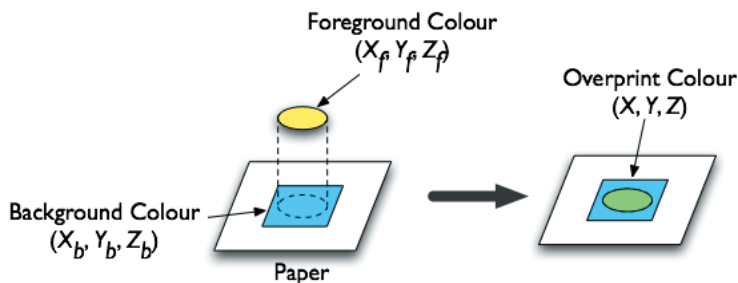


Figure 2: Spot colour overprint described in terms of background and foreground colours

We proposed a method (Deshpande, 2010), which uses linear regression to model the relationship between the overprint colour (X, Y, Z) and the product of the background colour (X_b, Y_b, Z_b) and the foreground colour (X_f, Y_f, Z_f) .

It was found that power regression is better choice (see Figure 8) than linear regression for predicting the spot colour overprints. Figure 3 depicts a strong correlation between the measured overprint colour and the product of the background and the foreground colours, with the correlation coefficient 0.99.

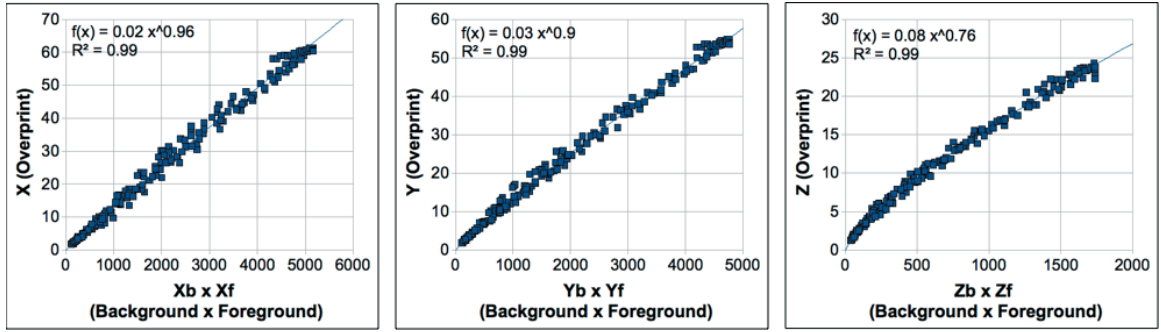


Figure 3: Data fitting - Measured overprint colour vs. the product of background and foreground colours

The overprint model predicts a resulting colour (X, Y, Z) from the product of the background colour (X_b, Y_b, Z_b) and the foreground colour (X_f, Y_f, Z_f) as follows:

$$\begin{aligned}
 X &= j_x \times (X_b \times X_f)^{k_x} \\
 Y &= j_y \times (Y_b \times Y_f)^{k_y} \\
 Z &= j_z \times (Z_b \times Z_f)^{k_z}
 \end{aligned}
 \tag{1}$$

where:

- [X_b Y_b Z_b]: Tristimulus values of background colour.
- [X_f Y_f Z_f]: Tristimulus values of foreground colour.
- [j_x, j_y, j_z]: Scaling factors of foreground colour depending on dot area.
- [k_x, k_y, k_z]: Exponents of foreground colour depending on dot area.

We found that the coefficients (scaling factors and exponents) are dependent on the foreground colour. They can be calculated from the ink step-wedge chart of the foreground colour. The ink step-wedge chart provides ink reflectance characteristics transparency. This is explained in detail in the implementation section. The above equation can be used recursively to calculate colour printed by multiple inks, for example 3-inks, 4-inks and so on.

3. Method

A 6-colour test chart is used to evaluate the model. It includes four process inks (C, M, Y, K) and two spot colours, Pantone 157C and Pantone 330C.

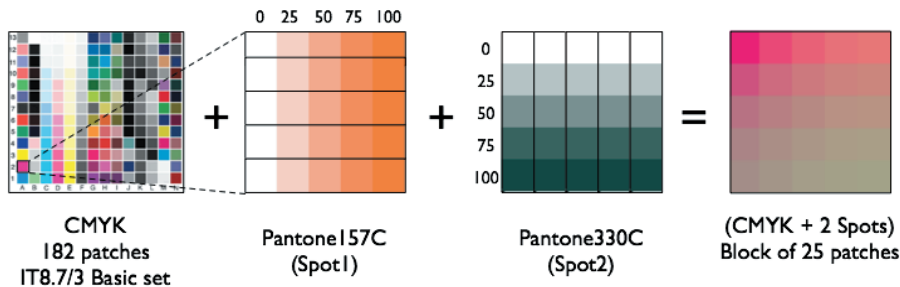


Figure 4: Design of the 6-colour test chart

To design this chart, we started with the basic set of IT8.7/3 CMYK chart (182 patches). On each CMYK patch, we added solid and tints (0%, 25%, 50%, 75% and 100%) of each spot colour (Figure 4). This gives a set of 25 colour patches for each CMYK basic colour resulting in a total of 4550 patches.

The ink step-wedge chart was used to characterise each ink separately in terms of its opacity. This chart uses ramps of inks printed over white, grey and black backgrounds (Figure 5). The model coefficients are derived from the ink step-wedge chart of the foreground colour.

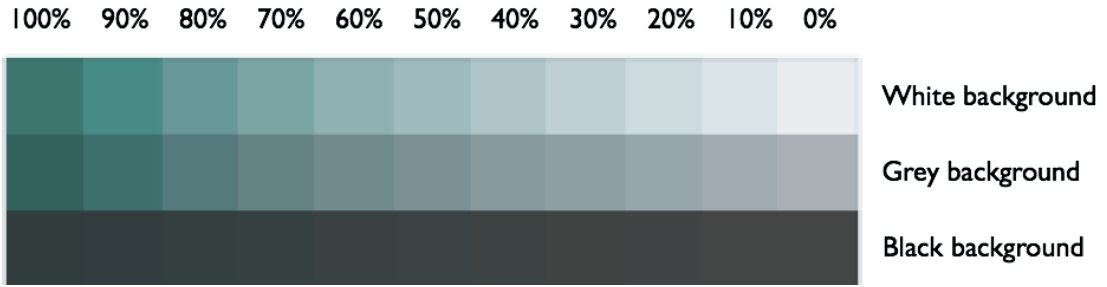


Figure 5: Ink step-wedge chart for Pantone 330C ink

3.1 Printing specifications

Printing process used in this study was the Offset printing with Mitsubishi New DAIYA 306 press. Three different substrates were used as shown in Table 1. These were all coated papers, representing different weights.

Table 1: Specifications of substrates

Substrate	Weight (gsm)	L*	a*	b*	Whiteness
Mitsubishi "MYU Coat NEOS"	157	94	1	-1	86
Hokuetsu "Pearl Coat N"	127.9	94	1	-1	84
Nihon "Be-7"	122	96	1	-1	89

Toppan standard inks were used with the following sequence: *K - C - M - Y - Spot Colour1 (PMS 157C) - Spot Colour2 (PMS 330C)*. All inks were printed with 150 lpi (lines per inch) screen ruling and the following screen angles: *K = 45, C = 15, M = 75, Y = 90, PMS 157C = 30 and PMS 330C = 60*.

These specific two spot colours are selected because they have very different spectral reflectances. *Spot Colour1* is a representative of pastel colours and *Spot Colour2* is a dark colour. Thus, we covered both light and dark spot colours to evaluate the model.

The test charts and ink step-wedge charts were measured using an X-Rite Spectrolino. Overprint coefficients were calculated from the ink step-wedge chart for the foreground colour. Power regression is applied to predict the overprint colours. Model predictions were compared to the actual measurements of overprint colours.

4. Implementation

This section includes step-by-step guidelines to implement the model for predicting the colour of 2-inks overprint. It can be easily extended to more than 2-inks overprint.

Let's assume we are printing two special inks with the following ink sequence: *Spot1 - Spot2*, and we want to predict the overprint colour resulting from a combination of 40% *Spot1* and 60% *Spot2*. Here, a background colour is 40% *Spot1* and foreground colour is 60% *Spot2*. We can predict the overprint colour as follows.

(A) Print and measure the ink step-wedge chart for each ink

Print the ink step-wedge charts for *Spot1* and *Spot2*. This chart should include the following colours at the minimum: the substrate, solid black, solid ink printed over white, grey and black backgrounds and at least one tint patch of the ink printed over white, grey and black backgrounds. For example, the ink step-wedge chart in Figure 3 consists of ink ramps of 0% to 100% in 11 steps over white background (plain substrate), grey background (50% black) and black background (solid black). Measure the tristimulus values (*X, Y, Z*) of each patch in the ink step-wedge chart.

(B) Calculate the overprint coefficients for the foreground colour from ink step-wedge chart

Calculate the overprint coefficients (*j_x, j_y, j_z, k_x, k_y and k_z*) for the foreground colour, which is 60% *Spot2* ink. This is done by applying the model equations to the ink step-wedge chart of *Spot2* ink as follows.

Measure the ink step-wedge chart

Measure the tristimulus values (X, Y, Z) of all patches in the ink step-wedge chart for the foreground colour (*Spot2*). Now, we have the measurements of 60% *Spot2* over white, grey and black backgrounds. We are going to apply the overprint model to these patches to calculate the coefficients. These patches (marked as 1, 2 and 3 in Figure 6) are treated as the resultant overprint colours.

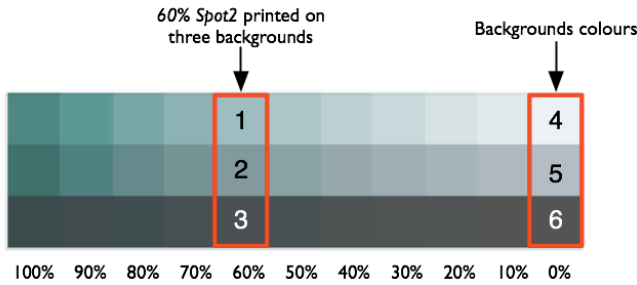


Figure 6:
Ink step-wedge chart - *Spot2* ink printed on three background

Table 2 shows the background colour and foreground colour for each of three overprint colours.

Table 2: Background and foreground colours for each overprint colour

Overprint Colour [X, Y, Z]	Background Colour [X_b, Y_b, Z_b]	Foreground Colour [X_f, Y_f, Z_f]
60% <i>Spot2</i> over white (Patch 1)	Substrate (Patch 4)	60% <i>Spot2</i> over white (Patch 1)
60% <i>Spot2</i> over grey (Patch 2)	Grey (Patch 5)	60% <i>Spot2</i> over white (Patch 1)
60% <i>Spot2</i> over black (Patch 3)	Solid Black (Patch 6)	60% <i>Spot2</i> over white (Patch 1)

For example, consider 60% *Spot2* on grey background (X, Y, Z). Here, the background colour (X_b, Y_b, Z_b) is the colour of grey, which is patch number 5 in Figure 6 and the foreground colour (X_f, Y_f, Z_f) is the 60% *Spot2* printed over white, which is patch number 1 in Figure 6. Similarly, we can find the background and the foreground colours for the remaining two overprint colours.

Now, we have the measured tristimulus values of all three resulting overprint colours and their background and foreground colours. We can use the model equations to calculate the coefficients.

Calculate the overprint coefficients for the required dot area

Using a set of three patches for 60% *Spot2*, apply the power regression to calculate the scaling factors (j_x, j_y, j_z) and constants (k_x, k_y, k_z) as shown in the following equation.

$$\begin{aligned}
 X &= j_x \times (X_b \times X_f)^{k_x} \\
 Y &= j_y \times (Y_b \times Y_f)^{k_y} \\
 Z &= j_z \times (Z_b \times Z_f)^{k_z}
 \end{aligned} \tag{2}$$

where:

[$X Y Z$]: measured tristimulus values of the overprint colour patch.

[$X_b Y_b Z_b$]: measured tristimulus values of background colour.

[$X_f Y_f Z_f$]: measured tristimulus values of foreground colour.

[j_x, j_y, j_z]: Scaling factors for 60% *Spot2*.

[k_x, k_y, k_z]: Exponents for 60% *Spot2*.

All tristimulus values can be obtained from the measurements of the ink step-wedge chart as described above. This is further demonstrated with an example in **Appendix I**. If 60% dot area is not printed in the ink step-wedge chart of *Spot2*, then obtain the tristimulus values of 60% *Spot2* by interpolating the existing measurements. For example, calculate the tristimulus values of 60% *Spot2* over white, by interpolating the existing measurements of ink ramp over white background. You can calculate the model coefficients for any intermediate dot area by interpolating the existing measurements. Once the overprint coefficients are calculated, the next step is to find out the product of the background colour 40% *Spot1* and the foreground colour 60% *Spot2*.

(C) Calculate the product of background colour and foreground colour

Tristimulus values of background colour, 40% Spot1, can be obtained from the measurements of ink step-wedge chart of Spot1 ink (40% Spot1 printed on plain substrate). Similarly, tristimulus values of foreground colour, 60% Spot2, are obtained from the measurements of ink step-wedge chart of Spot2 ink (60% Spot2 printed on plain substrate). If the required dot area is not printed in the ink step-wedge chart, say 24%, then it can be obtained by interpolating the existing measurements. If tristimulus values of background colour are $[X_b, Y_b, Z_b]$ and those of foreground colour are $[X_f, Y_f, Z_f]$, then calculate the product of two colours: $[X_b \times X_f]$, $[Y_b \times Y_f]$, $[Z_b \times Z_f]$.

(D) Calculate the resulting colour

Apply the model equations to calculate the resulting colour XYZ using the overprint coefficients (j_x, j_y, j_z, k_x, k_y and k_z) obtained in Step (B).

$$\begin{aligned}
 X &= j_x \times (X_b \times X_f)^{k_x} \\
 Y &= j_y \times (Y_b \times Y_f)^{k_y} \\
 Z &= j_z \times (Z_b \times Z_f)^{k_z}
 \end{aligned}
 \tag{3}$$

where

$[X_b, Y_b, Z_b]$: measured tristimulus values of background colour.

$[X_f, Y_f, Z_f]$: measured tristimulus values of foreground colour.

$[j_x, j_y, j_z]$: Scaling factors for foreground colour 60% Spot2.

$[k_x, k_y, k_z]$: Exponents for foreground colour 60% Spot2.

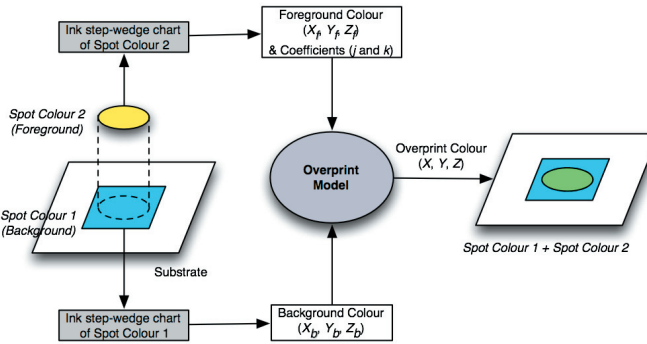


Figure 7: Implementation of the overprint model for 2-inks combination

5. Results

Figure 8 shows the model accuracy of linear regression and power regression for all papers. It is evident that power regression has improved the accuracy of predictions.

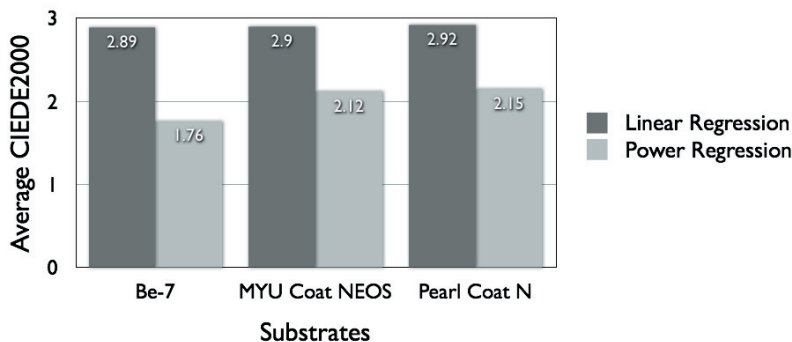


Figure 8: Improvement in model accuracy using power regression

The 6-colour test chart was printed on three substrates. Average CIEDE2000 values between the measured and the predicted overprint colours were calculated for three different combinations: *Spot1 + Spot2*, *CMYK + Spot1* and *CMYK + Spot2*. Results for each substrate are shown in Figure 9. Model accuracy is acceptable with all average CIEDE2000 values below 2.5.

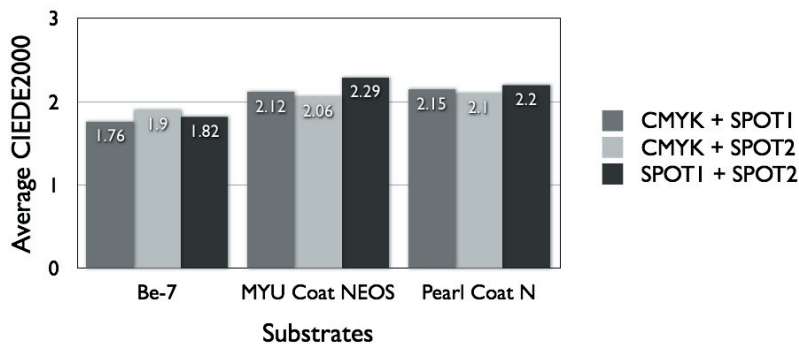


Figure 9: Summary of results for power regression method

Since every ink is defined separately by printing the ink step-wedge chart, there is no need to print combinations of individual inks. For a given library of spot colours, once we measure the ink step-wedge chart for each ink, then we can predict the overprint colour resulting from any combination of inks in the library.

6. Conclusion

This paper addresses the issue of predicting solid and halftone overprints of spot colours. A regression method for calculating scaling parameters for predicting spot colour overprints was evaluated. This provides relatively simple method, which requires small number of inputs. The overprint model shows very good accuracy with average CIEDE2000 values between the predicted and measured overprint colours below 2.5.

This method can be used for different applications like previewing spot colour overprints on monitor using pre-media software and matching spot colour overprints on digital printing and proofing devices. Simplicity of the model makes it suitable for ICC workflow and PDF/X documents.

This paper also describes a step-by-step procedure to implement the overprint model for predicting 2-inks overprints. As the next phase, we are studying the effect of dot percentage of foreground colour on the accuracy of model.

Acknowledgement

We would like to thank Toppan printing for printing the test charts and providing substrates for this project.

References

- Chung, R., Riordan, M. and Prakhya S. (2008) *Predictability of spot colour overprints. Advances in Printing and Media Technology, VI. XXXI, p. 373-380*
- Deshpande, K. and Green, P. (2010) *A simplified method of predicting the colorimetry of sot colour overprints, Proc. 18th Color Imaging Conference: Color Science and Engineering Systems, Technologies, and Applications, p 213-216, San Antonio, Texas*
- Hersch R.D., Collaud, F. Crete, F. and Emmel, P. (2004) *Spectral prediction and dot surface estimation models for halftone prints, IS&T/SPIE Electronic Imaging Symposium, Conf. Imaging IX: Processing, hardcopy and Applications, SPIE Vol. 5293, pg. 356-369*
- Hersch, R.D. and Crete, F. (2005) *Improving the Yule-Nielsen modified spectral Neugebauer model by dot surface converages depending on the ink superposition conditions, IS&T/SPIE Electronic Imaging Symposium, Color Imaging X: Processing, Hardcopy and Applications, SPIE Vol. 5667, pg. 434-445*
- Van De Capelle, J.P. And Meireson, B. (1997) *A new method for characterising output devices and its fit into ICC and HIFI colour workflows, Proc. 5th IS&T/SID Col. Imag. Conf., pg. 66-69*

Viggiano, J.A.S. (1990) *Modelling the colour of multi-coloured halftones*, Proc. TAGA, pg. 44-62.

Viggiano, J.A.S. and Prakhya, S. (2008) *Prediction of overprint spectra using trapping models: A feasibility study*, TAGA 2008, Rochester, NY:2008 TAGA student chapter.

Appendix I: Calculation of the coefficients (scaling factors and exponents)

Figure 10 shows an example of calculation of the model coefficients in a spreadsheet application (Microsoft Excel). If we are printing 60% Spot2 on top of 40% Spot1, then we can calculate the coefficients from the ink step-wedge chart of Spot2 ink. Here, 60% Spot2 is a foreground colour.

Scaling factors and exponents are calculated from the measured tristimulus values of the overprint colours and their respective background and foreground colours. Formula used to calculate each coefficient is given. Power regression can also be applied using trend lines by plotting the measured overprint colour against the product of background and foreground colours (See Figure 3).

	A	B	C	D	E	F
1						
2	Description	Notation	60% Spot2			
3			Over white	Over grey	Over black	
4	Measured overprint colour	X	65.28	28.33	4.80	
5		Y	60.33	26.92	4.82	
6		Z	31.34	15.05	3.18	
7	Measured background colour	X _b	84.60	35.09	4.80	
8		Y _b	87.50	36.33	4.87	
9		Z _b	73.27	30.26	3.59	
10						
11	Measured foreground colour	X _f	65.28	65.28	65.28	
12		Y _f	60.33	60.33	60.33	
13		Z _f	31.34	31.34	31.34	
14						
15	Product of background and foreground colours	X _b x X _f	5522.69	2290.68	313.34	
16		Y _b x Y _f	5278.88	2191.79	293.81	
17		Z _b x Z _f	2296.28	948.35	112.51	
18						
19	Description	Notation	Value	Formula		
20	Scaling Factors	j _x	0.026	=EXP(INTERCEPT(LN(C3:E3),LN(C12:E12)))		
21		j _y	0.034	=EXP(INTERCEPT(LN(C4:E4),LN(C13:E13)))		
22		j _z	0.090	=EXP(INTERCEPT(LN(C5:E5),LN(C14:E14)))		
23	Exponents	k _x	0.907	=SLOPE(LN(C3:E3),LN(C12:E12))		
24		k _y	0.872	=SLOPE(LN(C4:E4),LN(C13:E13))		
25		k _z	0.753	=SLOPE(LN(C5:E5),LN(C14:E14))		
26						

Figure 10: Calculation of the model coefficients in Microsoft Excel

Extended color gamut printing for flexo packaging

*Alexandra Pekarovicova*¹, *Veronika Lovell*², and *Paul D. Fleming*¹

¹ Center for Ink and Printability, Western Michigan University, CEAS
4601 Campus Dr., A-231 Parkview, Kalamazoo, MI 49008-5462, USA

E-mail: a.pekarovicova@wmich.edu

² SUN Chemical Corporation, 30110 S Wixom Rd., Wixom, MI 48393, USA

E-mail: veronica.lovell@sunchemical.com

Abstract

Typically, the higher price of the ECG ink systems can offset expenses associated with the use of the specialty spot color inks when a properly studied and designed ink set is completed based on specific customer requirements. However, there is lack of information about extended gamut ink systems, what types of inks and ink sets and color sequences are optimal to use in the flexographic print processes. In this work, different water based extended gamut mono-pigmented and two pigmented ink sets, several packaging substrates, multiple press setups and ink sequences were studied in order to better understand the behavior of these specially designed color ink sets on the presses. The ink characteristics were also evaluated based on present printing and graphic industry standards. ECG ink systems widen the reachable color space on the press. It was observed that the final performance is dependent on many of the studied factors. The transparency and color properties of the inks can dictate the proper ink sequence which can then lead to even larger enhancement of the color gamut of specific ink set. Other printability properties can be controlled with the use of different substrate types and varnishes and better knowledge of the ink behavior on the press. The use of different ink systems, mono vs. two-pigmented, also offer various advantages, such as coverage of unusual areas of the color space or better control of the ink hues.

Keywords: Extended color gamut (ECG), process colors, mono and two pigmented inks, flexo packaging, overprint varnish, mottle

1. Introduction

Flexo printing is still competing with gravure and lithography to create equal or better print quality (Cole, 2010). However, it is gaining customers especially, in the packaging and labels sector, due to various innovations such as direct laser engraving of flexo plates, digital imaging systems (Taylor, 2010), or implementing of continuous sleeves (Meade, 2010), tight registration on problematic surfaces, better process control, reduction of waste, and increasing productivity (Sharkey, 2009). Multicolor flexo presses are able to deliver more vivid imagery than presses with a fewer stations. It was found that standard four color set can only cover about 60% of Pantone® spot color set (Thompson, 2010). Especially violets, greens and oranges are very difficult to match. Flexo packaging inks tend to use a wider range of pigments, which may be organic, inorganic, process color, process colors enriched with extra color stations using spot colors. The graphics may be enriched with metallic, pearlescent, opalescent and special effect pigments. This represents a huge number of pigments, leading to different special effects, brands, logos, or PMS matched inks, which provide enriched design, but at the same time all these inks need to be stored at the printer's location.

Printers will have lower inks inventory if they will go back and use color sets including process colors and extra spot colors to enrich the color gamut (Moran, 2010; Aberly, 2006), and at the same time enjoy benefit of richer, more saturated colors. In such case, the make-ready times could be shorter, because each job uses the same ink set and there is no need for proofing of spot colors. The Munsell book of colors mechanism was employed to extend flexo color gamut by using adjacent colors to CMYK, such as orange, green and violet instead of yellow, magenta and cyan (Spitzinger, 2000). Extended gamut is printed by Hexachrome, employing six different inks, Pantone six color patented process, or by Opaltone®, employing seven different colors, (CMYK+RGB), cyan, magenta yellow, black and primaries red, green, and blue (Buystedt, 2003; Osmond and Buystedt, 2005; Buystedt (A), 2004; Buystedt (B), 2004; Tolliver-Nigro (A), 2007). Opaltone is able to reproduce 2,800 different colors (note this is a discrete number of spot colors, as we will see below even simple process colors can print many more colors than this within a specified tolerance, Chovancova-Lovell, 2009). FM six is an approach using frequency modulated screening, CMYK set and two additional colors,

which are taken depending on the need from a set of blue, orange and green (Thompson, 2010). The benefit of using extended gamuts is that such system can better reproduce brand colors, and at the same time reduce the inventory of spot color inks (Tolliver-Nigro (B), 2007; Ellis, 2010). Usually, large printers develop their extended color gamut ink sets with their ink supplier, thus the information is kept secret. The aim of present work was to confirm the benefits and drawbacks of one or two-pigmented orange, green and violet ink sets and find out the color gamut differences when applying different print sequences, such as CMYK OGV versus YOMGCVK.

2. Methods

2.1 Substrates

Four different label substrates were used: two coated ones, 54lb semi Gloss Litho and a proprietary coated (PCS) label stock, one non-coated, and Fasson® 2.6 mil pearl white top coated bi-axially oriented polypropylene film (BOPP).

Two one side coated label stock paper substrates and one non coated label stock paper substrate along with one label BOPP film were used in the study. Roughness of the substrates was measured on Parker Print Surf (PPS, Messmer Ltd) instrument using soft backing and 500 kPa clamping pressure. PPS Porosity was also measured on Parker Print Surf (Messmer Ltd) instrument using 500 kPa clamping pressure. Specular gloss was measured at 75° geometry, using a ProfilePlus Technidyne instrument. Caliper was measured using ProfilePlus Technidyne instrument. Brightness was measured at Technidyne Brightimeter Micro S-5. Properties of substrates used are listed in the Table 1. Semigloss Litho, Non-coated and BOPP were backed with release liner.

Table 1: Optical and physical properties of substrates

Property	Semi Gloss Litho (One side coated)	Non-coated	One side coated	BOPP (Bi-oriented polypropylene)
Roughness [μm]	1.52 \pm 0.04	3.1 \pm 0.2	1.41 \pm 0.01	0.77 \pm 0.02
Porosity [mL/min]	5.64 \pm 1.42	72.34 \pm 5.66	4.86 \pm 0.27	3.89 \pm 0.69
Brightness [% GE]	84.4 \pm 0.5	88.3 \pm 0.5	86.1 \pm 0.4	90.6 \pm 0.6
Specular gloss at 75 °[%]	60.5 \pm 6.4	20.9 \pm 0.3	72.3 \pm 0.4	99.3 \pm 0.4
Caliper [μm]	145 \pm 2	82 \pm 3	64 \pm 2	144 \pm 3

2.2 Test charts

Two test charts were applied; one ECI 2002R chart for cyan, magenta, yellow and black (CMYK) colors only, with 1798 patches. The other was a specially designed test chart contained CMYK and spot colors orange, green and violet (OGV) patches containing solids, halftones of one, two, three, up to 400% total coverage area overprints. Total number of patches at the chart was 1560 (Figure 1).

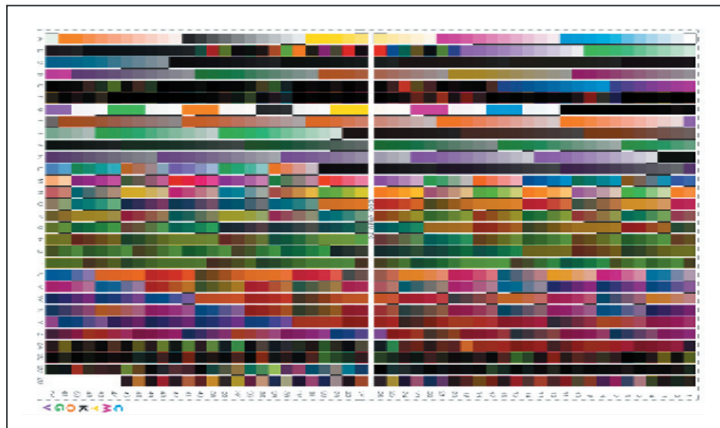


Figure 1: ECG chart with 7 channels, CMYK+OGV

2.3 Print trials

An eight -station AL20L3 Mark Andy 2200 flexo 10 inch label press with a BST Pro Mark registration system equipped with a Power Scope 3000 video camera (Pro Mark Edition) was employed for printing. The press speed was 200 fpm. Inks were printed in order YMCK, YMCK+ OGV with two different OGV ink sets, and YOMGCVK with two different OGV ink sets with or without overprint varnish (Ashland 9709 high gloss/high scuff resistance varnish). CMYK inks were compliant with FIRST requirements (Hershey, 2010). Two different ink sets included single pigmented orange, green and violet, and the other two pigmented OGV set. All inks were made by Sun Chemical. A screen ruling of 150 lpi was set for the 067 DFQ flexo plates, with screen angles for cyan 7.5 °; magenta 67.5 °; yellow 82.5 °; black 37.5 °; orange 7.5 °; violet 82.5 ° and green 67.5 ° to avoid the moiré effect in non imposing colors. Black and magenta stations were equipped with 800 lpi anilox rollers with 2.8 BCM (4.5 µm, Kattumenu, 2008) cell volume, rest of the stations had anilox rollers 600 lpi, resolution and 3.8 BCM (17.3 µm) cell volume.

2.4 CIELAB color measurement

The reflectance spectra and CIELAB values were measured with the help of a scanning spectrophotometer (X-Rite i1/iO) with 45°/0° geometry. ProfileMaker 5.0.9 Packaging version was used to create ICC output profiles for each ink set /substrate combination. ColorThink Pro 3.0 was employed to calculate color gamut volumes from ICC profiles and Color Think Pro 3.0 and Profile Editor 5.0 were used for the illustration of the gamut volumes.

2.5 Mottle

Visual print mottle measurements were made using Prufbau Verity IA Mottle Analysis. Areas of interest (100% tone of CMYK OGV) were scanned with an HP scanner. In each case, a patch area of 32.4mm² was analyzed. The mottle was measured on all substrates, and all solid patches. Cumulative mottle of all solid colors was calculated as a sum of individual mottle values for each color for a particular substrate.

Table 2: Press trial #1

Run	Substrate	Inks sequence	Varnish
1a	Semigloss Litho	YMCK + GOV (One Pigment Inks)	N
1b	Semigloss Litho	YMCK + GOV (One Pigment Inks)	Y
2a	Non Coated	YMCK + GOV (One Pigment Inks)	N
2b	Non Coated	YMCK + GOV (One Pigment Inks)	Y
3a	One Side Coated	YMCK + GOV (One Pigment Inks)	N
3b	One Side Coated	YMCK + GOV (One Pigment Inks)	Y
4a	One Side Coated	YMCK + GOV (Two Pigmented Green)	N
4b	One Side Coated	YMCK + GOV (Two Pigmented Green)	Y
5a	Semigloss Litho	YMCK + GOV (Two Pigmented Green)	N
5b	Semigloss Litho	YMCK + GOV (Two Pigmented Green)	Y
7a	BOPP	YMCK + GOV (One Pigment Inks)	N
7b	BOPP	YMCK + GOV (One Pigment Inks)	Y
8a	BOPP	YMCK + GOV (Two Pigmented Green)	N
8b	BOPP	YMCK + GOV (Two Pigmented Green)	Y

Table 3: Press trial #2

Run	Substrate	Inks sequence	Varnish
1	Semigloss Litho	YMCK	Y
2	Semigloss Litho	YMCK+ OGV (Single Pigment Inks)	Y
3	Semigloss Litho	YMCK+ OGV (Two Pigmented Inks)	Y
4	Semigloss Litho	YOMGCVK (Two Pigmented Inks)	Y
5	Semigloss Litho	YOMGCVK (Single Pigment Inks)	Y

2.6 Ink color and transparency

The selected flexographic process inks were tested for color and transparency based on the ISO/CD 2846-5. The standard specifies these attributes when printed under specified flexographic printing conditions. Colorimetric conformance is verified by printing each ink on the reference substrate as a finished product.

The APCO II/II sheets were used to proof the solid ink patches for the color measurements and Leneta Form 5NT-32C was used to assess the transparency of the inks as shown in Figure 2. Viscosity of the inks was adjusted to 22-25 sec on EZ #2 cup. Proofs were produced on Flexiproof 100 with 800 lpi, 2.8 BCM (4.5 μm) anilox. Three best uniformly produced proofs were then measured and averages of the measurements were calculated.

All of the process inks showed compliance with the ISO 2846-5 for color and transparency as well as the spot colors when tested for transparency.

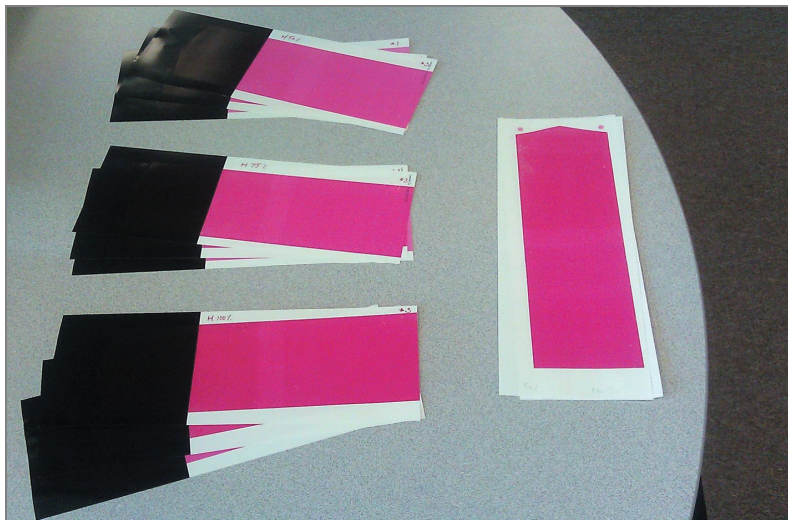


Figure 2: ISO 2846-5 complaint prints of Magenta ink

3. Results

The narrow web flexo press was used to print two synthetic test charts, the four color ECI 2002R chart and extended gamut chart with 1560 patches of single color tone steps of CMYK OGV, orange, green, and violet on three different label paper substrates. The printed test chart was in some cases over-coated with a clear varnish. Two trials were executed. In the first trial, focus was oriented towards differences between varnished and non-varnished print, and print quality of CMYK OGV charts. In the second print trial, the differences between CMYK and CMYK OGV for one pigmented and two pigmented OGV inks were studied along with the changes, caused by an altered sequence of the inks.

The varnish has a different level of effect on diverse types of substrates. Varnish decreased overall mottle on all colors across all of the substrates. Mottle average values and standard deviations for all the colors are listed in the Table 4. Because of the nature of measurement, calculating the mottle from the pixel values, it was expected that yellows will have lowest and blacks the highest mottle, which was also confirmed. Highest mottle was found on black of non-coated substrate printed without varnish (sample 2a), being 325 AU (arbitrary units), which decreased dramatically after varnishing to 92 AU. The lowest black mottle was found at 2.4 AU with sample 8b, BOPP substrate, printed CMYK OGV. The lowest overall mottle was found at yellow with the low of non detectable mottle (5b and 7b), and high of 12.7AU in sample 2a. Yellow mottle of sample 2a decreased after varnishing to 3.4 AU. Green mottle was measured on single pigmented and spot color green. As shown in the Table 4, the largest green mottle 8.1 AU, was found on non-coated substrate (2a), but it was greatly reduced by the application of the varnish to 1.47 AU. Lowest green mottle 0.01AU was found at sample 7b, BOPP varnished sample, with single pigment green. Overall, there were no significant differences in the mottle for single pigmented and spot color green. Cumulative mottle for all colors is illustrated for every substrate in Figure 3. Smallest cumulative mottle was found at the BOPP varnished substrate 8b.

Table 4: Verity IA Mottle (in AU) for solid colors, numbers 1-8 as in the Table 2

Sample	1a	1b	2a	2b	3a	3b	4a	4b	5a	5b	7a	7b	8a	8b
Magenta AvG	1.26	0.23	3.60	3.30	0.62	0.45	0.21	0.28	0.26	0.31	0.52	0.36	0.39	0.50
Magenta StDev	1.34	0.05	0.85	0.99	0.40	0.13	0.13	0.06	0.23	0.01	0.04	0.01	0.05	0.00
Cyan AvG	0.16	0.08	3.30	0.18	0.16	0.14	1.48	0.12	0.12	0.12	0.16	0.15	0.12	0.12
Cyan StDev	0.10	0.07	1.70	0.08	0.04	0.06	1.87	0.00	0.04	0.02	0.13	0.03	0.01	0.07
Yellow AvG	0.04	0.04	12.65	3.45	0.13	0.08	0.21	0.05	0.01	0.00	0.08	0.00	0.80	0.02
Yellow StDev	0.04	0.04	0.78	0.49	0.00	0.04	0.01	0.07	0.01	0.00	0.02	0.00	0.71	0.03
Black AvG	6.25	3.85	325.00	92.35	6.20	6.00	3.55	5.55	5.45	4.20	4.75	3.65	4.95	2.45
Black StDev	3.75	1.34	162.63	7.00	3.68	0.85	0.35	2.19	0.49	2.83	0.49	0.64	2.12	0.07
Green AvG	0.08	0.08	8.10	1.47	0.09	0.13	0.06	0.12	0.07	0.05	0.13	0.01	0.08	0.04
Green StDev	0.01	0.00	5.94	0.76	0.06	0.06	0.01	0.07	0.10	0.03	0.03	0.01	0.02	0.00
Orange AvG	0.07	0.06	17.20	2.20	0.09	0.10	0.05	0.09	0.05	0.11	0.04	0.06	0.06	0.10
Green StDev	0.03	0.01	8.20	0.71	0.01	0.02	0.01	0.06	0.05	0.01	0.03	0.03	0.04	0.03
Violet AvG	0.40	0.53	6.90	3.20	0.46	0.92	0.51	1.30	0.44	0.62	0.28	0.45	0.74	0.76
Violet StDev	0.04	0.12	1.98	0.71	0.01	0.04	0.04	0.14	0.16	0.01	0.04	0.06	0.37	0.26

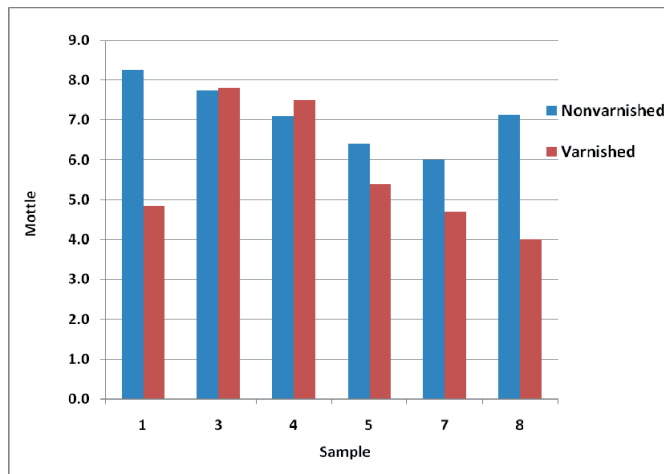


Figure 3: Cumulative average mottle across all solid colors (CMYK+OGV), numbers 1-8 as in the Table 2

Sample 2a with cumulative mottle 376.7 AU and 2b 106.1 AU are not shown in the Figure 3. Figure 4 shows achieved color gamuts for different substrate- ink-varnish combination. As illustrated in Figure 4, varnished prints achieved a larger color gamut volume than non varnished for all prints and substrates, the largest difference 3.4% was found at BOPP printed with monopigmented OGV (Figure 4, sample 7). On an average, varnished prints had larger gamut by 1.6%. BOPP varnished substrate with two pigmented green ink (Figure 5, sample 8) achieved largest color gamut volume with 490,485 CCu, followed by BOPP varnished, two pigmented green with 479,596 CCu (Figure 5, sample 7), followed by one-side coated, varnished with 464,702 CCu, and Semigloss Litho varnished 458,482CCu. The Color Gamut Volume can be interpreted as the number of colors that can be printed with the device/ink set combination with a tolerance of $\sqrt{3}$ (Chovancova-Lovell, 2009). The larger gamut for BOPP was expected, because that substrate was practically non-porous, very smooth and the brightest from all of the substrates (Table 1). Also, one side coated had

better color gamut than Semigloss Litho, but also smoothness and porosity were slightly better on that substrate than found on Semigloss Litho (Table 1). Overall, OGV ink set with two pigmented green achieved larger color gamut than single pigmented ink set, which led to introducing second print trial, involving two sets of additional inks, one and two pigmented orange, green and violet. Because the positive effect of varnish was already shown, the second trial was run only with the varnish over-coating. Also, the effect of substrate was demonstrated in Trial 1, thus it was not reexamined any further. Semigloss Litho was used as the sole substrate for Trial 2. Focus was oriented to compare the four-color ink set to seven color sets, using single pigmented and two pigment inks. Also, a change of order of printing individual inks from CMYKOGV to YOMGCVK (Figure 7) sequence was tested. Color green spot and single pigmented inks were the same as previously used, additional two pigmented orange and violet were applied.

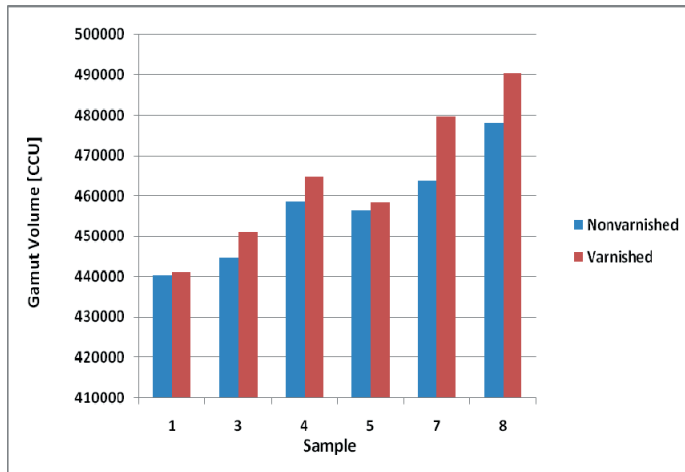


Figure 4: Gamut volume of different substrates printed CMYK OGV with and without varnish, numbers 1-8 as in the Table 2

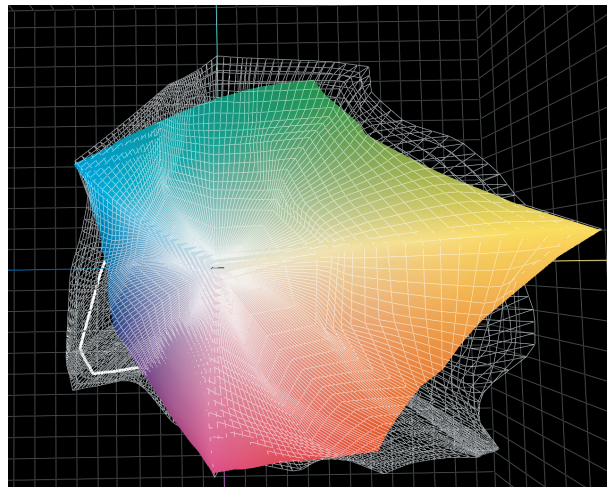


Figure 5: Comparison of 4-color CMYK (true color) and 7-color single pigmented inks YOMGCVK (wireframe)

The gamut volumes of all print situations are illustrated in Figure 6. The color gamut of four color CMYK print was 400,511 CCu (Figure 6). Seven color print, CMYKOGV with single pigmented OGV inks resulted in 28% increased color gamut with 512,493 CCu. Similar run, CMYKOGV with two pigmented OGV inks resulted in color gamut of 499,276 CCu, thus 25% increase against four color one. The change of colors order based on their transparency from CMYKOGV to YOMGCVK was leading to further increase of color gamut, 34% increase (539,321 CCu) for single pigmented inks, and 30% increase, to 523,913 CCu for spot color OGV inks (Figure 6). Thus, set of single pigmented inks delivered better result than two pigmented OGV inks. The gamut illustration of CMYK and the largest gamut of YOMGCVK for single color is illustrated in Figure 5. When only the ECG situation is taken, it can be seen that the change of color sequence for single pigmented inks resulted in 5.2% increase in color gamut, and for two pigmented OGV inks, the increase was 4.9% (Figure 7).

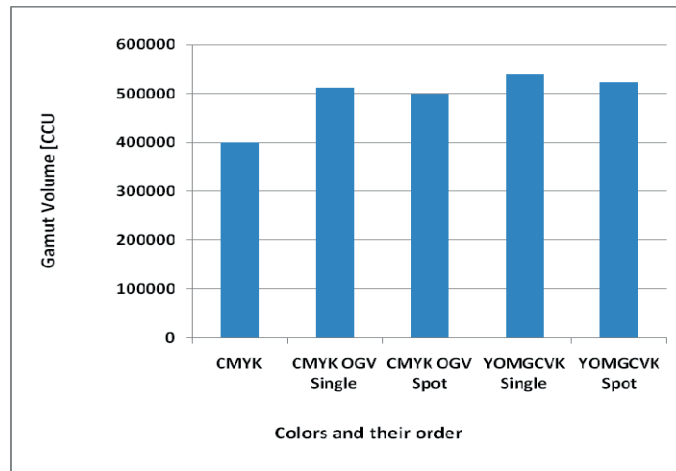


Figure 6: Gamut volume of 4-color ink set printed on Semigloss Litho substrate with CMYK, seven color set printed in order CMYK OGV, and YOMGCVK. Additional inks were either single pigmented or two pigmented OGV inks

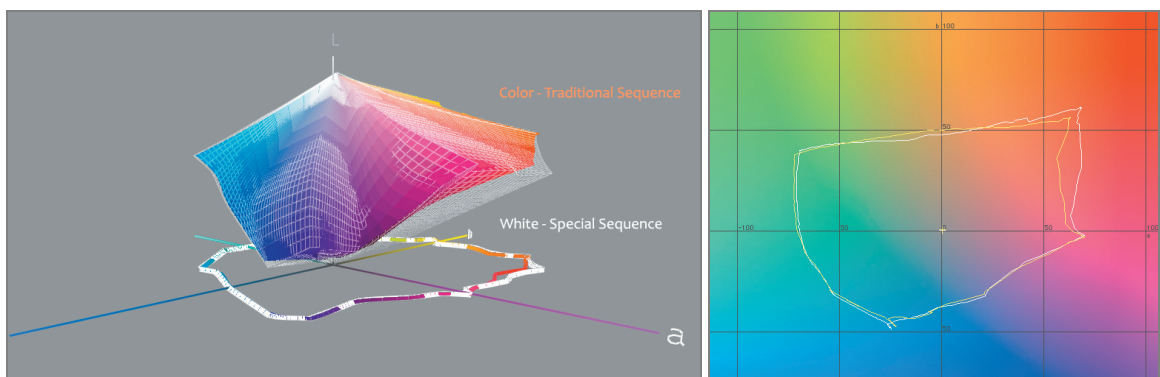


Figure 7: The single pigmented ink system shows 5.2% enhanced color gamut in the orange-red area achieved by changing the print ink sequence to YOMGCVK. 2-D projection is illustrated at L=50

4. Discussion

There is a definitely known fact that an extended color gamut (ECG) ink set extends the color gamut in specific areas of the color spectrum, depending on the choice of extra pigments in the extra ink sets. However, prior to working with additional colors, it is crucial to optimize color gamut with process colors first (Chung, 2006). In our work, a FIRST recommended CMYK water based ink set was used. It was found that substrate plays great role in determining the color coverage of each set. The smoother and less porous the substrate surface is, the more uniform dots are created and more homogeneous overprints are achieved resulting in higher color coverage. The color coverage was increased by 2-8% going from the less smooth to the smoother substrate, and the highest color gamut was obtained for BOPP film.

The achievable color coverage was increased in all instances when the varnish was applied. Increased color gamut due to varnish is attributed due to reduction of scattering of the light on the print surface (Stanton, 2006), thus possibly by increased reflection from the composite ink/varnish layer. As the varnish introduces a clear coating layer on top of the inks, higher gloss is attained (data not shown), along with much lower mottling, which happened with all print conditions (Figure 4).

The largest difference in color gamut was found between the 4-color print and 7-color print using single pigmented inks with the special print sequence (Figure 6), and the largest contributors to increased color gamut were green and violet inks. Single pigmented inks delivered larger color gamut than two pigmented inks. When compared print order CMYK OGV and YOMGCVK, it is obvious that the increase of gamut is connected with overprinting, thus trapping of the colors and the effect shows mainly in the red- orange - yellow area for single pigmented ink system. In the two pigmented ink system, the order change CMYK OGV to YOMGCVK caused its main gamut increase in yellow- orange-red and yellow- green area (data not shown).

5. Conclusion

Four color CMYK and seven color CMYKOGV flexo water based inks were printed on different paper and film label substrates with or without varnish. It was confirmed that the higher substrate quality (higher smoothness, lower porosity) increases achievable color gamut. Also, the positive effect of varnish was shown. Varnish enhances light reflection and at the same time makes it more uniform, which shows in increased color gamut and decreased mottling. Two and one pigmented ink systems were tested. Single pigmented inks reached better color coverage than two pigmented ones. Change of ink order from CMYK OGV to YOMGCVK further enhanced color gamut of both systems by about 5%, which is attributed to ink trapping issues and ink transparencies.

References

- Aberly D., Stansbury S., (2006), *Prepress prep for 10-deck printing*, *Flexo*, 31, 2, 22-24.
- Buystedt M., (2003) *The search for an extended color gamut, flexo print*, *Ink Maker*, 81, 9, 14-16, 22.
- Buystedt M., (A) (2004), *The growing colour gamut, Labels and Labelling*, (2), 117-118.
- Buystedt M., (B) (2004), *Extending the color gamut*, *Flexo*, 29 (3), 40-42.
- Cole S., (2010) *Partners in time, Converting today*, 25 (6), 13-17.
- Chung R., Hsu F. (2006) *Gravure Process Color Gamut Optimization*, 2006 TAGA Conference Proceedings, 430-442.
- Ellis R.: (2010), *Proofing for Flexo and Packaging with Multi-color Profiles*, *Flexo*, 6, 46-47.
- Hershey J.M., (2010), *First methodology takes a 'by-the-numbers' approach*, *Package Printing*, 57 (6), 28-29.
- Meade R., (2010), *Flexo sets out its stall*, *Flexo Tech*, 111, 19-25.
- Moran R., Bonawandt C.R., (2010), *The premium package: Produced at the right time in the right place: FFTA forum*, *Flexo* 35, 6, 6-8.
- Osmond P.K., Buystedt M., (2005), *Printing beyond CMYK*, *Flexo* 30, 4, 62-64.
- Sharkey P., (2009), *The golden age of flexo*, *Flexo*, 34, 11, 30-32.
- Spitzinger M.R., (2000), *The reproduction of extended gamut colors for flexographic printing using the mechanism of the Munsell book of colors*, *Flexo*, 9, 20-34.
- Stanton A., Bohan M., (2006), *The Effects of Coatings on Color Gamuts in Lithography*, 2006 TAGA Proceedings, 236-256.
- Taylor M., (2010), *Print show UK- Part 2, Converting Today*, 24, 4, 20-22.
- Thompson S., Design 2 print blog, (2010), http://www.i2mls.com/i2mls_WebSite/D2P_Blog/Entries/2010/3/12_Extended_Gamut.html, accessed May 5, 2011
- Tolliver-Nigro H., (A) (2007), *Going beyond the benefits of flexo: Extended gamut inks*, *Ink Maker*, 85, (5), 14-16.
- Tolliver-Nigro H., (B) (2007) *Flexo: A market in transition*, *Ink Maker*, 85 (4), pp. 14-18.

Evaluation of quality for color halftone

Li Yang

Innventia AB, Drottning Kristinas väg 61, SE-114 86 Stockholm, Sweden

E-mail: li.yang@innventia.com

Abstract

In this work we present the fundamental aspects regarding quantitative quality evaluations of colour halftone. It begins with the basics of ink-transfer and ink-setting of various printing technologies. Ink-paper interaction in forms of ink spreading and ink-penetration and its impacts on colour reproduction are specially addressed.

Keywords: colour tone reproduction, ink-spreading and ink penetration, physical and optical dot gain

1. Introduction

Print quality is a complex concept which depends on the underlying physical or optical phenomena as well as the characteristics of human visual system such as visual acuity and contrast sensitivity etc. The physical evaluations often consists of a set of quality-matrix, such as optical density (also called as print density), gloss, printing mottle, colour gamut, dot gain, print-through etc. Each of the matrix elements relates to one or a few underlying physical phenomena. Therefore, in practice a subset of the quality matrix is often chosen, depending on the need of application. For example, to evaluate ink-paper interaction, dot gain, line raggedness, strike through, and colour gamut often are some of the quantities in addition to the commonly used quantities like optical density, because these quantities are closely related to ink-spreading and ink penetration.

In the present paper, we present a collection of research works concerning the physical evaluations of print quality in colour tone reproduction. This report is organized as the following. In the next section, we describe briefly the fundamentals of ink-transferring for conventional and digital printing presses. It follows of the section describing processes of ink-setting. Then we present examples showing how print quality is affected by these physical processes, in forms of dot gain, ink-penetration, etc.

2. Ink transferring

Ink transferring and ink setting are the major processes of printing, which dominate different prospects of print quality: optical density, print-through, dot gain etc. The mechanism of ink transferring differs significantly from one printing technology to another. For illustration purposes, offset and inkjet are used as the representative technologies for the conventional and digital technologies. Nevertheless, most of the conclusions and findings presented here are applicable even for other printing technologies.

2.1 Offset

Offset is a commonly used printing technique for large volume productions, where the inked image is transferred or "offset" from a plate to a rubber blanket, then to the printing surface (Kippan, 2001). When used in combination with the lithographic process which is based on the repulsion of oil and water, a flat (planographic) image carrier or plate is employed. On the plate image elements receive ink from the ink rollers, while non-printing areas attract a water-based film (fountain solution), keeping the non-printing areas free from ink.

Figure 1 is a schematic drawing of offset system (left), in which ink transferring is achieved by mechanical pressure, from the printing plate to the rubber blanket and in turn from the blanket to paper. At each time of the ink transferring the dots get squashed a little bit due to pressure and the diameter of the printed dot increased. Consequently, the dots (or the true dot percentage, a) become bigger on the paper than on the plate (the nominal dot percentage, a_0). Nevertheless, at the final stage of the ink-transferring wherein ink splitting occurs, ink dots may experience a count-effect. Ink filament expands in length while exiting, at the same time exerts a force (ink tack) on the ink dot, pulling the ink off the dots on paper until the filament breaks. This explains the observation of unusually small and even negative dot gain for the light tones of the offset (Yang and Lundström, 2007).

2.2 Inkjet

Ink transfer of ink jet is completely different from the conventional printing technologies. There is no mechanical contact between the inking device (the printing head) and the paper. Rather ink is jetted out in form of tiny droplets by pressure pulses regulated by electrical pulse (voltage) that results in either volume deformation (shear of piezocrystal) or thermal bubble expansion inside the print head. On the right half of Figure 1 it depicts the operational principles of an ink pressure chamber surrounded by walls of piezocrystal. When + and - voltages are applied the walls bend (b) and push an ink droplet out of the nozzle. When the walls bend inwards because of reversed voltages (c), the ink inside the ink chamber contracts, causing the ink droplet breaks from the nozzle and is jetted out.

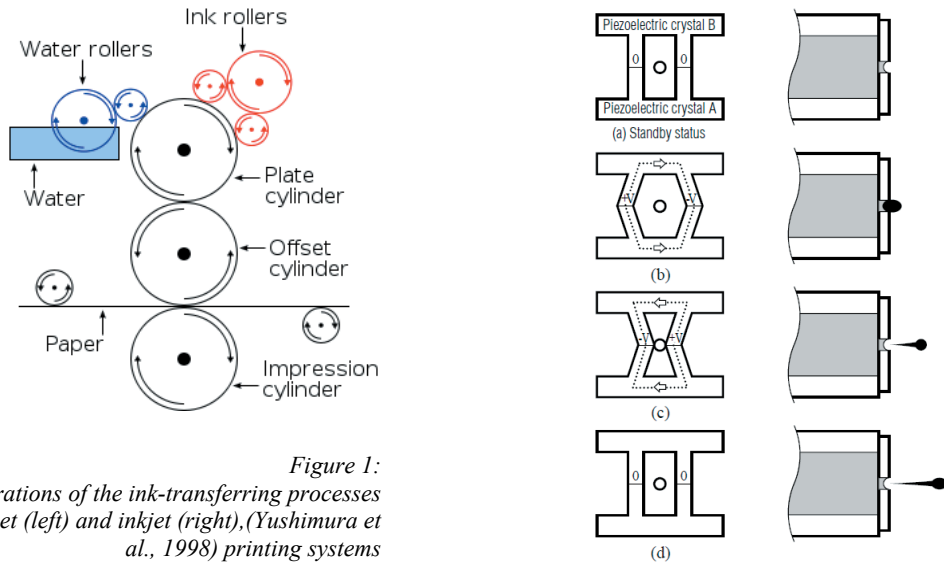


Figure 1:
Illustrations of the ink-transferring processes
for offset (left) and inkjet (right), (Yushimura et
al., 1998) printing systems

There are a few factors originated from the ink transfer process, which are potential sources of physical dot gain. The fluctuation of the electrical pulses (waveform) is one of the sources for size- and speed variations of ink droplets. The print head comprise of a matrix of nozzle. Variation of the nozzle opening influences naturally the volume of ink droplet and in turn the dot-size. Moreover, ink jetting and the formation of ink droplet depend strongly on the ink viscosity. When the ink viscosity is sensitive to the temperature, variation in operational temperature may lead to unexpected dot gain characteristics.

3. Ink setting

After exiting the printing nip in offset ink dots continue to set (often known as ink setting), this occurs both vertically (ink penetration) and horizontally (ink spreading), which increases the dot diameter. This effect is more pronounced for prints on uncoated grades like newsprint than on coated grades. In addition to the paper properties, ink transferring and ink setting depend also on press parameters, rubber blanket used, ink properties and even fountain solutions. These parameters and materials' properties contribute naturally to the physical dot gain in one way or other. Ink-setting is particularly important for inkjet. It is actually one of the key factors that govern the quality of inkjet print. The initial dot size on paper depends on the speed (the kinetic energy) of the droplet that strikes the paper substrate in addition to the volume of the droplet. Fluctuations in droplet size and speed lead to the fluctuations in dot size and physical dot gain. After the ink droplet lands on the paper surface, ink-setting process follows, namely the ink (pigment or dye) is adsorbed to the paper surface. Ink-setting is a 3-dimensional process. Governed by surface tension of the ink droplet and surface energy of the paper substrate, ink spreads on the paper surface while it is absorbed vertically into the paper, driven by the capillary force of the paper's pore structure. Figure 2 highlights the major processes involved in ink-setting on coated surface (Kettle et al., 2010; Lamminmaki et al., 2010). The time lengths of these processes vary dramatically from microsecond (ms) to hundreds of seconds or even hours.

The colour tone of inkjet print relates closely to the movements of the ink droplets, namely ink-spreading in x-y plane and ink-penetration along z-direction. These movements are of critical importance for the quality of print as well as the productivity of the printing operation. The ink colorant needs to be immobilized quickly on

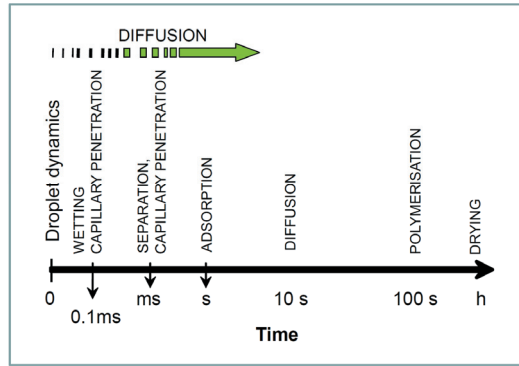


Figure 2: Time scale of ink-setting processes (Kettle et al., 2010)

on the surface of paper and to separate from the ink solvent. However too quick ink absorption into the paper sheet can frequently lead to poor print quality, for instance low optical density and print gloss, severe strike through etc. On the other hand, if the ink absorption is not quickly enough, it will cause drying problem. This in turn, results in lateral ink-spreading (physical dot gain or line broadening) colour on colour bleed, and edge raggedness, etc. Therefore, the requirements of ink setting are contradictory and an appropriate trade-off between these two effects is needed (Svanholm, 2007). This has been normally achieved by either sizing or surface coating, which modify the sheet's porosity and absorbency characteristics.

3.1 Ink spreading

From a print quality point of view, the most important physical processes of ink-setting are ink spreading and ink penetration. Among these two, ink-spreading is the major source of physical dot gain, while ink penetration affects mainly colour saturation (optical density), gloss and print through.

Ink spreading is governed by ink-paper interaction that is often characterized by so-called contact angle. As shown in Figure 3, an ink droplet on the paper substrate creates three interfaces, solid-liquid, solid-gas, and liquid-gas. The movement of the ink droplet on the paper surface depends on the interfacial energies: γ_{sg} for solid-gas sometimes known as surface energy of the solid, γ_{sl} for solid-liquid, and $\gamma = \gamma_{lg}$ for liquid-gas which is also known as surface tension of the liquid. In equilibrium, these interfacial energies satisfy the Young Equation

$$\cos \theta_c = \frac{\gamma_{sg} - \gamma_{sl}}{\gamma} \quad [1]$$

In the expression θ_c is the contact angle.

Equation [1] indicates that the value of the contact angle depends on the surface energy (γ_{sg}) of the substrate, provided that the substrate's surface is smooth, nonporous, non-absorptive, and homogeneous. When the surface energy of the substrate equals to the interfacial energy of the solid-liquid, namely $\gamma_{sg} = \gamma_{sl}$, the contact angle equals to 90° . The contact angle is otherwise bigger or smaller than 90° depending on the relative interfacial energies, $\gamma_{sg} - \gamma_{sl}$. It is obvious that the behaviour of ink spreading, characterized by the contact angle, can be altered by surface treatment like coating or sizing because of modified interfacial energies.

Contact angle is often used as the major descriptor for the wettability of the solid surface. The surface is said to be hydrophilic as the front of the ink droplet will advance (spreads) on the surface, when the contact angle is smaller than 90° . The surface is said hydrophobic when the contact angle is greater than 90° . Furthermore, the surface is called super-hydrophobic if the contact angle is 150° or higher.

For a porous material like paper, there is another physical process, ink-penetration, occurring in parallel and competing with the process of ink-spreading. Penetrating into the porous structure of the paper, the volume of the ink droplet on the paper surface continuously decreases. This makes the ink-droplet on paper deviates from the presumption of the Young Equation. Consequently, the value of the contact angle is no longer constant along time as reported in published works (Debeljak et al., 2010).

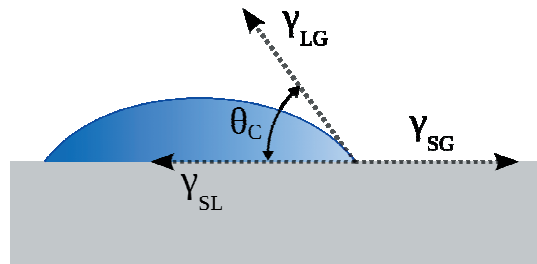


Figure 3: Contact angle and interfacial energies between ink droplet, air and paper. L-liquid (ink), S-solid (paper), G-gas (vapor and air)

One has to be with cautious when applying the Young model to print on paper, because the paper surface is seldom smooth in addition to paper is porous and absorptive. Besides the physical quantities, like interfacial energies, topological structure of the paper surface also plays an important role in the surface wettability. For paper of rough surface, the contact angle may locally be smaller than 90° at some positions (hydrophilic), even though the global (average) contact angle is bigger than 90° (hydrophobic) and vice versa. This leads to preferred wetting paths on the surface, for instance along the surface fibres of plain paper. This also causes irregular dot shapes and rough line edges compared to their digital origins. To reduce the impact of the paper surface’s topology, calendering is often needed in paper making.

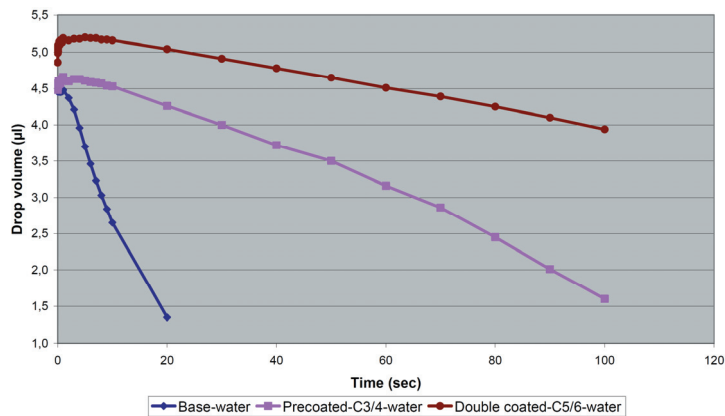


Figure 4: Volume decreases of water droplets along time on the base paper, pre-coated and double-coated substrates (Zeyringer et al., 2010)

3.2 Ink-penetration

The rate of ink penetration into the pores of the paper substrate, equalling to the volume of the ink transportation per unit time (l^3s^{-1}), is described by Darcy’s law,

$$\frac{dV}{dt} = - \frac{KA\Delta P}{\eta L} \tag{2}$$

The Darcy’s law says that the rate of ink penetration is linearly proportional to the permeability of the substrate, K , the effective pressure difference (ΔP) over the length L , as well as the area of cross section of the pore, A , but inversely proportional to the viscosity of the ink, η , and the transport (penetration) length, L . In case of external pressure, ΔP , should be regarded as the sum of external pressure and the capillary pressure. Figure 4 shows the volume decreases of the ink (water) droplets on paper surfaces, along the time, as the consequence of ink penetration (Zeyringer et al., 2010). Except for the initial seconds when the ink droplet oscillates in shape directly after its landing on the paper surfaces, the ink volumes decrease linearly along time for all of the papers, indicating a constant rate of ink penetration into each of the substrates. It is obvious that the ink penetrates much faster into the base paper than into the pre-coated and double-coated papers, because of higher porosity and much better connectivity between the pores (effective porosity) in the base paper. On the contrary, there are many dead end pores in the coating layers, blocked by fine pigment and latex particles, hindering the passage of the ink/water. This also explains why coating layers reduce ink-penetration as seen in Figure 5 (right).

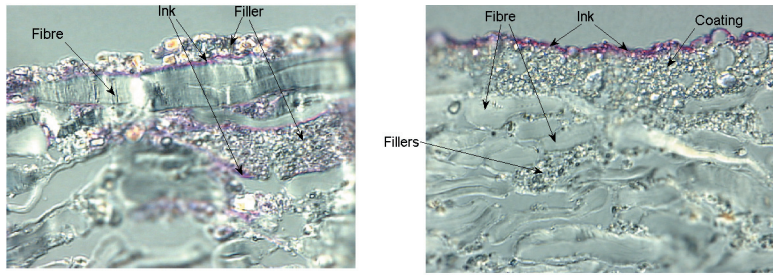


Figure 5: Microscopic view of ink-setting for inkjet printings on plain paper (left) and coated paper (right) (Svanholm, 2007)

Figure 5 depicts the microscopic view of the cross section of inkjet ink penetrating into two commercial papers, one coated and one uncoated office paper. As seen, the ink penetrates deeply into the structure of the uncoated which is of an open structure. Besides, depending on the flowing path, the depth of the ink penetration varies. According to the theoretical study (Ridgway et al., 2001), the ink moves favourably along fibres' surface rather than fills the pores along its way. Therefore, the ink can reach rather deep into the bulk. On the contrary, the ink is accommodated by the coating layer of the coated paper hence no penetration into the base paper occurs.

Besides surface coating used for producing high paper grades, lower grades of paper as for instance, newsprint, office paper and other uncoated grades, employ other solutions which cost much less than coating. One of the solutions is sizing with starch or chemicals which close up the open paper structure of the uncoated. This reduces both the porosity and the permeability of the paper, which, according to Darcy's law, will reduce the ink penetration. This in turn can reduce print quality problem like print through, cockling, etc. The commonly used size agents are starch and polyvinyl alcohol, PVOH (Svanholm, 2007). Figure 6 shows the microscopic views of cross section of the ink jet prints. These two paper-substrates have identical material compositions except for sizing. With the same volumes of ink applied by the inkjet, it is obvious that the ink penetration is significantly reduced in the internally sized paper.

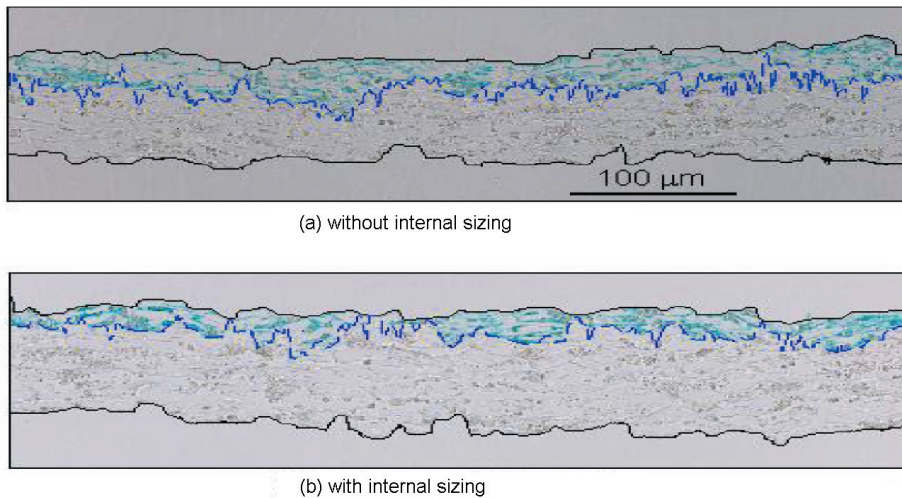


Figure 6: Dependence of ink-penetrations on internal sizing for uncoated hand-sheets. The papers have the identical paper-making materials but sizing (Yang et al., 2005)

4. Results and discussions

4.1 Ink spreading and dot gain

In-plane ink spreading causes deviation of the printed-dot size (dot percentage) from its nominal value. This deviation is often called geometrical or physical dot gain as it stands for the true area-difference, very frequently area-extension. Quantitative knowledge of ink spreading or dot gain provides one with insight into the printing processes (Yang and Lundström, 2007). Be aware of that the true dot area differs from the so called effective dot area because the latter comprises even the optical dot gain.

The physical dot gain varies non-linearly with the nominal dot percentage, but subjects to the constraints at zero and full-tone percentages. One may express their relationship in a hyperbolic form (Yang, 2004),

$$\Delta\sigma_{phy} = (\beta - 1)\sigma_0(1 - \sigma_0) \quad [3]$$

where σ_0 is the nominal dot percentage and β a parameter depending on the entire printing system: the press, the ink and the paper. For a well controlled printing system with fixed press's settings and the fixed ink and paper combination, β is nearly a constant and can thus be used for calibrating the printing system as demonstrated by the researchers (Emmel and Hersch, 2002; Hersch et al., 2005 and 2008).

Optical dot gain is an optical illusion rather than a true dot-area extension. It originates from lateral light scattering inside the paper substrate. As the consequence, a photon that enters the substrate at an inked area (ink dot) has a probability to enter and exit from non-inked areas and vice versa. The probability increases when the incident point moves close to the border (edge) of the dot. Having passed once through the ink area, the exiting photon is coloured even its exiting point is outside of the ink dot. Hence, perceptually, the adjacent area surrounding the dot appears to have the similar colour as the inked area.

Quantitative determination of dot gain, physical and optical, needs tools. Physical and optical dot gains co-exist in the conventional measurements using for example optical densitometer or spectrophotometer. It is hence difficult to separate one type from another without using the tools. There are basically two types of methods for separating physical dot gain from the optical. For the first type, one needs physical model that deals properly with the major optical phenomena, to mention some, lateral light scattering, fluorescence, and interfacial reflections (Hersch and Hébert, 2006; Yang, 2010). Another type of tool bases on image processing technique or image thresholding (Engeldrum, 1994; Arney et al., 1995; Nyström, 2009). By careful choosing the threshold, the inked area (dots) can be separated from the non-inked ones. Figure 7 displays the physical dot gain, determined with these types of methods. More extensive description on these tools is beyond the scope of the present work and will be published elsewhere.

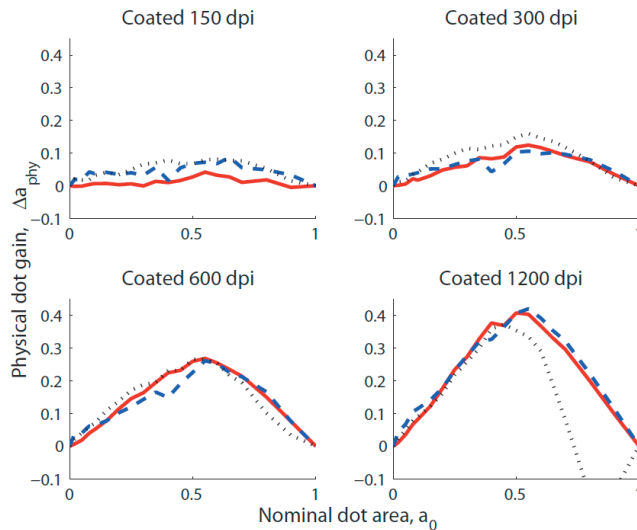


Figure 7: Physical dot gain of halftones (magenta) of different screen resolutions. Solid time: the spectral-model-based approach; dashed line: the transmission scan; and the dotted line: the image-analysis-based method (Nyström and Yang, 2009)

Dot gain causes lower light reflection or higher optical density, because of light absorption by ink dots. Mathematically, one may sub-divided the measured spectral reflectance into two parts,

$$R(\sigma_0, \Delta\sigma_{phy}, \lambda) = R_{MD}(\sigma_0, \lambda) - \Delta R(\sigma_0 + \Delta\sigma_{phy}, \lambda) \quad [4]$$

In this expression, R_{MD} is the reflectance computed with the Murray-Davies model which includes neither physical nor optical dot gain. Following the proceeding discussions, the total effect of dot gain comprises two components: physical and optical dot gain, namely

$$\Delta R(\sigma_0 + \Delta\sigma_{phy}, \lambda) = \Delta R_{phy}(\sigma_0 + \Delta\sigma_{phy}, \lambda) + \Delta R_{opt}(\sigma_0 + \Delta\sigma_{phy}, \lambda) \quad [5]$$

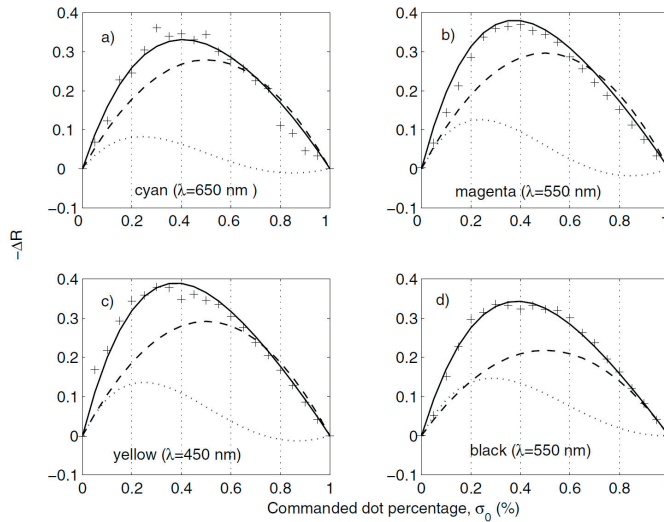


Figure 8: Effects of dot gain on reflectance values computed employing the physical model (Yang, 2004). ΔR_{phy} : the physical dot gain (dashed lines); ΔR_{opt} : the optical dot gain (dotted lines); and $\Delta R = \Delta R_{phy} + \Delta R_{opt}$: the total dot gain (solid lines). The measurements are marked with +

Figure 8 shows the example of applying the physical model based approach. As expected the physical dot gain (dashed lines) has a hyperbolic form with its maximum at $\sigma_0=50\%$, while for optical dot gain (dotted lines) its maximum is shifted to lower nominal dot percentage, $\sigma_0 < 50\%$, because the optical dot gain responds to the true physical dot size, $\sigma = \sigma_0 + \Delta\sigma_{phy}$ rather than the nominal one. The computation (solid lines) of the total dot gain agrees well with the measured (cross, +).

4.2 The effects of ink penetration on colour tone reproduction

In terms of print quality, there are a few clear drawbacks of ink penetration. Print through or more precisely strike through is one of the severe drawbacks of ink penetration, particularly for water-based inkjet inks. For offset, instead of the ink pigment, the ink oil penetrates deeply into the paper and turns the penetrated portion of the paper substrate into half-transparent. In either way, the printed pattern becomes clearly visible on the reversal side, which disturbs reading. Strike through is one of the two components of print through. Another component is known as show through, which is originated from insufficient opacity of the paper substrate. Show through occurs when the paper's opacity is too low to prevent the feature printed on the next page from being visible through the paper.

Reduced optical density or colour gamut is another severe drawback of ink penetration. Figure 9 displays the optical densities of the prints on the substrates shown in Figure 6. Obviously, the prints on the sized paper (less ink-penetration) have higher optical densities in the absorption bands of the inks. The explanation is straight forward. Inkjet inks are transparent and of little light scattering. Paper making materials (fibres and fillers), on the other hand, have very strong light scattering and serve as the base for light reflection of the print. In the case of less ink penetration, the ink concentrates in a thinner layer that lies closely to the top of the paper. The light has then higher possibility to pass through the whole inked layer before it hits the paper-making materials and is reflected. This results in through light absorption and in turn higher optical density.

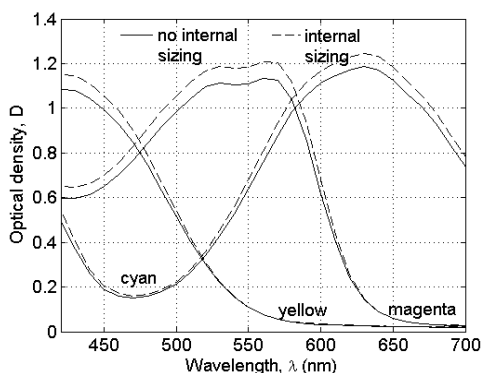


Figure 9: The optical densities of the prints on the substrates shown in Figure 6. The prints of less ink-penetration (with internal sizing, dashed lines) have higher optical densities than those of deeper ink penetration (solid lines, without internal sizing)

On the contrary, in the case of deeper ink-penetration, the same amount of ink is now distributed in a thicker layer of ink-paper mixture. As the consequence, the light is more likely to be scattered (reflected) by the fibres and fillers before it passes through the whole inked layer. Consequently, the absorption to the light is less sufficient, which makes the printed colour less saturated or lower optical density.

It is generally difficult to evaluate the pure effects of ink penetration on halftone print by experimental means, because one can hardly obtain two halftones that differ only in ink-penetration. Other impacts such as different ink-spreading or physical dot gain may play a role as well. To avoid the complexity in the assessment on the impacts of ink-penetration, comparative studies of solid tones on two commercial paper grades: office paper (uncoated) and photo gloss (coated) were conducted. The prints were created with inkjet using water-based inks. To minimize the influence from the substrates' colours, these two substrates were particularly chosen so that they are very similar in colour before print, see Table 1. The colour differences between the print solids on these substrates are also collected in Table 1. As shown, the colour difference between the coated photo gloss paper and the office paper is barely noticeable ($\Delta E=1.32$). However, the differences increase dramatically after printing, between $\Delta E=12.3$ -25, depending on the printed colours. As only the solid prints are compared, the colour differences arise mainly from the ink penetration.

Table 1: Colour differences (ΔE) between the coated photo gloss paper and the office copy-paper and the solid prints on the substrates

	Paper	cyan	magenta	yellow	black	red	green	blue
ΔE	1.32	12.37	19.30	23.67	13.44	24.92	22.59	20.75

To better appreciate the impacts of ink-penetration on the colour reproduction, the colours of the prints on the respective papers are shown in the chromaticity diagram, Figure 10. The colours of the solid prints are connected by the dashed lines for the office paper and by the solid lines for the coated photo gloss paper. As the areas within the respective lines represent the colour gamut of the prints, it is evident that ink penetration (office paper) reduces significantly the colour gamut. In addition to the solid tones, the colour differences for halftones may as well be estimated using the chromaticity diagram. The pair-wise arrows in the diagram, connected by the line stretch, correspond to the same nominal dot percentage but on different substrates. Obviously, the colour difference or the length of the stretch line grows with increasing ink-coverage, indicating severer impact of ink penetration for the darker tones.

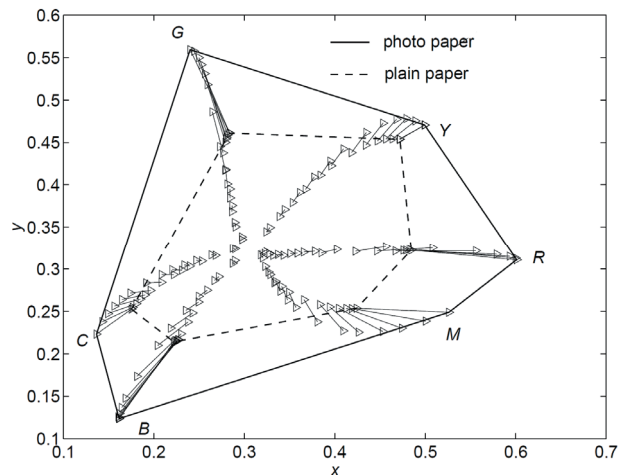


Figure 10: The areas in the chromaticity diagrams, spanned by the prints on plain paper (dashed line) and photo gloss paper (solid line). The pair-wise points corresponding to the same (nominal) dot percentages but different substrates are connected by Δ - Δ . The characters, C, M, Y, R, G and B are the abbreviations of the primary and the secondary colours

References

- Arney, J., Engeldrum, P.G. and Zeng, H. (1995), *An Expanded Murray-Davies Model of Tone Reproduction in Halftone Imaging*, J. Imaging Sci. Technol. 39, pp. 502-508.
- Debeljak, M., Brëko, S., Hladnik, A. and Gregor-Sveteć, D. (2010), *Comparison of ultraviolet inkjet printing on different synthetic fibrous papers*, Tappi J. 9, p 17.

- Emmel, P. and Hersch, R.D. (2002), *Modeling Ink Spreading for Color Prediction*, J. Imaging Sci. Technol. 46, pp. 237-246.
- Engeldrum, P.G. (1994), *The color between the dots*, J. Imaging Sci. Technol. 38, pp. 545–551.
- Hersch, R.D., Emmel, P., Collaud, F. and Cr  t  , F. (2005), *Modeling Ink Spreading for Color Prediction*, J. Electronic Imaging 14, pp. 33001-12.
- Hersch, R.D. and H  bert, M. (2006), *Interaction between Light, Paper and Color Halftones: Challenges and Modelization Approaches*, in Proc. IS&T 3rd European Conference on Color in Graphics, Imaging and Vision (CGIV), pp. 1-7.
- Hersch, R.D., Brichon, M., Bugnon, T. and H  bert, M. (2008), *Deducing Ink Spreading Curves from Reflection Spectra Acquired Within Printed Color Images*, J. Imaging Sci. Technol. 53, pp. 030502-7
- Kettle J., Lamminm  ki, T.T. and Gane, P.A.C. (2010), *A review of modified surfaces for high speed inkjet coating*, Surf. Coating Tech. 204, pp. 2103-2109.
- Kippan, H. (2001), *Handbook of print media*, Springer-Verlag.
- Lamminm  ki, T.T., Kettle, J.P., Puukko, P.J.T., Ridgway, C.J. and Gane, P.A.C. (2010), *The role of ink component diffusion during absorption into inkjet coatings*, in Proc. 11th Tappi Advanced Coating Fundamentals Symposium, pp. 195-214.
- Nystr  m, D. (2009), *High Resolution Analysis of Halftone Prints: A Colorimetric and Multispectral Study*, PhD thesis, University of Link  ping, Sweden.
- Ridgway, C.J., Schoelkopf, J., Matthews, G.P., Gane, P.A.C. and Jamesz, P.W. (2001), *The Effects of Void Geometry and Contact Angle on the Absorption of Liquids into Porous Calcium Carbonate Structures*, J. Colloid Interface Sci. 239, pp.417-431.
- Svanholm, E. (2007), *Printability and ink-coating interactions in inkjet printing*, PhD thesis, Karlstad University, Sweden.
- Yang, L. (2004), *A unified model of optical and physical dot gain in print color reproduction*, J. Imaging Sci. Technol. 48, pp. 347-353.
- Yang, L., Fogden, A., Pauler, N., S  vborg,   . and Kruse, B (2005), *A novel method for studying ink penetration of a print*, Nordic Pulp & Paper Res. J., 20, pp. 399-405.
- Yang, L., Fogden, A., Pauler, N., S  vborg,   . and Kruse, B (2006), *Studying Ink Penetration with Microscopic and Spectroscopic Techniques*, J. Imaging Sci. Technol. 50, pp. 327-332.
- Yang, L. and Lundstr  m, N. (2007), *Physical dot gain of offset: understanding and determination*, Nordic Pulp Pap. Res. J. 22, pp. 388-393.
- Yang, L. (2010), *Probabilistic spectral model of color halftone incorporating substrate fluorescence and interface reflections*, J. Opt. Soc. Am. A 27, pp. 2115-2122.
- Yoshimura, K, Kishimoto, M. and Suemune, T. (1998), *Inkjet printing technology*, OKI Tech. Rev. 64, pp. 41-44.



The impact of optical brightener on the color perception of halftones

Michael Dattner¹, Daniel Bohn², Peter Urban²

¹ BST-International GmbH
Heidsieker Heide 53
D-33739 Bielefeld, Germany
E-mail: michael.dattner@bst-international.com

² Bergische Universität Wuppertal
Rainer Gruenter Straße 21
D-42119 Wuppertal, Germany
E-mails: bohn@uni-wuppertal.de; purban@uni-wuppertal.de

Abstract

Fluorescent-brightening-agents (FBAs) in substrates have a major impact on the perception of color and particularly on the perception of halftone prints. The main objective is to describe the illumination-dependent interaction of brightened substrates and inks as well as colorants in general.

Therefore, the characteristic behavior of FBAs and inks and their combination in the UV wavelength range must be considered additionally to the effects in the visible range.

Measurements of identical samples on brightened substrates show significant differences in their spectra if different illuminations are used. Factually, these effects cannot be compensated by the solely consideration of the particular illumination-type with the classical calculation of tristimulus values (XYZ) and the corresponding $L^*a^*b^*$ -values. The related CLIELAB-color differences that occur between these samples have a maximum of 7.02 DeltaE*ab units, if they are measured with the illuminations close to A and D65, respectively.

A physically founded mathematical description of the mentioned complex interactions is presented. These interactions are directly correlated to the absorption of printed samples, which can be observed especially within the UV-range. All discovered spectral conclusions will be used to adjust the classical approach of converting spectra to $L^*a^*b^*$ -values, by considering the effects of FBAs on the perception of halftone prints.

Keywords: optical brightener, fluorescent brightening agents, perception of color, metamerism, color stimulus, spectral reflexion, halftones

1. Introduction

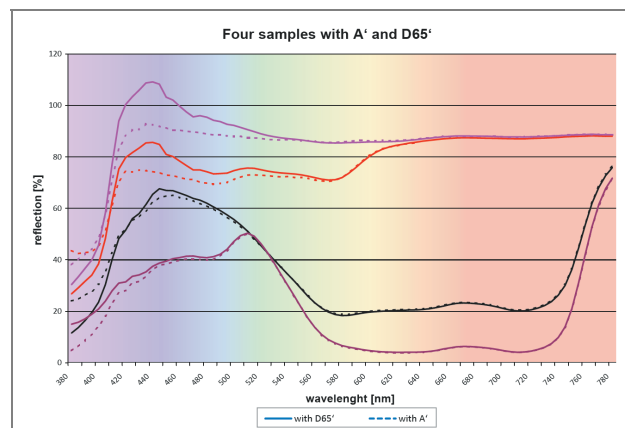


Figure 1: The influence of different illuminations on spectra of brightened samples

Optical brighteners - fluorescent brightening agents (FBAs) - in substrates have a major impact on the perception of color and particularly on the perception of halftone prints. The main objective is to describe the illumination-dependent interaction of brightened substrates and inks as well as colorants in general.

Therefore, the characteristic behavior of FBAs and inks and their combination in the UV wavelength range must be considered additionally to the effects in the visible range.

Measurements of identical samples on brightened substrates show significant differences in their spectra if different illuminations are used (Figure 1). Factually, these effects cannot be compensated by the solely consideration of the particular illumination-type with the classical calculation of tristimulus values (XYZ) and the corresponding $L^*a^*b^*$ -values (coordinates in the CIELAB-color-space).

Figure 2 illustrates the CLIELAB-color differences ΔE^*_{ab} with a maximum of 7.02 units, which occur between samples, that are measured with the illuminants A and D65, respectively. For the ΔE^*_{ab} calculation, the corresponding spectra are converted to $L^*a^*b^*$ -values according to the established approach (CIE, 1971) using the 2°-standard observer and the standard illuminant D65.

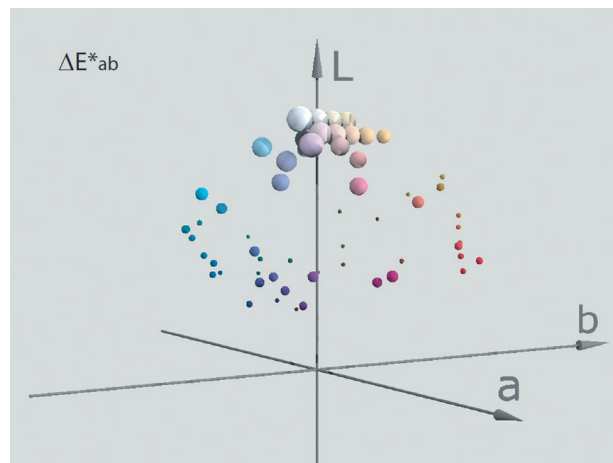


Figure 2: The influence of different illuminations on brightened samples in ΔE^*_{ab} -units

Within the present article, a physically founded mathematical description of the mentioned complex interactions is presented. These interactions are directly correlated to the absorption of printed samples, which can be observed especially within the UV-range. All discovered spectral conclusions will be used to adjust the classical approach of converting spectra to $L^*a^*b^*$ -values, by considering the effects of FBAs on the perception of halftoneprints.

2. State of the scientific knowledge

To classify the achieved results, established knowledge concerning metamerism, the consideration of FBA-effects and colorimetric issues are introduced in the following. All research in this article is directly related to them.

2.1 Metamerism

According to DIN 5033-1, two color stimuli with different color stimulus functions are termed “metamer”, if they lead to identical color stimulus specifications ($L^*a^*b^*$ -values) with one illumination, but to different $L^*a^*b^*$ -values with another illumination. Two “absolute-identical” samples show the same spectral reflexion and appear in the same way with every illumination for every observer (Din, 1992). Related issues concerning the reproduction of identical color stimulus specifications by different spectra (in the visible wavelength range concerning one illumination) are analysed for example by URBAN (Philip Urban, 2005). The effects of FBAs are explicitly excluded in URBANs study.

2.2 Existing approaches for considering the influence of optical brightener

It is documented and explored that the effects of different FBAs in various printing substrates lead to individual, illumination-dependent effects with unprinted and fully printed surfaces (T. Götze et al., 2003), (P.Green, E. Loser, 2008), (J. Zwinkels, 2008). The optical behaviour of halftone samples on brightened substrates, is also empirically determined (F. Geßner A. Kraushaar, 2006), (B. Fiebrand, 2007), (H. Pertler U. Bertholdt, 2007), but not physically founded described, until now.

2.3 Colorimetric issues

The well known tristimulus value (XYZ) calculation considers sample-reflexion and relative spectral power distribution of illuminations and CIE standard observer in the wavelength range between 380 nm and 780 nm (CIE, 1971). The illumination-dependent effects caused by brightened substrates are not being considered, yet.

3. Results

There are strong correlations concerning FBA-effects between unprinted substrates and halftone prints. Unprinted laboratory substrate once brightened and once unbrightened (but no further differences) measured with an UV-intense illumination and D65' (simulation of the CIE-standard illuminant D65) shows the characteristic excitation- and emission-behavior of the involved FBA (Figure 3).

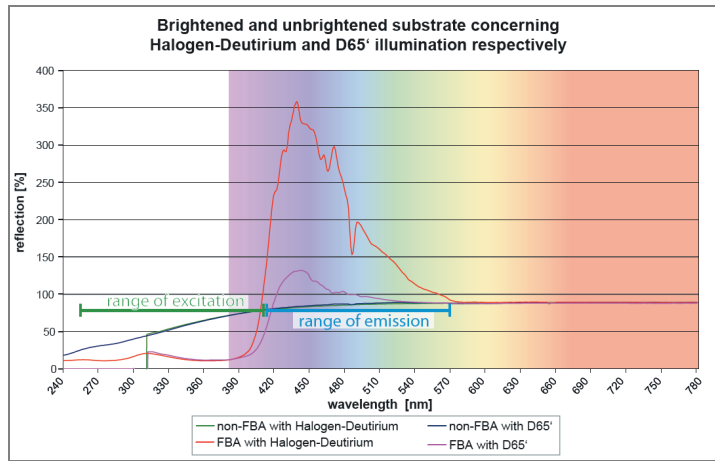


Figure 3: Absorption behaviour of a typical FBA

Unprinted brightened substrate measured twice - once with and once without UVcut-filter - provides all necessary information about the relevant effects of the FBA. This is used to calculate the spectral impact of this brightener on the spectral data of halftone samples measured with UVcut-filter (which eliminates the FBA-effects). Furthermore, spectral information of halftone samples printed on substrate without FBAs (APCO II/II) as well as printed on the mentioned brightened substrate (with warranted identical conditions) allows a physically founded mathematical description of the effects. For the modulation of the illumination-dependent interaction of FBAs and inks, the characteristic absorptions of optical brighteners and inks as well as their combination are relevant. The FBA-activity, as mentioned above, is not limited to the visible wavelength range, but also takes place in the UV-range. Therefore, especially the individual absorption of inks in the UV-range (Figure 4) is as important as it is in the visible wavelength range.

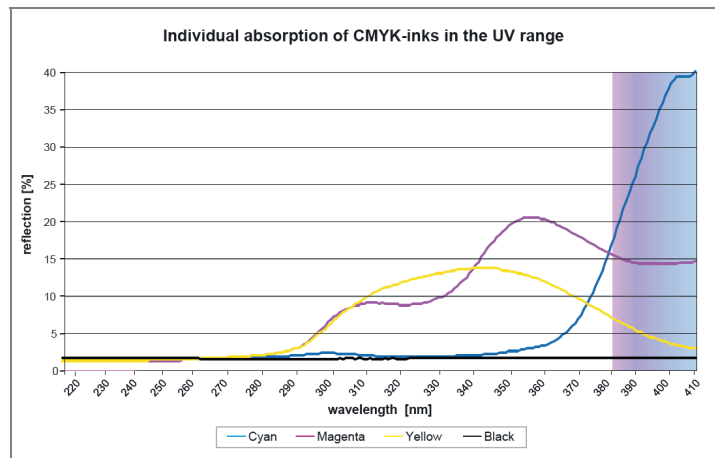


Figure 4: The individual absorption behavior of inks in the UV range

The ink absorption in the invisible UV-range weakens the excitation of the FBA and weakens consequently (and additionally to the absorption of the inks in the visible range) also the FBA-emission and therefore the corresponding optical effects. There are e.g. yellow and black having similar absorptions around 450 nm (where the main FBA-emission usually takes place) if printed on APCO, but different spectra in this range (Figure 5: marked area), if printed on brightened substrate. This is because the corresponding FBA-effect is particularly influenced by the individual absorption of yellow and black in the wavelength range of the FBA-excitation (280 nm - 400 nm).

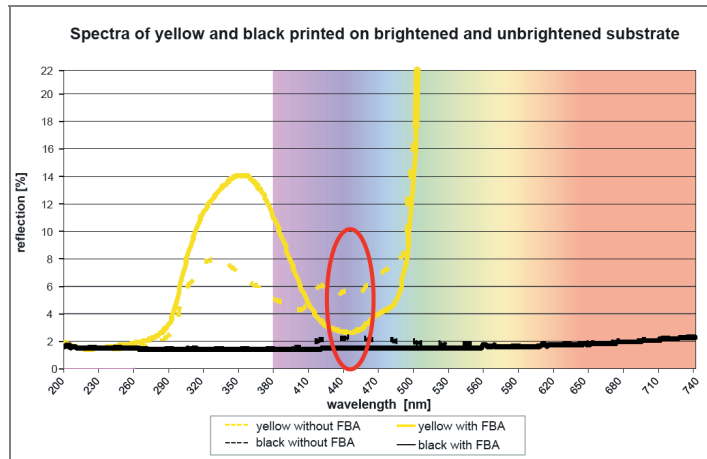


Figure 5: Spectra of yellow & black printed on brightened and unbrightened substrate (the FBA-emission range is marked)

These starting points initiate this survey which ends up with an extension of the metamerism-comprehension to a spectral-based description of the interaction between FBAs and screen-printed inks as well as the consideration of the identified effects in colorimetric issues. First of all, the experimental setup and the used materials are presented in the following.

3.1 Test environment

An UV-Vis spectrophotometer is used to determine spectral information in the visible and particularly in the UV-range (250 nm - 780 nm) of halftone prints. Several light sources and optical filters are used to generate measurements concerning various illuminations, including the simulations A', D50' and D65' of the CIE standard illuminations A, D50 and D65. Finally Figure 6 (left) shows evenly distributed spectra (in the relevant wavelength range of excitation and emission of FBAs, printed on unbrightened substrate) of 65 samples, which were identified in a large sample set shown in Figure 6 (right). All presented results are achieved concerning these halftone combinations of the involved primary printing colors (CMY).

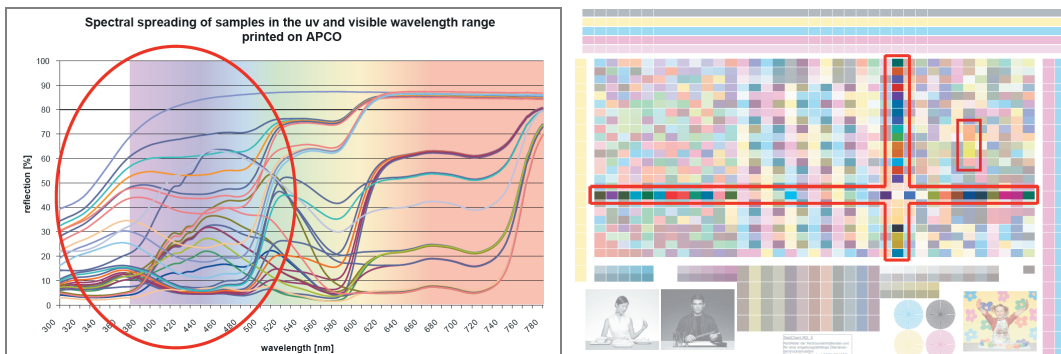


Figure 6: Spectra of samples printed on APCO II/II and the sample-positions on the developed test chart

3.2 Extension of the metamerism-comprehension

Based on the consideration of the UV-range, it can be shown that metamerism effects take place even though the spectral data of two samples are identical in the visible range (to the greatest possible extent concerning one particular illumination), if these sample-spectra are different in the UV-range. Their spectral data differ

unmistakably also in the visible range, if another illumination is used for the measurement (Figure 7). This is because of the distinct relative power distributions of the illuminations and the corresponding different excitation of the FBA, which is affected by the individual absorption of the samples in the UV-range.

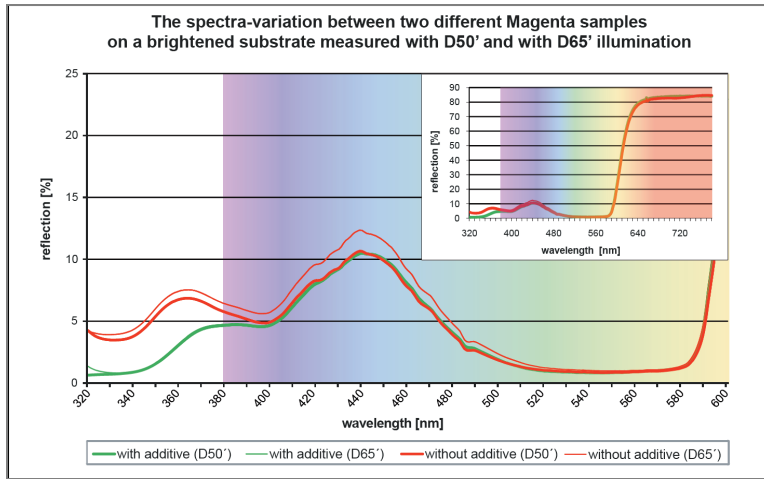


Figure 7: The spectra-variation between two different Magenta samples with identical ink-film-thickness on a brightened substrate measured with D50' and the same samples measured with D65' illumination

The two samples shown in Figure 7 are a standard magenta once admixed with an UV-absorbing additive, and once without additive. The $L^*a^*b^*$ -values of these samples differ concerning D50' only by 0.25 ΔE^*ab -units, while the CIELAB color difference of the same samples concerning D65' is at 4.22 ΔE^*ab -units. This result confirms the necessity to adjust the metamerism-definition by extending the relevant wavelength range of the established visible range by the UV-range. This extension reconfirms the statements “metamer” and “absolute-identical” of DIN 5033-1.

3.3 A physically founded description of the interaction between illumination, optical brighteners and inks

Spectral information of halftone samples printed on substrate without FBAs as well as printed on brightened substrate with identical conditions ($\beta_{APCO}(\lambda)$ and $\beta(\lambda)$ respectively) allows a physically founded mathematical description of the occurring perception-effects (Figure 8).

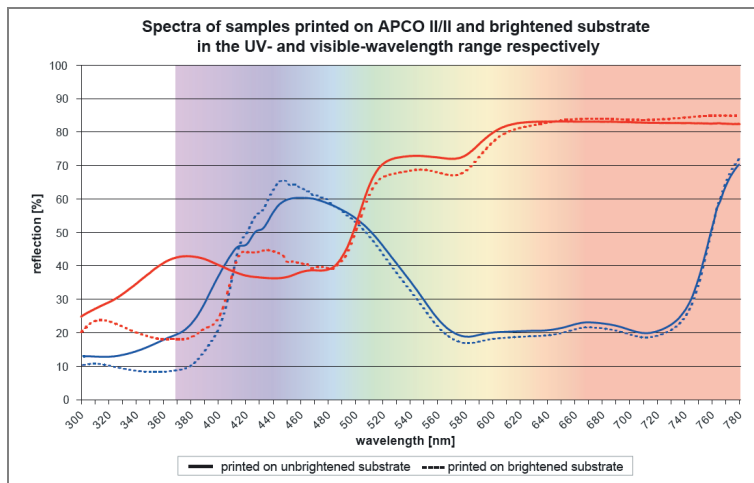


Figure 8: Spectra of two samples printed on APCO II/II and brightened substrate

The formula which describes the mentioned spectral influence of FBAs is defined by equation (3.1). The calculation of theoretical values $\beta_{calc}(\lambda)$ of halftone samples printed on brightened substrate is based on measurements with UVcut-filter $\beta^{UVcut}(\lambda)$ (where the effects of the FBAs in the visible range are eliminated) (Figure 9).

Therefore, the correspondence between spectra of unprinted brightened substrate measured once with and once without UVcut-filter is included for considering the brightener effects of printed samples. This correspondence can be described by the wavelength dependent brightener factor $B(\lambda)$ (M. Dattner, 2011), (P. Urban et al., 2009).

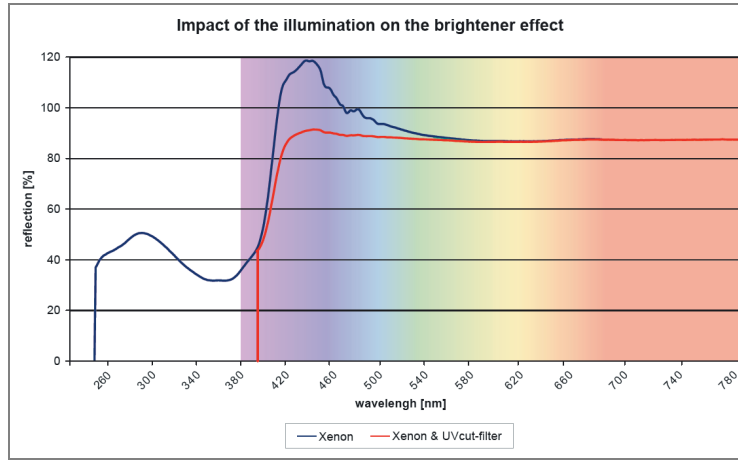


Figure 9: Spectra of brightened substrate measured once with and once without UVcut-filter

$$\beta_{calc}(\lambda) = \beta^{UVcut}(\lambda) \cdot (1 + B(\lambda) \cdot \eta) \quad [3.1]$$

with the mentioned brightener factor $B(\lambda)$ which is defined by:

$$B(\lambda) = \beta_{PW}(\lambda) - \beta_{PW}^{UVcut}(\lambda) \quad [3.2]$$

and with η as a weighting factor, which is defined by:

$$\eta = \frac{\Delta A_R \cdot (1 + D_K)}{\Delta A_{PW}} \cdot \Delta S \quad [3.3]$$

Equation 3.3 includes the area-differences ΔA_{PW} and ΔA_R between $\beta_{APCO}(\lambda)$ and $\beta(\lambda)$, which are defined as a Riemann integration concerning the wavelength range of the FBA-excitation for unprinted and printed samples respectively with step size $\Delta\lambda$:

$$\Delta A = \sum_{300nm}^{410nm} |\beta_{APCO}(\lambda) - \beta(\lambda)| \cdot \Delta\lambda \quad [3.4]$$

Furthermore D_K is defined by the difference between $\beta_{APCO}(\lambda)$ and $\beta(\lambda)$ concerning the wavelength range of the main emission of the FBA for printed samples (in this case at 430 nm):

$$D_K = |\beta_{APCO}(430nm) - \beta(430nm)| \quad [3.5]$$

Finally ΔS is defined by the weighted area-difference between the relative spectral power distributions $S^{UVcut}(\lambda)$ and $S(\lambda)$ of two illuminations as a Riemann integration concerning the wavelength range of the FBA-excitation:

$$\Delta S = \sum_{300nm}^{410nm} |S^{UVcut}(\lambda) - S(\lambda)| \cdot 3 \cdot \Delta\lambda \quad [3.6]$$

Remark:

ΔS is calculated concerning the relative spectral power distribution of the actually used illumination with UVcut-filter and the illumination, wherefore the FBA effects should be predicted. The relative spectral power distribution of the actually used illumination without UVcut-filter is solely included in the brighter factor $B(\lambda)$.

The strong dependency between the area-differences ΔA and ΔS with the factor η for weighting the brightener $B(\lambda)$ shows the physically founding of this approach. Consequently, the impact of the absorption of inks in the UV-range in interaction with the excitation-absorption of the FBA is as well as included as the impact of the relative spectral power distributions of various illuminations.

3.3 Adjusted colorimetric approach

As shown in Figure 2, the consideration of the various relative spectral power distributions of different illuminations without adjusting the corresponding reflectance spectra is not successful within the calculation of color stimulus specifications ($L^*a^*b^*$ -values), if FBAs are involved. Calculating $\beta_{calc}(\lambda)$ via equation (3.1) for halftone samples printed on brightened substrate, by using measurement-data generated with UVcut-filter and the illumination-dependent brightener factor $B(\lambda)$ adjusted to the desired illumination, solves this problem. No further adjustments are necessary to provide reliable color difference estimations via CIELAB- ΔE^*ab even though FBAs are involved and the illumination used for the measurement is different to the illumination, which is relevant for color-validations.

3.4 Achieved quality in calculations

Figure 10 shows the accuracy of the mathematical implementation concerning spectral data.

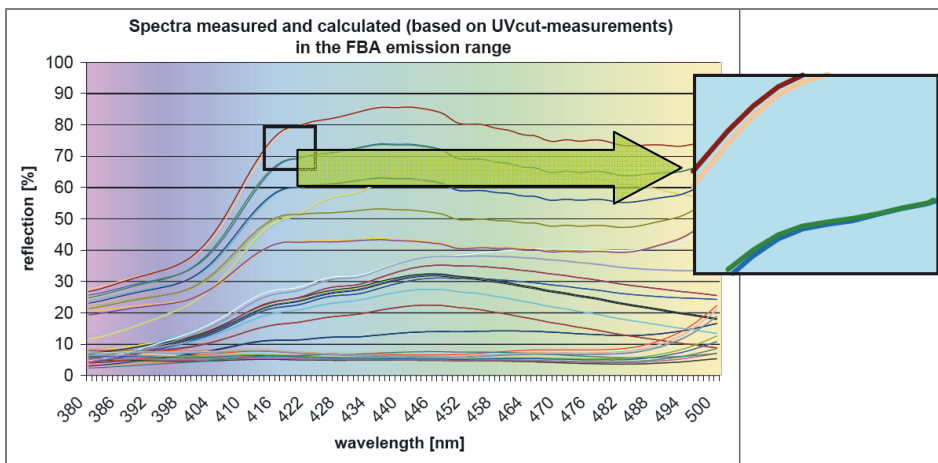


Figure 10: Measured and predicted spectra concerning the relevant wavelength range (Note: the zoom-in window shows the nearly perfect match)

The concerning CIELAB- ΔE^*ab values affirm the shown accuracy in the spectral calculations. Figure 11 illustrates the CLIELAB-color differences ΔE^*ab up to 1.50 units (0.52 units in average), which occur between measured and predicted spectra.

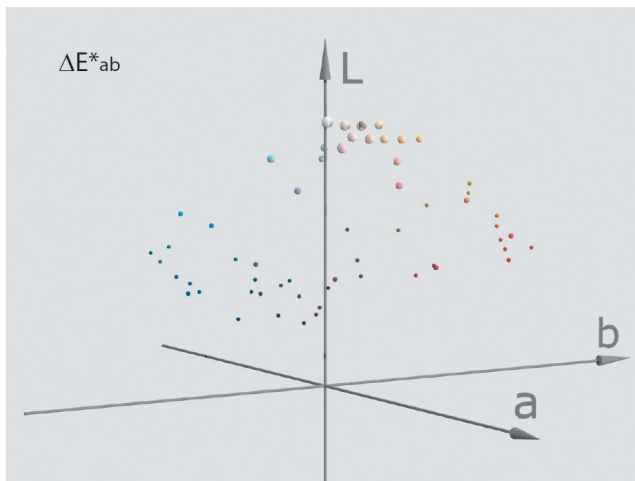


Figure 11: Color difference between measured and predicted spectra in ΔE^*ab -units

4. Conclusions

FBA will no longer be unconsidered and hidden by measurements with UVcut-filter at the colorimetric cross-validation of printing products. The influence of FBAs is considered by the introduced spectral estimation of illumination-dependent effects within the interaction of brightened substrates and inks (or colorants in general). Since the introduced approach is solely based on spectra (and no further information concerning involved primary colors or covering-details), it can be used to estimate the color perception of arbitrary samples independent of the measurement-light-source and the illumination at which the samples should be validated. Therefore, reliable color difference estimations via CIELAB- ΔE^*_{ab} are provided even though FBAs are involved and the main measurements are done with an UVcut-filter.

In order to find a fully physically based description of the brightener effects, it is necessary (at this point) to include the desired spectra in the calculations (equation 3.4), but this information is only relevant for one single scalar weighting factor. Therefore, the legitimacy of the introduced approach is given and offers the basis for further studies.

5. Outlook

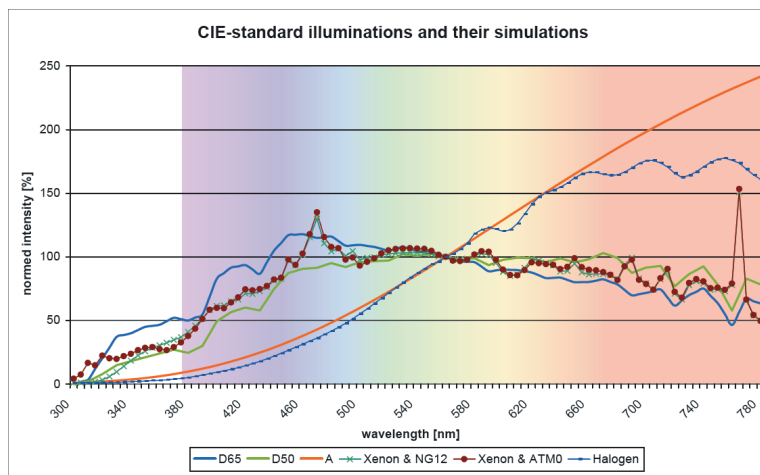


Figure 12: The CIE standard illuminations A, D50 and D65 and the corresponding simulations A', D50' and D65'

Further research will provide approaches, where the spectra which should be calculated within the color prediction are not contained in the calculation itself. A practice-oriented approach will additionally focus only on the visible spectrum which is measurable with commercial handheld equipment and will be founded on the results of the here presented study.

Finally, the actual CIE standard illuminations A, D50 and D65 will be considered in the shown mathematical description. The used relative spectral power distributions of these standard illuminations are well-fitted by available light sources and optical filters (A', D50' and D65' in Figure 12), but the final adoption to the standard illuminations is not yet verified.

References

- H. Pertler U. Bertholdt, 2007, Farbvergleich und Farbmessung an fluoreszierenden Proben der Druckindustrie. *FOGRA, Forschungsbericht*, Nr. 60.053
- P. Urban J. Rodriguez H. Mantler M. Dattner, 2009, Colour prediction model on basis of the wavelength dependent area coverage including the scattering of light and optical brightener. *IARIGAI*, 36:161-169
- M. Dattner, 2011, *Spektrales Farbvorhersagemodell für den Rasterdruck auf Basis der wellenlängenabhängigen Flächendeckung*. PhD thesis, Bergische Universität Wuppertal
- DIN. *Deutsches Institut für Normung*, 1992, *DIN 5033 'Farbmessung'*. Beuth Verlag, Berlin
- T. Götze W. Alber K. Erhard, 2003, Optimierung des Einsatzes optischer Aufheller bei der Erzeugung graphischer Papiere. *PTS-Forschungsbericht*

- B. Fiebrand, 2007, Optische Aufheller in Proof- und Druckpapieren, Versuche über die Einflüsse auf die Mess- und Drucktechnik mit praktischen Tipps zur Umsetzung, bvdM-Broschüre
- P. Green E. Löser, 2008, Estimating the Spectral Reflectance of Fluorescent Offset Papers for Varying Illuminants. *Digital Futures 2008, The Royal Photographic Society*
- F. Geßner A. Kraushaar, 2006, Farbmanagement für Drucke auf aufgehellten Papieren. *FOGRA, Forschungsbericht*, Nr. 32.144
- Philip Urban, 2005, Metamere und multispektrale Methoden zur Reproduktion farbiger Vorlagen. PhD thesis, Technische Universität Hamburg
- J. Zwinkels, 2008, Surface Fluorescence: the only Standardized Method of Measuring Luminescence. *Standardization and Quality Assurance in Fluorescence Measurements, Springer-Verlag Berlin Heidelberg*, 1:163-192
- CIE. *Experten-Ausschuß E-1.3.1*, 1971, *Colorimetry; optical recommendations of the International Commission on Illumination (CIE)*. Bureau Central de la CIE, Paris





5

*Environment,
publishing and society*

Printing and environmental sustainability

Ivana Bolanča Mirković¹, Igor Majnarić¹, Sandra Mustać², Zdenka Bolanča¹

¹ University of Zagreb, Faculty of Graphic Arts

Getaldićeva 2, HR-10000 Zagreb, Croatia

E-mails: ivana.bolanca@grf.hr; igor.majnarić@grf.hr; zdenka.bolanca@grf.hr

² BSc student, University of Zagreb, Faculty of Graphic Arts

Getaldićeva 2, HR-10000 Zagreb, Croatia

E-mail: sandra.mustac@gmail.com

Abstract

The impact of the printing process on the environment is significant. This paper explores the voltage of reverse roller in indirect electrophotography printing in the field of 0V to -250 V on the life end of the printed products through the efficiency of recycling. In addition, the quality of color reproduction is discussed. For the printing is used: uncoated woodfree paper, double-sided coated paper and Soho coated paper.

Characteristic of the results of image analysis handsheets made from recycled fibers prints obtained by changing the voltage of reverse rollers from 0 to -200V is reduced in the total dirt spot number and increasing in the dirt spot area. The efficiency of recycling is the highest for printing on uncoated paper, then on Soho coated paper, and the worst on double-sided coated paper. The quality of fullcolored prints observed through the volume gamut of prints gives reverse results.

This is just part of a comprehensive study involving all six separate stages of electrophotography printing synchronal performed. In this study the use of experimental design and creation of statistical models in the direction of optimization process and environmental sustainability follows.

Keywords: environmental sustainability, digital printing, voltage of reverse roller, quality of prints, recycling

1. Introduction

The concept of environmental sustainability refers to the systematic conditions that should not be disturbed by human activities either at a global or regional level more than the planet allows. At the same time all the natural resources must not be depleted, and have to be sufficient for the next generations. These two requirements should be in balance with the third one regarding sustainability which refers to the principle of ethics and fairness.

Ecological flexibility is the capacity of an eco-system to overcome certain disruptions without irreversible losses to conditions of its balance. Ecological space is the amount of energy, resources and territory which can be used in environmentally sustainable way, and ecological footprint points this out. Environmentally more sustainable product system and demands of sustainable conditions will result in production and consumption that are in the system of contemporarily industrial society and sustainability. The term of sustainability is significant for the development, and it includes energy and material flows, closed loop systems, clean technologies, economical and social factors, implementation of society values and quality. Therefore, the switching to sustainability is large and complex process of technological, economical and society innovation in which many differences have to adjust and find their place.

Environmental awareness, health and safety factor have an important role in identification of printing technologies for the future. In order to increase effectiveness of resource usage and effectiveness of environmental management system, life cycle assessment of the product has to be considered and included in planning and projecting, starting from early stage of design.

The level of environmental awareness is present in printing industry, which enables making the right choices. Significance of making the right choice is in the field of printing substrates (substrates with high content of secondary raw material, substrates made from total chlorine-free process), inks (lower solvent content level biodegradable inks, formulation with more renewable raw material), printing (clean technologies, preparation of printing forms with no wastewater which contains chemicals from the process, cleaning agents for machine elements which are based on renewable resource) and postpress finishing (binding process can be specified to enable full recycling of paper content without glue contamination).

The main component of the waste is paper used in the preparation of the printing process. Due to preparatory process for offset printing machine overall paper consumption is by 3.7 times higher for smaller editions in relation to a digital offset printing machine (Kadam S. R., Evans M. E., Rothenberg S. 2009). The offset printing inks are present with the amount of about 2.7g per one print at smaller editions, and are decreased as the edition increases. The amount of ink that goes to waste is less in digital offset printing than in conventional process.

Shown results are a part of an extensive research of the relevant factors in technological process of digital electrophotography printing, simply defined by the terms of tamping, exposure and developing. In this paper, the influence of changing the voltage of the reverse rollers in relation to reproduction quality, and in relation to the last phase of the lifecycle and properties of recycled fibers are discussed. So far, the process of recycling is studied a lot. The domain of influential process factors is being researched: the kind and the amount of chemicals used in various process stages, pH values and fiber suspension consistency, temperature of suspension, the time of disintegration, hydrodynamic flotation factors (Thender K., Pugh R.J., 2004; Zhao Y. et al. 2004; Azevedo M.A.D. et al., 1999, Luo Q. 2003). Machildon and co-authors and Magda have researched the efficiency of the flotation in relation to size, shape and surface characteristics of dispersed particles of printing dye, the volume of the air and the size of the air bubbles (Machildon L. et. al. 1999; Magda J.J. 1999). In the described issues the most of the studies were dedicated to hydrodynamic factors of recycling process, the influence of chemical and physical system conditions to the process efficiency, while the influence of printing techniques and graphic materials were less studied (Carre B., Magnin L., 2004; Manning A., Fricker A., Thompson R., 2006; Bolanca Mirkovic I., Bolanca Z., 2005; Schiller A. 2008). According to gained results the contribution of this paper is determining the influence of the conditions in digital indirect printing based on electrophotography using liquid toner ElectroInk on the quality of the prints and characteristics of recycled fibers, which presents the contribution to determinants for further development within the meaning of sustainability in that area.

2. Experimental

For the printing HP Indigo TurboStream machine based on indirect electrophotography is used. The printing form contains following elements: standard CMYK RGB wedge in the range from 10-100 screen value, textual positive and negative microelements, standard wedge for production of ICC profile and 3D gamut, and standard ISO illustration for visual control. The prints are made on paper with Soho coat for digital printing, both side coated and uncoated paper for conventional offset printing. The bases of the papers have the same chemical composition of the paper raw materials and the difference is in the coating.

After the calibration of the machine, the printing is followed, with the correction of the voltage of reverse roller, for the next voltages: 0V, -50V, -125V, -200V and -250V.

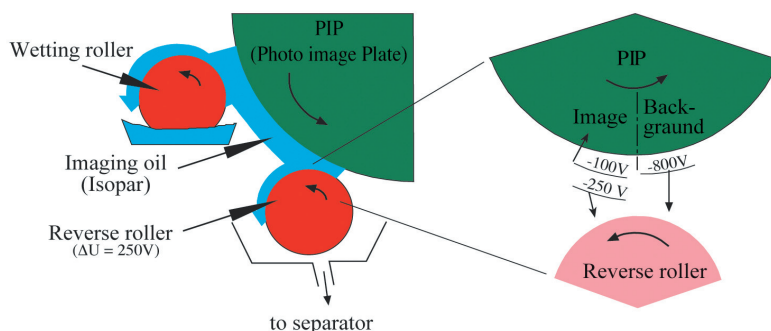


Figure 1: Indirect electrophotography printing

Tamping of photoconductor is the initial phase of electrophotography process. The next phase is exposing, which is carried out with the laser head which forms four light rays at once. The third stage in the indirect electrophotography is developing. It is conducted in three separate parts: the development with the processing drum, developing with reverse rollers and fixing with squeegee roller. All these aforementioned distinct phases are performed synchronized and they are the subject contented of our project, within which are researches presented in this paper.

This is followed by spectrophotometric analysis made with X-Rite SwatchBook and ColorShop 2,6 application. From ICC profile with the use of MONACO Platinum programe the gamut of prints is established. In the paper the curve of reproduction, ΔE CIE Lab and 2D and 3D gamut of the reproduction are shown.

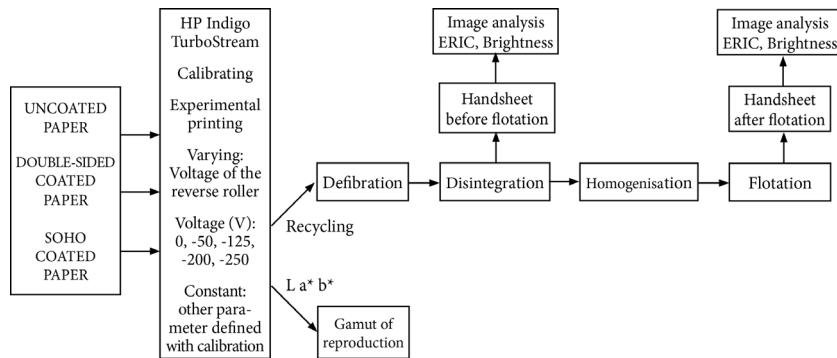


Figure 2: Workflow

For recycling of the prints alkaline chemical deinking flotation is used. In the process the next chemicals are used: sodium hydroxide 1%, hydrogen peroxide 1%, sodium silicate 2%, DTPA 0,2%, and surface active substance 0,4%. Consistency of the suspension in the phase of disintegration is 10%, while in the flotation phase the consistency is 0,6%. The time of the disintegration is 10 minutes, and the time of the flotation is 8 minutes (Bolanča Mirkovic I., Bolanča Z. 2005). After the disintegration and flotation laboratory handsheets are made with the use of standard sheet former Rapid- Köthen, according to INGEDE Method 1 and ISO 5269-2 (ISO 5269_2). On this laboratory handsheets using spectrophotometer Technidyne Color Touch 2 model ISO, before and after flotation brightness (ISO 2470) and effective residual ink concentration are measured (TAPPI T 567 pm-97). According to the recycling process phases image analysis is made with the use of SpecScan® Apogee System software in accordance with TAPPI standard method (TAPPI T 563 pm-97).

3.Results and discussion

Figure 3 shows the results of image analysis from handsheets made of fibers from different phases of recycling prints obtained by varying the voltage of reverse rollers in indirect electrophotography printing with HP Indigo TurboStream.

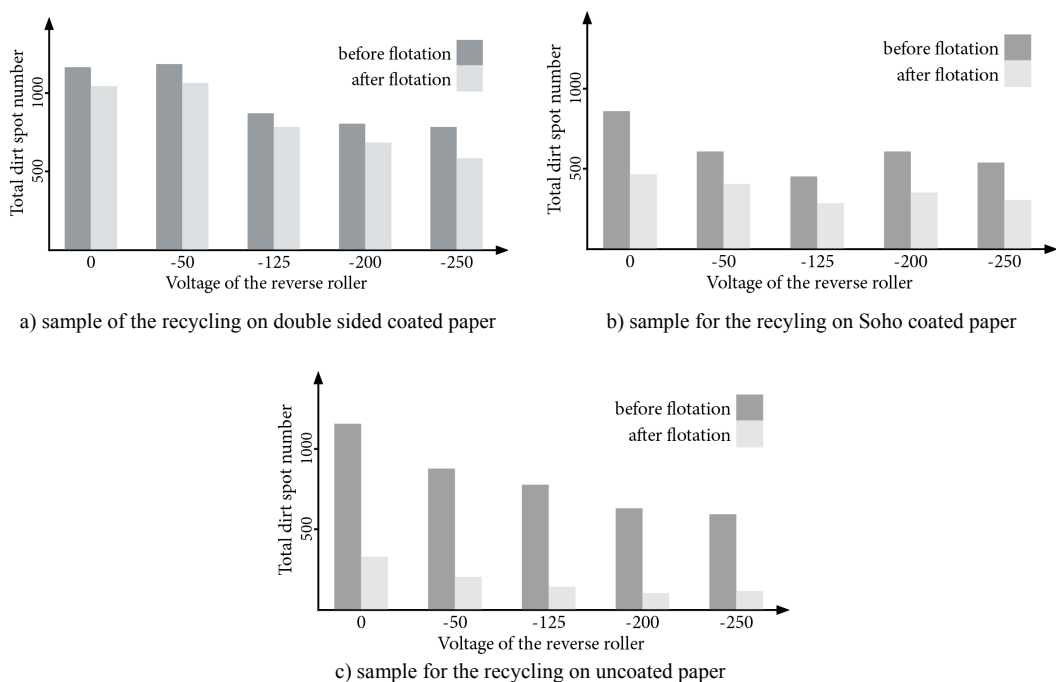


Figure 3: Total dirt spot count versus voltage of reverse rollers and types of the printing substrate

The common characteristic found in results is the reduced of total dirt spot number by variation of voltage reverse rollers from 0 V to -200 V. The results are dependent on the substrate characteristics.

In used printing substrates there is no difference in the chemical composition of the raw paper, but in the finishing process in relation to the coating. For double-sided coated paper prints, standard for offset printing, efficiency of the deinking flotation procedure ranges from 10-26% depending on the voltage of reverse rollers in the recycling samples printing process. Slightly higher recycling efficiency (33-47%) is achieved by using the paper with Soho coating which is specially adjusted for indirect electrophotographic printing. The best efficiency of recycling (75-84%) is achieved by using woodless uncoated offset paper.

The coating of paper is a significant factor of the recycling process effectiveness. The fact must be acknowledged that the coating process assists in dispersing the fillers in the coating. In recycling process dispersants are at time surface active and together with alkali can lead to acceptable ink detachment from the coated paper. These species can hydrophilize ink containing agglomerates and hinder flotation efficiency as well as contribute to unwanted foam generation and/or stability.

The coating of paper is a significant factor of the recycling process effectiveness. The fact must be acknowledged that the coating process assists in dispersing the fillers in the coating. In a recycling process at time, dispersants are surface active and together with alkali can lead to acceptable ink detachment from the coated paper. On uncoated paper the adhesion of printing ink to paper depends on paper properties such as surface structure, fibre type, ash content and drying mechanism of the chosen printing process.

These species can hydrophilise ink containing agglomerates and hinder flotation efficiency as well as contribute to unwanted foam generation and stability.

On the uncoated paper, the adhesion of printing ink to paper depends on paper properties such as surface structure, fiber type, ash content and drying mechanism of the chosen printing process.

The results show the opposite relationship between the voltage of reverse rollers in indirect electrophotographic printing of samples for recycling and dirt spot area (Figure 4).

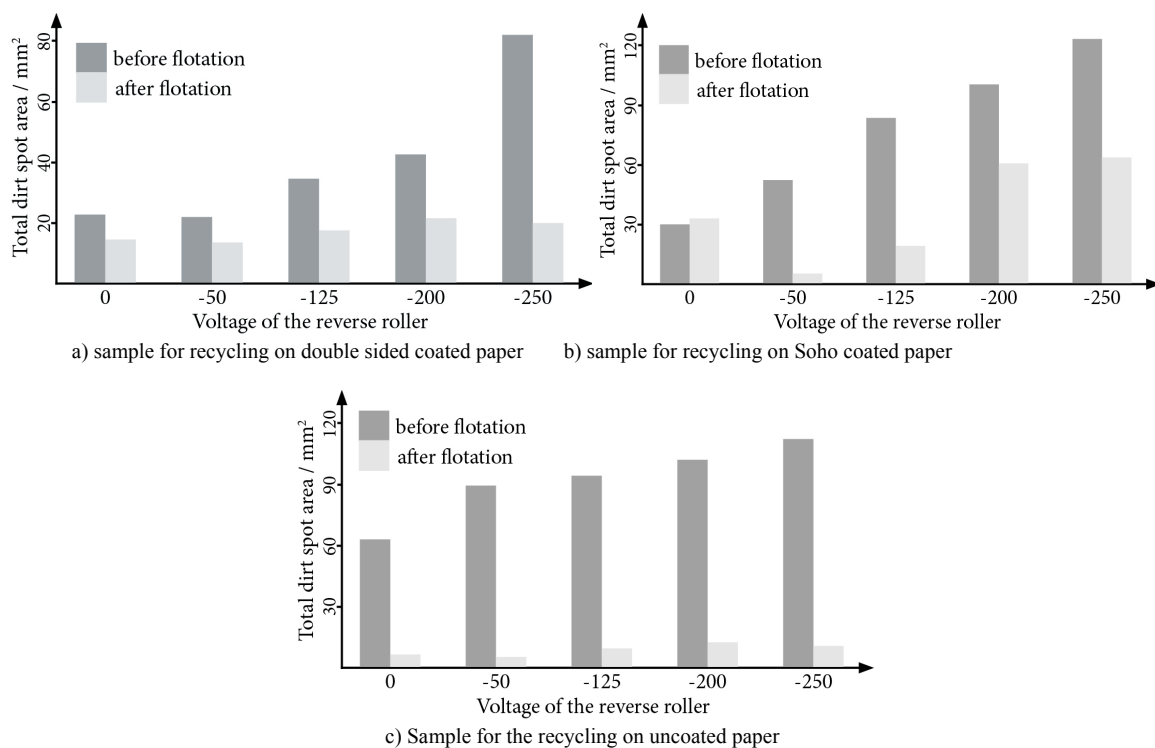
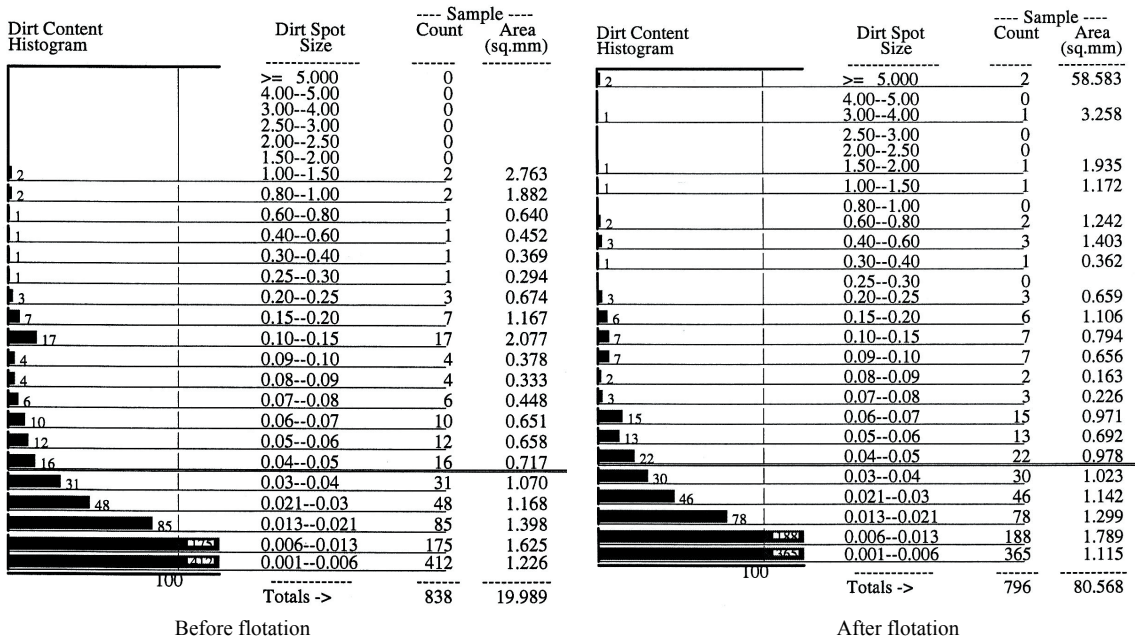


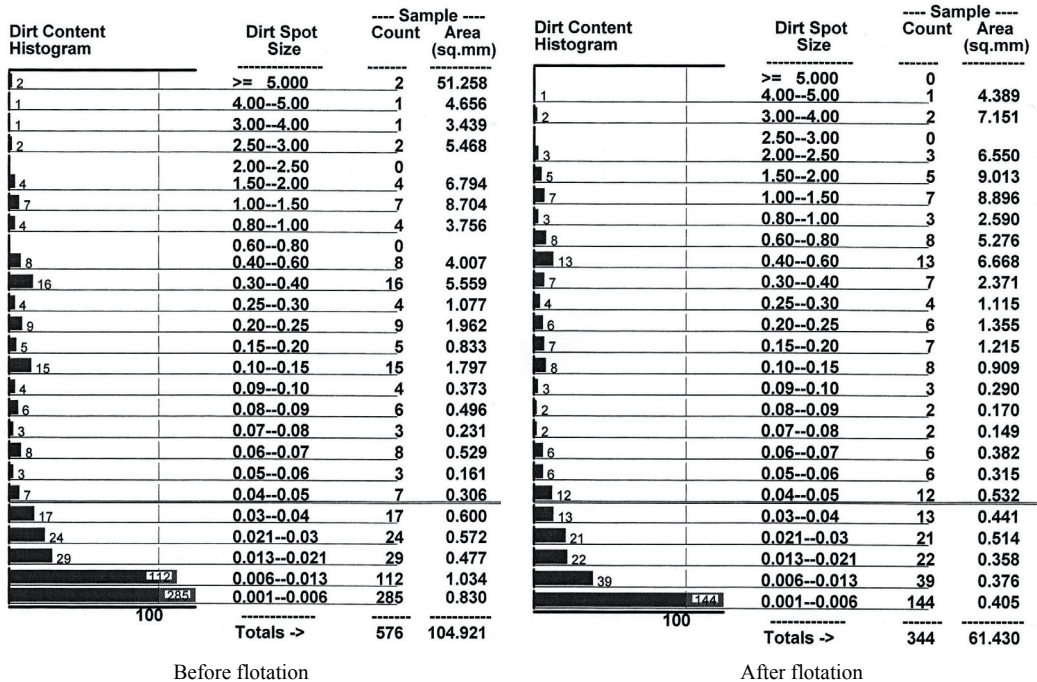
Figure 4: Total dirt spot area versus voltage of reverse rollers and printing substrate types

With increasing of the negative voltage of reverse rollers in the printing, the total dirt spot area on the handsheets made from recycled fibers is increased. In this case the impact of the printing substrate on re-

cycling is also proven. Thus, recycling of prints made with the -250V voltage of reverse rollers, efficiency to reduce dirt spot area of the substrate with a Soho coating is 48%, for the surface with double-sided coating designed for offset printing is 75% and for uncoated woodfree paper is about 90%. Reduce of total dirt spot number with increase of total dirt spot area indicates the increase in the size of individual particles. For better monitoring and interpretation of the deinking flotation mechanism, Figure 5 shows the dirt spot histograms for dirt spot size from 0001-0006 to $\geq 5 \text{ mm}^2$

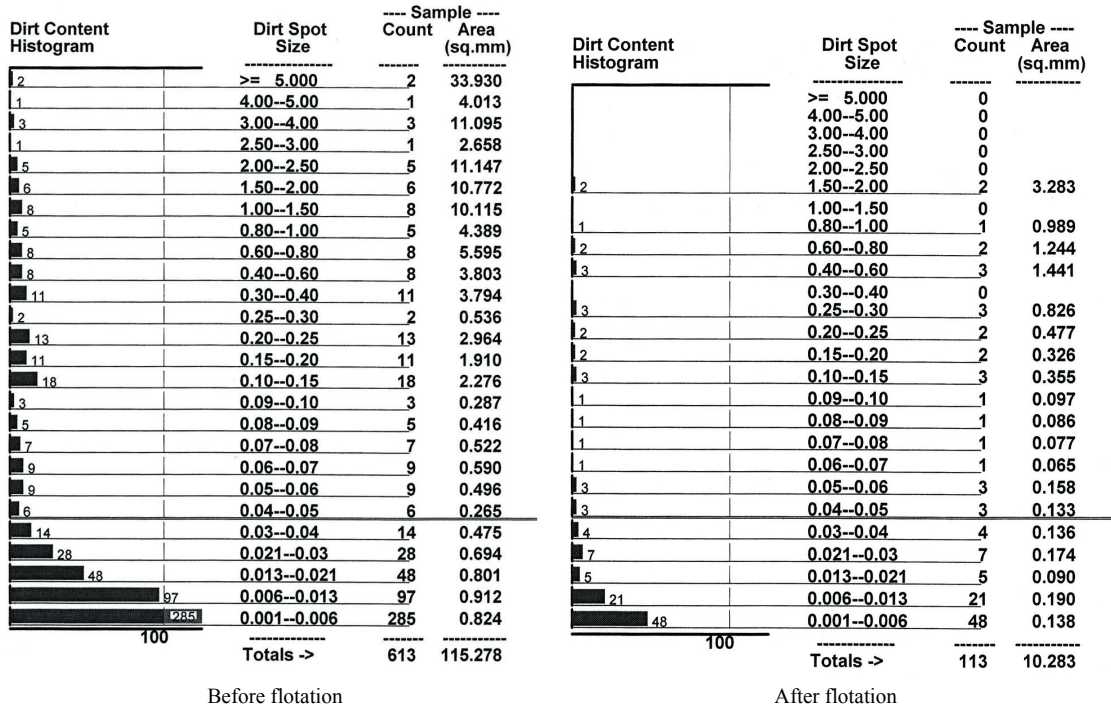


a) sample for recycling on double sided coated paper



b) sample for the recycling on Soho coated paper

The research results show that the larger negative voltage of the reverse roller formed larger flat dirt spot areas, sometimes larger than 5 mm^2 . Handsheets made from the fibers after the disintegration of prints on uncoated woodfree paper have the greatest number of such spots (141-199) depending on the voltage of the transmission drum, while such spots can be at least expected if the double-sided coated paper prints are used for recycling.



c) sample for the recycling on uncoated paper

Figure 5: Dirt content histograms for handsheets made from recycled print fibers with the reverse rollers voltage of -200V

On the prints made on woodfree uncoated paper and Soho coated paper the efficiency of recycling process in comparing the total dirt spot area in the total of $\geq 0.04 \text{ mm}^2$, and the total of $< 0.04 \text{ mm}^2$ is almost equal. For prints on uncoated woodfree paper recycling efficiency is around 90%, while for the prints on Soho coated paper efficiency is about 42%. Recycling specifics of prints in the described experimental conditions are significant for prints on the double-sided coated paper for offset printing, referring to the good efficiency of about 82% for the recycling when it comes to spots in the $0.04 - \geq 5.000 \text{ mm}^2$ for prints made at reverse roller voltage of -200 V and a very inefficient flotation efficiency for spots in the class size of $0.001-0.04 \text{ mm}^2$ should be pointed out. Given that this is the efficiency of removing the spots below 1%, this is probably due to fragmentation of large particles and the inability of flotation methods for their removal as well.

Results of image analysis are further tracked and verified through the measurement of effective residual ink concentration and brightness. The highest brightness have handsheets made from recycled fibers prints on Soho coated paper (Brightness102) and the value is slightly increased by increasing the negative voltage values of the transfer roller in printing the recycling samples.

Handsheets made from recycled fibers of prints on double-sided coated paper have a slightly lower brightness (brightness around 85) which is almost changed compared to the voltage of recycling samples. Effective residual ink concentration decreases for handsheets after flotation in comparison to those before flotation. Correlation between effective residual ink concentration and brightness is determined.

Given that the purpose of this paper is establishing links between the end of life of the printed product, the quality of prints with the ultimate goal of process optimization in the domain of suitable environment is shown below. As indicators of reproduction quality of a certain stage in the process of indirect electro-photography process, two dimensional and three-dimensional reproduction Gamut are shown.

Table 1: Volumes of gamut $V_{CIE L^* a^* b^* CCU}$

Sample	Voltage 0	Voltage -125 V	Voltage -250 V
Uncoated paper	382.434	517.113	546.834
Double-sided coated paper	551.702	730.174	762.139
Soho coated paper	424.572	581.387	618.448

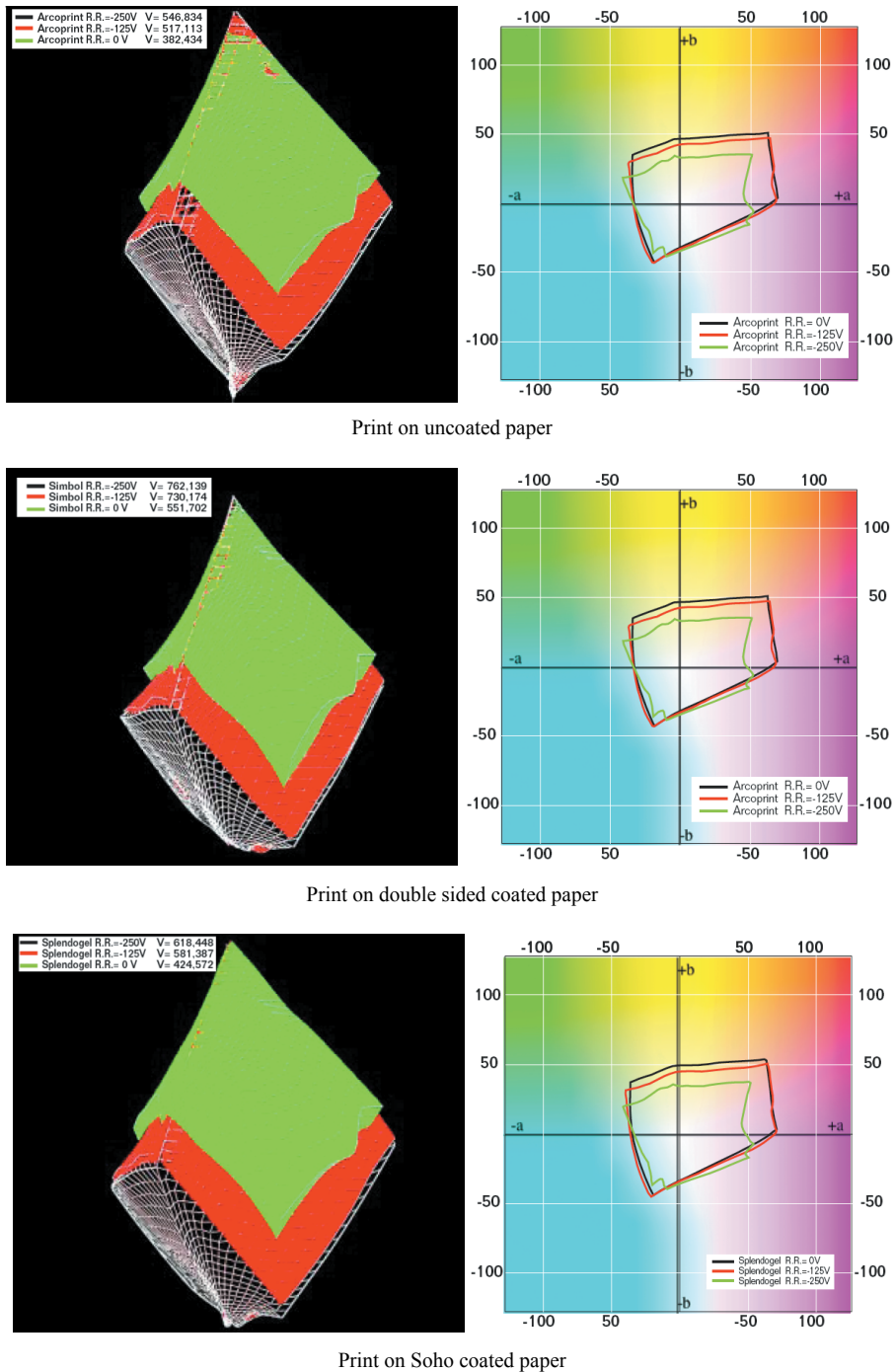


Figure 6: Gamut of print, obtained by using the voltage of reverse roller of 0 V, -125 V and -250 V on Soho coated paper

The largest reproduction gamut is achieved at a voltage of the reverse rollers - 250 V on the double-sided coated substrate. For this substrate is specific that the central part of gamut body at a voltage of 0 V has the best reproduction of green and blue tones. Increasing the voltage leads to a smaller reduction in reproduction of blue, and increase in the reproduction of magenta, red, yellow and green. In relation to the research, the minimum reproduction gamut is achieved at uncoated substrate. In the typical cross-sections there is a change in magenta, red, yellow and light green, increasing the voltage from 0V to -125 V. Voltage from -250V causes the change in tones containing a higher percentage of the yellow.

Gamuts obtained by reproduction on Soho coated paper are very similar in characteristic cross-sections to those on uncoated paper. The difference is noticed in light and dark shades, because the ink is better accepted on Soho coated surface.

4. Conclusion

Based on the results of image analysis a reduction in total dirt spot number and increasing the dirt spot area for voltage change of reverse rollers from 0 to -250 V for indirect electrophotography on recycled print samples is proven. This general trend show prints on all used substrates.

Flotation deinking efficiency is dependent on the voltage of reverse rollers (0V-250V) in indirect electrophotography printing of samples and on the characteristics of the substrate as follows: double-sided coated paper 10-26%, Soho coated paper 33-47% and uncoated woodfree paper 75-84%.

The largest brightness have handsheets made from recycled fibers of prints on Soho coated paper. The research results in the context of reproduction quality indicators of the observed phase of indirect electrophotography process are as follows: the largest gamut is realized with printing on double-sided coated paper, followed by reproduction gamut on the Soho coated paper and the smallest gamut is achieved with reproduction on uncoated paper.

Given that the indirect electrophotography printing is complex process, with six separate, synchronous phases, the needs and characteristics of graphic material, along with a number of factors in the field of chemical deinking flotation (if the life end of printed products is followed) should be considered. In the further research experimental design will be used and statistical models will be created to obtain information about optimizing in the direction of environmental sustainability in this area.

References

- Azevedo M.A.D., Drelich J., Miller J.D.,(1999) The effect of pH on pulping and flotation of mixed office wastepaper, *J.Pulp Pap. Sci.* 25(9):317(1999),66-72
- Bolanaca Mirkovic I., Bolanca Z., (2005), Optical properties of deinked pulp, *Journal of Imaging Science and Technology*, 49(3)(2005)284-292
- Carre B., Magnin L. (2004) Digital prints: A survey of the various deinkability behaviours, 7th Research Forum on Recycling PAPTAC-TAPPI, Quebec Canada
- Carre B., Magnin L., Galland G., Vernac Y., (2003), Printing process and Deinkability, *Das Papier*, 12 (2003) 41-45
- ISO 2470, Paper, board and pulps- Measurement of diffuse blue reflectance factor (ISO brightness)1999
- ISO 5269-2 Pulp-Preparation of laboratory sheets for physical testing, Part 2. Rapid Köthorn method
- Kadam S.R., Evens M.E., Rothenberg S., (2009) A comparative study of the environmental aspects of lithographic and digital printing processes, GATF, Rochester
- Luo Q., Deng Y., Zhn j., Shin WT., (2003), Foam Control Using a Foaming agent Spray: A Novel Concept for Flotation Deinking of Waste paper, *Ind. Eng. Chem. Res.* 42. 3578-3583
- Machildon, M., Lapointe, B., Chabot, L.,(1999) The influence of particulate size in flotation deinking of newsprint, *Pulp Pap. Can.* 90(4):90(1)
- Magda J.J., Lee J.Y.,(1999), A critical examination of the role of ink surfacehydrophobicity i flotation deinking, *Tappi J.*, 82(3): 97(1999),139-145
- Manning A., Fricker A., Thompson R., (2006) Deinking of Indigo prints using high-intesity ultrasound, *Surface Coatings International* 89B2
- Schiller A. (2008) Deinkability of UV prints into ink formulation, Final COST Conference, Bordeaux
- TAPPI T 563 pm-97, Equivalent Black Area (EBA) and count of visible dirt in pulp, paper and paperboard by image analysis
- TAPPI T 567 pm-97, Determination of effective residual ink concentration by infrared reflectance measurement
- Theander K., Pugh R.J.,(2004), Surface chemicals concepts of flotation deinking, *Colloids and Surfaces A: Physicochem. Eng. Aspects* 240 (2004)
- Zhao Y., Deng Y., Zhu J.Y., *Progress in Paper Recycling* 14(1):41(2004).

Development of innovative sustainable printing practices to reduce VOCs emissions in the SMEs printing industry based on BREF best available techniques

Markus Johannes Müller, David Pérez, Vicente de Gracia, Alejandro Fuentes, Susana Otero

Technological Institute of Optics, Colour and Imaging, AIDO
C/ Nicolás Copérnico 7-13, E-46980 Paterna (Valencia), Spain
E-mail: dperez@aido.es

Abstract

Printing SMEs are usually out the scope of the Best Available Techniques (BATs) defined in the STS (Solvent Treatment Surface) BREF. In addition, the BATs implementation produces technical imbalances which became in a productivity and quality decrease, so the BATs are abandoned and the environmental impact doesn't decrease. The objective of this research is to develop innovative sustainable printing practices to reduce VOCs emissions in the Printing SMEs, while keeping the quality and productivity of their processes.

The research had the next specific objectives: Study of the current impact of BATs in the Printing SMEs; Determination of the main BATs to reduce VOCs in the Printing SMEs and the barriers to implement them; Development of Sustainable Practices for an optimal implementation of critical BATs; Development of a Tool to achieve a successful implementation.

The European SMEs printing companies need a technical support to understand and implement the BATs, especially Sheet Fed Offset SMEs, which are out of the scope of the legislations. The critical information for SMEs Sheet Fed Offset companies is how to reduce the use of IPA and how change from Mineral to Vegetable Inks. A innovative procedure to change from mineral oils inks to vegetable inks has been developed in four steps: Preconditions, Study of printing condition with mineral oil based inks, Implementation, Conformance printing. This Best Practices can reduce the use of mineral oil inks in 100%. A innovative procedure to achieve IPA reduction has been developed in three steps: Preconditions, Housekeeping and New Additives and Machinery. Housekeeping practices reduced IPA concentration to a maximum of 8 vol. % in this manner New Additives and Machinery can reduced IPA concentration to a maximum of 5 vol.% in this manner; in some cases even further up to 0 vol.%. The information showed in the developed eTool can facilitate the implementation of the developed Best Practices.

Keywords: sustainable printing, VOCs emissions, IPA reduction

1. Introduction

More than 95% of the printing companies are Sheet Fed Offset SMEs, so they are usually out of the scope of the Best Available Techniques (BATs) defined in the STS (Solvent Treatment Surface) BREF. However, their global environmental impact is similar or, even, bigger than which is produced by the big companies.

In addition, the BATs implementation produces technical imbalances which became in a productivity and quality decrease, due to the lack of specialized environmental and technical expertise. Then, the BATs are abandoned and the environmental impact doesn't decrease.

The objective of the present research is to develop innovative sustainable printing practices to reduce VOCs emissions in the European SMES Industry, while keeping the quality and productivity of the printing processes.

The research has followed the next specific objectives:

- Study of the current impact of BATs in the European Printing Industry
- Determination of the main BATs to reduce VOCs in the SMEs Printing Industry and the barriers to implement them
- Development of Sustainable Practices for an optimal implementation of critical BATs
- Development of a Tool to achieve a successful implementation

2. Methods

2.1 European survey

Development of an European Survey, which involves printing companies, consultants and public bodies to determine the current impact of the BATs in the European printing industry.

2.2 Survey results analysis

Determination of the most important BATs for European SMEs printing industry, based on the results of the study, with the next criteria:

- Potential environmental improvements
- Problems on its implementation
- Grade of implantation at a European Level

2.3 Development of innovative practices for reducing VOCs

- Desk and sector research; Based on documentation, own experience and direct contacts with sector stakeholders.
- Sustainable practices determination; Definition of the optimal methodologies for implementing BATs
- Validation; The sustainable practices were validated in 9 selected Spanish, Dutch and Czech companies with the following methodology:
 - To implement the selected BAT by means of the sustainable practices defined in the previous step.
 - To evaluate the results, by means of the next two kinds of test:
 - I. A printing test including quality control image, which evaluates the printing result before and after the implementation of BATs.
 - II. Environmental impact analysis of the productive process, before and after the implementation of BATs.
- Implementation strategy

Determination of the best way to communicate the optimal methodologies to SMEs printing companies in order to facilitate their implementation.

3. Results

3.1 European Survey results

More than 500 European Printing stakeholders (printing houses, consultants, public bodies) contributed to the survey, which was managed with an online tool which allowed to obtain the next conclusions:

- The knowledge of the BREF Document is small in the European Printing Industry (10%). The knowledge of BATs is higher but it is also small (30%)
- Dutch printing companies are better informed about BREF Document, and especially about BATs than Spanish and Czech ones, where the percentage of informed companies is near to 10%. Some experience should be transferred from Holland to the rest of countries
- Near to 50% of the European Printing companies which work with other Heat-Set Offset, Cold-Set Offset, Flexography and Packaging Gravure are informed about BATs.
- However, the knowledge of BATs in Sheet Fed Offset and Publication Gravure European Printing Companies is smaller.
- It's needed to extend the knowledge of Vegetable Inks, Replacement or Optimizing of IPA in Sheet Fed Offset companies and provide them with technical instructions to use them successfully and provide the companies with process managements tools in order to overcome the economical problems
- It's needed to continue the dissemination of the benefits and ways to controlling the hardness and cooling the dampening solution, especially in the lower level European Printing companies, placed in Western Europe and Mediterranean regions

- UV curing inks and High solid adhesives alternatives are partially implanted because a small percentage of companies have used them.
- Electron beam (EB) inks, Retention inks and Co-extrusion to replacement of the necessary varnish are not known in the European Printing Industry, and they are not implanted at all.
- Water-based inks, varnishes and adhesives are known in the European Printing Industry, and they are partially implanted because 50% of companies are using or have used them. We can state that there exist implementation problems because an important number of companies have abandoned them.
- UV Curing Varnishes and Solvent-free adhesives alternatives are known in the European Printing Industry, and they are implanted in a number of companies. Some of them have some problems when using this BAT

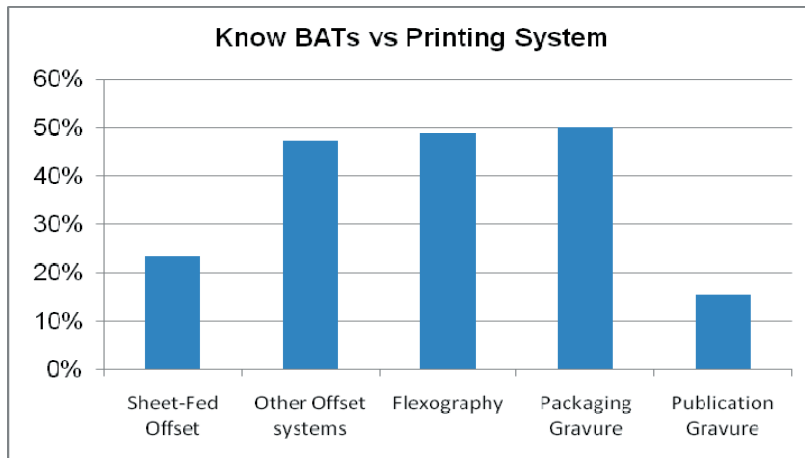


Figure 1: Knowledge of Best Available Techniques (BATs) vs Printing System

3.2 Survey results analysis

According to the conclusions of “BATs Implantation in the European Printing Industry” Report” and the experience of the members of the Consortium, it has been to prioritize the next BATs:

1. Vegetable inks

- They are well known in the European Printing Industry
- Vegetable Inks produces environmental improvements in the European Printing Companies which are using them
- The main problem related with their implementation BAT are the technical problems.

According to this information, it’s needed to extend the knowledge of vegetable Inks and provide the companies with technical instructions to use them successfully.

2. Replacement of IPA

- Replacement of IPA is well known in the European Printing Industry
- Replacement of IPA produces environmental improvements in the Sheet Fed European Printing Companies which are using them
- There exist a big technical problem related with this BAT.

According to this information, it’s needed to extend the knowledge of Replacement of IPA and provide the companies with technical instructions to use them successfully. The experience developed in Holland should be transferred to the rest of Europe.

3. Optimizing of IPA

- Optimizing of IPA is **well known** in the European Printing Industry
- They **produces environmental improvements** in the Sheet Fed European Printing Companies which are using them
- There exist a big **technical problem** related with this BAT

According to this information, it's needed to extend the knowledge of Optimizing of IPA and provide the companies with technical instructions to use them successfully. The experience developed in Holland should be transferred to the rest of Europe.

4. Ceramic, metal and hydrophilic distributing and plate rollers

- Ceramic, metal and hydrophilic distributing and plate rollers are not so known in the European Printing Industry, and they are not fully implanted because a big number of companies have not used them. A small number of companies have abandoned this BAT or are using them with problems. An important percentage of Sheet Fed Offset companies are using them successfully and could provide information about their working procedures.
- They produce environmental but specially technical improvements in the Sheet Fed European Printing Companies which are using them
- The main problems related with this BAT are the technical implementation and economical problems.

According to this information, although this BAT is not so known, it's needed to extend the knowledge of Ceramic, metal and hydrophilic distributing and plate rollers and provide the companies with process managements tools in order to get an economical from the technical improvements and overcome the economical problems which exists. The rest of BATs, "controlling the hardness of the dampening solution" and "cooling the dampening solution" are not consider as priority because they are well known in the European Printing Industry, and they're highly implanted because a big number of companies are using them OK. A small number of companies have abandoned this BAT or are using them with problems.

So, the main effort of this Consortium will be make in developing best practices procedures in the mentioned priority BATs implementation.

3.3 Innovative practices for reducing VOCs

3.3.1 The use of **vegetable inks** needs a procedure to make a correct change from mineral oil inks to be successfully implemented in four steps:

Step 1: Preconditions

- Ensure that the board fully backs the ink substitution plan;
- Those responsible on-site (chief operators / foremen) must be positive about the substitution plan;The printers should support the substitution plan;
- It may be desirable to inform important clients about the substitution plans;
- Ensure a good internal structure for communication, so that ink substitution can be discussed adequately;
- Provide regular information or education on the use of Vegetable Inks to ensure that employee motivation - especially that of printers -does not decrease;
- Ensure that there is sufficient external support in case of print problems or unclear matters (examples are your own suppliers and/or more generalist business sector consultants such as the KVGGO Dienstencentrum or AIDO);
- Check, based on the safety information sheets, whether your (new) inks do not contain (more) hazardous components than their predecessor(s);
- Take regular measurements of the quality of the damping solution, using the parameters of *temperature, IPA concentration, conductivity* and *acidity*. Ensure that the measured values are recorded on a registration-card per damping unit (in effect often per press);
- Define a reliable printing control parameters system supported by the appropriated equipment to control the colourimetry, densitometry and dot gain.

Step 2: Study of printing condition with mineral oil based inks

- **Test-form design:**The first test shall contain, at least, some elements to measure the $L^*a^*b^*$ and dot gain values of the mineral oil-based inks printing condition. It should contain, also, other elements that will not be measured but will help to check if the test printing is correct.

Minimum required elements

Solid tones. These patches will be used to measure which is the $L^*a^*b^*$ obtained with mineral oil-based inks in a regular print production.

Mid-tones. There is where the dot gain obtained with mineral oil-based inks will be measured.

Recommended elements

Reference images. Representative reference images should be used to check the visual appearance of the test. In this case, we used some of the Roman 16 set (www.roman16.com) which is a perfect image collection for this purpose

Gray balance. The ECI bvdM Gray Control Strip should be used to check, visually, whether the gray color produced with CMY and K percentages are balanced.

Slur and doubling. During the test printing such defects must be controlled. These patches will not show lines if any of both defects are affecting to the printing press in any of its units

Pressure. This patch will not show a clear convergence of the lines if excessive pressure is applied in any printing unit.

Circumferential densities. The densities should be as equal as possible in the circumferential direction of all printing units. These patches should be measured during the test printing on the dashed line zones to check homogeneity

- **RIP settings and plate calibration** Plates of this test should be produced like any other normal print job, ie using the same dot gain compensation curves (actual and Intended press) as used in this printing condition. The printing condition is defined by a combination of variables: RIP settings (screen resolution, frequency, etc), printing press, ink series, paper type, etc. Except for the inks, the other variables must be kept stable during this procedure. To make the best accurate plates possible, it is recommended that the CtP system has been calibrated shortly before producing these plates. To do that, please, refer to the workflow or RIP vendor's manual. The ideal instrument for calibration is a plate measurement device like X-Rite PlateScope, X-Rite IC Plate or Techkon Spectroplate instead of densitometers or spectrophotometers of any kind.
- **Test printing** This first test shall be printed, simply, as a normal product with the usual production techniques and measurement devices (if any) of the company. The aim of this test is to get some copies of the OK print, so the the printing will end when the densities are correct or when the visual appearance of print match the color proof.
- **Density, $L^*a^*b^*$ color and dot gain measurements.** This test, as any other, shall be measured when be completely dry. Please let, at least, 10 to 20 hours to proceed to measuring it. Density and dot gain values should be measured using polarization filter and $L^*a^*b^*$ color values must not use any filter. The other measurement conditions will follow ISO 12647-2 specification: Device geometry: 45°/0° or 0°/45°, Bandwidth response: Status E, Backing: black, matt, L<5, Illuminant: D50, Observer: 2°
 - Density values will be used to validate the OK print. "a" and "h" elements should has equal densities in the entire print sheet. No more than a difference value as of 0,10D should be accepted in the circumferential direction
 - $L^*a^*b^*$ color If the previous density values were validated, then we will register the $L^*a^*b^*$ color obtained in the sheet measuring the six "a" elements. The values should be an average so this is the $L^*a^*b^*$ color obtained with the mineral oil-based inks

Step 3: Implementation of vegetable oil based inks

The best obtained ΔE against mineral inks will be automatically related to their wet density, obtaining the production densities to be used with the new inks. Finally, dot value shall be measured in order to compute which is the dot gain produced in this new printing condition for, later, make new compensation curves at RIP station.

The aim of this test is to find which is the ideal production density that fits with the visual appearance produced with the former mineral oil-based inks test.

- **Testform design**

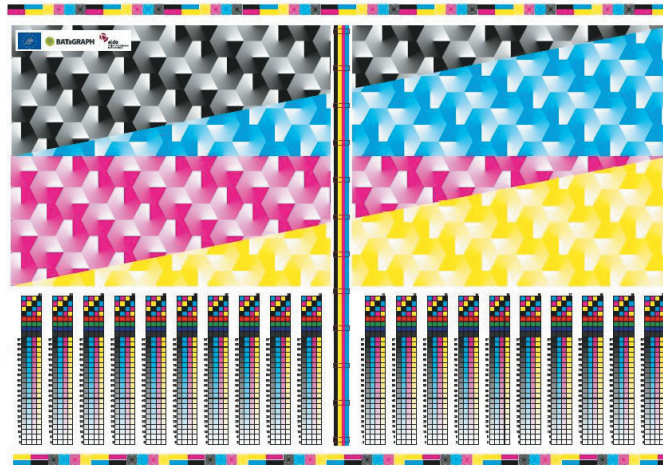


Figure 2: Inking test

The test should contain, the same way that the former one, some required elements and some others to help getting a good result

Minimum required elements

Unload ink area. This area will help to unload some ink. The aim is to get a slope in the density values at the later patches measurement from too high to too low density.

Solid and mid-tones. At this group of patches, density and $L^*a^*b^*$ values will be measured. Density values will be measured right after printing to register the wet production density. Will be preferred to take this data from the company instrument. In case of take the measurement will a manual device, please, make sure that a polarization filter is used. These patches, after drying, will be used, too, to take $L^*a^*b^*$ and dot gain measurements

Additional elements

Like in test 1, slur and doubling (f), pressure (g) and circumferential density control (h) patches should be used to check the test during print production.

- **RIP settings and plate calibration**

- The plates produced for this test shall be as best calibrated as possible. Please note that with this printed test we will compute the printing press actual dot gain, so we will need to deactivate any other RIP curve than plate calibration one in order produce linear plates.
- As said at point 1.2, please, refer to the workflow or RIP respective manual and use an appropriate measurement device.

- **Test printing**

- In order to get sloped densities we need to apply too much density in one side and decreasing until the other one. Contrary to common perception, the side where more ink has to be applied is where the unloading ink area has less influence.

- **Color versus density and dot gain measurements**

- As said before, density must be measured, in wet, at printing time. $L^*a^*b^*$ values must be taken after the printed test is completely dry. Please, let the test dry 10 to 20 hours, then start measuring $L^*a^*b^*$ values

Step 4: Conformance printing

- **Testform design**

Test 1 that been showed at point 1.1 of this procedure should be used.

- **Actual dot gain (printing press) compensation**

- **Validation Test printing**

Finally, the third test shall be printed using compensated plates as we saw above and applying production densities as we saw at point 2.7. If this procedure were followed as accurately as possible we should obtain a printed test that matches the former ink series visual appearance.

3.3.2 The BATs related to **IPA reduction** needs to an integrated implementation procedure to have a successful technical implementation in three steps:

Step 1: Basic (pre)conditions for successful reduction of IPA are created. These basic conditions are primarily the creation of good communication and a common basis of support within the company and the creation of an IPA-administration: Maintain a closed damping system;

- Take regular measurements of the quality of the damping solution, using the parameters of temperature, IPA concentration, conductivity and acidity. Ensure that the measured values are recorded on a registration-card per damping unit (in effect often per press).
- Ensure proper controls of the plate development process. In case of a negative result it is important to devise a solution together with the supplier.
- Calibrate the aerometer by performing your own test of the damping solution.
- Get informed on the quality of the (tap) water that is used to dilute the damping solution.

Step 2: Housekeeping. In the second step the machines that are currently in use are tuned and settings are adjusted and optimized. This is so-called good housekeeping. The IPA concentration can be reduced to a maximum of 8 vol. % in this manner

- Take care that automatic dosage systems have (rubber) caps on the IPA cans/drums to prevent unneeded evaporation;
- Start the IPA doser half an hour later than the damping solution mixer to ensure a better IPA measurement and dose;
- Isolate all piping leading to and from the damping system to prevent unneeded heating and evaporation (and accompanying energy loss);
- Always strive for minimal piping length for the damping system to prevent unneeded pollution or heating;
- Optimize the cooling of damping solution containing IPA by reducing the water temperature in steps of 0.25 °C to 8 °C in the sheet fed offset and 10 °C in the heatset;
- Consider raising the temperature of non-IPA containing damping solution (to around 10 to 12°C) to achieve faster evaporation of the damping solution;
- Use filter mats in the damping solution tank what will filter ink particles and paper dust from the recycled damping solution;
- Install (if financially feasible) a filtration system which will significantly decrease the 'age' of the damping solution (by up to 6 months in some cases).
- Ensure that the floater (IPA measurement device) of the conventional damping solution doser is always clean to prevent incorrect measurements (which are always deleterious to IPA use)
- Periodically clean all piping of the damping unit and the damping solution container to prevent unwanted pollution;
- Regularly replace the damping solution (often weekly);
- Removing glazing (paper dust, lime and leftover inks) from the rubber rolls in the damping unit as much as required to guarantee optimal damping solution use.
- Consider 'conserving' (especially for the weekend) the rubber rolls by injecting them with acidic etching gum;
- Regularly clean the metal roller to remove greasy washing solutions. This will significantly improve solution use;
- Check rubber rolls for any damage that cause inferior solution use. Proceed with early replacement if required;
- Check all rolls every 4 million print runs or once each quarter with regard to straight alignment to prevent friction of rolls - and therefore bad solution use;
- Consider outsourcing the regular maintenance of the printing press;
- When all previous measurements have been introduced: proceed with a step-by-step reduction of the IPA concentration in the damping solution to a maximum value of 8

Step 3: Further decrease of IPA in the damping solution. In the third step the IPA concentration is lowered through the addition of IPA-reducing damping solution additives and/or changes to the press. A requirement for this third step is that the existing machines are in optimal condition. This means that step three will only work if the measures in step one and two have been taken and are a continuous topic of attention. The IPA concentration can be reduced to a maximum of 5 vol.% in this manner; in some cases even further up to 0 vol.-%:

- Purchase water purifying equipment if much water is needed. Examples are reverse osmosis and nanofiltration;
- Replace conventional damping solution additives with IPA replacing additives. Ensure that you do this with the cooperation of your supplier. Then proceed to lower your IPA percentage to the lowest possible level (5 vol.% or lower) in a step by step manner;
- Replace the standard rubber damping rolls with rolls with a low hardness (24-30 Shore). Replacement is especially opportune when old rolls should be replaced anyway;
- Confer with your (press)supplier whether replacement of the standard chrome damping roll by specialized chrome, ceramic or copper roll would offer benefits for IPA reduction;
- Check with your supplier whether complete removal of the contact roll of the damping unit will have a positive effect on the performance. This has proven the case for certain types of presses);
- Check whether is it possible to run 'out of contact' on your presses;
- (If applicable) Check the rotation settings of the damping roll or the settings of your potentiometer.
- Consider using IR measuring equipment to ensure accurate dosage of IPA. N.B.: This equipment is very expensive and only beneficial when not striving for complete IPA elimination (which is currently quite possible);
- Consider (especially for large print runs and new presses) switching to ink cooling. This increases the stability of the print.
- Check with your supplier whether it is possible to change the alcohol based damping system to a non-alcohol based (film)damping system. This is a possibility for certain small format presses;
- Consider using digital print technology as an alternative to conventional offset techniques;
- Switch to waterless offset with the support of a skilled supplier

The validation process has shown the validity of the best practices in both aspects:

- Technical: keeping the productivity and the quality of the printing productions
- Environmental: reducing the VOCs emissions and the rest of the considered environmental parameters

3.4 Implementation strategy

STEP 1: CONDITIONS FOR SUCCESSFULLY ACHIEVING IPA REDUCTION Current User: wvz [Logout](#) Language | English ▾

[next phase](#)

1. Ensure that the board fully backs the IPA reduction plan.

Important conditions for successful IPA reduction are a sufficient common basis of support and good internal communications within the company. This applies for both the employer, who must strive for a safe and healthy working area and for the printers who must be able to work safely and in a healthy manner. There are also the chief operators/foremen who are responsible to the management and must lead by example. Taking everything into account, there are quite some layers within the organization that must support the IPA reduction policy.

Answer:

Resolve Date: (dd/mm/yy)

Responsible:

Comments:

2. Those responsible on-site (chief operators / foremen) must be positive about the reduction plan.

Important conditions for successful IPA reduction are a sufficient common basis of support and good internal communications within the company. This applies for both the employer, who must strive for a safe and healthy working area and for the printers who must be able to work safely and in a healthy manner. There are also the chief operators/foremen who are responsible to the management and must lead by example. Taking everything into account, there are quite some layers within the organization that must support the IPA reduction policy.

Figure 3: eTool Best Practice Module

An eTool has been developed in order to facilitate the implementation of the Best Practices developed, including the next three modules:

- Best Practices Implementation: best practice implementation module, step by step, in a guided and in an automated way. A registry of all pending and completed actions, dates and responsible is available.
 - A complete report is delivered about the Best Practices implementation and the correspondent Action Plan.
- Print quality control module: Allow remote verifications of the quality of the printed output in order to check that best practice implementation guidelines have been correctly adopted. The tool provides an automatical system to analyze the printing result according to ISO 12647-2 requirements. The tool provides a control patch to be measured by the company with an Eye One. The tool provides a measurement software application to be download in the own user PC These software application creates and xml. File which must be onload in the BATsGRAPH tool. The BATsGRAPH tool produce a measurement report to check the print quality.



Figure 4: eTool Print Quality Module

- Environmental control module Each company has a set of EcoIndicators aligned to each improvement process in order to verify the environmental improvement reached and monitor them. The BATsGRAPH tool produce a measurement report to check the print quality

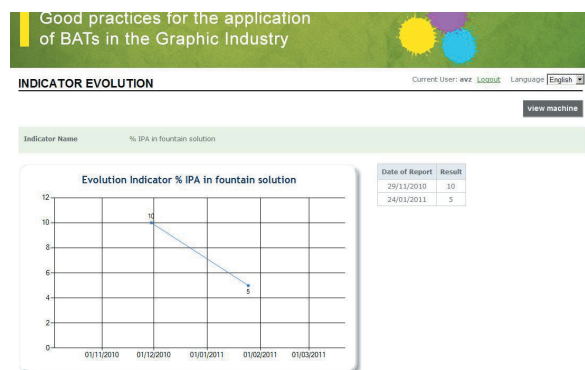


Figure 5: eTool Environmental Module

4. Conclusions

The European SMEs printing companies needs a technical support to understand and implement the BATs, especially Sheet Fed Offset SMEs, which are out of the scope of the legislations. The critical information for SMEs Sheet Fed Offset Companies is how to reduce the use of IPA and how change from mineral to vegetable inks.

A successful procedure to change from mineral oils inks to vegetable inks has been developed in four steps: Preconditions, Study of printing condition with mineral oil based inks, Implementation, Conformance printing.

This Best Practices can reduce the use of mineral oil inks in 100%. A innovative procedure to achieve IPA reduction has been developed in three steps: Preconditions, Housekeeping and New Additives and Machinery. Housekeeping practices reduced IPA concentration to a maximum of 8 vol. % in this manner New Additives and Machinery can reduced IPA concentration to a maximum of 5 vol.% in this manner; in some cases even further up to 0 vol.% The information showed in the developed eTool can facilitate the implementation of the developed Best Practices.

Acknowledgements

The development of this research has been possible thanks to the cooperation of the partners of the BATsGRAPH project, which are: KVG0 Dienstencentrum (Holland), ENVIROS (Czech Republic), FCV_RE (Spain) and Clean Technologies Center (Spain).

References

- (1) European Commission Directorate-general Joint Research Centre Institute for Prospective Technological Studies (2007). *Reference Document on Best Available Techniques on Surface Treatment using Organic Solvents*
- (2) Heidelberg (2008) *Dampening Solutions in Offset Printing*
- (3) Martinez Ayala (2010) *Technical Specifications Sheet Ink ECOGLOSS Serie*

Water conservation and approach to zero liquid discharge (ZLD) in a paper manufacturing plant - A case study

Anayath Rajendrakumar¹, Satyavolu V. Subrahmanyam², Senniappan Chinnaraj², Amrutharaj Harikrishnan¹, Kaipensery S. Rajesh², Kiran Prayagi, Palaniappan Karunanithi², Natarajan Baskaran²

¹ Print Media Academy, Heidelberg India
333, GST Road, Chrompet, IN-600 044Chennai, India
E-mail: rajendrakumar.anayath@heidelberg.com

² Tamilnadu Newsprint and Papers Ltd.
Kagithapuram, Karur Dist.- IN-639136, India

Abstract

Tamilnadu Newsprint and Papers Limited (TNPL) is India's largest bagasse based Integrated Pulp and Paper mill, having an installed capacity of 245,000 TPY Printing & Writing paper and poised to enhance its capacity to 4,00,000 TPY by middle of Year 2010. It used to consume about 70,000 m³/day and discharging 55,000 m³/day where 15,000 m³/day being accounted for evaporation losses.

TNPL has an installed capacity of 245,000 TPY Printing & Writing paper and enhancing its capacity to 4,00,000 TPY by middle of Year 2010 maintaining the same total fresh water consumption. It used to consume about 70,000 m³/day and discharging 55,000 m³/day where 15,000 m³/day being accounted for evaporation losses. The mill has determined to go for major water saving program along with pollution load reduction and developed a road map to go for Zero Liquid Discharge (ZLD) and same is presented and discussed in this paper.

Keywords: ZLD-Zero Liquid Discharge, ECF-Elemental Chlorine Free, D-Dioxide Extraction, ESP-Electro Static Precipitation, AOX-Adsorbable Oxygen Halide

1. Introduction

The pulp and paper industry is one of the highest water consumers among major chemical process industries. Using a well-diluted fiber suspension for manufacturing paper on wire is still the same from the day the paper was invented 2000 years ago. Water is also the medium where all the pulp and paper making process are carried out and it is also used as vehicle to transport the pulp in the mills from one unit operations to another. A major fraction of water used becomes contaminated during various processes. The water removes contaminants such as, Colloids, mineral ions, chromophoric groups, wood extractives, organic radicals, slime, stickies etc. This contaminated water (effluent) is treated and discharged later as waste water. In the 80's water consumption per ton of paper produced was as high as 250 m³/MT, and at present it ranges from 100 to 150 m³/MT.

The modern pulp and paper technologies have helped in closing the water circuits to generate less effluent. The concentration of contaminants causes problems in the process by way of erosion, corrosion and scaling etc., as water systems are closed and fresh water consumption minimized. In the past decade, considerable efforts were made in both national and international level to develop and operate closed loop configuration in the pulp and paper mills to minimize environmental impact on the surrounding ecosystem. The concept is being accelerated in the recent years due to increasing awareness about environmental among the public and consumers (Johnston *et al.*, 1996). The concept is accepted within the industry that close looping is essential for long term sustainable operations (Subhash Chandra, 1994, Senhorest, 1998, Ferguson and Finchem, 1997, Gleadow *et al.* 1997). Nonetheless, when water circuit is closed, concentration build-up of contaminants especially chlorides and other non-process elements cause problem in process operation by way of erosion, corrosion and scaling, forcing to purge or develop new systems to remove or reduce contaminates. TNPL has an installed capacity of 245,000 TPY Printing & Writing paper and enhancing its capacity to 4,00,000 TPY by middle of Year 2010 maintaining the same total fresh water consumption. It used to consume about 70,000 m³/day and discharging 55,000 m³/day where 15,000 m³/day being accounted for evaporation losses. The mill has determined to go for major water saving program along with pollution load reduction and developed a road map to go for Zero Liquid Discharge (ZLD) and same is presented and discussed in this paper. The efforts made in TNPL and its future plans are broadly classified into three phases and presented in Table 1.

Table 1: TNPL Road map for water conservation and pollution reduction

1.	Phase I	1. Water conservation and pollution reduction under mill development plan (Hard wood brown loop closure) 2. Eop recycling 3. Chloride removal in Chemical recovery plant 4. Reuse of paper machine water for bagasse storage, bagasse handling and washing
2.	Phase II	1. Filtration of clear filtrate in paper machine and reuse for high pressure showers 2. Chemical bagasse brown loop closing, recycling of gland cooling and pump sealing water 3. Close looping of SRP island 4. Close looping of Energy Island
3.	Phase III	Bleach plant waste water treatment using physico-chemical process followed by membrane separation

2. Research methods

2.1 Phase 1. Water conservation and pollution reduction under mill development plan (Hard wood brown loop closure)

TNPL has replaced 120 TPD Hardwood fibreline with 330 TPD Superbatch™ cooking system with oxygen delignification process and complete brown loop closure followed by $D_{HT} E_{OP} D$ medium consistency bleaching sequence. The washing system comprises of twin roll presses. The chemical bagasse line was integrated in to single line 550 TPD ECF ($D E_{OP} D$) medium consistency bleaching. The oxygen delignification and brown loop closer is under way in the bagasse line under mill expansion plan. MDP was implemented in the year 2008 and it became fully functional in the year 2009.

Historically, the pulp is transferred by low consistency pumping (2.5 to 3.5%). This means that for each dry ton of pulp, we are also pumping 96 to 97 m³ of water. In this process the water gets several contaminants like, colloids, ions, fines, pitch, chromophoric groups, sand and volatile odorous compounds that enter to other area together with the pulp. Higher consistency washers would reduce water and energy consumption for each dry ton of pulp produced. Implementation of medium consistency process using press washing in new hard wood line along with Oxygen delignification and ECF bleaching process is one of the major element, which reduced the water consumption and pollution load in the pulp mill (Pryke *et al*, 1998, Gulichsen, 1991). The average water consumption per day in the pulp mill is reduced from 44,092 m³ in the year 2007 to current quarterly average of 16,080 m³. As expected, the average consumption did not reduce in other areas like paper machine, utilities, SRP and energy side and the reduction is only 1.3%. However, overall water consumption in the mill has reduced significantly from 70,851 in the year 2007 to 42,810 m³ in the current quarter, as the pulp mill is the major consumer of water in the mill. The average water consumption per day has reduced by 31% in the beginning of 2009 when compared to 2007 and specific consumption per ton of product is 99 m³, 87 m³, 71 m³ and 57 m³ for 2007, 2008, up-to June 2009 and from July to September 2009 respectively.

Implementation of modern technologies and practices that are stated above have improved the process economics, like, improved yield, quality and reduced energy and water consumption per ton of the product. It also helped in improving the environmental performance of the mill which is evidenced in the present case in TNPL. Commissioning of new 330 TPD hardwood fibreline and 550 TPD chemical bagasse fibreline has improved the overall environmental performance of the mill. The overall pollution loads to the effluent treatment plant has come down in spite of the increased production. For example, in the high BOD stream, which is treated through anaerobic process followed by activated sludge process, the COD & BOD load is reduced from 83.63 TPD to 70.65 TPD and from 58.91 TPD to 35.91 TPD respectively. The reduction is 15.5% in case of COD load and 39.0% in case of BOD load. In case of Low BOD stream, which is treated directly in the activated sludge process, the BOD load has come down from 13.9 TPD to 7.6 TPD which is around 45.4%, however change is not significant in the COD load. The high COD/BOD ratio in the post MDP is low due to biodegradable nature of the effluent especially from bleach plant which joins this low BOD stream. The overall pollution load to effluent treatment pant i.e. both high and low BOD stream combined, has reduced by: Color 11.3%, Total solids 12.6%, Total dissolved solids 12.0%, COD 12.6% and BOD 40.3%.

The reduced water consumption and pollution load has improved over all performance of ETP and improved the mill final effluent discharge standards with respect to Color, Total solids, Total dissolved solids, COD and BOD. The discharge standard for the year 2009 per ton of product is: Color 10.0 kg, Total suspended solids 2.0 kg, COD 9.2 kg, BOD 0.1 kg and AOX 0.1 kg, which is comparable or even low against the values of one of the best mill in Europe i.e. Total suspended solids 1.6 kg, COD 18.6 kg, BOD 2.2 kg and AOX 0.15 kg (StoraEnso, EMAS Environmental Statement 2007, Imatra Mills, Finland).

2.1.1 Eop alkaline filtrate recycling

Replacing conventional CEH with ECF bleaching sequence in both hard wood and chemical bagasse fibrelines reduced the contribution of calcium hardness to wastewater. As result, the percent sodium level increased in final discharge effluent. Wastewater generated from Eop stage contains relatively high molecular weight organic compounds and sodium (Dence and Reeve, 1996), whereas, acid waste water contains mostly low molecular weight organics and inorganic salts, such as, calcium, magnesium, chlorides and sulphates etc., and it is not desirable to mix and concentrate inorganic substance with organic substances. Therefore, to reduce percent sodium level, alkaline extraction filtrate (E_{OP}) alone is being recycled fully in new hardwood fiber line and sent to soda recovery plant via brown-stock washing. Alkaline filtrate contains organic solids removed during extraction process, chromophoric compounds and AOX removed from the pulp. In addition to benefits stated above, reuse of E_{OP} filtrate may reduce organic solids level and colour compounds leaving the bleach plant.

Alkaline filtrate from filter, after recovery of suspended solids, going to the effluent drain is diverted to an intermediate tank installed for recycling alkaline filtrate. From intermediate tank, alkaline filtrate is pumped and used in post oxygen press for washing in place of hot water (Dilution factor 2 - 2.5).

Use of alkaline filtrate in PO press did not increase the alkali loss, Chlorine dioxide consumption at the same time resulted in saving of hot water (80°C) that was used earlier. Hot water used in the PO press, generated from Superbatch™ cooking process, was diverted to CBP ECF bleaching resulting in saving of 0.3 MT of LP steam per tone of pulp that is used for generating LP steam in CBP ECF. About 60m³/hr of excess hot water is pumped to CBP ECF plant, thereby reducing 1400 m³ of hot water generation using LP steam. Due to that LP steam consumption is reduced by 0.3 t/ton of pulp in bagasse ECF plant accounting annual saving of Rs 2.0 Cores.

2.1.2 Incremental impact of recycling

A key to successful recycling of extraction filtrate is in management of non-process elements and controlled purging of chlorides and potassium. Closing water circuit in pulp mill will impact chemical recovery system as it is sensitive to chlorides and potassium and increased concentrations of inorganic cations and anions may cause scale formation, deposits, plugging in super heater and corrosion resulting high chemical and steam demand. Therefore, it is necessary to purge chlorides and potassium, directly through ESP ash purging or selective leaching of chlorides in ESP ash by crystallization and recovery of sodium sulphate present in ESP ash.

2.3.1.1 Chloride removal in chemical recovery plant

The Sources of Non-process elements (NPEs) in TNPL are mainly from, in-coming process water which has a chloride content varying from 100 ppm to 300 ppm, and usage of wood with bark in pulping, entry of treated effluent in pulping street along with washed bagasse and recycling of extraction filtrate. Complete closure of brown loop in pulp mill warrant new systems to remove NPE's to avoid problems arising due to chlorides and potassium (Ferreira *et al*, 2003, www.hpdsystems.com).

In TNPL, chlorides in white liquor is about 24 - 28 gpl as NaCl and Chlorides in Recovery boiler ESP ash is about 24 - 28% as NaCl. Initially the chloride level was about 4-6% and increased gradually to 10% and then to 20% and presently to a level of 24-28%. The reasons for build up of chlorides are already stated in the beginning.

Solubility of chlorides in water is high compared to sulphates. For example, Sodium chloride dissolved readily in water but suppresses the solubility of sulphates. To confirm the same, laboratory studies were conducted using the above principle to separate chlorides and sulphates. A series of tests with varying amounts of ESP ash (Insoluble matter in water: 0.11%, Sulphates as Na₂SO₄:70.3%, Chlorides as NaCl: 24.2%, Potassium as K: 5.10%,

Carbonates as Na_2CO_3 :0.30%) in water viz 500, 600, 800, 1000 and 1200 gram per liter were prepared. The slurry is filtered. Both the cake and filtrate were analyzed for sodium sulphate, sodium chloride and Potassium (Table 2).

2.3.1.2 Components and process for chloride removal system:

Based on laboratory results, a system was designed at TNPL to remove the chlorides. The system consist of a tank with a capacity of 2 m³ with a slow speed agitator, a centrifugal pump, a decanter centrifuge with 2 m³ feed rate, Density control equipments and necessary instrumentation. ESP Ash slurry of 800 gpl to 1000 gpl is fed into a decanter centrifuge which separates undissolved sodium sulphate as a cake from the slurry. The separated sodium sulphate is fed to mixing tank of recovery boiler and the filtrate rich in chlorides and potassium is drained.

The system efficiency for Sulphate recovery from the ash was around 73.4%, while chloride removal from the ash was 90.4% and Potassium removal from the ash was 70.6 % (Table- 3). The major benefits from chloride removal system are; 1. Increased stability of mill operation having less frequent stoppages of boiler for washing, 2. Reduction of corrosion in the recovery boiler and 3. Increase of recovery boiler steam production. However, the filtrate drained contains un-recovered sodium sulphate and chlorides. It is proposed to recover the sodium sulphate by employing sulphate removal nano membrane systems, those are employed in Chlor-alkali plants (Sinclair and Western,1996, Sanhaber *et al* 2001, Davis and McElhinery, 2002).

Table 2: Laboratory analysis results of ESP as solubility studies

Cake analysis					
ESP ash In water, gpl	50	600	800	1000	1200
Na_2SO_4 , %	92.9	94.3	92.3	90.8	89.7
NaCl, %	1.87	2.45	3.84	5.14	6.43
Potassium as K, %	0.54	1.35	2.24	2.99	3.29
Sulphate recovery, %	12.0	34.2	60.6	79.1	89.1
Chloride removal, %	99.3	97.4	92.7	87.0	81.4
Potassium removal, %	99.0	93.3	79.7	64.1	54.9
Filtrate Analysis					
ESP ash In water, gpl	500	600	800	1000	1200
Na_2SO_4 , gpl	284.5	244.2	238.1	189.0	144.5
NaCl, gpl	109.6	131.5	157.8	197.3	236.7
Potassium as K, gpl	18.1	25.0	28.1	30.6	29.4

Table 3: Chemical composition of samples of ESP Ash, Centrifuged cake and filtrates

S. No	Compounds	Composition in %		
		ESP ASH	Centrifuged Cake	Filtrate
1	Sulphates as Na_2SO_4	70.7	90.9	191.3
2	Chlorides as NaCl	22.4	4.50	188.2
3	Potassium compounds as K	5.60	3.0	32.0

2.2.1.3 Reuse of paper machine water for bagasse storage, bagasse handling and washing

To reduce fresh water consumption as part of water conservation measure, nearly 9000 m³ treated effluent was used in the bagasse handling and storage area till June 2009. Treated wastewater contains relatively high TDS and enters into recovery cycle along with bagasse creating adverse impact on recovery process. Paper machine wastewater, which contains relatively low TDS, was identified as an alternate to treated effluent and it was clarified using one of the clarifier separately and pumped to bagasse handling and storage area for use.

The comparison of Paper machine wastewater and treated wastewater characteristics are given in the Table 4 Utilization of paper machine wastewater in bagasse storage and handling area has reduced hydraulic load on activated sludge process and reduced 0.87 TPD chlorides entering into process. Also total average fresh water consumption from 48804 m³ per day to 42810 m³.

Table 4: Comparison of treated and paper machine wastewater

S. No	Parameter	Unit	Treated effluent water	Paper machine effluent
1	Colour	Pt Co	235	108
2	Total Solids	ppm	1994	1130
3	Total Dissolved Solids	ppm	1950	1060
4	COD	ppm	194	221
5	BOD	ppm	4	30
6	Chlorides as Cl	ppm	780	200

2.2 Phase 2. Filtration of clear filtrate in paper machine and reuse for high pressure showers

Mill is procuring Algas filtration system to filter the clear filtrate to the tune of 5000 m³/day in paper machine I and II. It is proposed to reuse this filtered water in high pressure showers that would reduce the fresh water consumption of similar quantity.

2.2.1 Chemical bagasse brown loop closing, recycling of gland cooling and pump sealing water

TNPL has now embarked on a Mill Expansion Plan (MEP) involving reduction of the pollution load further by backward integration of ECF bleach plant of Chemical Bagasse Pulp. The current brown pulp operations in Bagasse fibreline are open and use drum washing system having brown stock washers followed by Decker washing. The Decker washer is currently integrated with ECF bleach line through Pre-thickener filter to increase the pulp consistency before it enters bleaching process. In backward integration, the drum washers will be replaced with press washers and Oxygen delignification will be introduced and close the brown loop. Current fresh water consumption in bagasse pulping and bleaching operations is about 30 m³/ton of pulp that is expected to come down to about 18 m³/ton after backward integration. Introduction of press washing, closing brown loop, introduction of ODL stage and recycling of extraction filtrate will reduce water consumption and pollution loads especially the colour and TDS. A dedicated system is being implemented for bagasse washing, wastewater reuse and recycling along with sludge handling system. Increasing the recycle ratio in the bagasse handling process will improve biogas generation due to increased COD concentration in the wastewater and reduced hydraulic loading in the reactors.

2.2.2 Close looping of SRP Island

In Chemical recovery plant, nearly 70 m³/hr of mill water is used for pump cooling and vacuum pump sealing and another 20m³/hr for lime kiln bearing cooling details are presented in Table – 5. The used water is let in to the drain. It is proposed to recover water and reuse for the process again. The pump sealing water used in the Alfa Evaporator will be pumped to old causticizer hot water tank and from Alfa evaporator -2 and Recovery boiler, water will be pumped to dissolver tank and then to lime kiln hot water tank. The water used for lime kiln bearing cooling will be diverted to lime kiln hot water tank. The vacuum pump sealing water contains some odour and further studies are underway to identify the appropriate point to use.

Around 300 m³/hr treated effluent is used in WLCD heat exchanger; Dregs filter vacuum pump & condenser, Mud filter vacuum pump & condenser and LMCD vacuum pump & condenser and let into drain Table - 6. In the proposed new system all the water after use will be collected in separate collection pit and will be pumped to proposed dedicated new mini cooling tower and then reused again in the system and will not be allowed to drain. The excess wastewater from paper machine will be used for the new make-up in the new cooling tower and it will eliminate around 300 m³/hr treated effluent use.

Table 5: Fresh water use in SRP

S. No	Equipment	Consumption m ³ /hr
1	Alfa Evaporator-1 Pumps cooling water	15
2	Alfa Evaporator-1 Vacuum pump sealing water	10
3	Alfa Evaporator-2 Pumps cooling water	20
4	Alfa Evaporator-2 Vacuum Pump sealing water	20
5	Recovery Boiler Pumps cooling water	5
6	Lime kiln bearing cooling water	20
7	Total discharge to drain	70

Table 6: Treated wastewater use in SRP

S. No	Equipment	Consumption m ³ /hr.
1	Dregs filter vacuum pump and condenser	50
2	Mud filter vacuum pump and condenser	100
3	LMCD vacuum pump and condenser	70
4	WLCD heat exchanger	80
5	Total discharge to drain	300

2.2.3 Close looping of energy island

Around 1000 m³ of treated wastewater is used in Boiler # 1, 2 & 3 for ash quenching and Vacuum Pump sealing and let into drain. It is planned to draw clarified paper machine waste water for pump sealing and ash quenching. And after filtering to remove coarse and fine materials the used water will be sent to clarifier along with papermachine effluent. Nearly 1000 m³ of water is currently drained from cooling tower as blow down water. Instead of draining from the cooling towers, the water will be drained from evaporator and used for vacuum sealing.

Close looping in SRP and Energy Island will eliminate the burden on effluent treatment system and ultimately facilitate the ZLD.

2.3 Phase 3. Treatment of acidic effluent from bleach plant (HW & CB ECF)

2.3.1 Pilot plant studies

The D_{HT} filtrate from HW ECF plant was treated with lime followed by soda ash and sent to a clarifier to precipitate Magnesium and Calcium salts, colloidal silica and some of the organics. Lime addition increased the pH to 11.0 to 11.5. The precipitated clarified sludge contains 50 to 55 % organics, 5 to 7 % silica, 30 to 40 % calcium as CaO and 4 % MgO that is found to be suitable for use in Cement plant along with lime sludge. The clarifier is free from hardness. This treatment reduces the COD to a level of 30 %, but TDS and Sodium level increase marginally. The pH is then adjusted to 3.5 to 4.0 using CO₂ or Hydrochloric acid to neutralise pH. The effluent is then passed through a 5 micron bag filter and treated with 100 ppm of FeSO₄, H₂O₂ (60 ppm) and Ammonium persulphate (90 ppm) and fed to a FACCO (Fenton activated carbon catalytic oxidation) reactor. This reactor consists of Stone pebbles, 0.3 to 3 mm in the bottom layer and catalyst impregnated activated carbon in the top layer. The effluent is allowed to pass downwards with air distribution at the bottom. The COD was found to reduce from 1807 to 760 ppm and colour from 540 to 200 ppm pre-filter to remove suspended solids and taken to a Membrane filtration unit, to remove dissolved organics (lignin compounds) and inorganic salts. The permeate COD was reduced from 1094 to 332 ppm (69.7 %) and TDS from 8756 to 2784 ppm (68.2 %). Colour gets reduced totally in this stage. The rejects can be further concentrated to get Sodium chloride, Sodium sulphate and other inorganic salts. The Organics, after concentration can be sent to Chemical recovery plant for incineration. Permeate from the above stage is further processed through RO system. RO accepts was found to contain negligible level of COD and lower TDS and hardness. An overall reduction of 88 generated @ 6500 m³ /day can be treated by the membrane separation process to get good quality water that will be used in the process replacing the fresh water. to 95 % was achieved after this stage.

3. Conclusion

The brown stock washing is based on the TwinRoll Press technology for achieving low alkali loss at minimum dilution factor resulting in substantial reduction in water consumption. The malodorous gases (Non Condensable Gases) are captured and burnt in the Lime Kiln of 170TPD commissioned under MDP. The Elemental Chlorine Free/Chlorine-dioxide (ECF) bleaching process replaces the conventional Elemental Chlorine - Hypo bleaching process bringing down the pollutants like color, COD and AOX significantly. By adopting the advanced pulping and bleaching processes in hardwood pulp processing, the water consumption is reduced from 60 m³/ton of pulp to 15 m³/ton of pulp. TNPL is first mill in India to implement recycling of Extraction filtrate (highly colored with high TDS Eop effluent) in the hardwood fibreline that minimises the pollution load significantly at source. The conventional Elemental Chlorine - Hypo bleaching process in bagasse line also is replaced with the Chlorine-dioxide bleaching to reduce the Color, Chloro-organics and COD generation at source. Other measures like reuse of paper machine wastewater, chloride removal also contributed to a great extend to improve the environmental performance of the mill. TNPL is currently under-

taking many measures like close looping of chemical bagasse brown loop, recycling of gland cooling and pump sealing in pulp mill, energy & SRP. Treatment for bleach plant acidic wastewater using physicochemical process followed by the membrane technology to reduce the pollution load to the barest minimum. Treatment of about 15000 m³/day having Cauvery river water quality with Ozone making it much more superior in quality irrigation water to meet the obligatory supply of irrigation water to farmers.

References

- Davis R. A. and J. E. McElhinery (2002). The advancement of sulphate removal from sea water in offshore waterflood operation. Corrosion 02314.
- Dence C.W. and C.W.D. Reeve (1996). Pulp bleaching Principles and Practice, Tappi Press, Atlanta, USA, Page - 756.
- Ferreira G. A. L., Soares, M.A.R. Egas A.P. and J. A. M. Castro J (2003). Selective removal of chlorine and potassium in kraft pulp mills. *Tappi Journal*. Vol(2) No.4,:21 - 25.
- Gleadow, P., Hastings, C., Richardsdon, B., Towers, M., and Uloth, V. (1997). Towards Closed Cycle Kraft Pulping: Canadian Mill StudiesP."A *PRICAN Miscellaneous Report 353*. Pulp and Paper Research Institute of Canada.
- Ferguson, K. and Finchem K. (1997). Effluent minimization technologies move pulp mills closer to closure. *Pulp and Paper*:71,3.
- Gullichsen J. (1991). Process internal measures to reduce pulp mill pollution load. *Water Science and Technology*: **24(3 & 4)**: 45-53.
- Johnston P.A., R. L Stringer, D. Santillo, A. A. Stepahenson, I.P. Labounskaia, and H. M.A. McCartney (1996). Towards zero – effluent pulp and paper production: The Pivotal role of totally chlorine free bleaching, Greenpeace International, Amsterdam, Technical Report 7/96.
- Pryke D.C., Winter P, Bouree G.R. and C. Mickowski (1998). Elemental chlorine free bleaching, Anthology of published papers (Edited by Katherine A. Kulas), Tappi Press, Atlanta, USA.
- Sanhaber W.M., K.Kream, T. Raab and H.Schwaiger (2001). Field test results of nanofilter application for separating almost saturated brine solution of vacuum salt production. ECC-Number. 26-28.
- Sinclair R. and R. Western (1996). Application of sulphate remove I technology in the Heron Cluster Field Rupert Sinclair, Shell UK Exploration & Production and Serck Baker Limited - Membrane Division.
- StoraEnso, EMAS Environmental Statement 2007, Imatra Mills, Finland.
- Subash Chandra (1998) Effluent minimization - A little water goes a long way. *Tappi Journal*:80(12):37-42.
- Henk B., A.J. Senhorst Lourens, Z. Richard P. and B. W. J. Luttmer (1997). A broad approach to water loop closure at papierfabriek doetinchem. Appendix Report. SPA-report 97006, RIZA- document 97.188X, Institute for Inland Water Management and Waste Water Treatment RIZA, Lelystad Papierfabriek Doetinchem, Doetinchem The Netherlands.



Analysis of JDF files

Thomas Hoffmann-Walbeck and Sebastian Riegel

Hochschule der Medien
Nobelstr. 11, D-70569 Stuttgart, Germany
E-mail: hoffmann@hdm-stuttgart.de

Abstract

In this paper a new tool of analyzing JDF files is presented. In general, one needs an XML-editor and the JDF specification to analyze the content of such a file. For non-specialist this is quite difficult, however. This projected tool tries to improve this situation by explaining the content of a JDF file with easy words. For that it uses a database with standard text blocks, adjusting those in some cases, triggered by specific JDF attributes. All JDF-nodes are reordered and assigned to the classical production areas prepress, press and postpress.

Keywords: job definition format, process integration, project management, java-tool

1. Introduction

Using the Job Definition Format one can define print products in a very flexible manner. Moreover, one can specify (almost) all production steps that are needed to produce previously specified products. Thus, it is not too surprising that the JDF specification is over 1000 pages and also fairly complicated. A JDF file is coded in XML, which means that it can be opened by XML-editors, as well by word processors and internet browsers. Even though it is easy to read the file, it is quite hard to understand it. See, for example, Figure 1, which shows a small part of an actual JDF-file, which has been taken from a production workflow. A net of product-, process- and process group-nodes that are linked by resources describes the interdependencies between the production steps quite accurately, but not very comprehensible for users, who normally classify their tasks in prepress, press and postpress. Figure 2 shows by an example the tree-like structure of JDF-nodes. The first two rows show product nodes, then there are two rows of process group nodes (*GrayBoxes* are double-outlined) and finally there are process nodes at the bottom. Figure 3 outlines an example of the input- and output-resource of a single process-node as defined in the JDF-specification (1). The process *ConventionalPrinting* represents the classical printing process with a physical printing form. The mandatory and optional resources are plotted as circles. The question marks denote an optional resource. JDF-files can get quite large. The code of Figure 1 is taken out of a JDF-file, which contains 38 JDF-nodes and 447 references to resources. When importing the file into a text processor it amounts to 98 pages.

```
<JDF Activation="Active" ID="Link081105_103004495_005678" JobPartID="1002" Status="Part"
Type="ConventionalPrinting" Version="1.3">
  <ResourcePool>
    <NodeInfo Class="Parameter" ID="Link081105_103004417_005661" NaturalLang="de" NodeStatus="Waiting"
      PartIDKeys="SignatureName SheetName" PartUsage="Implicit" SetupDuration="PT1H57M" Status="Available"
      TotalDuration="PT2H56M46S">
      ...
    </NodeInfo>
  </ResourcePool>
  <ResourceLinkPool>
    <NodeInfoLink Usage="Input" rRef="Link081105_103004417_005661" />
    <ColorantControlLink Usage="Input" rRef="r081105_104145405_001283" />
    <ConventionalPrintingParamsLink Usage="Input" rRef="r081105_104913377_013068" />
    ...
  </ResourceLinkPool>
</JDF>
```

Figure 1

JDF-files are changing over time. New JDF-nodes are generated during production; others, like the *GrayBoxes*, are deleted. For example, the JDF-file in Figure 2 is based on was 324 KB, while in an earlier production stage it had only amounted to 212 KB. Thus, any drawing of a JDF-tree represents only an intermediate snap-shot and might look inconsistent at first glance. This adds to the difficulty of analysing any JDF-file.

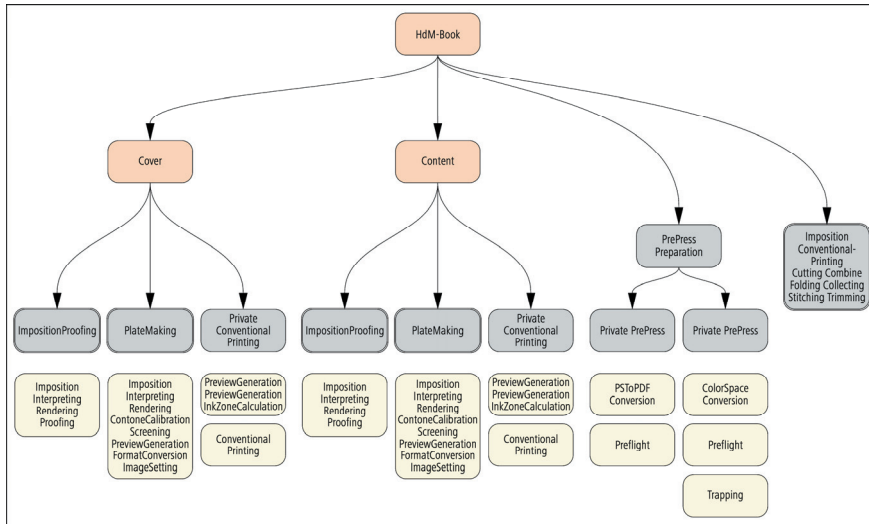


Figure 2

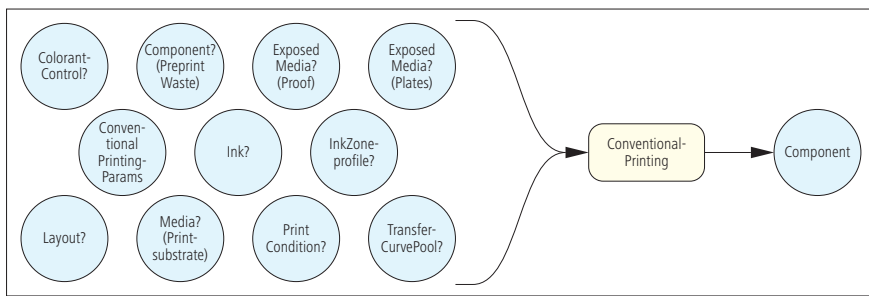


Figure 3

To ease the task of writing JDF-software, the *Interoperability Conformance Specifications (ICS)* have been specified by the CIP4, the *Cooperation for the Integration of Processes in Prepress, Press, and Postpress*. There are around a dozen papers that clarify the interfaces between common production areas in the graphical industry, such as MIS, Prepress and the like. For each interface different *levels* are defined, each dependent on the other. However, these papers do not make reading the specification superfluous. Quite in the contrary, the ICS-papers are based on the specification and must be read additionally.

There is a common misconception that only JDF programmers need to comprehend the structure and the content of a JDF file. There is no need, in fact, for an operator in a printing company to understand or even write such a file. In the daily work they normally fill in information about the product and about the production steps in a graphical dialog mask only. Generating and processing JDF files are done automatically in the in the background by the software.

But JDF workflow integration has to be configured individually for every print shop. This is caused by the fact that JDF potentially covers all parts of the business. Therefore major parts of the existing equipment have to be re-used for the JDF integration. And even if the JDF-devices are supposed to conform to ICS there are still plenty of imponderables causing JDF- conflicts between the software products of different vendors. In short: JDF-integration is far from being “plug ‘n play”.

Thus, somebody in a printing plant has to be responsible for this integration, namely the “workflow manager”. Furthermore, technicians from the equipment-supplier also help to specify the workflow. As a rule, those workflow managers, however, are not specialists in the internal structure of JDF files (at least in the beginning of an integration project), because it’s hard to become adept in this discipline. To make things even more difficult, there are very few text books available about JDF workflow, helping to elucidate JDF structures, such as those in (2) or (3)). And so the workflow manager has a problem, if a JDF interface between two JDF-compliant components won’t work properly. Even ascertaining which ICS-level a JDF-file is written in can be a difficult task.

There are, in fact, no simple support tools available to assist in such situations. XML-editors or even the CIP4 JDF Editor that can be downloaded from the CIP4-website are only helpful for those who can read JDF code. We are not aware of any software that explains JDF-content to non-programmers.

2. Folding parameter

Outlining a possible integration of specific JDF-modules can be quite demanding, but, on the other hand, it can be crucial for a workflow manager in a print shop. The difficulty is that it is not so easy to evaluate the quality of the information that is contained in a JDF file. The following example should explain what is meant by that: A JDF file for a folding machine can either contain simple administration data like the job-ID and the like or additionally useful presetting data. With the latter the file might simply contain the number of the imposition scheme according to the fold catalogue that is given in the JDF specification or it might specify the folding sequence and the exact fold positions. An imposition scheme, however, is not enough to preset the folding positions accurately (for example, if binding flaps are involved or if several folding sheets are positioned on one printing sheet). Figure 4 shows this situation. In any case, the vendor of a JDF-device will call the software JDF-compliant, even if the quality of the information is questionable. All in all, workflow managers have a hard time to evaluate the usefulness of a specific JDF interface before its implementation.

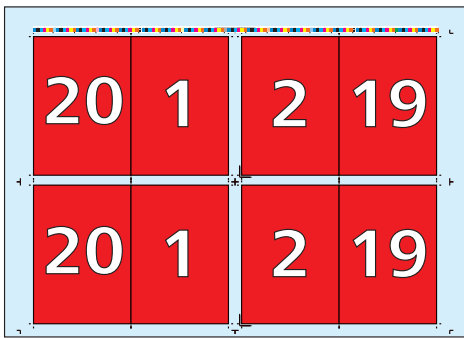


Figure 4

3. Software overview

Our approach here attempts to fill this gap. Software is presented that imports any JDF file and outputs a text-file explaining its content. The end-user might be only interested in a general overview about the content of the JDF file. On the other hand, the user might like to get more specific information about it, for instance in order to analyse the actual JDF code. In our software the textual output can be adjusted in three modes. In the basic mode the output only states the ICS Version that the JDF-file is written in and describes all JDF-nodes of the file in a few words, trying to avoid all specific JDF-notations (see Figure 5). The standard output additionally lists all input- and output resources; again, without using JDF-jargon (Figure 6). Finally, one can choose the option Expert Modus. In this case NodeIDs and the like are shown (Figure 7). Figure 8 shows the JDF-process ConventionalPrinting once again. Here our software generated the text automatically - not as in Figure 3, where the tree has been hand-drawn.

```

Summe Knoten = 38, Anzahl Produktknoten = 3, Anzahl Prepress Knoten = 16, Anzahl Press Knoten = 2
Anzahl Übergreifende Prozesse = 1, Anzahl privater JDFNodes = 16

Basic Modus ist eingeschaltet
ICSVersions = Base_L2-1.3 MIS_L2-1.3

---- PRODUKTBESCHREIBUNG ----
1) Endprodukt: HdM-Book
2) Endprodukt: Umschlag
3) Endprodukt: Innenteil

---- PREPRESS ----
4) Plattenausgabe (Beschreibung noch unvollständig)

5) Eine Kombination von mehreren Prozessen:
---Ausschießen (=Errechnung von Druckbögendaten aus Standbögen- und Seitendaten)
---Interpretieren (Teil eines RIP-Vorgangs)
---Rendern (=Umrechnung von Objektgrafiken in Pixelstrukturen)
---Prozesskalibrierung
...

```

Figure 5

```

Summe Knoten = 38
...
----- PRODUKTBESCHREIBUNG -----
1) Endprodukt: HdM-Book
Input:
  Informationen über den Auftraggeber. Auftragsname des Kunden: HdM-Book
  Vereinbarung zur Auslieferung oder Abholung von Druckprodukten oder von Proofs
  Terminplanung der Produktionschritte und Auslieferung
  Geplante Bindung des Druckproduktes
  Ein Produktteil
  Ein Produktteil
  Beschreibung, wie die Farben im Dokument in die Druckfarben umgerechnet werden
  Auflistung und Beschreibung aller Farben in dem Auftrag
Output:
  Das graphische Endprodukt
2) Teilprodukt: Umschlag
Input:
  Geplante Farbigkeit des Druckproduktes
  Beschreibung der Größe und Anzahl der Seiten des Druckproduktes
  Eigenschaften des geplanten Bedruckstoffs
  Terminplanung der Produktionschritte und Auslieferung
Output:
  Ein Produktteil
3) Teilprodukt: Innenteil
...
    
```

Figure 6

```

Summe Knoten = 38
...
----- PRODUKTBESCHREIBUNG -----
1)
JDF-Knoten von Typ Product Endprodukt: HdM-Book
Node ID = n_110513_20593231_007935
Hierarchietiefe = 0
JDF-Knoten Product
Input:
  CustomerInfo
  r_110513_20593246_007940
  Informationen über den Auftraggeber. Auftragsname des Kunden: HdM-Book

  NodeInfo
  r_110513_20593262_007952
  Terminplanung der Produktionschritte und Auslieferung

  Component
  r_110513_20593262_007957
  Ein Produktteil
...
    
```

Figure 7

```

Summe Knoten = 38
...
----- PRESS -----
20) Konventionelles Drucken (mit physischer Druckform)
Input:
  Terminplanung der Produktionschritte und Auslieferung
  Details über belichtete Platten oder Proofs
  Farbzonenvoreinstellungen
  Voransichtsbild Thumbnail
  Voransichtsbild Separation
  Festlegungen zum Bedruckstoff
  Standbogenbeschreibung
  Eigenschaften des Geräts Speedmaster CD 74-6L (HdM)
  Beschreibung der Druckfarbe bzw. Toners oder Lack
  Einige Transferkurven (Kalibrierungskurven) werden definiert
  Festlegungen zum konventionellen Druckprozess SheetFed
  Beschreibung, wie die Farben im Dokument in die Druckfarben umgerechnet werden DeviceCMYK
  Festlegungen zur Farbübertragung in der Druckmaschine
Output:
  Zwischenprodukt Druckbogen
...
    
```

Figure 8

The software consists of three parts:

- a) JDF import. Here nodes and resources as well as some of the values of their attributes are stored in a database
- b) Evaluation of the database. Here the information in the database is used to analyse the JDF. In particular, all tasks are divided into the common categories of prepress, press and postpress.
- c) In the last step the output file is generated in the txt-format, showing the explanations. For this part a second database is used that contains standard texts for all types of JDF node and for all resources.

Figure 9 shows a sketch of the general situation.

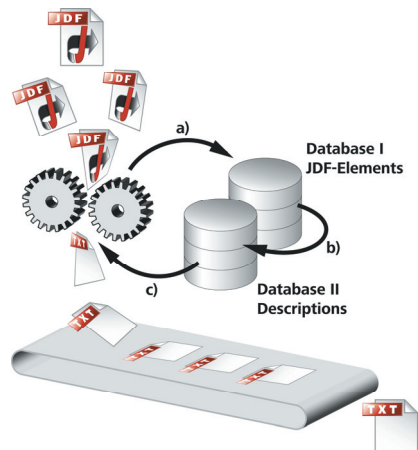


Figure 9

4. Coding details

JDF import is achieved by using the standard JAVA-library “JDFLibJ-2.1.4a,63” provided by the CIP4-organisation. It is based on two other libraries (Xerxes-J-2_9_0 and jakarta-commons-lang-2.3). Part of the actual source code that is used for importing the JDF file is seen in Figure 10 and 11. In Figure 10 the root node is read. All JDF nodes and JDF sub nodes are imported recursively in Figure 11. The IDs of the nodes as well as values of certain attributes are read from the file and stored in a database. For this research project, we used Microsoft Office Access as a database system. Furthermore, all the names of the resources that are used by the nodes either as input or as output are written into the database. Again, certain attributes (or even data that is stored in sub-elements of the resources) are stored in the database.

```
public class JDFAnalyse {
    ...
    public static void main(String[] args) throws Exception {
        try{
            //create JDF-Dokument
            JDFDoc.JDFDocument = JDFDoc.parseFile(InFileStorage);
            final JDFNode root = JDFDocument.getJDFRoot();
            KElement Ke = root;

            //Open data bases rsNodes, rsRes, rsND, rsRD
            ...
            //the main procedures
            importJDF(hierarchieiefe, Ke, rsNodes, rsRes);
            evaluateDB(rsND, rsRD, rsNodes, rsRes);
            exportText(bw, rsND, rsNodes, rsRes, rsRD);
            //Close OutFile and data bases
            ...
        }
        catch(java.lang.NullPointerException e){...}
    }
}
```

Figure 10

```
private static void importJDF(...) throws Exception{
    // Store certain attribute values into the data base
    ...
    // Store resources into data base
    ...
    //Search child nodes and analyse them recursively
    KElement[] KElementArray = Ke.getChildElementArray();
    ...
    for (inti = 0; i< KElementArray.length;i++){
        if (KElementArray[i].getNodeName()=="JDF"){
            ...
            Ke = KElementArray[i];
            importJDF(hierarchieiefe,Ke, rsNodes, rsRes); // Recursion
        }
    }
}
```

Figure 11

Input- and Output resources of a particular JDF node need not to be stored in the *ResourcePool* of that node, but rather can be located in different *ResourcePool* that is closer to the root node. In this way, resources can be shared by different nodes without duplicating them. In the *ResourceLinkPool* of a node, however, the IDs of all resources that the node uses are listed. Following these links, one acquires all the resources that a JDF node needs. We implemented another recursion for that task. In general, the resources have different attributes, of course, and some of those are stored into the database.

All outcomes of the analysis concerning the resource links are also stored in the database. Figure 12 shows parts of the database of an example. The second column references to the resource of the internal JDF-node number are given. The 4th column provides the resource name. The I/O-column defines for the resource links if they are input or output to the JDF node. The 6th column references the other database holding the standard text-blocks that describe the resources.

No	JDFNodeNumber	ID	Name	I/O	Description Number	Attribute1
1	1	...7940	CustomerInfo	1	219	HdM-Book
218	18	...7993	Media	1	134	Paper
219	18	...5604	ShapeCuttingParams	1	186	
220	18	...7997	ColorantControl	1	46	DeviceCMYK
221	18	...7990	ConventionalPrintingParams	1	59	SheetFed
222	18	...1698	FoldingParams	1	97	Falzartenkatalog: F4-1 F16-6 Falzpositionen sind angegeben

Figure 12

In the second step (*evaluateDB* in Figure 10) the database is used for analysing the JDF. In particular, each standard JDF node is assigned to one of the following categories: product, prepress, press, postpress and comprehensive processes. This can be done by using different attributes of the nodes like *Type*, *Types* and *Category*. One should note that the categories above are not set explicitly in JDF. Nodes of type *Combined* are also allocated to these categories. All private nodes are denoted as such in the database but ignored for further analysis. Figure 13 gives an example of a database containing information about JDF-nodes after evaluation of a specific JDF-file. The entries in column *ProductionArea* indicate the assignment of the JDF node to the categories above. Moreover certain JDF-nodes and resources are analyzed specifically.

NO	NodeID	JDFNodeName	JDFDescriptiveName	JDFCategory	DescriptionNumber	JDFNodeKind	ProductionArea	JDFHierarchie	JDFTypes
1	...7935	Product	HdM-Book		107	4	-1	0	
2	...7955	Product	Umschlag		107	4	-1	1	
3	...7998	ProcessGroup	Auto_CIP_CD74	MISPRES. PlateMaking	111	5	1	2	
6	...2116	Combined			110	3	1	3	Imposition Interpreting Rendering ContoneCalibration Screening PreviewGeneration FormatConversion ImageSetting
7	...8007	ProcessGroup	E10kFProof-24Zoll	MISPRES. Imposition Proofing	111	5	1	2	
14	...5685	Conventional Printing			51	1	2	3	

Figure 13

The third step is crucial. Here short textual explanations for all nodes and their resources are generated. The resource descriptions are sorted by the nodes that are using them, not by the nodes that contain them. All texts are short to keep the volume of the output-file readable for the end-user. All these short texts are stored in a separate database (Figure 14). In the previous program step the IDs of the text blocks have been determined (see Figure 13, column *DescriptionNumber*). The assignment of a node or a resource to a text block can be straight-forward. A JDF node of type *PSToPDFConversion*, for example, is always assigned to the same text block. In other cases the decision about which text block to choose might be more involved. A JDF node of type *Product* might represent the end-product or a product part (depending on the node hierarchy). Similarly a resource of type *media* can denote *paper* or *plates*. The textual descriptions will be chosen accordingly.

ID	Type	Description	ProductionArea	Kind
...
50	Trapping	Überfüllen / Unterfüllen	1	1
51	ConventionalPrinting	Konventionelles Drucken (mit physischer Druckform)	2	1
52	DigitalPrinting	Drucken auf einer Digitaldruckmaschine	2	1
53	Varnishing	Lackieren	2	1
...

Figure 14

Individual text blocks are sometimes generated for certain resources, depending on the values of the attributes. For example, for the resource *CustomerInfo* the job name is exported, if available. Another example is, that the user will be informed if the resource *FoldingParams* contains the imposition scheme number only or the actual folding sequences. Figure 15 shows the textual outcome in both cases.

a) Falzbeschreibung Falzartenkatalog: F4-1 F16-6, Falzpositionen sind angegeben
b) Falzbeschreibung Falzartenkatalog: F4-1 F16-6

Figure 15

5. Conclusions

The tool presented here is not a product, but rather a prototype. It is clear that further amendments and improvements can be carried out. For example, the JDF-nodes might be sorted altogether by the production areas of prepress, press and postpress instead of separating those for the different product parts first. Also, the partitioned resources have been be ignored, in particular those concerning the sheet layout.

We plan to enhance our tool so that it can output the JDF-tree in a graphical manner (as in Figure 2).

It is also clear that the analysis cannot produce the exactness of the JDF-description (without getting as involved as the JDF structure). It mirrors the difficulty of recompiling low-level machine code to a high-level source code. Nevertheless, we think that with some more effort this might become a useful tool for a workflow manager in a print shop.

References

- (1) Cooperation for Integration of Processes in Prepress, Press and Postpress (CIP4): (2009), JDF Specification, Release 1.4a, www.cip4.org
- (2) Wolfgang Kühn / Martin Grell, (2005), JDF, Springer Verlag, ISBN 978-3-540-23560-6
- (3) Thomas Hoffmann-Walbeck / Sebastian Riegel, (2009), Der JDF-Workflow, Verlag Beruf und Schule, ISBN 978-3-88013-675-5, French edition: Le Flux JDF, (2010) GamSys Software ISBN 978-2-8052-0089-2, US edition: JDF Workflow, (2011), Printing Industries Press



Multiple platform magazine publishing: integration of print and digital content in traditional magazine advertising

Natalia Gilewicz

Ryerson University
350 Victoria St., Toronto, Ontario, M5B 2K3, Canada
E-mail: ngilewic@ryerson.ca

Abstract

This descriptive study evaluates the opportunities taken by consumer magazine advertisers to link readers from the printed publication to some form of digital content. Through the lens of Integrated Marketing Communication (IMC), the benefits of interactively connecting to digital spaces are discussed. From a content analysis of five magazines, a total of 255 advertisements have been analyzed. Results show that including a URL in the advertisement is the most common way of connecting users to the digital space (87% of ads used this method). Newer technologies such as barcodes, social media and applications are much less frequent, ranging from 6-13%. The benefits of these technologies are discussed. The study concludes that while the increase in URL inclusion is positive, advertisers have an opportunity to further integrate multiple media platforms by connecting through new digital options.

Keywords: magazines, integrated marketing communication, 2D barcodes, interactivity

1. Introduction

Publishing has seen incredible change as a result of a quickly evolving digital landscape. Undoubtedly, the book, newspaper and magazine industries have been affected by digital content delivery. Few publishers would argue that they could continue to operate with the same strategic objectives of a few years past. In turn, the changes rooted in the growing digital marketplace also affect the advertising industries that use printed media as a vehicle. Increasingly, marketers are looking to maximize consumer exposure by using multiple media to promote their products and services.

In light of this, traditional approaches to marketing are being challenged with increasing requirements for integration. As such this research offers an alternative theoretical approach of Integrated Marketing Communication (IMC), which focuses not on separating the different categories of media but rather showing how they work together (Sheehan & Doherty, 2001). With a focus specifically on consumer magazines, the interconnectedness of print and digital content will be interrogated.

Research has shown that advertising campaigns that are integrated across multiple media platforms are more effective. This is sometimes called the multiplier effect (de Montigny, Cardarelli, Eadie, & Helvena, 2007). Magazines are in particular known for generating awareness about a product and prompting customers toward trial (de Montigny et al., 2007). As such, we can see that magazines offer some persuasive benefits in the multi-media mix for advertisers. Further, advertising effectiveness is often closely linked to reader involvement (Greenwald & Leavitt, 1984). Interactivity between multiple media platforms can increase user involvement and thus improve the effectiveness of an ad. This research will catalog whether advertisers are making use of this potential benefit and in what way they are doing so.

Given that there are benefits to advertising on multiple platforms, this descriptive research will explore how integrated magazine advertisements are with digital content in North America today. Through the lens of IMC, this paper will describe the current opportunities taken by advertisers to integrate print and digital content. The paper will categorize what methods are being used to move readers into the digital space. A more in depth analysis of ways to connect print and digital media will follow. Opportunities explored will include linking through promotional URLs, using social media to connect with consumers, as well as the use of 2D barcodes such as quick response (QR) codes.

Increasingly, publishers are aware of the impact of the digital space on their business. It is highly probable that digital content delivery will experience growth; for print this is unlikely (Picard, 2003). It is important that as publishers acquire further capabilities linking static printed content to dynamic digital content that they begin to pass the knowledge on to advertisers. In many cases magazines rely on advertising as a core

source of revenue. As such this paper is written from an advertising, not editorial, perspective. This approach will allow us to see whether magazines as an advertising medium are being properly integrated to move readers to other media spaces.

A similar study by Kanso & Nelson (2004) evaluated how well advertisements link to the products' corresponding websites by analyzing 196 advertisements across 6 magazines. Here the following nine benefits of using the Internet were explored: company information richness, feature information richness, ease of updating, collection of data, global exposure, customization, enhancement of customer-company relations, role playing (contests and games), and purchase facilitation. The study identified that advertisers need to better integrate magazines with online content. Only 30% of the ads contained a URL. Many of the ads assessed only presented the URL in small print, not featuring any link to digital content. Further, benefits such as gathering data from visitors were not exploited when a reader did click through to the webpage.

In addition to establishing whether improvements have occurred since the 2004 study, this research is necessary because the digital landscape has undergone tremendous change. Namely, the growth of social media has had a tremendous impact on the way in which we use the Internet. While past studies on web advertising are largely e-commerce focused, social media is starting to direct a trend toward community building (Luck & Moffat, 2009; Duncan & Moriarty, 1998). Further, technologies such as QR codes have altered the ways in which we can interact with a printed magazine, making interactivity far more immediate and thus the printed page more dynamic.

This improved ability to connect the printed advertisement to digital content in an engaging way speaks to the construct of interactivity - one of the common benefits of IMC. Interactivity has undergone significant transformation as a result of changes in technology. Thus it is important to firstly explore what is meant by interactivity in general. Following this we can look at interactivity from the IMC perspective more specifically.

One of the contributions of this research is to examine interactivity from an online standpoint, and relate it back to the printed medium. As such we can think about interactivity from a computer-mediated communication (CMC) perspective. Generally, definitions include the notion that two-way communication is present, and that the Web is able to facilitate many-to-many interaction. (Hoffman & Novak 1996; Rust & Oliver 1994; Venkatesh, Dholakia & Dholakia 1996). In a paper by Dholakia, Zhao, and Fortin (2000), a review of predominant definitions of interactivity distills the concept to six dimensions: user control, responsiveness, real-time interaction, connectedness, personalization and playfulness. Each of these are important to different degrees depending on the purpose of the website. In the product website category responsiveness, real - time interaction, and personalization are most important, while playfulness is the least (Dholakia et al., 2000). This is relevant to this research as a majority of magazine advertisements feature a product. Today's technology can help relate some of these digital benefits into the printed medium.

Further stressing the importance of interactivity is its positive influence on the consumer. Interactivity is seen as one of the key advantages to digital content (Dholakia et al., 2000). Wu (2005) and Wang (2010) found that interactivity improved attitudes towards a website. Even more promising, in a study by Jee and Lee (2002) interactivity improved not only the positive attitude towards the website, but also increased purchase intention. Similarly, Chen, Griffith, and Shen (2005) showed that interactivity improved trust, as well as online and offline purchase intention. Lastly, a study by Macias (2003) revealed that increases in interactivity had a positive impact on brand perception in advertising. As such it can be seen that interactivity has a role to play when we integrate magazine ads with digital content.

From the IMC perspective, interactivity is a rising theme as we begin to think of marketing as an opportunity to communicate not persuade (Duncan et al., 1998), in a world that increasingly desires two-way communication (Mangold & Faulds, 2009). In a review of the IMC literature, Luck and Moffat (2009) summarize some of these arising key themes - interactivity being one of them. Their synthesis poignantly states, "IMC is more than a process or activity within an organization. It is a system of beliefs or engagement, embedded in an organization's culture, underpinned by communication, driven by technology, and embraced by senior management." (p.321) In order to accomplish this, companies need to build relationships with clients. Allowing interactivity is one method of strengthening those bonds (Day & Montgomery, 1999).

While in this research the linkage to digital spaces is interrogated, the purpose is not to suggest that this constitutes interactivity. Rather, informed by the literature it can be seen that interactive environments are much easier to facilitate in the digital space. As such, moving magazine readers to these spaces is beneficial.

Further, new technologies, such as 2D barcodes, can integrate some of the above-discussed interactivity characteristics into the printed product. Thus, the current landscape of this interactive integration between media platforms will be examined.

2. Methods

This paper is a descriptive study that reviews how print advertisements are currently being linked to digital content. In order to determine the current landscape of print and online integration, a content analysis was conducted. Following a literature review, a list of publications was selected. This list represents a group of publishers that are experienced in the digital space across several topical categories shown in Table 1. While selecting early adopters will not reflect the current general standard of the industry, it is the intent of this research to quantify the best possible innovations that link magazine and online publishing. This group of 5 magazines represents 4 publishers. While, a greater number of publishers would be favourable, this research is conducted from an advertisers perspective. As such, the variety of ads is more important than the variety of publishers.

Table 1: Selected publications list

Selected Publications	Category
Sports Illustrated	Entertainment
Time	News and current events
Martha Stewart Living	Home and garden
Vogue	Beauty
Mac World	Technology

Following magazine selection, a content analysis was conducted. While, it was known that interactivity and connectivity to other media (and in particular to digital media) were being interrogated, the coding was formative and exploratory in nature. A larger number of categories were then consolidated into the final 4 categories (with sub categories explored in results): URLs, social media, applications, and 2D barcodes. This approach was used because the research is meant to describe the current landscape. Preexisting categories could lead to the omission of ways in which advertisers are linking online content. A total of 255 ads were coded. They represented 13 different types of products and services. The product and service categories used by Kanso et al., (2004) were also used here because they were well structured and enabled us to compare the studies.

3. Results

Given the importance of integrating multiple media for an effective advertising campaign, interactivity as a construct needs to evolve in the IMC discipline. Historically, the focus of interactivity by enlarge was in e-commerce (Luck et al., 2009). Today a broader community perspective is increasingly necessary to succeed (Duncan et al., 1998). The following section will describe what avenues of connecting users to digital spaces advertisers are using today, as well as looking at how they use them.

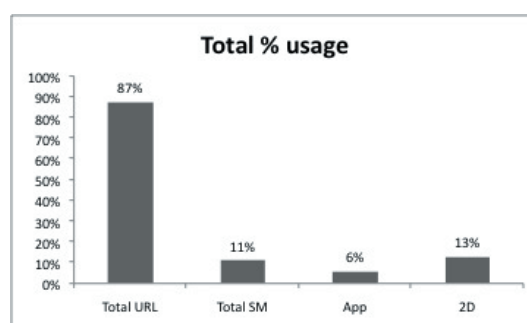


Figure 1: Total % usage

Given the 255 coded advertisements, Figure 1 demonstrates which of the four coded categories is most frequently occurring in all of the advertisements. Here we could see that URLs are by far the most common

method of providing a link to the digital space. The graph also shows a significant increase in the popularity of URLs from the previous study by Kanso et al., (2004) from 30% to 87% of total ads analyzed. Further, it can be seen that social media, applications, and 2D barcodes are currently limited in presence across this sample of publications.

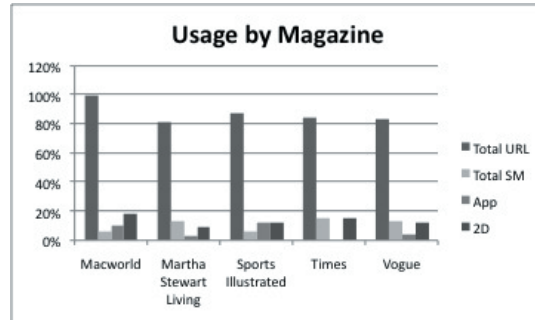


Figure 2: Usage by magazine

For this analysis 5 categories of magazines have been selected. While this research does not generalize a single magazine to represent an entire category some small differences between the publications can be observed. While the general trend in each magazine mirrors the average usage overall, the magazines performed best in different categories. All of the ads (100%) in Mac World, a technology magazine, had a URL present. Given the topic of the magazine it stands to reason that this would be the case. Mac World also had the highest usage of 2D barcodes (18%). Time, a news and current events magazine, had the highest linkage to social media. This is exceedingly relevant in this magazine category as professional news media institutions are constantly challenged by a growing public voice facilitated by social media (Rheingold, 2007). One could infer that publishers in this category are slowly starting to embrace this changing landscape. Sports Illustrated made best use of links to applications. The applications category included mobile applications as well as linkages to third party applications such as Apple’s iTunes store. An example of application uses in this category of magazines is the ability to track the scores and statistics of one’s favourite teams. Interestingly, Vogue (beauty) and Martha Stewart Living (house and home) displayed results that were most similar to the total usage percentages. These two publications account for the greatest number of advertisements (60% of all ads coded). Thus, given a greater sample of ads it is possible that the other publications would also mirror these results.

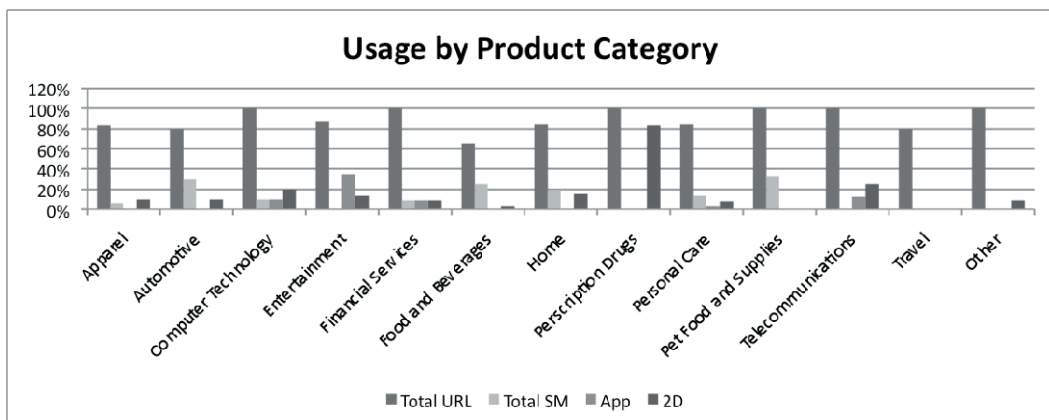


Figure 3: Usage by product category

The presence of connectivity was also categorized by product type (Figure 3). Here too the results closely resembled the overall usage. Aside from the use of URLs evident across all categories, entertainment products displayed the greatest number of ads featuring applications, technology had the highest 2D barcode presence, and food and beverage most often linked to social media.

In addition to describing the types of connections being used by the magazines, the opportunity to integrate multiple connections was examined. Figure 4 demonstrates the five most commonly occurring combinations of the coded categories. Not surprisingly, using just the URL in the ad is by far the most common choice.

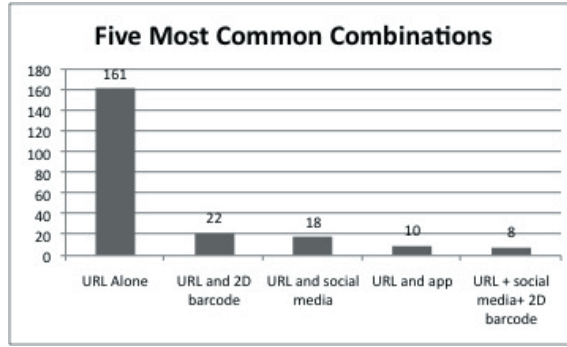


Figure 4: Five most common combinations

Given that more positive results are probable with higher levels of integration (de Montigny et al., 2007) this requires improvement. None of the advertisements used all 4 of the categories. In the online space it is increasingly common to see small icons for applications and social media along side QR codes. Thus there is a possibility that displaying all the options in the printed ad could occur in the future.

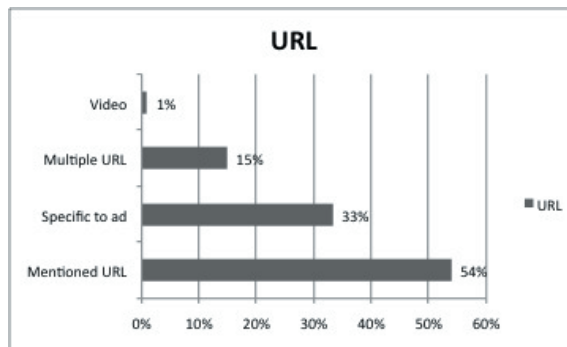


Figure 5: URL usage

Lastly figures 5 and 6 evaluate some details about the usage of URLs and 2D barcodes more specifically. Seemingly the usage of URLs has become more sophisticated. Figure 5 shows us that 33% of the ads are directing readers to a URL that is specific to a product. This means that the ad more immediately connects the page to the online counterpart. Another advantage here is that the URL can be campaign specific, which would thus allow the marketer to measure the effectiveness of the printed ad with better accuracy. Secondly, over half (54%) of the ads specifically prompted the readers to visit the website. This is an improvement from the high percentage of small and less impactful URLs in the Kanso et al. (2004) study.

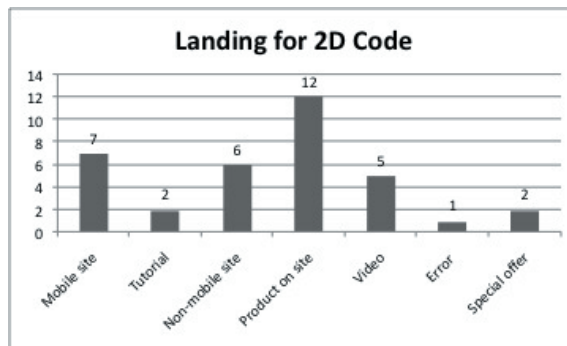


Figure 6: Landing for 2D Codes

Figure 6 allows us to interrogate the destination of the 2D barcodes present in the magazine. Much like URLs, one of the advantages of these barcodes is to be able to measure click-through. Here the number of barcodes that lead the user to the website (13) was almost the same as the number that lead to a product specifically (12). Surprisingly, of the 13 barcodes that directed users to the website, 6 did not have a mobile version of the site. Given that a majority of QR codes are scanned with a smartphone, this could be seen as a

mistake by the advertiser. While it is important to embrace this new technology, user experience is still a primary concern. Thus, viewing a non-mobile website on a phone could become a deterrent.

As can be seen, there has been vast improvement in the usage of URLs on magazine advertisements since the Kanso et al. (2004) study. Further, other technologies such as social media, 2D barcodes and applications are also being integrated into advertisements.

4. Discussion

The landscape of advertising media is quickly changing and becoming more interconnected. While print advertising has suffered criticisms, there are also studies that show many benefits to using print advertising—especially when it is integrated with other media. Magazines, for example, are exceptionally effective at persuading consumers, as well as having high retention rates (Dholakia et al., 2000). Pairing magazine advertising with online and/or television yields even more effective results (Dholakia et al., 2000). However the ways in which we are able to do this are quickly changing. Technological advancements affect the types of opportunities available to advertisers. In this study we describe which of these opportunities advertisers are currently using. Results reveal that while URL codes are being heavily utilized, other opportunities to connect are much less prevalent.

Studies have found a positive link toward brand perception resulting from a URL being included in an advertisement (Maddox & Gong, 2005). There are many benefits to having consumers link to a website from a magazine. The Internet offers several advantages such as: ease of updating, collection of data, global exposure, customization, enhancement of customer-company relations, role-playing, and purchase facilitation (Kanso, LeBlanc III & Nelson, 2005). However, simply stating a URL is not likely to yield results. Engagement and interactivity are key components to effective advertising (Greenwald et al., 1984). Consumers are not likely to visit a URL with no incentive or added benefit (Maddox et al., 2005).

The results in this study show that while a majority of advertisers seemingly agree that including a URL is advantageous (with 87% of ads containing a URL) fewer have taken the next step to take advantage of some of the above listed benefits of the Internet.

Using URLs effectively can help overcome one of the criticisms of print advertising - the inability to measure ad effectiveness. Having readers visit a unique campaign URL allows the advertisers to gauge the effectiveness of the ad, remembering that even with a unique URL present, few readers will actually visit the website. Further, advertisers can begin to explore further personalizing the URLs to individual users. Because magazines are mailed using subscribers lists which contain various reader information, each magazine can be customized. Many case studies (such as those published by Podi) show increased effectiveness with increased personalization. This level of personalization however, was not seen in this sample. Cost, campaign complexity and manufacturing restrictions are likely to prevent personalized URLs (PURLs) from becoming common in magazine advertising.

Additional technologies that further extend the advantages of the digital space are 2D barcodes, also known as mobile tags (Schmidmayr, Ebner & Kappe, 2008). As the adoption of smartphones grows exponentially, barcodes such as QR codes are becoming more common. This technology allows reader to take a picture of a barcode using special software (downloadable for free). The user is then directed to the information embedded in the barcode such as multimedia, websites, coupons and etc. Other applications of QR codes include ticketing and more recently location specific information (Schmidmayr et al., 2008). One of the advantages of QR codes over URLs is that they reduce the possibility of error (because the reader is not typing a URL) (Beck, 2011). Further there is a sense of immediacy as readers are instantly redirected to the additional content (Lisa & Piersantelli, 2008).

Given that only 13% of the advertisements in this sample contained barcodes, there is clearly an opportunity for growth in the area. However, much like in the case of the URL, it is the content presented through the barcode that makes it successful—just having a QR code is not enough to engage readers (Beck, 2011). Of all of the ads with 2D barcodes (33 in total), 12 directed readers to the product being advertised, while 13 simply directed them to the website home page. As the campaign information can be embedded in the barcode, there is no added measurement advantage from being more specific (as was the case with URLs). Thus the advantage of having the reader land on the product specifically is primarily ease of use. Further, barcodes present the possibility of taking users through to a buying decision by way of an offer. URLs can also direct

users to an online coupon, however, because QR codes are scanned with a phone, the reader is able to more easily save the coupon and bring it into the store (Funk, 2005). In this study only 2 QR codes directed readers to a special offer.

While the use of URLs and barcodes offers an opportunity to resolve some of the measurement problems that print campaigns have been criticized for, even more difficult to measure is the impact of social media on consumers. Social media is new to the marketing mix, with matrix measurements still in development. The number of users of social media sites such as Facebook, Twitter, and YouTube are staggering - Facebook alone has 500 million active users, half of whom use the site daily. (facebook.com) These sites are highly recognizable. There is no question that social media has captured a large portion of household entertainment time, the commercial applications of this however, are less evident. Only about 50% of the ads containing social media links in this study included URLs to the communities (the remaining just displayed icons).

Interestingly, social media, perhaps more so than the other technologies investigated here, most drastically reinforces the changes occurring in the IMC discipline. Though traditionally thought of as a one-way approach to information sharing, new paradigms in IMC are arising (Mangold et al., 2009). While communication has always been an integral part of creating a consistent message across multiple media, relationship management is increasingly becoming just as important (Luck et al., 2009). Social media sites offer an opportunity to build these relationships with and among customers (Mangold et al., 2009). Social media should be important to advertisers because is used by customers to search for information, get product feedback and evaluate purchase decisions (Lempert, 2006; Vollmer & Precourt, 2008).

Research shows that social media is engaging and interactive. This research along with other studies has investigated interactivity as a key success ingredient (Chen et al., 2005). Many publishers have done an excellent job at linking printed content to online social media outlets such as videos and blogs. However, from an advertising perspective there is room for improvement.

5. Conclusions

Involvement with digital media is ubiquitous in North America. Undoubtedly the magazine industry has been affected by the changes in our media consumption. Advertisers who use magazines as a media to promote their products need to integrate their campaigns to better involve the digital consumer. This descriptive study presents the current landscape of the ways in which magazine advertisements are connecting readers to digital spaces. The primary method seen here is the presence of URLs in the magazine advertisements, with 87% of all ads presenting a URL. However, emerging technologies such as 2D barcodes and social media are also present. One could expect that these new technologies will experience growth much in the same way that URLs have.

Analysis of the advertisements by magazine type as well as by product category shows no significant trends at this time. It is possible however that growth in this area will reveal future trends. As such a longitudinal approach to cataloging the ways in which readers can link to digital content would be beneficial. Further, more publications and a greater number of ads could reveal some trends.

Acknowledgements

I would first like to acknowledge the hard work of my research assistant Anna Whatman. Thank you for your dedication to this project. Further, I'd like to thank the Faculty of Communication and Design and the School of Graphic Communications Management at Ryerson University for their support, as well as IARIGAI for the opportunity to present this paper.

References

- Beck, K. (2011). Barcodes reach a new dimension. *CRM Magazine*, 15(1), 14-15.
- Chen, Q., Griffith, D. A., & Shen, F. (2005). The effects of interactivity on cross-channel communication effectiveness. *Journal of Interactive Advertising*, 5(2), 30-44.
- Day, G. S., & Montgomery, D. B. (1999). Charting new directions for marketing. *The Journal of Marketing*, 63, 3-13.
- de Montigny, M., Cardarelli, R., & Brown, M. (2007). Measuring Magazine Advertising Effectiveness And Synergies. Worldwide Readership Research Symposium. 233-242.

- Dholakia, R. R., Zhao, M., Dholakia, N., & Fortin, D. R. (2000). Interactivity and revisits to websites: A theoretical framework. *AMA Winter Conference Proceedings*, 2-19.
- Duncan, T., & Moriarty, S. E. (1998). A communication-based marketing model for managing relationships. *The Journal of Marketing*, 62(2), 1-13.
- Funk, J. L. (2005). The future of the mobile phone internet: An analysis of technological trajectories and lead users in the Japanese market. *Technology in Society*, 27(1), 69-83.
- Greenwald, A. G., & Leavitt, C. (1984). Audience involvement in advertising: Four levels. *The Journal of Consumer Research*, 11(1), 581-592.
- Hoffman, D. L., & Novak, T. P. (1996). Marketing in hypermedia computer-mediated environments: Conceptual foundations. *The Journal of Marketing*, 60(3), 50-68.
- Jee, J., & Lee, W. N. (2002). Antecedents and consequences of perceived interactivity: An exploratory study. *Journal of Interactive Advertising*, 3(1), 1-26.
- Kanso, A., LeBlanc III, H. P., & Nelson, R. A. (2005). Marketing more with less? lessons learned on how online advertising interacts with magazine advertising. *Journal of Website Promotion*, 1(3), 40-60.
- Lisa, S., & Piersantelli, G. (2008). Use of 2d barcode to access multimedia content and the web from a mobile handset. *Global Telecommunications Conference, 2008. IEEE GLOBECOM 2008. IEEE*, 1-3.
- Luck, E., & Moffatt, J. (2009). IMC: Has anything really changed? A new perspective on an old definition. *Journal of Marketing Communications*, 15(5), 311-325.
- Macias, W. (2003). A preliminary structural equation model of comprehension and persuasion of interactive advertising brand web sites. *Journal of Interactive Advertising*, 3(2), 36-48.
- Maddox, L. M., & Gong, W. (2005). Effects of URLs in traditional media advertising in china. *International Marketing Review*, 22(6), 673-692.
- Mangold, W. G., & Faulds, D. J. (2009). Social media: The new hybrid element of the promotion mix. *Business Horizons*, 52(4), 357-365.
- Picard, R. G. (2003). Cash cows or entrecote: Publishing companies and disruptive technologies. *Trends in Communication*, 11(2), 127-136.
- Rheingold, H. (2007). Using participatory media and public voice to encourage civic engagement. *The John D. and Catherine T. MacArthur Foundation Series on Digital Media and Learning*, , 97-118.
- Rust, R. T., & Oliver, R. W. (1994). The death of advertising. *Journal of Advertising*, 71-77.
- Schmidmayr, P., Ebner, M., & Kappe, F. (2008). What's the power behind 2D barcodes? Are they the foundation of the revival of print media. *Proceeding of I-KNOW'08 and I-Media '08*, 3-5.
- Sheehan, K. B., & Doherty, C. (2001). Re-weaving the web: Integrating print and online communications. *Journal of Interactive Marketing*, 15(2), 47-59.
- Venkatesh, A., Dholakia, R. R., & Dholakia, N. (1996). New visions of information technology and postmodernism: Implications for advertising and marketing communications. *The Information Superhighway and Private Households: Case Studies of Business Impacts*. 319-337.
- Wang, A. Digital ad engagement: Perceived interactivity as a driver of advertising effectiveness. *University of Connecticut*. 1-5
- Wu, G. (2005). The mediating role of perceived interactivity in the effect of actual interactivity on attitude toward the website. *Journal of Interactive Advertising*, 5(2), 45-60.

Local newspaper publishing: editorial structure and environmental effects - a case study

Malin Picha, Åsa Moberg

KTH Royal Institute of Technology
SE-100 44 Stockholm, Sweden

E-mail: picha@kth.se, asa.moberg@abe.kth.se

Abstract

Media companies operate in a dynamic environment where change is a constant. Pursuing change in a media company implies an opportunity to optimize processes on different levels. In order to meet these opportunities, as well as being proactive when it comes to environmental performance, we need to understand the current structure of media companies. Better understanding can lead to finding ways to optimize the workflow and to implement other improvements.

This study investigates the structure of the editorial processes and other processes regarding content production of a local newspaper in Sweden, Norrtelje Tidning. The objective is to analyze the workflow in order to discover how the different steps in the production process might affect potential environmental impact. Semi-structured interviews were undertaken to identify the process steps involved in the content production. Environmental data was then collected for each process step, and a screening environmental assessment with a life-cycle perspective was performed.

The major reasons for potential environmental impact related to content production at Norrtelje Tidning are travel and the use of electronic devices. These two areas are relevant to focus on when striving to reduce environmental impact on a general level.

Keywords: local newspaper, work process, environmental impact, media industry, life cycle assessment (LCA)

1. Introduction

1.1 Background

Media companies operate in a dynamic environment where change is a constant. This reality is due to a number of factors, for example business decisions, technical innovations, societal changes, legislation, or changing demands from consumers. Pursuing change in a media company implies an opportunity to optimize processes on different levels. In order to meet these opportunities, we need to understand the current structure of media companies and the existing editorial process steps. Better understanding can lead to finding ways to optimize the workflow and to implement other improvements.

A theme in the current political and social debate is the development of society in an environmentally, economically, and socially sustainable manner. The media sector, along with the entertainment sector, contributes yearly to 1-2% of global greenhouse gas emissions (Malmodin et al. 2010). Different incentives to facilitate environmental improvements are likely to become more common, and a proactive media company needs to consider and act upon its environmental performance.

“The ongoing ecological changes will strengthen the citizens’ awareness of environmental matters, also with respect to media. /.../ Media, both traditional and new, must carefully measure and assess the sustainability factors concerning their products and services, over their entire life cycles. /.../ There is a clear and growing demand for environmentally responsible and sustainable media.” (Teljas et al. 2007)

Several studies on the environmental impact of media products have been undertaken during the past years (e.g. Borggren et al. 2011; Moberg et al. 2010; Pihkola et al. 2010; Nors et al. 2009). When approaching printed media with a life-cycle perspective, research results show that the manufacturing of paper, as well as the printing process and home delivery of newspapers, are the main reasons for overall environmental impact. However, the work processes involved when producing media content also contribute to the total environmental impact (Kronqvist et al. 2010, Moberg et al. 2010).

Work processes in editorial newsrooms have been examined from a research perspective in earlier research, of which Sabelström Möller (2001) is considered the most relevant for this case study, because of her study of workflows. Sabelström Möller's research focuses mainly on the workflow of different types of content with regard to different publishing channels, especially printed versus electronic products and services within newspaper companies. In this study however, we will, unlike Sabelström Möller, investigate the editorial processes in connection to their place in the company structure, and not pay any special attention to the actual newspaper content.

1.2 Objectives

This study investigates the structure of the content production, such as editorial content production, and sales and advertisement production, of a local newspaper in Sweden. By content production we mean all work steps included in the task of filling a printed newspaper or a newspaper on the web with different types of content. This includes, for example, initiating news stories at editorial meetings, collecting background information, travelling to and performing interviews, writing stories, taking pictures, selling ad space, designing advertisements, and designing pages in the printed newspaper or on the web.

Our aim is firstly to understand and analyze the editorial processes and other processes regarding content production. Secondly, we aim to identify which steps in the processes are most important from an environmental perspective. The objective is to estimate the potential environmental impact related to the identified process steps, as well as in a larger setting where we include the newspaper company as a whole, which means not only activities connected directly to the daily workflow, but also management meetings, management travel and so forth. From a larger perspective, we hope to be able to suggest improvements both in the daily workflow and regarding environmentally preferable solutions in the company at large.

1.3 The studied company

The Swedish media market has changed considerably over recent years. Many smaller newspaper companies have been bought up by larger companies or merged into groups (Hadenius et al. 2008). The result of this long-term process is inevitably that the work conditions at these newspaper companies change. What these changes imply, on a more detailed level, has not been fully explored, even though we can assume some of these consequences.

The investigation presented here is based on a case study performed at Norrtelje Tidning in Sweden. Norrtelje Tidning is the main newspaper in Norrtälje and the surrounding municipality, located 70 km north of Stockholm. Norrtelje Tidning is published Monday through Friday, with a subscribed circulation of 14,500 copies (www.dagspress.se). The newspaper was founded in 1880 and belonged for 125 years to a group of political newspapers, Centertidningar AB, officially owned by the Swedish Agricultural Party.

In 2005, Centertidningar AB was purchased by the Stampen group. The purchase took place in two steps. Firstly, Norrtelje Tidning became an official part of Vestmanlands Läns Tidning (VLT) in Västerås in 2005; secondly both newspapers were consolidated into a group of politically Liberal newspapers together with Nerikes Allehanda in Örebro in 2007, which placed Norrtelje Tidning in a newspaper group called Promedia belonging to the newspaper conglomerate of Stampen, based in Gothenburg. In 2009, the yearly turnover of Promedia was 7.8 million euro, which can be compared to the total income of Stampen which in 2009 was about 539 million euro, according to Stampen Annual Report.

The process of purchases has naturally implied great changes for the newspaper company. As part of the agricultural press, Centertidningar AB, the newspaper was well-kept and worked very independently, according to interviews with management. In 1999, the new printing plant was built adjacent to the editorial premises in Norrtälje. Six years later, the printing plant became a part of Stampen-owned VTAB, together with printing plants located in the cities of Södertälje and Östersund. Distribution, in this case mainly home delivery of newspapers, has also been a part of Norrtelje Tidning, but in 2006 this business unit was moved over to Prolog, a separate company to which all Stampen's distribution companies in mid-Sweden now belong. With these changes in mind, Norrtelje Tidning has lost two of its three legs: the printing facility and the distribution business, leaving only the content production and sales department.

Another major change was the move of the customer service department to a central unit in Örebro. By 2008, all administration and economy work had left Norrtälje. Earlier, there was a substantial amount of advertisement production at Norrtelje Tidning. The newspaper also produced ads for other newspapers

located in Vallentuna, Nynäshamn, Södertälje, and Lidingö. In June 2009, the production of ads moved to Västerås. Today, the Norrtälje Tidning office consists of a publisher, ad sales department, a front office of three people, the editorial staff and the Head of environmental affairs. In addition, there are local offices in Rimbo and Hallstavik, with one journalist at each office.

At the time when Norrtälje Tidning belonged to Centertidningar AB, there were a total of 60 employees working in the Norrtälje office. In 2010, there were 40 people. Of the 20 people being laid off, many received offers to move to Örebro or Västerås to be able to continue working for the company. However, only a few of them accepted the offer. A consequence of these structural changes was that the office building was considered too large for its purposes. Therefore, one floor in the office building is now rented out to other businesses.

During the past years, the circulation of Norrtälje Tidning has been quite constant, around 15,000 copies with slight variations, depending on the economic situation in society as a whole. Around 300-400 people move into the municipality of Norrtälje every year. Since the town of Norrtälje is located in a popular district for tourism and with many summer homes, the municipality grows from 56,000 people to about 150,000 people in the summertime. This implies that Norrtälje Tidning is distributed to a lot more subscribers during the summer than during the rest of the year, and the company in charge of the newspaper home deliveries, Prolog, has a completely different set of routines in the summer than during autumn, winter and spring.

Norrtälje Tidning can be seen as a typical representative of the changing Swedish media market, with its consolidation into the Stampen group and reorganization in areas concerning print, distribution, customer services, economy, and ad production. In the case of Norrtälje Tidning, the consolidation with Stampen implied that part of the administrative work as well as advertisement production and other departments were transferred to Örebro and Västerås. Moving part of the production processes to other geographic locations meant that money could be saved in rationalizations. At the same time, this could imply an increase in the amount of travel for the employees at Norrtälje Tidning.

Considering environmental work, however, Norrtälje Tidning is at the forefront compared to other Swedish media companies, according to the Head of Environmental Affairs. Norrtälje Tidning initiated its environmental work relatively early. In 1999, the printing plant was ISO-certified, mainly due to demands on a more environmentally adaptable printing process from the external printing customers. When the printing plant was certified, it was natural to move on to certify the newspaper company as a whole, according to the Head of Environmental Affairs.

In 2000, the newspaper company was certified, including the distribution. In 2006 the distribution unit moved from the newspaper company to the Stampen-owned firm Prolog, and in 2008 Prolog's entire distribution in Mälardalen was certified as well. The Stampen-owned media group Promedia, which includes 14 local newspapers in the area, will be certified during 2011, according to the plan.

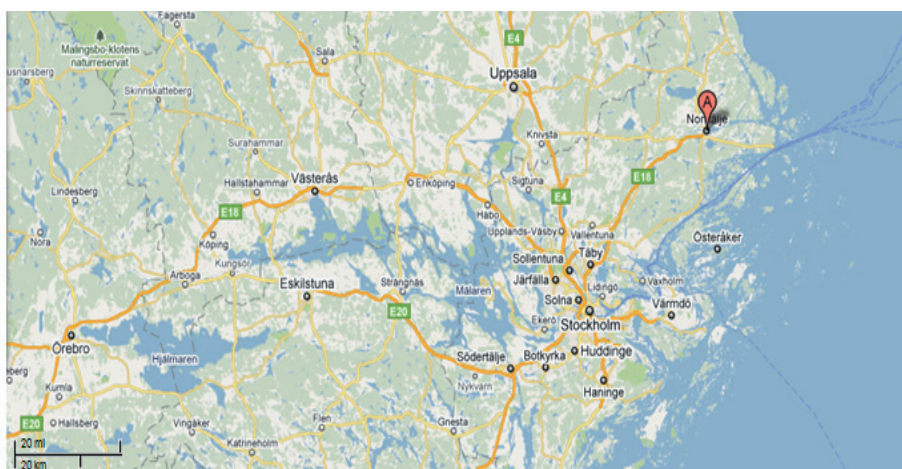


*Figure 1: The geographical area of Mälardalen, where Norrtälje is situated some 70 km north of Stockholm. The administration, economy and part of the marketing department of Norrtälje Tidning are located in Örebro (266 km driving distance from Norrtälje) and in Västerås (177 km driving distance from Norrtälje)
The map is reproduced with courtesy to Google Maps*

2. Methods

Semi-structured interviews were undertaken at Norrtelje Tidning during November and December 2010, with the Publisher, the Head of Advertisement, and with the Head of Environmental Affairs. These interviews resulted in an overview of the process steps and how they act together to form a content production process where the end product is daily content for the local newspaper, both for the printed newspaper and for the web edition. The information gained from the interviews was analyzed, using a computer processing modeling program. Environmental data was then collected for each process step, and this data was compared to every process step in the workflow. For each process step, the following environmental parameters were considered: Travel (distance, amount of people, mode), computer hours for laptops, computer hours for stationary computers, use of office material, use of other equipment, electricity use, meeting room hours, use of the editorial computer system, transport of goods, use of delivery firms, and person hours. Other data concerning environmental aspects was also collected and used in the overall environmental assessment, such as waste handling and travel to and from work, but these were examined more on a general company level and not for each separate process step.

A screening environmental assessment with a life-cycle perspective was performed for the overall work at Norrtelje Tidning based on figures for 2010. This was done to identify the major reasons for overall potential environmental impact, and to ensure that all important aspects were included. Life-cycle assessment (LCA) is an environmental assessment method for considering potential environmental impact and resources used throughout the whole life-cycle of a product or service, including raw material acquisition, production, use, and disposal/recycling (Baumann and Tillman 2004). In this particular case study, the system boundaries of the LCA were set to study the overall content production, meaning all processes related to producing newspaper content for the printed and web editions during one year. This also included administration, heating of office buildings, waste etc. These were examined more on a general company level and not for each separate process step. Manufacturing of paper, printing and distribution of the newspaper were not covered in this study.

The inventory of data was based on information for 2010 from the Head of Environmental Affairs regarding activities at Norrtelje Tidning and on data from the LCA database Ecoinvent 2.2 (Frischknecht et al. 2007). For the impact assessment, the ReCiPe Midpoint (H) method (Goedkoop et al. 2009), as provided in SimaPro 7.2, was used.

3. Results

3.1 Process Structure

As a result of the interviews, a number of process steps were identified and described, along with the inputs, outputs, and control mechanisms, according to the principles of the computer processing modeling program used in this study. The process steps were combined into a hierarchical structure with three segments. A total of 18 process steps were identified, including the three main segments: *Editorial content production* (six process steps), *Local editorial offices* (seven process steps), and the segment *Advertisement booking and advertisement production* (five process steps). The most central process steps in the *Editorial content production-segment* are shown in Figure 2.

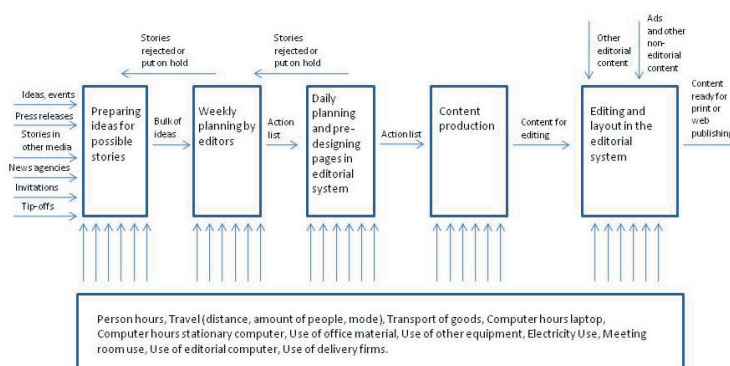


Figure 2: The most central process steps in the editorial content production segment.
For all process steps a number of environmental parameters were considered

3.2 Environmental parameters

Figure 3 illustrates how the total amount of person hours are distributed between the different process steps when looking at the production of one issue of the newspaper, printed and digital. From a process perspective, 24 percent of the total amount of person hours is spent on the process step called *News content production*. This includes background checks, preparations, travelling to interviews or performing telephone interviews, fact search, writing articles, proofreading et cetera. Twelve percent of the total amount of person hours is spent producing content for the sports pages. Another 12 percent is spent on the process step of *Sales by field salespeople* in Norrtälje. Eight percent is spent on *Preparing ideas for possible stories* and 6 percent on *Editing and layout*. *Booking of ads* takes up 5 percent of the total amount of person hours, and another 5 percent by *Production of ads in Västerås*.

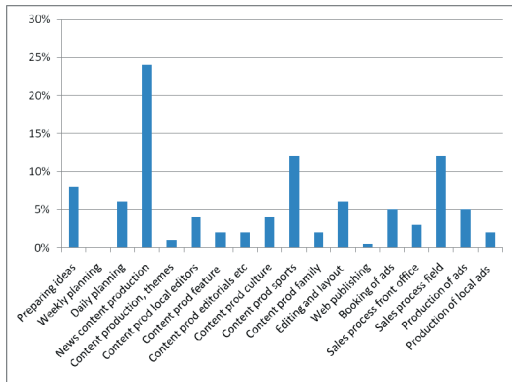


Figure 3: The percentages of the person hours that each specific process step has in relation to the total amount of person hours in all process steps.

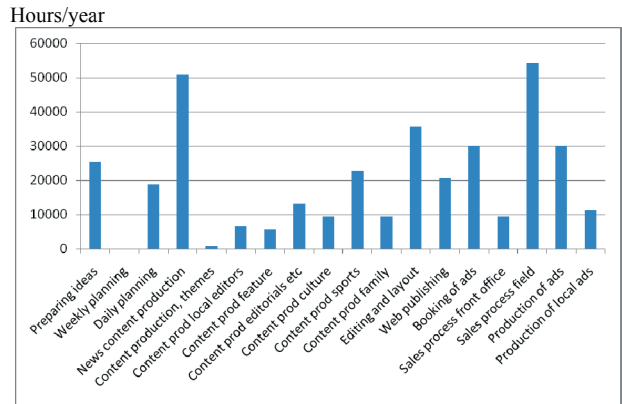


Figure 4: Hours of computer use per year, divided up on different process steps

When dividing up the hours of computer use on the different process steps, it is clear that the *Sales process by field sales people* and the *News content production* are using most of the computer time (Figure 4). There are also substantial differences between different areas of content production, such as feature material and sports.

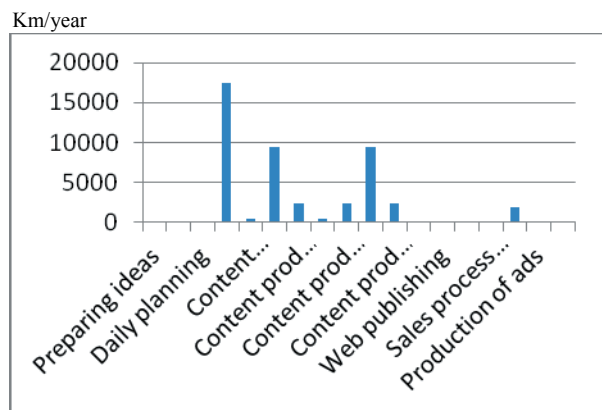


Figure 5: Yearly travel distance in km by car, divided up on different process steps

As can be seen in Figure 5, travel is mainly done by the editorial personnel in the process step of *News content production*, as well as content production in different segments such as the local editorial offices in Hallstavik and Rimbo, and the sports office. The editorial staff travels approximately 43 700 km by car every year. In the sales process, there is also a substantial amount of travel, even though these trips are relatively short and sometimes done by foot or by bicycle, according to the interviews done with the Head of Advertisement.

However, there is quite a large amount of travel to other cities, most importantly to Örebro and Västerås, where some of the other newspapers in Promedia are located, as well as business units connected to Norrtälje Tidning. These longer trips are mainly done by the management team for the purpose of business meetings,

either internally within the company, or with external partners. These management trips are illustrated in Figure 6, and data regarding these trips was collected from Norrtelje Tidning as well as discussed during the interviews with management representatives. The total distance travelled by management by car is 13 730 km per year. This can be compared to the distance travelled for the purpose of content production, approximately 43 700 km, and local sales activities, approximately 1 790 km, per year.

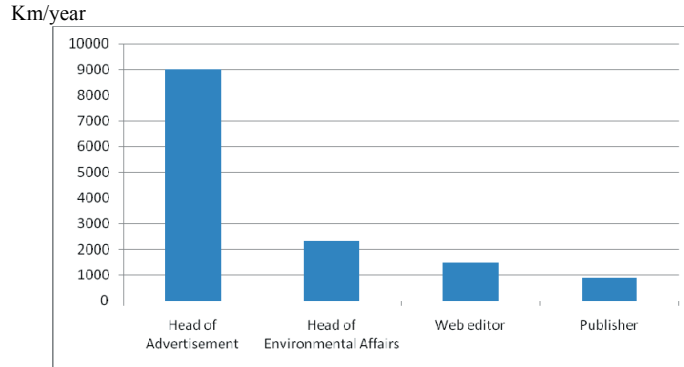


Figure 6: Yearly management trips. The Head of Marketing travels by train or by bus, which is not included here

3.3 Screening LCA

The results of the screening life-cycle assessment indicate that the major reasons for environmental impact from content production at Norrtelje Tidning were travel and the production of the electronic devices used at the company. These were the reasons for the major part of most of the different environmental categories studied, including e.g. climate change, eutrophication, and acidification. If considering the personnel's travel to and from work in the assessment, this proved to be a major reason for overall environmental impact. However, this result will not be considered here, since part of the environmental impact of these trips could be allocated to other purposes as well, such as driving kids to school, shopping on the way home etc.

The potential environmental impact related to Norrtelje Tidning is of course very specific for this company and dependent on the context in which this company exists. One of the relevant prerequisites from an environmental perspective is that Norrtelje Tidning uses electricity from hydro power only. Furthermore, Norrtelje Tidning reuses heat which is produced in the printing process at the printing plant next door. In the assessment made in this study, the reused heat was assumed to be without environmental impact - only the additional heat from district heating produced from biofuel was added to the overall environmental impact.

In order to test the importance of the use of hydro power for electricity, we altered this to a European electricity mix. The results then changed, and the electricity use became the major reason for the overall potential environmental impact of the content production.

4. Discussion

As mentioned in the introductory section of this article, the newspaper company in this study, Norrtelje Tidning, has undergone some major changes during the past years. In a period lasting over several years, Norrtelje Tidning was taken over and consolidated into a larger newspaper group. In this study, it has been interesting to consider what the consolidations in the company structure have meant for the editorial production processes, and how the workflow has changed in relation to this. As an example, the changes implied that part of the administrative work as well as advertisement production and other departments were transferred to the cities of Örebro and Västerås. Moving part of the production processes to other geographic locations meant that money could be saved in rationalizations. The consolidation has resulted in a reduction of staff and of floor space in the newspaper building, which would mean that heating and cooling were reduced as well as the use of electricity.

Results from the interviews undertaken in this case study show that the travel for administrative reasons to either Västerås or Örebro has increased due to the consolidation with Stampen. It is mainly the managers at different levels that tend to travel there. The increase in the amount of travel has in turn consequences for the environmental impact of the newspaper. Before the newspaper company was consolidated into Stampen, the employees had no reason at all to travel to the cities of Örebro and Västerås. After the consolidation, mana-

gement travels there at least a few times per week, almost exclusively by car, according to the interviews with management. As an exception, the Head of Marketing always travels to Västerås or Örebro by bus or by train. This is due to personal preferences and not necessarily because of environmental concerns.

With travel being a major reason for potential environmental impact, alternative solutions for travelling to meetings in other cities where Stampen-related departments are located could be further looked into by the company and the Stampen group. One such alternative might be technical solutions for meeting at a distance. This could also increase work quality, since employees have a chance to participate in some meetings where they otherwise would not have had the money or time to travel (Räsänen et al 2010). Other alternatives could be car-pooling, or looking into the possibilities of increasing the use of public transportation.

In this particular case, the other major reason for potential environmental impact is the use of electronic devices. When buying new electronic devices, the environmental performance could be regarded. In this study, general data for the production of stationary computers, laptops and computer screens were used. With less environmental impact in the supply chain, the overall performance would improve. Furthermore, by asking for devices with good environmental performance, the market demand for improvement is strengthened.

5. Conclusions

This investigation shows that it is feasible to make a structured description of the editorial process steps of a local newspaper, in order to analyze and understand the workflow. It is also possible to estimate the potential environmental impact related to the different steps in the production process. In this study, we have identified the process steps of the content production of Norrtelje Tidning and how these process steps piece together. Secondly, we have estimated the potential environmental impact related to the overall content production at Norrtelje Tidning and discussed the main reasons for environmental impact in relation to the different process steps.

The major reasons for potential environmental impact related to content production at Norrtelje Tidning are travel and the use of electronic devices. These two areas are relevant to focus on when striving to reduce environmental impact on a general level. The editorial staff travels approximately 43700 km yearly by car, local sales personnel travel yearly 1790 km by car, and management travels yearly 13730 km by car. The latter is an immediate effect of the consolidation into the media group of Stampen, which implies travel to management meetings in other cities. In order to reduce potential environmental impact, as well as time and money spent on travelling, we suggest looking into technical solutions for meetings at a distance, car-pooling or increasing the use of public transportation. When buying new electronic devices, we also suggest that the environmental performance could be regarded.

Acknowledgements

The case study presented here, is part of an inter-disciplinary research project undertaken within the framework of the KTH Centre for Sustainable Communication (CESC) at the Royal Institute of Technology. Industrial partners in this project are The Swedish Media Publishers' Association, and the two media groups Bonnier and Stampen. We would like to thank Norrtelje Tidning for making it possible for us to conduct our study there. In particular Anders Häggström, Katarina Ekspång and Niclas Pärni were very helpful in providing necessary data and personal insights. Our thanks also go to research engineer David Nord who participated in the first part of the project gathering and modeling environmental data. Furthermore, we are grateful to professor Nils Enlund and visiting professor Johan Stenberg for all their helpful support and good advice in this research project, as well as when writing this article.

References

- Baumann, H., Tillman, A-M. (2004) *The Hitch Hiker's Guide to LCA*, Lund: Studentlitteratur.
- Borggren, C., Moberg, Å., Finnveden, G. (2011) *Books from an environmental perspective - Part 1: Environmental impacts of paper books sold in traditional and internet bookshops. International Journal of Life Cycle Assessment. Volume 16, No 2, pp 138-14.*
- Frischknecht, R., Jungbluth, N., Althaus, H-J., Doka, G., Heck, T., Hellweg, S., Hirschler, R., Nemecek, T., Rebitzer, G., Spielmann, M., Wernet, G. (2007a) *Overview and Methodology. Data v2.0. ecoinvent report No. 1, Swiss Centre for Life Cycle Inventories, Dübendorf. Data as implemented in SimaPro 7.1.8.*

- Goedkoop, M., Heijungs, R., Huijbregts, M., De Schryver, A., Struijs, J., van Zelm, R., (2009) *ReCiPe 2008. A life cycle impact assessment method which comprises harmonized category indicators at the midpoint and the endpoint level. First edition. Report I: Characterization 6 January 2009. Ministry of Housing, Spatial Planning and Environment (VROM).*
- Hadenius, S., Weibull, L., Wadbring, I. (2008) *Massmedier: Press, radio och tv i den digitala tidsåldern. Helsingborg: Ekerlids Förlag.*
- Kronqvist, M., Löfgren, C., Sturges, M., Teleman, A. (2010) *Miljöbedömning av mediekanalerna papperstidskrift och Internetpublicering. Inventari rapport nr 97.*
- Malmödin, J., Moberg, Å., Lundén, D., Finnveden, G., Lövehagen, N. (2010) *Greenhouse Gas Emissions and Operational Electricity Use in the ICT and Entertainment & Media Sectors. Journal of Industrial Ecology, Special Issue: Environmental Applications of Information & Communication Technology, Volume 14, Issue 5.*
- Moberg, Å., Johansson, M., Finnveden, G. & Jonsson, A. (2010) *Printed and tablet epaper newspaper from and environmental perspective - A screening life cycle assessment. Environmental Impact Assessment Review 30(2010), pp. 177-191.*
- Nors, M., Behm, K., Dahlbo, H., Pajula, T., Pihkola, H., Viluksela, P. & Wessman, H. (2009) *Carbon footprint of print products. KCL Carbon Footprint Publication, 23 April 2009. Research report.*
- Pihkola, H., Nors, M., Kujanpää, M., Helin, T., Kariniemi, M., Pajula, T., Dahlbo, H., Koskela, S. (2010) *Carbon footprint and environmental impacts of print products from cradle to grave - Results from the LEADER project (Part 1). VTT Research Notes 2560.*
- Räsänen, M., Moberg, Å., Picha, M., Borggren C. (2010) *Meeting at a distance: Experiences of media companies in Sweden. Technology in Society 32, p 264-273.*
- Sabelström Möller, K. (2001) *Information categories and editorial processes in multiple channel publishing. Doctoral Thesis in Media Technology and Graphic Arts, KTH, Stockholm: Sweden.*
- Stampen (2009) *Annual Report 2009.*
- Teljas, C., Jonsson, A., Enlund, N. (2007) *Drivers of change in media channels. Where News? Report No. 6, Darmstadt: IFRA.*

References accessed on the web

www.dagspress.se (December 2010)

Social media in print - a publishing system for communities

Timo Kuula, Maiju Aikala, Jouko Hyvääkä, Anu Seisto

VTT Technical Research Centre of Finland
P.O. Box 1000, FI-02044 VTT, Finland
E-mails: timo.kuula@vtt.fi, maiju.aikala@vtt.fi

Abstract

The paper and printing industry are experiencing declining volumes and they are looking for new possibilities to develop their business. We studied the acceptability of one possible service product: the community publishing concept, where communities were offered a possibility to produce printed products from content that exists in digital format.

A pilot system for community publishing was developed based on the requirements of the participating communities. The project's scope of a networked way of working with community publishing required a new electronic system to be created as the current market offering did not provide a suitable tool for this purpose. The developed community publishing system was based on a freely available content management system, which allows content upload, creation and basic editing among the community members simultaneously.

The communities tested the pilot system, and they all ended up with a printed publication. Based on the community interviews, the use of the community publishing system is most suitable for communities that have motivation and culture for sharing content, and also publishing it both in printed and digital format. A clear vision of the content and target group of the publication is needed for the long-term use of the community publishing system.

Keywords: social media, publishing, print media, user-centric approach, activity theory

1. Introduction

Radical changes are taking place in the paper and printing industries as a result of increasing digitalization and changes in the use of media. For example, social media services in different forms have been a rising trend for several years. One proof of that is the incredible popularity of communal web-based services such as Facebook and Twitter. Even though there is a myriad of services available for different focus groups, the possible need of a community to produce printed products together has not been taken into account. For the industry, looking at ways to offer print products through social media services is an excellent possibility to get an understanding of the needs regular people have related to print products and publishing.

Media creation in the past can be simply classified in two categories: the *personal media* people created themselves, such as photographs and home videos, and the *media created by professional organizations*, such as newspapers, magazines and television programs. The number of broadband Internet connections and people's familiarity with computers and the Internet has grown in the last decade. This increased familiarity together with social media tools have resulted in the fact that the consumer tools for creating media are household items, and the means for sharing and publishing the media content are widely available and utilized. Thus, the concept of personal media has expanded and become even more significant.

Even though there is not yet a commercially available service for several members of a community to produce a printed product together, several services with a fairly similar approach do exist. To present a few of them, in Lulu (www.lulu.com) it is possible to publish books and calendars not only for one's own purposes but also for sale through the service. Similarly, in services such as MagCloud (www.magcloud.com), Printcasting (www.printcasting.com) and Scribd (www.scribd.com) anyone can publish magazines and offer them not only for consumers but also for advertisers. JPG Magazine (www.jpgmag.com) on the other hand has a different approach, as it publishes a collection of photographic art with a different theme on every issue. On their home page they describe the service by inviting anyone to join in the process of producing the magazine. There is also an example of a travel guide service that seeks for people interested in writing stories into the guide books that they publish (www.vivatravelguides.com). Out of the large amount of services, the approach in Wikipedia comes fairly close to the concept in this research project, as anyone can take part in content creation and it is possible to create a printed version of selected contents. Furthermore, Google Docs chat feature (previously known as Google Wave) allows multiple people to edit a single document, even simultaneously.

The idea of community publishing can be described as follows: “*Community publishing is about ‘grassroots activity’ by groups that produce narrative content. In contrast to chatting, bulletin board discussion, or role-play, community publishing is therefore a constructionist activity specifically aimed at storytelling and sharing experiences in a community setting, as well as learning and using new skills regarding publishing*” (Turpeinen, 2003). The aim of this research project was to pilot one possible community publishing concept idea. The target group in the concept idea was small communities, where the members of the community share a hobby and are friends together. User-centric approach as a research method was utilized in the project, and this paper especially focuses on users’ (community members’) viewpoint in the co-creation process.

2. User-centric approach and cultural-historical perspective

A *user-centric approach* was utilised in the research. The user-centric design process should start at the very early stages of the project, usually when the initial concept for the product or system is being formulated. The ISO standard determines four activities that should be repeated iteratively until the system meets the requirements (ISO 9241-210:2010):

- ◆ Understanding and specifying the context of use
- ◆ Specifying the user requirements
- ◆ Producing design solutions
- ◆ Evaluating the design.

In the iterative design approach, feedback from users becomes a critical source of information. Iteration allows preliminary design solutions to be tested against real world scenarios, with the results being fed back into progressively refined solutions. The first activity, understanding and specifying the context of use, includes the characteristics of the intended users, the tasks the users are to perform, and the environment in which the users are to use the system. Specifying the user and organizational requirements should define the allocation of functions: the division of system tasks into those performed by humans and those performed by technology. Producing design solutions involves developing design proposals, making the design solutions more concrete using simulations, models, etc., presenting the design solutions to users and allowing them to perform tasks, altering the design in response to user feedback, and managing the iteration of design solutions. Evaluation of designs against requirements can be used to provide feedback which can be used to improve the design, to assess whether user and organizational objectives have been achieved, and to monitor long-term use of the product or system. (ISO 9241-210:2010.)

In the development process of the community publishing system, these four activities were included in the process. After recruiting the communities for testing the concept idea, they were interviewed in order to get an understanding of the communities and their needs for the publishing system. This information was taken into account in the development of the system. The communities then had a period of five weeks to work with the publishing system and create their own publications in digital format. After that the layouts were made up, the publications were printed and the communities were interviewed again for feedback.

To understand the publishing needs of the chosen communities and to develop a publishing system that effectively support communities’ activities, it was necessary to examine the activities from a broader, *cultural-historical* perspective. Based on this approach, a model of *activity system* (Figure 1) was used as a framework for interviews with the communities.

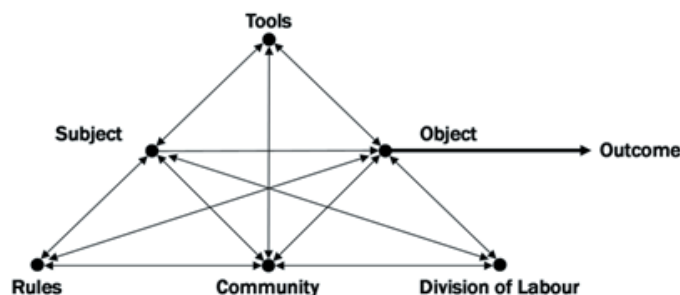


Figure 1: Activity system model (Engeström, 1987)

In the model, the *subject* refers to the individual or sub-group whose agency is chosen as the point of view in the analysis. The *object* refers to the 'raw material' or 'problem space' at which the activity is directed and which is molded and transformed into outcomes with the help of physical and symbolic, external and internal mediating instruments, including both *tools* and signs. The *community* comprises multiple individuals and/or sub-groups who share the same general object and who construct themselves as distinct from other communities. The *division of labour* refers to both the horizontal division of tasks between the members of the community and to the vertical division of power and status. Finally, the *rules* refer to the explicit and implicit regulations, norms and conventions that constrain actions and interactions within the activity system.*

The different elements of the activity system model were included in the interview themes and questions. According to cultural-historical activity theory, culture is present in the form of tools that mediate human activity, and in all the symbolic forms that have accumulated over the social group's history (Cole & Engeström, 2006). Thus, a historical overview of the development of the communities (past - present - future) was also included in the interviews.

3. The communities

Three different communities were recruited for the development and user testing of the community publishing system - *Badamtam's kennel*, *Lions Club Kisko* and "*Food Club*", a group of four families that enjoy cooking and eating together. The chosen communities differed from each other by their size, age, activities, organization and publishing needs. All three communities were located in Southern Finland, were quite small in terms of members, and the nature of activity was hobby-like with emphasis on social interaction and friendship. Two of the communities had only little experience in publishing (*Lions Club Kisko* and *Food Club*), whereas one already had a website, a Facebook group and printed materials (*Badamtam's*).

Descriptions of the communities:

Badamtam's, founded 1992, is a kennel and a community for dachshund breeding and coordinating dog activities. *Badamtam's* is actively involved in national and international dog shows and their dogs are also used in hunting and agility. *Badamtam's* has bred about 200 dogs that are located around the world and there is frequent contact between the dog owners and other dog hobbyists. The kennel is located in Siuntio.

Lions Club Kisko was founded in 1971 and is part of the international Lions Club organisation. Following the international Lions motto "we serve", *Lions Club Kisko* wants to profile themselves as a local service organisation for the approximately 2,000 people living in Kisko. The purpose of their activity is to help and support locals who are in need of help and organise recreational activities. To fulfil this purpose, fund-raising is an important activity for the club as well. For the members of *Lions Club Kisko*, social interaction, friendship, good manners and loyalty are important factors that are emphasised within the club.

Food Club, is a small community of four families living in Somero. The first meeting of this very informal community was in the beginning of 2009, soon after a couple members of the community had visited Italy and discussed the Italian eating culture. The idea of this culture is to meet and eat quite regularly with family and friends in someone's home or in a restaurant. The inclusion of children, i.e. the whole family, in the activities is important. *Food Club* wants to create a Finnish version of this culture.

All the communities considered that the printed publication would complement the digital material of the communities. The more formal communities, *Badamtam's* and *Lions Club Kisko*, considered the web pages a necessity. The role of the web page was seen as an updated information channel, whereas the printed publication could be published more seldom, for example once a year, based on a specific theme such as a year book. On the other hand, *Food Club* considered the printed publication more as a memory, a physical object that would be easy to store and that could also be handed to close relatives. The digital format was also important because "*scrapbooking is easier in digital format than by traditionally cutting and pasting*".

All the communities valued print products. For example, one's own article or picture in a printed publication is much more appreciated than the ones on the web. The result is in line with the findings of our earlier research (Forsell et al., 2007, Vihavainen et al., 2007). Also, the communities saw printed media as an effective means to give recognition to contributors, enhance the commitment of community members and to show gratitude. On the other hand, some community members questioned their own skills to produce high

quality content for a printed publication. A community magazine could be used instead of a business card. The printed product could also be something else than a magazine-like publication, for example a case-specific brochure.

Major challenges in community publishing were seen in encouraging several members of the community to take part in the publishing process, in addition to the scheduling. This obviously is a common challenge in many communities. In some cases, also technical skills were identified as a possible challenge, as some members of the pilot communities were not very experienced computer users.

4. Community publishing system

The study's scope of a networked way of working with community publishing required a new kind of electronic system to be created as the current market offering did not provide a suitable tool for this purpose. The created portal allows content upload, creation and basic editing among the community members simultaneously. Different articles can also be tagged into different categories by the user's own keywords and category titles. The privacy of the content can be defined to be limited to the community members only or to be open for others to use in their personalized publications. An automatic tool for creating a publication ready for press was not implemented in this pilot project. Instead, Adobe InDesign was used to create printable publications from the communities' electronic material situated in the web portal.

Existing publishing tools are often designed assuming there is only one person acting as the chief editor (who might even work off-line) and she/he usually has years of experience using a desktop publishing tool. Compared with that kind of working practice, a significant difference in this pilot project can be seen in the ideology where every member of a community is able to contribute to the publication work concurrently with the other community members. The idea is depicted in Figure 2.

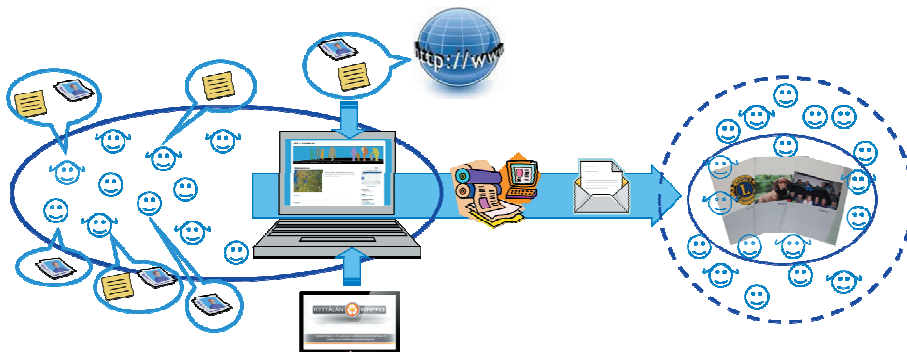


Figure 2: The community publishing process

In order to understand the necessary and desired features of the publication system, the communities were interviewed prior to developing the pilot demonstration system. All three communities emphasized the most important features to be the ease of use and Finnish language for the user interface. Additionally, Badamtam's pointed out the publication system had to work in Windows and Mac environments and also in English to allow the use of publications in international dog shows and events. Food Club reminded about the importance of privacy when dealing with personal content.

Comments regarding the ease of use already limited system development away from an "Adobe InDesign" look-alike tool. The interviews revealed several other useful boundary conditions, too. For instance, the system features should consist of

- ◆ Web-access
- ◆ Blogging-style discussion forum
- ◆ Archive for food recipes/articles/stories etc.
- ◆ Simple image editor
- ◆ Public section accessible to every Internet user
- ◆ Password protected section for registered members only

The system should also include a possibility to divide content into different categories. Thus, with this kind of earmarking it would be easy to collect and select different kinds of publications from the original community's content basket. The publication could, for instance, include only travel stories or the publication could be organized based on themes such as *starters*, *main courses*, *desserts*. The system design included also general requirements based on common practices with web services. These include a firewall setup, security, a backup system etc.

All of the above requirements were channeled towards freely available software due to the nature of the targeted communities. With all these conditions in mind, a web portal was created and an address *compub.vtt.fi* (community publishing) was registered for it. Although freely available software modules exist in the world, they still need to be integrated together in order to make the whole system work as expected. Possible license restrictions and copyright issues must of course be checked and taken into account before doing any modifications to the modules and even before starting to use them.

From the user point of view, a quite essential feature (or software module) is the content editor. The project's plan was to use Google Wave as a base for the real-time editor and then create missing software blocks, such as *PDF exporting* into the tool. Unfortunately, Google suspended Wave's development in August 2010 and thus the project was also forced to give up that direction. A required step was taken towards more mature and long-term development tools and the community publishing system was built based on a content management system (CMS). CMS is a common term for a system used for managing a content related work in a collaborative environment. The system usually consists of:

- ♦ a database for storing the actual data (user information, text, images, sound files etc.)
- ♦ a human interface
- ♦ a control system for access rights; who can modify or access the content

There is a significant amount of content management systems freely available; consult e.g. Drupal (<http://drupal.org/>), Joomla! (<http://www.joomla.org/>), eZ Publish (<http://ez.no/>) and over 50 others. Among all of these, WordPress (<http://wordpress.org/>) was selected as the platform for this pilot demonstration system. WordPress, since its first release in 2003, has gained popularity amongst software developers and still has frequent updates. As the community publishing portal is web based and was designed not to require installing any client software, it works seamlessly in both Windows and Mac environments. The portal is meant to be used with a modern web browser. Old web browsers, such as Internet Explorer 6 can also be used, although the usability is then very poor.

5. Experiences from the design process

The community publishing system was a new way of interacting within the communities. Thus, the 5-week testing period was required in order to make the system familiar to the users, although the actual time spent for making a publication varied from one day (Food Club) to couple of weeks (Badamtam's and Lions). All communities had one person, the owner, who took the main responsibility on the content collection, although the final content was agreed on together and created by more than one community member. For example, with Lions Club Kisko one person typed all the texts into the system but the content of the publication was discussed in several meetings. With Badamtam's, the owner organized roles for community members for content creation but all authors put their articles into the system themselves.

According to Activity system model (Figure 1), *division of labour* is one of the main elements in collaborative human activities, such as in community publishing. If we look at the creation of printed publication with the community publishing tool as an 'activity' from the viewpoint of Activity system, it became evident that Badamtam's had the best ability to organize their actions, and in this case, successfully perform collaborative document editing. The dog-owner community already possessed the culture of sharing and combining information.

It also became obvious that a clear vision of the content and target group of the publication is needed in order to become motivated in the long-term use of the community publishing system. This ultimately relates to *object* and its *outcome*, which are the crucial elements of the Activity system and define the meaning and motivation for the activity (see Engeström 1987). The object, the actual printed publication, needs to guide the activity of the community, and the final outcomes must fulfil the need behind the object.

Lions Club Kisko partly lacked the *reason*, even though the need and motivation for enhancing information about the club in the Kisko area was recognised. The reason for the object and its outcomes (publication and its uses) was still unclear, thus the creation of the publication was mentioned to be an extra burden for the community members. The lack of publishing experience and technical skills also affected so that Lions Club Kisko did not see the system as a very suitable tool for them. Interestingly, the testing period seemed to enhance the need to create the club's own website.

For the very small, informal community of Food Club the motivation for collecting recipes and publishing them in some format was clear, but it was mentioned that the system could be simpler than the pilot system. In the end, despite the clear motivation, the community publishing system would be a nice "bonus" for Food Club, but not a very significant tool.

The ease of use of the pilot system depended strongly on the experience and the technical skills of the users. For some of them, the use of web-based services and other computer applications was part of their everyday life, and thus, the use of the pilot system was fairly easy. The other extreme group of the users, the novices, consisted of people who use computers more randomly and mainly utilize Microsoft Office tools. For them, the pilot system seemed to be rather complicated to use at the beginning. The printed publication divided opinions: Lions Club Kisko and Food Club were satisfied, or even positively surprised, with the printed publications, whereas Badamtam's were more critical and pointed out several crucial targets for development. Due to the background of Badamtam's members, they had a very professional attitude towards the publication. Therefore they saw the main shortcomings in typography and layout, and they would require more finishing options in the form of templates.

The "blog-like writing" as performed within the pilot system seemed to serve well the needs of Badamtam's community. It was mentioned that the members of the community have the need to share their thoughts and it becomes easier to publish your own text when you see others write as well. Many of the members had previously sent long emails to the owner of the kennel in order to share ideas and get answers to questions. The use of a community publishing system would help especially new dog owners to get valuable information from the more experienced members of the community. The system would also make it easier to update and share the puppy buyer's guide which had been delivered as a PDF file or in printed format.

6. Summary

From the three participating communities Badamtam's kennel fulfills all the three key requirements. Badamtam's is the largest community in this study and its members vary from the dog experts to new dog owners. The new dog owners are very interested in collecting information, experience and tips from other dog owners. Thus, the community has a need for sharing information. They have experience in publishing both in digital and in print format, and many of the community members take also actively part in the chats for dog owners, thus, the content creation and sharing is not a problem. It is also important for a kennel's success and reputation to inform possible puppy buyers profoundly about kennel's activities by publishing in different ways. The publishing is seamlessly linked to other activities of the community, and the outcomes of publishing are supporting the activities.

Food Club and Lions Club Kisko were not quite as confident about regular publication as Badamtam's. From the above mentioned key requirements, Food Club has the culture of sharing and they are able create the content but they don't have a clear need. The publication is more like a bonus for the community. Lions Club Kisko, on the other hand, has a need for the publication both in the form of a homepage and as a leaflet. This need is still emerging however, and publishing is not seen as crucial for the community (yet). Additionally, they don't trust themselves in the content creation, and the ability to use technology varies within the community.

One major difference between the Lions Club Kisko and the other communities is the target group of the publication: Lions Club members want to give information to outsiders, but the main target group for Badamtam's and Food Club is themselves. For Lions Club, this is probably one reason behind their lack of trust on content creation and their wish to use a professional writer. One important element for successful publishing seems to be the personal importance and meaningfulness of the community's activity. For Badamtam's community members, dogs are close family members, thus dog-related activities are personally very meaningful. The need for publishing derives from this meaningfulness of activity.

7. Conclusions

The project's scope of a networked way of working with community publishing required a new kind of electronic system to be created as the current market offering did not provide a suitable tool for this purpose. Existing publishing tools are often designed assuming there is only one person acting as the chief editor and she/he usually has years of experience using a desktop publishing tool. Compared with that kind of working practice, a significant difference in this pilot project can be seen in the ideology where *every member of a community is able to contribute* to the publication work concurrently with the other community members.

For successful use of the publishing system, the community

- ♦ should have a *need* for producing a printed publication,
- ♦ should have a *culture of sharing* information,
- ♦ members should be ready to *create content* themselves. The ability to create content includes the ability to *use suitable technology* for content creation.

These requirements are especially important, when community begins to work with the publishing system; they lower the threshold of implementation within the community. The pilot version of a community publishing system was developed in this study. There are some additional requirements which must be fulfilled before this kind of demonstration application can be commercialized.

- ♦ The application should have good documentation and instructions on how to use it in order to cover different kinds of user groups. Getting started with the system should be easy enough for all kinds of users with a minimal amount of instructions.
- ♦ The application should have at least a few selectable layout templates for the printable publications and the initial layout proposal from the application should be fully automatic. It should also be possible for a community to create their own templates and it should be possible to share them easily in public.
- ♦ The possibility to add ready-made content by other hobbyists should also be taken into consideration in the development of the community publishing system. The possibility to compose a publication from ready-made articles from others sharing the same interest would significantly lower the hurdle and effort of creating a publication and thus increase the demand.

Acknowledgements

This research project was funded by Forestcluster Ltd.

References

- Cole, M. & Engeström, Y. (2006). *Cultural-Historical Approaches to Designing for Development*. In Valsiner, J. & Rosa, A. (eds.). *The Cambridge Handbook of Sociocultural Psychology*. Cambridge University Press. pp. 484-507.
- Engeström, Y. (1987). *Learning by expanding: An activity-theoretical approach to developmental research*. Helsinki: Orienta-Konsultit Oy.
- Forsell, M., Grenman, K. & Ylisiurua M. (2007). *Linking print and web based on community needs. Collaborating over Paper and Digital Documents(CoPADD), 2nd International Workshop, November 9th*.
- International standard ISO 9241-210:2010(E) (2010). *Ergonomics of human-system interaction - Part 210: Human-centred design for interactive systems*.
- Turpeinen, M. (2003). *Co-Evolution of Broadcasted, Customized and Community-Created Media*. In: Lowe, G. F. & Hujanen, T. (eds.). *Broadcasting & Convergence: New Articulations of the Public Service Remit*. Nordicom, Göteborg, 2003.
- Vihavainen, S., Sarvas, R., Näsänen, J. & Grenman, K. (2007). *User centric approach for designing cross media applications in personal photography. iarigai Advances in Printing and Media Technology, Vol. XXXIV, pp. 375-385*.

* Source: <http://www.edu.helsinki.fi/activity/pages/chatanddwr/activitysystem/>



Exchange rates for media currencies

*Ulf Lindqvist, Anna Viljakainen, Hannu Kuukkanen,
Paula Järvinen, Pekka Siltanen*

VTT Technical Research Centre of Finland
P.O. Box 1000, FI-02044 VTT, Finland
E-mail: firstname.surname@vtt.fi

Abstract

Understanding advertising impact of media and comparative media currencies are the bases of intelligent marketing investment decisions. Inter-media currencies are exchange rates for buying and selling media advertising space in different media. The reason for building media exchange rates is to find better measures for advertising impact: one media and cross-media. There are several ongoing projects in number of global media markets for building inter-media currencies as they are considered a growth factor for an industry that has a high dependence on advertising revenue. The objective of this research was to investigate how to increase comparability between media currencies in Finland and get more qualitative elements added to media surveys that are said to yield mainly quantitative results.

Keywords: media advertising, media currency, exchange rate, media survey

1. Introduction

Media currencies are used for buying and selling media advertising space and airtime. Usually each type of media has its own currencies, which measure quantity rather than quality. Such currencies have been built for traditional media, but the radical transformation towards the digitalisation of media calls for an inter-medial currency. The comparability between media metrics and getting deeper into the qualitative elements of different media would benefit both media buyers and sellers.

In 2010 media advertising spending in Finland excluding production costs reached over 1300 million Euros. Advertising revenue is the main source of income for most types of media, but it is very sensitive to market economy fluctuations because during an economic downturn marketers make quite heavy cutbacks in marketing budgets. Media advertising spending suffered a severe setback following the global financial crisis. In effect, spending on advertising both in Finland and around the globe began to drop in November 2008, TNS Gallup (2011). The recession has accelerated the gradual shift of advertising spending from traditional media towards online media. The challenge is that for most media advertising revenue is the sole source of income (urban and pick-up papers, outdoor media, commercial radio), or a significant part of revenue (50 - 80 % for commercial TV, 30 % for printed magazines, and 55 % for printed newspapers) Statistics Finland (2010) and Association of Finnish Advertisers (2010). However, at present online advertising revenue does not provide sufficiently revenue for media to cover the costs of production and distribution of media content across different platforms, Antikainen & al. (2010). Inter-media currencies are being built internationally, but we are still lacking an inter-media currency in Finland, mainly because of the small size of the market. Building an inter-media currency with the research methods available is extremely expensive.

At present, there are four existing media currencies in the Finnish media markets: the National Readership Survey (NRS) for printed media, TV Audience Measurement (TAM), the National Radio Listening Survey (KRT), and Outdoor Impact for outdoor media. There are also a number of other media surveys that are widely acknowledged and utilised, but which do not hold the position of a currency. Media currencies are measured using different methodologies and were initiated to serve the respective type of media. The differences lie in the depths of the data, as well as how and what data is gathered; i.e. relating to the sample and sampling, the source and size of the sample, the data collection method, and the frequency of reporting. Each currency/survey is governed by its respective survey data owners. The data processing of currencies takes place in multiple planning programmes that are built on the basis of the needs of each type of media. There is criticism within the market, that existing media currencies and surveys measure quantity rather than quality. Similarly, they have been built for traditional media, but a radical transformation towards the digitalisation of the production, distribution and consumption of media across different platforms has recently

been observed. There is a shift towards inter-media within intra-media; i.e. newspapers are being published not only in paper format, but also on the Internet, mobile, in tablets, etc.

The comparability between media metrics and getting deeper into the qualitative elements of different media would benefit both media buyers and sellers. For publishers, this would bring about a deeper understanding of the value of the media being offered (qualities other than contact prices) and more detailed metrics for selling cross-media brands through different platforms. Marketers are interested in understanding from where they can get the best possible returns for their advertising investments. Comparable currencies would provide the tools to optimise a media mix as well as a proof of the effectiveness of different media used in a campaign.

The aim of our research project was to overcome the lack of a national inter-media currency, i.e. an exchange rate for buying and selling media advertising space in different media. The reason for building such exchange rates is to find better measures for cross-media advertising impact.

The project objective is twofold: 1) to increase comparability between existing media currencies; and 2) to get more qualitative elements added to media surveys that are said to yield mainly quantitative results. The first objective was carried out by examining whether one single inter-media currency can be achieved, or whether exchange rates between intra-media currencies could be developed. The second objective can be carried out by monitoring consumers' everyday media use and user experiences thereof. Comparability between media metrics and getting deeper insight into the roles of media in consumers' lives would benefit both media buyers and sellers. A project objective is also to develop a reporting and visualisation system - the tool and interface to exploit the integrated data.

2. Research methods

The project consortium consisted of media organisations, organisations measuring TV audience, radio listening and readership, media agencies and researchers. The consortium defined the most essential research questions relevant to integrate existing media currencies.

In the next step a data integration workshop was arranged with a broader panel of experts in order to define the expectations and objectives for media currency data integration, idiosyncrasies of existing currencies and mutual interfaces to other currencies.

Interviews were conducted with industrial representatives in spring 2010, and approximately 30 experts within the Finnish media sector were interviewed in total. The main objective of interviewing industrial representatives was to identify the needs of the media industry value network (i.e. media houses, media agencies, advertisers, research agencies) when building a comparative media currency for all media. Interviewees were responsible in their respective organisations for media sales/buying and/or people who used media surveys regularly in their occupations. A semi-structured interviewing method, a focussed interview, was used. In focussed interviews, the interviewing themes are set in advance for all interviews, although there might be variations in the actual questions and the order in which they are asked. Interviews lasted from one to one and a half hours, during which interviewees were asked to elaborate on the following themes of interests:

- What opportunities and benefits would an inter-media currency offer to the players in the media value network?
- What kind of threats would an inter-media survey have?
- What are the strengths and weaknesses of existing media currencies?
- What would be the strengths and weaknesses of an inter-media level currency?
- What kind of information in respect to media use is lacking in different planning approaches?
- What kind of information is needed from an inter-media-level survey?
- How is it possible to combine different media surveys, each of which has its own strengths and weaknesses?
- What would the survey have to be like to be able to benefit all parties utilising it?
- What is important in making media sales and buying more cost-efficient?
- What additional properties are needed in the data processing planning systems?
- What would be the ideal with regard to survey data if anything was possible?
- What are the relevant international examples to be benchmarked?

The data content of the existing media surveys were analysed. The media survey data content analysis was carried out based on detailed data descriptions and data contents examples from two companies. Different data fusion methods and their suitability were studied together with different alternatives for fusion architecture. Finally different mobile data collecting technologies and methods for visual analytics were analysed.

3. Results

During the first year of the research project the primary stress was on 1) examining the current state of the Finnish media currencies/surveys and their comparability, and 2) the industry wants and needs related to increasing media currency comparability.

Based on our findings, the industry needs and wants in respect to our project objective of building a comparative media currency for all media could be categorised under five general topics for which improvements are sought after: 1) the roles of different media in consumers' lives, 2) media currency comparability, 3) consumer behaviour and media experience, 4) media impact and effectiveness, and 5) marketing/advertising impact.

The topic of *roles of different media* related to such issues as what is the special characteristics and depth of media, what are the roles and touch points of media in consumers' everyday life, and how is the relationship built between media and consumer. *Media currency comparability* related to the industry need of increasing the calculated comparability and weights of ad space in different media. Relating to *consumer behaviour and media experiences*, a fundamental issue raised in interviews was that a better understanding is required as to how consumers interpret and interact with media in the situations they are in, and how they remember or value those encounters later on. Argumentations were based on notions that consumers' interpretation of media is situational, affected by the emotional states they are in, their values, attitudes, interests and motives, and that media experiences differ from the memory traces they leave behind. In respect to *media impact*, a common viewpoint was that media surveys should go beyond media encounter to long-term media impact, and that different media have different temporal effectiveness. A common subject in respect to *advertising impact* was the issue of having the right approach for consumer contact in each media, to increase the accuracy of the aim of the media. Inter-media metrics for giving factual evidence on the effectiveness of marketing and advertising activity (such as calculating ROI, Return On Investment) was in general focus.

Based on our findings, existing media currencies are collected using different methodologies and have been initiated to serve the respective medium. A media survey data content analysis from three media surveys (the TV Audience Measurement TAM, The National Radio Listening Survey KRT, and a cross-media survey TNS Atlas) was carried out in 2010 focusing on exploring what data is collected in these surveys, how much overlapping data are there in the surveys, and how commensurable the data are (Figure 1).

The findings of the analysis revealed that each system codes and classifies many similar things, but the naming, coding and classifications between them differs. The harmonisation of the code values and classifications is the first step towards commensurability.

At present, survey data is owned by different entities: TV Audience Measurement and The National Radio Listening Survey by Finnpanel Oy, The National Readership Survey by The Finnish Audit Bureau of Circulations, Outdoor Impact by JCDecaux Finland and Clear Channel Finland, the cross-media survey TNS Atlas and the online audience measurement tool TNS Metrix by TNS Gallup. The integration of data owned by different entities requires technical, statistical, business and legal issues to be extensively considered and negotiated.

The *technical issues* relate to questions whether it is possible to fuse data from the existing databases and what tools are needed in doing so. *Statistical issues* relate to the algorithms that should be used in order to ensure the validity of the analysis based on the combined database. *The legal issues* relate to the legal challenges that are faced when combining information from different databases that contain personal information. The *business issues* relates to a necessary task to be accomplished at a very early stage, i.e. the development of a business model commonly agreed by everyone willing to go forward with data integration and the development of an end product. A business model will determine what data fusion strategies and architectures will be chosen.

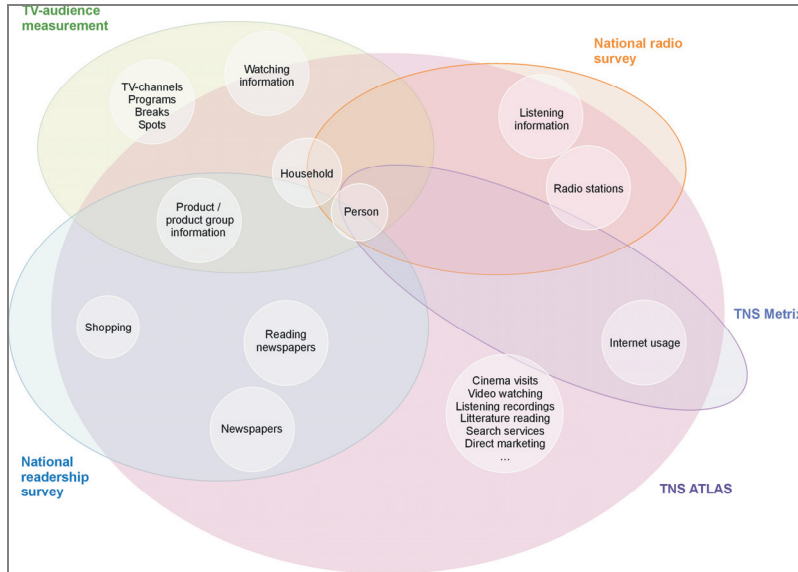


Figure 1: Overview of existing media survey companies' data content

Following our findings, there are several fusion architecture alternatives for the media industry to choose from. A *common database* would have shared tools for data collection, analysis and reporting, and each partner would use the same database with similar tools. A *shared data model* would mean that each partner would have its own database, all of which share a common data model. In this model partners would exchange data in a similar format, and use similar tools for data collection, analysis and reporting, but could also use and develop their own tools. A *data exchange model* would mean that each partner would have its own databases, which would be modelled in their own ways. The data would be shared and exchanged with partners through a common data exchange model and data transformations. Each partner would have its own tools for data collection, analysis and reporting. In a *shared reporting model* each partner would have its own database, and the data models would be harmonised in such a way that makes it possible to create shared reports; for example, by agreeing on data formats and similar classifications to code values meaning the same things. And finally, a *data partition model* would mean that each company keeps the data relating to its core business to itself, while the rest would be stored in a common database. For instance, individuals and their background information and shared objects of interest would be in the shared storage, and the media usage data is in the possession of each partner.

In order to implement any of the architectures above, an fusion algorithm for implementing the fusion must be selected. Data fusion means basically the matching of databases from two surveys at the respondent level. Fusion requires the surveys to have common variables: usually demographic, geographical, or relating to media usage, etc. The goal is to add new variables from the donor database to the recipient database, based on the similarity of the common variables (Figure 2). There are several well known algorithms for matching the surveys. Currently we are planning to compare two matching algorithms: standard nearest neighbour algorithm and predictive isotonic fusion (Soong R. & Montigny M, 2003).

Our findings show, that there are certain drivers for the media industry to merge media currency and survey data: 1) to enrich the media data of each partner; 2) to get more comparable media metrics for buying and selling media; 3) to share the costs of collecting data that certain data owners are missing; 4) to save on the costs of overlapping work in data collection, management, analysis and reporting; and 5) to be able to jointly develop new tools and methods for data collection, analysis and reporting.

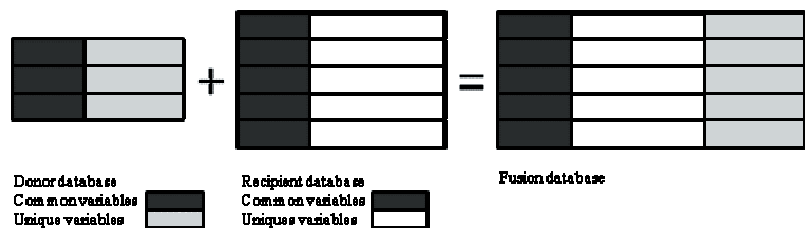


Figure 2: Data fusion

In 2011 a proof of concept will be developed to specify whether data fusion is possible, and under what conditions. Based on the proof of concept, a research objective is to examine whether one single currency (i.e. an inter-media currency) can be achieved, or whether each media have their own currencies that are scaled against one another using exchange rates (i.e. intra-media currencies of readerships of publications, viewing and listening figures, and contacts). An inter-media currency would mean that all intra-media currencies would be evaluated and rated equally. An exchange rate would mean that the measurements of all intra-media currencies would be executed differently and scaled against one another. Furthermore, each medium would retain its own currency, which would be updated following its own cycles and methodologies. An exchange rate exists and develops based on the changes made in each currency. The groundwork which must be done in order to move forward with either of these two alternatives is the harmonisation of data.

4. Conclusions

There are financial, political, and technical reasons that have generated existing media currencies that are similarly affecting the level of cooperation in negotiations related to integrating media surveys. Integration of media data is far from an easy task in any media market, since maintaining media neutrality while paying regard to the differing interests of the parties involved is challenging. It is challenging, because such an effort has to involve all parties from the media industry value network - media buyers, media sellers, and media data owners.

In the efforts of unifying media currencies in media markets at least the following questions should be of prime concern:

- Under what conditions is data integration possible (technical, statistical, business, and legal issues)?
- What needs to be harmonised in existing media data to enable data integration?
- Which can be achieved: inter-media currency or exchange rates between intra-media currencies?
- What is the state-of-the-art of media surveys and how can the strengths of existing media currencies utilised?
- What is the extent and benefit for data or knowledge transfer among the players in the media value network?
- How will media outside existing surveys (e.g. new media such as blogs or social media) be considered?
- What are strategically the key issues to be measured?
- How are media impact and effectiveness compared, how are they valued?
- How is qualitative data on media-use collected cost-efficiently?
- Who are the administrators and/or owners of a new inter-media level data?
- How can the quality of the inter-media currency or exchange rates be verified and ensured?
- What is the data processing tool for an integrated database?

Building exchange rates for media currencies in any market is a challenging and multidimensional task. In the beginning of such an effort it might involve slowness and perhaps an absence of clear-cut modes of operations. As such, openness, cooperation, and interaction between the parties involved should be of prime concern, and should be maintained by any means necessary. From the very beginning setting clear-cut and prioritising objectives, as well as listing and commonly agreeing the key questions to be solved in the process are of utmost importance.

Acknowledgements

The study was partly financed by the Finnish Funding Agency for Technology and Innovation (TEKES). The following companies and organisations have participated in the study: Dagmar Oy, Finnpanel Oy, The Finnish Newspapers Association, Sanoma Television Oy / Nelonen Media, TNS Gallup Oy.

References

- Antikainen, H., Kuusisto, O., Bäck, A., Nurmi, O., Viljakainen, A., (2010). VTT GT Report 1/2010. (In Finnish) Association of Finnish Advertisers (2010).
<http://www.mainostajat.fi/mliitto/sivut/mainonnanmerkitysmnk.pdf>
http://virtual.vtt.fi/virtual/nextmedia/Deliverables-2010/D1.4.1.1%20Mobime%20Building%20Exchange%20Rates%20for%20Media%20Currencies-MOBIME%202010_%20Final%20Report.pdf
http://www.stat.fi/ajk/tiedotteet/2010/tiedote_014_2010-12-08_en.html
- Soong, R. & de Montigny, M., (2003). Does fusion-on-the-fly really fly?, *in* 'ARF/ESOMAR Week of Audience Measurement'.
- Statistics Finland (2011), Statistical Yearbook of Finland 2010.
- TNS Gallup (2011) Media Intelligence. <http://www.tns-gallup.fi/index.php?k=12701>
- Viljakainen A., Järvinen, P., Siltanen, P., Kuukkanen, H., Lindqvist, U., Pajukanta, J., Peltola, J. (2010), Building Exchange Rates for Media Currencies MOBIME, Next Media Report, 2010.

Index of authors

- Afara, Imadeddine 167
 Aikala, Maiju 411
 Alecrim, Viviane 59
 Anokhina, Evgeniya 285
 Apró, Magdolna 209
- Bablyuk, Evgeniy 285
 Baskaran, Natarajan 379
 Bauer, Wolfgang 27, 93
 Baumann, Reinhard 247
 Bircher, Fritz 69, 79
 Blayo, Anne 237
 Blohm, Erik 21, 59
 Böddicker, Alexander 51
 Bohn, Daniel 349
 Bois, Chloé 237
 Bolanča Mirković, Ivana 361
 Bolanča, Zdenka 361
 Borbély, Ákos 87
- Carrabina, Jordi 221
 Chandak, Praveen 143
 Chaussy, Didier 237
 Chen, Ping-hsu 11
 Chinga-Carrasco, Gary 21
 Chinnaraj, Senniappan 379
 Chung, Robert 11
 Claypole, Timothy 103
 Csoka, Levente 143
- Dattner, Michael 349
 Deger, Wolfgang 247
 Deshpande, Kiran 323
 Diaz, Juan 271
 Dörsam, Edgar 167, 175, 303
 Dryga, Marina 285
 Dziallas, Holger 247
- Enlund, Nils 3
 Enns, Eugen 247
 Erho, Tomi 159
 Euler, Thorsten 175
- Fässler, Florian 69
 Fedutina, Maria 303
 Feirer, Verena 93
 Fergen, Immanuel 175
 Fleming, Paul 331
 Friedl, Herwig 93
 Fuentes, Alejandro 369
- (de) Gracia, Vicente 253, 271, 369
 Gane, Patrick 123, 133, 191
 Gerstner, Philip 133
 Gilewicz, Natalia 395
 Golob, Gorazd 231, 293
 Gonzalo Diaz, Elkin 221
 Gooran, Sasan 317
 Görgényi-Tóth, Pál 309
 Green, Phil 323
 Grozdits, George 143
- Haas, Martin 175
 Harikrishnan, Amrutharaj 379
 Haslebacher, Philipp 69
 Hauptman, Nina 231
 Herranz, Nuria 271
 Hirn, Ulrich 27, 93
 Hoffmann-Walbeck, Thomas 387
 Hübler, Arved 51
 Hübner, Gunter 103, 261
 Hyväkkä, Jouko 411
- Izdebska, Joanna 201
- Järvinen, Paula 419
 Jašúrek, Bohumil 277
 Jewell, Eifion 103
 Johansson, Per-Åke 59
 Juuti, Mikko 123
- Kaljunen, Timo 159
 Kaplanová, Marie 277
 Karlović, Igor 153
 Karunanithi, Palaniappan 379
 Keränen, Mikko 159
 Kiran, Prayagi 379
 Klamann, Marianne 59
 Klanjšek Gunde, Marta 183, 231, 277
 Kohl, Albert 247
 Kokko, Annaleena 159
 Kondratov, Alexandr 285
 Kukkamo, Vesa 191
 Kunnari, Vesa 159
 Kurmakaev, Evgeny 175
 Kuukkanen, Hannu 419
 Kuula, Timo 411
- Lechthaler, Markus 27
 Lindqvist, Ulf 419
 Lofthus, Jon 59
 Lovell, Veronika 331

- Maček, Marijan 231
 Majnarić, Igor 361
 Marmet, Philip 69
 Maurer, Chris 51
 Moberg, Åsa 403
 Moginov, Rostislav 43
 Muck, Tadeja 231
 Müller, Markus 253, 271, 369
 Mustač, Sandra 361
- Namedanian, Mahzian 317
 Nayoze, Christine 237
 Novaković, Dragoljub 153, 209
 Novotny, Erzsebet 153, 309
 Nowack, Dietmar 51
- Örtegren, Jonas 59
 Otero, Susana 253, 271, 369
- Pallarès, Jofre 221
 Panák, Ondrej 277
 Pekarovicova, Alexandra 331
 Pérez, David 369
 Petersen, Ingmar 103
 Petriaszwili, Georgij 111
 Picha, Malin 403
 Plevnjak, Janja 231
 Podsiadło, Halina 201
 Poznyak, Eva 43
 Prayagi, Paritosh 51
 Pyryev, Yuriy 111
- Rajendrakumar, Anayath 379
 Rajesh, Kaipensery Swaminathan 379
 Ramon, Eloi 221
 Rättö, Peter 21
 Renner, Johannes 69, 79
 Ridgway, Catherine 123, 191
 Riegel, Sebastian 387
 Rotar, Bojan 293
 Rozman, Jana 183
- Schanda, János 5
 Schlegel, Gert 69, 79
 Schmitt-Lewen, Martin 175
 Schnitzlein, Markus 51
 Seisto, Anu 411
 Siegel, Frank 247
 Siltanen, Pekka 419
 Sipiläinen-Malm, Thea 159
 Sonnenschein, Joachim 175
 Starešinič, Marica 231
 Subrahmanyam, Satyavolu Venkata 379
 Szabolcs, Pál 209
 Szentgyörgyvölgyi, Rozália 87, 309
- Šulc, Damjan 293
- Tåg, Carl-Mikael 123
 Terés, Lluís 221
 Toiviainen, Maunu 123
 Tomić, Ivana 153
- Urban, Peter 349
 Urban, Philipp 167, 303
 Urbas, Raša 183, 231
- Vališ, Jan 277
 Vermeulin, Alice 35
 Vidmar Tjaša 231
 Vieille-Grosjean, Laurette 35
 Vila, Francesc 221
 Viljakainen, Anna 419
 Vincent, Rémi 237
- Willert, Andreas 247
 Willfahrt, Andreas 261
- Yang, Li 339
- Zhang, Hai 133
- Žveglič, Maša 231